UNIVERSIDADE DE LISBOA

FACULDADE DE CIÊNCIAS

Reconstituição Paleoclimática e Paleoambiental em Estuários com Base no Registo Micropaleontológico de Foraminíferos: Relação com Indicadores de Escala Local, Regional e Global

Doutoramento em Geologia
Especialidade Paleontologia e Estratigrafia

João Carlos Jorge Moreno

Tese orientada por:
Doutor Francisco Manuel Falcão Fatela
Doutor Eduardo Leorri Soriano
Doutor Alejandro Cearreta Bilbao

Documento especialmente elaborado para a obtenção do grau de doutor

2017

UNIVERSIDADE DE LISBOA

FACULDADE DE CIÊNCIAS

Reconstituição Paleoclimática e Paleoambiental em Estuários com Base no Registo Micropaleontológico de Foraminíferos: Relação com Indicadores de Escala Local, Regional e Global

Doutoramento em Geologia

Especialidade Paleontologia e Estratigrafia

João Carlos Jorge Moreno

Tese orientada por:

Doutor Francisco Manuel Falcão Fatela

Doutor Eduardo Leorri Soriano

Doutor Alejandro Cearreta Bilbao

Júri:

Presidente:

- Professora Doutora Maria da Conceição Pombo de Freitas

Vogais:

- Doutor Guillermo Francés Pedraz
- Doutora Antje Helga Luise Voelker
- Doutor Francisco Manuel Falcão Fatela
- Doutor Ricardo Machado Trigo

Documento especialmente elaborado para a obtenção do grau de doutor

Instituição Financiadora: Fundação para a Ciência e a Tecnologia

2017

“My reasons for taking this less-travelled road were many. One is the inevitable thrill of discovery when you wander into new areas. More importantly, you also avoid the danger of being too comfortable in too narrow a niche. I truly believe the sayings that there is no hope for the satisfied man and that without fear there is no learning. (…) I also think that many of the most significant discoveries in science will be found not in but between the rigid boundaries of the disciplines: the terra incognita where much remains to be learned. It’s not a place that’s hidebound by practice and ritual. I have always tried to keep moving between fields of study.”

John Allen “Jack” Eddy, 1999 (Interview with Jack Eddy, conducted by Spencer Weart, April 21, 1999)

Acknowledgments

I would like to express my deepest gratitude to Professor **Francisco Fatela**, my supervisor, and to my co-supervisors Professor **Eduardo Leorri** and Professor **Alejandro Cearreta** for all the support and insight. Many thanks for the valuable discussions, suggestions and revisions of manuscripts and for their patience throughout the development of this dissertation. And, above all, for their inestimable friendship.

I am sincerely grateful for the advantage to be part of this research group, for its scientific honesty and interdisciplinary view, which allowed me to explore some “less-travelled roads”. In this, I include all the co-authors of the papers presented herein – **Maria Cristina Cabral**, **David Reide Corbett**, **Rui Taborda**, **Ricardo Machado Trigo**, **Mário Abel Gonçalves**, **Juan José Gómez-Navarro**, **Rudolf Brázdil**, **Manuel João Ferreira**, **José Maria De la Rosa**, **Inês Pereira**, **Maria de Fátima Araújo**, **Maria da Conceição Freitas**, **Ana Medeiros**, **Teresa Valente**, **Lúcia Guise** and **William H. Blake** –, who wisely guided me in the process. For each of them, my thanks!

I thank also to **Vera Lopes** and **Ana Rita Figueiredo** for the laboratory support, to **Maria Quintela**, **Anabela Cruces**, **João Cascalho**, **Catarina Fradique**, **Celso Pinto**, **Tanya Silveira**, **Francisca Rosa**, **Catarina Guerreiro**, **Raquel Cardoso** for the field work assistance, and to **Telmo Nunes**, from the Unidade de Microscopia da Faculdade de Ciências da Universidade de Lisboa, for the technical support SEM images.

I would like to acknowledge **Guillermo Francés**, **Ronal E. Martin**, **Peter Langdon**, **Dereck Booth** and all the anonymous reviewers for their remarks that improved the final manuscripts, and **Carla Neves** for proofreading.

I thank to **Filipa Moreno** who closely followed, advised and encouraged me throughout my graduate work and my life.

I thank to **FCT** – Fundação para a Ciência e a Tecnologia – for financing this work, through a PhD grant (SFRH/BD/87995/2012).

Finally, I thank my family and my friends for always being around during this exciting and intense journey.

Abbreviations and Acronyms

AD – *Anno Domini*
ACL – Average Chain Length of n-alkanes
AMO – Atlantic Multidecadal Oscillation
AMS – Accelerator Mass Spectrometry
ANC – Vila Praia de Âncora (Minho coast)
AO – Arctic Oscillation teleconnection index
APA – Agência Portuguesa do Ambiente
AR – Assessment Reports of the Intergovernmental Panel on Climate Change
avg. – Average
BFR – Brominated Flame Retardants
bmsl – below mean sea-level
BP – Before Present
Br_{org} – Organobromine
Br_{inorg} – Inorganic Bromine
[Br] – Soil/Sediment Bromine content
[Br_{org}] – Soil/Sediment Organic Bromine content
C – Carbon
CA – Correspondence Analysis
ca. – circa
cal yr BP – Calibrated year Before Present
CCN – Cloud Condensation Nuclei
CE – Coefficient of Efficiency
C_{fb} – Temperate climate, without dry season and warm summer
CM – Camarido (Minho coast)
CME – Coronal Mass Ejections
COI – Cone of Influence
C_{org} – Organic Carbon
CP – Railway Bridge sampling transect (Minho estuary)
CPC – Climate Prediction Center
C_{sa} – Temperate climate, with dry season and hot summer
CR – Cosmic Rays
CRS – Constant Rate of Supply model
CRVV – Comissão de Viticultura da Região dos Vinhos Verdes
CT – Connecticut
CWT – Continuous Wavelet Transform
DA – Dark Ages
DM – Dalton Minimum
DW – Durbin-Watson test
EA – East Atlantic Oscillation teleconnection index
EA/WR – East Atlantic/Western Russia teleconnection index
ECHO-G – Global model
EDM – Entre-Douro-e-Minho
EDXRF – Energy-Dispersive X-Ray Fluorescence Spectrometry
EHWS – Extreme High Water Spring
ERIK1 – Model simulation dataset
ET – Evapotranspiration
Expl. Var. – Particular component variance
FA – Factor Analysis
FAZ – Foraminiferal Assemblage Zone

GCR – Galactic Cosmic Rays
GEC – Global Electric Circuit
GHD – Grape Harvest Dates
G_i – Groundwater inflow
GLE – Ground Level Enhancement events
G_o – Groundwater outflow
GS – Growing Season
GST – Growing Season Temperatures
GSTmax – Growing Season mean maxima temperatures (March to August)
HHWS – Highest High Water Spring
HLW – Highest Low Water
HZ – Hydrographic Zero
IC – Ion Chromatography
ICNB – Instituto da Conservação da Natureza e da Biodiversidade
IGME – Instituto Geológico y Minero de España
IP – Iberian Peninsula
IPCC – Intergovernmental Panel on Climate Change
IPMA – Instituto Português do Mar e da Atmosfera
IR – Infrared band
ITCZ – Intertropical Convergence Zone
JJA – June, July and August
LASP – Laboratory for Atmospheric and Space Physics
LHW – Lowest High Water
LIA – Little Ice Age
LOI – Loss-on-ignition
Low Sal. spp. – Percentage distributions of the group of low-salinity benthic foraminiferal species
MAM – March, April and May
MAMJJA – March, April, May June, July and August
MCA – Medieval Climatic Anomaly
MHHW – Mean Highest High Water
MHW – Mean High Water
MHWN – Mean High Water Neap
MHWS – Mean High Water Spring
min–max – Minimum–maximum
MM – Maunder Minimum
MM5 – Mesoscale model
Mod.-Brackish spp. – percentage distributions of the group of Brackish/Moderate-Brackish benthic foraminiferal species
Mod.+Normal Sal. spp. – Brackish/Moderate plus Brackish-to-Normal salinity benthic foraminiferal species
MSL – Mean sea-level
MtL – Mean tide level
MWR – Minho Wine Region
NAE – North Atlantic European sector
NAO – North Atlantic Oscillation index
NASA – National Aeronautics and Space Administration
NASA/ARC – National Aeronautics and Space Administration/Ames Research Center
NF – Number of Foraminifera
NIST – National Institute for Standards and Technology
NOAA – US National Oceanic and Atmospheric Administration
Normal Sal. spp. – Percentage distributions of the group of Brackish-to-Normal salinity benthic foraminiferal species
NRLTSI2 – TSI estimation model
NSR – Nossa Senhora do Rosário, Lima estuary
NSR_L – Nossa Senhora do Rosário transect, Lima estuary

$[O_3]$ – Ozone concentration
OC – Organic Carbon
OIV – International Organisation of Vine and Wine
OM – Organic Matter
[OM] – Soil/Sediment Organic Matter content
OWDA – Old World Drought Atlas
P – Precipitation
p – p-value
P–ET – Precipitation minus Evapotranspiration
PAR – Photosynthetically Active Radiation
PDSI – Palmer Drought Severity Index
PiC – Pinelas transect (Minho estuary)
PM – Particulate Matter
PMF_M – Ponte Vila Nova de Milfontes transect (Mira estuary)
PMOD – Composite solar irradiance record (Physikalisch-Meteorologisches Observatorium Davos analysis of satellite data
PR – Pedras Ruivas transect (Minho estuary)
Prp.Totl. – Total amount of the explained variance
PSU – Practical Salinity Unit (1 psu = 1 gram of salt per 1000 grams of water)
PWP – Present Warm Period
QBOs – Quasi-Biennial Oscillations
r – Correlation coefficient
RCM – Regional Climate Model
RE – Reduction of Error
REDFIT – Spectral Analysis software
RMSD – Root Mean Squared Deviation
RMSE – Root Mean Squared Error
RSD – Relative Standard Deviation
RWP – Roman Warm Period
R_z – Wolf sunspot indices
S – Number of Species
[S] – Salinity
Sal. – Salinity
SA – Solar activity
SAT – Surface Atmospheric Temperature
SATIRE – TSI estimation model
SCA – Scandinavian teleconnection index
SCR – Solar Cosmic Rays
SD – Standard Deviation
SEP – Solar Energetic Particles
S_i – Surface water inflow
SM – Spörer Minimum
S_o – Surface water outflow
SORCE – Solar Radiation and Climate Experiment
SPI – Standardized Precipitation Index
SSI – Solar Spectral Irradiance
SST – Sea-surface Temperature
STG – Stepwise Thermogravimetric Procedure
S^{to} - Santo
TAR – Terrigenous/Aquatic Ratio of n-alkanes
T_i – Tidal inflow
TIMED – Thermosphere, Ionosphere, Mesosphere Energetics and Dynamics NASA exploratory mission
T_o – Tidal outflow
TOC – Total Organic Carbon

TRO_S – Troia transect (Sado estuary)
TSI – Total Solar Irradiance
V – Water Volume
VIS – Visible radiation
VM – Vilar de Mouros
VNC – Vila Nova de Cerveira (Minho coast)
vs. – versus
UE – European Union
USA – United States of America
USGS – United States Geological Survey
UV – Ultraviolet radiation
XWT – Cross Wavelet Transform
WDC – World Data Center
WM – Wolf Minimum
WMO – World Meteorological Organization
WP – Wine Production
WPG – Wine Production Gaps
WSN – Wolf Sunspot Number
WTC – Wavelet Coherence Transform
XWT – Cross Wavelet Transform
Yr – Year
$\Delta V/\Delta t$ – Change (Δ) in water volume (V) per unit of time (t)

Abstract

In recent years, many studies have sought to produce high-quality paleoclimatic reconstructions for the late Holocene based on high-resolution (annual or decadal) biological and/or chemical proxies, both providing a great amount of information on climate variability and change over the last two millennia. In this context, salt marsh sedimentary records have previously proved to be particularly suitable in unravelling anthropogenic impacts on coastal ecosystems from those caused by climate variability and other natural stressors, at local and regional scales, with intertidal benthic foraminifera providing consistent responses to the latter, specifically to relative sea-level change.

This dissertation focuses on showing evidence of climatic variability and change from a collection of multiple proxy studies combining marsh benthic foraminifera assemblages, wine production (WP), grape harvest dates (GHD), bromine (Br) contents in tidal marsh sediments, and different datasets ranging from the last decades, using instrumental (temperature–precipitation) records, to the past two millennia, by means of reconstructions (temperature, Total Solar Irradiance – TSI and North Atlantic Oscillation – NAO) and regional model (temperature–precipitation) simulations, with the aim of reconstruct the paleoclimate history of the west coast of Portugal for the past 2000 years. Simultaneously, the sensitivity of marsh benthic foraminifera to climate change induced by solar activity (SA) – via hydrological balance (controlling the salinity baseline of the high marsh environment) – is assessed, to show their reliability as a paleoclimatic proxy to be integrated in forthcoming studies. For that, the foraminiferal records from two dated sedimentary cores collected in the northwest (Caminha salt marsh; Minho River) and southwest (Casa Branca salt marsh; Mira River) Portuguese coast have been carefully examined and compared. Since the marshes' development in the 1300s, two compositionally distinct tidal marsh foraminiferal assemblages have been found, dominated by *Haplophragmoides manilaensis* and *Trochamminita salsa/irregularis* in the NW (Caminha) and by *Jadammina macrescens* and *Trochammina inflata* in the SW (Casa Branca), in accordance with their respective climate types. A number of revealed common key changes in the main assemblages' composition has been attributed to larger scale climatic shifts, particularly as regards the transitions firstly from the Medieval Climatic Anomaly (MCA) to the Little Ice Age (LIA), and next from the LIA to the Current Warm Period (CWP) in the Iberian Peninsula, as well as to major temperature–precipitation excursions throughout the LIA and directly correlated with sustained negative phases of the NAO index in periods of lowest SA, known as Grand Solar Minima. It is also found, throughout the application of spectral and cross wavelet methods, that in the time span analyzed (from the 1300s to present), the signals of solar forcing in both foraminiferal and

paleoclimatic records were intermittent, with the regional climate modulated by the solar secular Gleissberg cycle, especially after AD 1700–1750, following the Maunder Minimum (1645–1715).

Besides, an important – and unexpected – feedback is achieved concerning Br in the sedimentary record from the two salt marshes. It is found that Br enrichment peaks, and its connection with organic matter (OM) – promoted by the climate-driven marsh dynamics involving the production/release of volatile Br compounds (as methyl bromide – CH_3Br) to atmosphere – can be diagnostic, to some degree, of Grand Solar Minima and enhanced volcanic activity during those Grand episodes of SA. The CH_3Br has an ozone (O_3) depleting potential of 0.6, and belongs to Class I O_3-depleting substances. Its multiple anthropogenic sources were subjected to phase-out under the Montreal Protocol and its amendments, the reason why natural emissions, as the ones from salt marshes, have become progressively more important contributors to stratospheric O_3 loss processes. According to the results of the current work, based on the available knowledge about Br–OM relationships in terrestrial and marine ecosystems and moreover compatible with a wider recognized latitudinal (North-to-South) rising gradient on the salt marshes' CH_3Br emissions, it is plausible to assume (i) a switch in the marshes' Br source/sink dynamic in response to future major excursions of SA and (ii) an increased total flux of CH_3Br under a continued global warming trend.

Overall, the novelty of this PhD dissertation lies in showing a broader role of marsh benthic foraminifera as indicators of changes in the climate system triggered by SA. Therefore, and not disregarding the great amount of effort still required in their improvement, the results presented here have some meaningful implications, namely on (i) a better understanding of patterns and causes of late-Holocene climatic variability in the west Iberian margin, (ii) the estimate of local and regional changes in hydro-climate and temperature in response to future solar variability, despite the current scenario of anthropogenic climate change, (iii) the research of trends and exposure of naturally produced brominated compounds in salt marshes worldwide, and (iv) the setting up of Br as a paleoclimate proxy linked to SA.

Resumo

A emergência de questões relacionadas com o aquecimento global e as mudanças climáticas, em termos de disponibilidade de recursos e desenvolvimento sustentável, reforçou o interesse pelas Paleociências. Daí resultou a publicação de um número crescente de estudos visando obter reconstruções e interpretações paleoclimáticas para o Holocénico superior, com base em indicadores (*proxies)* biológicos e químicos de alta resolução (à escala anual e da década). Estes *proxies*, preservados em arquivos naturais como os sedimentos, as árvores ou o gelo, facultam informação relevante sobre a variabilidade e mudanças climáticas ocorridas nos últimos 1000 a 2000 anos, ou até num passado muito mais remoto. Permitem-nos assim ampliar consideravelmente a perspetiva acerca do funcionamento do sistema climático fornecida pelos registos históricos e instrumentais dos dois últimos séculos. Neste âmbito, os registos sedimentares dos sapais têm provado ser particularmente adequados para distinguir entre impactes antrópicos e efeitos naturais em ambiente costeiro, à escala local e regional, recorrendo ao estudo dos foraminíferos bentónicos da zona entre marés e à interpretação da resposta consistente perante a variabilidade do clima, e de forma mais específica, as alterações do nível médio do mar. A distribuição das associações de foraminíferos de sapal surge nitidamente relacionada com a altitude (acima do nível médio das marés) e o tempo de submersão do sedimento onde vivem, garantindo o seu enorme potencial de aplicação como indicadores paleoambientais. Para além desta relação inequívoca, as espécies dominantes encontram-se condicionadas pela geoquímica dos sedimentos e das águas intersticiais, refletindo a influência marinha (hidrodinâmica) no interior de cada estuário.

Esta tese fornece registos de variabilidade e mudanças climáticas para o período pré-industrial, a partir de um conjunto de artigos já publicados (**Capítulos 2** a **8**) ou em fase de revisão interpares (**Capítulos 9** e **10**), onde se combina a utilização de vários *proxies*, nomeadamente as associações de foraminíferos bentónicos de ambientes de sapal, as datas do início das vindimas (GHD), a produção de vinho (WP) e os teores de bromo (Br) em solos e sedimentos de sapal, com o objetivo de reconstruir a história paleoclimática da costa oeste de Portugal continental nos últimos 2000 anos. Simultaneamente, procura-se contribuir para o conhecimento da sensibilidade dos foraminíferos bentónicos, registada nos sedimentos, perante os agentes forçadores do clima, designadamente a atividade solar, por ação do balanço entre precipitação e evapotranspiração (P–ET), responsável pelo nível de base de salinidade do alto sapal, bem como mostrar a sua eficácia como *proxy* climático, passível de ser considerado e integrado em estudos futuros. Para tal, os registos de foraminíferos de duas sondagens de sedimentos, uma na costa noroeste (sapal de Caminha, rio Minho) e outra na costa sudoeste (sapal de Casa Branca, rio Mira) de Portugal, foram

estudados, datados e comparados. Foi possível detectar um conjunto de modificações-chave comuns, quer nos registos sedimentares (foraminíferos e geoquímica), quer noutro tipo de registos (e.g., WP), relacionadas com variações climáticas de larga escala, sobretudo no que se refere à transição da Anomalia Climática Medieval para a Pequena Idade do Gelo na região da Península Ibérica. As variações de temperatura e precipitação de âmbito local, ocorridas durante a Pequena Idade do Gelo, surgem, por sua vez, correlacionadas com fases negativas do índice de Oscilação do Atlântico Norte (NAO), que ocorreram durante grandes mínimos de atividade solar.

Verifica-se que desde o início da sua formação, desde o século XIV até ao presente, os sapais de Caminha e Casa Branca evoluíram sob uma influência climática diferenciada, à semelhança do padrão climático que observamos hoje nestas duas regiões da costa W portuguesa. Esta diferenciação encontra-se expressa pelas associações dominantes de foraminíferos do alto sapal. Sob condições de salinidade muito baixa, como as que se registaram em Caminha, no baixo estuário do rio Minho (a 3,5 km da foz), são essencialmente compostas pelas espécies aglutinadas *Haplophragmoides manilaensis* e *Trochamminita salsa/irregularis*, enquanto em Casa Branca, no estuário médio do rio Mira (a 13,0 km da foz), a maior influência marinha é revelada pelas associações dominadas por *Jadammina macrescens* e *Trochammina inflata*. Este contraste na microfauna parece refletir uma tendência de longo-prazo para o ganho da ET sobre a P, no balanço hidrológico na região SW, levando à prevalência de condições de maior salinidade em Casa Branca.

A aplicação dos métodos de análise espectral e de coerência espectral e fase revelou que, para o mesmo período (séc. XIV à atualidade), o registo dos sinais solares nestes *proxies* (espécies de salinidade normal, na região NW, e *T. inflata*, na região SW) é descontínuo e que o ciclo secular de Gleissberg (50–80 anos) parece ter tido um papel importante na modulação climática regional; nomeadamente a partir de AD 1700–1750, ou seja, após o Mínimo de Maunder (1645–1715).

Por último, a análise e a interpretação dos teores de Br, juntamente com a matéria orgânica (MO), ao longo do registo sedimentar das duas sondagens permitiu formular algumas conclusões significativas: os picos de concentração máxima de Br nos sedimentos, bem como a interdependência Br/MO – em estreita conexão com a dinâmica do sapal promovida pelo clima – podem evidenciar períodos de Grandes Mínimos de atividade solar e concomitante (elevada) atividade vulcânica. O CH_3Br, composto volátil de Br, pertence à classe I das substâncias destruidoras de O_3, com potencial de destruição de 0.6. Como as suas fontes antrópicas têm vindo a ser progressivamente eliminadas, no cumprimento do Protocolo de Montreal, as emissões naturais de CH_3Br – entre elas as dos sapais – têm hoje maior importância relativa nos processos de destruição do O_3 estratosférico. De acordo com os resultados da presente investigação – fundamentados no conhecimento disponível sobre a formação de compostos organobromados em ecossistemas terrestres e marinhos, e compatíveis com a observação do aumento das taxas de emissão de CH_3Br pelos sapais em função de um gradiente latitudinal (Norte–Sul) de crescente

temperatura – é plausível assumir (i) uma alternância no papel destes ambientes como fonte–sumidouro de Br em resposta a futuros episódios relevantes da atividade solar e (ii) um aumento do fluxo total de CH_3Br num cenário de continuado aquecimento global.

Acima de tudo, a inovação do trabalho compilado nesta tese consiste na revelação de uma vertente, ainda pouco explorada, do papel dos foraminíferos bentónicos de sapal como indicadores de mudanças climáticas induzidas pela dinâmica da atividade do Sol. Os resultados apresentados podem, por isso, ter algumas implicações pertinentes, quer na estimativa de mudanças locais e regionais na temperatura e no ciclo hidrológico, em face da futura variabilidade solar, quer na pesquisa de tendências e exposição a compostos organobromados em sapais de todo o mundo, bem como no reconhecimento do papel do Br como *proxy* de alterações paleoclimáticas ligadas à atividade solar.

Contents

Acknowledgments iii
Abbreviations and Acronyms v
Abstract ix
Resumo xi
Contents xv
List of Figures xxi
List of Tables xxix
List of Appendices xxxi
List of Plates xxxiii
1 Introduction 1
1.1. Motivation and objectives 1
1.2. Sun's activity, Earth's climate and biogeochemical markers of past environmental change 3
1.2.1. A coupled solar–terrestrial system affecting biosphere 3
1.2.2. A variable Sun 6
1.2.3. Solar–terrestrial climate interaction 12
1.2.4. Mechanisms of Sun–climate interaction 14
1.2.5. Solar signals in climate and geological records 21
1.3. Research material 24
1.3.1. Tidal marsh settings and sediments 24
1.3.2. Marsh foraminifera 28
1.3.3. Grape harvest dates and wine production 29
1.3.4. Bromine 34
1.4. Dissertation outline 36
References 40
2 Salinity and water temperature assessment of the tidal marshes from the W Portuguese coast, as an ecological tool to paleoenvironmental reconstructions based on foraminifera and ostracoda assemblages 53
ABSTRACT 53
Resumo 54
2.1. Introduction 55
2.2. Regional setting 56
2.3. Methods 57

2.4. Results 58
2.4.1. Marsh sediment interstitial water 58
2.4.1.1. Minho estuary 58
2.4.1.2. Tejo estuary 59
2.4.1.3. Mira estuary 60
2.4.2. Tidal marsh flooding water 60
2.4.2.1. Minho estuary 60
2.4.2.2. Mira estuary 60
2.5. Discussion 61
2.6. Conclusions 64
Acknowledgments 65
References 65
3 High marsh foraminiferal assemblages' response to intra-decadal and multi-decadal precipitation variability, between 1934 and 2010 (Minho, NW Portugal) 69
ABSTRACT 69
3.1. Introduction 70
3.2. Regional setting 71
3.3. Material and methods 73
3.4. Results and discussion 75
3.4.1. Tidal marsh surface foraminiferal assemblages 75
3.4.2. High marsh short sediment core assemblages 79
3.5. Conclusions 84
Acknowledgments 85
References 85
4 Grape harvest dates as indicator of spring-summer mean maxima temperature variations in the Minho region (NW of Portugal) since the 19th century 95
ABSTRACT 95
4.1. Introduction 96
4.2. Study area 98
4.3. Materials and methods 98
4.3.1. Grape harvest dates and weather information from documentary sources 98
4.3.2. Climate instrumental data and proxies 99
4.3.3. Statistical analysis 100
4.3.3.1. Seasonal reconstruction target 100
4.3.3.2. Regional temperature reconstruction prior to instrumental data 102
4.4. Results 102
4.4.1. The Minho GHD series and other documentary weather-related data 102

4.4.2. Relationships between Minho GHD and temperature/precipitation 104
4.5. Discussion 107
4.5.1. Minho grape harvest dates and climate variables (temperature and precipitation) 107
4.5.2. Teleconnection patterns influence on temperatures and grape harvest dates 108
4.5.3. Linking solar activity to Minho GSTmax 112
4.6. Conclusion 115
Acknowledgments 115
References 116
5 Records from marsh foraminifera and grapevine growing season temperatures reveal the hydro-climatic evolution of the Minho region (NW Portugal) from 1856–2009 123
ABSTRACT 123
5.1. Introduction 124
5.2. Study area 126
5.3. Materials and methods 128
5.4. Results 129
5.5. Discussion 130
5.6. Conclusions 137
Acknowledgments 137
References 137
6 A bi-proxy paleoclimatic reconstruction for the Entre-Douro-e-Minho region, northwest Portugal, from 1626 to 1820 – A search for evidence of solar forcing 155
ABSTRACT 155
6.1. Introduction 156
6.2. Data 159
6.2.1. WP data 159
6.2.2. Sediment cores 159
6.2.3. Additional reconstructed and simulated climate series 160
6.3. Methods 160
6.3.1. WP reconstruction 160
6.3.2. Spectral analysis 161
6.3.3. Wavelet analysis 162
6.4. Results 162
6.4.1. WP series 162
6.4.2. High marsh benthic foraminiferal assemblages 163
6.4.3. Spectral analysis 166
6.5. Discussion 168
6.5.1. Potential links between SA, climatic variables and proxies 168

6.5.1.1. WP1 period (1626–1709 years): sun-climate impacts on WP and benthic foraminifera 169
6.5.1.2. Historical events as potential drivers for the two WPGs in the WP1 period 171
6.5.1.3. WP2 and WP3 periods (1713–1794 years) 173
6.5.1.4. WP4 (1795–1820 years) and the Dalton Minimum 174
6.5.2. Cycles in paleoclimatic proxies and their relationship to SA 176
6.6. Conclusions 177
Acknowledgments 177
References 177
7 Marsh benthic Foraminifera response to estuarine hydrological balance driven by climate variability over the last 2000 yr (Minho estuary, NW Portugal) 185
ABSTRACT 185
7.1. Introduction 186
7.2. Study area 187
7.3. Surface foraminiferal distribution at the Caminha marsh 188
7.4. Materials and methods 190
7.4.1. Foraminifera 190
7.4.2. Sedimentology and geochemistry 190
7.4.3 Chronology 191
7.4.4. Historical and instrumental records 192
7.5. Results 193
7.6. Discussion 196
7.6. Conclusions 205
Acknowledgments 205
References 206
8 Bromine enrichment in marsh sediments as a marker of environmental changes driven by Grand Solar Minima and anthropogenic activity (Caminha, NW of Portugal) 219
ABSTRACT 219
8.1. Introduction 220
8.2. Materials and methods 223
8.2.1. Study area 223
8.2.2. Sampling and analytical procedures 225
8.2.2.1. Sediment surface samples 225
8.2.2.2. Water samples 226
8.2.2.3. Sediment core 226
8.2.3. Solar activity and paleotemperature data 227
8.2.4. Chronology 227
8.3. Results and discussion 228

8.3.1. Br concentrations in surface samples 228
8.3.2. Br variability in core sediment samples 232
8.3.2.1. Relationships with OM content 232
8.3.2.2. Br enrichment peaks in association with solar cycles 233
3.2.3. Br enrichment linked to anthropogenic activity 237
8.4. Conclusions 239
Acknowledgments 240
References 240
9 Bromine soil/sediment enrichment in tidal salt marshes as a potential indicator of climate changes driven by solar activity: New insights from W coast Portuguese estuaries 247
ABSTRACT 248
9.1. Introduction 248
9.2. Regional setting 250
9.2.1. NW coast 250
9.2.2. SW coast 252
9.3. Materials and methods 253
9.3.1. Water and sediment samples 253
9.3.2. Solar activity, temperature and precipitation climatic modelled data 255
9.3.3. Chronology 255
9.4. Results and discussion 256
9.4.1. Br^- in surface and interstitial water samples 256
9.4.2. Br–OM relationships in marsh surface environments 258
9.4.3. Br temporal trends in SW (Mira estuary) and NW (Minho estuary) coasts 261
9.4.3.1. Comparing Br enrichment in relation to the long-term OM storage ability from salt marshes in their soils/sediments 261
9.4.3.2. Br enrichment peaks in association with Grand Minima of solar activity 266
9.5. Conclusions 268
Acknowledgments 269
References 269
10 Marsh benthic foraminiferal evidence for environmental changes driven by the sun-climate coupling: application to the western coast of Portugal from the 14th century to present 279
ABSTRACT 280
10.1. Introduction 280
10.2. Regional setting 282
10.3. Materials and methods 283
10.3.1. Sampling and analytical techniques 283
10.3.1.1. Sediment coring 283

10.3.1.2. Chronology 284
10.3.1.3. Geochemical and sedimentological analyses 284
10.3.1.4. Multivariate (Factor) analysis (FA) 284
10.3.1.5. Reconstruction of solar activity and climate simulations 285
10.3.1.6. Spectral (REDFIT) analysis 285
10.3.1.7. Coherence-cross wavelet (WTC) analysis 285
10.4. Results 286
10.4.1. Foraminiferal, geochemical and sedimentological evidence from the Casa Branca coring site at the Mira River lower estuary 286
10.4.1.1. Characterization of the high marsh foraminiferal assemblages 286
10.4.1.2. Statistical evidence provided by Factor analysis 286
10.4.1.3. Geochemical and sedimentological tracers 287
10.4.1.4. Spectral analysis (REDFIT) of the benthic foraminiferal time series 291
10.4.1.5. WTC analysis: marsh benthic foraminifera and sun–climate variables 291
10.5. Discussion 292
10.5.1. Identifying foraminifera-based paleoclimatic trends in the west coast of Portugal 292
10.5.1.1. Casa Branca (southwest) and Caminha (northwest) salt marshes settlement as inferred from their foraminiferal record 292
10.5.1.2. Foraminiferal trends on Casa Branca (and Caminha) and their relationship with the physical factors influencing the P–ET balance of high marsh(es) 293
10.5.1.3. Potential proxies of dust events associated to drier conditions in the southwest coast of Portugal: examining the role of Trochammina inflata 295
10.5.2. Identifying imprints of the solar–terrestrial climate link in the Casa Branca coastal salt marsh environment 300
10.6. Conclusions 303
Acknowledgments 303
References 304
11 Concluding remarks **315**
11.1. General conclusions 315
11.2. Prospective 320
Appendices **321**
Appendix A1. Systematic List 321
Appendix A2. List of the scrutinized local/regional newspapers. 332

List of Figures

Figure 1.1. The earth's geosphere and biosphere interact and are interrelated through (i) climatic processes and (ii) the hydrological and biogeochemical cycles, with the sun as the dominant source of all external energy. Diagram designed by James A. Tomberlin, USGS. (https://pubs.usgs.gov/pp/p1386a/plate-earthsystem.html). **4**

Figure 1.2. Estimate of the global annual mean Earth's energy budget (NASA). This energy budget diagram shows the best understanding of energy flows into and away from the Earth. Arrows designate the schematic flow of energy in proportion to its importance. The numbers correspond to percentages of the overall mean amount of energy that reaches the Earth, i.e., 340.4 Wm^{-2}. Over the last 15 years, measurements show that the Earth's energy budget is not quite balanced. There has been a net ~0.2% of energy absorbed per year. (https://science-edu.larc.nasa.gov/energy_budget/pdf/ERB_Litho_Edits_Percent_2016_v7.pdf). **5**

Figure 1.3. Schematic view of the components of the global climate system (bold), their processes and interactions (thin arrows) and some aspects that may change (bold arrows) (from Baede et al., 2001). In such a complex system everything may affect everything, but to different degrees (Benestad, 2006). **6**

Figure 1.4. (From left to right); A drawing of the full disk of the spotted Sun made in Florence, Italy, by Galileo using a small telescope at about 2 o'clock in the afternoon of August 20, 1610. The solar disk seen in white light from the SOHO spacecraft on October 28, 2003. A close-up, colour-added view of the dark centres (umbrae) of sunspots; the less-dark, magnetically-formed penumbrae that generally encircle them (image taken with the Swedish 1-meter high-resolution solar telescope, at La Palma observatory - Canary Islands - credit: Eddy, 2009). A view of the Sun in March 28, 2001, showing high solar activity; the colour table has been altered to enhance the appearance of the faculae (white regions) which are hotter than sunspots (red-black regions) (image credit: NASA/Goddard Space Flight Center Scientific Visualization Studio). On the right, the sunspot groups observed each year, from 1826 to 1843, by Samuel H. Schwabe (1844), leading him to the discovery of the sunspot cycle (Hathaway, 2010). **7**

Figure 1.5. The yearly-sunspot number record since the beginning of telescopic observations until 2007 (Eddy, 2009). The Schwabe cycle is quite evident and obvious trends in the longer-term overall level of solar activity. One can see also that the amplitude of the Schwabe cycle varies significantly, from the almost spotless mid-1600s–1715 period (known as the Maunder Minimum) to the very high cycle 19, probably in relation to the secular Gleissberg cycle. **7**

Figure 1.6. The X9-class solar flare of December 5, 2006, observed by the Solar X-Ray Imager aboard NOAA's GOES-13 satellite (available at https://science.nasa.gov/science-news/science-at-nasa/2008/15dec_solarflaresurprise). **8**

Figure 1.7. Sunspot numbers for solar cycles 22, 23 and 24, showing a clear weakening trend (from Hathaway NASA/ARC) (https://solarscience.msfc.nasa.gov/predict.shtml) (left). On the right, the recent solar cycle 24 is represented here by the sunspot number, with the black line representing the monthly averaged data and the blue line a 13-month smoothed version of the monthly averaged data; the forecast for the rest of the solar cycle is given by the red line. As can be seen, cycle 24 is double peaked, similarly to the last two solar maxima, around 1989 and 2001 (http://www.swpc.noaa.gov/products/solar-cycle-progression). **9**

Figure 1.8. The known PMOD composite satellite-era TSI record (named for the institute in Davos, Switzerland that produces the data), spanning from 1978–present, shows peak-to-peak TSI variability of ~0.1% in each of the three solar cycles observed during the space-borne measurement record, with that variability being in-phase with solar activity. The colours indicate the binary selections of different instruments used in the creation of the composite. The right-hand vertical scale indicates the more accurate currently-accepted absolute value (after Kopp, 2016). **9**

Figure 1.9. Some TSI-reconstruction models providing estimates of solar variability for the last 400 years (after Kopp, 2016). **10**

Figure 1.10. Picture showing some fundamentals of the radioisotopes ^{14}C and ^{10}Be in the Earth's system. Both are produced by nuclear reactions of GCR particles with the atmospheric gases (Masarik and Beer, 2009), but after production their fate is very different (system effects). While ^{10}Be attaches to aerosols and is transported within a few years to ground (Heikkilä et al., 2009), ^{14}C oxidizes to CO_2 and enters the global C cycle, exchanging between atmosphere, biosphere, and the oceans (Siegenthaler, 1983) (after Steinhilber et al.,

2012). John Eddy (1976) was the first to recognize the strong inverse correlation between the production of the cosmogenic radionuclides and SA. **11**

Figure 1.11. (Left) Layers of the Earth's atmosphere (troposphere, stratosphere, mesosphere and thermosphere), showing the temperature difference with increasing altitude from Earth for both solar minimum and solar maximum periods, the atmospheric penetration of the various spectral wavelengths, the density of oxygen, nitrogen and carbon dioxide with increasing altitude from the Earth, and the approximate height within the D, E and F levels of the ionosphere (credit: John Emmert/NRL, NASA) https://science.nasa.gov/science-news/science-at-nasa/2010/15jul_thermosphere. (Right) Graphic showing also the ionosphere, overlapping the mesosphere and thermosphere; parts of the ionosphere overlap with magnetosphere, shaped by the solar wind's interaction with the Earth's magnetic field. The yellow line shows the response of air temperature to increasing height (credit: Encyclopædia Britannica, Inc.). **13**

Figure 1.12. SSI as inferred from the SORCE and TIMED satellite observations between April 22, 2004 and July 23, 2010. A – Average SSI for that period; B – Typical altitude of absorption in the Earth's atmosphere for each wavelength; C – Relative variability (peak-to-peak/average) for solar cycle variations, inferred from measurements obtained between April 22, 2004 and July 23, 2010. Spectral regions where the variability is in phase with the solar cycle (denoted, for instance, by the sunspot number or the TSI) are marked in red, while blue represents ranges where the variability measured by SORCE is out of phase with the solar cycle; D – SSI absolute variability, which peaks strongly in the near UV (after Ermolli et al., 2013). **15**

Figure 1.13. Schematic of the "bottom-up" mechanism (1), arising from the absorption at the surface of VIS/IR energy variations (yellow arrow) and of the "top-down" mechanism (2–4), arising from the absorption of UV energy variations in the stratosphere (red arrow). The charged particles contribution, including electrons as well as ions of all species and covering particles of both solar/heliospheric and galactic origin (EPPs), is also represented (after Thiéblemont and Matthes, 2015). **16**

Figure 1.14. Scheme of the Hadley and Walker circulation, both related to the trade wind system. The positions of the rising and sinking air are given by the dark blue arrows. Rising air is related to cloud formation and precipitation, thus these areas are often wet; sinking air results in drier conditions at the surface. Light brown represent the Walker circulation that owes its origin to the gradient of sea surface temperatures along the equator in the Pacific Ocean. The colours on the globe correspond to mean precipitation from the Global Precipitation Climatology Project for 1979–2008. The blues and greens show regions of heavier rains (available at https://www.meted.ucar.edu/). **17**

Figure 1.15. The positive (at left) and negative (at right) NAO phases and their connection to the stratospheric and oceanic circulations (http://www.whoi.edu/page.do?pid=8915&tid=3622&cid=24777). **19**

Figure 1.16. (Left) Main CR (including SEP and GCR) impacts on the Earth's atmosphere. CR are the main source of ionisation in the lower atmosphere. The GEC is distributed over the whole Earth. GLE – Ground Level Enhancement events (a special class of SEP events, characterized by higher energy of solar particles that can extend up to ~1–10 GeV, which are high enough to induce cascades of secondary particles in the atmosphere, just as GCR do. Thus, the ionizing atmospheric effect of GLE events is expected to be noticeable in the lower atmosphere (Usoskin et al., 2011) (after Seppälä et al. (2014). (Right) Schematic representation of the global electric circuit (GEC) and its interaction with energetic cosmic particles and the tropospheric cloud system. When GCR (*blue arrows*) and other highly energetic particles of solar and cosmic origin (*black arrows*) penetrate the terrestrial atmosphere, they create ion pairs and by that change the ionospheric electrical potential and the atmospheric vertical column resistance. The electrical charges transported by the vertical currents (indicated by *red arrows*) accumulate on airborne aerosols as well as on droplets and ice crystals at cloud tops and bottoms and potentially change the cloud physical properties. Variations in the solar wind, and in the solar magnetosphere's extend, modulate the atmospheric flux of energetic cosmic particles, being able of exerting this way an indirect influence on the Earth's cloud system and climate (after Rzesanke et al., 2013). **21**

Figure 1.17. Several reconstructions for the mean temperature of the Northern Hemisphere. All reconstructions were 30-year low-pass filtered, and scaled to the smoothed instrumental series by the variance and mean over the common period AD 1865–1973 (more details in Xing et al., 2016, from which this Figure was reproduced). **23**

Figure 1.18. (Left) $\Delta\ ^{14}C$–derived R_z (Wolf sunspot indices) estimate (solid squares) and global temperature model predictions (curve) (after Jirikowic and Damon, 1994). (Right) Estimated annual mean sunspot numbers from 1610 to 1750; dashed lines are decade's estimates, crosses are peak estimates and triangles are Wolf's estimated dates of maxima for an assumed 11.1-year solar cycle (after Eddy, 1976). **23**

Figure 1.19. Typical cross-marsh zonation, displaying the physical factors influencing vegetation (after Carter, 1988). HLW – Highest low water; MHWN – Mean high water neap; MHW – Mean high water. **25**

Figure 1.20. World map of coastal wetlands (after Scott et al., 2014). **25**

Figure 1.21. (Left) Caminha salt marsh in the Minho lower estuary (NW coast); (Right) Ponte de Vila Nova de Milfontes salt marsh in the Mira lower estuary (SW coast). **26**

Figure 1.22. Fine-grained, organic-rich sediments from the Caminha tidal marsh. **27**

Figure 1.23. *Sarcocornia* sp. (with water-retaining, succulent parts) from the Mira lower estuary (SW coast) by opposition to *Juncus maritimus* (non-succulent) from the Minho estuary (NW coast). **27**

Figure 1.24. Ancient tall-trained vine systems. A – "Ramada" or "latada" (http://arturpastor.tumblr.com/image/103491586558); B and C – "Arjões"; D – "Enforcado" or "uveiras" (http://arturpastor.tumblr.com/image/103481986553); E and F – Tall vineyard harvest (http://vryebeelde.blogspot.pt/2014_02_01_archive.html; http://4.bp.blogspot.com/). **31**

Figure 1.25. The S. Martinho de Tibães monastery (Tibães, Braga, NW of Portugal). (Left) Aerial view taken from south of the whole set. (Right) Northern general view of the Tibães monastery (Photos available at http://www.patrimoniocultural.gov.pt/pt/patrimonio/patrimonio-imovel/pesquisa-do-patrimonio/classificado-ou-em-vias-de-classificacao/geral/view/73612). **32**

Figure 1.26. (Left) Entrance to the Chapter's Room of the S. Martinho de Tibães monastery (Photo available at http://mosteirodetibaes.org/pagina,232,245.aspx). (Right) View of the Chapter's Room where the Congregation of St. Benedict of Portugal and the Province of Brazil met every three years on the third day of May (the feast day of the Holy Cross) to elect the General, the Abbots and all prelatures of each monastery. It is also in this occasion that the account reports (*Estados*) of the three preceding years were presented to the Congregation (Photo available at http://www.vortexmag.net/portugal-37-monumentos-que-deve-visitar-pelo-menos-1-vez-na-vida/5/). **32**

Figure 1.27. (Left) Some of the local papers systematically scrutinized in this research. (Right) Several newspaper articles reporting extreme weather and climatic events, rogation ceremonies and information on grape harvesting. **33**

Figure 1.28. Diagram for historical–climatological analysis (after Brázdil, 2002). **34**

Figure 1.29. Source and sink fluxes of methyl bromide: 1996 and 2010 (after Yvon-Lewis and Butler, 2015). **35**

Figure 2.1. Location of studied salt marsh transects along the W coast of Portugal, in the estuaries of Minho (PR – Pedras Ruivas), Tejo (Ros – Rosário) and Mira (PMF – Ponte de Vila Nova de Mil Fontes). **56**

Figure 2.2. Sampling profiles of studied transects of Pedras Ruivas (PR – Minho), Rosário (Ros – Tejo) and Ponte de V.N. Mil Fontes (PMF – Mira), showing the measured spring and autumn salinity of sediment interstitial water. **59**

Figure 2.3. Example of water salinity variation along tidal flat, low marsh and high marsh, during the spring tide flooding, in the Minho and Mira low estuaries. **61**

Figure 2.4. Seasonal salinity profiles of Minho low estuary under summer and spring season conditions. **62**

Figure 3.1. A – Location of study area in Portugal. B – Minho estuary and Coura tributary. Green area represents the Caminha tidal marsh. **72**

Figure 3.2. ^{210}Pb (A) and ^{137}Cs (B) activities down-core FCPw1. ..... **75**

Figure 3.3. Correspondence analysis plot of samples showing correlation with environment variable submersion time – TSubm. Dotted ellipse groups of low marsh samples (right), standing out the transitional zone (smallest ellipse), and dashed ellipse (left) groups of high marsh samples. **76**

Figure 3.4. Correspondence analysis plot of samples restricted to highest low marsh and high marsh samples. **77**

Figure 3.5. Correspondence analysis plot of species and submersion time –TSubm. High marsh species are aligned at the left side of diagram where salt marsh species (*T. inflata* – TrInf and *J. macrescens* – JaMac) occupy the upper part, and dominant brackish high marsh species (*T. salsa/irregularis* – TrSai, *H. manilaensis* – HaMan, *H. wilberti* – HaWil, *Haplophragmoides* sp. – HapSp and *P. limnetis* – PsLim) group in the lower part (dotted ellipse). **77**

Figure 3.6. Annual precipitation recorded in Minho region from 1994 to 2010. The precipitation normal (average of 30 year records) was calculated by the authors from the series of data available in Minho region weather stations for hydrological years 1981–2010 (http://snirh.inag.pt). **78**

Figure 3.7. Average winter precipitation (DJFM) for the hydrological years 1934–2010 *vs.* NAO index (r = −0.70)..... **80**

Figure 3.8. Relationship between smoothed average precipitation (solid line) and foraminiferal data; top axis – precipitation (mm) and number of foraminifera per cm^3 (solid circle); bottom axis – percentage of "normal-" (stars) and "low-" salinity (open squares) foraminiferal groups; average precipitation 1934–2010 (dashed line) **82**

Figure 3.9. Annual precipitation in the Minho region and historical record of floods (after local newspapers archives and Gonçalves, 2009, 2011); black arrows indicate severe floods, grey arrows indicate moderate floods and white arrows means no information about flood severity; figures indicate the number of floods in the hydrological year..... **83**

Figure 3.10. Comparison of the three phases, defined after precipitation data from Minho region. Box-plots represent the mean, the extreme values, the first and third quartiles; dashed line represents the average precipitation from 1934 to 2010..... **84**

Figure 4.1. A – Location of the Portuguese Demarcated Minho Wine Region (MWR). B – Map of the Viana do Castelo and Braga districts (Minho region) in the more extended Minho Wine Region (MWR; grey area). . **100**

Figure 4.2. A – Z-scores of the GHD recorded in newspapers from the Minho region, covering 16 municipalities (grey line); GHD 11-year running averages (black line; + periods of delayed, GHD; − periods of early GHD). B – Number of *pro-pluvia* events documented in the set of 41 local and regional newspapers reviewed for the Minho region. **103**

Figure 4.3. Calibration and verification results of the GHD composite with March–August Braga mean maxima temperatures (reconstruction – black; instrumental data – grey). **105**

Figure 4.4. A – March to August mean maxima temperatures (instrumental - dashed line; reconstructed - grey line; reconstructed 11-year running averages - black line). B – Averaged mean maxima temperatures for the GHD z-score periods (instrumental - grey number; reconstructed - black numbers). C – GHD 11-year running average periods (+ periods of delay GHD; − periods of early GHD). **106**

Figure 4.5. A – March to August mean maxima temperature anomalies for the Braga meteorological station (grey line) and 11-year running average (black line). B – March to August SCA index. C – June EA/WR index. D – July EA/WR index. E – August EA/WR index (indices raw data in grey lines and indices 11-year running averages in black lines). **112**

Figure 4.6. A – March to August mean maxima temperatures (instrumental - dashed line; reconstructed - grey line; reconstructed 11-year running averages - black line). B – Global mean annual temperature anomalies (after Jones et al., 2013) in grey line and 11-year running averages in black line. C – TSI – Total Solar Irradiance (after Krivova et al., 2010; Ball et al., 2012 and Yeo et al., 2014) in grey line; and 11-year running averages in black line. **114**

Figure 5.1. A – Geographical location of the Portuguese Demarcated Minho Wine Region (MWR). B – Delimitation of Minho Wine Region (MWR; grey area) and Viana do Castelo and Braga. C – Sampling location of core FCPwAR in Caminha tidal marsh (Minho estuary, NW Portugal)..... **127**

Figure 5.2. Percentage distribution of benthic foraminifera in core FCPwAR. Years (cal. AD): Age in calendar years AD; FAZ: foraminiferal assemblages' zones. **131**

Figure 5.3. Changes in foraminiferal assemblages including percentages of the strongly brackish (oligohaline to mesohaline) marsh species group (Low Sal. spp.); percentages of the moderately brackish-to-normal salinity (polyhaline to euhaline) marsh species group (Mod.– Salt marsh spp.); as well as March to August mean temperature maxima (GSTmax, after Moreno et al., 2016); average temperature maxima (Avg. Temp.) for GHD z-score periods (after Moreno et al., 2016); and annual precipitation records for Minho and Lima (after Fatela et al., 2014). Broken lines represent overall means and thick solid lines represent eleven-year running averages for the environmental parameters. **132**

Figure 5.4. Schematic diagram of water balance in a salt marsh (adapted from Nuttle, 1988). P – Precipitation; ET – Evapotranspiration; S_i – surface water inflow; G_i – groundwater inflow, T_i – tidal inflow; S_o – surface water outflow; G_o – groundwater outflow; T_o – tidal outflow. **133**

Figure 5.5. A – March to August mean maximum temperature (GST) anomalies from Braga meteorological station (41º33′ N; 08º24′ W). B – Growing season (March to August) SCA index. C – June EA/WR index. D – Percent abundance of low salinity (oligohaline to mesohaline) marsh foraminiferal species group. Thick black lines represent the eleven-year running average. Negative GST anomalies associated with positive growing season SCA and June EA/WR anomalies (shaded area in A–C) are reflected by the dominance of foraminiferal species characteristic of oligohaline–mesohaline conditions from the 1960s–1990s (shaded area in D). ... **136**

Figure 6.1. A – Geographical location of the Benedictine monasteries network established in the Entre-Douro-e-Minho (EDM) region (after Marques, 2011). The S. Martinho de Tibães monastery (Braga) was the head of the Benedictine Order in Portugal since 1569. It was in Tibães that, at every three years, the Orders' General Chapter meetings took place, in which the account reports (*Estados*) were presented. Bold dots represent the analyzed monasteries' wine productions; B – Location of core FCPwAR1 in the Caminha tidal marsh (Minho estuary, NW Portugal)..... **157**

Figure 6.2. The Apocalypse of Lorvão, an early medieval (1189) illuminated manuscript from the *scriptorium* of the S. Mamede do Lorvão monastery (Central Portugal) and based on the 8th century codex *Commentarium in Apocalypsin* by Beatus of Liébana, shows the grape harvesting and other agricultural work according to the practices of the 12th century (in *Commentarium in Apocalypsin* of S. Mamede do Lorvão, Arquivo Nacional da Torre do Tombo Book 44, C.F.160, p 172v). **158**

Figure 6.3. A – Wine production (WP) composite time series represented as deviations of the mean (%) for six Benedictine monasteries from the Entre-Douro-e-Minho (EDM) region. The periods WP1 to WP4 are distinguished based on differences of WP averages (arithmetic means) at the 99% level; B – Total solar irradiance (TSI) time series (Krivova et al., 2010); MM – Maunder Solar Minimum; Extended Maunder Minimum after Vaquero and Trigo (2015); C – Representation of the three solar dynamo natural oscillations in TSI raw data: black line - secular oscillation, grey line - semi-secular, dashed line - bi-decadal oscillation (after Duhau and Martínez, 2012); D – GST_Europe – European growing season temperatures (March to August) reconstruction (Xoplaki et al., 2005); black thicker line - 5 years running average; E – GST_NW IP ERIK1- NW Iberian (Ib) growing season temperatures (March to August) simulation (Gómez-Navarro, 2011, 2012); black thicker line - 5 years running average; F – NW Ib Temp JJA ERIK1 - NW Iberian summer temperatures simulation (Gómez-Navarro et al., 2011, 2012); black thicker line - 5 years running average; G – NW Ib Precip. JJA ERIK1 - NW Iberian summer precipitation simulation (Gómez-Navarro et al., 2011, 2012); black thicker line - 5 years running average..... **164**

Figure 6.4. Summary of benthic foraminiferal data in core FCPwAR. Age (yr cal. AD) – age in calendar years AD; Salt marsh spp. – percentage distributions of the group of brackish salt marsh benthic species; Low Sal. spp. – percentage distributions of the group of low-salinity benthic species; Mod.-Brackish spp. – percentage distributions of the group of Brackish/Moderate-Brackish benthic species; Normal Sal. spp. – percentage distributions of the group of Brackish-to-Normal salinity benthic species; Mod.+Normal Sal. spp. – Brackish/Moderate plus Brackish-to-Normal salinity benthic species; FAZ – foraminiferal assemblage zones.. ..... **165**

Figure 6.5. A – Lomb-Scargle periodogram of WP series for the 1713–1821 period; B – REDFIT periodogram of brackish/normal salinity species (*J. macrescens*, *T. inflata*, *T. comprimata*, *S. lobata* and *P. guaratibaensis*) for the period AD 1654–2010. The two statistically significant peaks registered at 59 years and 13 years are set at 96.8% level..... **166**

Figure 6.6. Results of the cross wavelet transform (XWT) and wavelet coherence (WTC). A) and B) Benthic foraminifera (*J. macrescens*, *T. inflata*, *T. comprimata*, *S. lobata* and *P. guaratibaensis)* (this work) *vs.* TSI (Krivova et al., 2010) for AD 1654–2010; C) and D) Benthic foraminifera *vs.* the NAO index (Luterbacher et al., 2002); E) and F) Benthic foraminifera *vs.* simulated annual temperature for NW IP (Gómez-Navarro et al., 2011, 2012). The color scale is proportional to the wavelet cross-correlation power. The black arrows indicate the relative phase relationship, with horizontal right-pointing arrows representing in-phase relationships and left-facing arrows denoting anti-phase; arrows pointing straight down indicate that the first series leads ahead the second by 90 degrees; arrows pointing vertically upward means the second series leads the first by 90 degrees. In all panels the black thick line is the 5% significance level using the red noise model. Shaded areas represent the cone of influence (COI) where edge effects may distort the results, so regions outside are discarded. **167**

Figure 6.7. Wine production (WP) composite time series for six Benedictine monasteries from the Entre-Douro-e-Minho (EDM) region (line) and number of new planted vines (black bars). Time series represented as deviations of the mean (%), considering the Tibães, Rendufe, S.^{to} Tirso (Casa/Passais), Pombeiro, Paço de Sousa and Palme monasteries (after Marques, 2011)..... **169**

Figure 6.8. Triennial grain (maize and rye) tithe series from the Tibães parish churches from 1683 to 1813 (after Oliveira, 1979). WPG2 corresponds to the major gap on the Entre-Douro-e-Minho regional WP time series. **173**

Figure 7.1. Location of core FCPw1 in the Caminha tidal marsh (Minho estuary, NW Portugal). **188**

Figure 7.2. Age model for the core FCPw1 and estimated 2σ errors, based on six AMS-^{14}C dates, performed on total organic sediment, and ^{210}Pb chronology. The data interpolation was obtained with Bchron 3.2 software. The lowermost 10 cm has been extrapolated from the Bchron calculation between 81 and 91 cm depth by linear regression. **192**

Figure 7.3. Percentage distribution of benthic foraminifera in core FCPw1. Age (yr AD) – age in calendar years AD; Salt marsh spp. – distributions of the group of brackish salt marsh benthic species; Low Sal. spp. – distributions of the group of low-salinity benthic species; NF – number of foraminifera per cm^3; FAZ – foraminiferal assemblage zones; Litos in – periods of continental lithogenic inputs to the shelf (see references in the text and Appendix 7.5); Clime Pe. – Climate periods in the last 2 millennia (see references in the text); Solar Irr. Anomaly – solar irradiance anomaly using a 22-yr running average reconstruction (after Steinhilber et al., 2012); Solar Ev. – Solar events (see references in the text); T anomal. – Temperature anomaly using a 10-yr running average reconstruction (after Martín-Chivelet et al., 2011). **197**

Figure 7.4. Sedimentological, geochemical and summary of benthic foraminiferal data in core FCPw1. Age (yr AD) – age in calendar years AD; Salt marsh spp. – percentage distributions of the group of brackish salt marsh benthic species; Low Sal. spp. – percentage distributions of the group of low-salinity benthic species; NF – number of foraminifera per cm3; FAZ – foraminiferal assemblage zones; Litos in – periods of continental lithogenic inputs to the shelf (see references in the text and Appendix 7.5); Clime Pe. – Climate periods in the last 2 millennia (see references in the text); Solar Irr. Anomaly – solar irradiance anomaly using a 22-yr running average reconstruction (after Steinhilber et al., 2012); T anomal. – Temperature anomaly using a 10-yr running average reconstruction (after Martín-Chivelet et al., 2011). **200**

Figure 7.5. Relationship between foraminiferal data and Standardized Precipitation Index (12-months: SPI_12), after Moreira et al. (2012), from Porto (Serra do Pilar: 41º08′19.20″ N–08º36′09.68″ W). A – number of foraminifera per cm^3; B – percentage of "normal" (stars) and "low" salinity (open squares) species; C – number of severe and extreme droughts (grey bars) calculated with the SPI_12, grouped in intervals of *ca.* 30 yrs., from 1864 to 1894, 1895 to 1922, 1923 to 1953 and 1982 to 2010; D – SPI_12 time series, from hydrological year 1863/1864 to 2007/2008), grey column represents the field of severe and extreme droughts (SPI ≤ −1.5)..... **204**

Figure 8.1. A – Location of the study area in Portugal. B – Location of Minho estuary bottom sediment samples and water analyzed for geochemistry. C – Minho estuary and Coura tributary sampling. Dark grey area represents the Caminha tidal marsh. Estuarine water samples CM – Camarido, VNC – Vila Nova de Cerveira and VM – Vilar de Mouros. Surface sediment and interstitial water sampling transects PR – Pedras Ruivas, CP – railway bridge and PiC – Pinelas. FCPw1 – sediment core location. **224**

Figure 8.2. Age model for the core FCPw1 and estimated 2σ errors, based on six AMS–^{14}C dates, performed on total organic sediment, and ^{210}Pb chronology. The data interpolation was obtained with Bchron 3.2 software. **228**

Figure 8.3. FCPw1 core data of bromine (Br), organic matter (OM), Br/OM ratio, lead (Pb) and summary of benthic foraminiferal assemblages (dashed line: distribution of salt marsh species; solid line: distribution of low-salinity marsh species); solar activity – solar irradiance anomaly using a 22-year running average reconstruction (after Steinhilber et al., 2012); temperature anomaly – 10-year running average reconstruction (after Martín-Chivelet et al., 2011); grey bars – solar minima events (references in the text); PWP – Present Warm Period; LIA – Little Ice Age; MCA – Medieval Climatic Anomaly. **232**

Figure 8.4. A – Production and use of lead in gasoline from *ca.* 1935 to 1995; B – Estimated use of bromine in leaded gasoline, based on data in A (adapted from Thomas et al., 1997). **238**

Figure 8.5. World consumption phase-out of methyl bromide (raw data source: United Nations Environment Programme, Ozone Secretariat, Data Access Centre). **238**

Figure 9.1. A – Study areas general location; B – Minho and Lima estuaries (NW coast); C – Sado estuary (SW coast); D – Mira estuary (SW coast). The location of the complete sampling set is also indicated. This includes thirteen surface sampling transects across the four tidal salt marshes (where both interstitial waters and sediments have been collected), and the two sediment cores obtained in the high marsh zones of the Caminha (FCPw1; Minho estuary; 1.55 m above mean sea-level; 41º52′37.0″ N and 8º49′28.0″ W) and Casa

Branca (FWCBr1.4; Mira estuary; 1.74 m above mean sea-level; 37º40′03.7″ N and 8º43′12.7″ W) salt marshes. **251**

Figure 9.2. Cl^-/Br^- mass ratios *vs.* Cl^- concentrations of (surface and interstitial) water samples and potential sources (zones and theoretical limits from Panno et al., 2006). A – Clusters of freshwater (riverine), marine, and impacted water samples (i.e., tidal and salt marsh interstitial waters) are indicated. B – Clusters of interstitial waters from NW and SW coastal salt marshes. Marine water samples are in the same group as the SW coast salt marshes interstitial waters. A group of three anomalous samples (TRO_P7, NSR_P1 and PMF_P6) is also identified. The diamond represents a typical marine sample. **257**

Figure 9.3. Bromine and organic matter (OM) contents of superficial tidal salt marsh sediment transects from Minho, Lima, Sado and Mira estuaries..... **260**

Figure 9.4. FWCBr1.4 and FCPw1 cores geochemical data: Br (mg/kg), OM (%) and Br/OM ratios. Other data represented are: TSI anomaly using a 21-year running average reconstruction (Steinhilber et al., 2012); volcanic radiative forcing (black bars) after Crowley (2000); cumulative precipitation and annual temperature (31-year running averages) for NW coast (black lines and top axis) and SW coast (grey lines and bottom axis) of Portugal (Gómez-Navarro et al., 2011). DM – Dalton Minimum; MM – Maunder Minimum; SM – Spörer Minimum; WM – Wolf Minimum. **264**

Figure 9.5. Conceptual model for the Br cycling in the W Portuguese coast saltmarshes, including the most important elements influencing the Br pool in soils/sediments (P – Precipitation; T – Temperature; PAR – Photosynthetically Active Radiation; ET – Evapotranspiration; S_i – Surface water inflow; S_o – Surface water outflow; G_i – Ground water inflow; T_i – Tidal water outflow; T_o – Tidal water outflow; [S] – Salinity; [OM] – Soil/Sediment Organic Matter content; $[Br_{org}]$ – Soil/Sediment Organic Bromine content)..... **265**

Figure 10.1. A – Study areas general location; B – Minho estuary (northwest coast); C – Mira estuary (southwest coast). The location of the two sediment cores is also indicated: FCPw1 (Caminha, Minho estuary; 1.55 m above mean sea-level; 41º52′37.0″ N and 8º49′28.0″ W) and FWCBr (Casa Branca, Mira estuary; 1.74 m above mean sea-level; 37º40′03.7″ N and 8º43′12.7″ W)..... **282**

Figure 10.2. A – Summary of dominant benthic foraminifera data in the southwest (SW) FWCBr core. B – Percentage distributions of the groups of brackish-to-normal salinity (black line) and brackish-low salinity benthic species (grey dashed line) in the northwest (NW) FCPw1 core; C – Accumulated annual precipitation simulation ERIK1 (Gómez-Navarro et al., 2011, 2012) - northwest Iberia black line; southwest Portugal grey line; D – Annual temperature simulation ERIK1 (Gómez-Navarro et al., 2011, 2012) - northwest Iberia black line; southwest Portugal grey line; E – annual North Atlantic Oscillation (NAO) index reconstruction (Luterbacher et al. 2002). - 21 years running average; Purple shadows represent Grand Solar Minima; Yellow bars represent drier/dust periods; Black arrows mark the *T. inflata* episodes in FWCBr; Age (yr cal. AD) – age in calendar years AD..... **288**

Figure 10.3. Factor analysis (FA) of the *T. inflata*, geochemical and sedimentological data from the FWCBr core. Biplots showing: A – Factors F1 *vs*. F4; B – Factors F2 *vs*. F4; C – Factors F3 *vs*. F4. ..... **289**

Figure 10.4. A – *Trochammina inflata* occurrence in the southwest (SW) FWCBr core; B – Zr/Rb ratio (black line); Zr/Al ratio (gray line); C – Percentage of coarse silt fraction; D – Percentage of medium silt fraction; E – Rb/Al ratio (black line); K/Al rato (dashed line); F – K/Zr ratio; G – Accumulated annual precipitation (black line) and annual temperature simulation (gray line) ERIK1 (Gómez-Navarro et al., 2011, 2012) for southwest Portugal; H – annual North Atlantic Oscillation (NAO) index reconstruction (Luterbacher et al., 2002) - 21 years running average; Purple shadows represent Grand Solar Minima; Yellow bars represent drier/dust periods; Black arrows mark the *T. inflata* episodes; Age (yr cal. AD) – age in calendar years AD. **290**

Figure 10.5. A – REDFIT periodogram of *T. inflata*; B – REDFIT periodogram of *J. macrescens;* both for the AD 1323–2012 period. The statistically significant peaks registered at 70, 29 and 23 years are set at 97.4% level. **291**

Figure 10.6. Results of the cross wavelet coherence transform (WTC; Grinsted et al., 2004) for the AD 1323–2012 period. A) *T. inflata vs.* TSI; B) NAO index *vs.* TSI; C) TSI *vs.* simulated annual temperature for southwest Portugal; D) *T. inflata vs.* simulated annual temperature for southwest Portugal; E) Comparison of WTC results obtained for southwest coast (AD 1323–2012; this work) with the ones for northwest coast (AD 1610–2010; Moreno et al., submitted, [Chapter 6]): *T. inflata vs.* TSI (FWCBr core) and benthic foraminifera brackish/saltier species *vs.* TSI (FCPw1 core). The color scale is proportional to the cross wavelet coherence correlation power. The black arrows superimposed on the representation indicate the relative phase relationship, with horizontal right-pointing arrows representing in-phase relationships and left-facing arrows denoting anti-phase; arrows pointing straight down indicate that the first series leads ahead the second by 90 degrees; arrows pointing vertically upward means the second series leads the first by 90 degrees. In all panels the black thick

line is the 5% significance level using the red noise model. Shaded areas represent the cone of influence (COI) where edge effects may distort the results. **302**

Figure 11.1. Main paleoclimate evolution characteristics of the NW and SW coasts as defined based on the down-core studies. **319**

List of Tables

Table 2.1. Temperature and Salinity of Marsh Sediment Interstitial Water and Estuarine Water. PR – Pedras Ruivas; Ros – Rosário; PMF – Ponte De V.N. Mil Fontes; LT – Low Tide; HT – High Tide. **58**

Table 3.1. Caminha tidal marsh salinity of sediment interstitial water (except PR1 and CP1). **78**

Table 3.2. ^{210}Pb CRS chronology supported by ^{137}Cs and total Pb concentrations of Caminha high marsh sediment core top (FCPw1). **79**

Table 4.1. Pearson correlation coefficients (GHD z-score normalized data *vs.* March to August mean maxima temperatures, for the period 1941–2009; MAM – March, April and May; JJA – June, July and August; MAMJJA – March, April, May June, July and August. **101**

Table 4.2. Linear regression model calibration and verification statistics, for two independent periods: r squared (r^2), r-bar squared (r^2), root mean squared error (RMSE), reduction of error (RE) statistic, coefficient of efficiency (CE), and Durbin-Watson (DW) statistic. Statistics for the overall period (1856–2009): $r^2 = 0.55$; r^2 adjusted = 0.54; DW = 1.60. ..... **105**

Table 4.3. Correlations of the prominent teleconnections patterns and monthly mean maxima temperature for the Braga weather station and growing season mean maxima temperature (1950–2009). MAMJJA – March, April, May June, July and August; AO – Arctic Oscillation index, NAO – North Atlantic Oscillation index, EA – Eastern Atlantic index, EA/WR – East Atlantic/Western Russia Oscillation index, SCA – Scandinavian Oscillation index, SCA_MAMJJA – Scandinavian Oscillation index mean for the growing season months. **111**

Table 5.1. Caminha intertidal salinity range of sediment interstitial water (‰) **127**

Table 6.1. Pearson correlation coefficients between 1629–1821 triennia of wine production raw data ($p < 0.05$). **161**

Table 6.2. WP Reconstruction: calibration/verification statistics. **161**

Table 7.1. Radiocarbon ages data determined in the Laboratory “Beta Analytic Inc.”. (AMS – standard delivery). **191**

Table 7.2. Summary of micropaleontological and sedimentological data. The values represent the average (bold) and the range; Low Sal. spp. % – low-salinity species group; Salt marsh spp. % – “normal”-salinity species group; NF – number of foraminifera; S – number of species; assemblages dominant species (bold). **194**

Table 8.1. Radiocarbon age data determined in the Laboratory “Beta Analytic Inc.” (AMS – standard delivery). **228**

Table 8.2. Geochemical data from Minho estuary. A – Surface and marsh interstitial water; B – Surface sediments. **229**

Table 8.3. Geochemical and foraminiferal assemblage data from sediment core FCPw1. ..... **236**

Table 9.1. Bromide concentrations in surface water (river freshwater, estuarine and coastal seawater) samples and in marsh interstitial water samples (Minho, Lima, Sado and Mira tidal salt marshes). **256**

Table 9.2. Bromine and organic matter contents in the surface sediment cross-shore transects from the Minho, Lima, Sado and Mira intertidal domains (tidal flat, low marsh and high marsh). **259**

Table 10.1. Summary of the main characteristics of the two studied regions in the west coast of Portugal. **283**

Table 10.2. Factor analysis (FA) based on the geochemical and sedimentological proxies chosen in estimating the respective riverine and aeolian contribution. **289**

Table 11.1. Climate types of the NW and SW Portuguese coasts and main features, as defined based on the studies performed at the marshes surface and estuaries. **316**

List of Appendices

Appendix 3.1. Marsh foraminiferal reference list for those species mentioned in the text. **90**

Appendix 3.2. Foraminiferal data from the top core FCPw1 – Caminha tidal marsh. **91**

Appendix 3.3. Foraminiferal data from surface sediment of Caminha tidal marsh (samples carrying less than 34 individuals and the species representing less than 2% of the assemblage were excluded). **91**

Appendix 3.4. Precipitation data from the Portuguese sectors of Minho and Lima river basins. **92**

Appendix 3.5. $^{210}Pb_{Excess}$ and ^{137}Cs content (Bq kg^{-1}) in the FCPw1 core. **92**

Appendix 4.1. GHD data – Grape Harvest Dates z-score from Minho region (1856–2009). GSTmax reconstructed data - growing season maxima temperatures reconstruction from Minho region (2009–1856). **121**

Appendix 4.2. Calibration and verification results of the grape harvest dates composite with March–August Braga maxima temperatures. Temp. rec. - temperature reconstructed (ºC); Temp. obs. - temperature observed (ºC). **122**

Appendix 5.1. Age model for the core FCPw1 and estimated 2σ errors, based on six AMS–^{14}C dates, performed on total organic sediment, and ^{210}Pb chronology. The data interpolation was obtained with Bchron 3.2 software (after Moreno et al., 2014). **142**

Appendix 5.2. Dead foraminiferal assemblage percentages from FCPwAR Caminha tidal marsh core. **143**

Appendix 5.3. Systematic list of Caminha tidal marsh foraminiferal species, including ecological distribution synthesis and plates. **144**

Appendix 6.1. Benedictine wine production in litres (bold- reconstructed values). **183**

Appendix 6.2. Percentage distribution of benthic foraminifera in core FCPwAR1. Age (yr AD) – age in calendar years AD; Salt marsh spp. – distributions of the group of low-salinity benthic species – Low Salinity spp.; – distribution of the group of moderate-brackish benthic species; Mod. Brackish spp. – distribution of the group of brackish-to-normal salinity benthic species; Brackish to Normal Salinity spp.; – distribution of the group of brackish-to-normal salinity benthic species plus the group of moderate-brackish benthic species; Mod. Brackish+Brackish-to-normal Salinity spp. **184**

Appendix 7.1. $^{210}Pb_{Excess}$ and ^{137}Cs content (Bq kg^{-1}) in the FCPw1 core – Caminha tidal marsh. **213**

Appendix 7.2. Foraminiferal data (%) from core FCPw1 – Caminha tidal marsh. **214**

Appendix 7.3. Sedimentological and geochemical data from core FCPw1 – Caminha tidal marsh. **215**

Appendix 7.4. Data from organic geochemistry proxy core FCPw1 (after De la Rosa et al., 2012) – Caminha tidal marsh. **216**

Appendix 7.5. Chronology of main floods and paleofloods from the Iberian Atlantic and NW Portuguese regions. **216**

Appendix 7.6. Foraminifera faunal list from core FCPw1 – Caminha tidal marsh. **217**

Appendix 8.1. Comparative values of the measured and certified concentrations of geological standard reference materials (SRM 2704 and SRM 1646). **245**

Appendix 8.2. $^{210}PbExcess$ and ^{137}Cs content (Bq kg^{-1}) in the FCPw1 core – Caminha tidal marsh. **245**

Appendix 8.3. Organic matter data from the core FCPw1 (after De la Rosa et al., 2012) – Caminha tidal marsh. **246**

Appendix 9.1. Age model for the core FWCBr and estimated 2σ errors, based on two AMS ^{14}C dates, performed on total organic sediment, and ^{210}Pb and ^{137}CS chronology. The data interpolation was obtained with Bchron 4.1 software. **277**

Appendix 9.2. Geochemical data from the FWCBr sediment core (Casa Branca salt marsh; Mira estuary). **278**

Appendix 10.1. Percentage distribution of benthic foraminifera in Casa Branca marsh cores. Age (yr AD) – age in calendar years AD; H. spp. – *Haplophragmoides* spp..... **311**

Appendix 10.2. Aeolian and fluvial geochemical indicators in the Casa Branca marsh core. Age (yr AD) – age in calendar years AD..... **312**

Appendix 10.3. Relative percentage distribution of the sand and silt (coarse and medium) fractions in Casa Branca marsh cores. Age (yr AD) – age in calendar years AD. **313**

Appendix A1. Systematic List. **313**

Appendix A2. List of the scrutinized local/regional newspapers. **332**

List of Plates

Plate 3.1. Scale bar 100 µm. 1a *Trochamminita salsa* (Cushman and Brönnimann, 1948), single areal aperture specimen; 1b and c *Trochamminita salsa* (Cushman and Brönnimann, 1948), irregular specimen with backward multiple areal apertures. 2 *Haplophragmoides manilaensis* Andersen 1953; 3 *Haplophragmoides wilberti* Andersen 1953; 4 *Haplophragmoides* sp.; 5a *Tiphotrocha comprimata* (Cushman and Brönnimann, 1948), ventral view; 5b *Tiphotrocha comprimata* (Cushman and Brönnimann, 1948), apertural view; 6a *Pseudothurammina limnetis* (Scott and Medioli, 1980), free specimen; 6b *Pseudothurammina limnetis* (Scott and Medioli, 1980), plant debris attached specimen. **93**

Plate 3.2. Scale bar 100 µm. 1a *Trochammina inflata* (Montagu, 1808), dorsal view; 1b *Trochammina inflata* (Montagu, 1808), ventral view; 1c *Trochammina inflata* (Montagu, 1808), apertural view. 2a *Miliammina fusca* (Brady, 1870); 2b *Miliammina fusca* (Brady, 1870), apertural view. 3a *Saccammina* sp.; 3b, *Saccammina* sp., apertural view; 4a *Psammosphaera* sp.; 4b *Psammosphaera* sp., pores/apertures detail; 5 *Paratrochammina guaratibaensis* Brönnimann, 1986, ventral view. 6 *Siphotrochammina lobata* Saunders, 1957, ventral view. 7a *Jadammina macrescens* (Brady, 1870), ventral view; 7b *Jadammina macrescens* (Brady, 1870), dorsal view. **94**

Plate 5.1. Scale bar 100 µm. 1a – *Trochamminita salsa/irregularis* (Cushman & Brönnimann, 1948),with a single aperture in the last chamber; 1b,c – *T. salsa/irregularis* irregular forms with backward secondary apertures in the last chamber; 2 – *Haplophragmoides manilaensis* Andersen, 1953; 3 – *Haplophragmoides wilberti* Andersen, 1953; 4 – *Haplophragmoides* sp.; 5a – *Tiphotrocha comprimata* (Cushman & Brönnimann, 1948), ventral face and oral view; 5b – *T. comprimata*, detail of secondary apertures; 6a – *Pseudothurammina limnetis* (Scott & Medioli, 1980), apertural view of a free specimen; 6b – *P. limnetis* sessile specimen attached to a marsh plant debris. **152**

Plate 5.2. Scale bar 100 µm. 1a – *Trochammina inflata* (Montagu, 1808), dorsal face; 1b – *T. inflata*, ventral face; 1c – *T. inflata*, apertural view; 2a – *Milliammina fusca* (Brady, 1870); 2b – *M. fusca*, apertural view; 3 – *Paratrochammina guaratibaensis* Brönnimann, 1986, ventral face; 4 – *Siphotrochammina lobata* Saunders, 1957, ventral face; 5a – *Jadammina macrescens* (Brady, 1870), ventral face; 5b – *J. macrescens*, dorsal view; 6 – *Polysaccammina ipohalina* Scott, 1976. Scale bar 50 µm for plate figure 6..... **153**

1 Introduction

"We have to bear in mind that tests of agglutinated Foraminifera were built by the industry of the protoplasm and we may compare this action with the building of nests by birds or webs by spiders. These nests or webs are so characteristic for the species (…) that built them that we could, if necessary, characterise each species by means of those nests or webs. In some way this is also done in the case of agglutinated Foraminifera…"

J. Hofker in PRIMITIVE AGGLUTINATED FORAMINIFERA (1972), p.1.

1.1. Motivation and objectives

Past foraminiferal research may be seen as encompassing two phases, the descriptive and the interpretive, that partially overlap (Jones, 2014). The first began with the early formal descriptions of foraminiferal species dating back to the late 18th to 19th centuries (e.g., Walker and Boys, 1784; d'Orbigny, 1826, 1843; Brady, 1876, 1884), while the second started with the first use of foraminifera in biostratigraphy in the late 19th century (Grzybowski, 1896, 1898, 1901). It continued in the 20th century, escorted by advances in the understanding of foraminiferal ecology, oceanography, paleoecology, paleoceanography and paleoclimatology. In the second half of the 20th century, the studies of Fred Phleger became a fundamental benchmark in the pioneered research into foraminiferal ecology (e.g., Phleger, 1951, 1954, 1960, 1965), leading to the conclusion that the modern foraminiferal distribution can be used as an analogue for the past distributions recorded in sediments. After that, foraminifera won a relevant role in paleoclimatology, in which they become one of the most extensively used proxies for paleoclimatic variations, in an effort of extending back in time the observational or instrumental meteorological data of the past *ca*. two centuries. The extreme sensitivity of foraminifera to changing environmental conditions has led to the development of techniques to understand past sea-level fluctuations, monsoons and hurricanes, using their specific characteristics to create paleoclimatic records with higher resolution, or the study of other kind of events like tsunamis (Nigam, 2005; Mamo et al., 2009).

In coastal transitional environments, such as salt marshes, the foraminiferal research of the last three decades was developed mainly for the purpose of reconstructing past environments in relation to sea-level fluctuations, with marsh foraminifera starting to be routinely used as sea-level proxies (see Barlow et al., 2013, for a review). In turn, there are few approaches exploring different marsh foraminifera applications as climate-change proxies (e.g., De Rijk, 1995; Hippensteel et al., 2002; Fatela et al., 2014; Moreno et al., 2014), namely to demonstrate their quick and measurable response to climate variability and change at several time-scales, and thus showing the value of marsh foraminifera-based analysis in the interpretation of past climates.

Benthic foraminiferal records in salt marshes are archives of environmental changes, where a local/regional or even global climatic signature can be obtained. They can provide evidence on how climate triggers regional hydrological changes in precipitation, runoff or groundwater flux because salinity strongly influences the species' distributions. Also the precipitation–evapotranspiration (P–ET) marsh balance can be estimated by the dominance of species/assemblages representative of either saline or brackish waters. In this analysis, short- and long-term hydrological changes must be considered to attain reliable paleoenvironmental signatures. Within this context, progress was made on the full set of foraminiferal proxies (e.g., Phleger, 1970; Cearreta, 1988, 1998; Alve, 1991; Murray, 1991, 2000, 2006; De Rijk, 1995; Nigam et al., 1995; Hayward et al., 1999; Cronin et al., 2000; Karlsen et al., 2000; Hippensteel et al., 2002; Debenay and Guiral, 2006; Khare et al., 2008), but much work remains in outlining which species are best for which kinds of issues. To achieve this knowledge, one has to ascertain the major variability's sources that mediate or control the foraminiferal species' response.

The scientific (and public) interest in paleoclimate has considerably grown as issues on abrupt climate change, past climate responses to elevated levels of atmospheric CO_2, and internal climate variability became urgent, in order to better characterize the anthropogenic impact on Earth's climate system (Smerdon and Pollack, 2016). As regards the last 2000 years, the separation of externally (e.g., solar) forced *versus* internal climate variability has been a key motivation (e.g. Schurer et al., 2013; Mann et al., 2014; Frankcombe et al., 12015), with implications for how each contribute to decadal-to-secular variability and, ultimately, to future climate change, all this accompanied by attempts to collect more proxies and understand the signals they contain (Smerdon and Pollack, 2016). Likewise, under the present scenario of global warming, scientific concern goes to the impact of rising temperatures on the hydrological cycle, leading to shifts on the local/regional precipitation regimes and to an expected increase in the frequency (and intensity) of extreme weather events, such as storms, snowfall, floods, heatwaves and droughts, threatening food and energy supply, as well as human safety and health (e.g., Sutherst, 2004; Tebaldi et al., 2006; Kang et al., 2009). In this context, paleoclimatic reconstructions, along with climatic modelling, not only have increasingly provided better insights into how the climate system operates on time-scales that cannot be captured by the instrumental period, allowing the analysis of large-scale patterns of temperature and humidity–precipitation (e.g., Wanner et al., 2014), but also played a major role on the ability to properly forecast future climate variability and change (Valdes, 2011; Smerdon and Pollack, 2016), in which solar forcing represents a source of uncertainty (Chiodo et al., 2016).

The major goal of the research assembled in this dissertation lies on establish an unedited relationship between climatic indices and the paleoecology of marsh benthic foraminifera, contributing by this way to increase the knowledge on the west Iberian margin's paleoclimatic

evolution in the context of the northeast Atlantic region. To fulfil this objective, several benchmarks were defined:

a) to relate the recent (20th and 21st centuries) evolution of the foraminiferal assemblages present in the sedimentary record from different temperate salt marshes of the west Portuguese coast with available instrumental data and the main modes of atmospheric circulation – North Atlantic Oscillation (NAO), the East Atlantic/Western Russia Oscillation (EA/WR), the Scandinavian Oscillation (SCA) – and the Atlantic Multidecadal Oscillation (AMO);

b) to search and scrutinize documentary sources, such as newspapers and municipal and religious archives, providing evidence on climate variability and weather-related extremes, as well as their socio-economic and political impacts;

c) to compare the material found in b) with the high-resolution marsh foraminifera-based paleoclimatic reconstruction of the west Portuguese coast, in order to corroborate the foraminiferal response to climatic and atmospheric forcing as well as to the cycles of solar activity (SA), as far back in time as possible;

d) to assess the influence of a recognized long-term North–South climatic gradient along this coast, featuring climate-driven singularities on the paleoenvironmental evolution of its estuarine systems over the last 2000 years;

e) to find out, based on the current research, new consistent paleoclimate proxies to be applied in future reconstructions.

1.2. Sun's activity, Earth's climate and biogeochemical markers of past environmental change

"Everything is based on energy. Energy is the source and control of all things, all value, and all the actions of human beings and nature. (…) When energy sources are rich, economies, knowledge and aspirations grow; when energy sources are all being used as fast as the Earth receives them, activities, values, and aspirations settle into a steady pattern. So it has been throughout the history of humanity and nature."

H.T. Odum and E.C. Odum in ENERGY BASIS FOR MAN AND NATURE (1976), p.1.

1.2.1. A coupled solar–terrestrial system affecting biosphere

The terrestrial biosphere, considered as one of the most critical and complex components of the climate system (Overpeck et al., 2003), has evolved over *ca.* 4 billion years as a balanced bio-geological system ultimately sustained by solar energy (e.g., Lorenzo et al., 2016) (Figure 1.1). Consequently, all life forms and processes on Earth, including human societies, exist within an intricate network of global energy flows (Karl, 2014), which is at the core of ecosystem analysis (Odum, 1968).

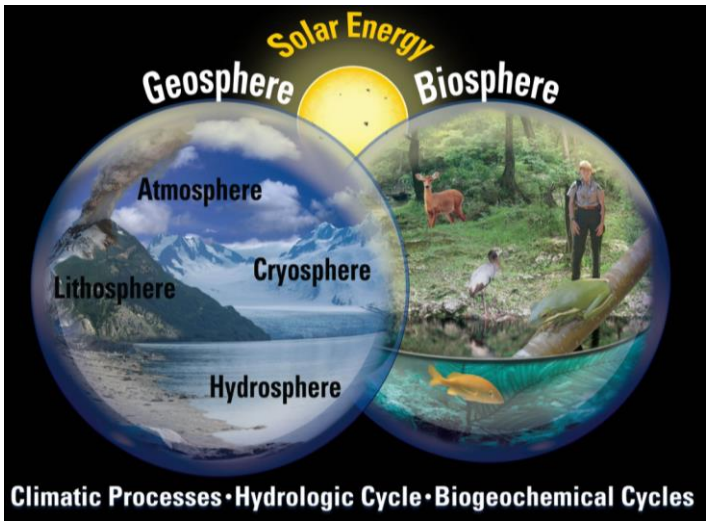

Figure 1.1. The earth's geosphere and biosphere interact and are interrelated through (i) climatic processes and (ii) the hydrological and biogeochemical cycles, with the sun as the dominant source of all external energy. Diagram designed by James A. Tomberlin, USGS (https://pubs.usgs.gov/pp/p1386a/plate-earthsystem.html).

Energy not only plays a role in ordering and maintaining complex systems; it could also regulate their origin, evolution, and fate. Living or non-living, dynamical systems use flows of energy to endure. Whether stars, bacteria or civilization, it is energy that not only sustains the structural integrity of open, non-equilibrated systems, but also keeps them working, helping them, at least locally and temporarily, to avoid a disordered state (of high entropy) demanded by the second law of thermodynamics (Chaisson, 2008, 2014, 2015).

The Earth is a mixed living and non-living system, an open system interacting with its atmosphere and with matter and energy in space (Miller and Miller, 1989). At the present stage of our planet's evolution (when the heat flux generated internally is only 0.03% of total energy budget at the surface), the Earth's global energy budget (Figure 1.2) is dominated by the incoming solar radiation that is dropped mainly into the external surface layers of atmosphere, upper ocean and biosphere, from which it is then re-radiated (Chaisson, 2014). For a stable climate, a balance is required between the incoming (solar) and outgoing (infrared) radiation. In this context, and since the Sun is known to be a variable star, any fluctuation in its total energy output (or luminosity) affects, at some level, the climate. However, this is further modulated by internal factors and processes, such as oscillations in the ocean–atmosphere system, volcanic eruptions, atmospheric content of greenhouse gases, cloud cover, or ice and vegetation cover (Tiwari and Ramesh, 2010), as represented by the bold arrows in Figure 1.3, making even more demanding to detect solar influence on the background of the atmosphere's internal variability. In fact, and despite the incontestably Sun's full potential to affect climate, "establishing both how the output of the Sun varies and how such variations influence Earth's climate have proved tricky", quoting Solanki (2002), with many aspects still poorly understood. This makes the Sun–climate connections one of the most challenging issues in the today's climate science.

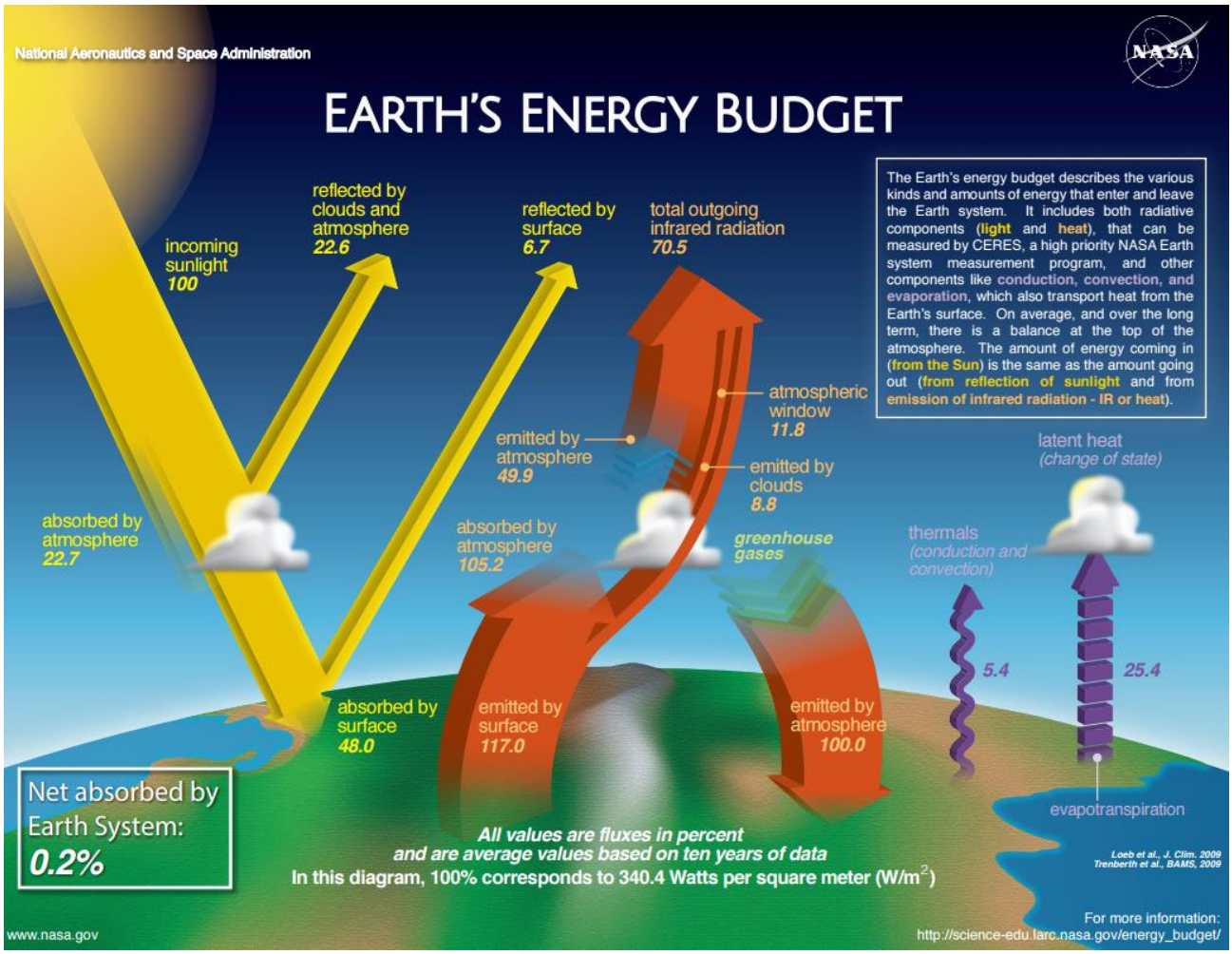

Figure 1.2. Estimate of the global annual mean Earth's energy budget (NASA). This energy budget diagram shows the best understanding of energy flows into and away from the Earth. Arrows designate the schematic flow of energy in proportion to its importance. The numbers correspond to percentages of the overall mean amount of energy that reaches the Earth, i.e., 340.4 Wm^{-2}. Over the last 15 years, measurements show that the Earth's energy budget is not quite balanced. There has been a net ~0.2% of energy absorbed per year (https://science-edu.larc.nasa.gov/energy_budget/pdf/ERB_Litho_Edits_Percent_2016_v7.pdf).

A comprehensive understanding of the influence of solar variability on the Earth's climate requires knowledge on (i) the short- and long-term solar variability, (ii) solar-terrestrial interactions, and (iii) the mechanisms determining the Earth's climate system's response to these interactions (Rind, 2002). Hence, behind the question: *What is the solar influence on climate?*, there is an extremely wide range of complex physical and chemical processes that, as stated by Lilensten et al. (2015), "can be imagined as multiple links of a long chain extending all the way from the solar interior to the Earth's surface". All this only recently began to be investigated within a framework of more active collaborations across scientific disciplines, which is the case, for instance, of the international CAWSES and CAWSES-II science program (e.g., Seppälä et al., 2014; Tsuda et al., 2015) and of the COST Action ES1005 (Lilensten et al., 2015; http://www.tosca-cost.eu), both already finished.

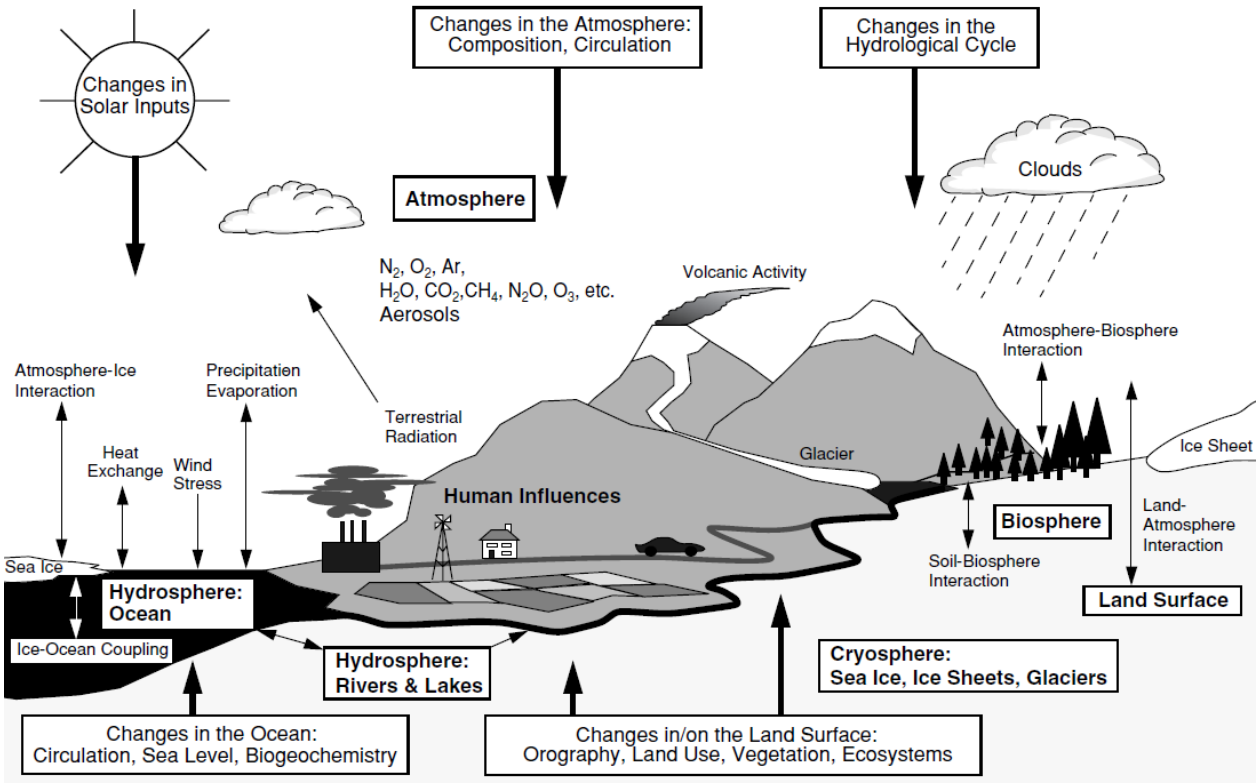

Figure 1.3. Schematic view of the components of the global climate system (bold), their processes and interactions (thin arrows) and some aspects that may change (bold arrows) (from Baede et al., 2001). In such a complex system everything may affect everything, but to different degrees (Benestad, 2006).

1.2.2. A variable Sun

Solar variability occurs on a wide range of time-scales, mainly as a result of (i) the Sun's evolution, driven by conditions in its core and (ii) the Sun's magnetic field produced through dynamo operation in the interior, strongly time-dependent. Without such dynamics phenomena like sunspots and coronal loops, faculae and solar flares, the solar wind and prominences, the solar cycle and irradiance variability, would be unknown to us (Solanki et al., 2006). All these features are described collectively under the designation of solar activity (SA), from which sunspots (Figure 1.4) were the first to receive attention. This happened in the early 17th century, after the Galileo's invention of the telescope, when their existence was demonstrated beyond doubt (e.g., Benestad, 2006). As a result, sunspots provide the longest direct record of SA, being used to describe it in a universal but arbitrarily-defined index, the Wolf sunspot number (WSN), since 1848 (e.g., Hoyt and Schatten, 1997; Eddy, 2009).

The long-time SA monitoring revealed that solar variations appear usually quasi-periodically (e.g., Schwabe, 1844; Wolf, 1861; Hoyt and Schatten, 1997), which is strikingly illustrated by the number of sunspots visible on the solar disc at any time (Figure 1.5). As one can see in the time series graph of Figure 1.5, a minima-and-maxima fluctuation is readily apparent, describing a regular but elastic, self-regenerating (Grandpierre, 2004), cycle that can vary from 9 to 14 years, with a mean of approximately 11 years, i.e., the 11-year solar (sunspot) cycle, also called Schwabe cycle

(Schwabe, 1844). This is but one aspect of a complex 22-year magnetic fluctuation (the Hale cycle, the true cycle of SA), in which the magnetic polarity of the Sun reverses and then returns back to the original state (Hale et al., 1919). Both cycles are included in the Sun's long-term variations (Tiwari and Ramesh, 2010), along with the 33–35-year Brückner cycle (Brückner, 1890), as well as lower frequency cycles, hard to recognize due to the lack of instrumental data, but evident indirectly based on proxies for SA (e.g., sunspots, faculae or cosmogenic isotopes like ^{14}C and ^{10}Be), such as the 88-year Gleissberg cycle (Gleissberg, 1939), the 208-year De Vries/Suess cycle (De Vries, 1958; Suess, 1980), the 970-year Eddy cycle (Eddy, 1976), and the 2300-year Hallstatt cycle (Damon and Sonett, 1991) and even a 100,000-year cycle (Sharma, 2002).

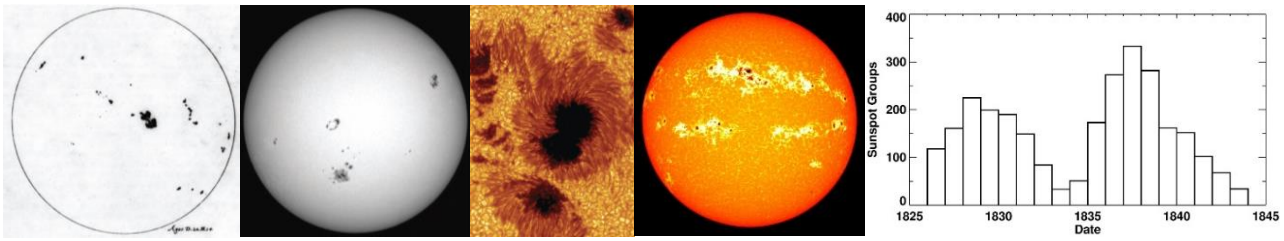

Figure 1.4. (From left to right); A drawing of the full disk of the spotted Sun made in Florence, Italy, by Galileo using a small telescope at about 2 o'clock in the afternoon of August 20, 1610. The solar disk seen in white light from the SOHO spacecraft on October 28, 2003. A close-up, colour-added view of the dark centres (umbrae) of sunspots; the less-dark, magnetically-formed penumbrae that generally encircle them (image taken with the Swedish 1-meter high-resolution solar telescope, at La Palma observatory – Canary Islands – credit: Eddy, 2009). A view of the Sun in March 28, 2001, showing high solar activity; the colour table has been altered to enhance the appearance of the faculae (white regions) which are hotter than sunspots (red-black regions) (image credit: NASA/Goddard Space Flight Center Scientific Visualization Studio). On the right, the sunspot groups observed each year, from 1826 to 1843, by Samuel H. Schwabe (1844), leading him to the discovery of the sunspot cycle (Hathaway, 2010).

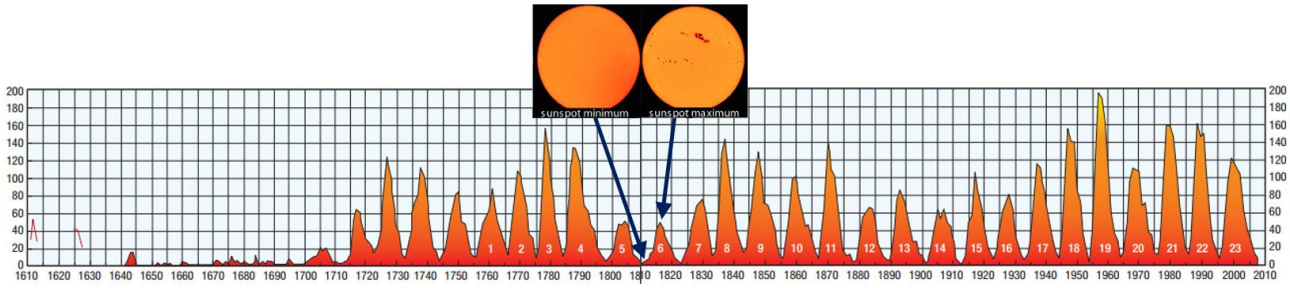

Figure 1.5. The yearly-sunspot number record since the beginning of telescopic observations until 2007 (Eddy, 2009). The Schwabe cycle is quite evident and obvious trends in the longer-term overall level of solar activity. One can see also that the amplitude of the Schwabe cycle varies significantly, from the almost spotless mid-1600s–1715 period (known as the Maunder Minimum) to the very high cycle 19, probably in relation to the secular Gleissberg cycle.

From the preceding long-term 11-year cycle's modulations, the main one is the Gleissberg cycle, first postulated by Wolf (1862) and confirmed by Gleissberg (1939). The Gleissberg cycle signals were also found in solar irradiance (Reid, 1987), aurorae (Siscoe, 1980; Feynman and Fougere, 1984) and ^{14}C and ^{10}Be (Beer et al., 1994; McCracken et al., 2001) records and solar energetic particles (SEP) events (Reames, 2004). Ogurtsov et al. (2002) revealed the complexity of this cycle that seems to present a wide frequency band with a double structure: 50–80-year (Lower Gleissberg) and 90–140-year (Upper Gleissberg) periodicities, for which Le and Wang (2003), by

examining the periodic properties in yearly mean sunspot numbers using wavelet transform, found average periods of 53 years and 101 years, respectively.

On short-term time scales (minutes to days), the Sun shows a diversity of non-stationary phenomena, caused by eruptive events together with strong releases of energy, e.g., flares accompanied by coronal mass ejections (CME), although the relation is not one to one. During these events, charged particles – SEP – can be accelerated, which, when reaching the Earth, affect atmosphere's physicochemical and electrical properties (Usoskin and Krivova, 2012; Velinov et al., 2013). Such Sun's processes are related to the 11-year cycle: moderate flares and CME may occur several times a day in different regions of the Sun nearby a solar maximum, while long and uninterrupted periods of quiet Sun are usual for a solar minimum. Though, strong solar flares can occasionally happen in the very late phase of the solar cycle, just before the minimum phase, as, for instance, a burst of activity in mid-December 2006 (Figure 1.6; Usoskin and Krivova, 2012).

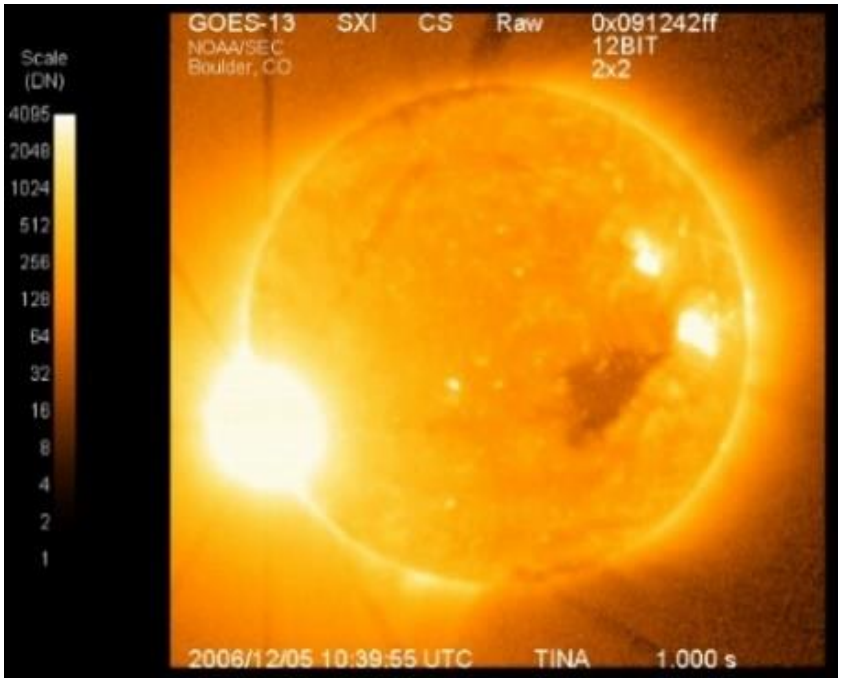

Figure 1.6. The X9-class solar flare of December 5, 2006, observed by the Solar X-Ray Imager aboard NOAA's GOES-13 satellite (available at https://science.nasa.gov/science-news/science-at-nasa/2008/15dec_solarflaresurprise).

Individual 11-year solar cycles, which by convention run from one sunspot minimum to the next, are identified by number, beginning arbitrarily with the cycle 1 (1755–1766). The most recently completed cycle was the 23 (which reached a minimum in 2007), and we are now over 7 years into the cycle 24 (Figure 1.7). This started in December 2008, following a solar minimum that lasted longer than average and reached record low levels of solar and magnetic activity (Solomon et al., 2010). In turn, cycle 24 has had, right from the start, a low level of activity, with only a brief peak in the Northern Hemisphere in 2011, and another peak in the Southern Hemisphere in 2014 (Pesnell, 2016).

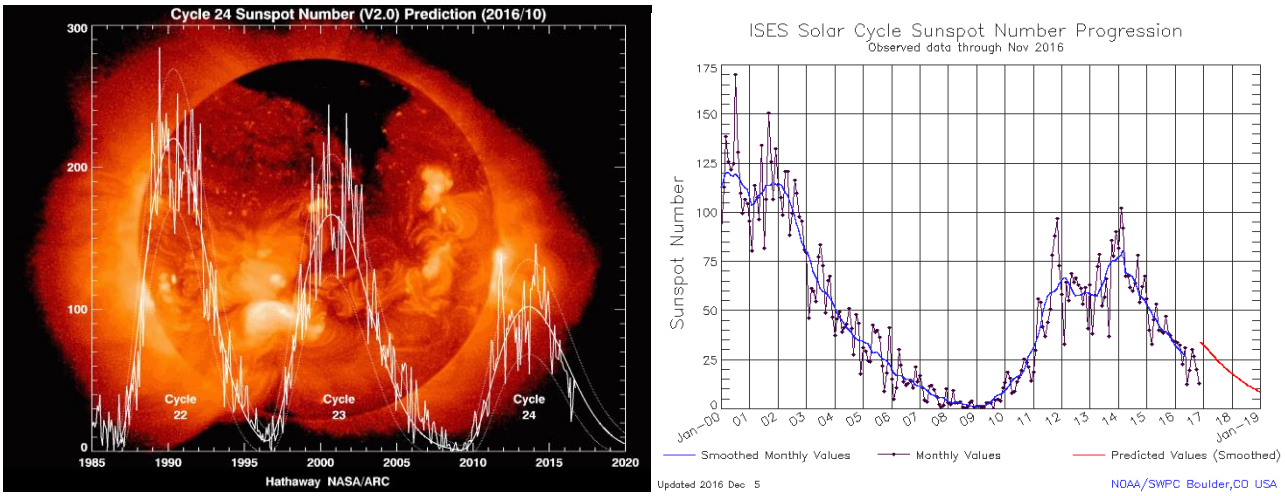

Figure 1.7. Sunspot numbers for solar cycles 22, 23 and 24, showing a clear weakening trend (from Hathaway NASA/ARC) (https://solarscience.msfc.nasa.gov/predict.shtml) **(left)**. On the **right**, the recent solar cycle 24 is represented here by the sunspot number, with the black line representing the monthly averaged data and the blue line a 13-month smoothed version of the monthly averaged data; the forecast for the rest of the solar cycle is given by the red line. As can be seen, cycle 24 is double peaked, similarly to the last two solar maxima, around 1989 and 2001 (http://www.swpc.noaa.gov/products/solar-cycle-progression).

The variation of magnetic activity during the 11-year solar cycle affects not only "magnetic" quantities (e.g., magnetic flux or sunspot number), but as well the Sun's radiative output, which becomes modulated in phase with the solar cycle (Solanki et al., 2006). An accurate measure of this output is the wavelength-integrated radiation flux illuminating the Earth at its average distance from the Sun, i.e., the total solar irradiance (TSI). Spacecraft measurements of the TSI have been made since 1978, evidencing a clear relationship between the solar cycle and TSI (Figure 1.8).

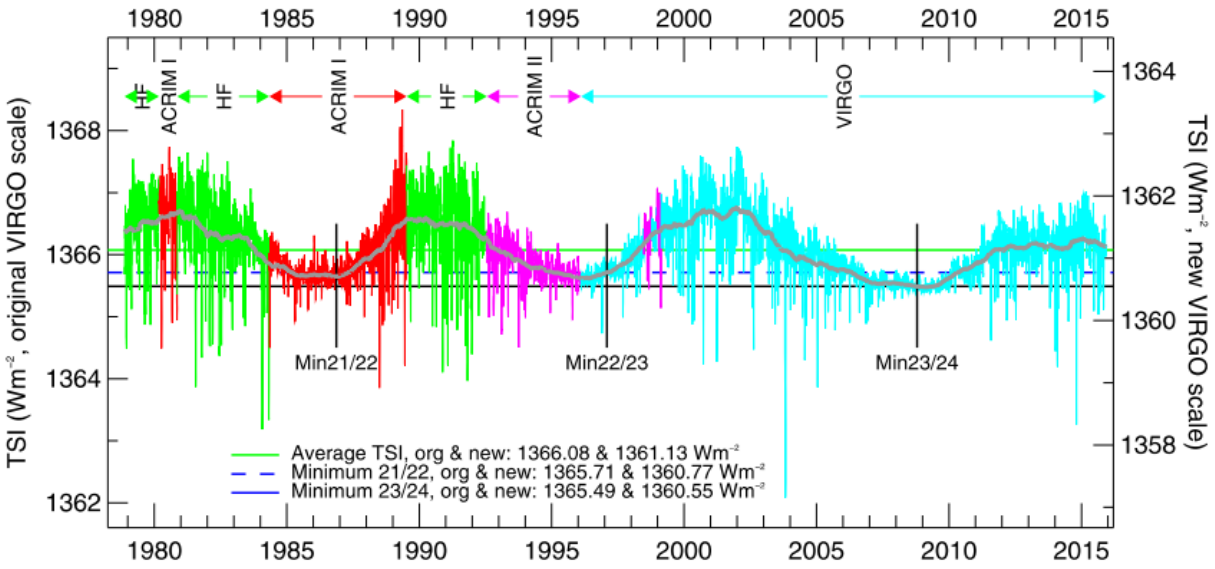

Figure 1.8. The known PMOD composite satellite-era TSI record (named for the institute in Davos, Switzerland that produces the data), spanning from 1978–present, shows peak-to-peak TSI variability of ~0.1% in each of the three solar cycles observed during the space-borne measurement record, with that variability being in-phase with solar activity. The colours indicate the binary selections of different instruments used in the creation of the composite. The right-hand vertical scale indicates the more accurate currently-accepted absolute value (after Kopp, 2016).

Hence, solar irradiance variability can be (i) modelled by correlating the current *ca.* 38-year direct TSI observations with sunspots plus other indices representative of solar-surface magnetic features as faculae, and then (ii) reconstructed by applying those correlations to historical indices of these solar features: 100-years records for faculae and, as referred above, over 400-years for sunspots (Kopp et al., 2016). Several TSI reconstruction models, given estimates of solar variability for the 1610 to present period, are shown in Figure 1.9. A historical TSI reconstruction based on SATIRE models (blue line of Figure 1.9; Krivova et al., 2010; Ball et al., 2012; Yeo et al. 2014), and earlier available online in the webpage of the Laboratory for Atmospheric and Space Physics (LASP) was used in this dissertation (**Chapter 6**). This historical reconstruction, which is updated annually, has meanwhile been replaced by the most recent TSI estimation, the NRLTSI2 model (red line of Figure 1.9), described by Coddington et al. (2015).

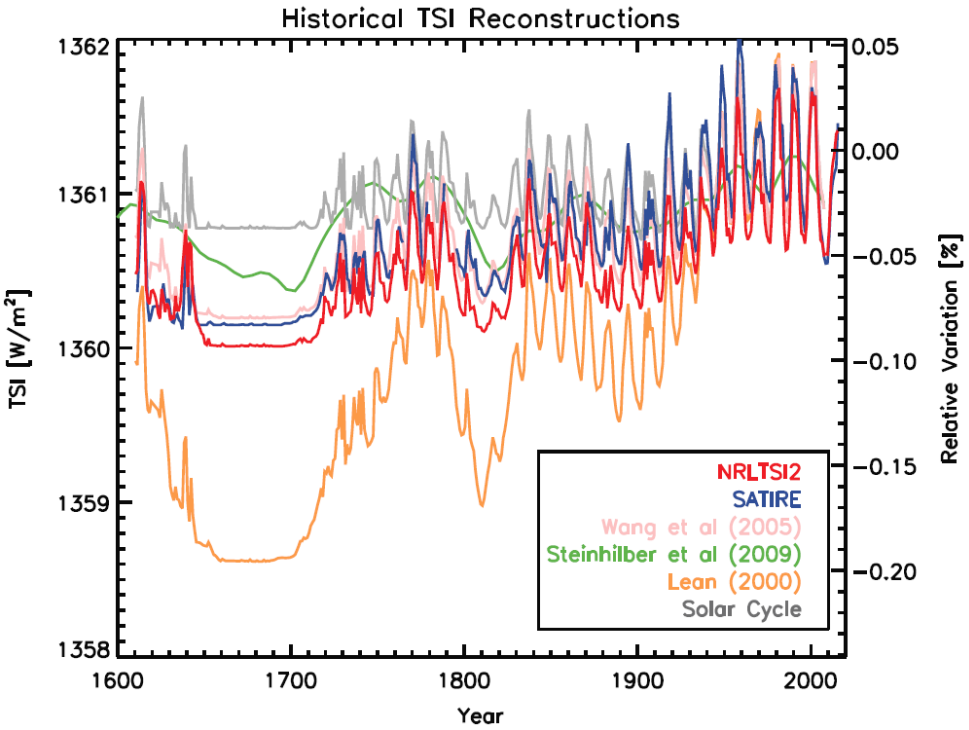

Figure 1.9. Some TSI-reconstruction models providing estimates of solar variability for the last 400 years (after Kopp, 2016).

To reconstruct SA backward over many millennia, cosmogenic isotopes produced in the Earth's atmosphere by nuclear reactions of GCR particles with atmospheric nitrogen (^{14}N) and oxygen (^{16}O), and stored in polar ice cores and tree rings (Figure 1.10), offer the sole opportunity (e.g., Stuiver and Quay, 1980; Bard et al., 1997; Beer, 2000; Steinhilber et al., 2009, 2012). Steinhilber et al. (2012) combined different ^{10}Be ice core records from Greenland and Antarctica with the global ^{14}C tree ring record to derive total solar irradiance for the last 9400 years, which can then be used as a proxy of SA to identify solar imprints in climatic-related records, as it was done in this research, where the TSI reconstruction of Steinhilber et al. (2012) was used in **Chapters 7** to **10**.

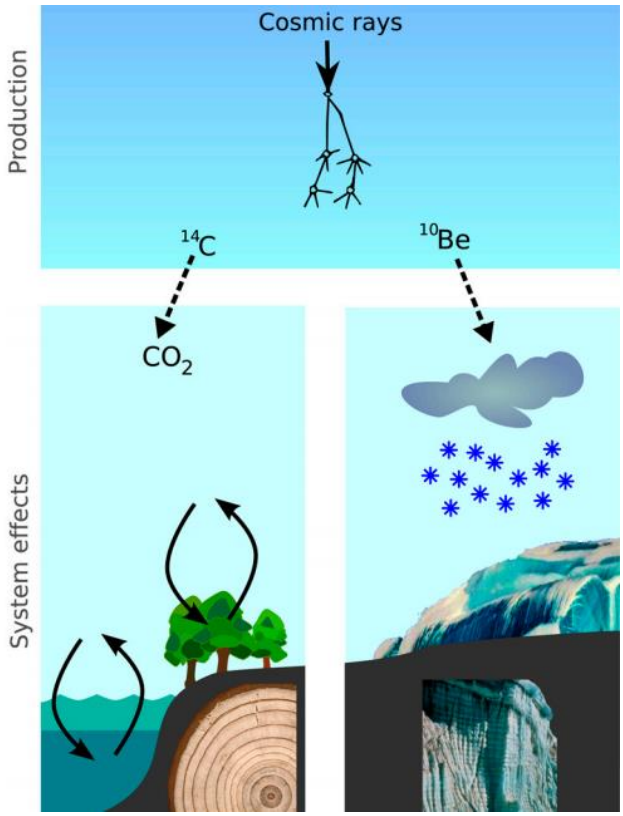

Figure 1.10. Picture showing some fundamentals of the radioisotopes ^{14}C and ^{10}Be in the Earth's system. Both are produced by nuclear reactions of GCR particles with the atmospheric gases (Masarik and Beer, 2009), but after production their fate is very different (system effects). While ^{10}Be attaches to aerosols and is transported within a few years to ground (Heikkilä et al., 2009), ^{14}C oxidizes to CO_2 and enters the global C cycle, exchanging between atmosphere, biosphere, and the oceans (Siegenthaler, 1983) (after Steinhilber et al., 2012). John Eddy (1976) was the first to recognize the strong inverse correlation between the production of the cosmogenic radionuclides and SA.

The analysis of cosmogenic data agreed with the identification of both prominent variabilities on time-scales longer than 11-years, as mentioned above, and the presence of low and high SA states, referred to as *Grand Minima and Maxima* in the sunspot record (Beer et al., 2012). The most recent episodes are the well-known Maunder Minimum (1645–1715), the Dalton Minimum (1790–1820), today not viewed as a Grand episode (e.g., Duhau and Martinez, 2012), and the Modern Maximum (1950–2009). By analysing these longer than 400-years cosmogenic records, further episodes were discovered, namely the Spörer Minimum (1450–1550) and the Wolf Minimum (1280–1350) – all comprised in the time frame of the current research –, with Grand Minima being classified, according to their duration, as Maunder- (short; 30–90 years) and Spörer- (long; > 110 years) type (e.g., Stuiver and Braziunas, 1989; Usoskin et al., 2007). Recently, a set of works, presenting the latest findings on the Sun's distinct modes of operation, has been published (e.g., Usoskin et al., 2014, 2016; Inceoglu et al., 2015; Vecchio et al., 2017), leading to the assumption that the occurrence of a Grand Minima mode with reduced solar activity is a result of the complex superposition of systematic long-term activity cycles, and cannot be explained by random fluctuations of the regular mode. The possible existence of a separate Grand Maximum mode, corresponding to an unusually active Sun is also proposed, with the Modern Maximum being "a rare

or even unique event, in both magnitude and duration, in the past three millennia" (Usoskin et al., 2014). According to Usoskin et al. (2016), Grand Minima and Maxima occurred intermittently over the past nine millennia, with clustering near lows and highs of the Hallstatt cycle, respectively. Vecchio et al. (2017) obtained slightly different results, attesting that the Gleissberg and Suess cycles are strongly involved in Grand Minima generation. Their findings suggest that while the Grand Minima time sequence is mostly defined by coupling between the Gleissberg and Suess/De Vries cycles, the latter represents the variability time-scale of the most intense and longest Spörer-like Minima. Excluding these extreme cases, SA is well confined within a relatively narrow range.

1.2.3. Solar–terrestrial climate interaction

The Sun, in conjunction with the Earth's motion along its orbit, rules changes in the solar–terrestrial environment (Tsuda et al., 2015). The solar energy continuously provided by the Sun can be mainly divided into (i) the solar (electromagnetic) radiation comprised of infrared (IR), visible (VIS), ultraviolet (UV), and X-rays (Figure 1.11, left), and (ii) the solar wind, which is a high-speed flow of plasma (low-energy charged) particles (Tsuda et al., 2016). The solar radiation maximizes at the equator (on the contrary of the solar wind's energy/particle inflow that converges into the polar regions), where atmospheric disturbances are actively produced in the troposphere, further exciting various types of atmospheric waves, which propagate upward in the middle atmosphere (stratosphere plus mesosphere) carrying energy and momentum up into the thermosphere (Tsuda et al., 2016; Figure 1.11). Solar radiation is dominated by the VIS/IR emissions from the Sun's surface (the photosphere), which are constrained, on decadal, centennial and millennial time-scales, to small changes in effective solar surface temperature and potential (Lockwood, 2012). Greater variations are seen in UV emissions (Lean et al., 1997), arising from the lower solar atmosphere (the chromosphere) and influencing the Earth's middle atmosphere (Figure 1.11). Even more variable are X-rays and extreme UV emissions originated in the upper solar atmosphere (the corona) and causing significant changes in the Earth's thermosphere, ionosphere and magnetosphere (Figure 1.11, right), especially during major solar flare events (e.g., Le et al., 2011).

The quasi-steady flow of the solar wind is also modified by CME, which accelerate energetic coronal and solar wind particles to very high energies in SEP events, and cause geomagnetic storms during subsequent impacts on Earth (Tsuda et al., 2015). Observations have suggested that SEP forcing may affect wave propagation, zonal mean temperatures, and zonal winds in the Northern Hemisphere winter stratosphere (Seppälä et al., 2013). The energy transferred by the solar wind to the terrestrial atmosphere is very much smaller than both the solar radiation energy and energies involved in the Earth's atmosphere; still, the near-Earth space ("geospace") environment (mesosphere, thermosphere, ionosphere and magnetosphere) responds in a non-linear way to the solar wind and may cause damage to a sophisticated ''high tech'' civilization (Singh et al., 2010).

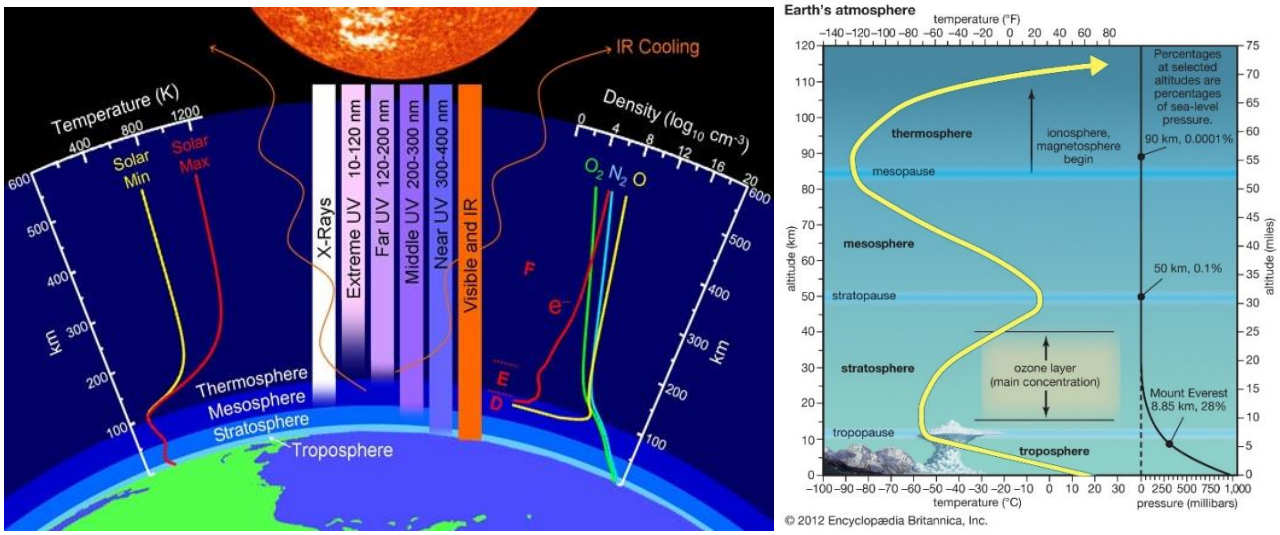

Figure 1.11. (Left) Layers of the Earth's atmosphere (troposphere, stratosphere, mesosphere and thermosphere), showing the temperature difference with increasing altitude from Earth for both solar minimum and solar maximum periods, the atmospheric penetration of the various spectral wavelengths, the density of some chemical species with increasing altitude from the Earth, and the approximate height within the D, E and F levels of the ionosphere (credit: John Emmert/NRL, NASA) https://science.nasa.gov/science-news/science-at-nasa/2010/15jul_thermosphere**. (Right)** Graphic showing also the ionosphere, overlapping the mesosphere and thermosphere; parts of the ionosphere overlap with magnetosphere, shaped by the solar wind's interaction with the Earth's magnetic field. The yellow line shows the response of air temperature to increasing height (credit: Encyclopædia Britannica, Inc.).

Furthermore, GCRs (even highly energetic particles than SEP, but mostly originated outside solar system and constantly impinging on planetary atmospheres) can also influence the ionization and, therefore, aspects as electrical conductivity, the global electric circuit (GEC; see Figure 1.17) or nucleation rates in cloud lightening discharges (Singh et al., 2010), affecting terrestrial climate (Singh et al., 2011). Moreover, wide agreement exists that ionization due to GCR and SEP, with the latter important only in the sub-polar and polar terrestrial atmosphere (Velinov et al., 2013), influences chemical processes leading to O_3 creation/depletion in the stratosphere (see Rozanov et al., 2012 for a review). Research on such relationships has leaded to the proposal of O_3 as a mediator of GCR influence on climate, with Kilifarska (2013) suggesting a new mechanism translating the stratospheric O_3 influence down to the surface.

As changes in the Earth's atmosphere occur, owing to variations in solar forcing (or in response to enhanced anthropogenic activity), the Earth's energy balance is altered and this affects its dynamics. Phenomena as solar flares, CME, geomagnetic storms and atmospheric waves represent solar short-term variability, with time-scales from minutes to weeks, while periodic variations such as semi-annual or quasi-biennial oscillations and the 11-year cycle occur at longer ones. Also, the Sun–Earth system is subjected to long-term alterations in solar irradiance (total and spectral irradiance – TSI/SSI), O_3 depletion, and in turn, climate change. Some of the new investigation on the Sun–Earth interaction has specially underlined on the short-term (weather) and long-term (climate) variability of SA and its effects/responses in geospace and Earth's environment,

aiming to improve the current knowledge of solar–terrestrial relationships impacting life and society (Tsuda et al., 2015).

1.2.4. Mechanisms of Sun–climate interaction

The major difficulty in the way of solar variability's recognition as a cause of climate change, has long been the absence of a generally suitable mechanism for the interaction. This field of research has a long history, starting with the investigation of the impacts of variation in the TSI to climate, which, as previously seen, occur over a broad span of time-scales, from which the most evident is its modulation in-phase with the 11-year cycle (Seppälä et al., 2014). The new TSI value for the contemporary solar cycle-average is 1361.0 Wm^{-2} (Kopp and Lean, 2011; Kopp, 2016), with the long-term stability of the space-based TSI measurement record high enough to trace changes of about 0.1% from the solar minimum to the maximum during recent decades (e.g., Fröhlich, 2006), thus having only a slight influence on the current changes that are being observed in the climate system (e.g., Lean and Rind, 2008).

Furthermore, the major topics of research have extended lately to studies of solar spectral irradiance (SSI) variations as well as of energetic particles (including solar protons, energetic electrons from the magnetosphere and GCR) and their impacts on the atmosphere and the potential links to regional climate effects. Specifically, the interest in SSI (which has not been continuously monitored until recently) was somewhat due to the SORCE mission's results (Ermolli et al., 2013). These showed that while the VIS and near IR bands' variability hardly surpasses 0.5% over a solar cycle, much larger relative variability of SSI occurs below 400 nm, in the UVs, where changes from ~7% to more than 100% over a solar cycle are observed (Figure 1.12), which can result in major changes in the middle and upper atmospheres, where these wavelengths are almost entirely absorbed, throughout radiative heating and stratospheric O_3 photochemistry (Ermolli et al., 2013). Therefore, although the UV radiation shortward of 400 nm represents less than 8% of the TSI (Krivova et al., 2006), its variability may have a substantial impact on climate, although via indirect mechanisms as explained below. Contrasting, the VIS and IR bands, having (i) the largest contribution to the TSI, (ii) minor variations over the solar cycle, and (iii) no absorption in the atmosphere, but in some well-defined IR bands, directly heat the Earth's surface and the lower atmosphere. The large amount of solar flux at the VIS and IR bands implies that small flux changes can prompt important terrestrial consequences. The impact of the variability of these bands on climate is expected to be small, though it may involve amplification mechanisms (Ermolli et al., 2013). Finally, cosmic rays (CR), including SEP events and GCR, or associated global atmospheric electric circuit (GEC) variations, can influence the formation of clouds and therefore control the total energy transferred from the Sun to the Earth's atmosphere (Dorman, 2012).

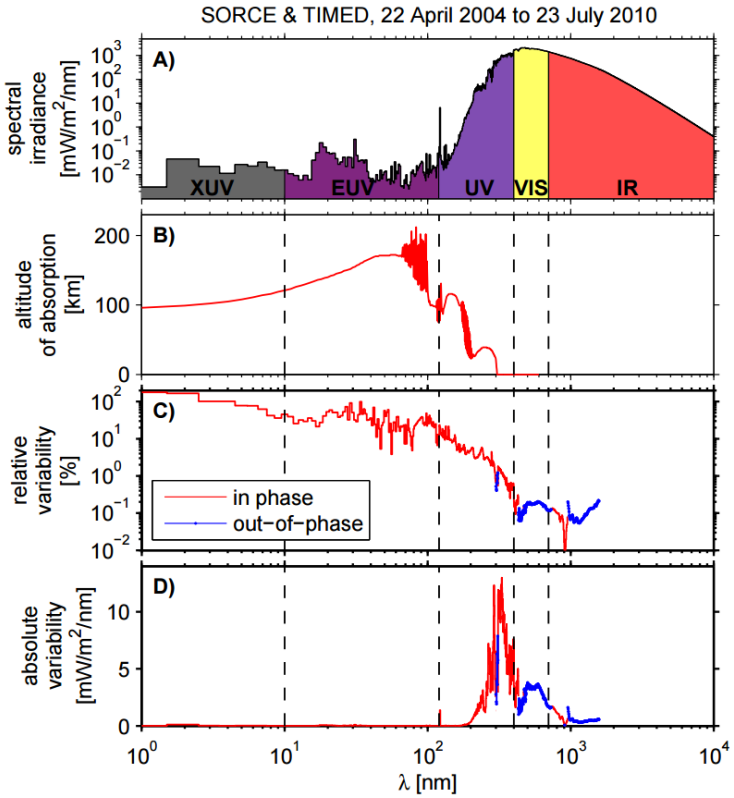

Figure 1.12. SSI as inferred from the SORCE and TIMED satellite observations between April 22, 2004 and July 23, 2010. **A –** Average SSI for that period; **B –** Typical altitude of absorption in the Earth's atmosphere for each wavelength; **C –** Relative variability (peak-to-peak/average) for solar cycle variations, inferred from measurements obtained between April 22, 2004 and July 23, 2010. Spectral regions where the variability is in phase with the solar cycle (denoted, for instance, by the sunspot number or the TSI) are marked in red, while blue represents ranges where the variability measured by SORCE is out of phase with the solar cycle; **D –** SSI absolute variability, which peaks strongly in the near UV (after Ermolli et al., 2013).

In view of the previous, the question of whether the influence of solar variability in the troposphere is "bottom-up", i.e., forced by solar heating of the surface, or "top-down", i.e., primarily driven from the stratosphere, has been formulated (Roy, 2013). Accordingly, the mechanisms suggested to explain the projection of solar irradiance variability onto regional climate fall roughly into (i) variations in the TSI leading to changes in heat input to the lower atmosphere, (ii) variations in the SSI, namely in the UV, coupled to changes in $[O_3]$, that affect the heat budget of the stratosphere, and (iii) variations in the solar wind and the flux of energetic particles, as illustrated in Figure 1.13. The main problems arise, in many instances, in establishing the physical link between the small magnitude of the forcing and the alleged response (Rind, 2002). The works of Gray et al. (2010) and Lockwood et al. (2012) offer a comprehensive view on possible links between SA and terrestrial climate.

(i) The "bottom-up" mechanism – TSI effect

TSI (VIS/IR) is the best known source of solar forcing into the Earth's atmosphere and despite the small initial perturbation (1.3 Wm^{-2} over a solar cycle; Kopp and Lean, 2011) it provides the

energy needed for the climate system, though encompassing amplifying dynamical and thermodynamical mechanisms, as the so-called “bottom-up”, mainly comprising the uptake of solar heat by the oceans (Figure 1.13).

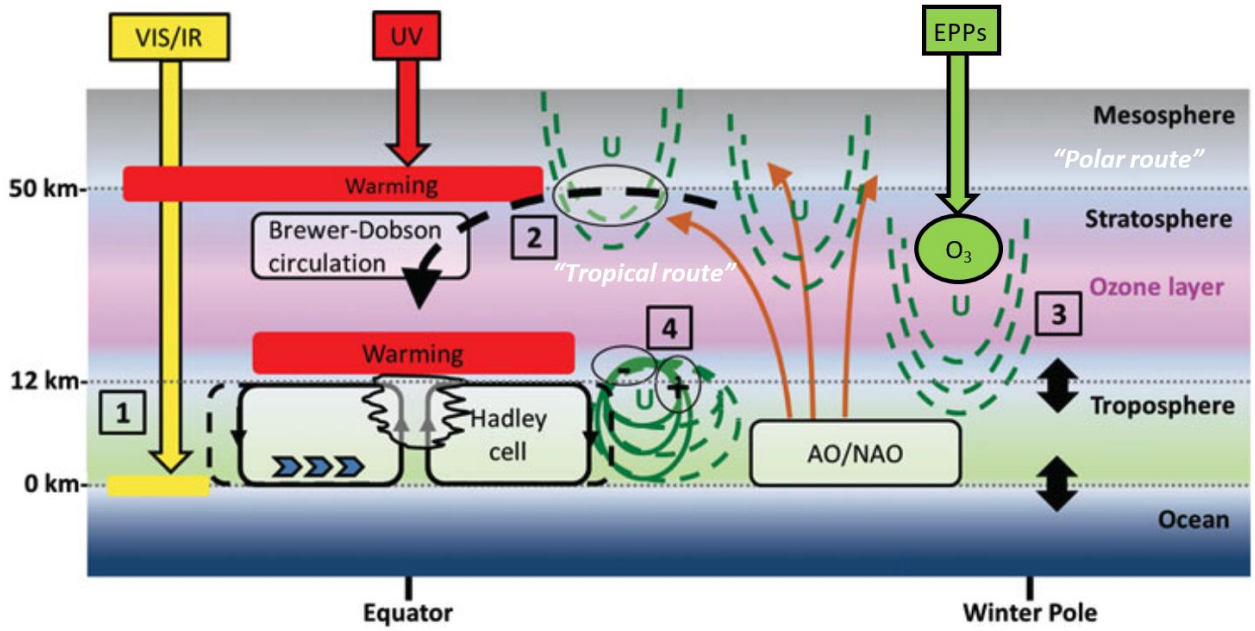

Figure 1.13. Schematic of the “bottom-up” mechanism (1), arising from the absorption at the surface of VIS/IR energy variations (yellow arrow) and of the “top-down” mechanism (2–4), arising from the absorption of UV energy variations in the stratosphere (red arrow). The charged particles contribution, including electrons as well as ions of all species and covering particles of both solar/heliospheric and galactic origin (EPPs), is also represented (after Thiéblemont and Matthes, 2015).

The “bottom-up” mechanism involves atmosphere–ocean coupling and interaction with incoming solar radiation at the surface in the relatively cloud-free areas of the subtropics. Peaks in solar forcing (solar maxima) produce greater energy input to the ocean surface in these areas, releasing more water vapour into the atmosphere, which converges in the precipitation zones (Intertropical Convergence Zone, ITCZ; blue arrows in Figure 1.13). Water vapour carries latent heat that is released upon condensation, typically in deep convective clouds in the tropics. This release of energy fuels the tropical zonal (Walker) and meridional (Hadley) overturning tropical circulations (Figure 1.14). The latter is characterized by an ascending branch near the equator and subsidence in the subtropics (black filled stream contours in Figure 1.13). A strengthening of the Hadley-type circulation, and associated colder sea-surface temperatures (SST), for solar maximum has thus been suggested (van Loon et al., 2007). A strengthened atmospheric circulation increases subtropical subsidence, which induces even fewer clouds in subtropical regions and more incoming solar radiation, providing this way a positive feedback and an amplification of the initial circulation perturbation (Gleisner and Thejll, 2003; Meehl et al., 2009). The clear solar signals attribution and details of the “bottom-up” mechanism are still under discussion (Thiéblemont and Matthes, 2015).

The TSI (and solar cycle variation in TSI) is the main solar influence so far considered in the Assessment Reports (AR) of the Intergovernmental Panel on Climate Change (IPCC) and included in climate models (Seppälä et al., 2014). The latest AR (AR5; IPCC, 2013) included some climate model simulations applying the novel (lower) TSI value from Kopp and Lean (2011), which means the estimate for the global radiative forcing from TSI has been decreasing since previous IPCC reports. Therefore, solar forcing cannot account for the overall warming trend in global mean air surface temperatures in the past 25 years and contributed only about 10% in the past 100 years (Lean and Rind, 2008). This small solar forcing contribution to recent climate change is supported by statistical evidence that human-induced effects on global mean air surface temperatures prevail over natural (solar and volcanic) forcings (Imbers et al., 2013).

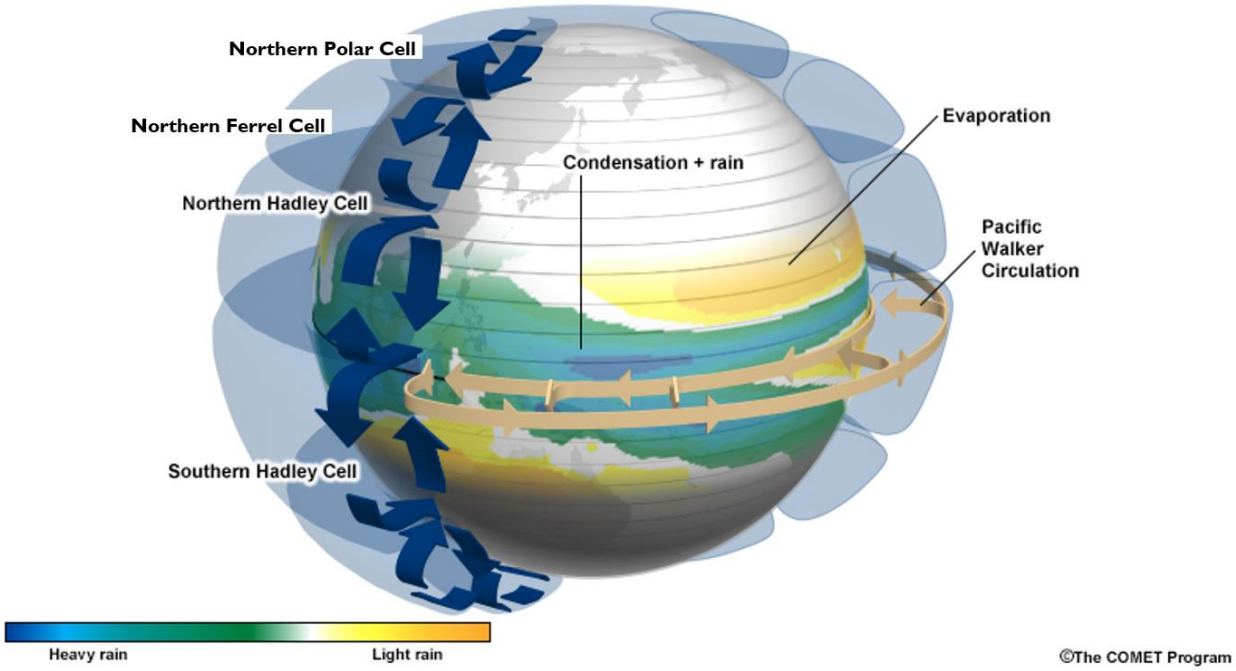

Figure 1.14. Scheme of the Hadley and Walker circulation, both related to the trade wind system. The positions of the rising and sinking air are given by the dark blue arrows. Rising air is related to cloud formation and precipitation, thus these areas are often wet; sinking air results in drier conditions at the surface. Light brown represent the Walker circulation that owes its origin to the gradient of sea surface temperatures along the equator in the Pacific Ocean. The colours on the globe correspond to mean precipitation from the Global Precipitation Climatology Project for 1979–2008. The blues and greens show regions of heavier rains (available at https://www.meted.ucar.edu/).

Succeeding the relatively high SA over the past decades (Modern Grand Maximum, which occurred during solar cycles 19–23, i.e., 1950-2009; Usoskin et al., 2014) and the low 2008–2009 solar minimum (already mentioned), a new interest arose on the potential climate impacts of TSI changes from future Grand Minima, with some works suggesting minor impacts of future solar extreme episodes on the global warming trend (e.g., Anet et al., 2013; Meehl et al., 2013). However, others propose that abrupt changes in atmospheric dynamics have occurred as a response to solar minimum events in the past, linked not to the TSI, but to the SSI (e.g., Martin-Puertas et al., 2012), as argued in the next item.

(ii) "Top-down" mechanism – UV effect

The SSI forcing in the Earth's atmosphere – by fluctuation of UV radiation – is the main driver in the indirect "top-down" mechanisms by affecting the chemical–dynamical coupling of the stratosphere to the underlying tropospheric climate (Figure 1.13) via interactions with O_3 (Tsuda et al., 2015). Such kind of pathways are needed to explain the transfer of the solar signal from the stratosphere to the surface, since UV radiation, as previously shown (Figure 1.11), is absorbed in the middle and upper atmospheres and thus no direct outcome is predictable on regional climate (Thiéblemont and Matthes, 2015).

Considering the "top-down" mechanisms, under solar maximum phases (red band in Figure 1.13) direct variations in SSI and indirect variations in O_3 in response to solar UV variability (increased ozone absorption and more ozone production through oxygen photolysis), modify the vertical and horizontal temperature structure, causing dynamical responses in the stratosphere and troposphere (e.g., Haigh, 1994, 1996). Such modifications on thermal gradients and hence in the wind systems (dashed green contours), lead to changes in the vertical propagation of the planetary waves that drive the global circulation (brown filled arrows) and their interaction with the mean flow (transparent ellipse) so that the stratospheric overturning circulation slows down (black dashed arrow, 2), and the initial westerly wind anomalies amplify and propagate poleward and downward through the winter season (evolution of green contours). The latter strengthens the stratospheric circumpolar cyclonic vortex (3), which ultimately impacts the regional climate at mid- and high-latitudes through stratosphere–troposphere coupling processes (e.g., Gerber et al., 2012). This version of the "top-down" mechanism is also known as the "polar route" (Kodera and Kuroda, 2002). A different one has also been suggested by Haigh et al. (2005), i.e., the "tropical route" prompted by the secondary warming maximum signal observed in the lower tropical stratosphere (red band), and resultant from adiabatic warming combined with increased O_3 heating due to the deceleration of stratospheric overturning circulation. Modeling studies have revealed that this temperature anomaly in the lower tropical stratosphere can cause a weakening and a poleward shift of the upper troposphere/lower stratosphere subtropical jet (dashed green contours), as well as an expansion of the Hadley cell (Thiéblemont and Matthes, 2015).

Both approaches have been used to explain the observed surface climate response to solar variability at mid- and high-latitudes, particularly, as plausible drivers of the Artic Oscillation (AO) and/or North Atlantic Oscillation (NAO) (e.g., Huth et al., 2007; Figure 1.13). The NAO is a main source of variability for North Atlantic climate on annual to multidecadal time-scales (e.g., Hurrell, 1995, 1996), especially during the cold season months (November–April), which effect spreads from the tropics to the Arctic (e.g., Miettinen et al., 2011; Hurrell and Deser, 2009, 2015). For instance, the expression at the surface of a strengthened polar vortex during solar maxima is a positive phase of the NAO, which is associated to stronger-than-average surface westerlies, more northerly storm

tracks and milder winters in Europe and North America (Figure 1.15A). Conversely, at solar minima, a weaker polar vortex, with negative zonal wind anomalies extending to the surface, represents a negative phase of the NAO and therefore weaker westerlies and cold, snowy winters in Europe and North America (Lilensten et al., 2015; Figure 1.15B). Recently, a re-evaluation of the solar cycle–NAO link showed that this is characterized by a near 3-year lagged NAO response, superimposed on the inherent year-to-year NAO variability (Gray et al., 2013). Such finding suggests a further component to the solar influence on the NAO beyond direct atmospheric heating and its dynamical response, with atmosphere–ocean interactions over the North Atlantic Ocean as the most likely source for the NAO lag (e.g., Scaife et al., 2013; Andrews et al., 2015).

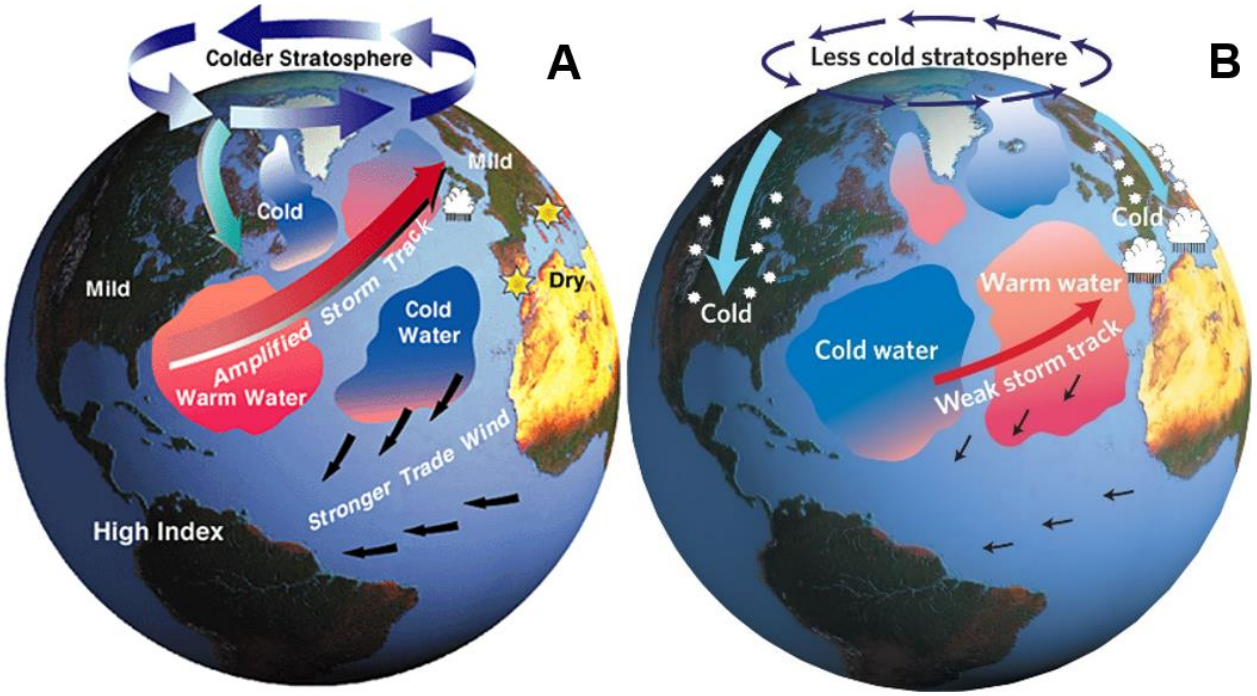

Figure 1.15. The positive (at left) and negative (at right) NAO phases and their connection to the stratospheric and oceanic circulations (http://www.whoi.edu/page.do?pid=8915&tid=3622&cid=24777).

The stratospheric response to the solar cycle is complex, involving dynamical processes and feedbacks which insight has however progressively evolved. Studies have suggested that the "top-down" and "bottom-up" mechanisms may in fact act in concert (Meehl et al., 2009), and that the combination of both ocean–atmosphere couplings and stratospheric processes is central to transfer solar irradiance variability into climate variability (Thiéblemont and Matthes, 2015).

(iii) CR modulation of clouds

The idea that cosmic ray changes could directly influence the weather and climate was firstly introduced by Ney (1959). Later on, Dickinson (1975), although with some scepticism, considered that modulation of GCR fluxes into the atmosphere by SA could affect cloudiness, thus providing a

viable driver for the terrestrial climate. In 1996, the discovery that the intensity of GCR correlates closely with variations of global cloud cover was announced, based on the available satellite data after 1983 (Svensmark and Friis-Christensen, 1997). This would be a very important effect because clouds modulate Earth's energy balance by altering the albedo and by increasing the IR greenhouse trapping effect. The balance between these two opposing effects is dependent on the cloud altitude: for low clouds the albedo effect controls (such that more cloud is a cooling effect), while for high-altitude clouds the greenhouse trapping effect dominates (so that more cloud gives warming) (Lockwood, 2012). It was suggested that this connection could be responsible for the observed correlations between variations in SA and terrestrial climate, with several works arguing that low-altitude global cloud cover shows an 11-year cycle variation, consistent with GCR modulation of the growth of cloud condensation nuclei – CCN (Svensmark and Friis-Christensen, 1997; Marsh and Svensmark, 2000, 2003; Kirkby, 2007). This idea about such direct GCR–cloud link has been much controversially discussed in the literature, with the main arguments against been summarized by Lockwood (2006). Regrettably, many steps are involved from the charging of nuclei and droplets to cloud formation and little is known quantitatively about the physical mechanisms involved (Rzesanke et al., 2013). So the question is: what mechanism might be responsible for a cosmic ray–cloud correlation?

Cosmic rays, including both SEP and GCR, are the highest source of ionisation in the troposphere, peaking at about 15 km altitude (Figure 1.16, left). Various microphysical mechanisms, which depend on the electrical state of the atmosphere, have been proposed, with these being mostly classified into two groups: (i) the ones which depend on the direct interaction between CR and the aerosol and cloud system (referred in the previous paragraph), and (ii) the ones which invoke an indirect connection between the ionizing radiation and the cloud system (Rzesanke et al., 2013). In the former, the formation of large ions, aerosol particles, cloud droplets and ice crystals is regarded as a direct result of the effect of the ionizing radiation on the cloud system (e.g., Marsh and Svensmark, 2000). Among the latter, a potential comprehensive mechanism has been proposed, suggesting that vertical electric currents in the atmosphere can modify cloud microphysics and thereby alter the properties of the cloud system (Tinsley, 2000; Tinsley and Yu, 2004). Some of the main aspects of this model are shown in Figure 1.16 (right). The flux of highly energetic particles of galactic origin (blue arrows) is modulated by the variations in the solar magnetic field, which in turn affects the ion pairs' concentration in the upper atmosphere. These are separated in the Earth's fair (no thunderstorm) weather electric field, which is created and upheld largely by the electrical activity of large storms within the ITCZ (Rzesanke et al., 2013).

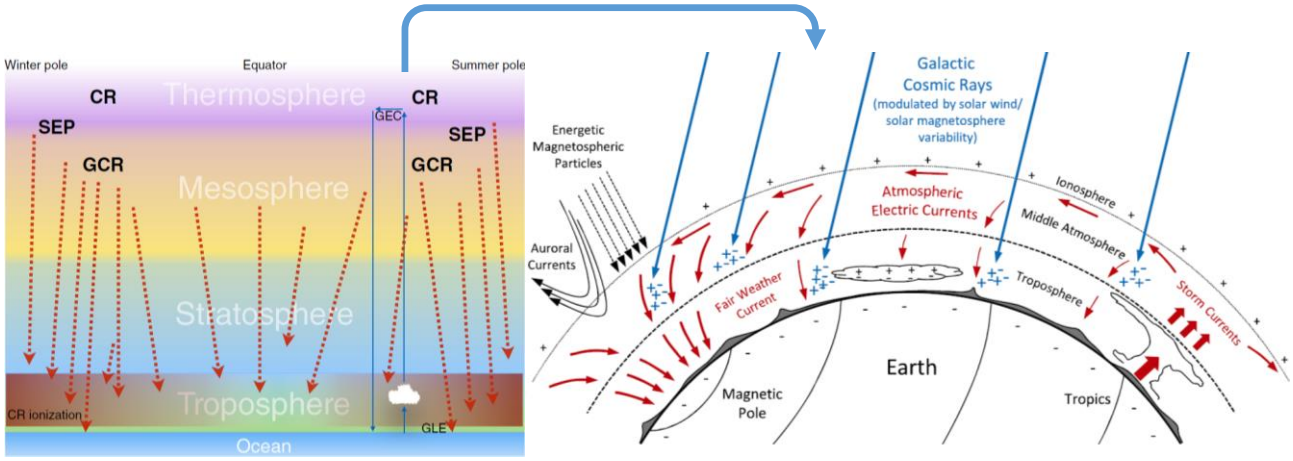

Figure 1.16. (Left) Main CR (including SEP and GCR) impacts on the Earth's atmosphere. CR are the main source of ionisation in the lower atmosphere. The GEC is distributed over the whole Earth. GLE – Ground Level Enhancement events (a special class of SEP events, characterized by higher energy of solar particles that can extend up to ~1–10 GeV, which are high enough to induce cascades of secondary particles in the atmosphere, just as GCR do. Thus, the ionizing atmospheric effect of GLE events is expected to be noticeable in the lower atmosphere (Usoskin et al., 2011) (after Seppälä et al. (2014). **(Right)** Schematic representation of the global electric circuit (GEC) and its interaction with energetic cosmic particles and the tropospheric cloud system. When GCR (*blue arrows*) and other highly energetic particles of solar and cosmic origin (*black arrows*) penetrate the terrestrial atmosphere, they create ion pairs and by that change the ionospheric electrical potential and the atmospheric vertical column resistance. The electrical charges transported by the vertical currents (indicated by *red arrows*) accumulate on airborne aerosols as well as on droplets and ice crystals at cloud tops and bottoms and potentially change the cloud physical properties. Variations in the solar wind, and in the solar magnetosphere's extend, modulate the atmospheric flux of energetic cosmic particles, being able of exerting this way an indirect influence on the Earth's cloud system and climate (after Rzesanke et al., 2013).

While the analysis of solar influence on terrestrial climate via changes in solar irradiance (TSI/SSI) is rather well-developed, the CR–cloud mechanisms have only beginning to take the first steps to be calculated, requiring more evidence before any can be considered both operational and effective. For the pathway via ion-induced CCN, it is needed to determine to what extent this might have a substantial effect in the context of other droplet growth mechanisms. For the mechanisms involving the GEC, more observational data on cloud edge properties are required, mostly on charge and droplet sizes (near the edges of clouds charge can accumulate and this can influence both evaporation of cloud droplets and interactions between them). All the cloud scenarios need to be evaluated within models of cloud microphysics incorporating the various complex interactions involved (Haigh, 2011).

1.2.5. Solar signals in climate and geological records

Assessment of climate variability and change depends significantly on the existence and accuracy of records of meteorological parameters, ideally consisting of long-time series of measurements made by a worldwide high-density network of well-calibrated instruments. In reality, the measurements with global coverage have only been made since the start of the satellite era, while reliable instrumental records just cover the past few centuries and are only available from a few locations, mostly in Europe (Haigh, 2007). In fact, on a local or regional scale, many instrumental series from individual stations exist, some of them reaching back the 17th century, as, for instance,

the temperature series of Central England (since 1659) or the precipitation series for Paris, France (since 1680), both referred by Brázdil et al. (2005). In the current dissertation, temperature–precipitation series of variable length have been used, for instance, a temperature series from the Braga (NW Portugal) weather station (**Chapter 4**). For longer periods, and in remote regions, records have to be reconstructed from natural archives (proxies), such as ice cores, sediments, tree rings, corals, pollens and speleothems – an example of the latter is the regional temperature reconstruction of Martín-Chivelet et al. (2011) used in **Chapters 7–8**, as well as from historical documentary sources (see section 1.3.3), complementing and generally providing support for evidence available from natural archives (Jones, 2008). Together, they allow us to reconstruct a multi-proxy history of climate conditions.

As previously mentioned, the Sun–terrestrial climate link has been hard to prove, as any working hypothesis must be supported by empirical evidence. Today, the variability on 11-year time-scales is well-established by the TSI measurement record and has been linked to similarly well-established Earth climate records – global and regional temperatures, sea-surface levels, O_3, ice, tree rings, and precipitation amounts (e.g., Lean and Rind, 2008; Gray et al., 2010) as well as historical records (e.g., Engels and van Geel, 2012) – indicating an influential Sun–climate connection (Kopp, 2016). Whether the long-term variations in the Earth's climate are related to changes in SA is much more uncertain, although those changes can be even more significant, as they might impacted more directly the Earth's climate in pre-industrial times, when natural influences dominated climate forcing (Kopp, 2016).

The last 2000 years correspond to a period of most accurate annually resolved dating, being characterized by boundary conditions (e.g., ice, ocean, and atmosphere) most alike to those of today (Mayewski and Maasch, 2006). Over this period, established, well-dated, proxy records of change in temperature (e.g., Mann and Jones, 2003) and precipitation (e.g., Yan et al., 2011) or both (e.g., Sánchez-López et al., 2016) are available. Two of the most relevant climatic events, the Medieval Climate Anomaly (MCA; *ca.* AD 900–1300) and the Little Ice Age (LIA; *ca.* AD 1350–1900), that have impacted the middle to high-latitudes during this time span (e.g., Grove, 1988) are quite evident in the temperature reconstructions gathered by Xing et al. (2016) for the Northern Hemisphere and presented in Figure 1.17. These were also the first to been linked to SA, namely to the Medieval Solar Maximum (AD 1100–1250; Jirikowic and Damon, 1994; Figure 1.18, left) and to the Maunder Minimum (MM, AD 1645–1715; Eddy, 1976; Figure 1.18, right). The MM is the only Grand Minimum covered by direct solar (and some relevant terrestrial) observations, forming a benchmark for other (Usoskin et al., 2015), and whose effects on climate have been documented in historical sources (Soon and Yaskell, 2003).

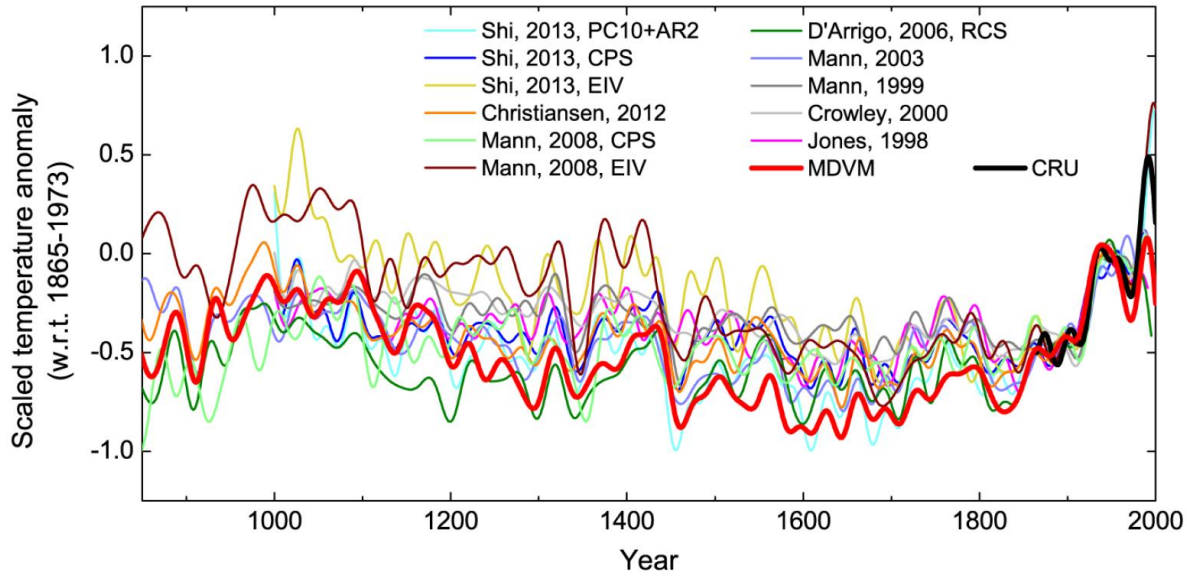

Figure 1.17. Several reconstructions for the mean temperature of the Northern Hemisphere. All reconstructions were 30-year low-pass filtered, and scaled to the smoothed instrumental series by the variance and mean over the common period AD 1865–1973 (more details in Xing et al., 2016, from which this Figure was reproduced).

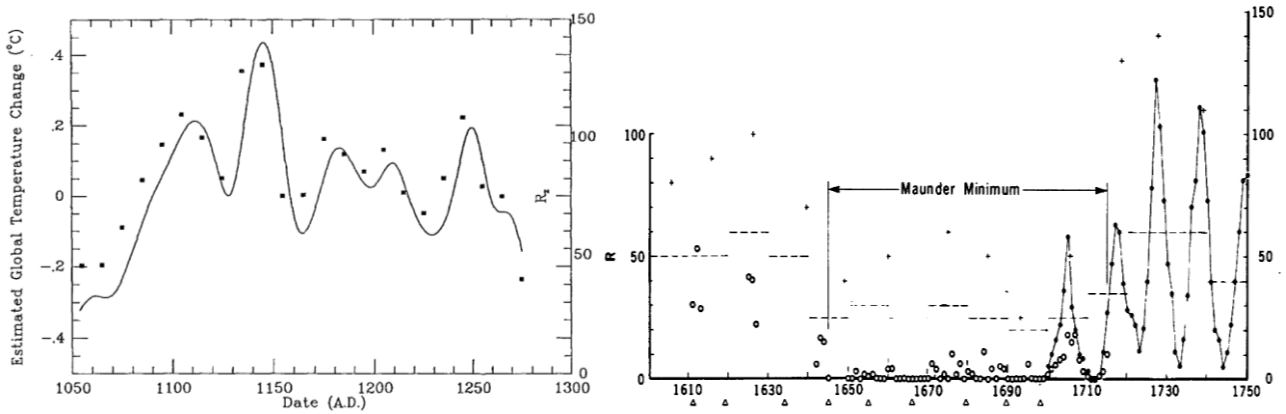

Figure 1.18. (Left) Δ ^{14}C–derived R_z (Wolf sunspot indices) estimate (solid squares) and global temperature model predictions (curve) (after Jirikowic and Damon, 1994). **(Right)** Estimated annual mean sunspot numbers from 1610 to 1750; dashed lines are decade's estimates, crosses are peak estimates and triangles are Wolf's estimated dates of maxima for an assumed 11.1-year solar cycle (after Eddy, 1976).

Since the first studies, much investigation from a range of natural archives has scrutinized solar-forced climate changes further back in the Holocene and beyond through comparisons of proxy climate data (including geochemical and biological records) with reconstructions of SA (e.g., Bond et al., 1997, 2001; Haltia-Hovi et al., 2007; Steinhilber et al., 2012; Galloway et al., 2013; Duan et al., 2014; Auer et al., 2015 and references therein). This has detected past changes in the Earth's climate system occurring simultaneously with changes in SA, mostly by using spectral and cross wavelet analytical techniques (as in the current research; **Chapters 6** and **10**). Thus, those results seem to support that the potential impact of solar variability on terrestrial climate also arises on multi-decadal to-secular and even longer time-scales, likely affecting, for instance, prehistoric human settlements (e.g., Magny, 2004). According to Engels and van Geel (2012), it is theoretically unlikely

that millennial-scale climate fluctuations are directly forced by TSI changes, the variability of which acts on a decadal to secular time-scale. But they also refer that “even weak forcing such as TSI might trigger long-term changes in the climate system when (a) present over a long time, (b) non-linear feedback mechanisms amplify the original forcing or (c) when certain thresholds are crossed”. Most of all, independent proxies’ studies have pointed towards a regional climate system that is sensitive to relatively small changes in SA.

Regrettably, two major drawbacks ascribed to the previous analysis are the following: by one side paleoclimate proxies may have chronological errors often leading to considerable temporal uncertainties in reconstructions and by the other, they are “noisy” (e.g., Turner et al., 2016). The latter means that they may also respond to other non-climatic factors (e.g., pests/diseases, availability of nutrients, competition, etc.), “contaminating” with irrelevant information the analysis. A standard procedure of assuming statistical relationships implicates the computation of a descriptive statistic (as the correlation coefficient; see **Chapter 4**), where a null hypothesis is tested and confidence levels are attributed to that statistic, or re-sampling techniques (as cross-validation; see **Chapters 4** and **6**, and Monte Carlo simulations; see **Chapters 6** and **10**). In Monte Carlo simulations a large number (10,000 or more) of artificial data are generated with properties similar to the original (real) data, by re-sampling these in a manner consistent with the null hypothesis: “The two quantities are not related”; the “new” surrogate data are, however, randomly arranged and by definition unrelated (Wilks, 2011). It is not possible to prove that the null hypothesis is wrong, but it is feasible to show that it is unlikely that it is true (Benestad, 2006).

However, the statistical analysis *per se* is unable to prove the existence of a physical link between two entities; so as to make robust assertions about relationships or certain behaviour it is required to formulate a hypothesis based on a physical explanation, and then apply the statistical analysis to test it (Benestad, 2006). The advances in solar–terrestrial physics research, summarized earlier in this chapter, have progressively (and will continue to) provide such a background information.

1.3. Research material

1.3.1. Tidal marsh settings and sediments

The strict definition of *salt marsh* is an intertidal area that is influenced largely by marine tidal cycles (Scott et al., 2014). Salt marshes’ vertical range is ruled by the tides, which outline the inundation time within different elevation ranges between mean sea-level (MSL) and the highest tides. Thus, the marsh environment is typically divided in low marsh (between highest low water – HLW | lowest high water LHW – and mean high water – MHW –, and high marsh (between MHW

and the highest high water – HHW), and lies at the ecotone between terrestrial, freshwater, and marine systems, as can be seen in Figure 1.19.

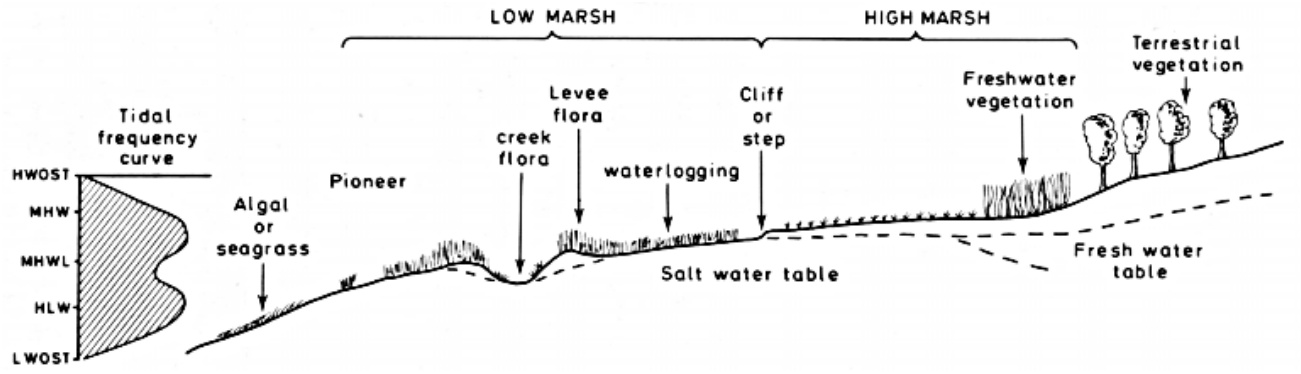

Figure 1.19. Typical cross-marsh zonation, displaying the physical factors influencing vegetation (after Carter, 1988). HLW – Highest low water; MHWN – Mean high water neap; MHW – Mean high water.

Globally, tidal (salt, brackish and freshwater) marshes are found in "small pockets or narrow bands" totalling today *ca*. 45,000 km^2, along the coastlines and estuaries of middle to high latitude regions, wherever wave energy is low and there is a surplus of fine sediment (Carter, 1988; Greenberg et al., 2006). The most widespread tidal marsh types are the temperate salt marshes, dominated by tall, salt-tolerant grasses and herbs with succulent (but also non-succulent; **Chapters 8** and **9**) stems or leaves, that predominantly occupy the mid-latitudes in both hemispheres (Scott et al., 2014; Figure 1.20).

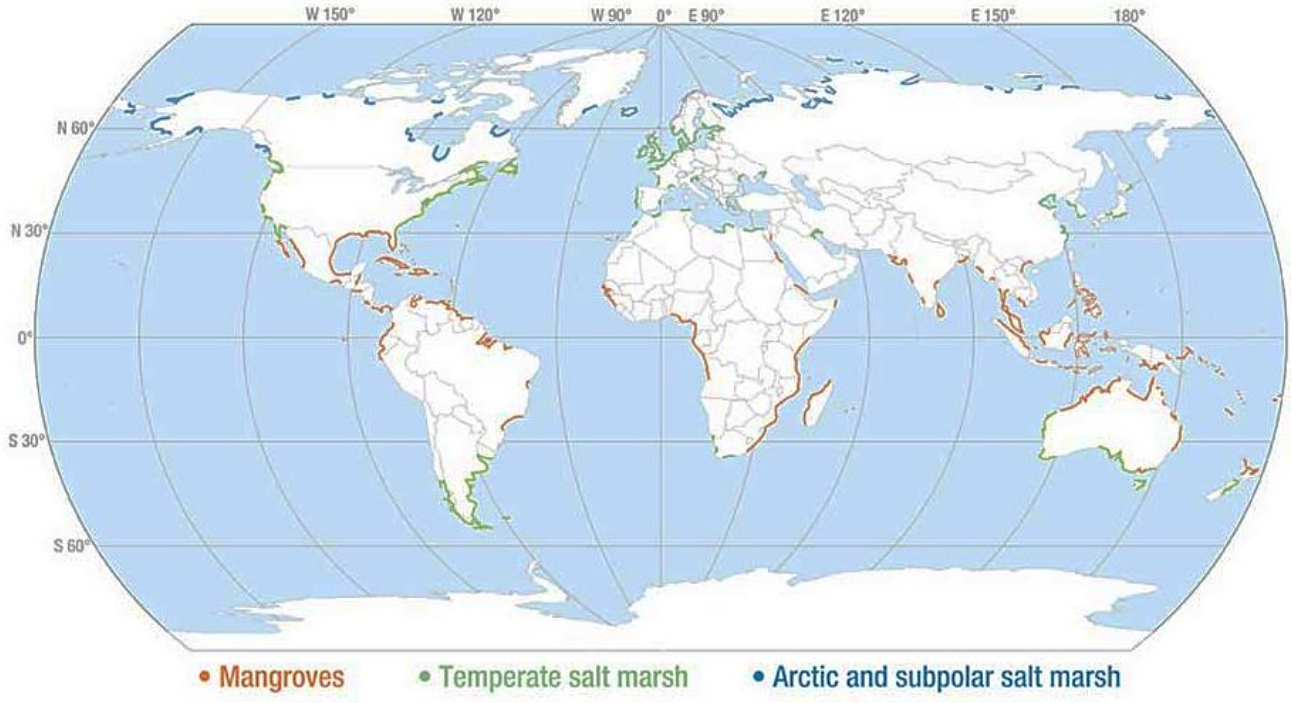

Figure 1.20. World map of coastal wetlands (after Scott et al., 2014).

Marshes of all types are among the most important and most biologically productive of all modern environments, providing a set of climate-regulating ecosystem services and a host of natural and provisioning services (Moffett et al., 2015; Figure 1.21). They also represent the most remarkable example of a system whose response to climate change may be controlled by biophysical feedback processes (also known as ecogeomorphic feedbacks; Fagherazzi et al., 2012), enhancing their resilience (e.g., surviving to MSL rise) in a very dynamic coastal environment (Kirwan et al., 2016). But, at the geological time scale, the life cycle of a salt marsh, i.e., the ratio between marsh extension and the rate at which the marsh is destroyed or built, is very ephemeral, with these landforms continually reworked by coastal processes within a few thousand years, in a rejuvenation process (Fagherazzi, 2013). Fagherazzi wrote: “Compared to the history of Earth, a salt marsh resembles a gorgeous butterfly. After emerging from the cocoon, it extends its wings under the morning sun, rises in the sky during the day, and when the night falls, it folds its wings and dies”. According to him, only very few locations have enough marsh area to survive common horizontal erosion rates of the order of 1 m/yr for more than 5000 years.

Figure 1.21. (Left) Caminha salt marsh in the Minho lower estuary (NW coast); **(Right)** Ponte de Vila Nova de Milfontes salt marsh in the Mira lower estuary (SW coast).

In fact, it has been detected that the intertidal system evolves quite rapidly from a low elevation, bare tidal flat (mud- or sand-) state to a high elevation, vegetated marsh state once a threshold elevation is surpassed; vegetation establishes and the sediment accumulation rate increases in a positive feedback (Wang and Temmerman, 2013). The marsh accretion may occur through the settling of particles delivered to the marsh during tidally induced floods, the direct capture of these particles by vegetation and the direct deposition of organic matter (OM) due to root growth and litter deposition (Mudd et al., 2010 and references therein).

Storms also play a key role in the sediment influx into the marsh environment (Davis, Jr. and FitzGerald, 2004), although they can be as well responsible for salt marsh loss (Tonelli et al. 2010). As a result of those various ways of sedimentation, tidal marsh sediments are characteristically

formed by a sub-equal combination of mud and plant debris, with small amounts of shell material, sand-size terrigenous particles and large plant fragments (Davis, Jr. and FitzGerald, 2004; Figure 1.22).

Figure 1.22. Fine-grained, organic-rich sediments from the Caminha tidal marsh.

Tidal marshes' biota (foraminifera included) are adapted to tolerate specific salinity levels and inundation times. Since tidal flooding frequency and average inundation times decrease with increased elevation, there is also often a change in plant and faunal communities, reflecting such gradients. To deal with this stressful setting, some interesting strategies have evolved, including, for instance, an alternative type (C_4) of photosynthetic mechanism, a well-developed rhizome and rooting system (to resist tidal action and bind the mud substrate) or succulence in plants (Carter, 1988). The latter is an important adaptation that contributes to the regulation of internal ion concentrations in many halophyte species, with these ones having enlarged water-filled cells in their tissues, which makes leaves or stems appear thicker than those of non-succulent plants (Karleskint, Jr. and al., 2010; Figure 1.23).

Figure 1.23. *Sarcocornia* sp. (with water-retaining, succulent parts) from the Mira lower estuary (SW coast) by opposition to *Juncus maritimus* (non-succulent) from the Minho estuary (NW coast).

Some studies have reported an increase in succulence with an increase in salinity, with some relationship found between succulence and optimal growth (e.g., Khan et al., 2005 and references

therein). Salinity is moreover important for the organic carbon (C_{org}) sequestration function of tidal marsh sediments, with implications for climate regulation (as its offers a potential to mitigate the atmospheric CO_2 increase related to global warming) and marsh accretion. Van de Broek (2016) reported largest total stocks in a freshwater and brackish tidal marsh and significantly lower in a saltwater marsh from the Scheldt estuary (Belgium–The Netherlands border), referring also that gradients in C_{org} concentrations with depth strongly vary between marsh types. This is the reason why these authors consider that a full record requires that sampling is carried out over the entire depth of the marsh sediments, as it has been done with OM in the present research (**Chapters 8** and **9**). Such assessments are important as, in tidal marshes, soil/sediment OM accumulation is a prime mechanism regulating marsh elevation, chiefly in the sediment deficient estuaries, thus contributing to these ecosystems' persistence over the rising sea-level (Langley et al., 2009; Kirwan et al., 2014). The threat for salt marshes with MSL rise can be further impacted by increased storm frequency and elevated CO_2 and warmer temperatures, all likely weakening the potential for persistence of tidal marshes. Though, a recent study (Kirwan et al., 2016) suggests an overestimation of marsh vulnerability to MSL rise due to a common underestimation of marshes' resilience by not entirely accounting for biophysical feedbacks known to accelerate accretion rates with MSL rise and the potential for marshes to transgress inland without finding natural or artificial obstacles. They thus concluded that the direct impact of MSL rise may not be a critical threat to many marshes over the next several decades.

1.3.2. Marsh foraminifera

Throughout the life cycle of a given marsh, the distribution of benthic foraminifera is constrained by their ecological tolerances and preferences. Many foraminiferal species are known for having narrowly defined niches (Murray, 1991, 2000), responding rapidly to changing environmental and climatic conditions. The marsh species, especially those colonizing high marshes are dependent on a myriad of natural stressors (e.g., flooding frequency and submersion time, salinity, pH, temperature, precipitation, solar irradiance, substrate and vegetation), all influencing the final assemblages' composition, although potential post-depositional modifications need to be considered.

Marsh foraminifera (Appendix A1) – the most characteristic are agglutinated, constructing tests from mineral and/or biogenic grains (e.g., quartz, mica, diatom frustules; Bradshaw, 1968; Scott et al., 2001; De Rijk, 1995) – provide an accurate zonation related to MSL (Scott and Medioli, 1978, 1980; Gehrels, 1994; Haslett et al., 1998; Hayward et al., 1999; Horton et al., 1999), and are normally well-preserved and easy to identify in buried and fossil marsh deposits (Scott and Medioli, 1980, 1986). Besides elevation, it was found that the next most significant factor controlling their distribution is salinity (Horton and Edwards, 2003; Hayward et al., 2004; Debenay et al., 2006; Horton and

Culver, 2008). This is ultimately dictated by the water steady balance on a tidal marsh, which equates total inflows (precipitation (P) + runoff + groundwater discharge + tides) with total outflows (evapotranspiration (ET) + drainage + groundwater recharge), plus or minus the change in storage (ground and surface water) within the marsh (i.e., its moisture-holding capacity, determined by the structure and composition of the substrate). Typically, interstitial salinity is equal to or greater than the flood water's salinity, changing with elevation, time, and climate (Morris, 1995). Whereas at lowest elevations within the marsh (flooded on every high tide cycle), interstitial salinity is kept close to that of the adjacent water, in the high marsh, immersed infrequently (for short periods of time by only highest high tides – HHW), interstitial salinity depends on the balance between P and ET (P–ET), being less than or greater than flooding water's salinity (e.g., Morris, 1995; Rabenhorst and Needelman, 2016). In cool temperate regions, interstitial salinity may range from 0 to 20‰ (1‰ = 1 psu – practical salinity unit) over one tidal cycle. In contrast, in hot (or cold) arid regions and warm climates (high atmospheric temperatures), interstitial salinity at higher elevations can increase far above that of tidal water due to evaporative water losses, leading to hypersaline conditions (50–60‰) (e.g., Webb, 1983; Scott et al., 2014). This interstitial salinity of the high marsh can also fluctuate considerably with time, but less temporal (and spatial) variations are expected to occur in colder climates (lower ET), assuming constant flood salinity (Morris, 1995).

Therefore, under the broad latitudinal gradient constraining temperate salt marshes (Figure 1.20), also more regional differences in summer temperatures and annual precipitation can be expected to influence inter-marsh distributions of benthic foraminifera in temperate high marsh zones, which is explored in **Chapters 2** and **10**. This might occur apart from the steep gradients of multiple environmental and ecological factors that characterize tidal marshes in estuaries (Craft, 2007), particularly the decreasing longitudinal coast–upper estuary salinity gradient, with salt marshes in the most seaward part over brackish marshes to freshwater tidal marshes (Van de Broek et al., 2016), as can be seen in **Chapter 10**.

1.3.3. Grape harvest dates and wine production

Historical and recent viticulture has been used in the research field of historical climatology (Pfister et al., 2001) as a source of knowledge on past climates. The cultivation of the vine (*Vitis vinifera*) that yields grapes for wine manufacture is particularly sensitive to climate variations (e.g., Brázdil et al., 2008). Temperatures and precipitations during the growing season, solar radiation, wind directions and intensities, and other climate variables, all influence the timing of the key grapevine phenological growth stages. The exact onsets and durations of those growth stages in turn influence the yields, qualities and, ultimately, the prices (Chevet et al., 2010). Such a relationship enables the use of historical viticultural data (e.g., the start date of the grape harvest – GHD – or records from wine quantity and quality) for the reconstruction of temperatures, namely of the growing

season (GS), and weather extremes in past times (Brázdil et al., 2008). While the potential of GHD as paleoclimate indicators has been extensively investigated in many publications, only a few studies using grapevine yield or wine quality exist (e.g., Bock et al., 2013). One reason, as pointed out by Pfister (1992), is the difficulty in obtaining long-term datasets on wine production (WP) or yields of grapevines.

In the previous context, ecclesiastical viticulture records were kept more systematically and seem to have survived better than those of individual secular owners. The current research utilizes the Benedictine hand-written records from 17th, 18th and 19th centuries, as regards WP, compiled by three Portuguese historians, Aurélio de Oliveira, Célia Taborda da Silva and Gonçalo Maia Marques. Their effort in making comprehensible hundreds of hand-writing pages from monastic Benedictine documents, as well as in summarizing and classifying the information contained in them, enabled the joint application of these valuable agricultural data with other paleoclimate proxies (**Chapter 6**).

The Benedictine Rule prescribed an ascetic diet which included the consumption of wine as a daily requirement, the reason why the Benedictine monasteries were heavily engaged in the successful production of wine. While repositories of knowledge, monasteries also promoted wide and meticulous investigation in order to obtain the best wines, a task with a double dimension – religious and material – since it was seen as a way of honouring the glory of God as well of "satisfying earthly needs" (Dias, 2005; Millon, 2013). In this context, the network of Benedictine monasteries settled in the Entre-Douro-e-Minho (EDM) region (NW of Portugal) became the major promoter of an innovative viticulture, owning a strategic vision that included the selection policy of grape varieties – focused on regional varieties, well adapted to the edapho-climatic conditions – to improve the quality of the finished product, the reconversion of vineyards (specially between the years 1775–1780) to take better advantage of sunlight exposure and relative humidity (e.g., exploring the trellis design and construction as an alternative/counterpart to the ancestral tall-trained vines; Figure 1.24) the improvement of winegrowing techniques (e.g., propagation by layering, in the search of more profitability of the productive potential of vineyards) and soils selection (e.g., introducing land terracing system for new vineyard plantations) (Oliveira, 1979; Silva, 1993; Marques, 2011). These monasteries were moreover true winemaking laboratories. As an example, in 1782–1784, the S. Martinho de Tibães monastery (Figure 1.25), the head of the Benedictine Order in the Kingdom of Portugal since 1569, and located within the *terroir* of *Vinhos Verdes*, hosted a wide-range experiment design implanting Douro varieties in its properties, in order to achieve greater autonomy in mature wines (Marques, 2011).

Figure 1.24. Ancient tall-trained vine systems. **A –** "Ramada" or "latada" (http://arturpastor.tumblr.com/image/103491586558); **B** and **C –** "Arjões"; **D –** "Enforcado" or "uveiras" (http://arturpastor.tumblr.com/image/103481986553); **E** and **F –** Tall vineyard harvest (http://vryebeelde.blogspot.pt/2014_02_01_archive.html; http://4.bp.blogspot.com/).

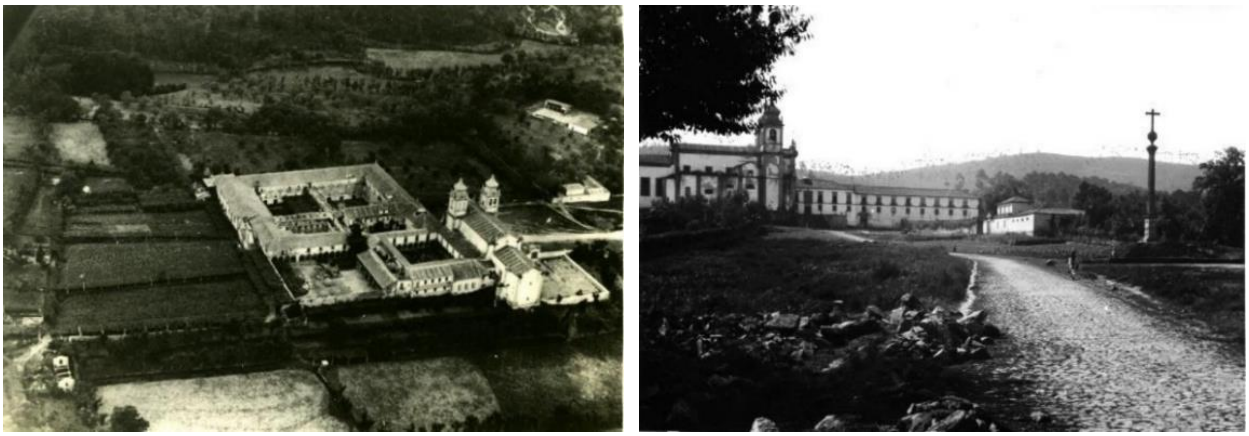

Figure 1.25. The S. Martinho de Tibães monastery (Tibães, Braga, NW of Portugal). **(Left)** Aerial view taken from south of the whole set. **(Right)** Northern general view of the Tibães monastery (Photos available at http://www.patrimoniocultural.gov.pt/pt/patrimonio/patrimonio-imovel/pesquisa-do-patrimonio/classificado-ou-em-vias-de-classificacao/geral/view/73612).

The wine records compiled by Oliveira (1979), Silva (1993) and Marques (2011) correspond to the data from the account reports (known as *Estados*) of six monasteries from the EDM region: Tibães, Rendufe, Santo Tirso, Pombeiro, Paço de Sousa and Palme covering the 1626–1820 period. The creation of those reports arose from a reorganization of the Order following a monastic-clerical crisis (the *Comendatários Crisis*), which started in 1566/67, aiming (among other things) more transparency in the financial matters (Dias, 1993, 2005). They were prepared by two monks elected by their peers and presented on a triennial basis in a meeting of the General Chapter of the Order, held at the S. Martinho de Tibães monastery (Figure 1.26; Marques, 2011).

Figure 1.26. (Left) Entrance to the Chapter's Room of the S. Martinho de Tibães monastery (Photo available at http://mosteirodetibaes.org/pagina,232,245.aspx). **(Right)** View of the Chapter's Room where the Congregation of St. Benedict of Portugal and the Province of Brazil met every three years on the third day of May (the feast day of the Holy Cross) to elect the General, the Abbots and all prelatures of each monastery. It is also in this occasion that the account reports (*Estados*) of the three preceding years were presented to the Congregation (Photo available at http://www.vortexmag.net/portugal-37-monumentos-que-deve-visitar-pelo-menos-1-vez-na-vida/5/).

According to Brázdil et al. (2005), a historical source on climate is "a document, i.e., a unit of information such as a manuscript, a piece of printed matter (book, newspaper, etc.), a picture or an artefact (e.g., a flood mark or an inscription on a house), which refers to weather patterns or impacts of climate". In this context, the climatological potential of local and regional newspapers, usually with a less than a weekly resolution, is enormous. They can offer rich narratives on climate-related phenomena (e.g., droughts, floods, storms, snowfalls, stages of vegetation), also including the organization of public prayers, i.e., rogation ceremonies (*rogativas*, e.g., Barriendos, 2005; or *rogos*, e.g., Alcoforado, 1999) directed to end stress-situations linked to long dry (*pro-pluvia* rogations) or wet spells (*pro-serenitate* rogations) threatening crops (Figure 1.27).

Figure 1.27. (Left) Some of the local papers systematically scrutinized in this research. **(Right)** Several newspaper articles reporting extreme weather and climatic events, rogation ceremonies and information on grape harvesting.

Descriptive documentary evidence is the basis for much of the research published on historical climatology, with these works producing high-resolution climate reconstructions containing time series of temperature-precipitation anomalies and natural disasters (Brázdil et al., 2005). Such an analysis usually comprises the steps represented in Figure 1.28.

It begins, in general, with the search and compilation of suitable documentary data or natural proxies capable of defining a high amount of climate variability such as temperature, precipitation,

etc., with all proxies then transformed into a time series considered with respect to a given reference period (Brázdil, 2002; Brázdil et al., 2005). A similar methodological approach has been used herein concerning the systematic scrutiny of a set of 68 historical newspapers published in the Portuguese Minho region between 1846 and the present-day (the full list is provided in the Appendix A2), totalling more than 34,200 individual newspapers, and allowing to gather valuable information, namely on grape harvesting (**Chapter 4**).

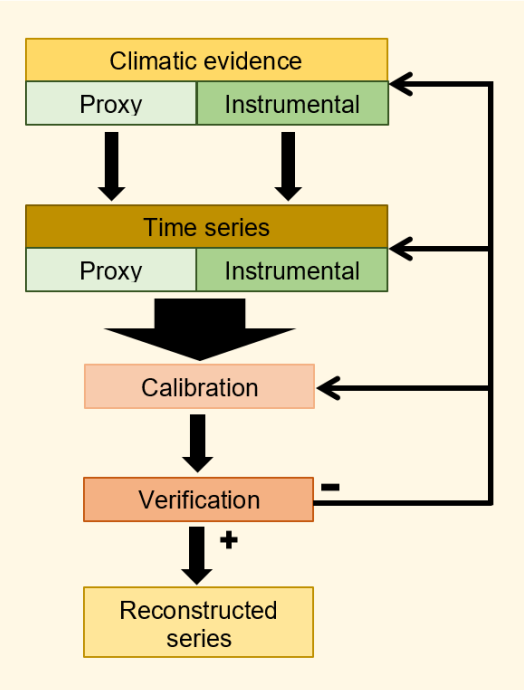

Figure 1.28. Diagram for historical–climatological analysis (after Brázdil, 2002).

1.3.4. Bromine

Bromine (Br) occurs naturally in the environment as soluble bromide (Br^-) salts (Br_{inorg}), but as well as (biogenic and abiotic) organobromine (Br_{org}) compounds, many of them synthetized by sessile marine organisms (e.g., sponges, seaweeds and corals) as part of their defensive arsenal (Gribble, 2010). They can be released to the atmosphere (more volatile) and ocean, though some Br_{org} moieties (more recalcitrant) might persist in the marine setting through sedimentation. Since it was found that OM in marine sediments is ubiquitously brominated, also organic sedimentation may be significant in the removal of Br_{inorg} from oceanic waters (Leri et al., 2014). In terrestrial and coastal soils and sediments, Br_{inorg} is subject to uptake by vegetation (Xu et al., 2004) as well as to conversion to Br_{org} through natural mechanisms (Leri and Myneni, 2012). Terrestrial organisms (e.g., lichens and fungi) also frequently contain Br_{org}, with bacteria remaining king of the biosynthesizers (Gribble, 2010). As a result, Br globally cycles between the oceans, atmosphere and land. But this natural cycling is distressed by the worldwide anthropogenic commercial application of Br_{org} compounds, namely of methyl bromide (CH_3Br), with global models suggesting that Br chemistry is

responsible for 5–15% of the loss of tropospheric O_3 (Von Glasow and Hughes, 2015). Global volcanic Br fluxes are comparatively poorly constrained (e.g., Aiuppa et al., 2005); however, recent analytical advances seem to assure that the next decades will see step change in our understanding of volcanic Br emissions (Mather, 2015).

Until the implementation of the Montreal Protocol, the Br budget of the stratosphere was largely controlled by the anthropogenic emissions of long-lived source gases as CH_3Br, e.g., from agricultural and industrial fumigation, fire-extinguishing agents' usage or combustion of leaded gasoline. But today natural emissions, such as those originated in coastal marshes (mostly via vegetation), become relatively more prominent as shown in Figure 1.29. The current knowledge on the atmospheric CH_3Br points out various sources and important sinks on land, in the ocean and in the atmosphere, as well as a computed lifetime of 0.8 years, against destruction by hydroxyl (OH) radicals in the troposphere, uptake by the ocean and consumption in soils. However, the calculated atmospheric budget is out of balance, with sinks outweighing sources (Montzka and Reimann, 2011). New findings continue to reveal earlier unidentified sources, which seem gradually to be closing the gap between calculated sources and sinks (Yvon-Lewis and Butler, 2015). Interestingly, the results of a recent study (Weinberg et al., 2015) performed in the Ria Formosa (South Portugal) suggest that seagrass meadows would cover a portion of 1.4–2.8% of the missing sources for CH_3Br reported in the most recent World Meteorological Organization report (36.1 Gg yr^{-1}; Montzka and Reimann, 2011).

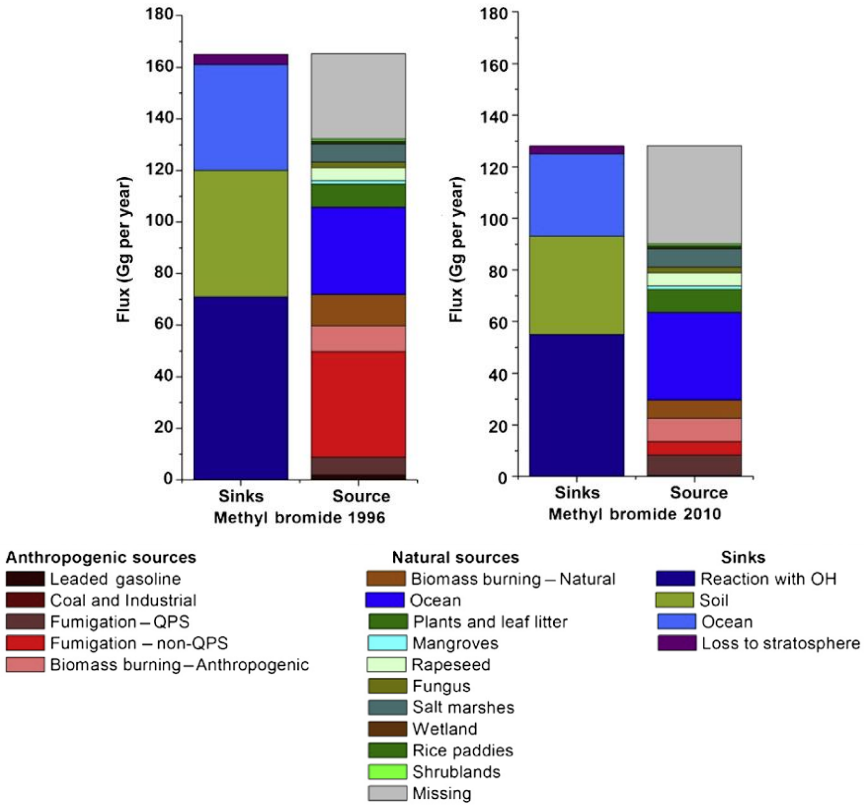

Figure 1.29. Source and sink fluxes of methyl bromide: 1996 and 2010 (after Yvon-Lewis and Butler, 2015).

In the previous context, the identification of couplings between the climate system and the biogeochemical processes that are able to impact atmospheric composition and chemistry is a crucial issue (Hughes et al., 2012). Coastal marshes with high abundance of C_{org} and biological activity, tidally inundated with Br^- rich seawater, have long been identified as global significant sources of CH_3Br (e.g., Rhew et al., 2000). All the subsequent investigation on this subject highlighted several key features, such as (i) marsh emissions derive mostly from vegetation and are species-dependent, being intrinsically related with plant's life cycle, (ii) they also show a strong climate dependence, linked largely to temperature – exponential dependence (Wishkerman et al., 2008) and insolation (available photosynthetically active radiation – PAR), not stopping with tidal inundation (Rhew et al., 2014), and (iii) decaying vegetation (abiotically or by fungi) releases as well measurable quantities of CH_3Br (e.g., Lee-Taylor and Holland, 2000). From these findings, maximum emissions would occur for plant material containing higher amounts of Br^- and decaying under warm and dry conditions. If this is expected to cause CH_3Br emission hotspots under a scenario of increased temperatures and extreme weather events, like heat waves and droughts (Gebhardt, 2008), it is plausible to assume the opposite under a scenario of both reduced temperatures and available PAR (like during Grand Solar Minima), allowing higher Br_{inorg} to be retained in marsh soils/sediments by natural bromination of OM. Supported by these relationships, Br has a strong potential (to be developed) as biogeochemical marker of past SA in salt marshes, as proposed in the current research (**Chapters 8** and **9**), with this one being a further example how and why ecosystems can shift from a net source to a sink (and vice-versa) as a result of changes in climate.

1.4. Dissertation outline

The present dissertation is outlined with this introductory chapter and a final one comprising the general conclusions and an outlook about future work (prospective). Its main body is divided in ten chapters, each one previously organized to be submitted to a peer-review scientific journal. This is the reason why they are self-contained and can be read independently. All include its own abstract, introduction, description of datasets and research methodologies, discussion and conclusions. The next focus paragraphs highlight the content of these main chapters.

Looking for more thorough foraminifera-based paleoenvironmental reconstructions in the northeast Atlantic domain, the modern marsh benthic foraminifera's geographical distribution in several west Portuguese estuaries is succinctly discussed in **Chapter 2**. In this chapter, a seasonal study of temperature and salinity, sampling estuarine and interstitial sediment waters from tidal marshes, was undertaken along the Minho (NW), Tejo and Mira (SW) estuaries. It has demonstrated the importance of the North–South climatic transition – from wet-Atlantic to Mediterranean – in determining the marsh assemblages' distribution of foraminifera (and ostracoda), mainly mirroring the existing water's salinity gradient. The interaction between the different environmental parameters

controlling the water balance on marshes seems to be of paramount importance regarding species composition's regulation. In this context, the knowledge on driven ecological parameters of modern assemblages (usually preserved in the fossil record), is fundamental to support reliable paleoclimatic and paleoenvironmental reconstructions. Therefore, the use of the modern assemblages requires caution because the fossil and subfossil records have a time-averaging overprint associated with taphonomic processes (physical reworking, dissolution, bioerosion and bioturbation) and also "(…) there is an inherent bias toward time-averaging because biological generation times, and therefore hard part inputs to sediment, normally occur over time scales much shorter than rates of burial. (…) Although high-frequency population dynamics are typically lost, time-averaged assemblages are more likely to be representative of long-term environmental conditions and community dynamics because the dominance of a particular set of environmental parameters increases with time while comparatively short-term (…) fluctuations are damped", quoting Martin et al. (2002).

Chapter 3 gives a first insight of the down-core processes for the instrumental period (AD 1934–2010), pointing to the high marsh benthic foraminifera's ability (Caminha salt marsh, Minho River estuary, NW of Portugal) to respond to short-term (intra-decadal and multi-decadal) fluctuations in precipitation, correlated with the winter NAO index, as a part of the North Atlantic climate dynamics. Positive precipitation anomalies increase the freshwater flooding and seepage at the intertidal zone and are recorded by the high marsh foraminiferal assemblages by means of an upsurge of the low-salinity species' abundance, like *Haplophragmoides manilaensis* (Andersen, 1953), *Haplophragmoides wilberti* Andersen 1953, *Trochamminita salsa/irregularis* (Cushman and Brönnimann, 1948) and *Pseudothurammina limnetis* (Scott and Medioli, 1980). Instead, a steady low precipitation throughout 4 to 5 years seems enough to significantly raise the presence of the high marsh normal-salinity species, namely *Trochammina inflata* (Montagu, 1808) and *Jadammina macrescens* (Brady, 1870).

The short-length of meteorological data time series has been a motivation to look for high-resolution (annual) historical proxy climatic indicators that could support, backward in time, climate-related responses from marsh foraminifera and more detailed paleoenvironmental reconstructions. **Chapters 4** to **6** all contribute to our understanding of such relationship (foraminifera–other proxies). Connecting climate and viticulture, GHD from several traditional European wine-producing regions have been compiled, allowing to open a six-centuries window for the study of past climate evolution in Europe, based on evidence of the strong link between GHD and growing season's temperature, which was also used to make several temperature reconstructions (Daux et al., 2012). Sustained by this well-recognized connection, the research from **Chapter 4** focus on to expand a climatic reconstruction of the northwest Minho region back to AD 1854, using GHD as a proxy of GS surface air mean maxima temperatures (GSTmax), which happens, as far as I know, for the first time for Portugal. This new 154-years GHD time series was built based on the records from a suite of local

and regional newspapers (1854–1978) and the annuals of a Wine Producers Cooperative (Ponte de Lima; 1978–2010). Additionally, the research includes a comparison with a global annual average temperatures trend (Jones et al., 2013) and an analysis of the regional climatic variability and change, as regards the GSTmax (1950–2009) association with the main large atmospheric teleconnection modes affecting the North Atlantic–European (NAE) sector, in which this region (Minho) is included. Persistent positive modes of spring-summer Scandinavian (SCA) and summer East Atlantic/Western Russia (EA/WR) patterns seem to have triggered lower GSTmax, particularly in the 1960s–1980s. The search for solar imprints' on the Minho region climate has identified the SCA mode as a promising link between the two, since it is significantly inversely correlated with both, the TSI and the GSTmax. Afterwards, in **Chapter 5,** the Minho GSTmax (1856–2010) is combined with data on benthic foraminiferal assemblages from the Caminha salt marsh to characterize the main hydro-climatic episodes in the region during the latter one and a half century. This work develops the hypothesis that marsh foraminifera respond to the complex and intricate variables' network that controls marsh evolution, and includes temperature as a key component of the environmental balance. Results emphasize that, in the brackish setting of the Minho estuary where foraminiferal species usually associated with low salinity prevail, higher GSTmax had an impact on marsh hydrological balance by enhancing ET and increasing interstitial water salinity. These conditions favoured the occurrence of marsh species like *J. macrescens* and *T. inflata*. The influence of the mentioned teleconnection patterns (SCA, EA/WR; 1950–2009) in this region climatic variability, in-phase with a positive precipitation anomaly (1958–1983), reduced the Caminha tidal marsh salinity, leading to the increase of low-salinity species: *T. salsa/irregularis*, *H. manilaensis*, *Miliammina fusca* (Brady, 1870) and *Miliammina* spp.

Motivated to go further back in time, **Chapter 6** introduces a triennial-resolved wine production (WP) series from 1626 to 1820 based on the Benedictine accounts from six monasteries of the Entre-Douro-e-Minho region (NW Portugal), as previously referred in this chapter, and a new benthic foraminiferal high-resolution record (AD 1654–1824) from the Caminha tidal marsh. Spectral analysis and wavelet-based methods were performed allowing the recognition of statistically significant periodicities at *ca.* 13-year and *ca.* 60-year, falling in the range of the Schwabe and Lower Gleissberg solar cycles. Wavelet analysis comparing these cycles in foraminifera with those in the TSI and the NAO index reconstructions, as well as a regional temperature climate model simulation revealed some highly coherent responses that can be linked to SA. The influence of the three solar dynamo natural oscillations (bi-decadal, semi-secular and secular) in the WP trend fluctuations is discussed as well as the likely climatic, socio-economic and political impacts on WP during the LIA, particularly in the Maunder and Dalton Minima.

In addition, **Chapter 7** provides a detailed (Caminha) marsh foraminifera-based reconstruction for the last two millennia (AD 140–2010), associated to sedimentological and

geochemical proxies, and supported by historical and instrumental climatic records. Based on this reconstruction is possible to infer brackish conditions persisting in the Minho estuary at least since AD 140. The intertidal sedimentary record highlights two main steps – tidal flat and marsh – in which the preservation of proxy data, namely benthic foraminifera, is quite distinct. The tidal flat assemblages are poorly preserved and often absent, in a baseline setting depleted in calcium carbonate ($CaCO_3$). Even so, it is clear that the residual assemblages are mainly composed by low-salinity species that persisted in the better preserved assemblages after the marsh establishment (AD 1380). As stated, estuarine evolution mainly occurred under brackish conditions, with flood events producing a drop in the foraminiferal density. However, drought periods are marked by an increase in the proportion of brackish-to-normal salinity marsh species, dominating the assemblages during the most severe dryer events recorded in the mid-20th century. The stronger influence of marine or fluvial conditions inside the estuary over the Roman Warm Period (RWP), MCA, LIA and the Present Warm Period (PWP) appears closely connected to climate variability (in dependence upon the fluctuations in SA). The hydrological balance recorded by the Caminha marsh foraminifera and sedimentological proxies is controlled by the atmospheric modes, reflecting the NE Atlantic climate dynamic, namely from the LIA to present.

Chapters 8 and **9** highlight the ability of total Br in marsh sediments to be used as a solar–climate proxy. Marshes play an important role on the biogeochemical cycling of elements at local, regional and even global scales and represent important land–ocean–atmosphere interfaces that allow to capture spatiotemporal variability in chemical fluxes. In these habitats, Br interacts with both halophytes and the relatively large OM pool of soils/sediments. In **Chapter 8** it is suggested that in the Caminha tidal marsh, the most prominent Br enrichment peaks in soils/sediments, between AD ~1300 and AD ~1800, were primarily due to dynamics' changes in the Br biogeochemical cycle, occurring in response to persistent environmental changes triggered by Grand Minima Episodes of SA during the LIA, ultimately weakening the marsh's role as a source for CH_3Br to atmosphere. Moreover, the Br pattern in sediments along the 20th century, may be related with the history of human-made organic brominated compounds and to its anthropogenic fingerprints in the tidal marsh environment. **Chapter 9** extends the previous investigation on Br cycling, to other W coast Portuguese estuaries. A difference in the size of the Br and OM pools of the marshes from the NW and SW coasts emerges, mostly triggered by distinct climatic conditions. Br temporal variability in the sediment record of two dated cores – from Caminha (Minho estuary) and Casa Branca (Mira estuary) high marsh zones – is interpreted in relation with SA oscillations, evidencing a fairly similar temporal Br enrichment pattern, with major peaks during Grand Minima or Minima-like episodes.

Chapter 10 presents a foraminifera-based paleoclimatic reconstruction for the W Portuguese coast during the last six centuries based on the integration of the SW Casa Branca (FWCBr core) and NW Caminha (FCPw1 core) records. As far as the true potential of salt marsh benthic

foraminiferal species as paleoclimate proxies is concerned, much more work remains in delineating which species are best for different kinds of problems. From this viewpoint, a more comprehensive assessment can be made using independent additional evidence as performed in this analysis, where *T. inflata* is suggested as a promising indicator of drier periods in the SW studied area, supported by geochemical and sedimentological proxies of aeolian large-dust inputs, with likely origin from the Sahara Desert, the largest global dust source. Although a sustained NW–SW microfaunal contrast has been found, the abundance of both the brackish-to-normal salinity foraminiferal group in the NW coast and *T. inflata* in the SW coast, seems to show a similar response to solar forcing.

References

Aiuppa, A., Federico, C., Franco, A., Giudice, G., Gurrieri, S., Inguaggiato, S., Liuzzo, M., McGonigle, A.J.S. and Valenza, M., 2005. Emission of bromine and iodine from Mount Etna volcano. Geochemistry, Geophysics and Geosystems 6, Q08008-8p.

Alcoforado, M.J., 1999. Variações climáticas do passado: chave para o entendimento do presente? Exemplo referente a Portugal (1675-1715). Territorium 6, 19–30.

Alve, E., 1991. Foraminifera, climatic change, and pollution: a study of late Holocene sediments in Drammens fiord, southeast Norway. The Holocene 1, 243–261.

Andersen, H.V., 1953. Two new species of Haplophragmoides from the Louisiana coast. Contributions from the Cushman Foundation for Foraminiferal Research 4, 21–22.

Andrews, B., Knight, J.R. and Gray, L.J., 2015. A simulated lagged response of the North Atlantic Oscillation to the solar cycle over the period 1960–2009. Environmental Research Letters 10, 054022-10p.

Anet, J.G., Rozanov, E.V., Muthers, S., Peter, T., Brönnimann, S., Arfeuille, F., Beer, J., Shapiro, A.I., Raible, C.C., Steinhilber, F., and Schmutz, W.K., 2013. Impact of a potential 21st century “grand solar minimum” on surface temperatures and stratospheric ozone. Geophysical Research Letters 40, 4420–4425.

Auer, G., Piller, W.E. and Harzhauser, M., 2015. Two distinct decadal and centennial cyclicities forced marine upwelling intensity and precipitation during the late Early Miocene in central Europe. Climate of the Past 11, 283–303.

Baede, A.P.M., Ahlonsou, E., Ding, Y. and Schimel, D., 2001. The Climate System: An Overview. In: Houghton, J.T., Ding, Y., Griggs, D.J., Noguer, M., van der Linden, P.J., Dai, X., Maskell, K. and Johnson, C.A. (Eds.), Climate Change 2001: The Scientific Basis. Contribution of Working Group I to the Third Assessment Report of the Intergovernmental Panel on Climate Change. Cambridge University Press, pp. 87–98.

Ball, W.T., Unruh, Y.C., Krivova, N.A., Solanki, S., Wenzler, T., Mortlock, D.J. and Jaffe, A.H., 2012. Reconstruction of total solar irradiance 1974-2009. Astronomy & Astrophysics 541, A27-15p.

Bard, E., Raisbeck, G., Yiou, F. and Jouzel, J., 2000. Solar irradiance during the last 1200 years based on cosmogenic nuclides. Tellus 52B, 985–992.

Barlow, N.L.M., Shennan, I., Long, A.J., Gehrels, W.R., Saher, M.H, Woodroffe, S.A. and Hillier, C., 2013. Salt marshes as late Holocene tide gauges. Global and Planetary Change 106, 90–110.

Barriendos, M. 2005. Variabilidad climática y riesgos climáticos en perspectiva histórica. El caso de Catalunya en Los siglos XVIII-XIX. Revista de Historia Moderna 23, 11–34.

Beer, J., Joos, C.F., Lukasczyk, C., Mende, W., Siegenthaler, U., Stellmacher, R. and Suter, M., 1994. ^{10}Be as an Indicator of Solar Variability and Climate. In: E. Nesme-Ribes (Ed.), The Solar Engine and Its Influence on Terrestrial Atmosphere and Climate. Springer-Verlag, Berlin, pp. 221–233.

Beer, J., 2000. Neutron monitor records in broader historical context. Space Science Reviews 93, 107–119.

Beer, J., McCracken, K. and von Steiger, R., 2012. Cosmogenic Radionuclides - Theory and Applications in the Terrestrial and Space Environments. Springer-Verlag Berlin Heidelberg, 426p.

Beer, J., McCracken K., Abreu, J., Heikkilä, U. and Steinhilber, F., 2013. Cosmogenic radionuclides as an extension of the neutron monitor era into the past: potential and limitations. Space Science Reviews 176, 89–100.

Benestad, R.E., 2006. Solar Activity and Earth's Climate. 2nd Edition, Springer, Chichester, UK, 316p.

Bock, A., Sparks, T.H., Estrella, N. and Menzel, A., 2013. Climate-induced changes in grapevine yield and must sugar content in Franconia (Germany) between 1805 and 2010. PLoS ONE 8(7): e69015. doi:10.1371/journal.pone.0069015.

Bond, G., Showers, W., Cheseby, M., Lotti, R., Almasi, P., deMenocal, P., et al., 1997. A pervasive millennial-scale cycle in North Atlantic Holocene and glacial climates. Science 278, 1257–1266.

Bond, G., Kromer, B., Beer, J., Muscheler, R., Evans, M. N., Showers, W., Hoffmann, S., Lotti-Bond, R., Hajdas, I. and Bonani, G., 2001. Persistent solar influence on North Atlantic climate during the Holocene. Science 294, 2130–2136.

Brady, H.B., 1870. Foraminifera. In: Brady, G.S., Robertson, D. and Brady, H.B. (Eds.), Ostracoda and Foraminifera of Tidal Rivers. Annals and Magazine of Natural History, Series 4, 6, pp. 273–306.

Brady, H.B., 1876. A monograph of Carboniferous and Permian foraminifera (the genus Fusulina excepted). Palaeontographical Society of London 30, pp. 1–166.

Brady, H.B., 1884. Report on the Foraminifera dredged by the H.M.S. Challenger during the years 1873–1876. Report on the Scientific Results of the Voyage of H.M.S. Challenger during the years 1873–1876. Zoology 9, pp. 1–814.

Bradshaw, J.S., 1968. Environmental parameters and marsh foraminifera. Limnology and Oceanography 13, 26–38.

Brázdil, R., 2002. Patterns in climate in Central Europe since Viking times. In: Wefer, G., Berger, W.H., Behre, K.-E. and Jansen, E. (Eds.), Climate Development and History in the North Atlantic Realm. Springer-Verlag, pp. 355–368.

Brázdil, R., Pfister, C., Wanner, H., von Storch, H. and Luterbacher, J., 2005. Historical climatology in Europe – the state of the art. Climatic Change 70, 363–430.

Brázdil, R., Zahradníček, P., Dobrovolný, P., Kotyza, O. and Valášek, H., 2008. Historical and recent viticulture as a source of climatological knowledge in the Czech Republic. Geografie 113, 351–371.

Brückner, E., 1890. Klimaschwankungen seit 1700. Geographische Abhandlungen 14, p. 325.

Carter, R.W.G., 1988. Coastal Environments – An Introduction to the Physical, Ecological and Cultural Systems of Coastlines. Academic Press, London, 617p.

Cearreta, A., 1988. Distribution and ecology of benthic foraminifera in the Santoña estuary, Spain. Revista Espanola de Paleontologia 3, 23–38.

Cearreta, A., 1998. Holocene sea-level change in the Bilbao estuary (north Spain): foraminiferal evidence. Micropaleontology 44, 265–276.

Chevet, J.-M., Lecocq, S. and Visser, M., 2011. Climate, grapevine phenology, wine production, and prices: Pauillac (1800–2009). American Economic Review: Papers and Proceedings 101, 142–146.

Chaisson, E.J., 2008. Long-term global heating from energy usage. EOS, Transactions American Geophysical 89, 253–254.

Chaisson, E.J., 2014. The natural science underlying big history. The Scientific World Journal 2014, ID 384912-41p.

Chaisson, E.J., 2015. Energy flows in low-entropy complex systems. Entropy 17, 8007–8018.

Chiodo, G., García-Herrera, R., Calvo, N., Vaquero, J.M., Añel, J.A., Barriopedro, D. and Matthes, K., 2016. The impact of a future solar minimum on climate change projections in the Northern Hemisphere. Environmental Research Letters 11, 034015-14p.

Coddington, O., Lean, J.L., Pilewskie, P., Snow, M. and Lindholm, D., 2015. A solar irradiance climate data record. Bulletin of the American Meteorological Society, DOI: http://dx.doi.org/10.1175/BAMS-D-14-00265.1, 1265–1282.

Craft, C., 2007. Freshwater input structures soil properties, vertical accretion, and nutrient accumulation of Georgia and U.S tidal marshes, Limnology and Oceanography 52, 1220–1230.

Cronin, T., Willard, D., Karlsen, A., Ishman, S., Verardo, S., McGeehin, J., Kerhin, R., Holmes, C., Colman, S. and Zimmerman, A., 2000. Climatic variability in the eastern United States over the past millennium from Chesapeake Bay sediments. Geology 28, 3–6.

Cushman, J.A. and Brönnimann, P., 1948. Additional new species of arenaceous foraminifera from shallow waters of Trinidad. Contributions from the Cushman Foundation for Foraminiferal Research 24, 37–43.

D'Orbigny, A., 1826. Tableau méthodique de la classe des Céphalopodes. Annales des Sciences Naturelles 7, 245–314.

D'Orbigny, A., 1843. Modèles des Foraminifères Vivants et Fossiles. 2nd edition. Cosson, Paris.

Damon, P.E. and Sonett, C.P., 1991. Solar and terrestrial components of the atmospheric ^{14}C variation spectrum. In: Sonett, C.P., Giampapa, M.S. and Mathews, M.S. (Eds.), The Sun in Time. University of Arizona Press, Tucson, pp. 360–388.

Darby, D.A., Ortiz, J.D., Grosch, C.E. and Lund, S.P., 2012. 1,500-year cycle in the Arctic oscillation identified in Holocene Arctic sea-ice drift. Nature Geoscience 5, 897–900.

Daux, V., Cortázar-Atauri, I.G., Yiou, P., Chuine, I., Garnier, E., Le Roy Ladurie, E., Mestre, O. and Tardaguila, J., 2012. An open-access database of grape harvest dates for climate research: data description and quality assessment. Climate of the Past 8, 1403–1418.

Davis, Jr., R.A. and Fitzgerald, D.M., 2004. Beaches and Coasts. Blackwell Publishing, Malden, Oxford, Victoria, 419p.

Debenay, J.-P. and Guiral, D., 2006. Mangrove swamp foraminifera, indicators of sea level or paleoclimate? Revue de Paléobiologie 25, 567–574.

Debenay, J.-P., Bicchi, E., Goubert, E. and Armynot du Châtelet, E., 2006. Spatio-temporal distribution of benthic foraminifera in relation to estuarine dynamics (Vie estuary, Vendée, W France). Estuarine, Coastal and Shelf Science 67, 181–197.

De Rijk, S., 1995. Agglutinated foraminifera as indicators of salt marsh development in relation to late Holocene sea level rise (Great Marshes at Barnstable, Massachusetts), Febo, Utrecht, 188p.

De Vries, H., 1958. Variation in concentration of radiocarbon with time and location on Earth, Koninklijke Nederlandse Akademie Van Weteschappen-Proceedings Series B-Physical Sciences 61, 94–102.

Dias, G.J.A.C., 1993. O mosteiro de Tibães e a reforma dos Beneditinos portugueses no séc. XVI. Revista de História 12, 95–132.

Dias, G.J.A.C., 2005. A Importância dos mosteiros no mundo do vinho. In Revista Douro: Estudos e Documentos, vol. 20. Porto, GEHVID, pp. 123–132.

Dickinson, R., 1975. Solar variability and the lower atmosphere. Bulletin of the American Meteorological Society 56, 1240–1248.

Dorman, L.I., 2012. Cosmic Rays in the Earth's Atmosphere and Underground, Kluwer Academic Publishers, Dordrecht, 865p.

Duhau, S. and Martinez, E.A., 2012. Solar dynamo transitions as drivers of sudden climate changes. INTECH, pp. 185–204.

Duan, F., Wang, Y., Shen, C.-C., Wang, Y., Cheng, H., Wu, C.-C., Hu, H.-M., Kong, X., Liu, D. and Zhao, K., 2014. Evidence for solar cycles in a late Holocene speleothem record from Dongge Cave, China. Scientific Reports 4, 5159-7p.

Eddy, J.A., 1976. The Maunder minimum. Science 192, 1189–1202.

Eddy, J.A., 2009. The Sun, The Earth, and Near-Earth Space. A Guide to the Sun-Earth System. National Aeronautics and Space Administration (NASA), 301p.

Engels, S. and van Geel, B., 2012. The effects of changing solar activity on climate: contributions from palaeoclimatological studies. Journal of Space Weather and Space Climate 2, A09-9p.

Ermolli, I., Matthes, K., de Wit ,T.D., Krivova, N.A., Tourpali, K., Weber, M., Unruh, Y.C., Gray, L.J., Langematz, U., Pilewskie, P., Rozanov, E.V., Schmutz, W., Shapiro, A., Solanki, S.K. and Woods, T.N., 2013. Recent

variability of the solar spectral irradiance and its impact on climate modelling. Atmospheric Chemistry and Physics 13, 3945–3977.

Fagherazzi, S., 2013. The ephemeral life of a salt marsh. Geology 41, 943–944.

Fagherazzi, S., Kirwan M.L., Mudd, S.M., Guntenspergen, G.R., Temmerman, S., D'Alpaos, A., van de Koppel, J., Rybczyk, J.M. Reyes, E. Craft, C. and Clough, J., 2012. Numerical models of salt marsh evolution: ecological, geomorphic, and climatic factors. Reviews of Geophysics 50, RG1002-28p.

Fatela, F., Moreno, J., Leorri, E., and Corbett, R., 2014. High marsh foraminiferal assemblages response to intra-decadal and multi-decadal precipitation variability, between 1934 and 2010 (Caminha, NW Portugal). Journal of Sea Research 93, 118–132.

Feynman, J. and P. Fougere, 1984. Eighty-eight year cycle in solar terrestrial phenomena confirmed. Journal of Geophysical Research 89, 3023–3027.

Frankcombe, L.M, England, M.H., Mann, M.E. and Steinman, B.A., 2015. Separating internal variability from the externally forced climate response. Journal of Climate 28, 8184–8202.

Fröhlich, C., 2006. Solar irradiance variability since 1978: Revision of the PMOD composite during solar cycle 21. Space Science Reviews 125, 53, doi:10.1007/s11214-006-9046-5.

Galloway, J.M., Wigston, A. Patterson, R.T., Swindles, G.T., Reinhardt, E. and Roe, H.M., 2013. Climate change and decadal to centennial-scale periodicities recorded in a late Holocene NE Pacific marine record: Examining the role of solar forcing. Paleogeography, Paleoclimatology, Paleoecology 386, 669–689.

Gebhardt, S., 2008. Biogenic Emission of Halocarbons. PhD Thesis, Johannes Gutenberg-Universität Mainz, 126p.

Gerber, E.P., Butler, A., Calvo, N., Charlton-Perez, A., Giorgetta, M., Manzini, E., Perlwitz, J., Polvani, L.M., Sassi, F., Scaife, A.A., Shaw, T.A., Son, S.-W. and Watanabe, S., 2012. Assessing and understanding the impact of stratospheric dynamics and variability on the Earth system. Bulletin of the American Meteorological Society 93, 845–859.

Gleisner, H. and Thejll, P., 2003. Patterns of tropospheric response to solar variability. Geophysical Research Letters 30, 1711-4p.

Gleissberg, W., 1939. A long-periodic fluctuation of the sun-spot numbers. Observatory 62, 158–159.

Grandpierre, A., 2004. Conceptual steps towards exploring the fundamental nature of our sun. Interdisciplinary Description of Complex Systems 2, 12–28.

Gray, L.J., Beer, J., Geller, M., Haigh, J.D., Lockwood, M., Matthes, K., Cubasch, U., Fleitmann, D., Harrison, G., Hood, L., Luterbacher, J., Meehl, G.A., Shindell, D., van Geel, B. and White, W., 2010. Solar influences on climate. Reviews of Geophysics 48, RG4001-53p.

Gray, L.J., Scaife, A.A., Mitchell, D.M., Osprey, S., Ineson, S., Hardiman, S., Butchart, N., Knight, J., Sutton, R. and Kodera, K., 2013. A lagged response to the 11 year solar cycle in observed winter Atlantic/European weather patterns. Journal of Geophysical Research: Atmospheres 118, 13,405–13,420.

Greenberg, R., Maldonado, J.E., Droege, S. and McDonald, M.V., 2006. Tidal marshes: a global perspective on the evolution and conservation of their terrestrial vertebrates. BioScience 56, 675–685.

Gribble, G., 2010. Naturally Occurring Organohalogen Compounds – A Comprehensive Update. Springer-Verlag, Vienna, 613p.

Grzybowski, J., 1896. Otwornice czerwonych ilow z Wadowic. Rozprawy Wydzialu Matemat.-Przyrod. Akad. Umiejetnosci w Krakowie 30, 261–308.

Grzybowski, J., 1898. Otwornice pokladow naftonosnych okolicy Krosna. Rozprawy Wydzialu Matemat.-Przyrod. Akad. Umiejetnosci w Krakowie 33, 257–305.

Grzybowski, J., 1901. Otwornice warstw inoceramowych okolicy Gorlic. Rozprawy Wydzialu Matemat.-Przyrod. Akad. Umiejetnosci w Krakowie 41, 219–286.

Haigh, J.D., 1994. The role of stratospheric ozone in modulating the solar radiative forcing of climate. Nature 370, 544–546.

Haigh, J.D., 1996. The impact of solar variability on climate. Science 272, 981–984.

Haigh, J.D., 2007. The sun and the earth's climate. Living Reviews in Solar Physics 4, 1–64 (URL accessed 03.12.13: http://www.livingreviews.org/lrsp-2007-2).

Haigh, J.D., 2011. Solar influences on climate. Grantham Institute for Climate Change Briefing paper Nº 5, 20p.

Haigh, J.D., Blackburn, M. and Day, R., 2005. The response of tropospheric circulation to perturbations in lower-stratospheric temperature. Journal of Climate 18, 3672–3685.

Hale, G.E., Ellerman, F., Nicholson, S.B. and Joy, A.H., 1919. The magnetic polarity of sun-spots. The Astrophysical Journal 49, 153–178.

Haslett, S. K., Davies, P., Curr, R. H. F., Davies, C. F. C, Kennington, K., King, C. P. and Margetts, A. J. 1998. Evaluating Late Holocene relative sea-level change in the Somerset Levels, southwest Britain. The Holocene 8, 197–207.

Haltia-Hovi, E., Saarinen, T. and Kukkonen, M., 2007. A 2000-year record of solar forcing on varved lake sediment in eastern Finland, Quaternary Science Reviews 26, 678–689.

Hathaway, D.H., 2010. The solar cycle. Living Reviews in Solar Physics 7, http://www.livingreviews.org/lrsp-2010-1 (accessed in 21/01/2017).

Hayward, B.W., Grenfell, H.R., Reid, C.M. and Hayward, K.A., 1999. Recent New Zealand Shallow-Water Benthic Foraminifera: Taxonomy, Ecologic Distribution, Biogeography, and Use in Paleoenvironmental Assessments. Institute of Geological and Nuclear Sciences monograph, vol. 21. Lower Hutt, New Zealand, 258 p.

Hayward, B. W., Scott, G. H., Grenfell, H. R., Carter, R. and Lipps, J.H., 2004, Techniques for estimation of tidal elevation and confinement (~salinity) histories of sheltered harbours and estuaries using benthic foraminifera: examples from New Zealand: The Holocene, v. 14, p. 218–232.

Heikkilä, U., Beer, J. and Feichter, J., 2009. Meridional transport and deposition of atmospheric ^{10}Be. Atmospheric Chemistry and Physics 9, 515–527.

Hippensteel, S.P., Martin, R.E., Nikitina, D., and Pizzuto, J.E., 2002. Interannual variation of marsh foraminiferal assemblages (Bombay Hook National Wildlife Refuge, Smyrna, De): Do foraminiferal assemblages have a memory? Journal of Foraminiferal Research 32, 97–109.

Horton, B.P., Edwards, R.J., Lloyd and J.M., 1999. UK intertidal foraminiferal distributions: implications for sea-level studies. Marine Micropaleontology 36, 205–223.

Horton, B.P. and Edwards R.J., 2003. Seasonal distributions of foraminifera and their implications for sea-level studies. SEPM Special Publication 75, 21–30.

Horton, B.P. and Culver, S.J., 2008. Modern intertidal foraminifera of the Outer Banks, North Carolina, USA and their applicability for sea-level studies. Journal of Coastal Research, 24, 1110–1125.

Hoyt, D.V. and Schatten, K.H., 1997. The Role of the Sun in Climate Change. Oxford University Press, 279p.

Hughes, C., Johnson, M., von Glasow, R., Chance, R., Atkinson, H., Souster, T., Lee, G.A., Clarke, A., Meredith, M., Venables, H.J., Turner, S.M. Malin, G. and Liss, P.S., 2012. Climate-induced change in biogenic bromine emissions from the Antarctic marine biosphere. Global Biogeochemical Cycles 26, GB3019-9p.

Huth, R., Bochníček, J. and Hejda, P., 2007. The 11-year solar cycle affects the intensity and annularity of the Arctic Oscillation. Journal of Atmospheric and Solar-Terrestrial Physics 69, 1095–1109.

Hurrell, J.W., 1995. Decadal trends in the North Atlantic Oscillation, Regional temperatures and precipitation. Science 269, 676–679.

Hurrell, J.W., 1996. Influence of variations in extratropical wintertime teleconnections on Northern Hemisphere temperature. Geophysical Research Letters 23, 665–668.

Hurrell, J.W. and Deser, C., 2009. North Atlantic climate variability: The role of the North Atlantic Oscillation. Journal of Marine Systems 78, 28–41.

Hurrell, J.W. and Deser, C., 2015. Northern Hemisphere climate variability during winter: Looking back on the work of Felix Exner. Meteorologische Zeitschrift 24, 113–118.

Imbers, J., Lopez, A., Huntingford, C. and Allen, M.R., 2013. Testing the robustness of the anthropogenic climate change detection statements using different empirical models. Journal of Geophysical Research: Atmospheres 118, 3192–3199.

Inceoglu, F. Simoniello, R., Knudsen, M.F., Karoff, C., Olsen, J., Turck-Chiéze, S., and Jacobsen, B. H., 2015. Grand solar minima and maxima deduced from ^{10}Be and ^{14}C: magnetic dynamo configuration and polarity reversal. Astronomy & Astrophysics 577, A20-10p.

IPCC, 2013. Climate Change 2013: The Physical Science Basis. Contribution of Working Group I to the Fifth Assessment Report of the Intergovernmental Panel on Climate Change [Stocker, T.F., D. Qin, G.-K. Plattner, M. Tignor, S.K. Allen, J. Boschung, A. Nauels, Y. Xia, V. Bex and P.M. Midgley (Eds.)]. Cambridge University Press, Cambridge, UK and New York, USA, 1535p.

Jirikowic, J.L. and Damon, P.E., 1994. The medieval solar activity maximum. Climatic Change 26, 309–316.

Jones, P., 2008. Historical climatology – a state of the art review. Weather 63, 181–186.

Jones, R.W., 2014. Foraminifera and their Applications. Cambridge University Press, 391p.

Jones, P.D., Parker, D.E., Osborn, T.J. and Briffa, K.R., 2013. Global and Hemispheric Temperature Anomalies–Land and Marine Instrumental Records. In: Trends: A Compendium of Data on Global Change. Carbon Dioxide Information Analysis Center, Oak Ridge National Laboratory, U.S. Department of Energy, Oak Ridge, Tenn., U.S.A. doi: http://dx. doi.org/10.3334/CDIAC/cli.002.

Kang, Y., Khan, S. and Ma, X., 2009. Climate change impacts on crop yield, crop water productivity and food security – A review. Progress in Natural Science 19, 1665–1674.

Karl, D.M., 2014. Solar energy capture and transformation in the sea. Elementa: Science of the Anthropocene 2: 000021, doi: 10.12952/journal.elementa.000021.

Karleskint, Jr., G., Turner, R. and Small, Jr., J.W., 20. Introduction to Marine Biology, 4th Edition, Brooks/Cole, Cengage Learning, Belmont, USA, 576p.

Karlsen, A.W., Cronin, T.M., Ishman, S.E., Willard, D.A., Kerhin, R., Holmes, C.W. and Marot, M., 2000. Historical trends in Chesapeake Bay dissolved oxygen based on benthic foraminifera from sediment cores. Estuaries 23, 488–508.

Khare, N., Nigam, R. and Hashimi, N.H., 2008. Revealing monsoonal variability of the last 2,500 years over India using sedimentological and foraminiferal proxies. Facies 54, 167–173.

Kilifarska, N.A., 2013.An autocatalytic cycle for ozone production in the lower stratosphere initiated by Galactic Cosmic rays, Comptes Rendus de l'Academie Bulgare des Sciences 66, 243–252.

Kirkby, J. 2007. Cosmic rays and climate. Surveys in Geophysics 28, 333–375.

Kirwan, M.L., Guntenspergen, G.R. and Langley, J.A., 2014. Temperature sensitivity of organic-matter decay in tidal marshes. Biogeosciences 11, 4801–4808.

Kirwan, M.L., Temmerman, S., Skeehan, E.E., Guntenspergen, G.R. and Fagherazzi, S., 2016. Overestimation of marsh vulnerability to sea level rise. Nature Climate Change 6, 253–260.

Kodera, K. and Kuroda, Y., 2002. Dynamical response to the solar cycle: Winter stratopause and lower stratosphere. Journal of Geophysical Research 107, 4749-12p.

Kopp, G., 2016. Magnitudes and timescales of total solar irradiance variability. Journal of Space Weather and Space Climate 6, A30-11p.

Kopp, G. and Lean, J.L., 2011. A new, lower value of total solar irradiance: evidence and climate significance. Geophysical Research Letters 38, L01706-7p.

Kopp, G., Krivova, N., Wu, C.J. and Lean, J., 2016. The impact of the revised sunspot record on solar irradiance reconstructions. Solar Physics 291, 2951–2965.

Krivova, N.A., Solanki, S.K. and Floyd, L., 2006. Reconstruction of solar UV irradiance in cycle 23, Astronomy and Astrophysics 452, 631–639.

Krivova, N.A., Vieira, L.E.A. and Solanki, S.K., 2010. Reconstruction of solar spectral irradiance since the Maunder Minimum. Journal of Geophysical Research: Space Physics 115, A12112-11p.

Langley, J.A., McKee, K.L., Cahoon, D.R., Cherry, J.A. and Megonigal, J.P., 2009. Elevated CO_2 stimulates marsh elevation gain, counterbalancing sea-level rise. Proceedings of the National Academy of Sciences (PNAS) 106, 6182–6186.

Le, G.-M. and Wang, J.-L., 2003. Wavelet analysis of several important periodic properties in the relative sunspot numbers. Chinese Journal of Astronomy & Astrophysics 3, 391–394.

Le, H., Liu, L., He, H. and Wan, W., 2011. Statistical analysis of solar EUV and X-ray flux enhancements induced by solar flares and its implication to upper atmosphere. Journal of Geophysical Research 116, A11301, doi:10.1029/2011JA016704.

Lean, J.L., Rottman, G.J., Kyle, H.L., Woods, T.N., Hickey, J.R. and Puga, L.C., 1997. Detection and parameterization of variations in solar mid and near-ultraviolet radiation (200–400 nm). Journal of Geophysical Research 102, 29,939–29,956.

Lean, J.L. and Rind, D.H., 2008. How natural and anthropogenic influences alter global and regional surface temperatures: 1889 to 2006. Geophysical Research Letters 35, L18701-6p.

Lee-Taylor, J.M. and Holland, E.A., 2000. Litter decomposition as a potential natural source of methyl bromide. Journal of Geophysical Research 105, 8857–8864.

Leri, A.C., Mayer, L.M., Thornton, K.R. and Ravel, B., 2014. Bromination of marine particulate organic matter through oxidative mechanisms. Geochimica et Cosmochimica Acta 142, 53–63.

Leri, A.C. and Myneni, S.C.B., 2012. Natural organobromine in terrestrial ecosystems. Geochimica and Cosmochimica Acta 77, 1–10.

Lilensten, J., de Wit, T.D. and Matthes, K., 2015. Earth's climate response to a changing Sun. EDP Sciences, Paris, 360p.

Lockwood, M., 2006. What do cosmogenic isotopes tell us about past solar forcing of Climate?. Space Science Reviews 125, 95–109.

Lockwood, M., 2012. Solar influence on global and regional climates. Surveys in Geophysics 33, 503–534.

Lorenzo, V., Marlière, P. and Solé, R., 2016. Bioremediation at a global scale: from the test tube to planet Earth. Microbial Biotechnology 9, 618–625.

Magny, M., 2004. Holocene climate variability as reflected by mid European lake-level fluctuations and its probable impact on prehistoric human settlements. Quaternary International 113, 65–79.

Mamo, B., Strotz, L. and Dominey-Howes, D., 2009. Tsunami sediments and their foraminiferal assemblages. Earth-Sciences Reviews 96, 263–278.

Mann, M.E. and Jones, P.D., 2003. Global surface temperatures over the past two millennia. Geophysical Research Letters 30, 1820, doi:10.1029/2003GL017814.

Mann, M.E., Steinman, B.A. and Miller, S. K., 2014. On forced temperature changes, internal variability, and the AMO. Geophysical Research Letters 41, 3211–3219.

Marques, G.N.R.M., 2011. Do vinho de Deus ao vinho dos Homens: o vinho, os Mosteiros e o Entre Douro e Minho. Dissertação de Doutoramento em História apresentada à Faculdade de Letras do Porto. Porto: FLUP. 524p.

Marsh, N. and Svensmark, H., 2000. Cosmic Rays, Clouds, and Climate. Space Science Reviews 94, 215–230.

Marsh, N. and H. Svensmark, H., 2003. Galactic cosmic ray and El Niño-Southern Oscillation trends in International Satellite Cloud Climatology Project D2 low-cloud properties. Journal of Geophysical Research 108, 4195-11p.

Martin, R.E., Hippensteel, S.P., Nikitina, D. and Pizzuto, J.E., 2002. Artificial time-averaging of marsh foraminiferal assemblages: linking the temporal scales of ecology and paleoecology. Paleobiology 28, 263–277.

Martín-Chivelet, J., Muñoz-García, M.B., Edwards, R.L., Turrero, M.J. and Ortega, A.I., 2011. Land surface temperature changes in Northern Iberia since 4000 yr. BP, based on $\delta^{13}C$ of speleothems. Global and Planetary Change 77, 1–12.

Martin-Puertas, C., Matthes, K., Brauer, A., Muscheler, R., Hansen, F., Petrick, C., Aldahan, A., Possnert, G., van Geel, B., 2012. Regional atmospheric circulation shifts induced by a grand solar minimum. Nature Geoscience 5, 397–401.

Masarik, J. and Beer, J., 2009. An updated simulation of particle fluxes and cosmogenic nuclide production in the Earth's atmosphere. Journal of Geophysical Research: Atmospheres 114, D11103-9p.

Mather, T.A., 2015. Volcanoes and the environment: Lessons for understanding Earth's past and future from studies of present-day volcanic emissions. Journal of Volcanology and Geothermal Research 304, 160–179.

Mayewski, P.A. and Maasch, K.A., 2006. Recent warming inconsistent with natural association between temperature and atmospheric circulation over the last 2000 years. Climate of the Past Discussions 2, 327–355.

McCracken, K.G., Dreschhoff, G.A.M., Smart, D.F. and Shea, M.A. 2001. Solar cosmic ray events for the period 1561-1994. 2. The Gleissberg periodicity. Journal of Geophysical Research 106, 21,599–21,609.

Meehl, G.A., Arblaster, J.M., Matthes, K., Sassi, F. and van Loon, H., 2009. Amplifying the Pacific climate system response to a small 11-year solar cycle forcing. Science 325, 1114–1118.

Meehl, G.A., Arblaster, J.M. and Marsh, D.R., 2013. Could a future "Grand Solar Minimum" like the Maunder Minimum stop global warming?. Geophysical Research Letters 40, 1789–1793.

Miettinen, A., Koc, N., Hall, I.R., Godtliebsen, F. and Divine, D., 2011. North Atlantic sea surface temperatures and their relation to the North Atlantic Oscillation during the last 230 years. Climate Dynamics 36, 533–543.

Miller, J.G and Miller, J.L., 1982. The Earth as a system. Behavioral Science 27, 313–322.

Millon, M., 2013. Wine: A Global History. Reaktion Books – Edible, London, UK, 175p.

Moffett, K.B., Nardin, W., Silvestri, S., Wang, C. and Temmerman, S., 2015. Multiple stable states and catastrophic shifts in coastal wetlands: progress, challenges, and opportunities in validating theory using remote sensing and other methods. Remote Sensing 7, 10184–10226.

Montagu, G., 1808. Supplement to Testacea Britannica. S. Woolmer, Exeter, 183p.

Montzka, S. A., and S. Reimann, 2011. Ozone-Depleting Substances (ODSs) and Related Chemicals. In: Ravishankara, A.R. et al. (Eds.), Scientific Assessment of Ozone Depletion 2010, Global Ozone Research and Monitoring Project–Report No. 52, World Meteorological Organization, Geneva, Switzerland, pp. 1–108.

Moreno, J., Fatela, F., Leorri, E., De la Rosa, J., Pereira, I., Araújo, M. F., Freitas, M. C., Corbett, R. and Medeiros A., 2014. Marsh benthic Foraminifera response to estuarine hydrological balance driven by climate variability over the last 2000 years (Minho estuary, NW Portugal). Quaternary Research 82, 318–330.

Morris, J.W., 1995. The mass balance of salt and water in intertidal sediments: results from North Inlet, South Carolina. Estuaries 18, 556–567.

Mudd, S.M., D'Alpaos, A. and Morris, J.T., 2010. How does vegetation affect sedimentation on tidal marshes? Investigating particle capture and hydrodynamic controls on biologically mediated sedimentation. Journal of Geophysical Research 115, F03029-14p.

Murray, J. W., 1991. Ecology and Palaeoecology of Benthic Foraminifera: Longman, Harlow, 397p.

Murray, J.W., 2000. Revised taxonomy, An Atlas of British Recent Foraminiferids. Journal of Micropalaeontology 19, 44p.

Murray, J.W., 2006. Ecology and Applications of Benthic Foraminifera. Cambridge University Press, Cambridge, UK, 426p.

Ney, E.P., 1959. Cosmic radiation and the weather. Nature 183, 451–452.

Nigam, R., 2005. Addressing environmental issues through foraminifera – case studies from the Arabian Sea. Journal of the Palaeontological Society of India 50, 25–36.

Nigam, R., Khare, N. and Nair, R.R., 1995. Foraminiferal evidences for 77-year cycles of droughts in India and its possible modulation by the Gleissberg solar cycle. Journal of Coastal Research 11, 1099–1107.

Odum, E.P., 1968. Energy flow in ecosystems: A historical review. American Zoologist 8, 11–18.

Ogurtsov, M.G., Kocharov, G.E., Lindholm, M., Meriläinen, J., Eronen, M. and Nagovitsyn, Y.A., 2002. Evidence of solar variation in tree-ring-based climate reconstructions. Solar Physics 205, 403–417.

Oliveira, A., 1979. A Abadia de Tibães (1630-1813): propriedade e exploração agrícola no Vale do Cávado no Antigo Regime. Dissertação de Doutoramento em História apresentada à Faculdade de Letras do Porto. Porto: FLUP. Vol. 2, 798p.

Overpeck, J., Whitlock, C. and Huntley, B., 2003. Terrestrial Biosphere Dynamics in the Climate System: Past and Future. In Alverson, K.D., R.S. Bradley and T.F. Pederson, Paleoclimate, Global Change and the Future. Springer-Verlag Berlin Heidelberg New York, pp. 81–111.

Pesnell, W. D., 2016. Predictions of solar cycle 24: How are we doing?. Space Weather 14, 10–21.

Pfister, C., 1992. Monthly temperature and precipitation in central Europe from 1525–1979: Quantifying documentary evidence on weather and its effects. In: Bradley, R.S. and Jones, P.D. (Eds.), Climate since A.D. 1500. Routledge, London, UK, pp. 118–142.

Pfister, C., Brázdil, R., Obrebska-Starkel, B., Starkel, L., Heino, R. and von Storch, H., 2001. Strides made in reconstructing past weather and climate. EOS – Transactions American Geophysical Union 82, 248.

Phleger, F.B., 1951. Ecology of Foraminifera, northwest Gulf of Mexico, Part 1, Foraminifera distributions. Geological Society of America Memoir 46, 88p.

Phleger, F.B., 1954. Ecology of Foraminifera and associated micro-organisms from Mississippi Sound and environs. Bulletin of the American Association of Petroleum Geologists 38, 584–647.

Phleger, F.B., 1960. Ecology and Distribution of Recent Foraminifera. The John Hopkins Press, Baltimore, 297p.

Phleger, F.B., 1965. Patterns of Marsh Foraminifera, Galveston Bay, Texas. Limnology and Oceanography 10, 169–180.

Phleger, F.B., 1970. Foraminiferal populations and marine marsh processes. Limnology and Oceanography 15, 522–534.

Rabenhorst, M.C. and Needelman, B.A., 2016. Soils of Tidal Wetlands. In: Vepraskas, M.J. and Craft, C.B. (Eds.), Wetland Soils. Genesis, Hydrology, Landscapes and Classification, 2nd Edition, CRC Press, Boca Raton, pp. 347–364.

Reames, D.V., 2004. Solar energetic particle variations. Advances in Space Research 34, 381–390.

Reid, G.C., 1987. Influence of solar variability on global sea surface temperatures. Nature 329, 142–143.

Rhew, R.C., Miller, B.R. and Weiss, R.F., 2000. Natural methyl bromide and methyl chloride emissions from coastal salt marshes. Nature 403, 292–295.

Rhew, R.C., Whelan, M.E. and Min, D.-H., 2014. Large methyl halide emissions from south Texas saltmarshes. Biogeosciences Discussions 11, 9451–9470.

Rind, D., 2002. The Sun's role in climate variations. Science 296, 673–677.

Roy, I., 2013. The role of the Sun in atmosphere–ocean coupling. International Journal of Climatology. DOI: 10.1002/joc.3713.

Rozanov, E., Calisto, M. Egorova, T., Peter, T. and Schmutz, W., 2012. Influence of the precipitating energetic particles on atmospheric chemistry and climate. Surveys in Geophysics 33, 483–501.

Rzesanke, D., Duft, D. and Leisner, T. 2013. Laboratory Experiments on the Microphysics of Electrified Cloud Droplets. In: F.-J. Lübken (Ed.), Climate and Weather of the Sun-Earth System (CAWSES). Highlights from a Priority Program, pp. 89–107.

Sánchez-López, G., Hernández, A., Pla-Rabes, S., Trigo, R.M., Toro, M., Granados, I., Sáez, A., Masqué, P., Pueyo, J.J., Rubio-Inglés, M.J. and Giralt, S., 2016. Climate reconstruction for the last two millennia in central Iberia: The role of East Atlantic (EA), North Atlantic Oscillation (NAO) and their interplay over the Iberian Peninsula. Quaternary Science Reviews 149, 135–150.

Scaife A.A., Ineson, S., Knight, J.R., Gray, L., Kodera, K. and Smith, D.M., 2013. A mechanism for lagged North Atlantic climate response to solar variability. Geophysical Research Letters 40, 434–439.

Schurer, A.P, Hegerl, G.C., Mann, M.E., Tett, S.F.B. and Phipps, S.J., 2013. Separating forced from chaotic climate variability over the past millennium. Journal of Climate 26, 6954–6973.

Schwabe, H., 1844, Sonnen-Beobachtungen im Jahre 1843. Astronomische Nachrichten 21, 233–236.

Scott, D.B. and Medioli, F.S., 1978. Vertical zonation of marsh foraminifera as accurate indicators of former sea-level. Nature 272, 538–541.

Scott, D.B. and Medioli, F.S., 1980. Quantitative studies of marsh foraminiferal distributions in Nova Scotia: their implications for the study of sea-level changes. Cushman Foundation for Foraminiferal Research, Special Publication 17, 59p.

Scott, D.B. and Medioli, F.S., 1986. Foraminifera as sea-level indicators. In: Van de Plassche, O. (Ed.), Sea-level Research: A Manual for the Collection and Evaluation of Data. Geobooks, Norwich, pp. 435–456.

Scott, D.B., Medioli, F.S. and Schafer, C.T., 2001. Monitoring in Coastal Environments Using Foraminifera and Thecamoebian Indicators. Cambridge University Press, Cambridge, UK, 177p.

Scott, D.B., Frail-Gauthier, J. and Mudie, P.J., 2014. Coastal Wetlands of the World Geology, Ecology, Distribution and Applications. Cambridge University Press, Cambridge, UK, 364p.

Seppälä, A., Lu, H., Clilverd, M.A. and Rodger, C.J., 2013. Geomagnetic activity signatures in wintertime stratosphere wind, temperature, and wave response. Journal of Geophysical Research 118, 2169–2183.

Seppälä, A., Matthes, K., Randall, C.E. and Mironova, I.A., 2014. What is the solar influence on climate Overview of activities during CAWSES-II. Progress in Earth and Planetary Science 1:24, 12p.

Sharma, M., 2002. Variations in solar magnetic activity during the last 200000 years: is there a Sun climate connection? Earth and Planetary Science Letters 199, 459–472.

Siegenthaler, U., 1983. Uptake of excess CO_2 by an outcrop-diffusion model of the ocean. Journal of Geophysical Research: Oceans 88, 3599–3608.

Silva, C.T., 1993. O Mosteiro de Ganfei. Propriedade, Produção e Rendas no Antigo Regime (1629-1683 e 1716-1822). MSc Thesis, Faculdade de Letras do Porto, Porto, FLUP, 284p.

Singh, A.K., Singh, D. and Singh, R.P., 2010. Space Weather: Physics, Effects and Predictability. Surveys in Geophysics 31, 581–638.

Singh, A.K., Singh, D. and Singh, R.P., 2011. Impact of galactic cosmic rays on Earth's atmosphere and human health. Atmospheric Environment 45, 3806–3818.

Siscoe, G.L., 1980. Evidence in the auroral record for secular solar variability. Reviews of Geophysics 18, 647–658.

Smerdon, J.E. and Pollack, H.N., 2016. Reconstructing Earth's surface temperature over the past 2000 years: the science behind the headlines, WIREs Climate Change 7, 746–771.

Solanki, S.K., 2002. Solar variability and climate change: is there a link?. Astronomy & Geophysics 43, 5.9–5.13.

Solanki, S.K., Inhester, B. and Schüssler, M., 2006. The solar magnetic field. Reports on Progress in Physics 69, 563–668.

Solomon, S.C., Woods, T.N., Didkovsky, L.V., Emmert, J.T. and Qian, L., 2010. Anomalously low solar extreme-ultraviolet irradiance and thermospheric density during solar minimum. Geophysical Research Letters 37, L16103-5p.

Soon, W. W.-H. and Yaskell, S.H., 2003. The Maunder Minimum and the Variable Sun-Earth Connection. World Scientific, Singapore, 278p.

Steinhilber, F., Beer, J. and Fröhlich, C., 2009. Total solar irradiance during the Holocene, Geophysical Research Letters 36, L19704-5p.

Steinhilber, F., Abreu, J.A., Beer, J., Brunner, I., Christl, M., Fischer, H., Heikkilä, U., Kubik, P.W., Mann, M., McCracken, K.G., Miller, H., Miyahara, H., Oerter, H. and Wilhelms, F., 2012. 9,400 years of cosmic radiation and solar activity from ice cores and tree rings. Proceedings of the National Academy of Sciences 109, 5967–5971.

Stuiver, M. and Quay P.D., 1980. Patterns of atmospheric ^{14}C changes. Radiocarbon 22, 166–176.

Stuiver, M. and Braziunas, T.F., 1989. Atmospheric 14C and century-scale solar oscillations. Nature, 338, 405–408.

Suess, H.E., 1980. The radiocarbon record in tree rings of the last 8000 years. Radiocarbon 22, 200–209.

Sutherst, R.W., 2004. Global change and human vulnerability to vector-borne diseases. Clinical Microbiology Reviews 17, 136–173.

Svensmark, H. and Friis-Christensen, E., 1997. Variation of cosmic ray flux and global cloud coverage-a missing link in solar-climate relationships. Journal of Atmospheric and Solar-Terrestrial Physics 59, 1225–1232.

Tebaldi, C., Hayhoe, K., Arblaster, J.M. and Meehl, G.A., 2006. Going to the extremes - An intercomparison of model-simulated historical and future changes in extreme events. Climatic Change 79, 185–211.

Thiéblemont, R. and Matthes, K., 2015. Solar influence on Earth's climate. Astronomy in Focus 11, 372–376.

Tinsley, B.A., 2000. Influence of solar wind on the global electric circuit, and inferred effects on cloud microphysics. Space Science Reviews 94, 231–258.

Tinsley, B.A. and Yu, F., 2004. Atmospheric Ionization and Clouds as Links between Solar Activity and Climate. In: Pap, J. and Fox, P. (Eds.), Solar Variability and Its Effects on Climate. Geophysical Monograph 141, AGU Press, Washington, DC, pp. 321–339.

Tiwari, M. and Ramesh, R., 2010. Sun: Climate Coupling on Sub-Decadal to Multi-Millennial Time Scales. In Gopalswamy, N., Hasan, S.S. and Ambastha, A. (Eds.), Heliophysical Processes. Springer-Verlag, Berlin, Heidelberg, pp. 251–269.

Tonelli, M., Fagherazzi, S. and Petti, M., 2010. Modeling wave impact on salt marsh boundaries. Journal of Geophysical Research 115, C09028-17p.

Tsuda, T., Shepherd, M. and Gopalswamy, N., 2015. Advancing the understanding of the Sun–Earth interaction-the Climate and Weather of the Sun–Earth System (CAWSES) II program. Progress in Earth and Planetary Science 2:28, 18p.

Tsuda, T., Yamamoto, M., Hashiguchi, H., Shiokawa, K., Ogawa, Y., Nozawa, S., Miyaoka, H. and Yoshikawa, A., 2016. A proposal on the study of solar-terrestrial coupling processes with atmospheric radars and ground-based observation network, Radio Science 51, 1587–1599.

Turner, T.E., Swindles, G.T., Charman, D. J., Langdon, P.G., Morris, P.J., Booth, R.K., Parry, L.E. and Nichols, J.E., 2016. Solar cycles or random processes? Evaluating solar variability in Holocene climate records. Scientific Reports 6, 23961-7p.

Usoskin, I., Solanki, S.K. and Kovaltsov, G.A., 2007. Grand minima and maxima of solar activity: new observational constraints. Astronomy & Astrophysics 471, 301–309.

Usoskin, I., Kovaltsov, G.A., Mironova, I.A., Tylka, A.J. and Dietrich, W.F., 2011. Ionization effect of solar particle GLE events in low and middle atmosphere. Atmospheric Chemistry and Physics 11, 1979–1988.

Usoskin, I. and Krivova, N., 2012. Climate and weather of the Sun-Earth system. In: Astronomy and Astrophysics, Vol. II, edited by Engvold, O., Stabell, R., Czerny, B. and Lattanzio, J. (Eds.), in Encyclopedia of Life Support Systems (EOLSS), pp. 397–424.

Usoskin, I., Hulot, G., Gallet, Y., Roth, R., Licht, A., Joos, F., Kovaltsov, G.A., Thébault, E., and Khokhlov, A., 2014. Evidence for distinct modes of solar activity. Astronomy & Astrophysics 562, L10-4p.

Usoskin, I., Arlt, R., Asvestari, E., Hawkins, E., Käpylä, M., Kovaltsov, G.A., Krivova, N., Lockwood, M., Mursula, K., O'Reilly, J., Owens, M.J., Scott, C.J., Sokoloff, D.D., Solanki, S.K., Soon, W. and Vaquero, J.M., 2015. The Maunder minimum (1645–1715) was indeed a Grand minimum: a reassessment of multiple datasets. Astronomy & Astrophysics 581, A95-19p.

Usoskin, I., Gallet, Y., Lopes, F., Kovaltsov, G. A. and Hulot, G., 2016. Solar activity during the Holocene: the Hallstatt cycle and its consequence for grand minima and maxima. Astronomy & Astrophysics 587, A150-10p.

Valdes, P., 2011. Built for stability. Nature Geoscience 4, 414–416.

Van de Broek, M., Temmerman, S., Merckx, R. and Govers, G., 2016. The importance of an estuarine salinity gradient on soil organic carbon stocks of tidal marshes. Biogeosciences Discussions, doi:10.5194/bg-2016-285.

Van Loon, H., Meehl, G.A. and Shea, D.J., 2007. Coupled air-sea response to solar forcing in the Pacific region during northern winter. Journal of Geophysical Research 112, D02108-8p.

Vecchio, A., Lepreti, F., Laurenza, M., Alberti, T., and Carbone, V., 2017. Connection between solar activity cycles and grand minima generation. Astronomy & Astrophysics 599, A58-12p.

Velinov, P.I.Y., Asenovski, S., Kudela, K., Lastovicka, Jan, Mateev, L., Mishev, A. and Tonev, P., 2013. Impact of cosmic rays and solar energetic particles on the Earth's ionosphere and atmosphere. Journal of Space Weather and Space Climate 3, A14-17p.

Von Glasow, R. and Hughes, C., 2015. Bromine. In: North, G.R., J. Pyle and F. Zang, Encyclopedia of Atmospheric Sciences, 6 Volume Set, Volume 1, pp. 194–200.

Walker, G. and Boys, W., 1784. Testacea minuta rariora nuperrime detecta in arena littoris Sandvicensis. (A collection of the minute and rare shells lately discovered in the sand of the sea shore near Sandwich.) G. Walker, London, printed by J. March.

Walker, G. and Jacob, E., 1798. In Adam's essays on the microscope, containing a practical description of the most improved microscopes; a general history of Insects. A description of 383 animalcula etc. 2nd edition with considerable additions and improvements by F. Kanmacher. Dillon and Keating, London, 712p., 32 pl.

Wang, C. and Temmerman, S., 2013. Does biogeomorphic feedback lead to abrupt shifts between alternative landscape states? An empirical study on intertidal flats and marshes. Journal of Geophysical Research: Earth Surface 118, 229–240.

Wanner, H. and Bütikofer, J., 2008. Holocene Bond Cycles: real or imaginary? Geografie-SbornÌk ČGS 113, 338–350.

Wanner, H., Mercolli, L., Grosjean, M. and Ritz, S.P., 2014. Holocene climate variability and change; a data-based review. Journal of the Geological Society 172, 254–263.

Webb, J.W., 1983. Soil water salinity variations and their effects on *Spartina alterniflora*. Contributions in Marine Science 26, 1–13.

Wilks, D.S., 2011. Statistical Methods in the Atmospheric Sciences, Volume 100, 3rd Edition (International Geophysics), Academic Press, USA, 704p.

Wishkerman, A., Gebhardt, S., McRoberts, C.W., Hamilton, J.T.G., Williams, J. and Keppler, F., 2008. Abiotic methyl bromide formation from vegetation and its strong dependence on temperature. Environmental Science and Technology 42, 6837–6842.

Wolf, R., 1861. Mittheilungen über die Sonnenflecken. Vierteljahrsschr. Nat.forsch. Ges. Zürich 12, 41–82.

Wolf, R., 1862. Mittheilungen über die Sonnenflecken. Vierteljahrsschr. Nat.forsch. Ges. Zürich 14, 119–131.

Xing, P., Chen, X., Luo, Y., Nie, S., Zhao, Z., Huang, J., et al., 2016. The Extratropical Northern Hemisphere Temperature Reconstruction during the Last Millennium Based on a Novel Method. PLoS ONE 11, e0146776. doi:10.1371/journal.pone.0146776. 19p.

Xu, S.P., Leri, A.C., Myneni, S.C.B. and Jaffe, P.R., 2004. Uptake of bromide by two wetland plants (*Typha latifolia L.* and *Phragmites australis [Cav.] Trin. ex Steud.*). Environmental Science and Technology 38, 5642–5648.

Yan, H., Sun, L., Wang, Y., Huang, W., Qiu, S. and Yang, C., 2011. A record of the Southern Oscillation Index for the past 2,000 years from precipitation proxies. Nature Geoscience 4, 611–614.

Yeo, K.L., Krivova, N.A., Solanki, S.K. and Glassmeier, K.H., 2014. Reconstruction of total and spectral solar irradiance from 1974 to 2013 based on KPVT, SoHO/MDI, and SDO/HMI observations. Astronomy & Astrophysics 570, A85-18p.

Yvon-Lewis, S. and Butler, J.H., 2015. Halogen Sources, Natural (Methyl Bromide and Related Gases). In: North, G.R., J. Pyle and F. Zang, Encyclopedia of Atmospheric Sciences, 6 Volume Set, Volume 1, pp. 228-232.

http://lasp.colorado.edu/home/sorce/data/tsi-data/ (assessed in 1/2/2017)

2 Salinity and water temperature assessment of the tidal marshes from the W Portuguese coast, as an ecological tool to paleoenvironmental reconstructions based on foraminifera and ostracoda assemblages

FRANCISCO FATELA [(1)(2)], JOÃO MORENO [(1)(2)] & M. CRISTINA CABRAL [(1)(2)]

[(1)] IDL – Instituto Dom Luiz, Universidade de Lisboa, Campo Grande, 1749-016, Lisboa, Portugal. Autor correspondente: ffatela@fc.ul.pt

[(2)] Departamento de Geologia da Faculdade de Ciências da Universidade de Lisboa, Campo Grande, 1749-016, Lisboa, Portugal

Published in: *Estudos do Quaternário* 14 (2016), 73–81

http://www.apeq.pt/ojs/index.php/apeq/article/view/211/241

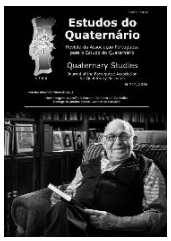

"The scientific discoveries of one generation are built upon the foundations laid by earlier workers."

J.W. Murray in ECOLOGY AND APPLICATIONS OF BENTHIC FORAMINIFERA (2006), p. 2.

ABSTRACT

A seasonal study of temperature and salinity of estuarine and sediment interstitial water of tidal marshes was undertaken along three estuaries of W Portuguese coast (Minho, Tejo and Mira).

The climatic N–S transition from wet Atlantic to Mediterranean features appear clearly imprinted in the distribution of tidal marsh assemblages, like foraminifera and ostracoda, mainly reflecting the water salinity gradient control.

The Minho low estuary tidal marsh tends to be flooded by estuarine water ranging from 0.5‰ to 32‰ in each tide cycle, even during dry seasons. However, the marsh hydrological balance sustains a more stable environment where the salinity of interstitial water measurements yielded 8‰ to 16‰. In contrast the Tejo and Mira salt marsh flooding waters record a narrow range between 33‰ and 36‰, in spring, and between 29‰ and 36‰ in autumn. The climatic control of evaporation/ precipitation balance produces an enhanced salinity

of marsh interstitial water that can reach hypersaline conditions, with maximum records of 53‰ in Tejo and 48‰ in Mira lower estuaries.

These environmental differences along the W Portuguese coast are recorded by the tidal marsh assemblages, namely foraminifera and ostracoda. In the low salinity Caminha salt marsh, living foraminifera are essentially composed by the agglutinated species *Haplophragmoides manilaensis*, *Miliammina fusca*, *Pseudothurammina limnetis Psammosphaera* sp. and *Trochamminita salsa/irregularis*. The modern ostracoda assemblage includes *Leptochytere baltica, Leptochytere psammophila, Leptocythere* sp. A and *Tuberoloxoconcha* sp. 1. In the Tejo and Mira salt marsh *Ammonia beccarii*, *Ammonia tepida*, *Haynesina germanica*, *Jadammina macrescens*, *Trochammina inflata*, are the dominant foraminifera and *Loxoconcha malcomsoni, Terrestricythere* cf. *elisabethae, Tuberoloxoconcha* cf. *atlantica* and *Xestoleberis labiata* prevail as well as many other more marine ostracoda species, such as *Basslerites teres* and *Leptocythere fabaeformis*.

This study highlights that the knowledge of driven ecological parameters of modern assemblages (usually preserved in fossil record), is fundamental to support reliable paleoclimatic and paleoenvironmental reconstructions.

Resumo

Avaliação da salinidade e da temperatura da água nos sapais da costa Oeste de Portugal, na perspectiva da reconstrução paleoambiental com base na ecologia de Foraminíferos e Ostracodos.

O registo sazonal da temperatura e da salinidade da água dos estuários e da água intersticial dos sedimentos de sapal nos rios Minho, Tejo e Mira, durante a enchente, integram o estudo das associações de foraminíferos e ostracodos actuais da costa Oeste de Portugal. Nestes trabalhos podemos observar a transição entre o padrão climático húmido do NO da Península Ibérica e o padrão mediterrâneo a SO.

O sapal do baixo estuário do rio Minho tende a ser inundado por águas com grande amplitude de salinidade, de 0.5‰ a 32‰ em cada ciclo de maré, que persiste mesmo nas estações mais secas. No entanto o balanço hidrológico do sapal contribui para um ambiente relativamente estável, onde os valores da salinidade da água intersticial variam entre 8‰ e 16‰.

No baixo estuário do rio Mira, a salinidade das águas que inundam os sapais durante a preia-mar varia apenas entre 33‰ e 36‰, na Primavera, e entre 29‰ e 36‰ no Outono. O balanço da evaporação/ precipitação no contexto climático do Sul produz um aumento da salinidade da água intersticial até à hipersalinidade, que atinge 53‰ nos sapais do Tejo e 48‰ nos do Mira.

Estas diferenças das condições ambientais ao longo da costa Oeste de Portugal estão reflectidas na composição das associações dos organismos de sapal, nomeadamente dos foraminíferos e dos ostracodos. Sob as condições de baixa salinidade registadas no sapal de Caminha, a biocenose de foraminíferos é composta essencialmente pelas espécies de carapaça aglutinada *Haplophragmoides manilaensis*, *Miliammina fusca*, *Pseudothurammina limnetis Psammosphaera* sp. e *Trochamminita salsa/irregularis*. A associação dos ostracodos actuais inclui as espécies *Leptochytere baltica, Leptocythere psammophila, Leptocythere* sp. A e *Tuberoloxoconcha* sp. 1. Nos sapais do Tejo e do Mira as espécies *Ammonia beccarii*,

A. tepida, *Haynesina germanica*, *Jadammina macrescens*, *Trochammina inflata*, dominam a associação de foraminíferos, enquanto *Loxoconcha malcomsoni*, *Terrestricythere* cf. *elisabethae, Tuberoloxoconcha* cf. *atlantica* e *Xestoleberis labiata* se destacam numa associação de ostracodos com diversidade de espécies de características mais marinhas, como *Basslerites teres e Leptocythere fabaeformis*.

A relação encontrada entre a salinidade e a composição das associações de foraminíferos e ostracodos, mostra que a caracterização dos factores ecológicos e das biocenoses (dos grupos que integram o registo fóssil) em análogos actuais, são determinantes para a reconstituição fiável da evolução paleoclimática e paleoambiental.

Keywords: salinity, tidal marshes, foraminifera, ostracoda, Portuguese W coast.
Palavras-Chave: salinidade, sapais, foraminíferos, ostracodos, Costa Oeste de Portugal.

2.1. Introduction

Estuaries are highly productive environments but they also undergo intense impacts of human activities during the last century. The intertidal fringe is often occupied by salt marshes that represent one of the most suitable environments to search for the record of regional and global forcing mechanisms. Actually the almost constant sedimentation, that builds these zones, often represents the most continuous post-glacial geological record available on shore (e.g., Davis and Fitzgerald, 2004).

Since the 1950s several researchers studied salt marshes aiming to define environmental proxies, like foraminifera and ostracoda, to be used in paleoclimatic and paleogeographic interpretations, namely within the context of global change evaluation (e.g., Phleger and Walton, 1950; Pujos, 1971; Scott and Medioli, 1980; Gehrels 1994; de Rijk, 1995; Hayward et al., 1999; Cearreta et al., 2000, 2007; Horne and Boomer, 2000; Sen Gupta, 2002; Horton and Edwards, 2006; Murray, 2006; Cabral and Loureiro, 2013). Such applications of microfossils record rests upon the Principle of Actualism, which states that the composition of the micro-organisms assemblages strongly depends on the environmental biotic and abiotic parameters thereby making them reliable proxies. Consequently, their interpretation must be supported by a robust and site specific data base built upon the study of temperature, salinity, pH, dissolved oxygen, and $CaCO_3$ content (among others) that constrains the distribution of modern living communities (e.g., Moreno et al., 2005, 2007; Leorri et al., 2008; Fatela et al., 2009; Loureiro et al., 2009; Valente et al., 2009; Cabral and Loureiro, 2013).

In this paper we present the results of synoptic measurements of estuarine and interstitial waters temperature and salinity seen as main ecological parameters to the control of living tidal

marsh assemblages along the west Portuguese coast (e.g., Moreno et al., 2006, 2007; Fatela et al., 2007, 2009; Cabral and Loureiro, 2013).

2.2. Regional setting

The W coast of Portugal faces the NE Atlantic and develops approximately from 37º00′ N to 41º50′ N and between 8º40′ W and 9º30′ W, over more than 700 km long, often interrupted by many estuaries. The estuaries of Minho, Tejo (Tagus) and Mira were selected from those where preserved tidal marshes can be found in the lower estuary section.

Tides present a semi-diurnal high-mesotidal regime along this coast. The tidal range varies between 2 m, during neap waters, and almost 4 m in spring waters but the astronomical tide levels are often incremented by storm surges (Taborda and Dias, 1991).

The Minho River defines the political border with Spain along 77 km, joining the regions of Minho and Galicia (Figure 2.1) and discharging to the sea through a barred estuary trending NNE–SSW. The dynamic tide is felt up to 40 km upstream, due to the large tidal range and to both the smoothness and low gradient of the Minho's outlet (Alves, 1996). The upstream limit of marine water influence is not consensual and disparate distances of 9 to 35 km have been found (Bettencourt et al., 2003; Moreno et al., 2005).

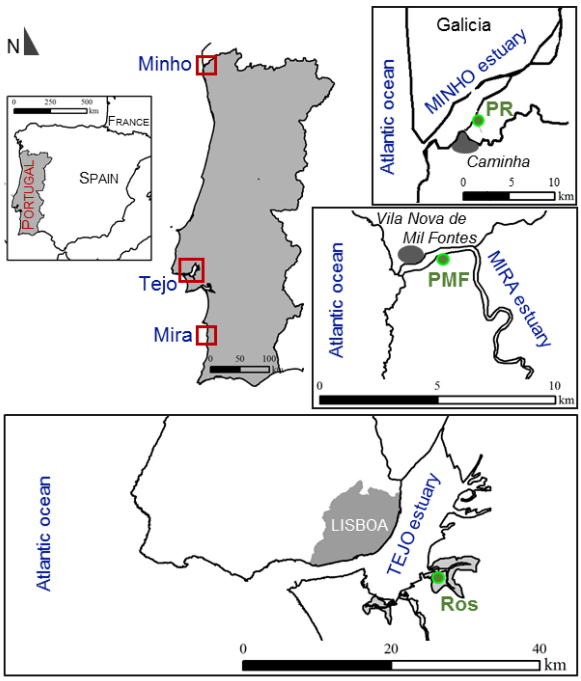

Estuary	Transect	Latitude	Longitude	Distance*
Minho	PR	N 41º 53' 18''	W 08º 49' 30''	4.0
Tejo	Ros	N 38º 40' 23''	W 09º 00' 45''	29.5
Mira	PMF	N 37º 43' 33''	W 08º46' 04''	2.0

* Distance to river mouth (km)

Figure 2.1. Location of studied salt marsh transects along the W coast of Portugal, in the estuaries of Minho (PR – Pedras Ruivas), Tejo (Ros – Rosário) and Mira (PMF – Ponte de Vila Nova de Mil Fontes).

The Minho watershed spans over 17,080 km^2 of igneous and metamorphic rocks basement, draining the rainiest region of Portugal. The average annual precipitation is *ca.* 1600 mm but exceptionally may reach 3500 mm (Fatela et al., 2014). The yearly average fluvial discharge is about 300 m^3/s and the winter peak discharge (December to March) usually exceeds 1000 m^3/s (Bettencourt et al., 2003).

The Tejo River has one of the largest estuaries of Western Europe, covering more than 325 km^2. Forty percent of this area emerges during low water spring. The hydrographical basin develops in Portugal and Spain over 81,310 km^2, occupied by a large variety of igneous, metamorphic, calcareous and detrital rocks. The average annual precipitation in the Portuguese sector of Tejo basin reaches *ca.* 900 mm. The fluvial average discharge is around 300 m^3/s, but may range out between 250 m^3/s and 5400 m^3/s under extreme dry or wet conditions (Bettencourt et al., 2003; ARH Tejo, 2011).

The dynamic tidal effects are felt up to a distance of 80 km upstream and the salt edges reaches 50 km upstream under the average flux of 300 m^3/s (Bettencourt et al., 2003).

Mira is an important river of SW Portugal whose hydrographical basin occupies an area of 1600 km^2 of mostly greywackes, pelites, slates, schists and conglomerates. The estuary extends from the mouth to SSE for almost 40 km of incised meanders, passing Odemira, where the dynamic effect of tide completely felts down (ICNB, 2008). Annual precipitation is around 645 mm, with a monthly average between 2.6 mm and 103 mm recorded in a series of 75 years. However, 0 mm is frequently record in summer (ICNB, 2008). The fluvial discharge ranges from 0 m^3/s during dry summers to 500 m^3/s in winter and spring rainy periods, leading to a yearly average fluvial discharge of 2.9 m^3/s. Tides are thus the main flow component in the Mira estuary (INAG, 2011).

2.3. Methods

Salinity and temperature of estuarine and sediment pore-water were measured along 3 low estuary transects in Minho (Pedras Ruivas – PR), Tejo (Rosário – Ros) and Mira (Ponte de Vila Nova de Mil Fontes – PMF) tidal marshes (Figure 2.1), under spring and autumn season conditions. The interstitial water was allowed to seep and accumulate inside perforated PVC tubes previously inserted into the sediment to a depth of 40 cm below the surface, following De Rijk (1995), and covered with aluminium foil between measurements. The salinity and temperature were also measured every 15 minutes, close to the marsh surface during the rising tide at PR (Minho) and PMF (Mira) transects. These measurements started just after the beginning of surface submersion and ended at high water slack, unless interrupted for safety reasons. Simultaneous measurement of the salinity and temperature of estuarine water has also been made close to the channel bottom, in high and low water during spring tide. Water parameters were measured using a multiparameters

Horiba U-22, a WTW LF 191 and 197i probes. The water salinity terms of limnetic, oligohaline, mesohaline, polyhaline, euhaline and hypersaline, used hereafter, follow the criteria defined by the Venice System (1959).

The altimetric data of the sampling profiles have been obtained using a Zeiss Elta R55 total station from a benchmark connected to the national altimetric datum (Cascais), using the GPS differential positioning combined with a regional geoid model and linked to local chart datum (e.g., Fatela et al., 2009).

2.4. Results

2.4.1. Marsh sediment interstitial water

2.4.1.1. Minho estuary

The temperature of Caminha marsh interstitial waters (PR) tends to have a stable pattern from tidal flat to high marsh. The main differences were found between spring (average: 11.5ºC) and autumn (average: 16.4ºC) temperatures, as shown in Table 2.1.

Table 2.1. Temperature and Salinity of Marsh Sediment Interstitial Water and Estuarine Water. PR – Pedras Ruivas; Ros – Rosário; PMF – Ponte De V.N. Mil Fontes; LT – Low Tide; HT – High Tide.

Temperature °C													
		PR1	PR2	PR3	PR4	PR5	PR6	PR7	PR8	PR9	PR10	LT	HT
MINHO	Spring		11.9			11.7	12.1	11.3	10.3			11.8	13.4
	Autumn					16.8	17.3	16.0	15.7		15.9	15.0	18.4
		Ros1	Ros2	Ros3	Ros4	Ros5	Ros6	Ros7	Ros8	Ros9	Ros10	LT	HT
TEJO	Spring	19.7			18.5					16.1			
	Autumn		15.2	14.4	14.0	14.5	12.6	14.1	14.3	13.7	13.6		13.0
		PMF1	PMF2	PMF3	PMF4	PMF5	PMF6	PMF7	PMF8	PMF9	PMF10	LT	HT
MIRA	Spring			16.9	17.2	16.1	16.3	14.7				18.2	17.7
	Autumn	16.3	16.0	15.2	15.1	14.9	14.5					15.7	17.0

Salinity ‰													
		PR1	PR2	PR3	PR4	PR5	PR6	PR7	PR8	PR9	PR10	LT	HT
MINHO	Spring		0.9			15.8	11.9	8.4	7.7			0.3	28.8
	Autumn					15.8	14.4	12.2	10.4		9.4	1.9	31
		Ros1	Ros2	Ros3	Ros4	Ros5	Ros6	Ros7	Ros8	Ros9	Ros10	LT	HT
TEJO	Spring	28.0			32.9					40.4			
	Autumn		31.6	33.2	33.1	39.5	31.8	28.4	52.9	45.7	23.6		29
		PMF1	PMF2	PMF3	PMF4	PMF5	PMF6	PMF7	PMF8	PMF9	PMF10	LT	HT
MIRA	Spring			37.0	23.2	43.3	30.6	11.7				32.8	35.8
	Autumn	33.8	33.7	35.9	42.0	47.5	28.8					29	36

The salinity measurements in the PR transect (Figure 2.2), under spring season conditions, yielded 0.9‰ in the subtidal domain, contrasting with low marsh values of 15.8‰ (PR5) and 7.7‰ of high marsh (PR10). This trend is maintained in autumn, but an increase in salinity values becomes clear (Figure 2.2) with 1.9‰ in the subtidal domain and 9.4‰ in the high marsh (PR10). The

maximum salinity of PR5 is the same as in spring but the other records of low marsh also arise (Table 2.1; Figure 2.2).

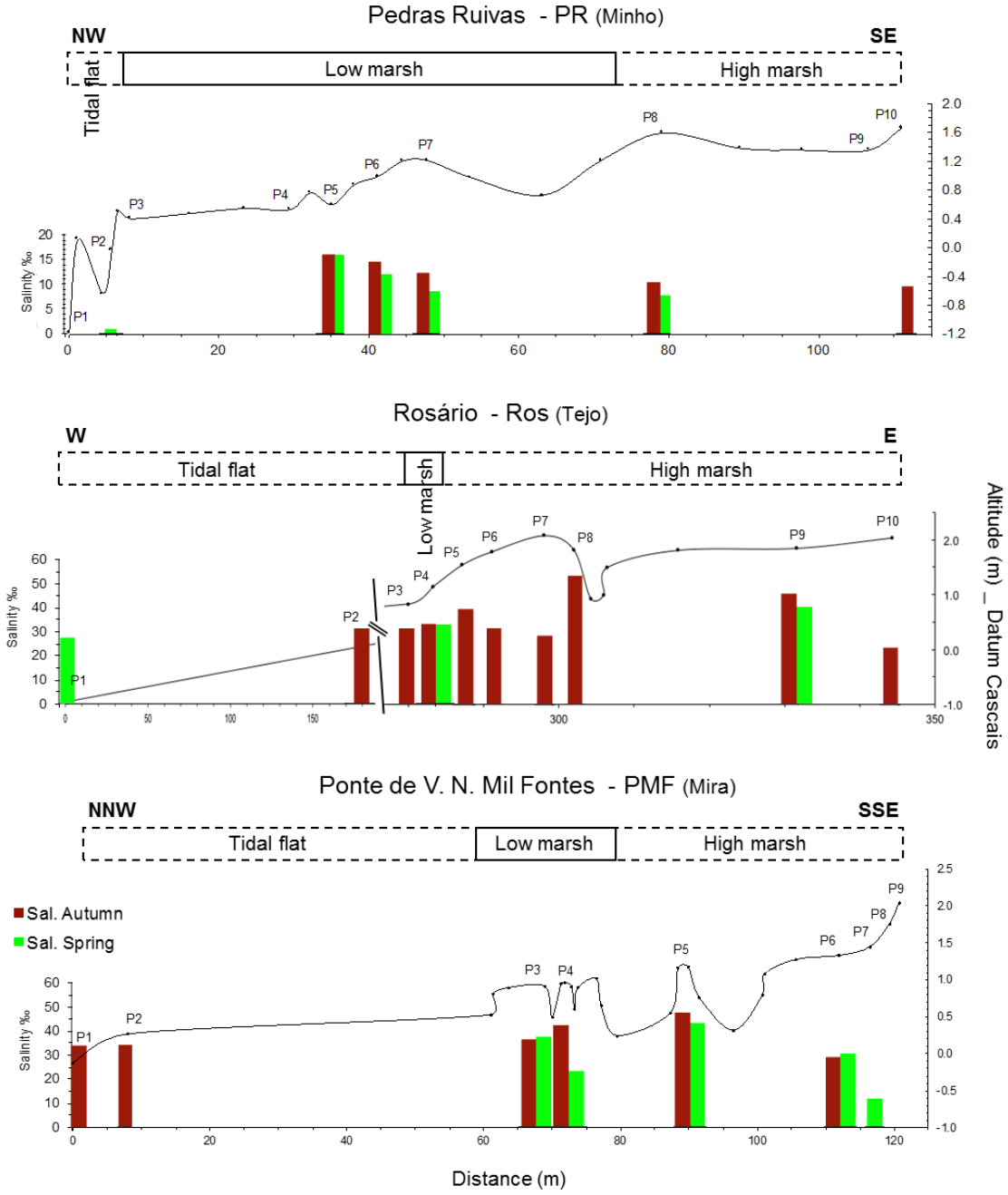

Figure 2.2. Sampling profiles of studied transects of Pedras Ruivas (PR – Minho), Rosário (Ros – Tejo) and Ponte de V.N. Mil Fontes (PMF – Mira), showing the measured spring and autumn salinity of sediment interstitial water.

2.4.1.2. Tejo estuary

At Rosário salt marsh the temperature of interstitial waters measured across the Ros transect is also very stable. The main differences are also related to season but reveal a reverse trend, when compared with Minho tidal marsh. The average temperature is higher in spring (18.1ºC) than in autumn (14.0ºC; Table 2.1).

The salinity measurements in the Ros transect (Figure 2.2), under spring season conditions, yielded 28‰ in the tidal flat (Ros1), 32.9‰ in the low marsh (Ros4) and 40.4‰ in the high marsh (Ros9). This direct relation of increasing salinity with altitude of the marsh surface is also clear in autumn (Figure 2.2), ranging from 31.6‰ in the tidal flat (Ros2) and 52.9‰ in the high marsh (Ros8). However, a significant drop to 23.6‰ is recorded at Ros10, in highest high marsh zone (Table 2.1).

2.4.1.3. Mira estuary

The stability of temperature in the marsh interstitial waters is also observed along the PMF transect (Table 2.1), with no significant difference between spring (average: 16.2ºC) and autumn (average: 15.3ºC) records.

The spring season salinity measurements in the PMF transect (Figure 2.2), yielded 32.8 ‰ in the subtidal domain, an average of 30.1‰ in the low marsh and a maximum of 43.3‰ (PMF5) in the high marsh. The relation of increasing salinity with altitude of the marsh surface is also clear in this transect, rising in autumn (Figure 2.2), except in the subtidal domain (33.8‰). Average salinity record rises to 38.9‰ in the low marsh and reaches new maximum of 47.5‰ (PMF5) in the high marsh. In both seasons a significant drop to 11.7‰ and 28.8‰, respectively, is recorded at the transition to highest high marsh zone (Table 2.1). All the sampling points from the highest high marsh were dry, in both spring and autumn campaigns, avoiding the measurement of interstitial water parameters.

2.4.2. Tidal marsh flooding water

2.4.2.1. Minho estuary

The Minho lower estuary records a wide range salinity twice a day (Moreno et al., 2005) resulting from the balance between river flow and tidal regime. The measurements close to the sediment surface across the PR transect, during its submersion by a spring tide, show that from the arrival of estuarine water at each sampling point until the complete flooding of the marsh, the salinity values at the sediment – water interface ranged from 0.5‰ to 31.6‰ in the tidal flat, 3.1‰ to 31.6‰ in the low marsh and 7.0‰ to 23.1‰ in the high marsh (Figure 2.3).

2.4.2.2. Mira estuary

In the Mira lower estuary the tidal regime do not force a marked wide range of salinity. Our records show that in autumn the salinity ranges between 28.6‰ and 35.5‰, and between 32.8‰ and 35.8‰ in spring season.

The measurements performed during a rising spring tide across the PMF transect, show that from the arrival of estuarine water at each sampling point until the complete flooding of the marsh,

the salinity values at the sediment – water interface range from 35.4‰ to 36.0‰ in the tidal flat, 35.0‰ to 39.8‰ in the low marsh and 35.4‰ to 36.5‰ in the high marsh (Figure 2.3).

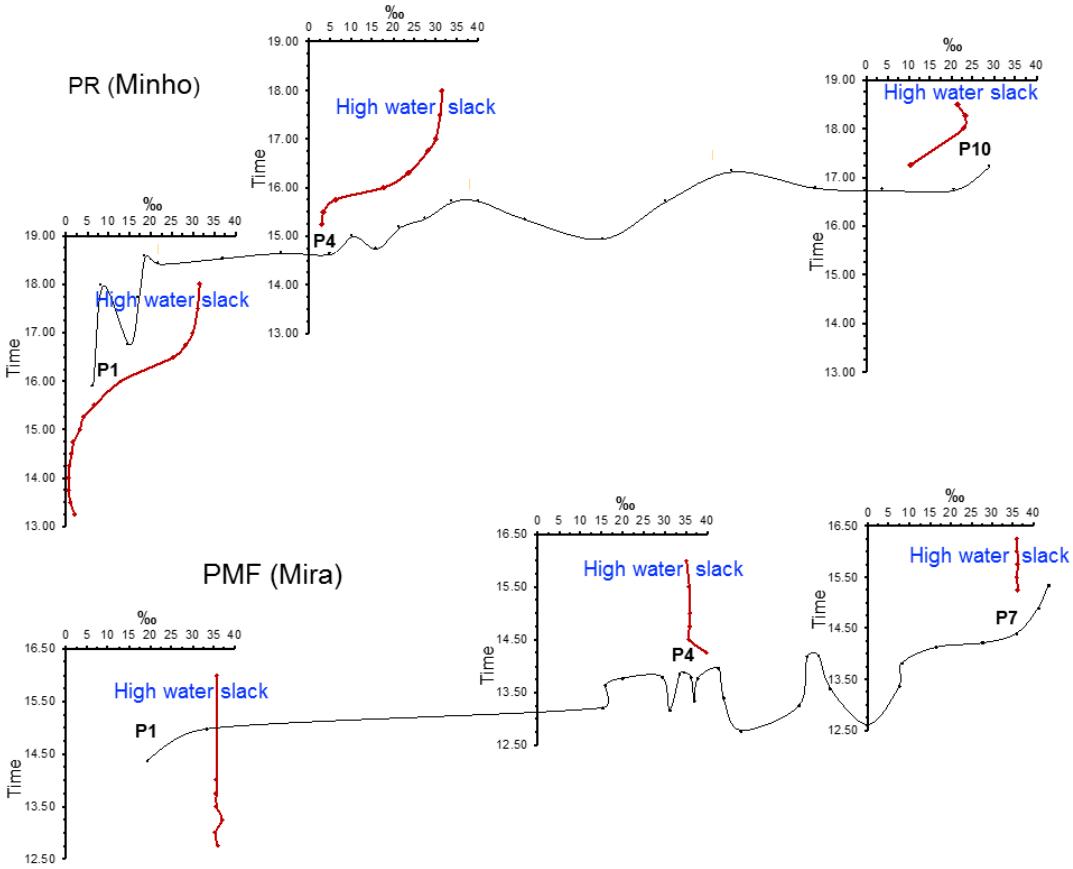

Figure 2.3. Example of water salinity variation along tidal flat, low marsh and high marsh, during the spring tide flooding, in the Minho and Mira low estuaries.

2.5. Discussion

A distinctive attribute of the W coast of Portugal is the transition from the warm and rainy Atlantic to the hot and dry Mediterranean climate across a distance of around 400 km, in a narrow range of latitude. That means that estuarine environments and hydrographic basin are constrained by a C_{fb} climate type (temperate, with warm summer and no dry season) at North, and C_{sa} climate type (temperate with hot and dry summers) at South (Peel et al., 2007).

The temperature of marsh sediment interstitial waters is quite stable across all transects for the same site and campaign. So when differences appear, they are directly connected with seasonality of climate in the temperate regions. The climatic fingerprint is also noted in the North to South increasing temperatures when the Caminha records are compared with Tejo and Mira marsh interstitial waters.

In the northern estuary of Minho River, the penetration of salt edge faces the resistance of lower basin morphology and of hydrological features resulting from the climate type mentioned above. On one hand, a widespread siltation has led to a very shallow estuary, with a very limited

volume to hold the tidal prism. On the other hand, the intense and long precipitation regime generates a persistent runoff. In summer, under spring tide conditions, the euhaline water (30‰ to 35‰) penetrates less than 5 km upstream during high tide (Moreno et al., 2005). However, at low tide the sea water is completely flush out, with prevailing oligohaline conditions (0.5‰ to 5‰) all over the lower estuary (Figure 2.4). In the rainy spring time, at spring high tide, the same domain is occupied by 29‰ to 26‰ waters (polyhaline), from the mouth to less than 5 km upstream. During low tide freshwater prevails and the most part of the estuary acquires limnetic conditions with 0‰ to 0.5‰ (Figure 2.4). Nevertheless, the daily salinity dynamic stress is considerably smoothed inside the marsh sediment. The salinity of tidal flooding waters is retained in the sediment pore water according to the submersion time, freshwater seepage from up-land and evaporation/precipitation balance. In the Caminha tidal marsh the highest salinity (mesohaline) is found in the transition from low to high marsh zone (Figure 2.3) as a result of a longer submersion with euhaline water. At the high water slack the top of high marsh tends to be flooded by polyhaline water, resulting from the less dense brackish mixture from Coura drainage, which is pushed onto the upland margin of Caminha tidal marsh. Moreover, interstitial high marsh water salinity is more affected by dilution with precipitation and freshwater inflow from surrounding land and groundwater.

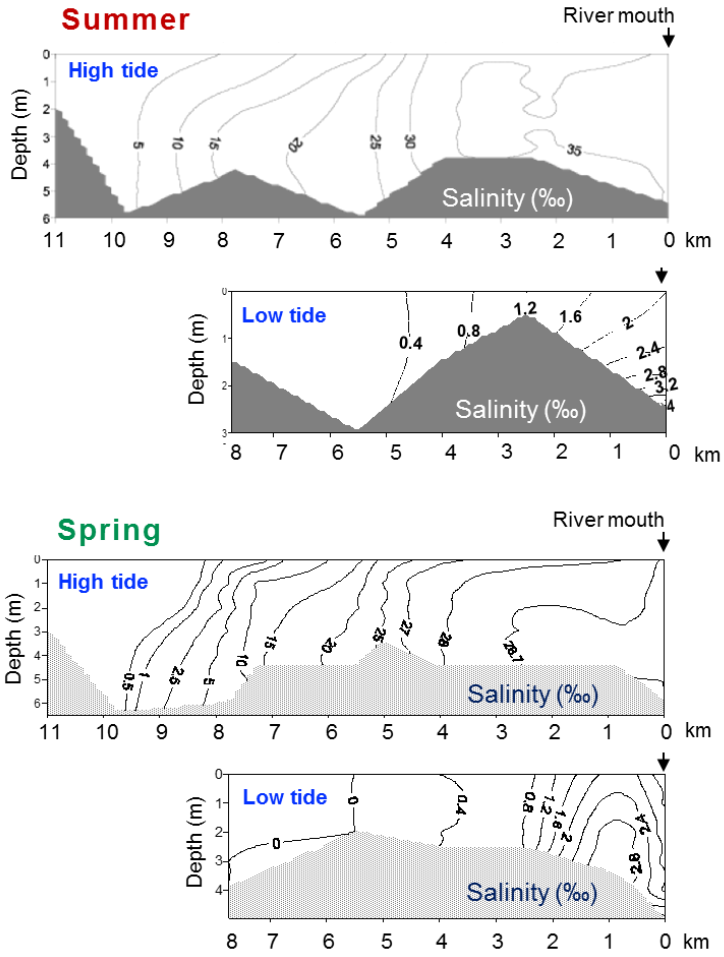

Figure 2.4. Seasonal salinity profiles of Minho low estuary under summer and spring season conditions.

In the Tejo and Mira marsh sediment interstitial waters the salinity values are higher than in Caminha tidal marsh. The low marshes of those southern estuaries are impregnated with euhaline waters that became hypersaline in the high marsh. There is a clear direct relation between pore-water (interstitial water) salinity and marsh surface altitude. However, altitude is not a factor by itself but reflects the true process reducing the time submersion by tidal flooding waters from tidal flat to the high marsh. After the tidal retreat the higher zones are exposed for a longer period where evaporation prevails due to the hotter and dryer season's conditions felt in southern estuaries.

The Mira lower estuary tends to preserve a body of euhaline water even in low tides (Blanton and Andrade, 2001). Under spring season conditions, low marsh may be covered by hypersaline water in the beginning of the flooding tide, tending to the euhaline conditions in the high tide (Table 2.1; Figure 2.3). This record reflects the importance of evaporation during low tide and the consequent precipitation of salt on the tidal flat and marsh surfaces. The rising tide dissolves this precipitated salt increasing significantly the salinity of the early flooding waters. By contrast in the Caminha tidal marsh we have recorded a gradual salinity increase, from limnetic to euhaline, in tidal flooding waters.

The Tejo and Mira salt marshes also record a relative decrease of pore-water salinity in the highest high marsh, suggesting that dilution by fresh-water inflow from surrounding land and groundwater in the upland transition may be present under the dryer conditions of C_{sa} climate type.

A seasonal cycle was found in the salinity of marsh interstitial water that leads to salt concentration in sediment during the dryer and hotter months (autumn records), and a dilution during the rainy and colder months (spring records), reflecting the evaporation/precipitation balance along the W coast.

Salinity is very important for the metabolism of organisms, namely by osmosis (Murray, 2006) and for the production of carbonated tests. This influence is very clear in the composition and distribution of foraminifera and ostracoda assemblages. They may tolerate a wide range of salinity, from limnetic to hypersaline conditions, but most species are found under euhaline conditions, where the assemblages exhibit the highest diversity (e.g., Haq and Boersma, 1978; Boomer and Eisenhauer, 2002; Sen Gupta, 2002; Frenzel and Boomer, 2005; Murray, 2006).

The salt marsh foraminiferal assemblages under low salinity conditions are essentially composed by agglutinated species. For instance, the Caminha salt marsh assemblages of living foraminifera include species like *Haplophragmoides manilaensis* Andersen, 1953, *Miliammina fusca* (Brady, 1870), *Pseudothurammina limnetis* (Scott and Medioli, 1980), *Psammosphaera* sp., *Trochamminita salsa/irregularis* (Cushman and Brönnimann, 1948) and *Polysaccammina ipohalina* Scott, 1976. When the salinity of marsh sediment rises till polyhaline to hypersaline conditions, as found in Tejo and Mira estuaries, they are replaced by *Ammonia beccarii* (Lineaus, 1758), *Ammonia tepida* (Cushmann, 1926), *Haynesina germanica* (Ehrenberg, 1840), *Jadammina macrescens*

(Brady, 1870), *Trochammina inflata* (Montagu,1808), *Tiphotrocha comprimata* (Cushman and Brönnimann, 1948)*, Paratrochammina guaratibaensis* (Brönnimann, 1986) and *Siphotrochammina lobata* Saunders, 1957, among other minor species (e.g., Hayward et al., 1999; Debenay et al., 2000; Scott et al., 2001; Sen Gupta, 2002; Moreno et al., 2006; Fatela et al., 2009, 2014). The same trend is clearly shown by Cabral and Loureiro (2013), among other authors, in the distribution of modern ostracoda assemblages. For instance, the brackish species found in the Caminha tidal marsh, like *Leptochytere baltica* Klie, 1929*, Leptocythere psammophila* Guillaume, 1976, *Leptocythere* sp*.* A and *Tuberoloxoconcha* sp. 1 are replaced by a diverse assemblage in the Tejo and Mira salt marshes, under euhaline to hypersaline conditions, composed by *Loxoconcha malcomsoni* Horne and Robinson, 1985, *Tuberoloxoconcha* cf. *atlantica* Horne, 1989, *Terrestricythere* cf. *elisabethae* Horne, Smith, Whittaker and Murray, 2004, *Xestoleberis labiata* Brady and Robertson, 1874 and many other more marine species such as *Basslerites teres* (Brady, 1869) and *Leptocythere fabaeformis* (G. W. Müller, 1894) (e.g., Loureiro et al., 2009; Cabral and Loureiro, 2013).

The knowledge of the influence of environmental parameters in the ecology of modern foraminifera, ostracoda, and many other groups, is a fundamental requirement to develop reliable paleoenvironmental reconstructions.

2.6. Conclusions

The different climatic features recognized from the N to the S of Portugal introduces significant differences in the hydrological balance of W coast estuaries. The contribution of freshwater drainage to the estuarine waters is reflected in the tidal marshes interstitial water parameters. The seasonal cycle is also well marked either the NW, under warm summers and no dry season (C_{fb} climate type) or the SW, under hot and dry summers (C_{sa} climate type).

The tidal flooding waters that cover the salt marshes are not homogeneous. In the Minho low estuary the salinity may range between limnetic to euhaline conditions in the same tidal cycle. However, in the interstitial water mesohaline conditions prevail, under both the spring and autumn seasons, showing that tidal marsh may offer a relatively stable environment when compared with the extreme daily salinity variation of the lower estuary.

In contrast, the Tejo and Mira salt marsh flooding waters tend to keep euhaline characteristics, although they can be slightly polyhaline in the rainy season. Such conditions and the control of evaporation/precipitation balance are responsible by an enhanced euhaline to hypersaline interstitial marsh waters.

These environmental contrasts are clearly reflected in the composition and distribution of tidal marsh assemblages. Namely, foraminifera and ostracoda that tend to be dominated by low-salinity

tolerant species in the low estuaries from NW and by high salinity tolerant species in the low estuaries of SW coast.

This data from Portuguese marshes represent a reliable support for the interpretation of the geological record in a regional, as well as global context, of paleoclimatic and paleoenvironmental reconstructions of east North Atlantic estuaries.

Acknowledgments

This paper is a contribution of the MicroDyn (POCTI/CTA/45185/2002) and WestLog (PTDC/CTE/105370/2008) projects, funded by the Fundação para a Ciência e a Tecnologia – FCT. João Moreno benefits from a PhD grant (SFRH/BD/87995/2012) from FCT. We would like to thank our colleagues Anabela Cruces, Filipa Moreno, João Cascalho, Catarina Fradique, Celso Pinto, Tanya Silveira, Francisca Rosa, Catarina Guerreiro, Vera Lopes, Raquel Cardoso and Ana Rita Figueiredo, among other for assistance laboratory and field work.

References

ALVES, A. 1996. *Causas e Processos da Dinâmica Sedimentar na Evolução Actual do Litoral do Alto Minho*. Unpublished PhD Thesis, Univ. Minho, Braga, Portugal. 442p.

ARH Tejo, 2011. *United Nations World Water Development Report. World Water Assessment Programme (UNESCO). The Tagus River Basin District – Portugal. Case Study*. Edited by Ministério da Agricultura, Mar, Ambiente e Ordenamento do Território / Administração da Região Hidrográfica do Tejo I.P.

BETTENCOURT, A., RAMOS, L., GOMES, V., DIAS, J.M.A., FERREIRA, G., SILVA, M. & COSTA, L. 2003. *Estuários Portugueses*. Ed. INAG – Ministério das Cidades, Ordenamento do Território e Ambiente, Lisboa. 311p.

BLANTON, J.O. & ANDRADE, F.A. 2001. Distortion of tidal currents and the lateral transfer of salt in a shallow coastal plain estuary (O estuário do Mira, Portugal). *Estuaries*, 24: 467–480.

BOOMER, I. & EISENHAUER, G. 2002. Ostracod faunas as palaeoenvironmental indicators in marginal marine environments. In: Holmes, J.A. and Chivas, A.R. (Eds.). *The Ostracoda applications in Quaternary Research*. American Geophysical Union, Washington, DC, Geophysical Monograph, 131: 135–149.

CABRAL, M.C. & LOUREIRO, I.M., 2013. Overview of Recent and Holocene ostracods (Crustacea) from brackish and marine environments of Portugal. *Journal of Micropalaeontology,* 32 (2): 135–159.

CEARRETA, A., IRABIEN, M.J., LEORRI, E., YUSTA, I., CROUDACE, I.W. & CUNDY, A.B., 2000. Recent anthropogenic impacts on the Bilbao estuary, N. Spain: Geochemical and microfaunal evidence. *Estuarine, Coastal and Shelf Science,* 50: 571–592.

CEARRETA, A., ALDAY, M., FREITAS, M.C. & ANDRADE, C., 2007. Postglacial foraminifera and paleoenvironments of the Melides Lagoon (SW Portugal): to-wards a regional model of coastal evolution. *Journal of Foraminiferal Research*, 37: 125–135.

DAVIS, R. JR. & FITZGERALD, D. 2004. *Beaches and Coasts*. Blackwell Publishing Company, 419p.

DEBENAY, J.–P., GUILLOU, J-J., REDOIS, F. & GESLIN, E. 2000. Distribution Trends of Foraminiferal Assemblages in Paralic Environments – A Base for Using Foraminifera as Bioindicators. In: Martin, R.E. (Ed.), *Environmental Micropaleontology - The Application of Microfossils to Environmental Geology*. Kluwer Academic/Plenum Publishers, pp. 39–67.

DE RIJK, S. 1995. Salinity control on the distribution of salt marsh Foraminifera (Great Marshes, Massachusetts). *Journal of Foraminiferal Research,* 25: 156–166.

FATELA, F., MORENO, J., MORENO, F., ARAÚJO, M.F., VALENTE, T., ANTUNES, C., TABORDA, R., ANDRADE, C. & DRAGO, T. 2009. Environmental constraints of foraminiferal assemblages distribution across a brackish tidal marsh (Caminha, NW Portugal). *Marine Micropaleontology*, 70 (1-2): 70–88.

FATELA, F., MORENO, J. & ANTUNES, C. 2007. Salinity influence on foraminiferal tidal marsh assemblages of NW Portugal: an anthropogenic constraint? *Thalassas,* 23: 51–63.

FATELA, F., MORENO, J., LEORRI, E. & CORBETT, R. 2014. High marsh foraminiferal assemblages response to intra-decadal and multi-decadal precipitation variability, between 1934 and 2010 (Caminha, NW Portugal). *Journal of Sea Research,* 93: 118–132.

FRENZEL, P. & BOOMER, I. 2005. The use of ostracods from marginal marine, brackish waters as bioindicators of modern and Quaternary environmental change. *Palaeogeography*, *Palaeoclimatology*, *Palaeoecology*, 225: 68–92.

GEHRELS, W.R., 1994. Determining relative sea level change from salt marsh foraminifera and plant zones on the coast of Maine, USA. *Journal of Coastal Research*, 10: 990–1009.

HAQ, B.U. & BOERSMA, A. 1978. *Introduction to marine micropaleontology*. Elsevier, 387p.

HAYWARD, B.W., GRENFELL, H.R., REID, C.M. & HAYWARD, K.A. 1999. Recent New Zealand shallow-water benthic foraminifera: taxonomy, ecologic distribution, biogeography, and use in paleoenvironmental assessment. *Institute of Geological & Nuclear Sciences monograph*, 21. Lower Hutt, New Zealand, 264p.

HORNE, D.J. & BOOMER, I. 2000. The Role of Ostracoda in Saltmarsh Meiofaunal Communities. In: Sherwood, B.R., Gardiner, B.G. and Harris, T. (Eds), *British Saltmarshes*, Forrest Text, Cardigan, for the Linnean Society of London, pp. 182-202.

HORTON, B.P. & EDWARDS, R.J. 2006. Quantifying Holocene sea-level change using intertidal foraminifera: lessons from the British Isles. *Cushman Foundation for Foraminiferal Research,* sp. pub. 40, 97p.

ICNB, 2008. *Plano de ordenamento do Parque Natural do Sudoeste Alentejano e Costa Vicentina; Estudo base – Etapa 1*. Instituto da Conservação da Natureza e da Biodiversidade, 287p.

INAG, 2011. Instituto Nacional da Água (http://www.inag.pt/estuarios/MenusEstuarios/Descri%C3%A7%C3%A3o/descricao_Mira.htm) 22.06.2011

LOUREIRO, I.M., CABRAL, M.C. & FATELA, F. 2009. Marine influence in Ostracod assemblages of the Mira River estuary: comparison between lower and mid estuary tidal marsh transects. *Journal of Coastal Research*, SI 56: 1365–1369.

LEORRI, E., HORTON, B.P. & CEARRETA, A. 2008. Development of a Foraminifera-Based Transfer Function in the Basque Marshes, N. Spain: Implications for Sea-Level Studies in the Bay of Biscay. *Marine Geology*, 251: 60–74.

MORENO, J., FATELA, F., ANDRADE, C., CASCALHO, J., MORENO, F. & DRAGO, T. 2005. Living Foraminiferal assemblages from Minho/Coura estuary (Northern Portugal): a stressfull environment. *Thalassas*, 21: 17–28.

MORENO, J., FATELA, F., ANDRADE, C. & DRAGO, T. 2006. Distribution of "living" *Pseudothurammina limnetis* (Scott and Medioli): an occurrence on the brackish tidal marsh of Minho/Coura estuary – Northern Portugal. *Révue de Micropaléontologie*, 49: 45–53.

MORENO, J., VALENTE, T., MORENO, F., FATELA, F., GUISE, L., & PATINHA, C. 2007. Calcareous Foraminifera occurrence and calcite-carbonate equilibrium conditions – a case study in Minho/Coura estuary (N Portugal*). Hydrobiologia,* 597: 177–184.

MURRAY, J.W., 2006. *Ecology and Applications of Benthic Foraminifera*. Cambridge University Press, 438p.

PEEL, M.C., FINLAYSON, B.L. & MCMAHON, T.A. 2007. Updated world map of the Köppen-Geiger climate classification. *Hydrology and Earth System Sciences,* 11: 1633–1644.

PHLEGER, F.B. & WALTON, W.R. 1950. Ecology of marsh and bay foraminifera, Barnstable, Massachussetts. *American Journal of Science,* 248: 274–294.

PUJOS, M. 1971. Foraminifères et thecamoebiens de la Gironde: leur intérêt dans la mise en évidence des biotopes estuariens. *Compte Rendus de l'Académie de Sciences de Paris*, 273: 1095–1097.

SCOTT, D.B. & MEDIOLI, F.S. 1980. Quantitative studies of marsh foraminiferal distribution in Nova Scotia: implications for sea level studies. *Cushman Foundation for Foraminiferal Research*, sp. pub. 17, 58p.

SCOTT, D.B., MEDIOLI, F.S. & SCHAFER, C.T. 2001. *Monitoring in coastal environments using foraminifera and thecamoebian indicators*. Cambridge Univ. Press, 177p.

SEN GUPTA, B. 2002. Foraminifera in marginal marine environments. In: Sen Gupta, B. (Ed.), *Modern Foraminifera*. Kluwer Academic Publishers: pp. 141–159.

TABORDA, R. & DIAS, J.M.A. 1991. Análise da sobre-elevação do nível do mar de origem meteorológica durante os temporais de 1978 e 1981. *Geonovas* sp. n. 1: 89–97.

VALENTE, T., FATELA, F., MORENO, J., MORENO, F., GUISE, L. & PATINHA, C. 2009. A comparative study of the influence of geochemical parameters on the distribution of foraminiferal assemblages in two distinctive tidal marshes. *Journal of Coastal Research*, SI 56; 1439–1443.

VENICE SYSTEM, 1959. The final resolution of the Symposium on the Classification of Brackish Waters. *Archivio di Oceanografia e Limnologia*, 11, supplement: 243–248.

3 High marsh foraminiferal assemblages' response to intra-decadal and multi-decadal precipitation variability, between 1934 and 2010 (Minho, NW Portugal)

Francisco Fatela [a,b,*], João Moreno [a,b], Eduardo Leorri [a,c], Reide Corbett [c]

[a] Universidade de Lisboa, Centro de Geologia_CeGUL, Campo Grande, 1749-016 Lisboa, Portugal

[b] Universidade de Lisboa, Faculdade de Ciências, Departamento de Geologia, Campo Grande, 1749-016 Lisboa, Portugal

[c] East Carolina University, Department of Geological Sciences, Greenville, NC 27858-4353, USA

Published in: *Journal of Sea Research* 93 (2014), 118–132

http://dx.doi.org/10.1016/j.seares.2013.07.021

"Microfossils are ideally suited to environmental studies because their short generation times allow them to respond quickly to environmental change."

R.E. Martin in ENVIRONMENTAL MICROPALEONTOLOGY (2000), p. xi.

ABSTRACT

Foraminiferal assemblages of Caminha tidal marshes have been studied since 2002 revealing a peculiar dominance of brackish species, such as *Haplophragmoides manilaensis*, *Haplophragmoides wilberti*, *Haplophragmoides* sp., *Pseudothurammina limnetis* and *Trochamminita salsa/irregularis* in the high marshes of the Minho and the Coura lower estuaries. The assemblage composition reflects low salinity conditions, despite the short distance to the estuarine mouth (~4 km). However, in May 2010, the presence of salt marsh species *Trochammina inflata* and *Jadammina macrescens* became very significant, likely a result of 5 consecutive dry years and a corresponding salinity rise in sediment pore water. Correspondence analysis (CA) groups the surface samples according to their marsh zone, showing a positive correlation with the submersion time of each sampling point. The brackish- and normal-salinity foraminiferal species appear separated in the CA. This observation was applied to the top 10 cm of a high marsh sediment core that corresponds to the period of instrumental record of precipitation and river flow in the Minho region. We found that river flow strongly

correlates with precipitation in the Lima and Minho basins. The longer precipitation record was, therefore, used to interpret the foraminiferal assemblages' variability.

Three main phases were distinguished along *ca.* 80 years of precipitation data: 1) negative anomalies from 1934 to 1957; 2) positive anomalies from 1958 to 1983; and 3) negative anomalies from 1984 to 2010. This last dryer period exhibits the precipitation maximum and the greatest amplitude of rainfall values. High marsh foraminifera reveals a fast response to these short-term shifts; low-salinity species relative abundance increases when precipitation increases over several decades, as well as in the same decade, in the years of heavy rainfall of dryer periods. High marsh foraminifera records the increase of freshwater flooding and seepage by 1) decreasing abundance and 2) increasing the dominance of low-salinity species. On the other hand, low precipitation over *ca.* 5 years increases the assemblage productivity and the relative abundance of normal-salinity species.

The negative correlation found between winter precipitation and the winter NAO index indicates that the Minho region is a part of the North Atlantic climate dynamics and demonstrates that the foraminiferal record from Caminha high marsh may be applied in high-resolution studies of SW Europe climate evolution.

Keywords: Modern foraminifera; high marsh; multi-decadal precipitation; SW Europe.

3.1. Introduction

The study of benthic foraminiferal assemblages from tidal marsh ecosystems undertaken in the last several decades clearly highlights their value as environmental proxies (e.g., Gehrels et al., 2001; Hayward et al., 1999; Martin, 2000; Martin et al., 2002; Murray, 1991, 2006; Phleger and Bradshaw, 1966; Phleger and Walton, 1950; Pujos, 1971, 1976; Scott et al., 2001; Sen Gupta, 2002).

The development of marsh foraminiferal studies has provided insights into paleoecological information, mainly concerned with climate dynamics, sea-level rise, and the evolution of coastal zones under natural or anthropogenic influence (e.g., Alve, 1995; Armynot du Châtelet et al., 2004; Callard et al., 2011; Cearreta et al., 2008; Fatela et al., 2007; Gehrels, 1994, 2000; Hippensteel et al., 2002; Horton and Edwards, 2006; Horton et al., 1999; Kemp et al., 2011; Leorri et al., 2010a, 2011; Moreno et al., 2005; Scott and Medioli, 1980). This micropaleontological information, when sufficiently preserved in the sedimentary record, tied to high precision instrumental data and analyzed with robust statistical analysis, can provide reliable paleoenvironmental reconstructions (e.g., Callard et al., 2011; Cearreta et al., 2002b, 2007, 2008; Diz et al., 2002; Gehrels, 1994; Gehrels et al., 2001; Hippensteel et al., 2002; Horton and Edwards, 2000, 2006; Kemp et al., 2009; Leorri et al., 2010b, 2011; Martin, 2000; Williams, 1994).

Climate, geological structures and lithology, and geomorphological conditions of the drainage basin and the hydrodynamics of an estuary control the marine influence in its lower reaches, imposing a geochemical signature in estuarine waters as well as in the marsh sediments and

interstitial waters. The composition and distribution of foraminiferal assemblages reflect these abiotic characteristics of a tidal marsh ecosystem, as well as their evolution controlled by regional and global changes and responding to anthropogenic impacts of the estuary over time (e.g., Alve, 1995; Armynot du Châtelet et al., 2004; Cearreta et al., 2000, 2002a,b; De Rijk, 1995; De Rijk and Troelstra, 1997; Diz et al., 2002; Fatela et al., 2007, 2009; Hayward et al., 1999; Kemp et al., 2011; Moreno et al., 2005, 2006, 2007). The contribution of tidal marsh foraminiferal assemblages to paleoenvironmental studies has been recognized worldwide (e.g., Callard et al., 2011; Fatela et al., 2009; Hayward et al., 1999; Horton and Murray, 2007; Kemp et al., 2011; Murray, 1971; Phleger and Walton, 1950), but when analyzed in detail, regional differences must be accounted for to achieve accurate interpretations (e.g., Callard et al., 2011; Fatela et al., 2009; Leorri and Cearreta, 2009; Leorri et al., 2008, 2010a, 2011).

The distribution of foraminiferal assemblages across a tidal marsh is linked to the tidal flooding (a direct constraint of ecological factors such as salinity and desiccation) that, in turn, correlates well with elevation. Foraminiferal assemblages gradually reduce the number of species from tidal flat (submersion time > 50%) to high marsh (submersion time < 6%) where *Trochammina inflata* (Montagu, 1808) and *Jadammina macrescens* (Brady, 1870) are usually dominant (e.g., Phleger and Bradshaw, 1966; Scott and Medioli, 1980; Sen Gupta, 2002) in the lower reaches of the estuaries (i.e., greater marine influence). This is not the case in the Minho and the Coura estuaries where high tide covers the marsh with brackish water. The high marsh foraminiferal assemblages are dominated by *Haplophragmoides manilaensis* (Andersen, 1953), *Haplophragmoides* sp., *Trochamminita salsa* (Cushman and Brönnimann, 1948), *Trochamminita irregularis* (Cushman and Brönnimann, 1948), and *Pseudothurammina limnetis* (Scott and Medioli, 1980) (see Fatela et al., 2007, 2009; Moreno et al., 2005, 2006). We believe that high marsh represents an extreme environment where foraminiferal species, though euryhaline and eurythermic, are at the limit of their environmental tolerance. Consequently, a global and regional overview of these proxies must be supported by regional or local studies.

3.2. Regional setting

The Minho River originates at Serra da Meira, in the province of Lugo (Spain). After approximately 300 km, the Minho River flows into the NE Atlantic, in the northwest coast of the Iberian Peninsula. It defines the political border between Portugal and Spain along the last 77 km of its course, dividing the Portuguese region of Minho and the Spanish region of Galicia (Figure 3.1).

The Minho watershed drains an area of 17,080 km^2 dominated by igneous and metamorphic rocks, namely granites, greywackes and schists. It drains the rainiest region of Portugal, where the average annual precipitation in the Portuguese basin is higher than 1600 mm, but may reach more than 3500 mm. The yearly average fluvial discharge is approximately 300 m^3/s and the winter peak

discharge (December to March) usually exceeds 1000 m^3/s, with a 100 year recurrence interval recorded at 6100 m^3/s (Bettencourt et al., 2003).

The Minho River discharges to the sea through a barred estuary trending NNE–SSW. It presents a semi-diurnal high meso-tidal regime with an astronomical tidal range of 2 m, during neap waters, and almost 4 m in spring tides. The high-water astronomic tidal levels are often accentuated by storm surges (Taborda and Dias, 1991). The dynamic tide is felt up to 40 km upstream, due to the large tidal range and the smoothness and low gradient of the Minho's outlet (Alves, 1996). The upstream limit of marine water influence has been reported between 9 km and 35 km (Bettencourt et al., 2003; Fatela et al., 2009). The lower estuary section just extends a few kilometers from the mouth and essentially behaves as "partially mixed" (Brown et al., 1991). This section is very shallow as a result of widespread siltation and, therefore, a significant part of the bottom emerges during low water spring tide. A large tidal flat and tidal marsh surface of around 6 km^2 have developed in the margins. The widest marsh expansion in the left margin of the Minho estuary occurs at the confluence with the Coura River (hereafter referred to as the Caminha tidal marsh – Figure 3.1). This site provides exceptional conditions to investigate the distribution of foraminiferal assemblages and their environmental constraints, from seasonal to decadal time scales (sedimentary record).

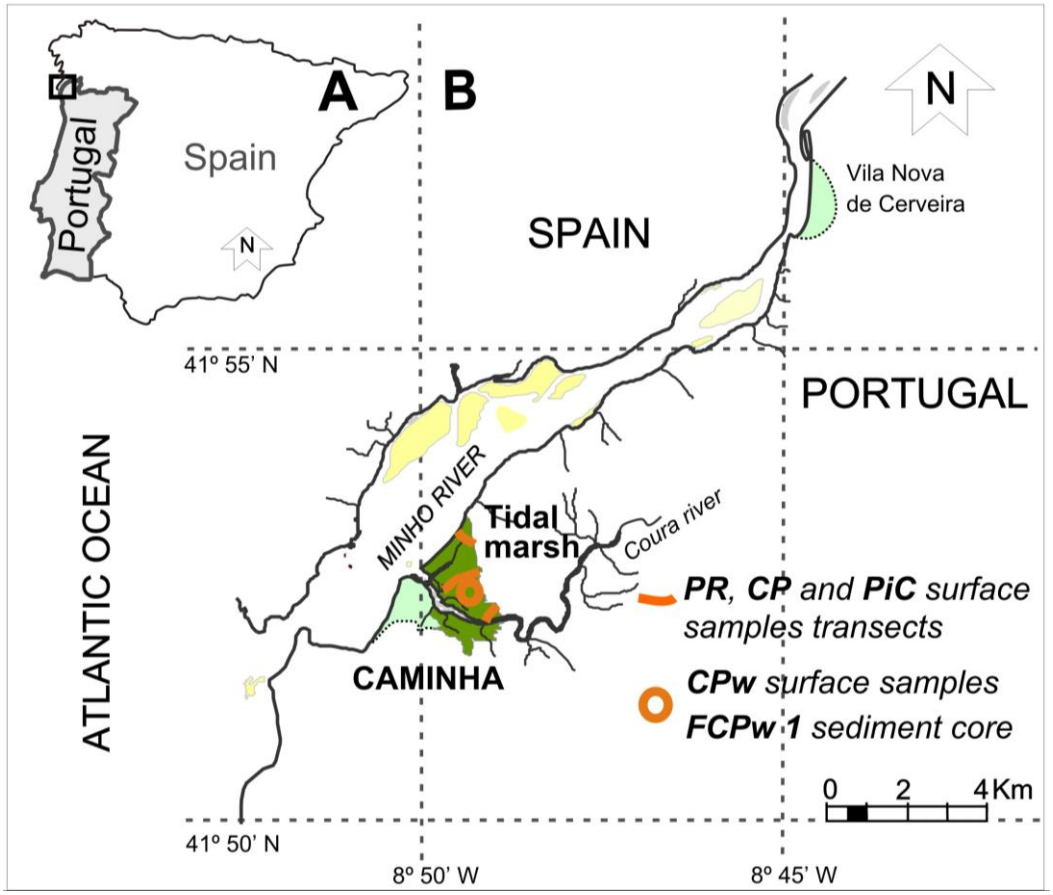

Figure 3.1. A – Location of study area in Portugal. **B –** Minho estuary and Coura tributary. Green area represents the Caminha tidal marsh.

3.3. Material and methods

Twenty eight surface sediment samples were collected in April (spring) 2002 along three transects: Pedras Ruivas (PR), Railway Bridge (CP) and Pinelas (PiC), which extends across the marsh, tidal flat and channel environments of both the Minho and Coura estuaries (Figure 3.1). A second set of eighteen samples was recovered in May 2010 close to the highest zone of the CP transect, in order to improve high marsh foraminiferal data. Each sample consists of 30 cm^3, from three 10 cm^3 aliquots of the topmost 1 cm sediment layer, taken with a cut-off syringe from a surface of approximately 0.25 m^2. Samples were immediately transferred to a plastic vial and immersed in alcohol (95%). Once in laboratory, samples were washed with tepid tap water through a 63 μm sieve to remove clay and silt material, and all the remaining residue was immersed for at least 1 h in a [1 g/L] Rose Bengal solution (e.g., Murray, 2006) to separate dead specimens from those considered to be live at the time of collection, and rewashed to eliminate excess stain. Foraminiferal collection was performed under a wet picking procedure using a micropipette. When possible, at least 100 dead and 100 living (stained) individuals were counted in each sample, such counting is fully adequate to characterize the low diversity assemblages of tidal marshes (Fatela and Taborda, 2002).

A set of one-meter-long replicate sediment cores were collected in the Caminha high marsh, 1.55 m above mean sea-level (MSL), with a manual Auger corer at 41º52′37" N and 8º49′28″ W (Figure 3.1). Each core was transferred to a PVC half pipe and wrapped with cling film to protect them during transport and avoid desiccation. In the laboratory, the cores were carefully sectioned into 1 cm samples for analyses, including micropaleontology and chronology. This work also includes the samples from the top 10 cm of the core that were also submitted to the procedure described above. Foraminiferal identification under binocular microscope followed Loeblich and Tappan (1988) to generic classification. The picked specimens of each sample were archived in the respective micropaleontological Plummer cell slide.

Correspondence analysis (CA) was performed in order to analyze the dead benthic foraminiferal distribution from the marsh surface samples. This analysis was performed using CANOCO software (version 4.5, Ter Braak and Smilauer, 2002). Data on submersion time of sampling sites were used as a co-variable. CA is based on the reduction of data dimensionality through the extraction of eigenvectors from its variance–covariance matrix. Each eigenvector represents an ordination axis and has an eigenvalue associated that corresponds to the proportion of the assemblages' total variance that it can explain. Most variability of assemblages' distribution is represented by the first two, or three, main ordination axes. The projection of data in the plane defined by two of these axes reveals a clear and objective affinity between groups of species and samples, if a natural pattern exists, enhanced by this reduction from multidimensionality to two or three dimensions (e.g., Hammer and Harper, 2006; Ter Braak, 1995). The interpretation of ordination axes may be simply based on the knowledge of environmental conditions, but if environmental data

are available they may be associated as a matrix of covariables, displaying their projection in the CA ordination diagram. We followed the method that first calculates the unconstrained ordination of samples and species and then the regression of the ordination axes on the environmental variables (Leps and Smilauer, 2007). The samples carrying less than 34 individuals and species representing less than 2% of the assemblage were excluded.

Temperature, salinity, dissolved oxygen (dO) and pH of sediment pore-water were measured along transects in sampling points during low water. The interstitial water seeped and accumulated inside sediment holes with a depth of *ca.* 40 cm below the surface, following De Rijk (1995). A few sampling sites did not supply any interstitial water. A synoptic control of the same parameters has also been made in estuarine water, during high and low water spring tide. Water parameters were measured with WTW probes (Cond 197i, Oxi 197i and pH 197i). In this work only salinity data are considered.

Surface sediment samples and core altitudes were obtained using a Zeiss Elta R55 total station from a benchmark connected to the national altimetric datum (Cascais), using the GPS differential positioning combined with a regional geoid model (Catalão, 2006) and linked to local chart datum. This datum – HZ (hydrographic zero) lies 2 m below the MSL of Cascais 1938.

Precipitation curves were built up from the month average recorded in the meteorological and hydrological stations from the Minho region. The available data from 54 weather stations of the Portuguese sectors of Minho River and Lima River basins were merged in order to obtain a representative record of the area (http://snirh.inag.pt).

Precipitation and river flow data were obtained from the monthly record of meteorological and hydrological stations from Portuguese sectors of Minho River and Lima River basins (http://snirh.inag.pt). Considering that both datasets exhibit a positive correlation and the precipitation record is more continuous, the available data from 54 weather stations were merged to obtain a representative curve of annual precipitation in the Minho region since 1930. In addition, NAO index data were collected from open access databases (Hurrell, 1995).

Dating recent marsh sediments usually rely on the determination of the vertical distribution of unsupported ^{210}Pb that allows ages to be ascribed to sedimentary layers based on its known decay rate. The total ^{210}Pb was measured by alpha spectroscopy following the methodology of Nittrouer et al. (1979). Unsupported ^{210}Pb ($^{210}Pb_{Excess}$) was determined by subtracting the ^{210}Pb activity supported by ^{226}Ra from the total ^{210}Pb activity, where the supported ^{210}Pb activity for a given core was assumed to be equal to the uniform background activity found at depth (Nittrouer et al., 1979). The chronology was derived using the constant rate of supply model (CRS; Appleby and Oldfield, 1992), as it is the most suitable in the region (Leorri et al., 2010b).

In order to support the ^{210}Pb derived chronology, we used ^{137}Cs (Smith, 2001) and total Pb concentrations (Leorri and Cearreta, 2009; Leorri et al., 2008). The radionuclide ^{137}Cs was determined by its gamma emissions at 662 keV (Figure 3.2). Samples were counted for 24 h to the depth of limit of fallout ^{210}Pb or ^{137}Cs, i.e., until activity concentrations of both radionuclides dropped below the minimum detectable (Leorri et al., 2010b).

3.4. Results and discussion

3.4.1. Tidal marsh surface foraminiferal assemblages

The first set of samples recovered in Caminha, close to the confluence of the Coura and the Minho Rivers (Figure 3.1 – PR, CP and PiC references), includes 7 samples from tidal flat, 13 from low marsh and 8 from high marsh settings (Fatela et al., 2009; Moreno et al., 2005). In order to improve the performance of a transfer function based on marsh benthic foraminifera to estimate the sea-level changes in northern Portugal (Leorri et al., 2011), a second set of 18 surface sediment samples was recovered from the high marsh (Figure 3.1 – CPw series).

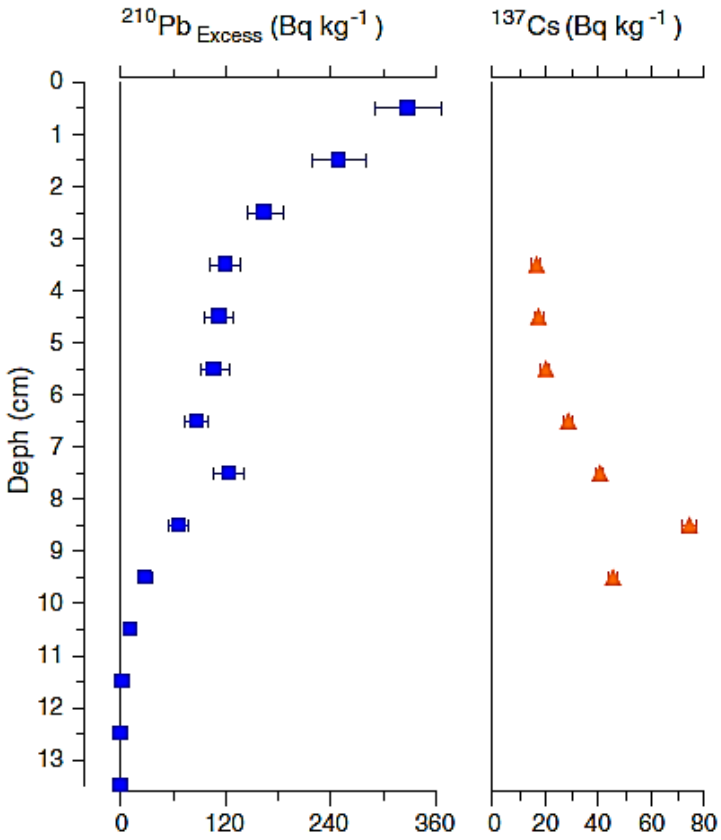

Figure 3.2. ^{210}Pb (A) and ^{137}Cs (B) activities down-core FCPw1.

Unconstrained CA analyses of dead foraminiferal assemblages from Caminha clearly separates the group of high marsh samples, in the left side of plot, from the group of low marsh and

tidal flat samples, in the right side (Figure 3.3). The latter group may also be subdivided into two subgroups: 1) samples located in the transition from low to high marsh (except PiC3, from a lower position), and 2) samples from low marsh and tidal flat (except PR7, located at the transition as the former subgroup). In fact, the projection of the submersion time of each sampling point, as a co-variable of the environmental data (calculated from the measured altitudes and tide levels, see Fatela et al., 2009), exhibits a long vector aligned with the first ordination axis. Therefore, we consider the time of submersion to be a significant ecological parameter forming 3 clusters: 1) high marsh zone (above mean high water – MHW) grouping the samples submerged less than 10% of the year, 2) highest low marsh (transitional zone, between MHW and MHW of neap tides) with submersion time between 28% and 14%, (PiC3 excluded) and 3) the low marsh and tidal flat samples (below MHW neap) submerged 24% to 98% of the time (PR7 excluded). The eigenvalues of axis 1 = 0.46 and axis 2 = 0.20, accounting 31% and 14% of assemblages data total variance, respectively; the first axis is well correlated with the environmental data (r = 0.77) as can be seen in Figure 3.3.

The new set of samples, from May 2010, perfectly integrates with the distribution of the initial sampling, collected across intertidal zone in April 2002 (Figure 3.3).

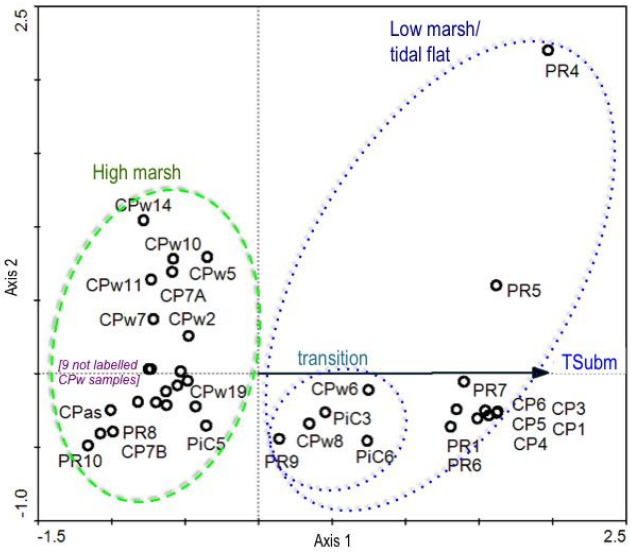

Figure 3.3. Correspondence analysis plot of samples showing correlation with environment variable submersion time – TSubm. Dotted ellipse groups of low marsh samples (right), standing out the transitional zone (smallest ellipse), and dashed ellipse (left) groups of high marsh samples.

Analyzing in detail the samples above the highest low marsh, we confirm that CPw6 and CPw8 groups with the samples of the transitional zone and all the other CPw samples fall within the high marsh zone, above MHW of 1.47 m (Figure 3.4). In this CA analysis, the eigenvalues of axis 1 = 0.26 and axis 2 = 0.19, account for 24% and 17% of the assemblages total variance, respectively; the first axis is also well correlated with the time of submersion (r = 0.95) as can be seen in Figure 3.4.

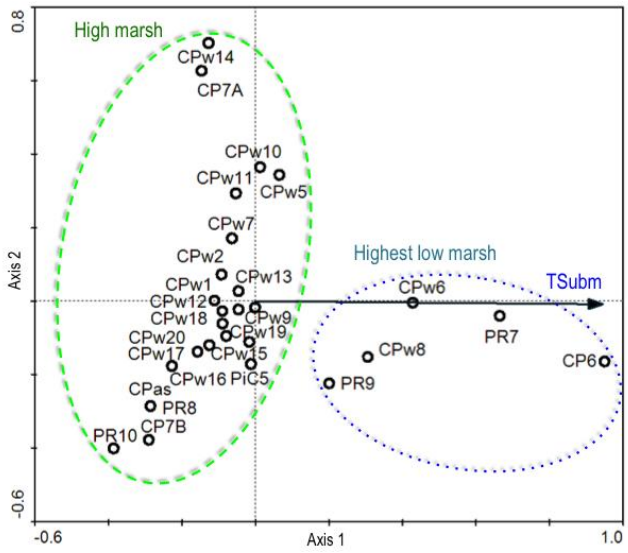

Figure 3.4. Correspondence analysis plot of samples restricted to highest low marsh and high marsh samples.

The CA plot of species also reflects time of submersion along axis 1 (Figure 3.5). Nevertheless, it must be pointed out that species from the high marsh zone group (above MHW of 1.47 m), plotted in the left side, exhibiting a clear division along axis 2, reflecting salinity differences (e.g., Fatela et al., 2007, 2009; Hayward et al., 1999; Moreno et al., 2005, 2006; Pujos, 1971). The brackish foraminiferal species like *H. manilaensis*, *H. wilberti*, *Haplophragmoides* sp., *T. salsa*, *T. irregularis*, and *P. limnetis* are distinctively separated from *T. inflata* and *J. macrescens*. All these species may be common or dominant in the high marsh zone (e.g., Hayward et al., 1999; Scott and Medioli, 1980). However, *T. inflata* and *J. macrescens* were absent in April 2002 from the Caminha high marsh, when foraminiferal assemblages were dominated by *H. manilaensis*, *Haplophragmoides* sp. and *P. limnetis* (Fatela et al., 2007, 2009; Moreno et al., 2005, 2006).

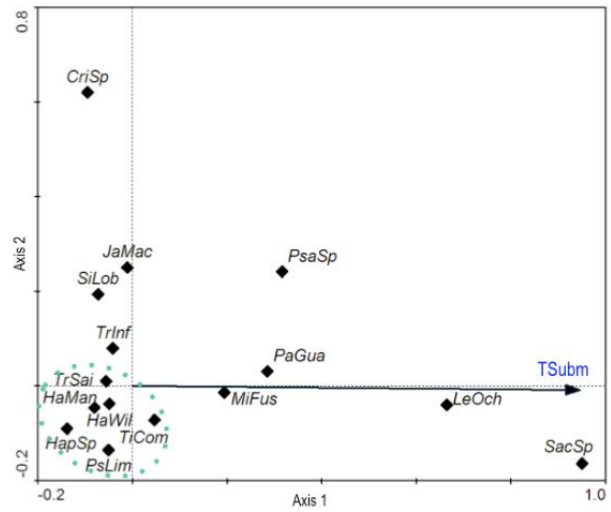

Figure 3.5. Correspondence analysis plot of species and submersion time –TSubm. High marsh species are aligned at the left side of diagram where salt marsh species (*T. inflata* – TrInf and *J. macrescens* – JaMac) occupy the upper part, and dominant brackish high marsh species (*T. salsa/irregularis* – TrSai, *H. manilaensis* – HaMan, *H. wilberti* – HaWil, *Haplophragmoides* sp. – HapSp and *P. limnetis* – PsLim) group in the lower part (dotted ellipse).

The significant difference between the two sampling periods can be explained by salinity changes of sediment interstitial waters, resulting from the regional precipitation patterns, drainage and short penetration of the salt wedge inside the Minho estuary (op. cit.). Thus, the significant presence of *T. inflata* and *J. macrescens* in May 2010, that may reach more than 40% of the high marsh assemblage (maximum values: 30% and 27%, respectively), may be seen as a result of a salinity increase in the Minho estuarine system. Unfortunately, the interstitial water could not be measured in May 2010, but in the following campaigns of October and April 2011, a general increase of salinity, relative to 2002, was effectively recorded (Table 3.1).

Table 3.1. Caminha tidal marsh salinity of sediment interstitial water (except PR1 and CP1).

		PR1*	PR2	PR3	PR4	PR5	PR6	PR7	PR8	PR9	PR10
2002	April	_	0.9	_	_	15.8	11.9	8.4	7.7	_	_
	October	1.9	_	_	_	15.8	14.4	12.2	10.4	_	9.4
2011	April	10.3	_	_	12.9	_	2.5	6.7	_	_	_
	October	1.1	_	18.6	14.7	20.9	18.5	9.5	_	_	_

		CP1*	CP2	CP3	CP4	CP5	CP6	CP7	CP7A
2002	April	4.4	15.4	_	13.0	14.1	13.4	7.2	_
	October	8.6	_	_	11.6	13.4	18.6	14.1	_
2011	April	7.1	16.3	_	6.2	18.2	13.8	_	10.1
	October	10.6	22.3	_	22.8	22.0	25.0	22.9	22.1

* Measurements taken at the subtidal environment, close to the water-sediment interface.

The compilation of precipitation data from the Minho region indicates that samples collected during April 2002 followed a period of several years with positive anomalies (precipitation above the average), whereas the May 2010 sampling period occurred at the end of a six-year negative anomaly (precipitation below the average; Figure 3.6).

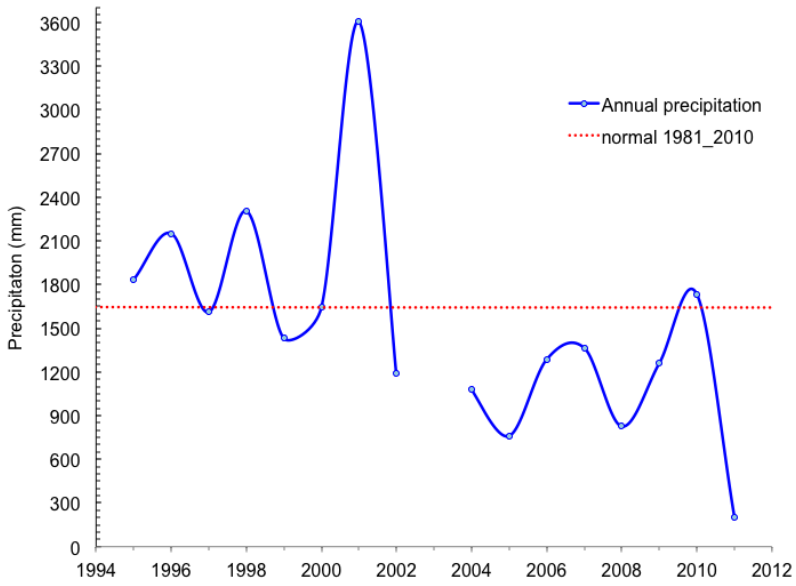

Figure 3.6. Annual precipitation recorded in Minho region from 1994 to 2010. The precipitation normal (average of 30 year records) was calculated by the authors from the series of data available in Minho region weather stations for hydrological years 1981–2010 (http://snirh.inag.pt).

The present work is based on dead foraminiferal assemblages that represent several generations of living assemblages, added consecutively over time, reflecting the mean environmental conditions of the previous years (Horton and Murray, 2006). Accordingly, these results suggest that dead foraminiferal assemblages from Caminha high marsh are able to record short period fluctuations on precipitation (Hippensteel et al., 2002) and thus, they may be applied to high-resolution studies of SW Europe climate evolution.

3.4.2. High marsh short sediment core assemblages

The precipitation measurements in the Minho and Lima river basins began in 1932. A consistent instrumental record for Minho region may be considered since 1934, corresponding to the top 8 cm of the sediment core (1934 to 2010; Table 3.2) collected in the Caminha high marsh (FCPw1). In this core, the $^{210}Pb_{Excess}$ presented a variable, but fairly linear natural logarithmic down-core profile. This pattern suggests relatively constant rates of deposition. However, an inflection at 8 cm depth in the $^{210}Pb_{Excess}$ pattern suggested a short term fluctuation in net deposition and therefore we applied the CRS model. The results derived from this model are supported by a subsurface maximum of total Pb at 7 cm depth ascribed to 1970 (see Leorri et al., 2008 for discussion and references). In addition, the ^{137}Cs maximum is found just below this depth, likely to be dominantly derived from nuclear weapons' testing, with peak fallout in 1963, supporting the ^{210}Pb chronology. However, the cesium peak seems to be slightly displaced downwards by post-depositional migration.

Table 3.2. ^{210}Pb CRS chronology supported by ^{137}Cs and total Pb concentrations of Caminha high marsh sediment core top (FCPw1).

Depth (cm)	Age (year CE)	Error
0-1	2010	0
1-2	2002	1
2-3	1995	2
3-4	1988	3
4-5	1983	4
5-6	1976	4
6-7	1970	5
7-8	1960	7
8-9	1934	10

During this period, the average precipitation is *ca.* 1890 mm for the hydrological year (October to September) and 960 mm for the winter months (December to March – DJFM). The NAO index correlated well with the winter precipitation regime ($r = -0.70$), reflecting the control of North Atlantic climate dynamics (e.g., Trigo et al., 2004) in the Minho region (Figure 3.7).

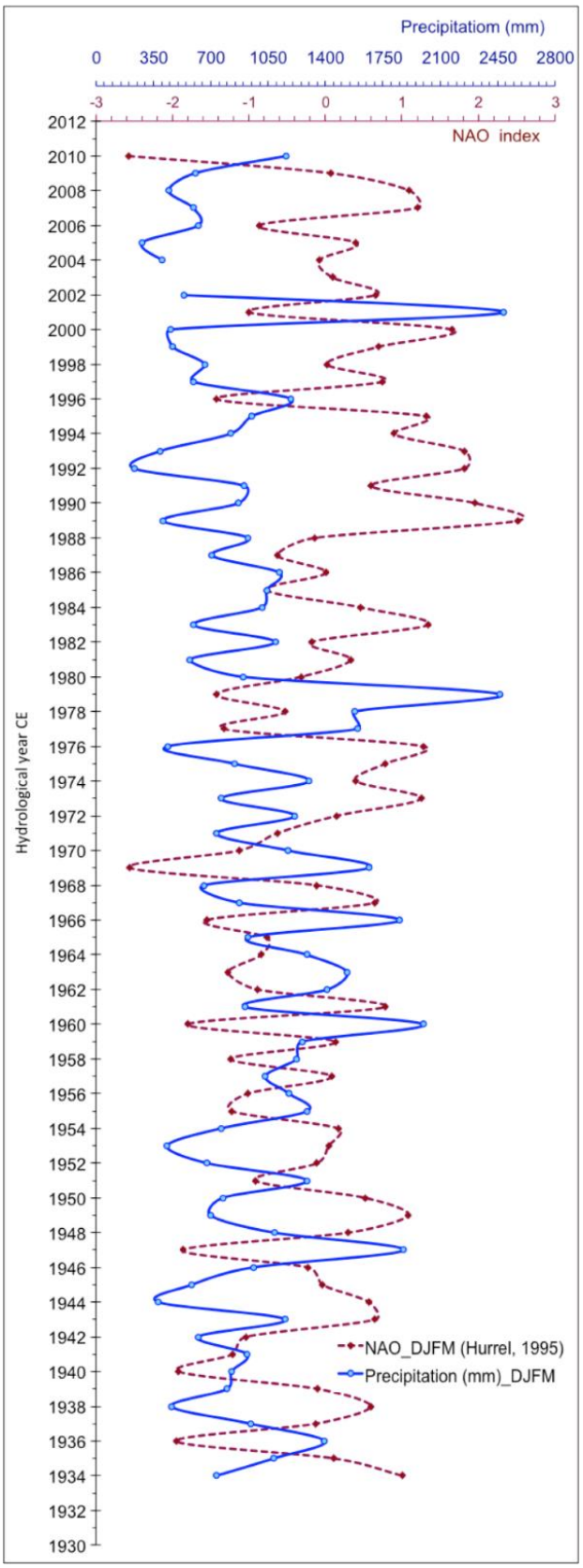

Figure 3.7. Average winter precipitation (DJFM) for the hydrological years 1934–2010 *vs.* NAO index (r = −0.70).

The temporal resolution of the core reconstructions cannot be directly compared to instrumental data. Besides the error associated with the dating methods, the foraminiferal

assemblage of each sediment sample represents an integration of several biocenoses over time, whereas the precipitation record provides a monthly resolution. Therefore, we used a 5-year running average for precipitation data (e.g., the precipitation value for 2010 corresponds to the average from 2010 to 2006, the precipitation of 2009 corresponds to the average from 2009 to 2005, and so on) to compare against ^{210}Pb-derived chronology for each sample (Figure 3.8). Three main distinctive phases can be assigned from this approach: 1) from 1934 to 1957 the precipitation was below the average of the instrumental record (1890 mm) showing negative anomalies, except in 6 of these years; 2) from 1958 to 1983 the smoothed precipitation curve is consistently above the average, exhibiting positive anomalies over these 25 years, except in 2 of the years; and 3) from 1984 to 2010, the precipitation tends to be below mean values, except for 6 of these years (Figure 3.8).

Over this period of almost 80 years covered by instrumental data, our core presents 8 samples semi-randomly distributed that allow a direct comparison. The density of benthic foraminifera (NF, number of individuals per cm^3) ranges between 160 and 250 from *ca.*1934 to *ca.* 1983, covering the first and second phases of the precipitation record (Figure 3.8). The rainfall drop that marks the beginning of the third phase seems to lead to an increase of NF, except *ca.* 1995 and *ca.* 2002. In spite of the negative precipitation anomalies that characterize this phase, a severe flood is recorded in the hydrological year of 1994, 2 severe floods in 1996 and 7 in 2001 (Gonçalves, 2009, 2011), the year that recorded the highest precipitation (3604 mm) since 1933 (Figure 3.9).

The highest NF value (498 individuals per cm^3) is recorded in the 2010 sample, after 6 consecutive years of negative anomalies that include the drier years of the instrumental record.

A positive correlation was found between precipitation and river flow in Minho region (r = 0.72 in Lima and r = 0.85 in Minho river basins). Thus, we may consider that the freshwater flooding of upper intertidal zones during longer periods adversely affects the assemblages' productivity (Figure 3.8).

The rainfall positive anomalies also lead to a decrease of high marsh salinity along with an increase of low-salinity foraminiferal species, as discussed in Section 3.4.1 (e.g., *H. manilaensis*, *T. irregularis*). These species exhibit a clear dominance (54–88% of the assemblage) since the beginning of the second phase (*ca.* 1960). The record of normal-salinity species (e.g., *T. inflata*, *J. macrescens*) starts *ca.* 1934, with a dominance of 59% and drops continuously during the second phase, characterized as a broad period of precipitation positive anomalies (Figure 3.8). However, this trend remains during the third phase where the normal-salinity assemblages exhibit lower relative abundance (Figure 3.8). It must be pointed out that we found the lowest average precipitation (1640 mm) and the minimum annual precipitation during this period (since 1933). However, this period also had the heaviest rainfall, responsible for a significant increase of severe floods in Minho region (Gonçalves, 2009, 2011), mainly between 1988 and 2001 (Figure 3.9). Some of these floods

occurred in dry years reflecting an enhanced instability in this third phase (1983–2010) when compared with the previous phases, as shown in Figure 3.10.

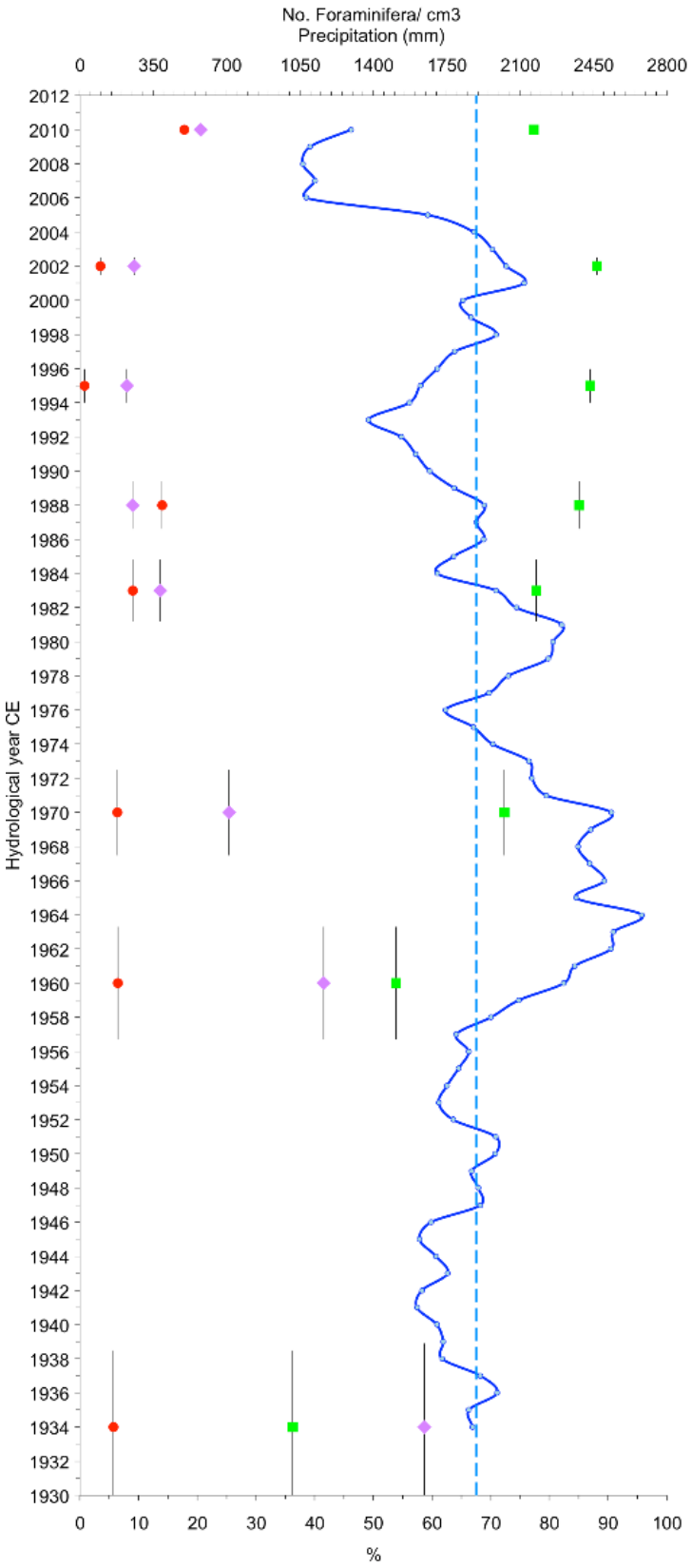

Figure 3.8. Relationship between smoothed average precipitation (solid line) and foraminiferal data; top axis – precipitation (mm) and number of foraminifera per cm³ (red circles); bottom axis – percentage of "normal-" (purple diamonds) and "low-" salinity (green squares) foraminiferal groups; average precipitation 1934–2010 (dashed line).

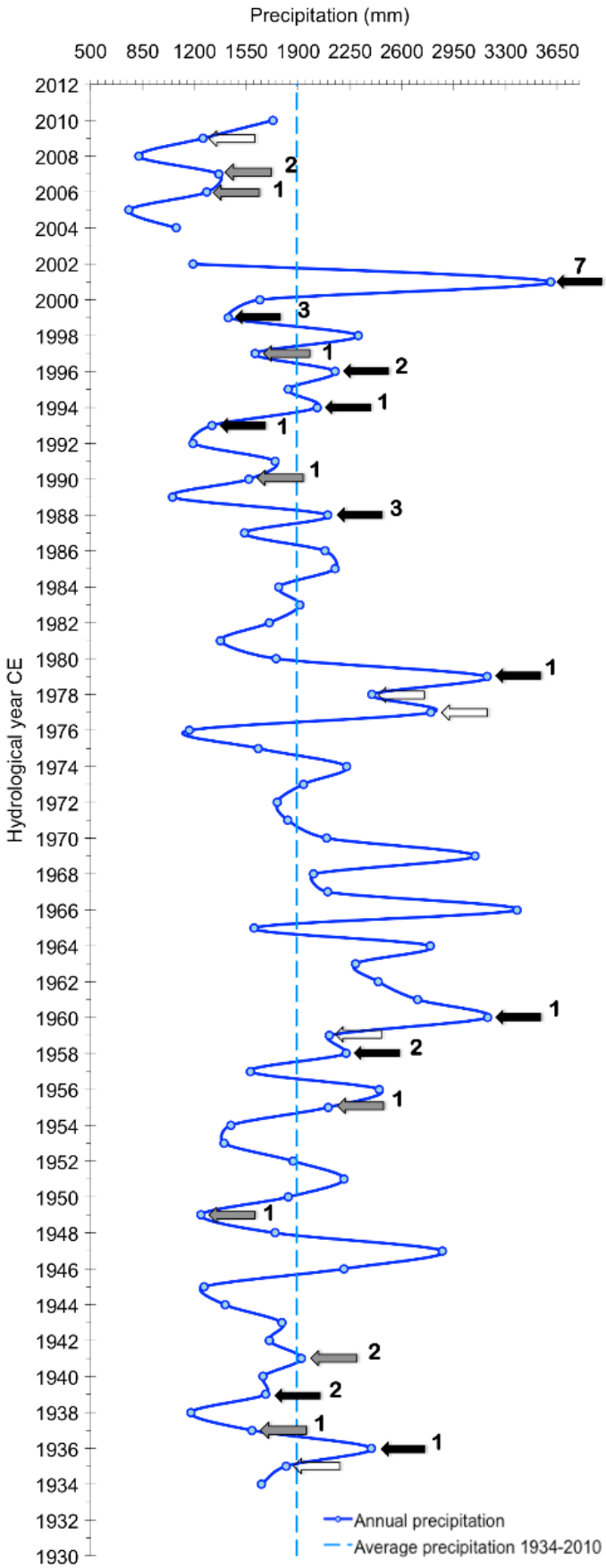

Figure 3.9. Annual precipitation in the Minho region and historical record of floods (after local newspapers archives and Gonçalves, 2009, 2011); black arrows indicate severe floods, grey arrows indicate moderate floods and white arrows means no information about flood severity; figures indicate the number of floods in the hydrological year.

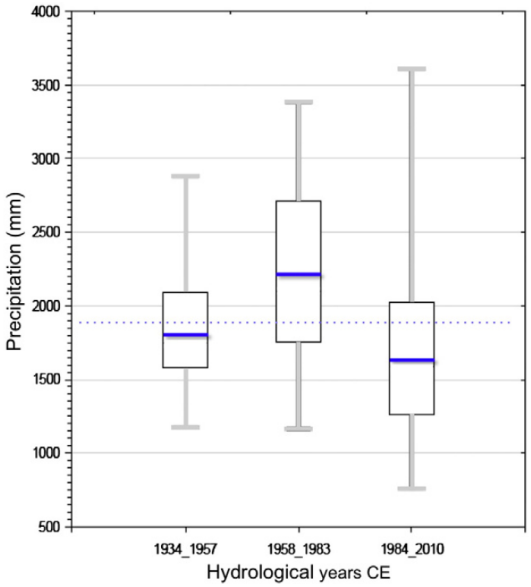

Figure 3.10. Comparison of the three phases, defined after precipitation data from Minho region. Box-plots represent the mean, the extreme values, the first and third quartiles; dashed line represents the average precipitation from 1934 to 2010.

The lowest relative abundances of *T. inflata* and *J. macrescens* mentioned above, *ca.* 1995 and 2002, are related with the occurrence of these severe floods. The normal-salinity species partially replace (21%) the low-salinity species at the top sample, as a consequence of the precipitation negative anomalies that mark the end of the third phase, from 2004 to 2010 (Figures 3.8 and 3.9). The tendency of low-salinity species predominance in the marsh sediment record since *ca.* 1960 may be seen as a consequence of the steady increase of precipitation as well as of flood events in the last dry phase.

3.5. Conclusions

This study is based on dead benthic foraminiferal assemblages from surface sediment and from the upper 10 cm of a core retrieved from the Caminha tidal marsh.

The 46 surface samples were obtained in two different campaigns: April 2002 and May 2010. Correspondence analysis (CA) integrates both sampling periods and defines 3 groups of samples according to foraminiferal assemblage distribution across the tidal marsh zonation, showing a significant correlation with submersion time. A separation between brackish and salt high marsh foraminiferal species groups is also clearly identified.

Dominant species in salt marshes like *T. inflata* and *J. macrescens* are absent in Caminha high marsh in April 2002, but became common in May 2010. This decrease of lower salinity assemblage (*Haplophragmoides* sp., *H. manilaensis*, *H. wilberti* and *P. limnetis*) dominance may be a direct consequence of the increase in marsh sediment interstitial water salinity, connected with a shift in regional precipitation regime over the 8 years that separate both samplings.

This observation was applied to the analysis of benthic foraminifera from the top 8 samples (0 to 10 cm depth) of a high marsh sediment core that corresponded to the period of instrumental record of precipitation and river flow in the Minho region. We found that river flow directly reflects precipitation on Lima and Minho basins ($r = 0.72$ and $r = 0.85$, respectively). The almost 80 years of precipitation record in the Minho region allows us to distinguish three main phases of 1) negative anomalies from 1934 to 1957, 2) positive anomalies from 1958 to 1983, and 3) negative anomalies from 1984 to 2010; however, this period exhibits the precipitation maximum of all instrumental record and the greatest amplitude of rainfall values.

Benthic foraminifera from high marsh zone quickly respond to these short-term variations. The direct relationship between the relative increase of low-salinity species and the increase of precipitation along several decades, as well as in the same decade, became clear in the years of heavy rainfall recorded during the dryer periods.

The positive anomalies of precipitation raise the freshwater flooding and seepage at the intertidal zone and are recorded by high marsh foraminiferal assemblages through 1) a reduced number of individuals per cm^3 of sediment, and 2) an increase dominance of low-salinity species (*H. manilaensis*, *H. wilberti*, *T. irregularis* and *P. limnetis*). On the other hand, a steady low precipitation throughout 4 or 5 years seems enough to increase the assemblage productivity and increasing the significant presence of high marsh normal-salinity species, namely *T. inflata* and *J. macrescens*.

The negative correlation found between Minho winter precipitation and the winter NAO index ($r = -0.70$) reflects its connection with the climate dynamics of the North Atlantic region pointing out that the record of benthic foraminifera from Caminha high marsh may have an important contribution to high-resolution studies of SW Europe climate evolution.

Acknowledgments

This work is a contribution of the WesTLog (PTDC/CTE/105370/ 2008) project, funded by the Fundação para a Ciência e Tecnologia – FCT, and a contribution to the IGCP Project 588, Northwest Europe working group of the INQUA Commission on Coastal and Marine Processes and the Geo-Q Zentroa Research Unit (Joaquín Gómez de Llarena Laboratory), Sociedad de Ciencias Aranzadi. Dr. Leorri was awarded the 2012 W. Storrs Cole Research Award. We thank the comments and suggestions of Dr. Guillermo Francés (University of Vigo, Spain) and Dr. Ronald E. Martin (University of Delaware, USA) that greatly improved this manuscript.

References

Alve, E., 1995. Benthic foraminiferal responses to estuarine pollution: a review. Journal of Foraminiferal Research 25, 190–203.

Alves, A., 1996. Causas e Processos da Dinâmica Sedimentar na Evolução Actual do Litoral do Alto Minho. Unpublished PhD Thesis, Universidade do Minho, Braga, Portugal.

Andersen, H.V., 1953. Two new species of Haplophragmoides from the Louisiana coast. Contributions from the Cushman Foundation for Foraminiferal Research 4, 21–22.

Appleby, P.G. and Oldfield, F., 1992. Application of ^{210}Pb to sedimentation studies. In: Ivanovich, M. and Harmon, R.S. (Eds.), Uranium Series Disequilibrium. Oxford University Press, Oxford, pp. 731–778.

Armynot du Châtelet, E., Debenay, J.-P. and Soulard, R., 2004. Foraminiferal proxies for pollution monitoring in moderately polluted harbors. Environmental Pollution 127, 27–40.

Bettencourt, A., Ramos, L., Gomes, V., Dias, J.M.A., Ferreira, G., Silva, M. and Costa, L., 2003. Estuários Portugueses. Ed. INAG – Ministério das Cidades, Ordenamento do Território e Ambiente. Lisboa, Portugal.

Brown, J., Colling, A., Park, D., Philips, J., Rothery, D., Wright, J., 1991. Waves, Tides and Shallow-Water Processes. Butterworth Heinemann/The Open University, Milton Keynes, UK.

Brady, H.B., 1870. Foraminifera. In: Brady, G.S., Robertson, D. and Brady, H.B. (Eds.), Ostracoda and Foraminifera of Tidal Rivers. Annals and Magazine of Natural History, Series 4, 6, pp. 273–306.

Brönnimann, P., 1986. *Paratrochammina* (*Lepidoparatrochammina*) *guaratibaensis* n. sp. from Brackish Waters of Brazil and a Check List of Recent Trochamminaceans from Brackish Waters (Protista: Foraminiferida). Revue Paléobiologie 5, 221–229.

Brönnimann, P., Whittaker, J.E. and Zaninetti, L., 1992. Brackish water foraminifera from mangrove sediments of southwestern Viti Levu, Fiji Islands, Southwest Pacific. Revue Paléobiologie 11, 13–65.

Callard, S.L., Gehrels, W.R., Morrison, B.V., Grenfell, H.R., 2011. Suitability of salt-marsh foraminifera as proxy indicators of sea level in Tasmania. Marine Micropaleontology 79, 121–131.

Catalão, J., 2006. Iberia–Azores Gravity Model (IAGRM) using multi-source gravity data. Earth, Planets and Space 58, 277–286.

Cearreta, A., Irabien, M.J., Leorri, E., Yusta, I., Croudace, I.W. and Cundy, A.B., 2000. Recent anthropogenic impacts on the Bilbao estuary, N. Spain: geochemical and microfaunal evidence. Estuarine, Coastal and Shelf Science 50, 571–592.

Cearreta, A., Irabien, M.J., Leorri, E., Yusta, I., Quintanilla, A. and Zabaleta, A., 2002a. Environmental transformation of the Bilbao estuary, N. Spain: microfaunal and geochemical proxies in the recent sedimentary record. Marine Pollution Bulletin 44, 487–503.

Cearreta, A., Irabien, M.J., Ulibarri, I., Yusta, I., Croudace, I.W. and Cundy, A.B., 2002b. Recent salt marsh development and natural regeneration of reclaimed areas in the Plentzia estuary, N. Spain. Estuarine, Coastal and Shelf Science 54, 863–886.

Cearreta, A., Alday, M., Freitas, M.C. and Andrade, C., 2007. Postglacial foraminifera and paleoenvironments of the Melides lagoon (SW Portugal): towards a regional model of coastal evolution. Journal of Foraminiferal Research 37, 125–135.

Cearreta, A., Alday, M., Irabien, M.J., Etxebarria, N. and Soto, J., 2008. Modern conditions and recent development of the Muskiz estuary: historical disturbance by the largest oil refinery of N Spain. Journal of Iberian Geology 34, 191–213.

Cushman, J.A. and Brönnimann, P., 1948. Additional new species of arenaceous foraminifera from shallow waters of Trinidad. Contributions from the Cushman Foundation for Foraminiferal Research 24, 37–43.

Debenay, J.-P., Guiral, D. and Parra, M., 2002. Ecological factors acting on microfauna in mangrove swamps. The case of foraminiferal assemblages in French Guiana. Estuarine. Coastal and Shelf Science 55, 509–533.

De Rijk, S., 1995. Salinity control on the distribution of salt marsh Foraminifera (Great Marshes, Massachusetts). Journal of Foraminiferal Research 25, 156–166.

De Rijk, S. and Troelstra, S.R., 1997. Salt marsh foraminifera from the Great Marshes, Massachusetts: environmental controls. Palaeogeography Palaeoclimatology Palaeoecology 130, 81–112.

Diz, P., Francés, G., Pelejero, C., Grimalt, J. and Vilas, F., 2002. The last 3000 years in the Ría de Vigo (NW Iberian Margin): climatic and hydrographic signals. The Holocene 12, 459–468.

Fatela, F. and Taborda, R., 2002. Confidence limits of species proportions in microfossil assemblages. Marine Micropaleontology 45, 169–174.

Fatela, F., Moreno, J. and Antunes, C., 2007. Salinity influence on foraminiferal tidal marsh assemblages of NW Portugal: an anthropogenic constraint? Thalassas 23, 51–63.

Fatela, F., Moreno, J., Moreno, F., Araújo, M.F., Valente, T., Antunes, C., Taborda, R., Andrade, C. and Drago, T., 2009. Environmental constraints of foraminiferal assemblages' distribution across a brackish tidal marsh (Caminha, NW Portugal). Marine Micropaleontology 70, 70–88.

Gehrels, W.R., 1994. Determining relative sea level change from salt marsh foraminifera and plant zones on the coast of Maine, USA. Journal of Coastal Research 10, 990–1009.

Gehrels, W.R., 2000. Using foraminiferal transfer functions to produce high-resolution sea-level records from salt-marsh deposits, Maine, USA. The Holocene 10, 367–376.

Gehrels, W.R., Roe, H.M. and Charman, D.J., 2001. Foraminifera, testate amoebae and diatoms as sea-level indicators in UK saltmarshes: a quantitative multiproxy approach. Journal of Quaternary Science 16, 201–220.

Gonçalves, G., 2009. Áreas inundáveis entre 1900 e 2007 em Arcos de Valdevez e Ponte da Barca, Portugal. Unpublished MSc Thesis. Universidade do Porto. Porto, Portugal.

Gonçalves, G., 2011. Percepção dos danos após inundação nos concelhos de Arcos de Valdevez e Ponte da Barca entre 1900 e 2007. Territorium 18, 231–238.

Hammer, Ø., Harper, D.A.T., 2006. Paleontological Data Analysis. Blackwell Publishing, Oxford, UK.

Hayward, B.W., Grenfell, H.R., Reid, C.M. and Hayward, K.A., 1999. Recent New Zealand shallow-water benthic foraminifera: taxonomy, ecologic distribution, biogeography, and use in paleoenvironmental assessment. Institute of Geological and Nuclear Sciences, Monograph, 21. Institute of Geological and Nuclear Sciences Limited, Lower Hutt, New Zealand.

Hippensteel, S.P., Martin, R.E., Nikitina, D. and Pizzuto, J.E., 2002. Interannual variation of marsh foraminiferal assemblages (Bombay Hook National Wildlife Refuge, Smyrna, DE): do foraminiferal assemblages have a memory? Journal of Foraminiferal Research 32, 97–109.

Horton, B.P. and Edwards, R.J., 2000. Quantitative paleoenvironmental reconstruction techniques in sea-level studies. Archaeology in the Severn Estuary 11, 105–119.

Horton, B.P. and Edwards, R.J., 2006. Quantifying Holocene sea-level change using intertidal foraminifera: lessons from the British Isles. Cushman Foundation for Foraminiferal Research, sp. pub. 40, 97p.

Horton, B.P. and Murray, J.W., 2006. Patterns in cumulative increase in live and dead species from foraminiferal time series of Cowpen Marsh, Tees Estuary, UK: implications for sea-level studies. Marine Micropaleontology 58, 287–315.

Horton, B.P. and Murray, J.W., 2007. The roles of elevation and salinity as primary controls on living foraminiferal distributions: Cowpen Marsh, Tees Estuary, UK. Marine Micropaleontology 63, 169–186.

Horton, B.P., Edwards, R.J. and Lloyd, J.M., 1999. UK intertidal foraminiferal distributions: implications for sea-level studies. Marine Micropaleontology 36, 205–223.

Hurrell, J.W., 1995. Decadal trends in the North Atlantic Oscillation: regional temperatures and precipitation. Science 269, 676–679.

Kemp, A.C., Horton, B.P., Corbett, D.R., Culver, S.J., Edwards, R.J., and Van de Plassche, O., 2009. The relative utility of foraminifera and diatoms for reconstructing late Holocene sea level change in North Carolina, USA. Quaternary Research 71, 9–21.

Kemp, A.C., Buzas, M.A., Horton, B.P. and Culver, S.J., 2011. Influence of patchiness on modern salt-marsh foraminifera used in sea-level studies (North Carolina, USA). Journal of Foraminiferal Research 41, 114–123.

Leorri, E., Cearreta, A., 2009. Recent sea-level changes in the southern Bay of Biscay: transfer function reconstructions from salt-marshes compared with data. Scientia Marina 73, 287–296.

Leorri, E., Horton, B.P. and Cearreta, A., 2008. Development of a foraminifera-based transfer function in the Basque marshes. Marine Geology 251, 60–74.

Leorri, E., Gehrels, W.R., Horton, B.P., Fatela, F. and Cearreta, A., 2010a. Distribution of foraminifera in salt marshes along the Atlantic coast of SW Europe: tools to reconstruct past sea-level variations. Quaternary International 221, 104–115.

Leorri, E., Cearreta, A., Corbett, R., Blake, W., Fatela, F., Gehrels, R. and Irabien, M.J., 2010b. Identification of suitable areas for high-resolution sea-level studies in SW Europe using commonly applied ^{210}Pb models. Geogaceta 48, 35–38.

Leorri, E., Fatela, F., Moreno, J., Antunes, C., Cearreta, A. and Drago, T., 2011. Assessing the performance of a foraminifera-based transfer function to estimate sea-level changes in northern Portugal. Quaternary Research 75, 278–287.

Leps, J. and Smilauer, P., 2007. Multivariate Analysis of Ecological Data Using CANOCO, Third edition. Cambridge University Press, Cambridge, UK.

Loeblich Jr., A.R. and Tappan, H., 1988. Foraminiferal Genera and Their Classification. Van Nostrand Reinhold Company, New York, USA.

Martin, R.E., 2000. Environmental Micropaleontology – The Application of Microfossils to Environmental Geology. Kluwer Academic/Plenum Publishers, New York, 481p.

Martin, R.E., Hippensteel, S.P., Nikitina, D. and Pizzuto, J.E., 2002. Artificial time-averaging of marsh foraminiferal assemblages: linking the temporal scales of ecology and paleoecology. Paleobiology 28, 263–277.

Montagu, G., 1808. Supplement to Testacea Britannica. S. Woolmer, Exeter, 183p.

Moreno, J., Fatela, F., Andrade, C., Cascalho, J., Moreno, F. and Drago, T., 2005. Living foraminiferal assemblages from Minho/Coura estuary (Northern Portugal): a stressful environment. Thalassas 21, 17–28.

Moreno, J., Fatela, F., Andrade, C. and Drago, T., 2006. Distribution of "living" *Pseudothurammina limnetis* (Scott and Medioli): an occurrence on the brackish tidal marsh of Minho/Coura estuary — Northern Portugal. Révue de Micropaléontologie 49, 45–53.

Moreno, J., Valente, T., Moreno, F., Fatela, F., Guise, L. and Patinha, C., 2007. Calcareous foraminifera occurrence and calcite-carbonate equilibrium conditions — a case study in Minho/Coura estuary (N Portugal). Hydrobiologia 597, 177–184.

Murray, J.W., 1971. Living foraminiferids of tidal marshes: a review. Journal of Foraminiferal Research 1, 153–161.

Murray, J.W., 1991. Ecology and Palaeoecology of Benthic Foraminifera. Longman Scientific and Technical, London, 397p.

Murray, J.W., 2006. Ecology and Applications of Benthic Foraminifera. Cambridge University Press, Cambridge, 426p.

Nittrouer, C.A., Sternberg, R.W., Carpenter, R. and Bennett, J.T., 1979. The use of ^{210}Pb geochronology as a sedimentological tool: application to the Washington Continental Shelf. Marine Geology 31, 297–316.

Phleger, F.B. and Bradshaw, J.S., 1966. Sedimentary environments in a marine marsh. Science 154, 1551–1553.

Phleger, F.B. and Walton, W.R., 1950. Ecology of marsh and bay foraminifera, Barnstable, Massachusetts. American Journal of Science 248, 274–294.

Pujos, M., 1971. Foraminifères et thecamoebiens de la Gironde: leur interêt dans la mise en évidence des biotopes estuariens. Compte Rendus de l'Académie de Sciences de Paris 273, 1095–1097.

Pujos, M., 1976. Écologie des foraminifères benthiques et des Thecamoebiens de la Gironde et du plateau continental Sud-Gascogne. Application à la connaissance du Quaternaire terminal, da la région Ouest-Gironde. Mémoires de l'Institut de Géologie du Bassin d'Aquitaine, 8. Institut de Géologie du Bassin d'Aquitaine, Bordeaux, France.

Saunders, J.B., 1957. Trochamminidae and certain Lituolidae (Foraminifera) from the recent brackish-water sediments of Trinidad, British West Indies. Smithsonian Miscellaneous Collections 134 (5), 1–16.

Scott, D.B. and Medioli, F.S., 1980. Quantitative studies of marsh foraminiferal distribution in Nova Scotia: implications for sea level studies. Cushman Foundation for Foraminiferal Research sp. pub. 17, 58p.

Scott, D.B., Medioli, F.S. and Schafer, C.T., 2001. Monitoring in Coastal Environments Using Foraminifera and Thecamoebian Indicators. Cambridge University Press, Cambridge, 177p.

Sen Gupta, B., 2002. Foraminifera in Marginal Marine Environments. In: Sen Gupta, B. (Ed.), Modern Foraminifera. Kluwer Academic Publishers, Dordrecht, The Netherlands, pp. 141–159.

Smith, J.N., 2001. Why should we believe ^{210}Pb sediment geochronologies? Journal of Environmental Radioactivity 55, 121–123.

Taborda, R. and Dias, J.M.A., 1991. Análise da sobre-elevação do nível do mar de origem meteorológica durante os temporais de 1978 e 1981. Geonovas, sp. n. 1, pp. 89–97.

Ter Braak, C.J.F., 1995. Ordination. In: Jongman, R.H.G., Ter Braak, C.J.F. and Van Tongeren, O.F.R. (Eds.), Data Analysis in Community and Landscape Ecology. Cambridge University Press, Cambridge, UK, pp. 91–173.

Ter Braak, C.J.F. and Smilauer, P., 2002. CANOCO reference manual and CanoDraw for Windows user's guide: software for canonical community ordination (version 4.5). Microcomputer Power, New York, USA.

Todd, R. and Brönnimann, P., 1957. Recent foraminifera and thecamoebina from the eastern Gulf of Paria. Contributions from the Cushman Foundation for Foraminiferal Research, Special Publication 6, pp.1–43.

Topping, R.M., 1973. Benthonic foraminifera from Puhoi estuary, Auckland. Unpublished B.Sc. (Hons) Thesis. University of Auckland, 39p.

Trigo, R.M., Pozo-Vázquez, D., Osborn, T.J., Castro-Díez, Y., Gámis-Fortis, S., Esteban-Parra, M.J., 2004. North Atlantic oscillation influence on precipitation, river flow and water resources in the Iberian Peninsula. International Journal of Climatology 24, 925–944.

Williams, H.F.L., 1994. Intertidal benthic foraminiferal biofacies on the Central Gulf Coast of Texas: modern distribution and application to the sea-level reconstruction. Micropalaeontology 40, 169–183.

Williamson, W.C., Medioli, F.S., Schafer, C.T., 1858. On the Recent Foraminifera of Great Britain. Ray Society, London, 107p.

Appendix 3.1. Marsh foraminiferal reference list for those species mentioned in the text.

Species		Citation
Haplophragmoides manilaensis Andersen	Plate 1, Fig. 2	*Haplophragmoides manilaensis* Andersen, 1953: p. 22, pl. 4, fig. 7, 8.
Haplophragmoides wilberti Andersen	Plate 1, Fig. 3	*Haplophragmoides wilberti* Andersen, 1953: p. 21, pl. 2, figs. 5, 6, pl. 3, figs. 9–16.
Haplophragmoides sp.	Plate 1, Fig. 4	
Jadammina macrescens (Brady)	Plate 2, Fig. 7a, b	*Trochammina inflata* (Montagu) var. *macrescens* Brady, 1870: p. 290, pl. 11, figs. 5a-c. *Jadammina polystoma* Bartenstein and Brand, 1938: p. 381, text-figs. 1–3. *Trochammina macrescens* Brady; Phleger and Walton, 1950: p. 281, pl. 2, figs. 6, 7. *Jadammina macrescens* (Brady); Murray, 1971: p. 41,pl. 13, figs. 1–5.
Miliammina fusca (Brady)	Plate 2, Fig. 2a, b	*Quinqueloculina fusca* Brady, 1870: p. 286, pl. 11, fig. 2a-c. *Miliammina fusca* (Brady); Horton and Edwards, 2006: p. 68, pl. 1, figs. 5a, b.
Paratrochammina guaratibaensis Brönnimann	Plate 2, Fig. 5	*Paratrochammina guaratibaensis* Bronnimann, 1986; Debenay et al., 2002: p. 531, pl. 2, figs. 11-14.
Lepidodeuterammina ochracea (Williamson)		*Rotalia ochracea* Williamson, 1858: p. 55, pl. 4, Fig. 112, pl. 5, Fig. 113. *Trochammina ochracea* (Williamson); Murray, p. 37, pl. 11, fig. 1-5. *Lepidodeuterammina ochracea* (Williamson); Loeblich & Tappan, p. 127, pl. 135, fig. 10-14.
Pseudothurammina limnetis (Scott and Medioli)	Plate 1, Fig. 6a, b	*Thurammina ? limnetis* Scott and Medioli, 1980: p. 43, pl. 1, figs. 1-3. *Pseudothurammina limnetis* (Scott and Medioli); De Rijk, 1995: p. 28, pl. 1, figs. 15, 16.
Saccammina sp.	Plate 2, Fig. 3a, b	
*Tiphotrocha comprimat*a (Cushman and Brönnima	Plate 2, Fig. 5	*Trochammina comprimata* Cushman and Bronnimann, 1948: p. 41, pl. 8, figs. 1-3. *Tiphotrocha comprimata* (Cushman and Brönnimann); Horton and Edwards, 2006: p. 69, pl. 2, figs. a-e.
Trochamminita salsa (Cushman and Brönnimann)	Plate 1, Fig. 1a, b, c	*Labrospira salsa* Cushman and Bronnimann, 1948, p.16, p l.3, fig. 5,6. *Alveophragmium salsum* (Cushman and Brönnimann). Todd and Bronnimann, 1957, p. 23, pl. 2, fig. 3• Trochamminita salsa (Cushman and Brönnimann). SAUNDERS1 957, p. 6, pl. 1, fig. 3-8. *Trochamminita irregularis* Cushman and Bronnimann, 1948, p. 17, pl. 4, fig. 1-3. - Saunders, 1957,p. 4, pl.2, fig. 3- 8. - Todd and Brönnimann 1957, p . 30,pl. 4, fig. 19-22.- Topping, 1973, p. 21, pl. 3, fig. 4-7.
Trochammina inflata (Montagu)	Plate 2, Fig. 1a, b, c	*Nautilus inflatus* Montagu, 1808: p. 81, pl. 18, fig. 3. *Trochammina inflata* (Montagu); Horton and Edwards, 2006: p. 69, pl. 2, figs. 8a-d.
Siphotrochammina lobata Saunders	Plate 2, Fig. 6	*Siphotrochammina lobata* Saunders, 1957: p. 9-10, pl. 3, fig. 1-2; Bronnimann et al., 1992, p. 31, pl. 4, fig. 1-2; De Rijk, 1995, p. 33, pl. 3, figs. 9, 11-13.
Psammosphaera sp.	Plate 2, Fig. 4a, b	

Appendix 3.3. Foraminiferal data from the top core FCPw1 – Caminha tidal marsh.

Core samples	*Cribrostomoides sp.*	*Haplophragmoides sp.*	*H. manilaensis*	*H. wilberti*	*J. macrescens*	*M. fusca*	*P. guaratibaensis*	*P. limnetis*	*T. comprimata*	*T. inflata*	*T. salsa / irregularis*	*S. lobata*	Undetermined	Foraminifera total number	Foraminifera num. species
0	0	24	57	6	0	18	0	5	0	18	10	0	3	141	7
1	3	10	84	0	0	19	0	0	3	11	17	0	4	151	7
2	6	3	70	0	1	27	3	3	0	3	14	1	7	138	9
3	13	87	0	0	0	3	0	2	3	6	11	1	8	134	11
4	1	0	74	0	0	2	3	1	6	6	14	0	10	117	8
6	6	0	77	17	4	6	2	1	5	4	5	0	3	130	10
7	0	0	44	7	18	8	2	1	3	18	18	5	6	130	10
8	3	0	22	6	13	8	3	0	1	56	17	2	7	138	10

Appendix 3.2. Foraminiferal data from surface sediment of Caminha tidal marsh (samples carrying less than 34 individuals and the species representing less than 2% of the assemblage were excluded).

	Cribrostomoides . sp.	*Haplophragmoides* sp.	*H. manilaensis*	*H. wilberti*	*J. macrescens*	*L. ochracea*	*M. fusca*	*P. guaratibaensis*	*Psammosphaera* sp.	*P. limnetis*	T. earlandi	*T.comp.*	*T. inflata*	*T. salsa / irregularis*	*Saccammina sp.*	*S. delicatula*	*S. lobata*	*H. germanica*	Foraminifera total number	Submersion time %
	CriSp	HapSp	HaMan	HaWil	JaMac	LeOch	MiFus	PaGua	PsaSp	PsLim	TeEar	TiCom	TrInf	TrSai	SacSp	SiDel	SiLob	HaGer		TSubm
PR1	0	1	0	9	0	1	71	0	0	0	0	0	3	0	0	0	0	0	96	100
PR4	0	0	2	0	6	3	41	0	5	0	3	0	0	0	0	9	0	2	85	51.8
PR5	1	1	7	0	3	1	92	0	1	0	2	0	0	0	4	5	0	3	121	48.9
PR6	0	0	0	25	0	0	95	1	2	2	0	0	0	0	0	0	0	0	133	30.7
PR7	0	3	0	1	3	1	89	0	2	3	0	0	0	0	0	0	0	0	109	19.8
PR8	0	28	112	3	0	0	3	0	0	26	0	0	6	23	0	0	0	0	210	5.7
PR9	0	0	13	0	0	0	16	0	0	4	0	2	0	1	0	0	0	0	39	13.5
PR10	0	17	18	0	0	0	0	0	0	4	0	0	0	0	0	0	0	0	49	4.2
CP1	0	0	0	0	0	0	60	0	0	1	0	2	0	0	0	0	0	0	66	98.1
CP3	0	0	1	2	0	0	126	0	1	1	0	0	0	0	0	0	0	0	141	50.5
CP4	0	0	0	1	0	0	51	0	0	0	0	0	0	0	0	0	0	0	56	32.8
CP5	0	0	0	0	0	0	55	0	0	0	0	0	0	0	1	0	0	0	56	31.2
CP6	0	0	0	0	0	0	48	2	0	2	0	1	0	0	5	0	0	0	59	23.9
CP7A	8	4	6	2	0	0	5	0	0	5	0	0	0	0	0	0	0	0	39	9.9
CP7B	0	14	0	0	0	0	2	0	0	6	0	0	0	7	0	0	0	0	43	7.9
CPas	0	1	10	0	0	0	1	0	0	0	0	0	0	4	0	0	0	0	34	6.0
CPw1	0	7	35	4	1	0	15	0	0	0	0	1	19	18	0	0	4	0	106	7.7
CPw2	0	34	12	13	18	0	23	0	0	0	0	0	17	4	0	0	1	0	130	8.2
CPw5	0	11	25	0	38	0	33	2	1	0	0	1	19	6	0	0	0	0	142	8.5
CPw6	2	6	6	2	2	0	72	1	0	2	0	4	7	4	0	0	0	0	111	15.5
CPw7	1	3	30	0	8	0	17	0	0	0	0	0	31	15	0	0	0	0	105	7.7
CPw8	0	0	14	2	0	0	66	0	0	13	0	16	9	12	0	0	0	0	140	15.1
CPw9	0	0	28	6	0	0	24	1	0	6	0	1	27	20	0	0	0	0	119	7.4
CPw10	0	0	17	0	28	0	26	0	0	0	0	1	16	34	0	0	7	0	132	8.2
CPw11	0	0	32	0	23	0	17	0	0	0	0	3	21	21	0	0	5	0	129	8.8
CPw12	0	7	31	0	3	0	17	0	0	6	0	2	21	27	0	0	0	0	123	7.1
CPw13	0	0	33	13	5	0	21	1	0	5	0	0	19	24	0	0	3	0	134	8.2
CPw14	20	0	45	2	13	0	14	0	1	0	0	0	12	8	0	0	7	0	126	7.9
CPw15	0	4	42	5	1	0	13	0	0	7	0	21	20	9	0	0	5	0	131	7.9
CPw16	0	8	51	3	2	0	11	0	0	11	0	3	19	8	0	0	0	0	124	6.8
CPw17	0	16	62	10	5	0	18	1	0	0	0	7	2	7	0	0	5	0	133	8.8
CPw18	0	0	50	10	6	0	21	0	0	1	0	13	13	17	0	0	4	0	142	7.9
CPw19	0	0	67	6	2	0	32	0	0	1	0	3	8	17	0	0	0	0	138	8.5
CPw20	0	0	53	10	3	0	20	0	0	1	0	0	9	32	0	0	0	0	131	8.8
PiC3	0	0	13	0	0	0	21	0	0	0	0	0	2	0	0	0	0	0	42	42.0
PiC5	0	0	204	19	0	0	92	0	0	0	0	3	0	36	0	0	0	0	397	6.6
PiC6	0	10	42	40	0	0	153	5	0	3	0	9	0	0	0	0	0	0	300	28

Appendix 3.4. Precipitation data from the Portuguese sectors of Minho and Lima river basins.

Precipitation data from Minho region

Hydrological years from 1933 to 2010

	Annual	RunAve (5 years)	Winter (DJFM)
2010	1733	1294	1157
2009	1260	1099	605
2008	826	1063	443
2007	1364	1122	593
2006	1286	1079	625
2005	760	1659	282
2004	1078	1880	402
2003	N/A	1968	N/A
2002	1193	2035	540
2001	3604	2118	2486
2000	1643	1828	455
1999	1430	1866	468
1998	2305	1986	665
1997	1610	1789	596
1996	2151	1705	1190
1995	1834	1625	949
1994	2028	1571	820
1993	1321	1377	392
1992	1192	1532	231
1991	1747	1602	906
1990	1568	1669	869
1989	1054	1786	409
1988	2100	1929	929
1987	1541	1892	708
1986	2084	1925	1116
1985	2150	1783	1041
1984	1772	1704	1012
1983	1912	1985	595
1982	1707	2082	1093
1981	1375	2300	574
1980	1754	2258	899
1979	3175	2234	2466
1978	2398	2044	1579
1977	2797	1952	1593
1976	1166	1744	437
1975	1633	1877	843
1974	2227	1970	1302
1973	1936	2143	763
1972	1759	2157	1212
1971	1832	2225	735
1970	2094	2535	1174
1969	3095	2437	1666
1968	2006	2376	658
1967	2099	2433	872
1966	3380	2501	1852
1965	1605	2367	929
1964	2792	2682	1287
1963	2288	2546	1532
1962	2441	2533	1412
1961	2709	2361	909
1960	3179	2309	1995
1959	2112	2094	1258
1958	2224	1961	1226
1957	1579	1796	1033
1956	2449	1854	1179
1955	2106	1806	1288
1954	1447	1752	761
1953	1400	1712	435
1952	1867	1781	678
1951	2212	1983	1287
1950	1834	1982	773
1949	1246	1869	698
1948	1745	1901	1088
1947	2876	1911	1876
1946	2210	1677	960
1945	1267	1620	584
1944	1407	1699	381
1943	1793	1754	1154
1942	1706	1631	623
1941	1925	1608	920
1940	1665	1702	827
1939	1682	1733	799
1938	1178	1728	462
1937	1589	1911	942
1936	2397	1991	1395
1935	1820	1856	1085
1934	1655	1874	734
1933	2093	N/A	1192
1932	(december value included in hydrol. year 1933)		

Appendix 3.5. $^{210}Pb_{Excess}$ and ^{137}Cs content (Bq kg^{-1}) in the FCPw1 core.

$^{210}Pb_{Excess}$ and ^{137}Cs content (Bq kg^{-1})				
Depth (cm)	$^{210}Pb_{Excess}$	Error	^{137}Cs	Error
0.5	328.8	38.3		
1.5	250.7	29.7		
2.5	166.1	20.9		
3.5	121.1	16.4	16.7	1.7
4.5	113.6	15.6	17.7	1.7
5.5	108.9	15.3	20.0	1.7
6.5	88.2	13.0	28.5	1.7
7.5	125.9	16.8	40.5	1.3
8.5	66.8	10.9	74.3	2.7
9.5	30.5	7.4	45.7	1.7
10.5	12.5	5.6		
11.5	5.0	4.9		
12.5	2.4	4.6		
13.5	2.1	4.6		

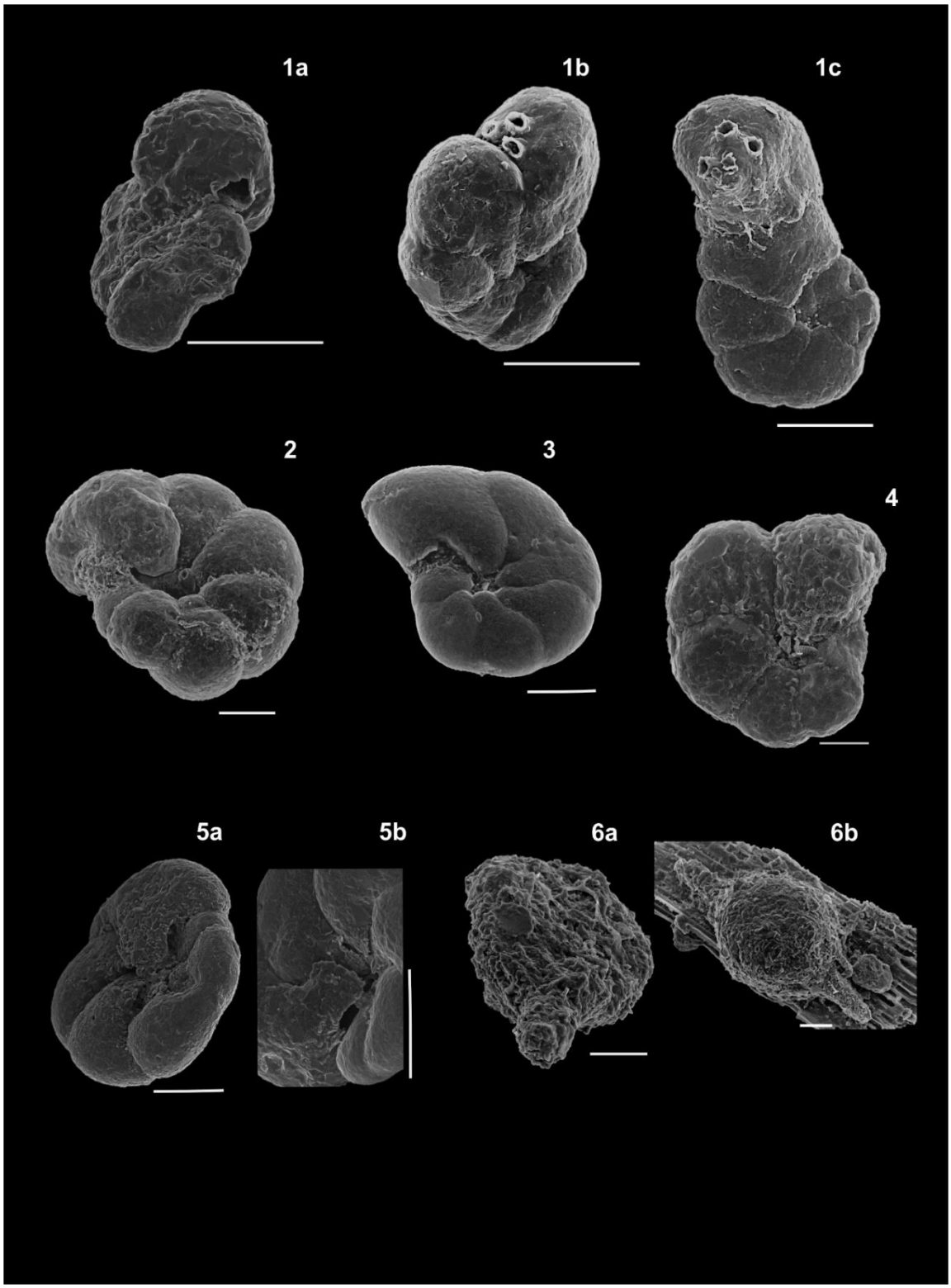

Plate 3.1. Scale bar 100 µm. 1a *Trochamminita salsa* (Cushman and Brönnimann, 1948), single areal aperture specimen; 1b and c *Trochamminita salsa* (Cushman and Brönnimann, 1948), irregular specimen with backward multiple areal apertures. 2 *Haplophragmoides manilaensis* Andersen 1953; 3 *Haplophragmoides wilberti* Andersen 1953; 4 *Haplophragmoides* sp.; 5a *Tiphotrocha comprimata* (Cushman and Brönnimann, 1948), ventral view; 5b *Tiphotrocha comprimata* (Cushman and Brönnimann, 1948), apertural view; 6a *Pseudothurammina limnetis* (Scott and Medioli, 1980), free specimen; 6b *Pseudothurammina limnetis* (Scott and Medioli, 1980), plant debris attached specimen.

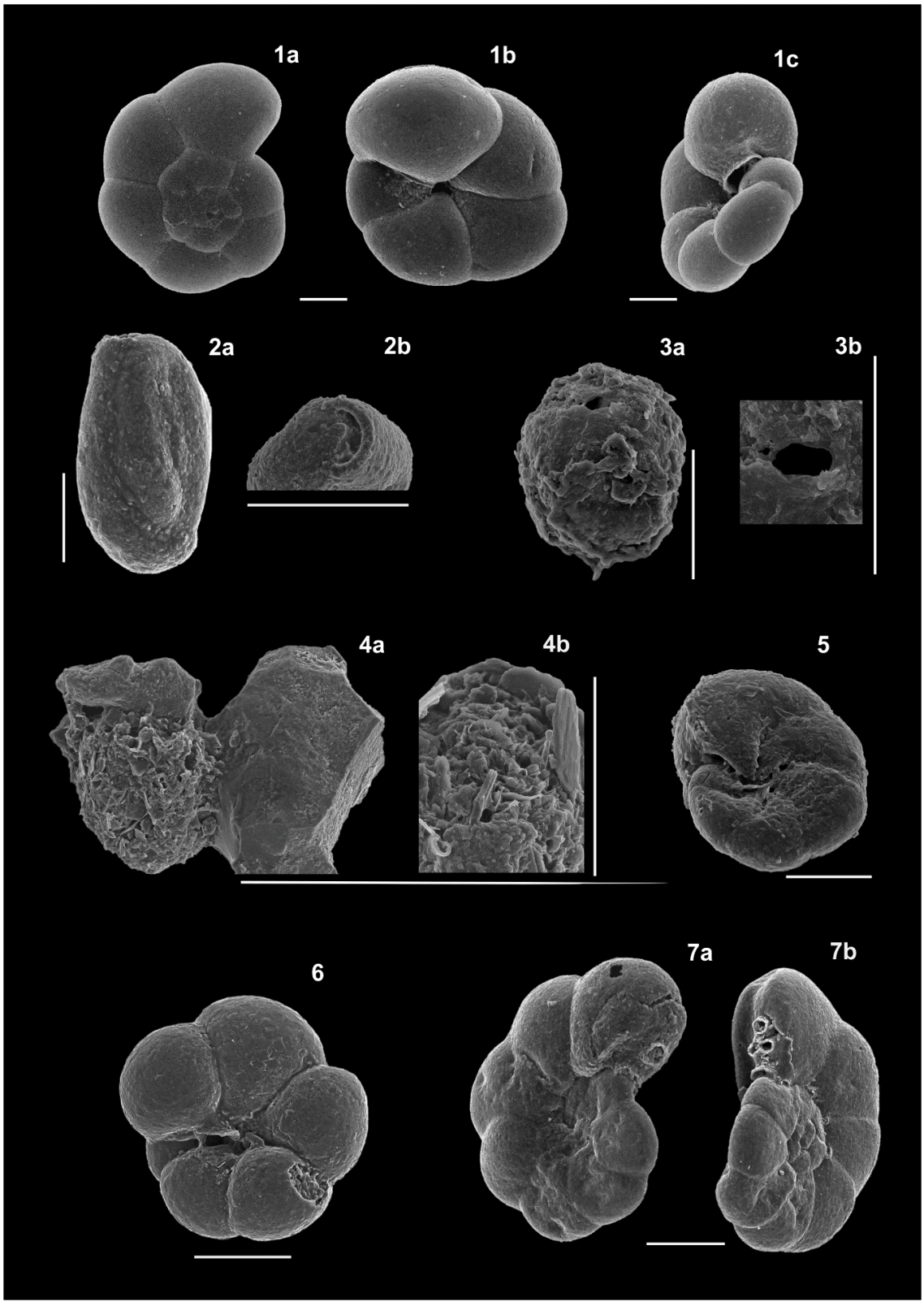

Plate 3.2. Scale bar 100 µm. 1a *Trochammina inflata* (Montagu, 1808), dorsal view; 1b *Trochammina inflata* (Montagu, 1808), ventral view; 1c *Trochammina inflata* (Montagu, 1808), apertural view. 2a *Miliammina fusca* (Brady, 1870); 2b *Miliammina fusca* (Brady, 1870), apertural view. 3a *Saccammina* sp.; 3b, *Saccammina* sp., apertural view; 4a *Psammosphaera* sp.; 4b *Psammosphaera* sp., pores/apertures detail; 5 *Paratrochammina guaratibaensis* Brönnimann, 1986, ventral view. 6 *Siphotrochammina lobata* Saunders, 1957, ventral view. 7a *Jadammina macrescens* (Brady, 1870), ventral view; 7b *Jadammina macrescens* (Brady, 1870), dorsal view.

4 Grape harvest dates as indicator of spring-summer mean maxima temperature variations in the Minho region (NW of Portugal) since the 19th century

J. Moreno [a,b], F. Fatela [a,b], F. Moreno [c], E. Leorri [d], R. Taborda [a,b], R. Trigo [e]

[a] IDL – Instituto Dom Luiz, Universidade de Lisboa, Campo Grande, 1749-016, Lisboa, Portugal

[b] Departamento de Geologia da Faculdade de Ciências da Universidade de Lisboa, Campo Grande, 1749-016, Lisboa, Portugal

[c] Independent researcher, Caminho da Portela, 4940-061 Bico PCR, Portugal

[d] East Carolina University, Department of Geological Sciences, Greenville, NC 27858-4353, USA

[e] DEGGE – Departamento de Engenharia Geográfica, Geofísica e Energia da Faculdade de Ciências da Universidade de Lisboa, Campo Grande, 1749-016 Lisboa, Portugal

Published in: *Global and Planetary Change* 141 (2016), 39–53

http://dx.doi.org/10.1016/j.gloplacha.2016.04.003

"Want the moonlight ripens the grapes." Portuguese adage used to describe someone who wants something impossible.

A. Moreira in PROVÉRBIOS PORTUGUESES (2003), p. 276.

ABSTRACT

This paper reports a climatic reconstruction approach for the Minho region (NW of Portugal) using grape harvest dates (GHD) as proxy of surface air temperature. This new GHD series was built based on the records from a set of local and regional newspapers (1854–1978) and the annuals of a Wine Producers Cooperative (1978–2010). The strong inverse correlation between Minho GHD and the mean maxima temperatures of the preceding March to August months (GSTmax), registered at the Braga weather station for the overlap period 1941–2009, allowed a reconstruction, with associated statistical uncertainties, of the regional GSTmax back to 1856. These were then used to characterize the main climatic episodes in the region during the last 154 years. The most noticeable feature that emerges from the comparison of the Minho GSTmax with the global annual average temperatures of Jones et al. (2013) is that these regional temperatures, in clear contrast with the global warming observed from around 1990 onwards, show no

noteworthy increasing trend. The influence of climatic variability was examined also in terms of the relations between GSTmax (1950–2009) and the main meteorological teleconnection patterns affecting the North Atlantic European sector where the Minho region is included. Data support the hypothesis that persistent positive modes of spring-summer Scandinavian (SCA) and summer East Atlantic/Western Russia patterns triggered lower GSTmax, especially in the 1960s–1980s. The search for solar imprints in the Minho region climate identified the SCA mode as a promising connection between the two, since it is significantly inversely correlated with both, the TSI and the GSTmax.

Like in other traditional European viticultural regions, the Minho GHD have shown to be a valuable tool for understanding the interactions between large-scale circulation modes and regional/local climatic conditions. Besides it will deliver a reliable assessment of climatic proxies from geological record, like tidal marsh benthic foraminiferal assemblages.

Keywords: Newspapers; grape harvest dates; growing season; maxima temperatures; teleconnection modes; TSI.

4.1. Introduction

The interest in past climate variability under the present scenario of climate change has led to various efforts to extend temperature reconstructions further back in time, particularly in Europe where archives and documentary sources abound. These reconstructions usually rely on a combination of instrumental data (only available for the last *ca.* 150 years), several kinds of historical records, archeological evidence and inferences from environmental proxies (e.g., Jones and Mann, 2004).

In this context, a number of studies have used dates of vine harvests as indicators of climate variability (e.g., Guerreau, 1995 and references therein). Following the pioneer works of Dufour (1870), Angot (1883) and, later on, Garnier (1955) or Le Roy Ladurie (1967), connecting climate and viticulture, grape harvest dates (GHD) have been gathered to generate temperature reconstructions for the past 400 to 500 years from the traditional European viticultural regions of France, Italy, Spain, Switzerland and Germany (e.g., Le Roy Ladurie and Baulant, 1980; Pfister, 1992; Chuine et al., 2004; Brázdil et al., 2005, 2008; Meier et al., 2007; Jones et al., 2009; Mariani et al., 2009; Kiss et al., 2011; Krieger et al., 2011; Maurer et al., 2011). However, similar quantitative reconstructions are lacking from Portugal, despite the long history of this Iberian country in winemaking and the fact that it is the current 11th wine-producer worldwide (OIV, 2015). This Portuguese viticultural heritage is reflected by > 250 native grape varieties as well as by the close link between wine and the historic expression of some local and regional cultural traditions. As stated by Stanislawski (1970), these ones are deeply embedded in the rural landscape, remaining at present much alive in the geographical identity of the country (e.g., Hooson, 1998; Correia, 2011).

It has been recognized that the onset and duration of all major grapevine phenological growth stages are interconnected and strongly dependent on climate conditions (e.g., Jones and Davis, 2000), because wine production is largely controlled by atmospheric forcing, mainly during the grapes growing season (GS), i.e., from budburst to harvest, when temperature is a major controlling factor. Indeed, temperature was used in the development of a number of climate indices linked to wine grape quality, such as the Latitude-Temperature Index (Kenny and Shao, 1992) and the Average Growing Season Temperature Index (Jones, 2006). Furthermore, on a global scale, it has long been considered that the optimal zones for viticulture are between either the mean annual 10–20ºC isotherms (e.g., de Blij, 1983) or the growing season 12–22ºC isotherms (Gladstones, 2004; Jones, 2006). In addition to temperature, annual precipitation and its seasonality is also a critical factor, affecting pest and disease pressure, fruit quality, vine balance and yield (Fraga et al., 2014; Keller, 2015). Excessive rainfall during the early GS has a negative effect by delaying growth, and precipitation during the late GS (particularly during the ripening period) may have a negative influence, diluting the grapes and producing lower relative sugar levels, thus lowering the alcohol content (e.g., Jones and Storchmann, 2001). In this sense, some modelling studies of Portuguese viticulture have included climatic variables to predict wine production (Gouveia et al., 2011) and yield (Santos et al., 2010a) in the famous Douro Port Wine Region. Likewise, extreme weather events, like hail, frost and heat waves during the GS, can have harmful impacts on vineyards, thus contributing to significant fluctuations in yield, wine quality and in the dates of harvest. Consequently, the overall grapevine growth cycle (including vegetative and reproductive cycles) is triggered by a combination of parameters such as surface air temperature, precipitation and solar radiation (e.g., Jones et al., 2005; Keller, 2015). In addition to this direct influence, other factors, as weather regimes or teleconnection climatic modes of oscillation (Wallace and Gutzler, 1981; Barnston and Livezey, 1987), may explain grape production and wine quality as they incorporate several components of climate in their typical atmospheric conditions. In Iberian Peninsula, such climatic stimuli and their effects have been studied before by Lorenzo et al. (2012) in Rías Baixas (NW of Spain) and by Fraga et al. (2014) in the northern Portuguese Minho Wine Region (MWR).

Amongst the vine-related biophysical indicators, GHD have attracted the attention of historical climatologists mainly due to the existence of these data in Europe since the “Middle Ages”. This (para)phenological information has resulted in long archives of dates, which, in general, correspond to the stage of full maturation of grapes. Owing to the strong control of temperature on grape ripening, these archived dates furnish a very concise record of growing season temperatures (GST; mean or maximum temperature averaged normally over April–August; Menzel, 2005). In fact, GST and GHD series present statistically significant correlations (e.g., Menzel, 2005; Daux et al., 2007; Meier et al., 2007; Maurer et al., 2011). Considering the whole body of evidence about the relationships between GHD and temperatures, the starting dates for grape harvests are currently

held as a consistent proxy for this meteorological variable and a source of climatological knowledge in the reconstruction of past climates (Brázdil et al., 2008).

The present work aims to take a step further towards a more comprehensive understanding of the climatic patterns in the MWR, derived from the compiled information about the beginning of the grape harvests. We do this by i) introducing a 154-year series of grape harvest dates for this region, ii) evaluating the potential of these data for temperatures reconstruction in the MWR by means of a linear product moment Pearson correlation methodology, iii) examining how the mean maxima temperatures of the GS (reconstructed from the Minho GHD series) have changed over the documented period (1856–2009), and iv) relating the main North Atlantic teleconnection modes and the oscillations in the total solar irradiance (TSI) with GSTmax changes.

4.2. Study area

The Minho region is a historical province, located in the NW of Portugal, that includes the Braga and Viana do Castelo districts. This region borders Galicia (Spain) in the north and the Atlantic Ocean in the west and covers 4700 km^2. The MWR, demarcated in 1908, is one of the oldest in the country land covering about 8800 km^2 and geographically coinciding with the "Vinho Verde" denomination of origin (Figure 4.1A and B). It is the Atlantic wet climate, with relatively high exposure to maritime winds, high annual precipitation (1200–2400 mm), mild summers (summer mean temperatures from 18 to 22ºC) and relatively low annual insolation (> 2500 h), that explains the MWR uniqueness and discrimination from other Portuguese wine regions (Fraga et al., 2014). The MWR possesses an irregular topography, ranging from 0 m to *ca.* 1500 m altitude, characterized by a compact valley system (Magalhães, 2008), in a geological setting of igneous and metamorphic rocks, including granites, quartz-diorites, greywackes and schists (IGME, 1986; Pereira et al., 1989). Benefiting from these local/regional climatic and geomorphological features, some traditional vine training systems (pergola, stakes, trellised vines and tall growing vines) have survived to modern times. These systems are a response to the high vegetative growth of vines and the need to isolate grapes from the ground to facilitate ripening and to diminish the risk of fungal diseases.

4.3. Materials and methods

4.3.1. Grape harvest dates and weather information from documentary sources

The time series of grape harvest dates for the Minho region was compiled from two documentary sources: 41 local and regional newspapers, from 1854 to 1978, and the annual records (unpublished) from the Ponte de Lima Wine Producers Cooperative (1978–2012), located in the Viana do Castelo district. As a result, the series was constructed from an ensemble of harvest dates chronicled at 16 municipalities from a total of 24 belonging to the Viana do Castelo and Braga districts

(Figure 4.1B). Just the newspapers from 1854 to 1855, 1860, 1883, 1933, 1946, 1951, and 1955 did not contain any reference to grapevine harvests, i.e., only about reducing the information gaps to *ca.* 5% of the total period considered. For a given year, we have stipulated the harvest starting date as the first news published about grape harvesting. Simultaneous to the GHD research, the newspapers were methodically reviewed for supplementary descriptive data as regards to meteorological events with potential meaningful impacts on those dates (e.g., floods, droughts, storms, snowfall, hail, etc.).

In Catholic countries like Portugal, the use of religious ceremonies constitutes an important source of information that can support historical climate reconstructions. The potential use of these rogations (i.e., "prayer, plea, request") as a climate proxy was recognized by Giralt (1958), and since then systematic records of these religious expressions, with traditional rituals appealing for the end of drought periods – *pro-pluvia* rogations/processions – or long wet/stormy spells – *pro-serenitate* rogations/processions, have often been used in historical climatology (e.g., Alcoforado et al., 2000; Domínguez-Castro et al., 2008). Rogations were indeed an institutional mechanism related to climate stress situations (e.g., Martín-Vide and Barriendos, 1995; Barriendos, 2005). They were ordered by ecclesiastical and municipal authorities when the harvests seemed to be threatened by drought or excessive rainfall. Thus, the occurrence of pro-pluvia and pro-serenitate ceremonies was also compiled.

In order to avoid redundancy, when the same meteorological or religious event was reported by several newspapers, it was included in the dataset as one entry. In total, near 34,200 individual newspapers were consulted for this study.

4.3.2. Climate instrumental data and proxies

Monthly and annual mean temperature measurements were obtained from a recent compilation of homogenized daily temperature time series (Santo et al., 2014). We were particularly focused on the national weather station 023, located at Braga (altitude 190 m; 41°33′ N, 08°24′ W; Figure 4.1B), with data ranging from 1941 to 2009. Besides its central location in the study area, this station was chosen because it has one of the oldest instrumental records in the Minho region.

Precipitation data were obtained from the monthly records of 54 meteorological and hydrological stations from the Minho region since 1930. Data from the Portuguese areas of the Minho and Lima River basins were integrated to create the longest and most representative record for the area (http://snirh.pt), covering the period 1932–2010. This 78-year precipitation series was used to compute the Standard Precipitation Index – SPI (McKee et al., 1993) with a freeware program (SPI_SL_6.exe) available at the National Drought Mitigation Center of the University of Nebraska-Lincoln, USA (http://drought.unl.edu). This index allows monitoring drought events, labelling their severity according to a classification scheme (from mild to extreme; McKee et al., 1993). It is widely applied due to its reliability and the relatively ease of comparison between diverse locations and

climates (http://drought.unl.edu). The SPI can be computed to quantify the precipitation deficit for multiple time scales, from 1 month (SPI_1) up to 72 months, although SPIs with time scales longer than 24 months may be unreliable (Guttman, 1999).

The monthly values of the major large-scale patterns (or teleconnections) for the Euro-Atlantic region (Barnston and Livezey, 1987) were also considered. Thus, the indices relative to the North Atlantic Oscillation (NAO), Arctic Oscillation (AO), East Atlantic Oscillation (EA), East Atlantic/Western Russia Oscillation (EA/WR) and the Scandinavian Oscillation (SCA) were taken from the Climate Prediction Center (CPC) at the National Centre of Environmental Prediction, USA (http://www.cpc.noaa.gov/data/teledoc/), and also from http://www.atmos.colostate.edu/ao/data/ao_index.html and http://climexp.knmi.nl/.

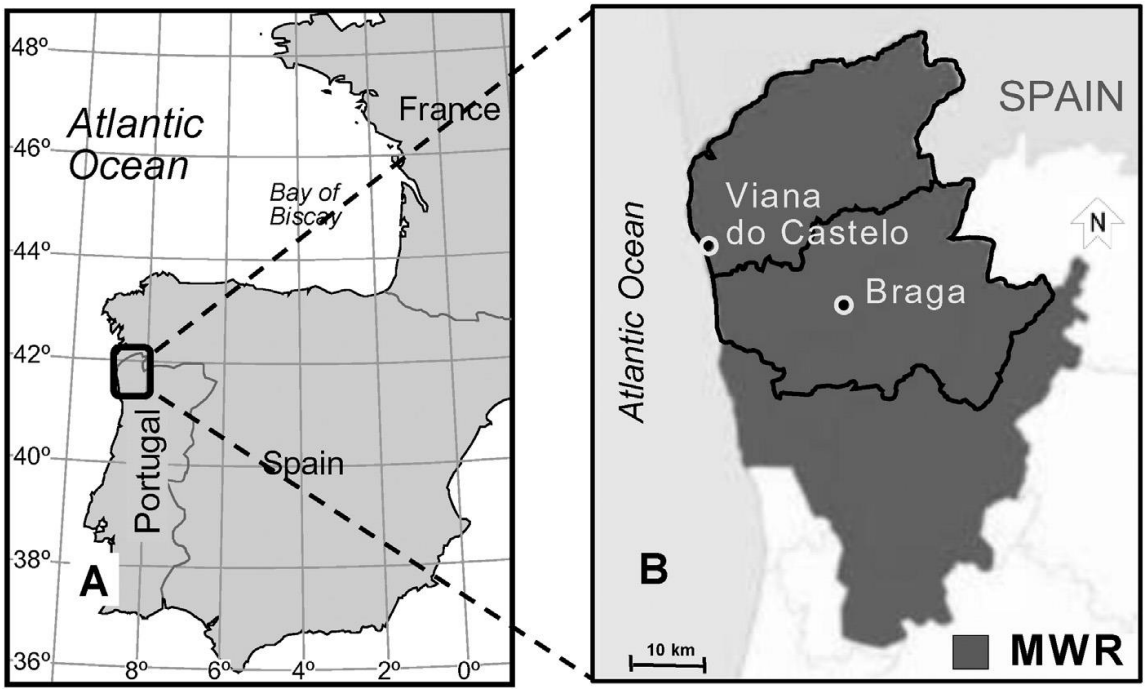

Figure 4.1. **A –** Location of the Portuguese Demarcated Minho Wine Region (MWR). **B –** Map of the Viana do Castelo and Braga districts (Minho region) in the more extended Minho Wine Region (MWR; grey area).

4.3.3. Statistical analysis

4.3.3.1. Seasonal reconstruction target

Climatic reconstructions using a proxy predictor like GHD can be efficiently conducted either with linear regression or process-based phenological models (e.g., Cortázar-Atauri et al., 2010). However, the latter are of difficult application because they require a detailed dataset of field observations concerning main grapevine phenophases (budbreak, flowering and ripening) in addition to harvest dates, which in practice, are hardly attainable. On the other hand, linear regression models are simple to design and they have been routinely demonstrated to be successful in delineating the relationships between this kind of data and climatic fluctuations (Etien et al., 2009).

Therefore, in an initial step, grape harvest calendar dates were defined as the number of days after August 21st, the earliest harvesting date of the entire series. In a second step, GHD were standardized to z-scores, using the equation:

$$z - \text{score} = \frac{GHD_i - \overline{GHD}}{\sigma} \qquad (1)$$

Where GHD_i is a specific GHD date, GHD is the mean date of the series and s is the standard deviation.

Then an 11-year running average was applied to the GHD normalized series to improve the signal to noise ratio in the data. Pearson product-moment correlation coefficients were computed, together with their significance levels for the period of time when both the instrumental data (temperature and precipitation) and the Minho GHD time series overlap (1941–2009), to determine the seasonal response (in terms of strength and linearity) of these data. This process was performed for a range of averaged values, from monthly data to semi-annual values (i.e., averaged values of 1, 2, 3, 4, 5, and 6 months), in order to ascertain the period(s) potentially providing the strongest correlation between the two variables (GHD *vs.* temperature/precipitation), and consequently, the best reconstruction target. In our case, this is identified as the mean maxima temperatures of the group of months from March to August – GSTmax –, as registered in Table 4.1. To our knowledge, this database includes the longest time span (68 years) of concomitant grape harvest dates and instrumental air temperatures (minimum, mean and maximum monthly averages) for the Minho region.

Table 4.1. Pearson correlation coefficients (GHD z-score normalized data *vs.* March to August mean maxima temperatures, for the period 1941–2009; MAM – March, April and May; JJA – June, July and August; MAMJJA – March, April, May June, July and August.

	Month	Bimester		MAM	JJA	MAMJJA
March	-0.46*	-0.57*		-0.69*		
April	-0.43*		-0.62*			
May	-0.54*	-0.67*				-0.74*
June	-0.52*		-0.55*			
July	-0.33**	-0.47*			-0.57*	
August	-0.37**					

*p < 0.001.
** p< 0.05.

4.3.3.2. Regional temperature reconstruction prior to instrumental data

The transformed Minho GHD time series was applied as a predictor in the reconstruction of the growing season (spring-summer) mean maxima temperatures back to 1856 in the MWR, using a linear regression model (least squared method). It is worth noting that the approach selected for this study has been largely used in dendroclimatology (e.g., Cook et al., 1994) and historical climatology (e.g., Brázdil et al., 2008; Leijonhufvud et al., 2010; Wetter and Pfister, 2011; Možný et al., 2012).

In order to remove the potential impact of outliers into the reconstruction, a least median of squares model was initially applied to the overlapping period (from 1941 to 2009) of GHD and monthly (maximum) temperature measurements. Following the criteria of Rousseeuw and van Zomeren (1990), the year 1949, the largest outlier, was excluded from the analysis. The model performance was assessed by means of a holdout cross-validation method, by dividing the overlap period in two subsets: the calibration and the verification periods. Calibration was made independently on both 1941–1976 and 1977–2009 periods while the verification was undertaken on the periods not comprised in calibration. This process was validated by some commonly used skill statistics: shared variance (r^2 and $\bar{r}^2$), root mean squared error (RMSE), reduction of error (RE) and coefficient of efficiency (CE) values (Cook et al., 1994). The coefficient of determination (r^2) ranges from 0 to 1, with higher values indicating less error variance, and typically values > 0.5 are considered acceptable; the lower the RMSE the better the model performance, with a value of 0 indicating a perfect fit; RE and CE values range from $-\infty$ to 1, with RE / CE = 1 being the optimal value and positive ones indicating regression skill relative to the climatology. An additional statistical approach – the Durbin-Watson (DW) test – was used for measuring the predictive ability and diagnosis of first-order autocorrelation within regression residuals (e.g., von Storch and Zwiers, 1999). To reconstruct the temperature for the whole studied period, the training set was developed using the data corresponding to the period 1941–2009. Parameters and statistical indicators of the final model performance are presented in the Results section.

4.4. Results

4.4.1. The Minho GHD series and other documentary weather-related data

The 154-years GHD time series for the Minho region covers the period between 1856 and 2009 (Figure 4.2; Appendix 4.1). Gaps result from missing information for 8 years, 4 in the 19th century (1854, 1855, 1860, and 1883) and 4 in the 20th century (1933, 1946, 1951, and 1955).

The 11-year running average of the Minho GHD series allows the identification of 6 periods: 3 distinctive periods of earlier harvest dates (dominated by negative values): 1856–1876, 1888–1899, and 1929–1952; and 3 periods of delayed harvest dates (dominated by positive values): 1876–

1888, 1900–1929, and 1952–2010. The latter is showing the most meaningful set of positive values, particularly between the 1960s and the 1980s (Figure 4.2).

Newspaper articles about *pro-pluvia* and *pro-serenitate* ceremonies in the Minho region were published mainly during the 19th century, becoming apparently less newsworthy thereafter. Despite this constraint, a total of 41 records of pro-pluvia religious ceremonies was found (Figure 4.2). They are predominantly related to negative GHD z-score values, or low positive values, in the years of 1887, 1895, 1926, and 1953, when 83% occurred during the GS months (March to August). It must be also pointed out that 17 (42%) of the pro-pluvia rogations are recorded in the 7 years that are preceded by several very negative z-scores of GHD, between 1856 and 1876 (Figure 4.2).

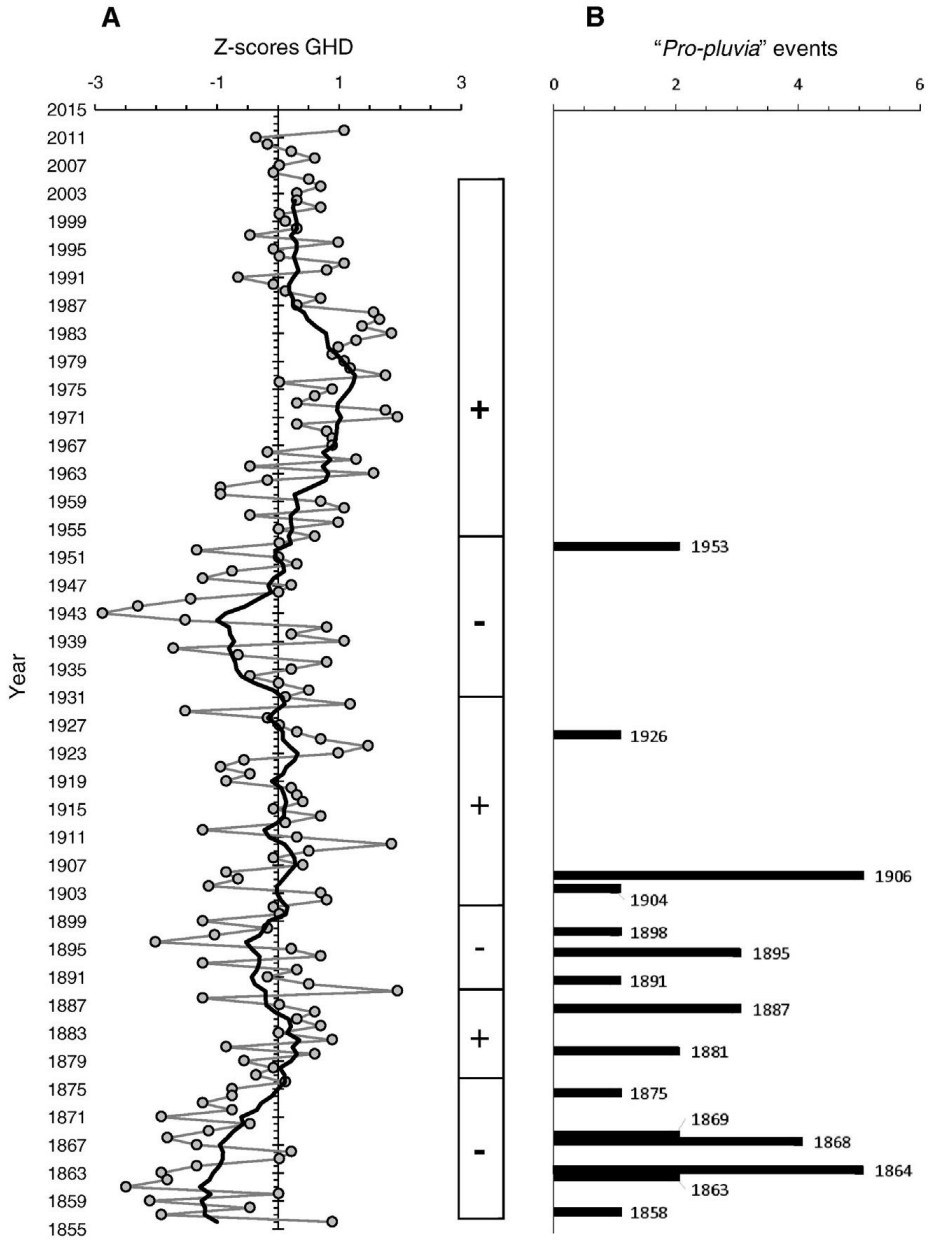

Figure 4.2. A – Z-scores of the GHD recorded in newspapers from the Minho region, covering 16 municipalities (grey line); GHD 11-year running averages (black line; + periods of delayed, GHD; − periods of early GHD). **B –** Number of *pro-pluvia* events documented in the set of 41 local and regional newspapers reviewed for the Minho region.

4.4.2. Relationships between Minho GHD and temperature/precipitation

The highest value concerning the Pearson correlation coefficients between the GHD series and the Minho region monthly precipitation was obtained for the month of June ($r = 0.21$; $p < 0.07$). An identical result ($r = 0.24$; $p < 0.05$) was found for the SPI_1 for the same month.

However, GHD values inversely correlate with spring and summer mean maxima surface air temperatures (Table 4.1). While the correlation between single months and a series of month combinations were calculated, the interval of March–August was selected as the "growing season period" for the Minho region. This interval yielded the most stable and strongest inverse correlation with GHD ($r = -0.74$; $p < 0.001$; Table 4.1). Adding September temperatures to the ones of the previous months (March–August) did not improve the correlation. This is due, as referred by Chuine et al. (2004) and Brázdil et al. (2008), amongst others, to the significant role played by late-spring temperatures, in contrast with September temperatures, which strongly impact the sugar content rather than the timing of the grape harvest. Grapevine harvest dates are also inversely correlated with mean annual temperatures yielding a linear correlation coefficient of $r = -0.57$ ($p < 0.001$). No significant correlation was found between GHD and autumn winter maxima temperatures. The same result (lack of significant correlation) was observed for minima temperatures. So, on the basis of this correlation analysis, the March–August mean maxima temperatures were chosen as the most accurate (best) climatic reconstruction target.

Though the length of the two sub-periods used in the calibration/ verification exercises (Figure 4.3) could be considered relatively short, the reconstruction skill statistics of Minho GHD against March–August mean maxima temperatures (Table 4.2) suggest a reliable model, using the ordinary least squares linear regression, to reconstruct the complete period (1856–2009). The proposed model explains 55% of the March–August mean maxima surface air temperature variance and satisfies the general criterion RE > CE > 0. The DW value of 1.60 indicates low first order autocorrelation in the reconstructed/measured residuals and that the reconstruction captures decadal variability relatively well. Similarly to earlier models, the variance unresolved by our model might be ascribed not only to other natural factors affecting the annual cycle of vines, but to human activities reflected in the grape harvesting date. Amongst them the personal judgement of the winegrower regarding the exact time of ripeness might be influential (more in the past than today due to technical progress).

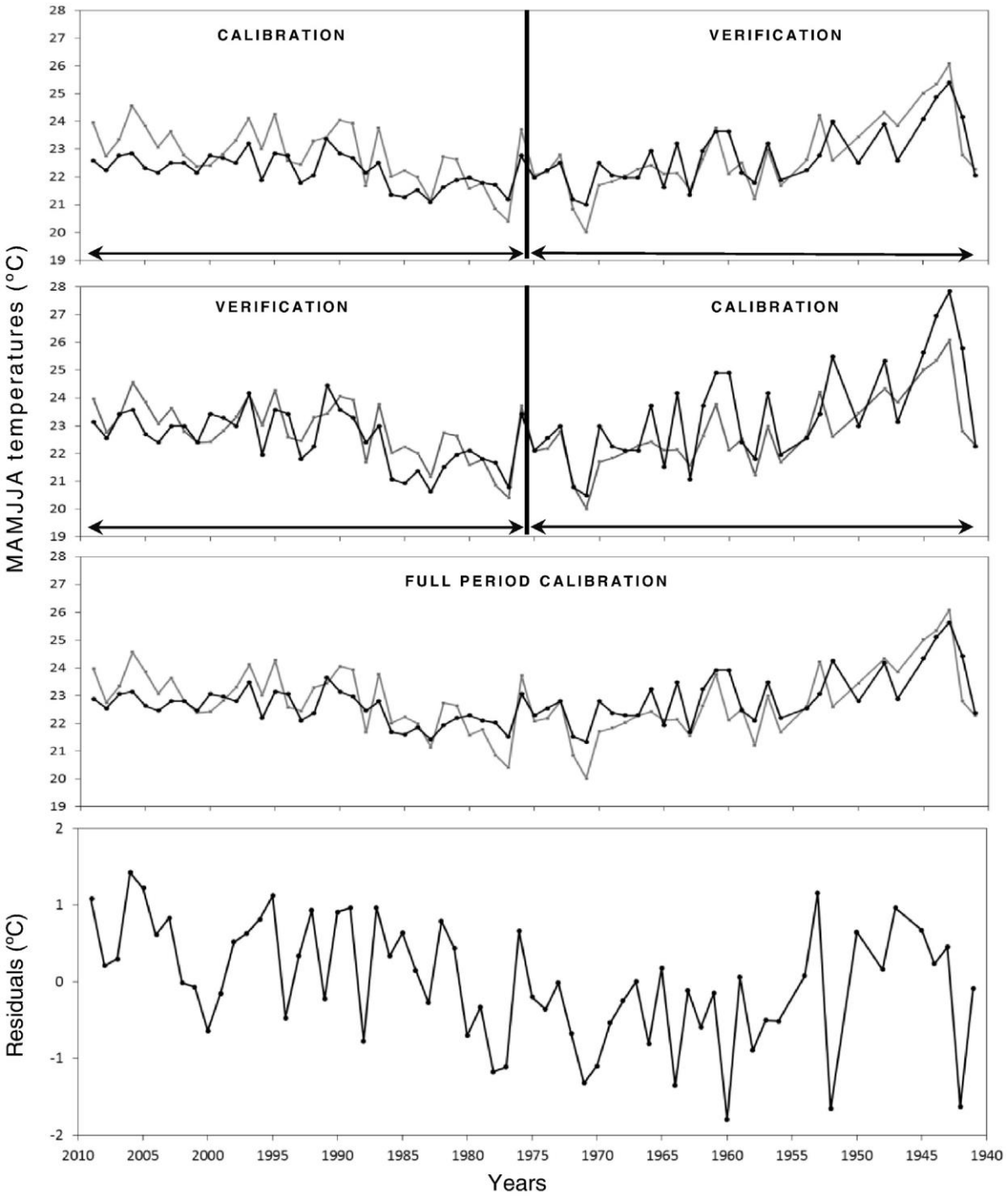

Figure 4.3. Calibration and verification results of the GHD composite with March–August Braga mean maxima temperatures (reconstruction – black; instrumental data – grey).

Table 4.2. Linear regression model calibration and verification statistics, for two independent periods: r squared (r^2), r-bar squared (r^2), root mean squared error (RMSE), reduction of error (RE) statistic, coefficient of efficiency (CE), and Durbin-Watson (DW) statistic. Statistics for the overall period (1856–2009): r^2 = 0.55; r^2 adjusted = 0.54; DW = 1.60.

Calibration statistics					Verification statistics					
Period	r^2	r^2 adjusted	RMSE	DW	**Period**	r^2	r^2 adjusted	RMSE	RE	CE
1941-1976	0.66	0.65	0.75	1.73	**1977-2009**	0.57	0.56	0.90	0.22	0.21
1977-2009	0.57	0.56	0.81	1.39	**1941-1976**	0.66	0.65	0.75	0.12	0.11

Therefore, the final regression equation for reconstructing March–August mean maxima temperatures in the Minho region is the following:

$$T_{max\ (Marsh\text{-}August)} = 23.07 - 0.89 \times GHD_{Minho} \qquad (2)$$

The standard predictive error is 0.78ºC. The reconstruction (raw data) for the pre-instrumental period back to 1856 (along with a 10-year running average) is displayed in Figure 4.4.

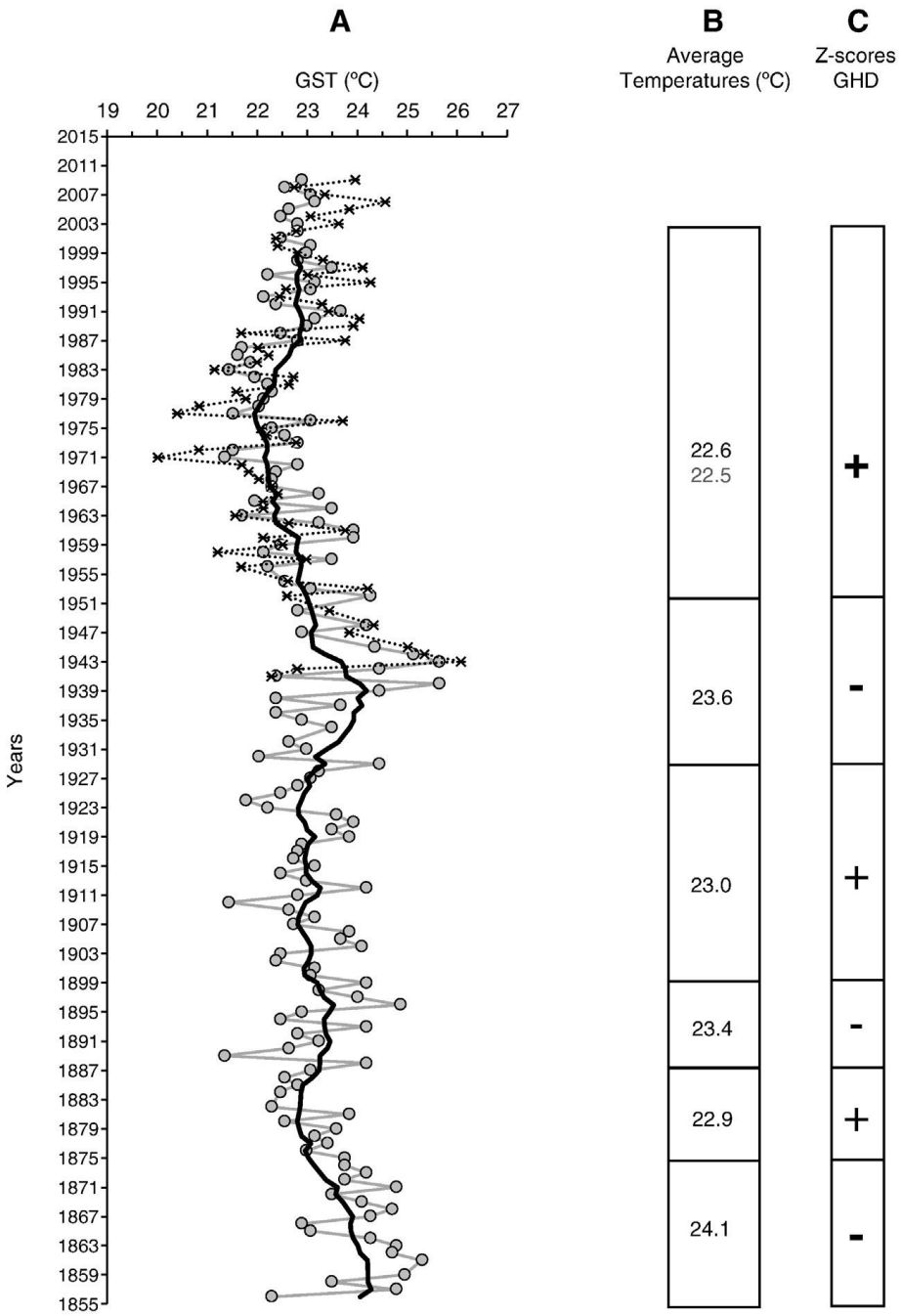

Figure 4.4. A – March to August mean maxima temperatures (instrumental - dashed line; reconstructed - grey line; reconstructed 11-year running averages - black line). **B –** Averaged mean maxima temperatures for the GHD z-score periods (instrumental - grey number; reconstructed - black numbers). **C –** GHD 11-year running average periods (+ periods of delay GHD; − periods of early GHD).

4.5. Discussion

4.5.1. Minho grape harvest dates and climate variables (temperature and precipitation)

Agricultural systems are managed ecosystems (Adams et al., 1998). However, climate is the main determinant on traditional crop production (not considering recent greenhouse agricultural production). While temperature and precipitation are both major controlling factors, in regions without pronounced water limitations, which is the case of the study area, temperature becomes the leading factor for grapevine growth, and hence for the date of the harvest (e.g., Jones and Davis, 2000). This is supported by the lack of strong correlations between Minho GHD and GS precipitation and it is in agreement with results elsewhere (e.g., Mariani et al., 2009; Dalla Marta et al., 2010). The delaying harvest effect detected in our data for June precipitation (1932–2010 Minho–Lima basin precipitation; $r = 0.21$; $p < 0.07$) has also been reported by Bock et al. (2013) in Germany. This might be linked to the general climatic influences for flowering, which occurs in the first weeks of June, and needs dry stable conditions to facilitate flower growing (Jones, 1999). A compatible result for the precipitation role in May–June was obtained by other researchers modelling the amount of Portuguese Douro wine production (Gouveia et al., 2011).

Specifically, grape harvest dates are dependent on climate over the whole GS, having shown to be strongly influenced by spring-summer maxima temperatures (e.g., Chuine et al., 2004). On the other hand, between October and early March vineyards are in a latency stage (inactive or dormant) during which the vine static mass is not impacted by temperature changes, unless intense frost occurs (Lorenzo et al., 2012). This means that the grapevine harvest will occur earlier with higher spring and summer temperatures, despite the impact of non-climatic (human) factors when planning these dates, like the winegrower verdict (Etien et al., 2009). Actually, GHD are more than just (para)phenological data, relating vine cycles stages, especially their timing, with weather and climate. They can also be considered historical data, and their variations through time can reflect an anthropogenic factor affecting harvest scheduling: modifications in cultivation methods and improvements in agricultural technology, cultural changes, political background or socio-economic context like wars, local conflicts or panics due to robberies or vineyard diseases (e.g., Schultz and Jones, 2010; Garnier et al., 2011). Regardless of the uncertainties arising from that sort of contingencies and the additional (and crucial) fact that the Minho GHD series outcomes from a composite of newspaper records about harvests from more than a dozen localities spread over an area of *ca.* 4000 km^2 – each one reflecting different edaphoclimatic conditions, i.e., the *terroir* or "the taste of the place" – the present model shows statistical predictive ability (Table 2). Although, it must be recognized that the reconstruction error is not as good as the one achieved by other phenological models (e.g., Kiss et al., 2011; Možný et al., 2012). The single outlier removed from the training set (year 1949) can be explained by a drought peak (SPI severe drought; Santos et al., 2010b) that was exacerbated by a summer heat wave, covering Western Europe (Della-Marta et al., 2007). While dry

heat is generally good for wine grapes, heat stress (temperatures above 35ºC) can severely damage grapevine leaves and grapes (Chuine et al., 2004). Heat waves may actually provoke later harvest dates by slowing down metabolic processes, delaying ripening and promoting withering (Gershunov et al., 2010; Dalla Marta et al., 2010). The elimination of this grape harvest date from the training set seems justified considering this contextualized information.

It follows from Figure. 4.4A that the model developed here is able to reproduce the maximum temperature inter-annual variability for the Minho region. It underestimates (colder than) the instrumental values between 1943 and 1950 and 2003–2009, and overestimates instrumental values (warmer than) between 1956 and 1980,with the exception of the years of 1959, 1965 and 1976 (Figure 4.4; Appendix 4.2). This offset between modelled and measured values could be a reflection of other regional influences (e.g., specific soils, topography, climate, landscape characteristics and biodiversity features) or changes in vineyard management techniques. Portuguese viticulture experienced a major transformation in the 1950s with the foundation of a national network of Cooperative Wineries, which brought technical support for the development of the wine sector (Parente, 2002). Furthermore, with the integration of Portugal in the European Economic Community (1986), a National Program Support was implemented in viticulture partially financed by the European structural funds (http://www.vinhoverde.pt). This might had impacted the viticulture after 1978 and during the early 1990s, respectively.

4.5.2. Teleconnection patterns influence on temperatures and grape harvest dates

A large fraction of the spatiotemporal variability of surface air temperature, precipitation and other climate variables is modulated by a complex interplay of large-scale atmospheric circulation modes (e.g., Trigo et al., 2002, 2008; Taboada et al., 2009; Gómez-Gesteira et al., 2011). These large-scale modes can persist from days to months typically covering vast geographical areas (Barnston and Livezey, 1987). The Minho region is located in a sector (North Atlantic European sector – NAE) characterized by the passage of cold frontal systems Associated with the storm track in the North Atlantic Ocean (Trigo, 2006), where the most active modes of low-frequency variability are the NAO, AO, EA, EA/WR and SCA. The EA pattern is structurally similar to the NAO but displaced south-eastward (Trigo et al., 2008).

Several recent studies have evaluated the impact of the preceding modes on the European climate and, more regionally, on the Iberian Peninsula, particularly on temperature and precipitation (Trigo et al., 2002; Taboada et al., 2009; Gómez-Gesteira et al., 2011). Taboada et al. (2009) obtained a significant inverse correlation between spring and summer temperatures and the SCA ($r = -0.57$, $p < 0.01$ and $r = -0.46$, $p < 0.01$, respectively), and between summer temperature and the EA/WR ($r = -0.32$, $p < 0.01$) using temperature data since 1960 from the Peinador weather station (Vigo, Galicia). They did not find significant correlations of spring (MAM) and summer (JJA)

temperatures with the NAO and EA, and concluded that these two teleconnection modes are not important in explaining inter-annual temperature variability in Galicia (Taboada et al., 2009). Likewise, Santo et al. (2014), investigating the teleconnections influence on seasonal temperature changing patterns in mainland Portugal since 1941, obtained stronger responses for the SCA pattern, showing that warm related Extremes were mostly associated with this mode in spring, summer and autumn seasons. According to these authors, this is compatible with the presence/absence of blocking patterns that control the SCA phase, as pointed out earlier by Barriopedro et al. (2006), and the occurrence of extreme temperature episodes in both winter and summer time in western Mediterranean (e.g., Trigo et al., 2004; Carril et al., 2008). Conversely, the NAO, being the most prominent Northern Hemisphere pattern, plays a minor role in shaping extreme (minima and maxima) temperatures in mainland Portugal affecting, although not noticeably, spring temperatures and impacting, more than any other teleconnection pattern, winter temperatures (Santo et al., 2014).

Analogous interactions were found in the present work between the main NAE sector teleconnection modes and the Braga GSTmax between 1950 and 2009. From the large number of possible results, Table 4.3 presents only those that are statistically significant, displaying that the highest linear (inverse) correlations were achieved with the SCA index. This is in accordance with what has been described for the SCA pattern and its relevance during spring and summer months in western Iberia (Lorenzo et al., 2012; Jerez and Trigo, 2013; Santo et al., 2014). A SCA positive phase is associated with below-normal spring and summer maxima temperatures in northwestern Portugal as a consequence of a high pressure system positioned over the Scandinavian Peninsula and two low pressure systems located over the northeastern Atlantic/western Europe and central Siberia, respectively. In summer, this situation usually results from a blocking anticyclone over Scandinavia and western Russia carrying warmer and drier conditions over Scandinavia and a southwards shift of the North Atlantic storm tracks accompanied by higher precipitation rates and lower temperatures over southern Europe (e.g., Mauri et al., 2014).

In summer, the NW of Portugal can be affected by two typical European heatwave patterns (Stefanon et al., 2012). One is the “Iberian” pattern triggered by warm air advection from northern Africa, which tends to be preceded by drought conditions at the same location as the heat wave, like the heat wave that affected Portugal and Spain in early August 2003 (Trigo et al., 2005). The other one is the “Western Europe” pattern, marked by a high pressure over central Europe, mostly centred over France, and a low pressure over the Atlantic Ocean, associated with a rainfall deficit in winter and spring in southern Europe. In 1949, when an extreme heat wave was recorded in the NW of Portugal, it had occurred after a prolonged period of several moderately to severe drought months (Moreira et al., 2012). Short-duration weather events, like heat waves, tend to occur around the annual peak of temperature in July and August, which can decisively impact grapevine ripening. In

this perspective, in the MWR the exclusive dark coloured recommended varieties (e.g., Alvarelhão, Amaral, Borraçal, Espadeiro, Padeiro, Pedral, Rabo-de-Ovelha and Vinhão; http://www.vinhoverde.pt), used in the production of the "Vinho Verde" denomination of origin, can be even more intensively affected, as soon as their berries get much hotter than the surrounding air temperature, resulting in shrivelled or sunburnt grapes.

Apart from the direct influence of temperature (and rainfall) on the annual growth cycle of grapevines, some authors have explored the relationships between European viticulture and the index that characterizes each teleconnection pattern, with special incidence on the NAO (e.g., Rodó and Comín, 2000; Esteves and Manso Orgaz, 2001; Dalla Marta et al., 2010; Krieger et al., 2010, 2011; Lorenzo et al., 2012). Those studies have accomplished mixed results, which is not unexpected since the NAO is primarily a wintertime mechanism. Mixed results also indicate why we have no success in establishing a robust statistical relationship between the NAO and Minho GHD. However, Herceg-Bulić and Kucharski (2014) demonstrated that the atmospheric circulation associated with the December to February NAO generates an SST anomaly pattern in the North Atlantic, which can slightly affect the atmospheric circulation over Europe between March and May. Dalla Marta et al. (2010) were able to find a significant inverse correlation between the winter NAO and budbreak and flowering dates, but not with harvest dates, confirming its diminishing influence over GS. Moreover, in the absence of significant correlations between winter precipitation and budbreak dates, they suggested that the role of the NAO could be mainly due to a reduction in cloud cover and consequently greater insolation than average for the positive NAO index phase. In contrast, Souriau and Yiou (2001), working with grapevine flowering dates of northeast France and Switzerland, based on the common observation that harvest occurs around 100 days after flowering, found significant inverse correlations of harvest dates with the winter and early spring NAO index. For the Minho region, we achieve some significant correlations between March mean maxima temperatures and GHD ($r = -0.48$; $p < 0.001$; Table 4.1) and between March mean maxima temperatures and the NAO and AO indices ($r = 0.37$ and $r = 0.40$, respectively; $p < 0.05$; Table 4.3). These results appear to suggest that the positive NAO and AO patterns (which generally operate in tandem) from the transition of winter to early spring might have a moderate influence on the Minho grape harvest dates through an increment of maximum temperatures and, thus, on an earlier onset of budbreak. Since optimal temperature requirements for breaking dormancy are grapevine variety-dependent (Lavee, 2000; Malheiro et al., 2013), a great deal of research is still required. The highest correlation between GHD and teleconnections was obtained for the SCA pattern of February ($r = 0.38$; $p < 0.05$), showing that this seems to be the leading pattern in the MWR during the heat forcing period to budburst (broadly a forcing temperature threshold of 10ºC in early spring is accepted for grapevines). However, it must be noted that buds of different varieties differ in their appearance at the end of the post-dormant stage, making it difficult to define the day of budburst in a uniform way (Lavee and May, 1997).

Table 4.3. Correlations of the prominent teleconnections patterns and monthly mean maxima temperature for the Braga weather station and growing season mean maxima temperature (1950–2009). MAMJJA – March, April, May June, July and August; AO – Arctic Oscillation index, NAO – North Atlantic Oscillation index, EA – Eastern Atlantic index, EA/WR – East Atlantic/Western Russia Oscillation index, SCA – Scandinavian Oscillation index, SCA_MAMJJA – Scandinavian Oscillation index mean for the growing season months.

	March	April	May	June	July	August	MAMJJA
AO_March	0.40						
AO_May			0.32				
AO_June				0.28			
AO_July					0.36		
AO_August						0.27	
NAO_March	0.37						
NAO_July					0.25		
EA_April		-0.31					
EA/WR_Ago							-0.30
SCA_March	-0.48*						
SCA_April		-0.35					
SCA_May			-0.61*				-0.44*
SCA_Jun				-0.52*			
SCA_July					-0.36		
SCA_Ago							
SCA_MAMJJA						-0.50*	-0.49*

* $p < 0.001$.
** $p < 0.05$.

Data regarding the EA/WR and SCA indices are only available after 1951. From the middle 1950s until the early 1990s, either the summer EA/WR index and the spring and summer SCA index show a tendency to a positive phase (Figure 4.5). Assuming their inverse correlation with maximum temperatures, and in combination with the positive precipitation anomaly recorded in the Minho region between 1958 and 1983, it is possible to explain the lowest GSTmax between the 1960s to the 1990s. It is also plausible to assume an opposite scenario for periods of higher GSTmax preceding 1950 (reconstructed), with particular emphasis for the period 1856–1875, when a high temperature peak on the decadal averaged temperatures was obtained (Figure 4.4). In such periods, a higher frequency and intensification of the Atlantic blocking (anticyclone bridge and anticyclone circulation over north Iberia with ridge to central Europe) and a negative SCA phase have hypothetically contributed to enhancing GSTmax in the Minho region.

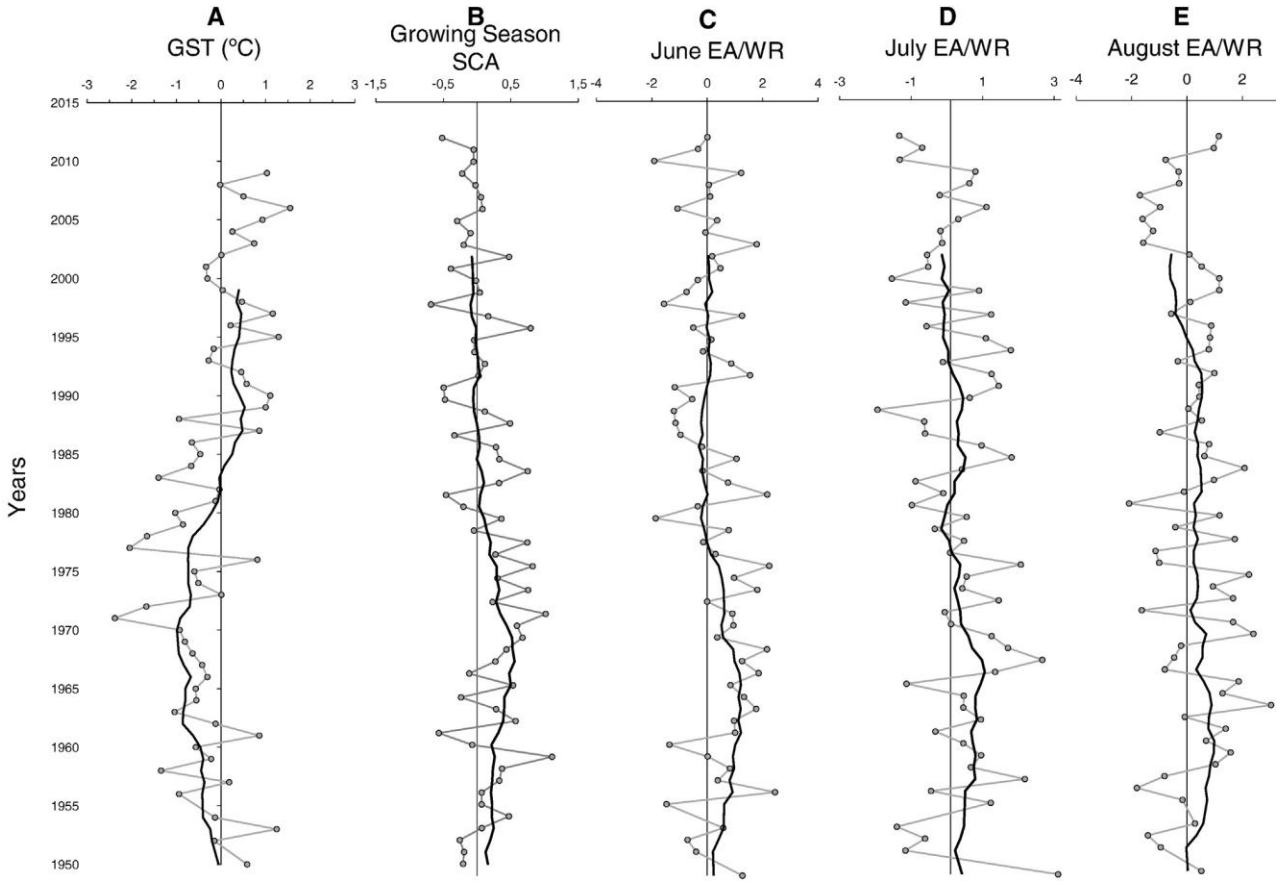

Figure 4.5. **A –** March to August mean maxima temperature anomalies for the Braga meteorological station (grey line) and 11-year running average (black line). **B –** March to August SCA index. **C –** June EA/WR index. **D –** July EA/WR index. **E –** August EA/WR index (indices raw data in grey lines and indices 11-year running averages in black lines).

4.5.3. Linking solar activity to Minho GSTmax

The Earth's climate variability appears to be organized in a wide range of spatiotemporal patterns. The input to this observed variability results from external forcing and the internal stochastic response to such a large and extremely complex coupled system (e.g., Le Mouël et al., 2009). The major external forcing of the climate system derives from the Sun. A solar signature has been found in global mean surface temperatures, with evidence directly related to two noticeably different features of the Sun's dynamics: its short-term irradiance fluctuations and secular patterns of 22-year and 11-year cycles (Scafetta and West, 2008). But the essential dynamics behind the Sun-Earth's climate linkage continues nowadays in the centre of an intense scientific debate.

An extensive review can be found, for instance, in Soon et al. (2015), outlining the points of general agreement and the aspects that still remain controversial. Nonetheless, it is recognized that solar forcing manifestations denote a strong spatial and seasonal variability (Usoskin et al., 2006), and this would be the reason why it might be illusive to seek a single global relationship between climate and solar activity (de Jager, 2005). Thus, Le Mouël et al. (2009) stated that a regional approach may allow one to identify specific forms of solar forcing, where and when the solar input is

most important. In line with this, it seemed worthwhile to attempt to identify a solar signal in the Minho GSTmax trend.

In Figure 4.6 the GSTmax time series (1856–2009) for the Minho region is displayed along with a mean annual global temperature anomalies curve (Jones et al., 2013) and a historical TSI series (Krivova et al., 2010; Ball et al., 2012 and Yeo et al., 2014). The inter-annual linear correlation between the two surface air temperature series is low ($r = -0.12$; $p < 0.05$), only improving when a 30-year moving average is used ($r = -0.59$; $p < 0.001$). Comparing the decadal variability (11-year average temperatures; black thick lines) we can, however, notice that the maximum discrepancy arises in the period near 1990 and thereafter, when the steeply rise on global temperatures is not observable in the Minho GSTmax. During this period, the solar influence has been positive; this because after the TSI increase registered early in the century, happening with the coming after 1924 of the Grand Maximum Episode of the 20th century (Duhau and Martínez, 2012), a period in which irradiance exhibits no multidecadal trend occurred (Figure 4.6C). This could be representative of a regional climate deviation from global trends, likely reflecting the fact that local processes, such as land-atmosphere coupling interactions, gain relevance in the summer, with greater impact on maxima temperatures (e.g., Jerez et al., 2012).

Also the inter-annual linear correlation with the TSI shows a low value ($r = -0.17$; $p < 0.05$), increasing at decadal and multidecadal scales: $r = -0.45$ ($p < 0.001$), $r = -0.57$ ($p < 0.001$) and $r = -0.65$ ($p < 0.001$) using successively 11-year, 22-year and 30-year moving averages. This seems to agree with both i) the suppression (by using correlation analysis) of any direct connection between intermittent Sun's irradiance changes and short-time (weekly and monthly) solar footprints on terrestrial temperatures (requiring other statistical approaches), which is due to the strong non-linear hydrodynamic interactions across the Earth's surface, and ii) the accepted longer term solar activity influence creating temperature oscillations for tens or even hundreds of years (Scafetta and West, 2003, 2007, 2008). This is also evident in the red noise spectrum of the Minho GSTmax (not shown) obtained using the REDFIT procedure of Schulz and Mudelsee (2002), where two periodic signals were detected above the 98.63% critical false-alarm level: a maximum spectral peak at 54.8 years followed by one located at 3.3 years, on the frequency bands of two well-known solar activity cycles: the Lower Gleissberg cycle (e.g., Ogurtsov et al., 2002) and the Quasi-Biennial Oscillations (QBOs; Bazilevskaya et al., 2014), respectively. These spectral analysis results appear to support a solar forcing with regards to Minho GHD, however this would need a more thorough analysis which falls outside of the scope of our research.

As it would be expected, the decadal global annual mean temperatures are directly correlated with TSI ($r = 0.88$; $p < 0.001$), while the Minho GSTmax show an odd opposite relationship. A possible explanation might come from the following hypothesis: the TSI influence on the Minho GSTmax mainly occurs via the modulation of the SCA oscillation mode. Table 4.3 results show significant

inverse correlations between GSTmax and the SCA oscillation mode during the spring-summer months in the Minho region. On the other hand, the SCA mode shows significant decadal and bi-decadal inverse correlations ($r = -0.63$ and $r = -0.76$, $p < 0.001$, using 11-year and 22-year running correlations, respectively) with TSI, for the period 1950–2012. This appears to indicate that during times of reduced solar activity the anticyclone blocking over Scandinavia (SCA positive phase) impacts the Minho region climate by dropping its spring-summer maximum temperatures. Under this scenario, we might hypothesize that the SCA oscillation establishes a potential robust linkage between solar activity and Minho GSTmax.

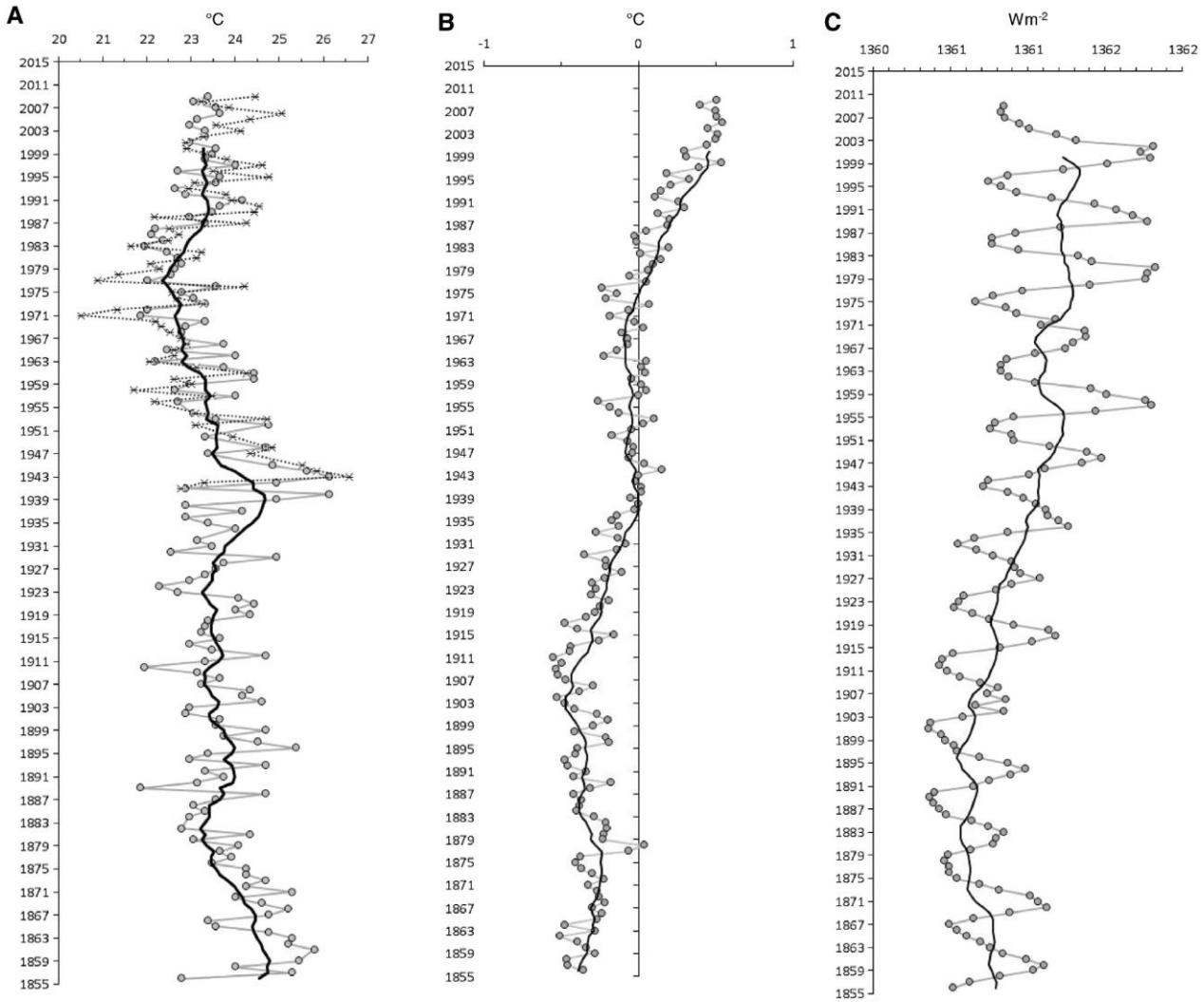

Figure 4.6. **A –** March to August mean maxima temperatures (instrumental - dashed line; reconstructed - grey line; reconstructed 11-year running averages - black line). **B –** Global mean annual temperature anomalies (after Jones et al., 2013) in grey line and 11-year running averages in black line. **C –** TSI – Total Solar Irradiance (after Krivova et al., 2010; Ball et al., 2012 and Yeo et al., 2014) in grey line; and 11-year running averages in black line.

Several studies emphasized blocking episodes as an essential aspect of variability in the North Atlantic circulation (e.g., Shabbar et al., 2001; Woollings et al., 2010a), with decadal variations of blocking parameters (frequency, intensity and location) being associated to various forcing factors, amongst them Sun's activity. Barriopedro et al. (2008) and Woollings et al. (2010b) detected a solar-

blocking relationship, involving an increase in Euro-Atlantic blocking during periods of solar minima. However, their investigation has mainly focused on the winter time NAO blocking. Thus additional work should be undertaken to fully understand the TSI modulation of the spring-summer blocking (SCA positive phase) effects on the GS temperatures regime of the NW of Portugal, so vital for a successful viticultural practice.

4.6. Conclusion

This study is the first report on long-term (154 years) grape harvest dates for the Minho Wine Region, in northwestern Portugal, built on documentary sources from local and regional newspapers and the proceedings archive from the Wine Cooperative of Ponte de Lima. This historical source of information resulted in a useful dataset that allowed, based on a simple linear regression model, to produce a high-resolution paleotemperature reconstruction. As in other European viticultural regions, it was found that GHD are strongly inversely correlated with the growing season (March–August) temperatures (mean maxima), being per se a good indicator of climate variability, namely surface air temperatures. Additionally, the Minho GHD (proxy of GSTmax) seem to reflect the complex interaction between different low frequency modes of atmospheric circulation and regional spring summer mean maximum temperature variation patterns, in which the SCA index mode has a special emphasis. Though it has not been found a direct relationship between TSI and GSTmax in the study area, the results of the correlation analysis evidenced that such an association could be reconciled by the effects of SCA blocking episodes, transferring the solar signal in winter climate to spring-summer seasons.

Finally, our findings give valuable insights to upcoming paleoclimate reconstructions of northwestern Iberia, will allow a reliable assessment of climatic proxies like from geological record, and may be applied to the grapevines production management in the Portuguese Minho Wine Region when facing the challenges of climate change scenarios.

Acknowledgments

This work is a contribution of the WestLog project (PTDC/CTE/ 105370/2008), funded by the Fundação para a Ciência e a Tecnologia – FCT. João Moreno acknowledges a FCT PhD grant (SFRH/BD/87995/ 2012). We are very grateful to Eng. Araújo Lopes for sharing his viticultural expertise, and to the Wine Cooperative of Ponte de Lima, in the person of Mr. Eduardo Martins, who kindly provided grape harvest dates from 1978 to 2009. We also kindly express our thanks to the two anonymous reviewers, who valuable comments greatly improve the manuscript, and to Carla Neves for the writing revision.

References

Adams, R.M., Hurd, B., Lenhart, S., Leary, N., 1998. Effects of global climate change on agriculture: an interpretative review. Clim. Res. 11, 19–30.

Alcoforado, M.J., Nunes, M.F., Garcia, J.C., Taborda, J.P., 2000. Temperature and precipitation reconstruction in southern Portugal during the late Maunder Minimum (AD 1675–1715). The Holocene 10, 333–340.

Angot, A., 1883. Etude sur les vendanges en France. Annales du Bureau Central Météorologique de France 29–120.

Ball, W.T., Unruh, Y.C., Krivova, N.A., Solanki, S., Wenzler, T., Mortlock, D.J., Jaffe, A.H., 2012. Reconstruction of total solar irradiance 1974–2009. Astron. Astrophys. 541 A27-15p.

Barriendos, M., 2005. Climate and culture in Spain, religious responses to extreme climatic events in the Hispanic Kingdoms (16th–19th centuries). In: Behringer, W., Lehmann, H. and Pfister, C. (Eds.), Cultural Consequences of the Little Ice Age (Kulturelle Konsequenzen der Kleinen Eiszeit). Vandenhoeck & Ruprecht, Gottingen, pp. 31–86.

Barriopedro, D., García-Herrera, R., Hernández, E., 2006. The role of snow cover in the Northern Hemisphere winter-to-summer transition. Geophys. Res. Lett. 33, L14708. http://dx.doi.org/10.1029/20006GL025763.

Barriopedro, D., Garcia-Herrera, R. and R. Huth, R., 2008. Solar modulation of Northern Hemisphere winter blocking. J. Geophys. Res. 113, D14118, doi:http://dx.doi.org/10. 1029/2008JD009789, 11p.

Barnston, A.G., Livezey, R.E., 1987. Classification, seasonality and persistence of low frequency atmospheric circulation patterns. Mon. Weather Rev. 115, 1083–1126.

Bazilevskaya, G., Broomhall, A.-M., Elsworth, Y., Nakariakov, V.M., 2014. A combined analysis of the observational aspects of the Quasi-Biennial Oscillation in solar magnetic activity. Space Sci. Rev. 186, 359–386.

Bock, A., Sparks, T.H., Estrella, N., Menzel, A., 2013. Climate-induced changes in grapevine yield and must sugar content in Franconia (Germany) between 1805 and 2010. PLoS One 8, e69015. http://dx.doi.org/10.1371/journal.pone.0069015.

Brázdil, R., Pfister, C., Wanner, H., 2005. Historical climatology in Europe — the state of the art. Climate Change 70, 363–430.

Brázdil, R., Zahradníček, P., Dobrovolný, P., Kotyza, O., Valášek, H., 2008. Historical and recent viticulture as a source of climatological knowledge in the Czech Republic. Geografie - Sbor Čes Geogr Spol 113, 351–371.

Carril, A.F., Gualdi, S., Cherchi, A., Navarra, A., 2008. Heatwaves in Europe: areas of homogeneous variability and links with the regional to large-scale atmospheric and SSTs anomalies. Clim. Dyn. 30, 77–98.

Chuine, I., Yiou, P., Viovy, N., Seguin, B., Daux, V., Le Roy Ladurie, E., 2004. Historical phenology: grape ripening as a past climate indicator. Nature 432, 289–290.

Cook, E.R., Keith, R., Jones, P.D., 1994. Spatial regression methods in dendroclimatology: a review and comparison of two techniques. Int. J. Climatol. 14, 379–402.

Correia, C.F., 2011. Historical Wines: Developing a Marketing Concept to Promote Portuguese Wines. Universidade Católica Portuguesa, MSc dissertation, 57p.

Cortázar-Atauri, G.I., Daux, V., Garnier, E., Yiou, P.N., Viovy, N., Seguin, B., Boursiquot, J.M., Parker, A.K., van Leeuwen, C., Chuine, I., 2010. Climate reconstructions from grape harvest dates: methodology and uncertainties. The Holocene 20, 599–608.

Dalla Marta, A., Grifoni, D., Mancini, M., Storchi, P., Zipoli, G., Orlandini, S., 2010. Analysis of the relationships between climate variability and grapevine phenology in the Nobile di Montepulciano wine production area. J. Agric. Sci. 148, 657–666.

Daux, V., Yiou, P., Le Roy Ladurie, E., Mestre, O., Chevet, J.M., Seguin, B., Chuine., I., Garnier, E., and Viovy, N., 2007. Temperature and grape harvest dates in France. In: P. Fontaine (Ed.), Global Warming, Which Impacts on the Vineyards, Dijon, France, 10p.

de Blij, H.J., 1983. Geography of viticulture: rationale and resource. J. Geogr. 82, 112–121.

de Jager, C., 2005. Solar forcing of climate.1: Solar variability. Space Sci. Rev. 120, 197–241.

Della-Marta, P.M., Luterbacher, J., von Weissenfluh, H., Xoplaki, E., Brunet, M., Wanner, H., 2007. Summer heat waves over Western Europe 1880–2003, their relationship to large-scale forcings and predictability. Clim. Dyn. 29, 251–275.

Domínguez-Castro, F., Santisteban, J.I., Barriendos, M., Mediavilla, R., 2008. Reconstruction of drought episodes for central Spain from rogation ceremonies recorded at the Toledo Cathedral from 1506 to 1900: a methodological approach. Glob. Planet. Chang. 63, 230–242.

Duhau, S., Martínez, E.A., 2012. Solar dynamo transitions as drivers of sudden climate changes. INTECH 185–204 http://dx.doi.org/10.5772/5181410.

Dufour, M.L., 1870. Notes sur le problème de la variation du climat. Bulletin de la Société Vaudoise de Sciences Naturelles 63, pp. 359–556 X.

Etien, N., Daux, V., Masson-Delmotte, V., Mestre, O., Stievenard, M., Guillemin, M.T., Boettger, T., Breda, N., Haupt, M., Perraud, P.P., 2009. Summer maximum temperature in northern France over the past century: instrumental data *versus* multiple proxies (tree-ring isotopes, grape harvest dates and forest fires). Clim. Chang. 92, 429–456.

Esteves, M.A., Manso Orgaz, M.D., 2001. The influence of climatic variability on the quality of wine. Int. J. Biometeorol. 45, 13–21.

Fraga, H., Malheiro, A.C., Moutinho-Pereira, J., Santos, J.A., 2014. Climate factors driving wine production in the Portuguese Minho region. Agric. For. Meteorol. 185, 26–36.

Garnier, M., 1955. Contribution de la phénologie à l'étude des variations climatiques. La Météorologie 4e série 40, pp. 291–300.

Garnier, E., Daux, V., You, P., García de Cortázar-Atauri, I., 2011. Grapevine harvest dates in Besançon (France) between 1525 and 1847: social out comes or climatic evidence? Clim. Chang. 104, 703–727.

Gershunov, A., Cayan, D.R. and Retornaz, B., 2010. California heat waves with impacts on wine grapes. In: Pavia, E.G., Sheinbaum, J. and Candela, J. (Eds.), The Ocean, the Wine, and the Valley: The Lives of Antoine Badan, pp. 205–224.

Giralt, R.E., 1958. En torno al precio del trigo en Barcelona durante el siglo XVI. Hispania 18, 38–61.

Gladstones, J.S., 2004. Climate and Australian Viticulture. In: Dry, P.R. and Coombe, B.G. (Eds.), Viticulture. Volume 1 - Resources. Winetitles, Second Ed., Adelaide, South Australia, pp. 90–118.

Gómez-Gesteira, M., Gimeno, L., deCastro, M., Lorenzo, M.N., Alvarez, I., Nieto, R., Taboada, J.J., Crespo, A.J.C., Ramos, A.M., Iglesias, I., Gómez-Gesteira, J.L., Santo, F.E., Barriopedro, D., Trigo, I.F., 2011. The state of climate in NW Iberia. Clim. Res. 48, 109–144.

Gouveia, C., Liberato, M.L., DaCamara, C.C., Trigo, R.M., Ramos, A.M., 2011. Modelling past and future wine production in the Portuguese Douro Valley. Clim. Res. 48, 349–362. http://dx.doi.org/10.3354/cr01006.

Guerreau, A., 1995. Climat et vendanges (XIVe-XIXe siècles): révisions et compléments. Histoire et Mesure. 10, pp. 89–147.

Guttman, N.B., 1999. Accepting the standardized precipitation index: a calculation algorithm. J. Am. Water Resour. Assoc. 35, 311–322.

Herceg-Bulić, I., Kucharski, F., 2014. North Atlantic SSTs as a sink between the wintertime NAO and the following spring climate. J. Climate 27, 186–201.

Hooson, D., 1998. The geographical identity of Portugal, with special reference to the works of Stanislawski. Finisterra XXXIII 65, 141–145.

IGME, 1986.Mapa geológico de la Peninsula Ibérica, Baleares y Canarias (1:1 000 000). Ed Instituto Geologico y Minero de España.

Jerez, S., Montávez, J.P., Gómez-Navarro, J.J., Jimenez, P.A., Jiménez-Guerrero, P., Lorente, R., González-Rouco, J.F., 2012. The role of the land-surface model for climate change projections over the Iberian Peninsula. J. Geophys. Res. 117, D01109. http://dx.doi.org/10.1029/2011JD016576 15p.

Jerez, S., Trigo, R.M., 2013. Time-scale and extent at which large-scale circulation modes determine the wind and solar potential in the Iberian Peninsula. Environ. Res. Lett. 8, 044035. http://dx.doi.org/10.1088/1748-9326/8/4/044035 11p.

Jones, G.V., 1999. Relationships between grapevine phenology, composition, and quality for Bordeaux, France. Arboreta Phaenologica 42, 3–7.

Jones, G.V., Davis, R.E., 2000. Climate influences on grapevine phenology, grape composition, and wine production and quality for Bordeaux, France. Am. J. Enol. Vitic. 51, 249–261.

Jones, G.V., Storchmann, K.-H., 2001. Wine market prices and investment under uncertainty: an econometric model for Bordeaux Crus Classés. Agric. Econ. 26, 115–133.

Jones, G.V., White, M.A., Cooper, O.R., Storchmann, K., 2005. Climate change and global wine quality. Clim. Chang. 73, 319–343.

Jones, G.V., 2006. Climate and terroir: impacts of climate variability and change on wine. In: Macqueen, R.W. and Meinert, L.D., (Eds.), Fine Wine and Terroir - The Geoscience Perspective Geoscience Canada Reprint Series Number 9. Geological Association of Canada, St. John's, Newfoundland, pp. 1–14.

Jones, P.D., Mann, M.E., 2004. Climate over the past millennia. Reviews of Geophysics, 42, American Geophysical Union, Paper No 2003RG2002/2004.

Jones, P.D., Briffa, K.R., Osborn, T.J., Lough, J.M., van Ommen, T.D., Vinther, B.M., Luterbacher, J., Wahl, E.R., Zwiers, F.W., Mann, M.E., Schmidt, G.A., Ammann, C.M., Buckley, B.M., Cobb, K.M., Esper, J., Goosse, H., Graham, N., Jansen, E., Kiefer, T., Kull, C., Kuttel, M., Mosley-Thompson, E., Overpeck, J.T., Riedwyl, N., Schulz, M., Tudhope, A.W., Villalba, R., Wanner, H., Wolff, E., Xoplaki, E., 2009. High-resolution palaeoclimatology of the last millennium: a review of current status and future prospects. The Holocene 19, 3–49.

Jones, P.D., D.E. Parker, T.J. Osborn, and K.R. Briffa. 2013. Global and Hemispheric Temperature Anomalies–Land and Marine Instrumental Records. In Trends: A Compendium of Data on Global Change. Carbon Dioxide Information Analysis Center, Oak Ridge National Laboratory, U.S. Department of Energy, Oak Ridge, Tenn., U.S.A. doi: http://dx. doi.org/10.3334/CDIAC/cli.002.

Keller, M., 2015. The science of grapevines. Anatomy and Physiology, second ed. Academic Press, 509p.

Kenny, G.J., Shao, J., 1992. An assessment of a latitude-temperature index for predicting climate suitability for grapes in Europe. Eur. J. Hortic. Sci. 67, 239–246.

Krieger, M., Lohmann, G., Laepple, T., 2010. Climate signatures of grape harvest dates. Clim. Past Discuss. 6, 1525–1550.

Krieger, M., Lohmann, G., Laepple, T., 2011. Seasonal climate impacts on the grape harvest date in Burgundy (France). Clim. Past 7, 425–435.

Krivova, N.A., Vieira, L.E.A., Solanki, S.K., 2010. Reconstruction of solar spectral irradiance since the maunder minimum. J. Geophys. Res. Space Phys. 115, A12112 11p.

Kiss, A., Wilson, R., Bariska, I., 2011. An experimental 392-year documentary-base multiproxy (vine and grain) reconstruction of May–July temperatures for Kőszeg, West- Hungary. Int. J. Biometeorol. 55, 595–611.

Lavee, S., May, P., 1997. Dormancy of grapevine buds — facts and speculation. Aust. J. Grape Wine Res. 3, 31–46.

Lavee, S., 2000. Grapevine (Vitis vinifera) growth and performance in warm climates. In: Amnon, E. (Ed.), Temperate Fruit Crops in Warm Climates. Springer Science + Business Media Dordrecht, pp. 343–366.

Leijonhufvud, L., Wilson, R., Moberg, A., Söderberg, J., Retsö, D., Söderlind, U., 2010. Five centuries of Stockholm winter/spring temperatures reconstructed from documentary evidence and instrumental observations. Clim. Chang. 101, 109–141.

Le Mouël, J.-L., Blanter, E., Shnirman, M., Courtillot, V., 2009. Evidence for solar forcing in variability of temperatures and pressures in Europe. J. Atmos. Sol. Terr. Phys. 71, 1309–1321.

Le Roy Ladurie, E., 1967. Histoire du Climat Depuis l'an Mil Champs Paris, 541p.

Le Roy Ladurie, E., Baulant, M., 1980. Grape harvests from the fifteenth through the nineteenth centuries. J. Interdiscip. Hist. 10, 839–849.

Lorenzo, M.N., Taboada, J.J., Lorenzo, J.F., Ramos, A.M., 2012. Influence of climate on grape production and wine quality in the Rías Baixas, north-western Spain. Reg. Environ. Chang. 12, 1–10.

Magalhães, N.P., 2008. Tratado de Viticultura - A videira, a vinha e "terroir". Esfera Poética, Portugal, 608p.

Malheiro, A.C., Campos, R., Fraga, H., Eiras-Dias, J., Silvestre, J., Santos, J.A., 2013. Winegrape phenology and temperature relationships in the Lisbon Wine Region, Portugal. Journal International des Sciences de la Vigne et du Vin 47, 287–299.

Mariani, L., Parisi, S., Failla, O., Cola, G., Zoia, G., Bonardi, L., 2009. Tirano (1624-1930): a long time series of harvest dates for grapevine. Ital. J. Agron. 14, 7–16.

Martín-Vide, J., Barriendos, M.V., 1995. The use of rogation ceremony records in climatic reconstruction: a case study from Catalonia (Spain). Clim. Chang. 30, 201–221.

Maurer, C., Hammerl, C., Koch, E., Hammerl, T., Pokorny, E., 2011. Extreme grape harvest data of Austria, Switzerland and France from A.D. 1523 to 2007 compared to corresponding instrumental/reconstructed temperature data and various documentary sources. Theor. Appl. Climatol. 106, 55–68.

Mauri, A., Davis, B.A.S., Collins, P.M., Kaplan, J.O., 2014. The influence of atmospheric circulation on the mid-Holocene climate of Europe: a data–model comparison. Clim. Past 10, 1925–1938.

McKee, T.B., Doesken, N.J., Kleist, J., 1993. The relationship of drought frequency and duration to time scales. 8th Conference on Applied Climatology. American Meteorological Society, Boston, pp. 179–184.

Meier, N., Rutishauser, T., Pfister, C., Wanner, H., Luterbacher, J., 2007. Grape harvest dates as a proxy for Swiss April to August temperature reconstructions back to AD 1480. Geophys. Res. Lett. 34, L20705. http://dx.doi.org/10.1029/2007GL031381.

Menzel, A., 2005. A 500 year pheno-climatological view on the 2003 heatwave in Europe assessed by grape harvest dates. Meteorol. Z. 14, 75–77.

Moreira, E.E., Mexia, J.T., Pereira, L.S., 2012. Are drought occurrence and severity aggravating? A study on SPI drought class transitions using log-linear models and ANOVA-like inference. Hydrol. Earth Syst. Sci. 16, 3011–3028.

Možný, M., Brázdil, R., Dobrovolný, P., Trnka, M., 2012. Cereal harvest dates in the Czech Republic between 1501 and 2008 as a proxy for March-June temperature reconstruction. Clim. Chang. 110, 801–821.

OIV, 2015. Global economic vitiviniculture data. Organisation Internationale de la Vigne et du Vin, Paris, France, 5p.

Ogurtsov, M.G., Kocharov, G.E., Lindholm, M., Meriläinen, J., Eronen, M., Nagovitsyn, Y.A., 2002. Evidence of solar variation in tree-ring-based climate reconstructions. Sol. Phys. 205, 403–417.

Parente, S.C., 2002. Adegas cooperativas na região demarcada dos vinhos verdes. Qualidade e estratégias comerciais. La multifuncionalidad de los espacios rurales de la Península Ibérica: Actas del IV Coloquio Hispano-Portugués de Estudios Rurales./ Coordenado por Ana Isabel García Arias, María Carmen Lorenzo Díaz, Edelmiro López Iglesias ISBN 84-600-9729-3.

Pereira, E., Ribeiro, A., Carvalho, G., Monteiro, H., 1989. Carta Geológica de Portugal (1:200 000), Folha 1. Ed. Serviços Geológicos de Portugal, Lisboa, Portugal.

Pfister, C., 1992. In: Bradley, R.S. and Jones, P.D. (Eds.), Monthly temperature and precipitation in central Europe 1525–1979: quantifying documentary evidence on weather and its effects, pp. 118–142 Climate since A.D. 1500. Routledge, London.

Rodó, X., Comín, F.A., 2000. Links between large scale anomalies, rainfall and wine quality in the Iberian Peninsula during the last three decades. Glob. Chang. Biol. 6, 267–273.

Rousseeuw, P.J., van Zomeren, B.C., 1990. Unmasking multivariate outliers and leverage points. J. Am. Stat. Assoc. 85, 633–639.

Santo, F.E., Lima, M.I.P., Ramos, A.M., Trigo, R.M., 2014. Trends in seasonal surface air temperature in mainland Portugal, since 1941. Int. J. Climatol. 34, 1814–1837.

Santos, J.A., Malheiro, A.C., Karremann, M.K., Pinto, J.G., 2010a. Statistical modelling of grapevine yield in the Port wine region under present and future climate conditions. Int. J. Biometeorol. 55, 119–131.

Santos, J.F., Pulido-Calvo, I., Portela, M.M., 2010b. Spatial and temporal variability of droughts in Portugal. Water Resour. Res. 46, W03503. http://dx.doi.org/10.1029/ 2009WR008071.

Scafetta, N., West, B.J., 2003. Solar flare intermittency and the Earth's temperature anomalies. Phys. Rev. Lett. 90, 248701. http://dx.doi.org/10.1103/PhysRevLett.90.248701 4p.

Scafetta, N., West, B.J., 2007. Phenomenological reconstructions of the solar signature in the Northern Hemisphere surface temperature records since 1600. J. Geophys. Res. 112, D24S03. http://dx.doi.org/10.1029/2007JD008437 10p.

Scafetta, N., West, B.J., 2008. Is climate sensitive to solar variability? Phys. Today 3, 50–51.

Schulz, M., Mudelsee, M., 2002. REDFIT: estimating red-noise spectra directly from unevenly spaced paleoclimatic time series. Comput. Geosci. 28, 421–426.

Schultz, H.R., Jones, G.V., 2010. Climate induced historic and future changes in viticulture. J. Wine Res. 21, 137–145.

Shabbar, A., Huang, J., Higuchi, K., 2001. The relationship between the wintertime North Atlantic Oscillation and blocking episodes in the North Atlantic. Int. J. Climatol. 21, 355–369.

Soon, W., Connolly, R., Connolly, M., 2015. Re-evaluating the role of solar variability on Northern Hemisphere temperature trends since the 19th century. Earth-Sci. Rev. http://dx.doi.org/10.1016/j.earscirev.2015.08.010.

Souriau, A., Yiou, P., 2001. Grape harvest dates for checking NAO paleoreconstructions. Geophys. Res. Lett. 28, 3895–3896.

Stanislawski, D., 1970. Landscapes of Bacchus: The Wine in Portugal. University of Texas Press, Austin, 210p.

Stefanon, M., D'Andrea, F., Drobinski, P., 2012. Heatwave classification over Europe and the Mediterranean region. Environ. Res. Lett. 7, 1–9.

Taboada, J.J., Lorenzo, M.N., Gimeno, L., 2009. Variabilidade e tendencias na escala sinóptica. Evidencias e Impactos do Cambio Climático en Galicia. Cap. 2, pp. 59–73 Xunta de Galicia.

Trigo, I.F., 2006. Climatology and interannual variability of storm-tracks in the Euro- Atlantic sector: a comparison between ERA-40 and NCEP/NCAR reanalyses. Clim. Dyn. 26, 127–143.

Trigo, R.M., García-Herrera, R., Díaz, J., Trigo, I.F., Valente, M.A., 2005. How exceptional was the early August 2003 heatwave in France? Geophys. Res. Lett. 32, L10701. http://dx.doi.org/10.1029/2005GL022410.

Trigo, R.M., Valente, M.A., Trigo, I.F., Miranda, P.M.A., Ramos, A.M., Paredes, D., Garcia- Herrera, R., 2008. The impact of north Atlantic wind and cyclone trends on European precipitation and significant wave height in the Atlantic. Ann. N. Y. Acad. Sci. 1146, 212–234.

Trigo, R.M., Trigo, I.M., DaCamara, C.C., Osborn, T.J., 2004. Climate impact of the European winter blocking episodes from the NCEP/NCAR reanalyses. Clim. Dyn. 23, 17–28.

Trigo, R.M., Osborn, T.J., Corte-Real, J.M., 2002. The North Atlantic Oscillation influence on Europe: climate impacts and associated physical mechanisms. Clim. Res. 20, 9–17.

Usoskin, I.G., Voiculescu, M., Kovaltsov, G.A., Mursula, K., 2006. Correlation between clouds at different altitudes and solar activity: fact or artifact? J. Atmos. Sol. Terr. Phys. 68, 2164–2172.

von Storch, H., Zwiers, F.W., 1999. Statistical Analysis in Climate Research. Cambridge University Press, Cambridge, 484p.

Wallace, J.M., Gutzler, D.S., 1981. Teleconnections in the geopotential height field during the Northern Hemisphere winter. Mon. Weather Rev. 109, 784–812.

Wetter, O., Pfister, C., 2011. Spring-summer temperatures reconstructed for northern Switzerland and southwestern Germany from winter rye harvest dates, 1454–1970. Clim. Past 7, 1307–1326.

Woollings, T., Hannachi, A., Hoskins, B., Turner, A., 2010a. A regime view of the North Atlantic Oscillation and its response to anthropogenic forcing. J. Clim. 23, 1291–1307.

Woollings, T., Lockwood, M., Masato, G., Bell, C., Gray, L., 2010b. Enhanced signature of solar variability in Eurasian winter climate. Geophys. Res. Lett. 37, L20805. http:// dx.doi.org/10.1029/2010GL044601 6p.

Yeo, K.L., Krivova, N.A., Solanki, S.K., Glassmeier, K.H., 2014. Reconstruction of total and spectral solar irradiance from 1974 to 2013 based on KPVT, SoHO/MDI, and SDO/ HMI observations. Astron. Astrophys. 570, A85 18p.

Internet sources
CVRVV — www.vinhoverde.pt/

http://drought.unl.edu
http://www.cpc.noaa.gov/data/teledoc/telecontents.shtml
http://www.atmos.colostate.edu/ao/Data/ao_index.html
http://climexp.knmi.nl/

Appendix 4.1. GHD data – Grape Harvest Dates z-score from Minho region (1856–2009). GSTmax reconstructed data - growing season maxima temperatures reconstruction from Minho region (2009–1856).

Year	Z-score GHD	GSTmax reconstructed	Year	Z-score GHD	GSTmax reconstructed	Year	Z-score GHD	GSTmax reconstructed
2009	0.20	22.9	**1959**	0.69	22.5	**1905**	-0.67	23.7
2008	0.59	22.5	**1958**	1.08	22.1	**1904**	-1.15	24.1
2007	0.01	23.1	**1957**	-0.47	23.5	**1903**	0.69	22.5
2006	-0.09	23.1	**1956**	0.98	22.2	**1902**	0.78	22.4
2005	0.49	22.6	**1954**	0.59	22.5	**1901**	-0.09	23.1
2004	0.69	22.5	**1953**	0.01	23.1	**1900**	0.01	23.1
2003	0.30	22.8	**1952**	-1.34	24.3	**1899**	-1.25	24.2
2002	0.30	22.8	**1950**	0.30	22.8	**1898**	-0.18	23.2
2001	0.69	22.5	**1949**	-0.76		**1897**	-1.05	24.0
2000	0.01	23.1	**1948**	-1.25	24.2	**1896**	-2.02	24.9
1999	0.11	23.0	**1947**	0.20	22.9	**1895**	0.20	22.9
1998	0.30	22.8	**1945**	-1.44	24.3	**1894**	0.69	22.5
1997	-0.47	23.5	**1944**	-2.31	25.1	**1893**	-1.25	24.2
1996	0.98	22.2	**1943**	-2.89	25.6	**1892**	0.30	22.8
1995	-0.09	23.1	**1942**	-1.54	24.4	**1891**	-0.18	23.2
1994	0.01	23.1	**1941**	0.78	22.4	**1890**	0.49	22.6
1993	1.08	22.1	**1940**	0.20	25.6	**1889**	1.95	21.3
1992	0.78	22.4	**1939**	1.08	24.4	**1888**	-1.25	24.2
1991	-0.67	23.7	**1938**	-1.73	22.4	**1887**	0.01	23.1
1990	-0.09	23.1	**1937**	-0.67	23.7	**1886**	0.59	22.5
1989	0.11	23.0	**1936**	0.78	22.4	**1885**	0.30	22.8
1988	0.69	22.5	**1935**	0.20	22.9	**1884**	0.69	22.5
1987	0.30	22.8	**1934**	-0.47	23.5	**1882**	0.88	22.3
1986	1.56	21.7	**1932**	0.49	22.6	**1881**	-0.86	23.8
1985	1.66	21.6	**1931**	0.11	23.0	**1880**	0.59	22.5
1984	1.37	21.9	**1930**	1.17	22.0	**1879**	-0.57	23.6
1983	1.85	21.4	**1929**	-1.54	24.4	**1878**	-0.09	23.1
1982	1.27	21.9	**1928**	-0.18	23.2	**1877**	-0.38	23.4
1981	0.98	22.2	**1927**	0.01	23.1	**1876**	0.11	23.0
1980	0.88	22.3	**1926**	0.30	22.8	**1875**	-0.76	23.7
1979	1.08	22.1	**1925**	0.69	22.5	**1874**	-0.76	23.7
1978	1.17	22.0	**1924**	1.46	21.8	**1873**	-1.25	24.2
1977	1.75	21.5	**1923**	0.98	22.2	**1872**	-0.76	23.7
1976	0.01	23.1	**1922**	-0.57	23.6	**1871**	-1.92	24.8
1975	0.88	22.3	**1921**	-0.96	23.9	**1870**	-0.47	23.5
1974	0.59	22.5	**1920**	-0.47	23.5	**1869**	-1.15	24.1
1973	0.30	22.8	**1919**	-0.86	23.8	**1868**	-1.83	24.7
1972	1.75	21.5	**1918**	0.20	22.9	**1867**	-1.34	24.3
1971	1.95	21.3	**1917**	0.30	22.8	**1866**	0.20	22.9
1970	0.30	22.8	**1916**	0.40	22.7	**1865**	0.01	23.1
1969	0.78	22.4	**1915**	-0.09	23.1	**1864**	-1.34	24.3
1968	0.88	22.3	**1914**	0.69	22.5	**1863**	-1.92	24.8
1967	0.88	22.3	**1913**	0.11	23.0	**1862**	-1.83	24.7
1966	-0.18	23.2	**1912**	-1.25	24.2	**1861**	-2.50	25.3
1965	1.27	21.9	**1911**	0.30	22.8	**1859**	-2.12	24.9
1964	-0.47	23.5	**1910**	1.85	21.4	**1858**	-0.47	23.5
1963	1.56	21.7	**1909**	0.49	22.6	**1857**	-1.92	24.8
1962	-0.18	23.2	**1908**	-0.09	23.1	**1856**	0.88	22.3
1961	-0.96	23.9	**1907**	0.40	22.7			
1960	-0.96	23.9	**1906**	-0.86	23.8			

Appendix 4.2. Calibration and verification results of the grape harvest dates composite with March–August Braga maxima temperatures. Temp. rec. - temperature reconstructed (ºC); Temp. obs. - temperature observed (ºC).

	Year	Temp. obs.	Temp. rec.	Residuals		Year	Temp. obs	Temp. rec	Residuals		Year	Temp. obs.	Temp. rec.	Residuals
Calibration	1941	22.28	22.06	0.22	Verification	1941	22.28	22.25	0.03	Full Period Calibration	1941	22.28	22.37	-0.09
	1942	22.80	24.17	-1.37		1942	22.80	25.78	-2.98		1942	22.80	24.43	-1.63
	1943	26.08	25.40	0.68		1943	26.08	27.84	-1.76		1943	26.08	25.63	0.45
	1944	25.35	24.88	0.47		1944	25.35	26.96	-1.61		1944	25.35	25.12	0.23
	1945	25.02	24.09	0.93		1945	25.02	25.64	-0.62		1945	25.02	24.34	0.67
	1947	23.85	22.59	1.26		1947	23.85	23.13	0.72		1947	23.85	22.88	0.97
	1948	24.33	23.91	0.42		1948	24.33	25.34	-1.01		1948	24.33	24.17	0.16
	1950	23.45	22.50	0.95		1950	23.45	22.98	0.47		1950	23.45	22.80	0.65
	1952	22.60	24.00	-1.40		1952	22.60	25.49	-2.89		1952	22.60	24.26	-1.66
	1953	24.22	22.77	1.45		1953	24.22	23.43	0.79		1953	24.22	23.06	1.16
	1954	22.62	22.24	0.38		1954	22.62	22.54	0.07		1954	22.62	22.54	0.08
	1956	21.68	21.89	-0.20		1956	21.68	21.95	-0.27		1956	21.68	22.20	-0.51
	1957	22.98	23.21	-0.22		1957	22.98	24.16	-1.18		1957	22.98	23.49	-0.50
	1958	21.22	21.80	-0.58		1958	21.22	21.81	-0.59		1958	21.22	22.11	-0.90
	1959	22.52	22.15	0.37		1959	22.52	22.40	0.12		1959	22.52	22.46	0.06
	1960	22.12	23.65	-1.53		1960	22.12	24.90	-2.78		1960	22.12	23.91	-1.80
	1961	23.77	23.65	0.12		1961	23.77	24.90	-1.13		1961	23.77	23.91	-0.15
	1962	22.63	22.94	-0.31		1962	22.63	23.72	-1.09		1962	22.63	23.23	-0.59
	1963	21.57	21.36	0.21		1963	21.57	21.07	0.50		1963	21.57	21.68	-0.12
	1964	22.13	23.21	-1.07		1964	22.13	24.16	-2.03		1964	22.13	23.49	-1.35
	1965	22.12	21.62	0.49		1965	22.12	21.51	0.60		1965	22.12	21.94	0.18
	1966	22.42	22.94	-0.53		1966	22.42	23.72	-1.30		1966	22.42	23.23	-0.81
	1967	22.28	21.98	0.31		1967	22.28	22.10	0.18		1967	22.28	22.28	0.00
	1968	22.03	21.98	0.06		1968	22.03	22.10	-0.07		1968	22.03	22.28	-0.25
	1969	21.83	22.06	-0.23		1969	21.83	22.25	-0.42		1969	21.83	22.37	-0.54
	1970	21.70	22.50	-0.80		1970	21.70	22.98	-1.28		1970	21.70	22.80	-1.10
	1971	20.02	21.01	-0.99		1971	20.02	20.48	-0.46		1971	20.02	21.34	-1.32
	1972	20.83	21.18	-0.35		1972	20.83	20.78	0.06		1972	20.83	21.51	-0.68
	1973	22.78	22.50	0.28		1973	22.78	22.98	-0.20		1973	22.78	22.80	-0.02
	1974	22.18	22.24	-0.06		1974	22.18	22.54	-0.36		1974	22.18	22.54	-0.36
	1975	22.08	21.98	0.11		1975	22.08	22.10	-0.02		1975	22.08	22.28	-0.20
	1976	23.72	22.77	0.95		1976	23.72	23.43	0.29		1976	23.72	23.06	0.66
Verification	1977	20.40	21.18	-0.78	Calibration	1977	20.40	20.78	-0.38		1977	20.40	21.51	-1.11
	1978	20.85	21.71	-0.86		1978	20.85	21.66	-0.81		1978	20.85	22.03	-1.18
	1979	21.78	21.80	-0.02		1979	21.78	21.81	-0.02		1979	21.78	22.11	-0.33
	1980	21.58	21.98	-0.39		1980	21.58	22.10	-0.52		1980	21.58	22.28	-0.70
	1981	22.63	21.89	0.75		1981	22.63	21.95	0.68		1981	22.63	22.20	0.44
	1982	22.73	21.62	1.11		1982	22.73	21.51	1.22		1982	22.73	21.94	0.79
	1983	21.15	21.10	0.05		1983	21.15	20.63	0.52		1983	21.15	21.43	-0.28
	1984	22.00	21.54	0.46		1984	22.00	21.36	0.64		1984	22.00	21.85	0.15
	1985	22.23	21.27	0.96		1985	22.23	20.92	1.31		1985	22.23	21.60	0.64
	1986	22.02	21.36	0.66		1986	22.02	21.07	0.95		1986	22.02	21.68	0.33
	1987	23.77	22.50	1.26		1987	23.77	22.98	0.78		1987	23.77	22.80	0.97
	1988	21.68	22.15	-0.47		1988	21.68	22.40	-0.71		1988	21.68	22.46	-0.77
	1989	23.93	22.68	1.25		1989	23.93	23.28	0.65		1989	23.93	22.97	0.96
	1990	24.05	22.85	1.20		1990	24.05	23.57	0.48		1990	24.05	23.14	0.91
	1991	23.43	23.38	0.05		1991	23.43	24.46	-1.02		1991	23.43	23.66	-0.22
	1992	23.30	22.06	1.24		1992	23.30	22.25	1.05		1992	23.30	22.37	0.93
	1993	22.45	21.80	0.65		1993	22.45	21.81	0.64		1993	22.45	22.11	0.34
	1994	22.58	22.77	-0.18		1994	22.58	23.43	-0.84		1994	22.58	23.06	-0.47
	1995	24.27	22.85	1.41		1995	24.27	23.57	0.69		1995	24.27	23.14	1.12
	1996	23.02	21.89	1.13		1996	23.02	21.95	1.06		1996	23.02	22.20	0.82
	1997	24.12	23.21	0.91		1997	24.12	24.16	-0.05		1997	24.12	23.49	0.63
	1998	23.32	22.50	0.81		1998	23.32	22.98	0.33		1998	23.32	22.80	0.52
	1999	22.82	22.68	0.14		1999	22.82	23.28	-0.46		1999	22.82	22.97	-0.15
	2000	22.42	22.77	-0.35		2000	22.42	23.43	-1.01		2000	22.42	23.06	-0.64
	2001	22.38	22.15	0.23		2001	22.38	22.40	-0.01		2001	22.38	22.46	-0.07
	2002	22.78	22.50	0.28		2002	22.78	22.98	-0.20		2002	22.78	22.80	-0.02
	2003	23.63	22.50	1.13		2003	23.63	22.98	0.65		2003	23.63	22.80	0.83
	2004	23.07	22.15	0.92		2004	23.07	22.40	0.67		2004	23.07	22.46	0.61
	2005	23.85	22.33	1.52		2005	23.85	22.69	1.16		2005	23.85	22.63	1.22
	2006	24.57	22.85	1.71		2006	24.57	23.57	0.99		2006	24.57	23.14	1.42
	2007	23.36	22.77	0.59		2007	23.36	23.43	-0.07		2007	23.36	23.06	0.30
	2008	22.75	22.24	0.51		2008	22.75	22.54	0.21		2008	22.75	22.54	0.21
	2009	23.97	22.59	1.38		2009	23.97	23.13	0.83		2009	23.97	22.88	1.08

5 Records from marsh foraminifera and grapevine growing season temperatures reveal the hydro-climatic evolution of the Minho region (NW Portugal) from 1856–2009

JOÃO MORENO[1, 2, 5], FRANCISCO FATELA[1, 2], EDUARDO LEORRI[1, 3] , FILIPA MORENO[4]

[1]IDL – Instituto Dom Luiz, Universidade de Lisboa, Campo Grande, 1749–016, Lisboa, Portugal

[2] Departamento de Geologia da Faculdade de Ciências da Universidade de Lisboa, Campo Grande, 1749–016, Lisboa, Portugal

[3] East Carolina University, Department of Geological Sciences, Greenville, NC 27858–4353, USA

[4] Independent researcher

[5] Correspondence author. E-mail: jcmoreno@fc.ul.pt

Published in: Journal of Foraminiferal Research 47 (2017), 208–218

doi:10.2113/gsjfr.47.2.208

"It is likely that abiotic environmental parameters are of greater importance than biotic factors in shaping the communities which live in variable environments such as marginal marine settings."

J. W. Murray in ECOLOGY AND PALAEOECOLOGY OF BENTHIC FORAMINIFERA (1991), p.2.

ABSTRACT

A hydro-climatic reconstruction is proposed for the Minho region (NW Portugal), integrating two different proxies: grape harvest dates (GHD) as a proxy of temperature variations, and benthic marsh foraminifera as a proxy of sediment interstitial-water salinity. The reconstructed and measured mean maximum temperatures (GSTmax) of grapevine growing season (March to August) were combined with data on benthic foraminiferal assemblages from the Caminha tidal marsh (Minho River estuary) to characterize the main hydro-climatic episodes in the region during the last 154 years. Results emphasize that, in the brackish setting of the

Minho estuary, where foraminiferal species usually associated with low salinity prevail, higher GSTmax had an impact on marsh hydrological balance by enhancing evapotranspiration and increasing interstitial water salinity. These conditions favoured the occurrence of marsh species like *Jadammina macrescens* and *Trochammina inflata*.

The influence of the North Atlantic European meteorological teleconnection patterns on recent climatic variability of the Minho region was also examined for the period from 1950–2009. Data support the hypothesis that persistent positive modes of spring-summer Scandinavian Oscillation Mode (SCA) and summer Eastern Atlantic/Western Russia Oscillation Mode (EA/WR) patterns triggered lower GSTmax, especially in the 1960s–1980s. Those conditions, in-phase with a positive precipitation anomaly (1958–1983), reduced the Caminha tidal marsh salinity, leading to the increase of low-salinity species: *Trochamminita salsa/irregularis*, *Haplophragmoides manilaensis*, *Miliammina fusca* and *Miliammina* spp.

Both proxies provide valuable tools for understanding the interactions between large-scale circulation modes and hydro-climatic conditions at regional and local scales.

5.1. Introduction

Coastal marshes are complex and dynamic ecosystems that can be characterized in several ways (Christian et al., 2000). They are among the most productive ecosystems with both ecological and economic value, from storm and flood protection (Mitsch & Gosselink, 2000a) to carbon sequestration (Chmura et al., 2003). One of the major drivers of change in coastal marshes is sea-level change (Christian et al., 2000), making these ecosystems susceptible to changes in the tidal frame (Kirwan et al., 2010) and therefore suitable environments to study former sea-levels (e.g., Gehrels, 1994; Hayward et al., 1999; Horton, 1999; Scott et al., 2001; Gehrels & Newman, 2004; Horton & Edwards, 2005; Fatela et al., 2009a; Leorri et al., 2010, 2011). However, climate change impacts on coastal marshes also include increased temperature, changes in rainfall distribution and freshwater inputs, operating at different spatiotemporal scales (Day et al., 2008). Deconvolving the contributions of these confounding factors is essential to reduce the uncertainty associated with reconstructions of environmental evolution and sea-level changes. While salinity and tidal range have been studied in relation to distributions of foraminiferal assemblages in coastal wetlands (e.g., Hayward et al., 2004), there are no similar studies regarding the effects of temperature based on foraminiferal assemblages while they are available for plant distributions.

Benthic foraminifera are excellent paleoclimatic proxies, because modern foraminiferal assemblages provide reliable analogues for understanding past environmental changes (e.g., Debenay et al., 2000; Sen Gupta, 2002; Murray, 2006). Paleoclimate research based on salt marsh foraminifera has been increasingly important since the pioneering works of Phleger (1965) and Scott & Medioli (1978, 1980). The role of marsh foraminifera as paleoenvironmental proxies is also highlighted by their use in reconstructing Holocene sea-levels (see references above). In this

context, Horton & Murray (2007) asserted that the importance of individual controls, such as flooding frequency (controlled by marsh elevation and tidal frame) and salinity, on foraminiferal distribution and abundance patterns varies temporally and spatially in salt marshes. Indeed, marsh elevation in relation to the tidal frame is a major control of the mechanisms of self-maintenance of these ecosystems, where environmental factors are directly related to the position and intensity of the interface between fresh and seawater. Elevation affects the salinity concentration, and therefore plant growth, nutrient cycling, and decomposition (Herbert et al., 2015), while turbidity and sediment load often decrease as fluvial sources become attenuated by seawater intrusion. Plant growth and reduced sediment availability can limit accretion and jeopardize the capacity for increases in elevation (Lovelock et al., 2015; Morris et al., 2016). However, there is evidence that vertical accretion of many salt marshes has kept up with mid- to late-Holocene rates of sea-level rise (0.6–1.7 mm/yr; Engelhart et al., 2009). Furthermore, positive feedback between climate, sea-level rise, and carbon emissions might produce a coastal wetland response that overcomes sea-level rise (Kirwan and Blum, 2011), making temperature a key factor if the marsh elevation in relation to the tidal frame is sustained over time. Consequently, flooding frequency and salinity can be important in different parts of the marsh or at different times. In addition, each species has its distinct response to environmental changes, allowing the identification of past climate driven shifts.

Unfortunately, long-term monitoring programs that could identify the influence of different factors on foraminiferal assemblages is time consuming and seldom funded, with temporal studies lasting three years at best (e.g., Hippensteel et al., 2002). On the other hand, the geological record can be calibrated against instrumental data; this is routinely done for sea-level studies where the instrumental data is used to test independently the most recent part of the geological record (e.g., Kemp et al., 2011), enhancing understanding of the different influences of these factors on the marsh evolution at different time scales.

When two different sets of modern analogues from the Caminha tidal marsh taken in 2002 and 2010 were compared, the foraminiferal assemblages had changed significantly. These results were connected to changes in the hydrology and alternating dry and wet periods (Fatela et al., 2014), subsequently related to changes in the depositional environment over the last 2000 years (Moreno et al., 2014). At the same time, changes in other proxies (like Bromine) were found to correlate with changes in total solar irradiance (TSI) for the same period (Moreno et al., 2015).

While the confounding effect of changes in tidal range and salinity has been studied (e.g., Culver et al., 2015), the influence of long term (decadal-scale) changes in temperature in the marsh ecosystem has not been addressed when studying foraminiferal assemblages. To understand the potential impact of this variable in the high marsh hydrological balance, and as a driver of coastal wetland change (as recorded in the plants communities), we compared a newly developed high-resolution foraminiferal record from the Caminha marsh with growing season mean maximum

temperatures (GSTmax) back to 1856, which were recently reconstructed by Moreno et al. (2016) for the Minho region (NW Portugal). Briefly, these authors used grape harvest dates (GHD), which are recognized as an important source of data to understand climate evolution in Europe (e.g., Brázdil et al., 2005, 2008), to reconstruct temperatures and the GSTmax series. So, this GHD series represents the mean maximum temperatures during the growing season between the months of March to August, based on the dependence of grape ripening on temperature (Menzel, 2005). These reconstructions are statistically supported by significant linear correlations between GST and GHD series (e.g., Menzel, 2005; Daux et al. 2007; Meier et al., 2007; Maurer et al., 2011) and are a recognized proxy for this meteorological parameter.

Our work is based on the hypothesis that marsh foraminifera respond to the complex and intricate number of variables that control marsh evolution and include temperature as a key component of the environmental balance. With this work we intend a) to contribute to the knowledge of the Minho region hydro-climatic dynamics through an innovative comparison of a newly reconstructed GSTmax (Moreno et al., 2016) with the high marsh benthic foraminiferal assemblage data; and b) to provide a better understanding of the hydrological balance in the Caminha tidal marsh, within the context of the main North Atlantic European meteorological teleconnection patterns between 1950 and 2009. This case study can be used as a reference to reduce uncertainties on paleoclimatic reconstructions based only on one driver.

5.2. Study area

The Minho River flows into the Northeast Atlantic, forming a natural border between Portugal and Spain, and the northern limit of the Minho Wine Region. Its estuary trends NNE–SSW and a large tidal flat and a tidal marsh (*ca.* 6 km^2) have developed close to the mouth. The widest marsh expansion occurs on the left margin, where the tributary Coura joins the Minho River, mentioned hereinafter as Caminha tidal marsh (Figure 5.1).

The Holocene sea-level in this coastal area presents two main phases: a) a fast relative sea-level rise from ~21 m below mean sea-level (bmsl) at *ca.* 9000 cal yr BP to ~5 m bmsl at *ca.* 7000 cal yr BP; and b) a relatively slow sea-level rise from *ca.* 7000 cal yr BP until present that equates to 0.7 mm/yr (Leorri et al., 2013). This trend in sea-level rise likely changed around 1920 (similar to Cascais; Antunes and Taborda, 2009), but the closest tide gauge located in A Coruna only has records since 1943 and suggests a new rate of 2.5 mm/yr (Leorri et al., 2013). While the Caminha marsh might have maintained elevation over the last several thousand years, it might have lost up to 15 cm over the last 150 years in relation to the tidal frame. However, the high marsh sampling site is flooded less than 7% of the time (Fatela et al., 2009a).

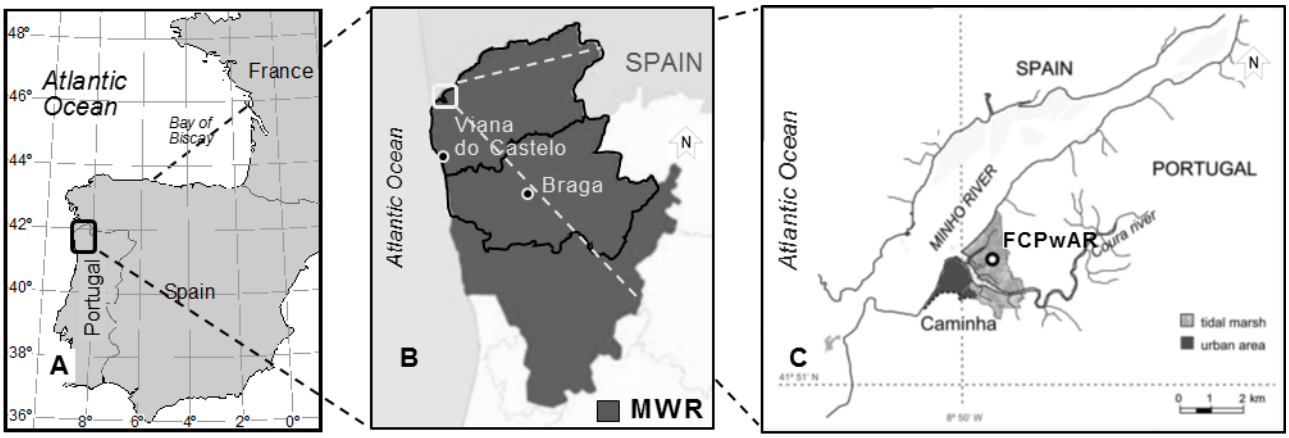

Figure 5.1. **A –** Geographical location of the Portuguese Demarcated Minho Wine Region (MWR). **B –** Delimitation of Minho Wine Region (MWR; grey area) and Viana do Castelo and Braga. **C –** Sampling location of core FCPwAR in Caminha tidal marsh (Minho estuary, NW Portugal).

The salinity of marsh-sediment interstitial waters is essentially brackish, exhibiting a wide range from limnetic to polyhaline (Venice system, 1959). The highest values were recorded in the transition from low to high marsh zone and during autumn (Table 5.1; Moreno et al., 2005, 2006; Fatela et al., 2009a). Environmental factors such as the concomitant undersaturation in calcite and low pH values of the interstitial waters limit calcareous foraminifera to very low proportions in the low marsh (min. = 0%, max.= 5%, avg.= 0.49%) and their absence in the high marsh zone (Moreno et al, 2007; Fatela et al., 2009a; Valente et al., 2009). The foraminiferal assemblages are almost exclusively composed by agglutinated species, whose distribution exhibits the following zonation: the high marsh IB sub-zone is dominated by *Haplophragmoides* sp. and *Haplophragmoides manilaensis* (Andersen, 1953); the low marsh zone II is characterized by the dominance of *Miliammina fusca* (Brady, 1870) but can be subdivided in an IIA upper part, where is followed by *Pseudothurammina limnetis* (Scott & Medioli, 1980), and in a IIB lower part defined by a subsidiary presence of *Psammosphaera* sp. (Fatela et al., 2009a).

Table 5.1. Caminha intertidal salinity range of sediment interstitial water (‰)

	Channel LT	Channel HT	Tidal flat	Low marsh	High marsh
Spring	0.1 - 7.1	24.4 - 30.7	0.1 - 16.3	2.2 - 18.2	1.6 - 10.1
Autumn	1.2 - 10.6	22.8 - 31.3	1.2 - 22.3	6.6 - 25.0	8.6 - 22.1

LT – low tide; HT – high tide

The presence of these species, as well as *Trochamminita salsa/irregularis* (Cushman & Brönnimann, 1948) and *Polysaccammina ipohalina* Scott, 1976, records also the low salinity conditions of the marsh environment (mainly limnetic to mesohaline). When the salinity of marsh

sediment rises to moderate to normal levels, those taxa are replaced by *Jadammina macrescens* (Brady, 1870), *Trochammina inflata* (Montagu,1808), *Tiphotrocha comprimata* (Cushman & Brönnimann, 1948), *Paratrochammina guaratibaensis* (Brönnimann, 1986) and *Siphotrochammina lobata* (Saunders, 1957), amongst other minor species (e.g., Hayward et al., 1999; Debenay et al., 2000; Scott et al., 2001; Sen Gupta, 2002; Fatela et al., 2009a,b, 2014).

5.3. Materials and methods

The FCPwAR core (30 cm long) was collected at the FCPw1 sediment core sampling site (Moreno et al., 2014) in the high marsh zone of the Caminha tidal marsh (altitude 1.55 m; 41º52′37″ N, 08º49′28″ W; Figure 5.1C). A PVC pipe was initially pushed into the sediment by hand, then carefully driven with a rubber hammer to minimize compaction. The core was kept refrigerated (*ca.* 4ºC) until it was sliced into 0.5 cm contiguous intervals, producing sixty samples (*ca.* 25 cm^3) that were analyzed for foraminifera. Samples were wet sieved to remove clay and silt material (63 μm mesh). The fraction greater than 63 microns was immersed for at least 1 hour in a [1 g/L] Rose Bengal solution (e.g., Murray, 2006) and rewashed to eliminate excess stain. This procedure allows discrimination between dead and live/stained (at time of collection) foraminiferal specimens. At least 100 dead individuals were wet picked with a micropipette from each sample, a number considered adequate to characterize the low-diversity assemblages of salt marshes (Fatela & Taborda, 2002). The details of the methodologies for micropaleontological analyses are described elsewhere (e.g., Fatela et al., 2014; Moreno et al., 2014). The chronology in this core is described in Moreno et al. (2014) and data are provided in Appendix 5.1. Briefly, the upper 14 cm of the core were dated using ^{210}Pb supported by ^{137}Cs and total concentrations of Pb, and the derived chronology was based on the constant rate of supply model (see Moreno et al., 2014 and references therein for further detail). Six additional samples (40–41 cm, 44–45 cm, 63–64 cm, 66–67 cm, 81–82 cm and 90–91 cm depth) were analyzed for radiocarbon content at Beta Analytic Inc. (USA). The final age-depth model was developed using BChron/R (Bchron 3.2; Haslett and Parnell, 2008; Parnell et al., 2008). Radiocarbon ages and the final model are provided in Appendix 5.1. While the studied period is within the ^{210}Pb range (4–6 times the half-life), the age error increases down-core and ages older than 100 years can be associated with large errors. The inclusion of the radiocarbon data minimizes the potential errors in the interpretation of the older ages.

The foraminiferal record was interpreted according to published ecological information (Appendix 5.3). Two main groups of species were established based on their salinity preferences: a) strongly brackish (oligohaline to mesohaline) –*H. manilaensis*, *T. salsa/irregularis* and *Miliammina* spp.; b) moderately brackish-to-normal salinity (polyhaline to euhaline) – *J. macrescens*, *T. inflata*, *T. comprimata*, *S. lobata*, *P. guaratibaensis*, *H. wilberti*, *P. limnetis*, and *P. ipohalina*.

The reconstruction of growing season mean maximum temperatures (GSTmax) for the Minho Region was obtained from a statistical linear model, based on documented grape harvest dates (GHD) (Moreno et al., 2016). The influence in temperature of two major large-scale patterns (or teleconnections) for the Euro-Atlantic region, the East Atlantic/Western Russia Oscillation (EA/WR) and the Scandinavian Oscillation (SCA) (Barnston & Livezey, 1987), was considered in the interpretation of the foraminiferal assemblages. The monthly values of EA/WR and SCA indices were retrieved from the Climate Prediction Center (NOAA) and the KNMI Climate Explorer websites.

5.4. Results

The core is dominated by high marsh foraminifera, with abundant *Trochamminita salsa/irregularis* (Cushman & Brönnimann, 1948), *Haplophragmoides manilaensis* (Andersen, 1953), *Haplophragmoides wilberti* Andersen, 1953, *Jadammina macrescens* (Brady, 1870) and *Trochammina inflata* (Montagu,1808), followed by *Polysaccammina ipohalina* Scott, 1976, and *Paratrochammina guaratibaensis* (Brönnimann, 1986) as subsidiary species, and *Tiphotrocha comprimata* (Cushman & Brönnimann, 1948), *Siphotrochammina lobata* (Saunders, 1957), *Pseudothurammina limnetis* (Scott & Medioli, 1980) and *Miliammina fusca* (Brady, 1870) occurring occasionally.

The sediment record of the Caminha marsh short core (FCPwAR) ranges from cal. AD 1650–2010, encompassing the late Little Ice Age (LIA) until present time. However, in this paper we analyzed only the top 16 cm that spans from the end of the Dalton Solar Minimum (DM) in the late 18th century (1790–1830; Komitov & Kaftan, 2004; Wagner & Zorita, 2005) to 2010.

FAZ II (16–8 cm depth) ranges from cal. AD 1824–1950. *Jadammina macrescens, T. inflata, and H. wilberti* followed by *T. comprimata, S. lobata* and *P. guaratibaensis* show a significant increases in percentage after the Dalton Solar Minimum (Figures 5.2 and 5.3), between cal. AD 1825–1860 (47–76%), and during two other well-marked periods, at cal. AD 1895 (41%) and 1935–1950 (46–50%). *Haplophragmoides manilaensis* (41–67%), associated with *T. salsa/irregularis* (10–18%), become the dominant species in two intercalated periods, between cal. AD 1880–1885 and 1900–1920 (Figures 5.2 and 5.3; Appendix 5.2).

FAZ I (8–0 cm depth) ranges from 1950–2010. In this FAZ, the marsh foraminiferal assemblage is dominated by *T. salsa/irregularis*, *H. manilaensis*, *M. fusca* and *Miliammina* spp. representing 63–83% of the assemblage. *Haplophragmoides wilberti* and *P. limnetis* are present as minor species. However, *T. inflata* is often well represented (5–20%), and a minor presence or the absence of *J. macrescens* and *S. lobata* should also be emphasized (Figure 5.2; Appendices 5.2 and 5.3).

5.5. Discussion

In salt marsh environments, soil or sediment salinity plays an important role determining zonation, productivity, and biogeochemical processes (Wang et al., 2007). In these ecosystems (traditionally divided into low, middle and high marsh zones in relation to the tidal frame) sediment salinity is mainly controlled by the net balance between evapoconcentration of tidally supplied salts and rainfall infiltration or groundwater flushing, particularly in the high marsh zone (e.g., Hughes et al., 2001). At higher elevations, the reduced frequency and duration of tidal flooding (less than 7% of time in the core site) intensifies the interaction between the tidal regime and climate that leads to both greater sediment salinity values and greater variability (Adam, 1990). This also accounts for the typical gradient of increasing sediment salinity from low to high marsh (e.g., Pennings & Callaway, 1992). Figure 5.4 summarizes the dominant hydrological factors influencing, at a regional scale, the water balance on salt marshes. A standard equation used to express this water balance is described by Mitsch & Gosselink (2000b):

$$P + S_i + G_i + T_i - ET - S_o - G_o - T_o = \Delta V/\Delta t \qquad (3)$$

where, P is the precipitation, S_i is the surface water inflow, G_i is the groundwater inflow, T_i is the tidal inflow, ET is the evapotranspiration, S_o is the surface water outflow, G_o is the groundwater outflow, T_o is the tidal outflow and $\Delta V/\Delta t$ is the change (Δ) in water volume (V) per unit of time (t) in the salt marsh. This water volume (V) is replaced, in a spatially and temporally varied pattern, by precipitation and tidal inundation contributing to the salinity trends (and moisture content) across the salt marsh, with maximum impact on the high marsh. Here the sediment salinity is determined primarily by the mutually opposing effects of P and ET, as stated above.

Salinity measurements carried out in the Caminha tidal marsh (Table 5.1) indicated a maximum salinity of interstitial water at the transition from the low marsh to the high marsh zone, particularly from late summer to early autumn (Moreno et al., 2005; Fatela et al., 2007, 2009a, 2014). The immediate implication of these results is that the pattern described above, of increasing salinity following the high marsh elevation trend (Adam, 1990), is not present in the Caminha tidal marsh. A depressed topographic surface between the top of the high marsh zone and the upland environment, associated with high freshwater inputs (P, S_i, G_i and, river flow; Figure 5.4), tends to induce lower interstitial salinity at the upper limit of the Caminha tidal marsh.

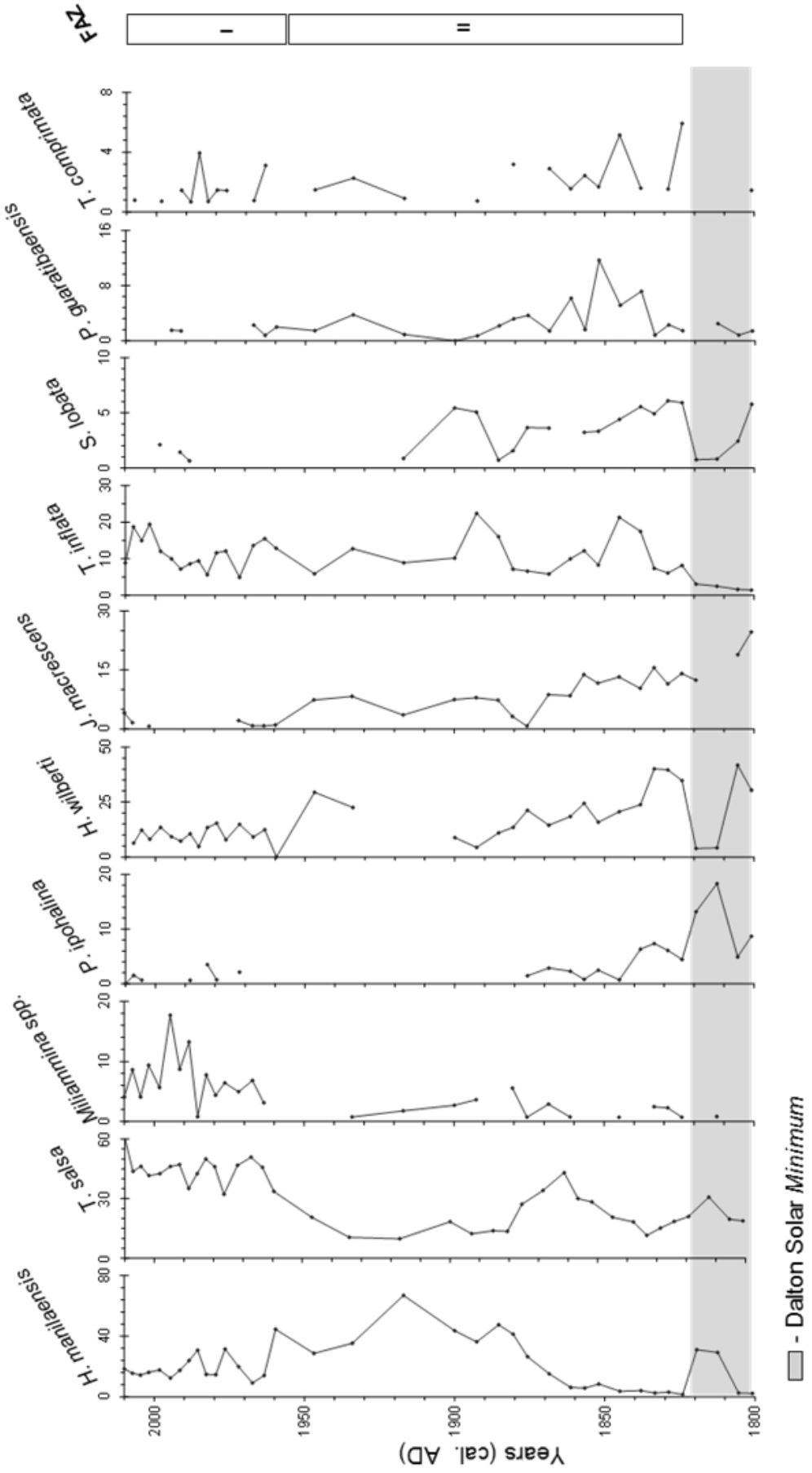

Figure 5.2. Percentage distribution of benthic foraminifera in core FCPwAR. Years (cal. AD): Age in calendar years AD; FAZ: foraminiferal assemblages' zones.

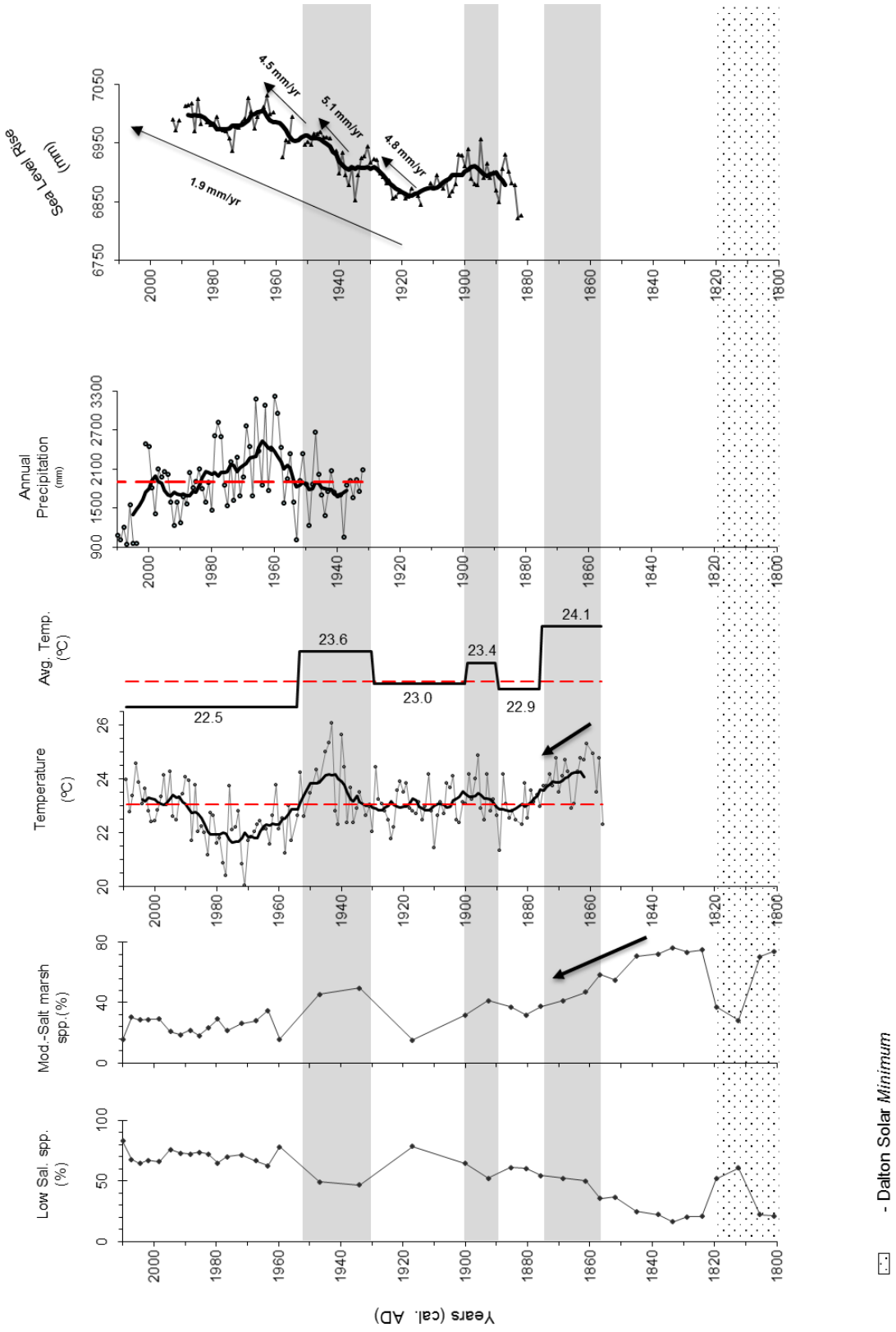

Figure 5.3. Changes in foraminiferal assemblages including percentages of the strongly brackish (oligohaline to mesohaline) marsh species group (Low Sal. spp.); percentages of the moderately brackish-to-normal salinity (polyhaline to euhaline) marsh species group (Mod.– Salt marsh spp.); as well as March to August mean temperature maxima (GSTmax, after Moreno et al., 2016); average temperature maxima (Avg. Temp.) for GHD z-score periods (after Moreno et al., 2016); annual precipitation records for Minho and Lima (after Fatela et al., 2014); and sea-level rise data from the Cascais tide gauge (http://www.psmsl.org/data/obtaining/rlr.annual.data/52.rlrdata). Broken lines represent overall means and thick solid lines represent eleven-year running averages for the environmental parameters; gray shading indicates intervals of above-average temperatures.

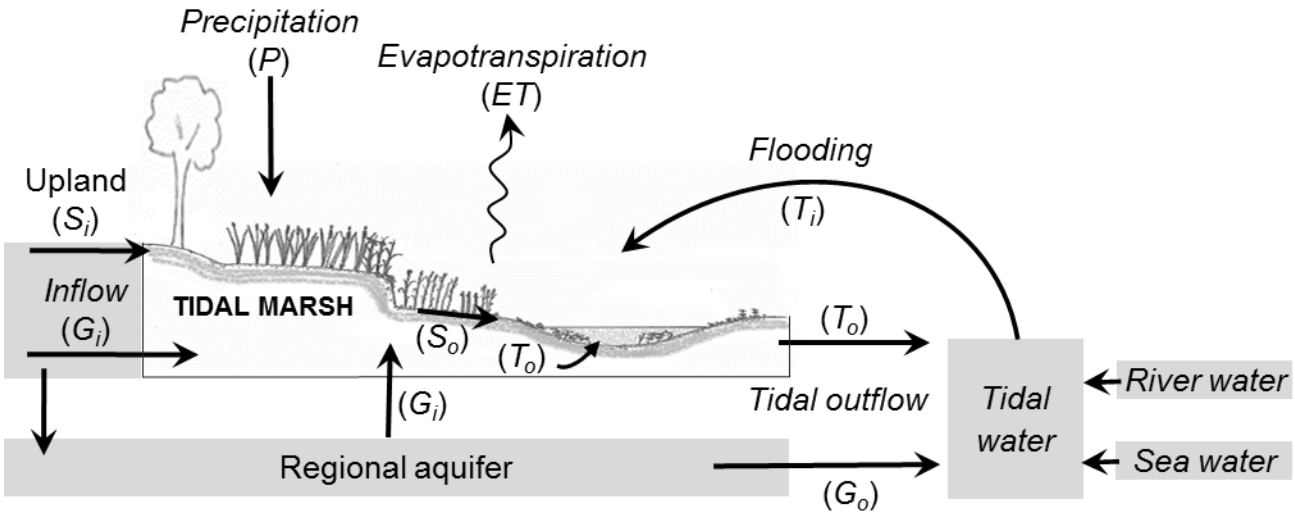

Figure 5.4. Schematic diagram of water balance in a salt marsh (adapted from Nuttle, 1988). P – Precipitation; ET – Evapotranspiration; S_i – surface water inflow; G_i – groundwater inflow, T_i – tidal inflow; S_o – surface water outflow; G_o – groundwater outflow; T_o – tidal outflow.

Similarly, benthic foraminifera showed that salinity is a clear ecological constraint on the composition of the high marsh assemblage (e.g., Fatela et al., 2009a; Appendix 5.3). The entire Caminha intertidal zone is a good example of a brackish environment where the dominant foraminiferal assemblages reflect low salinity conditions that range between limnetic to mesohaline in spring and between oligohaline to polyhaline in autumn. The low salinity results from the dilution of marine water in response to the combination of a) abundant rainfall and river flow (maximum precipitation often exceeds 2500 mm in the abundant nearby mountainous ranges during the wet season from October to March; Bettencourt et al., 2003), and b) limited penetration and residence of the salt water wedge within the estuarine basin (e.g., Moreno et al., 2005). This low salinity pattern has been consistent throughout the last 2000 years of estuarine and marsh development (Moreno et al., 2014). However, this brackish tidal marsh has experienced episodes of higher salinity. In fact, shifts towards the dominance of species that characterize polyhaline to euhaline marshes have occurred as a result of salinity increases on sediment interstitial waters, which have been connected in a previous work to a modification of the regional precipitation regime in the Minho region (Fatela et al., 2014). Other studies show that rainfall deficit (= precipitation minus evapotranspiration) controls sediment salinity on high marshes in two ways, regulating a) the seasonal and inter-annual patterns of soil/sediment salinity (e.g., De Leeuw et al., 1991) and b) the freshwater inflow to upland areas, including river systems that drain into tidal marshes (Wang et al., 2007).

Considering that salt accumulation in coastal marshes is also strongly affected by temperature, the GSTmax (reconstructed and instrumental) obtained from the Minho GHD time series provide a new climatic proxy to interpret salinity variations through time that can be extended beyond the historical records with the interpretation of foraminiferal assemblages (Figures 5.2 and 5.3).

Evapotranspiration is a temperature-dependent process, and consequently the temperature affects the maximum salinity of the marshes (Wang et al., 2007). Higher temperatures, associated with low precipitation rates, can prompt negative water balances (accelerating evapotranspiration rates), further increasing sediment salinities in high marsh areas that are not flushed daily by tides. In essence, the same factor (elevation) that reduces the amount of salt delivered by tidal flushing to the high marsh can also expose this environment to atmospheric conditions for longer during each tidal cycle. Ultimately, warmer and rainless growing seasons or droughts can considerably increase sediment salinities in the high marsh areas (Parker et al., 2011).

The 11-year moving average of the reconstructed GSTmax displays the highest values from 1856 to 1875 (avg. 24.1ºC ± 0.2ºC), concomitant with the later part of a longer period (in the geological record) marked by dominance of *J. macrescens, T. inflata,* and *H. wilberti*, associated with *T. comprimata, S. lobata* and *P. guaratibaensis* (Figures 5.2 and 5.3), that started at the end of the Dalton Solar Minimum. Note that errors are small for the most recent period but reach *ca.* 25 years for the 19th century dates and as much as 100 years for the older ages, as the geological record is limited by the chronology derived (mainly) from ^{210}Pb. Two other high GSTmax periods, 1890–1899 (avg. 23.4ºC ± 0.3ºC) and 1930–1953 (avg. 23.6ºC ± 0.2ºC), are in-phase (cal. AD 1893 and 1934–1947) with presence of foraminiferal assemblages dominated by species characteristic worldwide of polyhaline to hyperhaline salt marsh environments.

The GSTmax lowest average values were obtained for the period 1954–2010 (GSTmax reconstructed avg. 22.6ºC ± 0.1ºC; GSTmax instrumental avg. 22.5ºC ± 0.1ºC) with distinct minima between 1954 and 1988 (avg. 22.4ºC ± 0.1ºC; GSTmax instrumental avg. 22.1ºC ± 0.1ºC). Two additional low GSTmax periods can be distinguished, from 1876 to 1889 (avg. 22.9ºC ± 0.2ºC) and 1900 to 1930 (avg. 23.0ºC ± 0.1ºC). In these GSTmax low temperature periods, the low-salinity species assemblages (*T. salsa/irregularis*, *H. manilaensis*, *M. fusca* and *Miliammina* spp.) are dominant in the sedimentary record (1960–2010; 1900–1917; cal. AD 1881–1885). Moreover, some of the high GSTmax raw values can be related with extreme drought events referred to in literature during the 1940s (Domingos, 2006; Pires et al., 2010), 1960s, 1970s, and 1990s (Pires et al., 2010). This is also true in the analysis of severe and extreme drought events by Moreira et al. (2012), based on the 12-month Standardized Precipitation Index (i.e., SPI_12 ≤ –1.5) for Porto/Serra do Pilar meteorological station (1863–2007 precipitation series), for the years 1868, 1881, 1888, 1904, 1906, 1919 and 1921.

But some exceptions to this correlation can be identified. For instance, the high GSTmax (24.9ºC) of 1896 does not agree with the moderately wet conditions indicated by the SPI positive value of that year (SPI = 1.18). However, regional newspapers reported three religious events praying God for rain (*pro-pluvia* ceremonial) during the spring-summer season of 1896 (Moreno et al., 2016), suggesting that drought stress occurred during that interval. The lack of significant

correlation of GSTmax with SPI_12 Porto ($r = -0.07$, $p < 0.05$) and the weak inverse correlation with SPI_1 Minho ($r = -0.25$, $p < 0.05$) indicate that the occurrence of a high temperature period (high GSTmax) does not necessarily lead to a drought period.

Additionally, the dominance of low-salinity assemblages in the time span 1960–2010 is not consistent with the ~0.8ºC global mean temperature rise for the 20th century (Gómez-Gesteira et al., 2011; IPCC, 2014). Given the global warming trend, recorded in many locations of Portugal (Santo et al., 2014), we would expect a corresponding interstitial water salinity rise on the Caminha high marsh that would be reflected by the dominance of normal-salinity foraminiferal species, which is not the case. In fact, Santos et al.'s (2002) quantification of temperature rise for Portugal defines a differentiated pattern: steep for temperature minima and smaller for maxima. Moreover, the Minho GSTmax 11-year running averages exhibit a minimum for the period 1960–2010, which, together with a positive precipitation anomaly (1958–1983) for the Minho region (Fatela et al., 2014) must have been responsible for a different pattern in the water budget of the Caminha tidal marsh, by triggering ↑P and ↓ET (due to ↓T) in equation 3. This positive rainfall balance (= P–ET) on the marsh would lead to the prevalence of low salinity conditions, despite the global rising temperature, explaining the dominance of low-salinity foraminiferal species in this period (Figures 5.2 and 5.3).

Moreno et al. (2016) reported a correlation between GSTmax and the main teleconnection modes, which characterize the atmospheric circulation and temperature in the Minho region. That is, between the middle 1950s and the early 1990s, an inverse correlation was found for the positive phase of the Scandinavian Oscillation Mode (SCA – spring/summer) and the Eastern Atlantic/Western Russia Oscillation Mode (EA/WR – summer) indices compared to the GSTmax. We consider that the positive anomaly of the SCA and EA/WR lead to a negative anomaly of GSTmax, which added to a positive precipitation anomaly recorded in the Minho region between 1958 and 1983 (Fatela et al., 2014). These patterns are clearly reflected by the dominance of foraminiferal species characteristic of oligohaline to mesohaline conditions in the sedimentary record of the Caminha tidal marsh between the 1960s to 1990s (Figure 5.5). The opposite scenario can be asssumed for periods of higher GSTmax preceding 1950 (reconstructed), with particular emphasis on the period 1856–1875, where a peak in average temperatures occurred (Figure 5.3), which in turn is marked by the dominance of the moderately brackish-to-normal salinity foraminiferal assemblage, indicating polyhaline to euhaline conditions. In such periods, a higher frequency and intensification of Atlantic blocking (Trigo et al., 2005; Stefanon, 2012) and a negative SCA phase hypothetically contributed to enhancing GSTmax in the Minho region, amplifiying the evapotranspiration rate in the Caminha tidal marsh, and consequently raising the high marsh sediment salinity. This chain of events would have elicited a concomitant response from marsh foraminiferal assemblages, reflected in the increased proportion of normal-salinity species in this tidal marsh, which tends to be a brackish environment during most of the record examined.

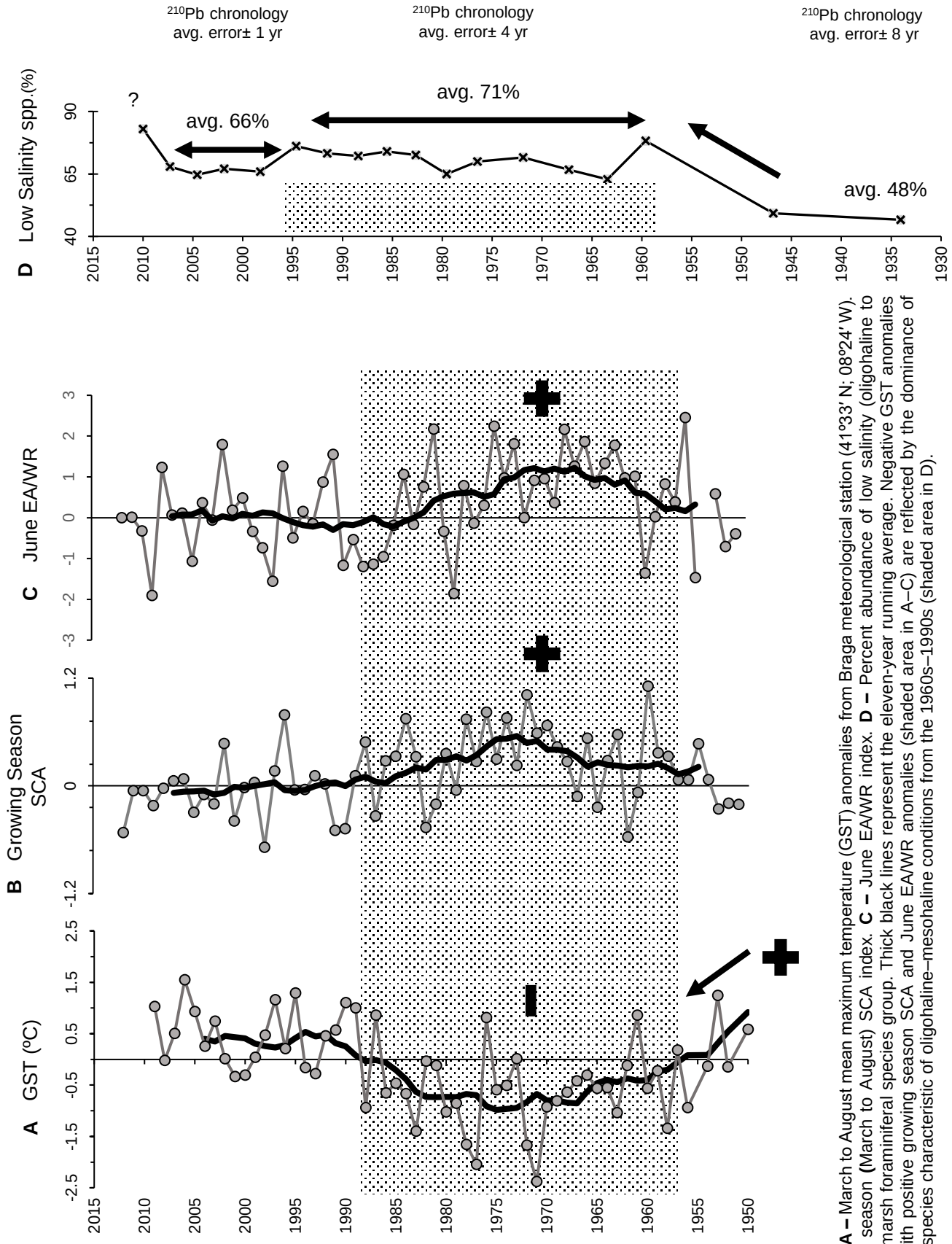

Figure 5.5. A – March to August mean maximum temperature (GST) anomalies from Braga meteorological station (41º33' N; 08º24' W). **B –** Growing season **(**March to August) SCA index. **C –** June EA/WR index. **D –** Percent abundance of low salinity (oligohaline to mesohaline) marsh foraminiferal species group. Thick black lines represent the eleven-year running average. Negative GST anomalies associated with positive growing season SCA and June EA/WR anomalies (shaded area in A–C) are reflected by the dominance of foraminiferal species characteristic of oligohaline–mesohaline conditions from the 1960s–1990s (shaded area in D).

Despite the increased rate of sea-level to *ca.* 2.5 mm/year (Leorri et al., 2013) detected in this region since 1943, the sampling site of Caminha high marsh zone is submerged less than 7% of the time. As indicated above, in this location (high in the tidal frame) elevation controls the salinity concentration, turbidity and sediment load. The last two factors are also controlled by the balance between seawater intrusion and river discharge, creating a complex interplay of climate variables in the hydrological balance (Figure 5.4). If, as suggested for other locations, salt marshes can maintain their elevation in relation to the tidal frame, the balance between seawater intrusion and river discharge and temperature would become the key factors that control marsh evolution and should be reflected by the foraminiferal assemblages.

5.6. Conclusions

High-resolution benthic foraminiferal data from the Caminha tidal marsh, in conjunction with a previously reconstructed March to August mean temperature maxima, allowed us to interpret the hydro-climatic evolution for the Minho region for the last 154 years (1856–2009). The Caminha tidal marsh foraminiferal assemblages seem to respond to the complex interaction between atmospheric circulation – associated with the precipitation regime (deficit/surplus) – and temperature variation patterns (low/high), affecting the water balance in the high marsh. An increase in the proportion of foraminiferal species, indicating normal salinity occurred in periods of rainfall deficit, associated with higher spring–summer mean temperature maxima (GSTmax), was observed. These high marsh foraminiferal species probably reflect saltier conditions on the marsh sediment of a strongly brackish environment, resulting from enhanced evapotranspiration.

These results highlight the importance of considering other factors besides sea-level changes when interpreting the geological record of coastal wetlands, as changes in the foraminiferal assemblages can reflect rainfall or temperature changes rather than imbalance between marsh elevation and the tidal frame.

Acknowledgments

This work is a contribution of the WestLog project (PTDC/CTE/105370/2008), funded by the Fundação para a Ciência e a Tecnologia – FCT. João Moreno acknowledges a FCT PhD grant (SFRH/BD/87995/2012).

References

Adam, P., 1990, Saltmarsh Ecology: Cambridge University Press. Cambridge, 461p.

Antunes, C., and Taborda, R., 2009, Sea level at Cascais Tide Gauge: Data, analysis and results: Journal of Coastal Research, SI 56, p. 218–222.

Barnston, A. G., and Livezey, R. E., 1987, Classification, seasonality and persistence of low-frequency atmospheric circulation patterns: Monthly Weather Review, v. 115, p. 1083–1126.

Brázdil, R., Pfister, C., and Wanner, H., 2005, Historical climatology in Europe—the state of the art: Climate Change, v. 70, p. 363–430.

Brázdil, R., Zahradníček, P., Dobrovolný, P., Kotyza, O., and Valášek, H., 2008, Historical and recent viticulture as a source of climatological knowledge in the Czech Republic: Geografie – Sbor Čes Geogr Spol, v. 113, p. 351–371.

Bettencourt, A., Ramos, L., Gomes, V., Dias, J. M. A., Ferreira, G., Silva, M., and Costa, L., 2003, Estuários Portugueses: INAG – Ministério das Cidades, Ordenamento do Território e Ambiente, Lisboa, 311p.

Chmura, G. L., Anisfeld, S. C., Cahoon, D. R., and Lynch, J. C., 2003, Global carbon sequestration in tidal, saline wetland soils: Global Biogeochemical Cycles, v. 17, p. 1111, doi:10.1029/2002GB001917

Christian, R. R., Stasavich, L., Thomas, C., and Brinson, M. M., 2000, Reference is a moving target in sea-level controlled wetlands. In: Weinstein, M.P. and Kreeger, D.A. (Eds.), Concepts and Controversies in Tidal Marsh Ecology: The Netherlands Kluwer Press, pp. 805–825.

Culver, S. J., Leorri, E., Mallinson, D.J., Corbett, D.R., and Shazili, N.A.M., 2015, Recent coastal evolution and sea-level rise, Setiu Wetland, Peninsular Malaysia: Palaeogeography, Palaeoclimatology, Palaeoecology, v. 417, p. 406–421.

Daux, V., Yiou, P., Le Roy Ladurie, E., Mestre, O., Chevet, J. M., Seguin, B., Chuine, I., Garnier, E., and Viovy, N., 2007, Temperature and grape harvest dates in France, *in* Global Warming, Which Impacts on the Vineyards: Fontaine P., Dijon, France, 10p.

Day, J. W., Christian, R. R., Boesch, D. M., Yáñez-Arancibia, A., Morris, J., Twilley, R. R., and Stevenson, C., 2008, Consequences of Climate Change on the Ecogeomorphology of Coastal Wetlands: Estuaries and Coasts, v. 31, no. 3, p. 477–491.

Debenay, J.–P., Guillou, J-J., Redois, F., and Geslin, E., 2000, Distribution trends of foraminiferal assemblages in paralic environments – A base for using Foraminifera as bioindicators, *in* R.E. Martin (ed.), Environmental Micropaleontology - The Application of Microfossils to Environmental Geology:. Kluwer Academic/ Plenum Publishers, p. 39–67.

De Leeuw, J., Van den Dool, A., De Munk, W., Nieuwehuize, J., and Beeftink, W. G., 1991, Factors influencing the soil salinity regime along an intertidal gradient: Estuarine Coastal and Shelf Science, v. 32, p. 87–97.

Domingos, S. I. S., 2006, Análise do índice de seca Standardized Precipitation Index (SPI) em Portugal Continental e sua comparação com o Palmer Drought Severity Index (PDSI): Unpublished MSc Thesis, Universidade de Lisboa, 53p.

Engelhart, S. E., Horton, B. P., Douglas, B. C., Peltier, W. R., and Tornqvist, T. E., 2009, Spatial variability of Late Holocene and 20th century sea level rise along the US Atlantic coast: Geology, v. 37, p. 1115–1118.

Fatela, F., and Taborda, R., 2002, Confidence limits of species proportions in microfossil assemblages: Marine Micropaleontology, v. 45, p. 169–174.

Fatela, F., Moreno, J., and Antunes, C., 2007, Salinity influence on foraminiferal tidal marsh assemblages of NW Portugal: an anthropogenic constraint?: Thalassas, v. 23, p. 51–63.

Fatela, F., Moreno, J., Moreno, F., Araújo, M. F., Valente, T., Antunes, C., Taborda, R., Andrade, C., and Drago, T., 2009a, Environmental constraints of foraminiferal assemblages distribution across a brackish tidal marsh (Caminha, NW Portugal): Marine Micropaleontology, v. 70, p. 70–88.

Fatela, F., Moreno, J., Antunes, C., Leorri, E., Taborda, R., Silva, A., Andrade, C., and Cearreta, A., 2009b, Foraminiferal assemblages distribution across the Sado estuary tidal marshes (SW Portugal): local assessment of regional palaeoenvironmental value. In: Flor Rodríguez, G., Gallastegui, J., Flor Blanco, G. and Martín Llaneza, J. (Eds.), Nuevas contribuciones al Margen Ibérico Atlantico, pp. 345–348.

Fatela, F., Moreno, J., Leorri, E., and Corbett, R., 2014, High marsh foraminiferal assemblages response to intra-decadal and multi-decadal precipitation variability, between 1934 and 2010 (Caminha, NW Portugal): Journal of Sea Research, v. 93, p. 118–132.

Gehrels, W. R., 1994, Determining relative sea level change from salt marsh foraminifera and plant zones on the coast of Maine, USA: Journal of Coastal Research, v. 10, p. 990–1009.

Gehrels, W. R., and Newman, S. W. G., 2004, Salt-marsh foraminifera in Ho Bugt, western Denmark, and their use as sea-level indicators: Danish Journal of Geography, v. 104, p. 49–58.

Gómez-Gesteira, M., Gimeno, L., de Castro, M., Lorenzo, M. N., Alvarez, I., Nieto, R., Taboada, J. J., Crespo, A. J. C., Ramos, A. M., Iglesias, I., Gómez-Gesteira, J. L., Santo, F. E., Barriopedro, D., and Trigo, I. F., 2011, The state of climate in NW Iberia: Climate Research, v. 48, p. 109–144.

Haslett, J., and Parnell, A., 2008, A simple monotone process with application to radiocarbon dated depth chronologies: Applied Statistics, v. 57, p. 399–418.

Hayward, B. W., Grenfell, H. R., Reid, C. M., and Hayward, K. A., 1999, Recent New Zealand Shallow-Water Benthic Foraminifera: Taxonomy, Ecologic Distribution, Biogeography, and Use in Paleoenvironmental Assessment: Institute of Geological & Nuclear Sciences monograph 21, Lower Hutt, New Zealand 264p.

Hayward, B. W., Scott, G. H., Grenfell, H. R., Carter, R., and Lipps, J.H., 2004, Techniques for estimation of tidal elevation and confinement (~salinity) histories of sheltered harbours and estuaries using benthic foraminifera: examples from New Zealand: The Holocene, v. 14, p. 218–232.

Herbert, E. R., Boon, P., Burgin, A. J., Neubauer, S. C., Franklin, R. B., Ardón, M., Hopfensperger, K. N., Lamers, L. P., and Gell, P., 2015, A global perspective on wetland salinization: ecological consequences of a growing threat to freshwater wetlands: Ecosphere, v. 6, p.1–43.

Hippensteel, S. P., Martin, R. E., Nikitina, D., and Pizzuto, J., 2002, Interannual variation of marsh foraminiferal assemblages (Bombay Hook National Wildlife Refuge, Smyrna, DE): do foraminiferal assemblages have a memory?: Journal of Foraminiferal Research, v. 32, p. 97–109.

Horton, B. P., 1999, The distribution of contemporary intertidal foraminifera at Cowpen Marsh, Tees Estuary, UK: implications for studies of Holocene sea-level changes: Palaeogeography, Palaeoclimatology, Palaeoecology, v. 149, p. 127–149.

Horton, B. P., and Edwards, R. J., 2005, The application of local and regional transfer functions to the reconstruction of Holocene sea levels, north Norfolk, England: The Holocene, v. 15, p. 216–228.

Horton, B. P., and Murray, J. W., 2007, The roles of elevation and salinity as primary controls on living foraminiferal distributions: Cowpen Marsh, Tees Estuary, UK: Marine Micropaleontology, v. 63, p. 169–186.

Hughes, C. E., Kalma, J. D., Binning, P., Willgoose, G. R., and Vertzonis, M., 2001, Estimating evapotranspiration for a temperate salt marsh, Newcastle, Australia: Hydrological Processes v. 15, p. 957–975.

IPCC, 2014, Climate Change 2014: Synthesis Report. Contribution of Working Groups I, II and III to the Fifth Assessment Report of the Intergovernmental Panel on Climate Change [Core Writing Team, Pachauri R. K., and Meyer, L. A. (Eds.)]: IPCC, Geneva, Switzerland, 151p.

Kemp, A. C., Horton, B. P., Donnelly, J. P., Mann, M. E., Vermeer, M., and Rahmstorf, S., 2011, Climate related sea-level variations over the past two millennia: Proceedings of the National Academy of Sciences, v. 108**,** p. 11017–11022.

Kirwan, M. L., Guntenspergen, G. R., D'Alpaos, A., Morris, J. T., Mudd, S. M., and Temmerman, S., 2010, Limits on the adaptability of coastal marshes to rising sea-level: Geophysics Research Letters, v. 37, L23401, http://dx.doi.org/10.1029/2010GL045489.

Kirwan M. L, and Blum L. K, 2011, Enhanced decomposition offsets enhanced productivity and soil carbon accumulation in coastal wetlands responding to climate change: Biogeosciences, v. 8, p. 987–993.

Komitov, B., and Kaftan, V., 2004, The Sunspot Activity in the Last Two Millennia on the Basis of Indirect and Instrumental Indexes: Time Series Models and Their Extrapolations for the 21st Century: Multi-Wavelength Investigations of Solar Activity Proceedings IAU Symposium No. 223, p. 113–114.

Leorri, E., Gehrels, W. R., Horton, B. P., Fatela, F., and Cearreta, A., 2010, Distribution of foraminifera in salt marshes along the Atlantic coast of SW Europe: tools to reconstruct past sea-level variations: Quaternary International, v. 221, p. 104–115.

Leorri, E., Fatela, F., Cearreta, A., Moreno, J., Antunes, C., and Drago, T., 2011, Assessing the performance of a foraminifera-based transfer function to estimate sea-level changes in northern Portugal: Quaternary Research, v. 75, p. 278–287.

Leorri, E., Drago, T., Fatela, F., Bradley, S., Moreno J., and Cearreta, A., 2013, Late Glacial and Holocene coastal evolution in the Minho estuary (N Portugal): implications for understanding sea-level changes in Atlantic Iberia: The Holocene, v. 23, p. 352–362.

Lovelock, C. E., Cahoon, D. R., Friess, D. A., Guntenspergen, G. R., Krauss, K. W., Reef, R., Rogers, K., Saunders, M. L., Sidik, F., Swales, A., and Saintilan, N., 2015, The vulnerability of Indo-Pacific mangrove forests to sea-level rise: Nature, v. 526, p. 559–564.

Maurer, C., Hammerl, C., Koch, E., Hammerl, T., and Pokorny, E., 2011, Extreme grape harvest data of Austria, Switzerland and France from A.D. 1523 to 2007 compared to corresponding instrumental/ reconstructed temperature data and various documentary sources: Theoretical Applied Climatology, v. 106, p. 55–68.

Meier, N., Rutishauser, T., Pfister, C., Wanner, H., and Luterbacher, J., 2007, Grape harvest dates as a proxy for Swiss April to August temperature reconstructions back to AD 1480: Geophysical Research Letters, v. 34, L20705, doi:10.1029/2007GL031381

Menzel, A., 2005, A 500 year pheno-climatological view on the 2003 heatwave in Europe assessed by grape harvest dates: Meteorologische Zeitschrift, v. 14, p. 75–77, doi:10.1127/0941-2948/2005/0014-0075.

Mitsch, W. J., and Gosselink, J. G., 2000a, The value of wetlands: importance of scale and landscape setting: Ecological Economics, v. 35, p. 25–33.

Mitsch, W. J., and Gosselink, J. G., 2000b, Wetlands: 3rd Edition, John Wiley and Sons, Inc. New York, 920p.

Moreira, E. E., Mexia, J. T., and Pereira, L. S., 2012, Are drought occurrence and severity aggravating? A study on SPI drought class transitions using log-linear models and ANOVA-like inference: Hydrological Earth System Sciences, v. 16, p. 3011–3028.

Moreno, J., Fatela, F., Andrade, C., Cascalho, J., Moreno, F., and Drago, T., 2005, Living foraminiferal assemblages from Minho/Coura estuary (Northern Portugal): a stressful environment: Thalassas, v. 21, p. 17–28.

Moreno, J., Fatela F., Andrade, C., and Drago, T., 2006, Distribution and new ecological data of *Pseudothurammina limnetis* (Scott and Medioli) on the brackish tidal marsh of Minho/Coura estuary, Northern Portugal: Révue de Micropaléontologie, v. 49, p. 45–53.

Moreno, J., Valente, T., Moreno, F., Fatela, F., Guise, L., and Patinha, C., 2007, Calcareous Foraminifera occurrence and calcite-carbonate equilibrium conditions – a case study in Minho/Coura estuary (N Portugal): Hydrobiologia, v. 597, p. 177–184.

Moreno, J., Fatela, F., Leorri, E., De la Rosa, J., Pereira, I., Araújo, M. F., Freitas, M. C., Corbett, R., and Medeiros A., 2014, Marsh benthic Foraminifera response to estuarine hydrological balance driven by climate variability over the last 2000 years (Minho estuary, NW Portugal): Quaternary Research, v. 82, p. 318–330.

Moreno, J., Fatela, F., Leorri, E., Araújo, M.F., Moreno, F., De la Rosa, J.M., Freitas, M.C., Valente, T., and Corbett, R., 2015, Bromine enrichment in marsh sediments as a marker of environmental changes driven by Grand Solar Minima and Anthropogenic activity (Caminha, NW of Portugal): Science of the Total Environment, v. 506/507, p. 554–566, doi:10.1016/j.scitotenv.2014.11.062

Moreno, J., Fatela, F., Moreno, F., Leorri, E., Taborda, R., and Trigo, R., 2016, Grape harvest dates as indicator of spring–summer mean maxima temperature variations in the Minho region (NW Portugal) since the 19th century: Global Planetary Change, v. 141, p. 39–53.

Morris, J. T., Barber, D. C., Callaway, J. C., Chambers, R., Hagen, S. C., Hopkinson, C. S., Johnson, B. J., Megonigal, P., Neubauer, S. C., Troxler, T., and Wigand C., 2016, Contributions of organic and inorganic matter to sediment volume and accretion in tidal wetlands at steady state: Earth's Future, v. 4, p. 110–121.

Murray, J. W., 2006, Ecology and Applications of Benthic Foraminifera: Cambridge University Press, Cambridge, 440p.

Nuttle, W. K., 1988, The extent of lateral water movement in the sediments of a New England salt marsh: Water Resources Research, v. 24, p. 2077–2085.

Parker, V., Callaway, J., Schile, L., Vasey, M., and Herbert, E., 2011, Climate change and San Francisco Bay-Delta tidal wetlands: San Francisco Estuary and Watershed Science, v. 9, p. 1–15.

Parnell, A., Haslett, J., Allen, J., Buck, C., and Huntley, B., 2008, A flexible approach to assessing synchroneity of past events using Bayesian reconstructions of sedimentation history: Quaternary Science Reviews, v. 27, p. 1872–1885.

Pennings, S. C., and Callaway, R. M., 1999, Salt marsh plant zonation: the relative importance of competition and physical factors: Ecology, v. 73, p. 681–690.

Phleger, F. B., 1965, Patterns of Marsh Foraminifera, Galveston Bay, Texas: Limnology and Oceanography, v. 10, p.169–180.

Pires, V. C., Álvaro, S., and Mendes, L., 2010, Riscos de secas em Portugal continental: Territorium, v. 17, p. 27–34.

Santo, F. E., Lima, M. I. P., Ramos, A. M., and Trigo, R. M., 2014, Trends in seasonal surface air temperature in mainland Portugal, since 1941: International Journal of Climatology, v. 34, p. 1814–1837.

Santos, F. D., Forbes, K., and Moita, R., 2002, Climate Change in Portugal. Scenarios, impacts and Adaptation Measures – SIAM: Gradiva, Lisboa, 456p.

Scott, D. B., and Medioli, F. S., 1978, Vertical zonations of marsh foraminifera as accurate indicators of former sea-levels: Nature, v. 272, p. 528–531.

Scott, D. B., and Medioli, F. S., 1980, Quantitative studies of marsh foraminiferal distributions in Nova Scotia: implications for sea level studies: Special Publication – Cushman Foundation for Foraminiferal Research, v. 17, 58p.

Scott, D. B., Medioli, F. S., and Schafer, C. T., 2001, Monitoring in Coastal Environments Using Foraminifera and Thecamoebian Indicators: Cambridge University Press, 177p.

Sen Gupta, B., 2002, Foraminifera in marginal marine environments, *in* Sen Gupta, B. (ed.), Modern Foraminifera: Kluwer Academic Publishers, p. 141–159.

Stefanon, M., D'Andrea, F., and Drobinski, P., 2012, Heatwave classification over Europe and the Mediterranean region: Environmental Research Letters, v. 7, p. 1–9.

Trigo, R. M., García-Herrera, R., Díaz, J., Trigo, I. F., and Valente, M. A., 2005, How exceptional was the early August 2003 heatwave in France?: Geophysical Research Letters, v. 32, L10701, doi: 10.1029/2005GL022410.

Valente, T., Fatela F., Moreno, J., Moreno, F., Guise, L., and Patinha, C., 2009, A comparative study of the influence of geochemical parameters on the distribution of foraminiferal assemblages in two distinctive tidal marshes: Journal of Coastal Research, SI 56, p. 1439–1443.

Venice system, 1959, The final resolution of the Symposium on the Classification of Brackish Waters: Archivio di Oceanografia e Limnologia, v. 11, supplement, p. 243–248.

Wagner, S., and Zorita, E., 2005, The influence of volcanic, solar and CO2 forcing on the temperatures in the Dalton Minimum (1790–1830): a model study: Climate Dynamics, v. 25, p. 205–218.

Wang, H., Hsiehb, Y., Harwella, M., and Huang, W., 2007, Modelling soil salinity distribution along topographic gradients in tidal salt marshes in Atlantic and Gulf coastal regions: Ecological Modelling, v. 201, p. 429–439.

http://www.cpc.noaa.gov/data/teledoc/telecontents.shtml
http://www.psmsl.org/data/obtaining/rlr.annual.data/52.rlrdata
http://climexp.knmi.nl/

Appendix 5.1. Age model for the core FCPw1 and estimated 2σ errors, based on six AMS–^{14}C dates, performed on total organic sediment, and ^{210}Pb chronology. The data interpolation was obtained with Bchron 3.2 software (after Moreno et al., 2014).

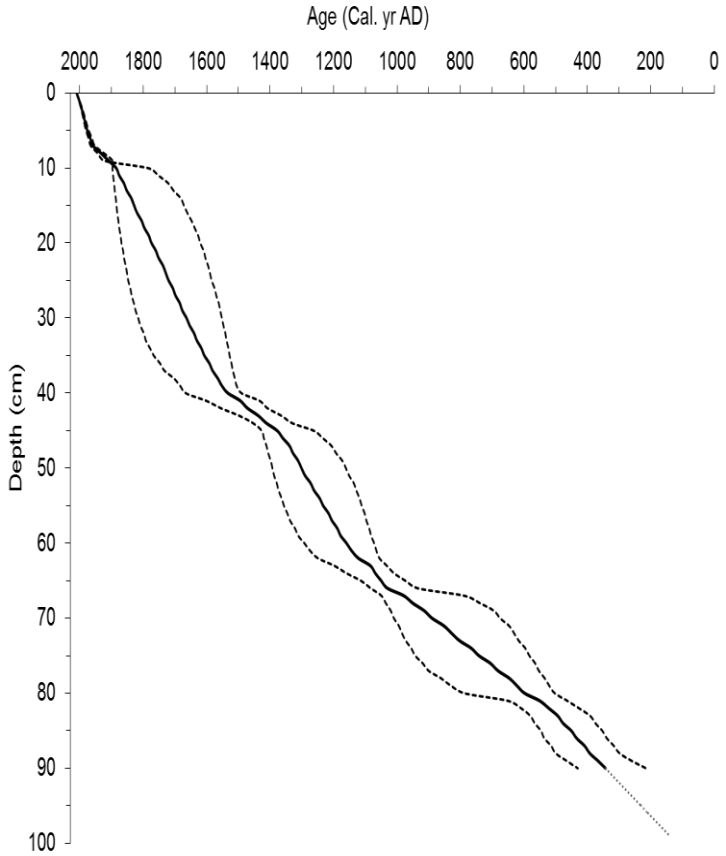

Depth (cm)	$^{210}Pb_{Excess}$	error	^{137}Cs	error
0.5	328.8	38.3		
1.5	250.7	29.7		
2.5	166.1	20.9		
3.5	121.1	16.4	16.7	1.7
4.5	113.6	15.6	17.7	1.7
5.5	108.9	15.3	20.0	1.7
6.5	88.2	13.0	28.5	1.7
7.5	125.9	16.8	40.5	1.3
8.5	66.8	10.9	74.3	2.7
9.5	30.5	7.4	45.7	1.7
10.5	12.5	5.6		
11.5	5.0	4.9		
12.5	2.4	4.6		
13.5	2.1	4.6		

^{210}Pb Excess and ^{137}Cs content (Bq kg−1)

Sample	Depth (cm)	δ^{13}C ‰	Conventional radiocarbon age	Δ^{14}C ‰	Calibrated years AD (2 Sigma range)
CM 41	40-41	-26.7	380 ± 30 BP	-46.20±3.6	1490 to 1666
CM 45	44-45	-26.8	650±35 BP	-84.57±3.9	1330 to 1453
CM 64	63-64	-25.9	1010±50 BP	-122.49±1.9	1032 to 1197
CM 67	66-67	-25.9	1030±34 BP	-124.97±1.9	934 to 1082
CM 82	81-82	-25.8	1570±40 BP	-181.66±1.9	463 to 650
CM 91	90-91	-27.2	1760 ± 30 BP	-196.80±3.0	215 to 429

Radiocarbon ages data determined in the Laboratory "Beta Analytic Inc.". (AMS - Standard delivery)

Appendix 5.2. Dead foraminiferal assemblage percentages from FCPwAR Caminha tidal marsh core.

Depth (cm)	Age (cal. AD)	*H. manilaensis*	*T. salsa*	*M. fusca* + *Miliammina* spp.	*J. macrescens*	*T. inflata*	*P. limnetis*	*H. wilberti*	*T. comprimata*	*S. lobata*	*P. guaratibaensis*	*P. ipohalina*	Brackish to "Normal" Salinity group	Low Salinity group
0.0	2010	18.4	60.5	4.1	4.1	8.8	2.7					0.0	15.6	83.0
0.5	2007	15.6	43.8	8.6	1.6	18.8	1.6	6.3	0.8			1.6	30.5	68.0
1.0	2005	14.3	46.3	4.1		15.0	0.7	12.2				0.7	28.6	64.6
1.5	2002	16.1	41.6	9.4	0.7	19.5	0.7	8.1					28.9	67.1
2.0	1998	17.7	42.6	5.7		12.1	0.7	13.5	0.7	2.1			29.1	66.0
2.5	1995	12.3	46.2	17.7		10.0		9.2			1.5		20.8	76.2
3.0	1992	17.4	47.1	8.7		7.2		7.2	1.4	1.4	1.4		18.8	73.2
3.5	1988	23.8	35.1	13.2		8.6	0.7	10.6	0.7	0.7		0.7	21.9	72.2
4.0	1986	30.7	42.5	0.8		9.4		4.7	3.9				18.1	74.0
4.5	1983	14.8	50.0	7.7		5.6		13.4	0.7			3.5	23.2	72.5
5.0	1980	14.6	46.0	4.4		11.7		15.3	1.5			0.7	29.2	65.0
5.5	1976	31.4	32.1	6.4		12.1		7.9	1.4				21.4	70.0
6.0	1972	19.9	46.8	5.0	2.1	5.0	2.1	14.9				2.1	26.2	71.6
6.5	1967	9.1	50.8	6.8	0.8	13.6	1.5	9.1	0.8		2.3		28.0	66.7
7.0	1963	14.0	45.7	3.1	0.8	15.5	2.3	12.4	3.1		0.8		34.9	62.8
7.5	1960	44.6	33.7		1.0	12.9		0.0			2.0		15.8	78.2
8.0	1947	28.7	20.6		7.4	5.9		29.4	1.5		1.5		45.6	49.3
8.5	1934	35.3	10.5	0.8	8.3	12.8		22.6	2.3		3.8		49.6	46.6
9.0	1917	67.0	9.8	1.8	3.6	8.9			0.9	0.9	0.9		15.2	78.6
9.5	1900	43.5	18.4	2.7	7.5	10.2		8.8		5.4	0.0		32.0	64.6
10.0	1893	36.2	12.3	3.6	8.0	22.5		4.3	0.7	5.1	0.7		41.3	52.2
10.5	1885	47.4	13.9		7.3	16.1		10.9		0.7	2.2		37.2	61.3
11.0	1881	41.3	13.5	5.6	3.2	7.1		13.5	3.2	1.6	3.2		31.7	60.3
11.5	1876	26.5	27.2	0.7	0.7	6.6		21.3		3.7	3.7	1.5	37.5	54.4
12.0	1869	15.2	34.1	2.9	8.7	5.8	1.4	14.5	2.9	3.6	1.4	2.9	41.3	52.2
12.5	1861	6.2	43.1	0.8	8.5	10.0		18.5	1.5		6.2	2.3	46.9	50.0
13.0	1857	5.7	30.1		13.8	12.2		24.4	2.4	3.3	1.6	0.8	58.5	35.8
13.5	1852	8.3	28.3		11.7	8.3		15.8	1.7	3.3	11.7	2.5	55.0	36.7
14.0	1845	3.7	20.6	0.7	13.2	21.3		20.6	5.1	4.4	5.1	0.7	70.6	25.0
14.5	1838	4.0	18.3		10.3	17.5		23.8	1.6	5.6	7.1	6.3	72.2	22.2
15.0	1833	2.5	11.5	2.5	15.6	7.4		40.2		4.9	0.8	7.4	76.2	16.4
15.5	1829	3.1	15.3	2.3	11.5	6.1		39.7	1.5	6.1	2.3	6.1	73.3	20.6
16.0	1824	1.5	18.5	0.7	14.1	8.1		34.8	5.9	5.9	1.5	4.4	74.8	20.7

Appendix 5.3. Systematic list of Caminha tidal marsh foraminiferal species, including ecological distribution synthesis and plates.

Most of foraminiferal species living in brackish environments are agglutinated forms regarded as typical of salt marshes (e.g. Phleger, 1970; Murray, 1991, 2006; Sen Gupta, 2002).

This appendix intends to illustrate and describe their general ecology, listing the 11 agglutinated most representative species of the Caminha tidal marsh (Minho estuary). Generic names are in accordance with Loeblich and Tappan (1988) and are listed alphabetically.

***Haplophragmoides manilaensis* Andersen, 1953; Plate 5.1, fig. 2.**

1953 *Haplophragmoides manilaensis* Andersen, p. 22, pl. 4, figs. 7-8.

1957 *Haplophragmoides bonplandi* Todd and Brönnimann, p. 23, pl. 2.

1980 *Haplophragmoides bonplandi* Todd and Brönnimann, 1957 - Scott and Medioli, p. 40, pl. 2, fig. 4-5.

General ecology: Interspecific variability in this species is wide and an intergradational series can be observed between *H. manilaensis* and *Haplophragmoides wilberti*, as described by De Rijk (1995a). Its presence is associated to low-saline conditions, usually above mean high water marsh zones. Several studies indicate that the distribution of *H. manilaensis* is controlled by local salinity conditions, with it favouring brackish environments at the rear of marshes or lower elevation areas associated with freshwater seeps (Scott and Medioli, 1980; Scott and Leckie, 1990; De Rijk, 1995a, b; De Rijk and Troelstra, 1997). Some sites, with elevations above mean highest high water (MHHW), are characterized by the dominance of *H. manilaensis* (Cahill et al., 2015). The Caminha high marsh zone is dominated by the *H. manilaensis* (20% to 96%) association, which can also include *Haplophragmoides* sp. (up to 28%) and a strong presence of *P. limnetis* (up to 68%). This association ranges in elevation between mean high water (MHW) and mean high water spring (MHWS) (Fatela et al., 2009a).

***Haplophragmoides wilberti* Andersen, 1953; Plate 5.1, fig. 3**

1953 *Haplophragmoides wilberti* Andersen, p. 21, pl. 2, figs. 5-6, pl. 3, figs. 9-16.

1999 *Haplophragmoides wilberti* Andersen, 1953 - Hayward et al., pl. 1, figs. 25-26

General ecology: It is generally common to abundant in brackish salt marshes associated with decreasing salinity conditions, living intertidally, above mean sea-level and most abundantly above mean high water. This species is dominant in brackish high marshes from New Zealand (Hayward et al., 1999, 2004) and Alve and Murray (1999) reported its presence under a salinity range of 10–27‰, in marginal marine environments of southern Scandinavia. In Caminha tidal marsh *H. wilberti* shows always a subsidiary occurrence in the high marsh zone, extending its presence to the upper part of low marsh (Fatela et al., 2009a).

***Jadammina macrescens* (Brady, 1870); Plate 5.2, figs. 5a, b**

1870 *Trochammina inflata* (Montagu) var. *macrescens* Brady, p. 290, pl. 11, figs. 5a-c.

1938 *Jadammina polystoma* Bartenstein and Brand, p. 381, text-figs. 1-3.

1950 *Trochammina macrescens* Brady - Phleger and Walton, p. 281, pl. 2, figs. 6-7.

1971 *Jadammina macrescens* (Brady) - Murray, p. 41, pl. 13, figs. 1-5.

General ecology: *Jadammina macrescens* is a widely distributed species, with a presence common to abundant in high marshes above MHW, where moderate to high salinity conditions prevails, but also may occur in adjacent intertidal marginal marine environments (Murray, 2013). It shows a high ability to adapt to various conditions and to occupy any environment fast although, it prefers the more marine habitats of the salt marshes with higher salinities (De Rijk, 1995a). After Hayward et al. (1999) their associations -*Trochammina*, *Jadammina*, *Trochammina-Elphidium*- are high salinity-related above mean high water zones. However in marginal marine southern Scandinavia tolerates a range of salinity from 10 to 28‰ (Alve and Murray, 1999). Being one of the most tolerant species to subaerial exposure, its relative abundance is very useful in sea-level change studies. In fact, its distribution reflects the elevation of the depositional environment in relation to the highest high water level, where it may represent 100% of the foraminiferal assemblages (Scott and Medioli, 1978, 1980). *Jadammina macrescens* is limited to an episodic presence in surface sediments of the Caminha tidal marsh, but it is dominant in the Lima estuary (Fatela et al., 2007, 2009a) and in the high marshes of the SW Portuguese coast, where it can reach codominance even at the low marsh zone (Fatela et al., 2009b, and authors unpublished data). It was also recorded by Camacho et al. (2015) in a marsh of the Guadiana estuary (SE Portuguese coast).

***Miliammina fusca* (Brady, 1870); Plate 5.2, fig. 2a, b**

1870 *Quinqueloculina fusca* Brady, p. 286, pl. 11, figs. 2a-c.

2006 *Miliammina fusca* (Brady) - Horton and Edwards, p. 68, pl. 1, figs. 5a-b.

General ecology: *Miliammina fusca* is a very common species in the upper to middle estuary channels and tidal flats and dominant in most salt marshes, often expanding its presence in marine marginal environments (e.g., Hayward et al., 1999; Murray, 2013). This cosmopolitan species dominates the continental end-member at the referred paralic environments, and is associated with direct freshwater influence (e.g., Debenay and Guillou, 2002). It's a wide range euryhaline species that may tolerate salinities of < 1-35‰ (Murray, 2013). De Rijk, 1995b found no correlation between its abundance and salinity (De Rijk, 1995b), but Debenay et al. (2002, 2004) found it more abundant in low salinity areas in French Guiana and it seems characteristic of low salinity estuaries to Hayward et al. (2004). Under temperature and salinity experimental conditions it grew at all salinities tested (12‰, 22‰, 36‰), but was most abundant at salinity 12‰ and it did least well at 12ºC (Goldstein and Alve, 2011). In Canada it is considered a cool tolerant species (Scott and Medioli, 1980). It is regarded as an indicator of the low-mid marsh zone characteristic of the daily-flooded salt marsh areas (De Rijk, 1995a; Varekamp et al., 1992) and the most ubiquitous agglutinated shallow-water species (Murray and Alve, 1999). The brackish low marsh studied in Caminha, is essentially a *M*. *fusca* zone, but can be subdivided in an IIA

upper part, where it is followed by *Pseudothurammina limnetis*, and in an IIB lower part defined by a subsidiary presence of *Psammosphaera* sp. (Fatela et al., 2009a). In the Lima estuary it is codominant in the assemblages with *Ammobaculites* spp. from flats and with *J. macrescens* and *T. inflata* from low to high marsh transition at salinities ranging from 1.1‰ to 21‰ (Fatela et al., 2009b). Mentioned as one of the most ubiquitous agglutinated species in the Guadiana estuary (SE Portuguese coast), dominates the mid-low environments in the upper reaches of the estuary (Camacho et al., 2015).

***Paratrochammina* (*Lepidoparatrochammina*) *guaratibaensis* Brönnimann, 1986; Plate 5.2, fig. 3**

2002 *Paratrochammina guaratibaensis* Brönnimann, 1986 - Debenay et al., p. 531, pl. 2, figs. 11-14.

General ecology: It is a brackish species that compose the dominant association, with *T. inflata,* in the upper intertidal zone, at the transition to dry fields in mangrove swamps of French Guiana (Debenay et al., 2002).

***Polysaccammina ipohalina* Scott, 1976; Plate 5.2, fig. 6**

1976 *Polysaccammina ipohalina* Scott, p. 318, pl. 2, figs. 1-4.

1980 *Polysaccammina ipohalina* Scott, 1976 - Scott and Medioli, p. 38, pl. 2, figs. 8-9.

General ecology: It has a low occurrence (less than 1%) in surface marsh sediments of both NW and SW Portuguese estuaries. It can be seen associated with low-salinity indicators like *H. manilaensis* (e.g., Semensatto Junior, 2006) or equally in association with *J. macrescens* and *T. inflata,* like in Guadiana's southeast Portugal estuary (e.g., Camacho et al., 2015). However, and following Scott (1976), *P. ipohalina* appears to be limited to brackish-water marshes and its occurrence with other marsh species such as *T. inflata* and *J. polystoma* should indicate a brackish marsh environment in subsurface sediments. In fact, in Caminha salt marsh, *P. ipohalina* gets its greatest relevance in the FCPwAR core sediments, reaching 18% of the assemblages, *ca.* -17 cm, in association with *H. manilaensis* and *T. salsa/irregularis*, two low-salinity indicators.

***Pseudothurammina limnetis* (Scott e Medioli, 1980); Plate 5.1, figs. 6a, b**

1980 *Thurammina* ? *limnetis* Scott and Medioli, p. 43, pl. 1, figs. 1-3.

1995a *Pseudothurammina limnetis* (Scott and Medioli) - De Rijk, p. 29, pl. 1, figs. 15-16.

General ecology: It is a common species in salt marsh areas above mean high water (De Rijk, 1995a), but also occurs in low abundance in the lowered salinity upper reaches of enclosed harbours and tidal flats of New Zealand (Hayward et al., 1999). *Pseudothurammina limnetis* revealed an important contribution to the characterization of IB and IA2 subzones of high marsh from present brackish environments of Caminha tidal marsh. Its occurrence can represent up to 68% of living assemblage under a possible optimum of salinity between 8‰ and 14‰, strongly contrasting with published data, where *P. limnetis* tends to be associated to higher salinity values and always in low proportions. This unusual dominance under such environmental conditions was seen as a new ecological data of *P. limnetis*. Its dominance at the Caminha high marsh must

also be stressed because no previous record of *P. limnetis* was found in the European coastal environments (Moreno et al., 2006). That dominance in the Caminha high marsh is shared with the *H. manilaensis* (20% to 96%) association, which can also include up to 28% of *Haplophragmoides* sp. (Moreno et al., 2006; Fatela et al., 2009a). This association ranges in elevation between MHW and MHWS (Fatela et al., 2009a). This species occurs in low abundance (< 2%) in the SW Portuguese marshes at the middle to lower estuaries (authors unpublished data).

***Siphotrochammina lobata* Saunders, 1957; Plate 5.2, fig. 4**

1957 *Siphotrochammina lobata* Saunders, p. 9-10, pl. 3, figs. 1-2.

1992 *Siphotrochammina lobata* Saunders, 1957 - Brönnimann et al., p. 31, pl. 4, figs. 1-2.

1995a *Siphotrochammina lobata* Saunders, 1957 - De Rijk, p. 33, pl. 3, figs. 9, 11-13.

General ecology: This primarily marsh/mangal species is found from north Carolina, USA, to French Guiana, with marginal marine occurrences in Tobago and Brazil (Murray, 2013). Its distribution from high to upper marsh, showed a slight positive correlation with salinity (De Rijk, 1995a). *Siphotrochammina lobata* is referred in association with *A. mexicana* and *H. wilberti* as representative of the high- and intermediate-salinity marshes (Culver and Horton, 2005). This species tend to occur in surface sediments mainly with percentages lower than 5%, but it may however be codominant in the high marsh associations, with *T. inflata* and *J. macrescens* in the NW and SW Portuguese marshes.

***Tiphotrocha comprimata* (Cushman and Brönnimann, 1948); Plate 5.1, figs. 5a,b**

1948a *Trochammina comprimata* Cushman and Brönnimann, p. 41, pl. 8, figs. 1-3.

2006 *Tiphotrocha comprimata* (Cushman and Brönnimann) - Horton and Edwards p. 69, pl. 2, figs. a-e.

General ecology: It is mainly a marsh species found only in the Atlantic, from southern Scandinavia to Portugal and from Canada to Brazil (Murray, 2013). It is an indicative species of upper and high marsh above MHW, preferably in marine-influenced areas (De Rijk, 1995a; De Rijk and Troelstra 1997). Therefore, it can be dominant at the transitional high marsh zone just below the MHW (Sen Gupta, 2002). The range of salinity tolerated in marginal marine southern Scandinavia is 20-28‰ (Alve and Murray, 1999). This species is better represented in transitional and high marsh zones of Portuguese NW coast of Minho and Lima estuaries (Fatela et al., 2007, 2014) than in the southwestern ones (authors unpublished data). Referred as rare in the living assemblages of Guadiana estuary (Camacho et al., 2015).

***Trochammina inflata* (Montagu, 1808); Plate 5.2, figs. 1a-c**

1808 *Nautilus inflatus* Montagu, p. 81, pl. 18, fig. 3.

2006 *Trochammina inflata* (Montagu, 1808) - Horton and Edwards, p. 69, pl. 2, figs. 8a-d.

General ecology: This is the typical mid marsh species, widely distributed throughout the Atlantic and Pacific oceans including the marginal marine settings (Murray, 2006, 2013). It is common to abundant above MHW in New Zealand salt marshes and frequently, comprises > 80% of faunas at about MHWS (Hayward et al., 1999). Its distribution of maximum abundance suggests more tolerance to lower salinity than *J. macrescens* in brackish-water environments (Hayward et al., 1999). *Trochammina inflata* can be codominant with *J. macrescens* in the living and dead assemblages, however in the Portuguese southwestern marshes it tends to be less abundant when they occur together (Fatela et al., 2009b; authors unpublished data). This species is absent at the high marsh of the Minho estuary during periods of high average annual precipitation, but it became significant, after a set of consecutive dry years that lead to the sediment interstitial salinity rise (Fatela et al., 2014).

***Trochamminita salsa/irregularis* (Cushman and Brönnimann, 1948); Plate 5.1, fig. 1a-c**

1948b *Labrospira salsa* Cushman and Brönnimann, p.16, p l.3, figs. 5-6.

1957 *Alveophragmium salsum* (Cushman and Brönnimann) - Todd and Brönnimann, p. 23, pl. 2, fig. 3.

1957 *Trochamminita salsa* (Cushman and Brönnimann) - Saunders 1957, p. 6, pl. 1, figs. 3-8.

1999 *Trochamminita salsa* (Cushman and Brönnimann) - Hayward et al., p. 217, pl. 1, figs. 30-32.

1948b *Trochamminita irregularis* Cushman and Brönnimann, p. 17, pl. 4, fig. 1-3.

1957 *Trochamminita irregularis* Cushman and Brönnimann - Saunders, p. 4, pl. 2, figs. 3-8.

1957 *Trochamminita irregularis* Cushman and Brönnimann - Todd and Brönnimann, p. 30, pl. 4, figs. 19-22.

General ecology: This species is abundant in the New Zealand brackish upper reaches of estuaries and in the mouth of small streams towards the limits of salt water intrusion. It is more abundant in the intertidal lower salinity environments, but may also live subtidally (Hayward et al., 1999). It is considered by Hayward (2014) as the foraminiferal species most tolerant to low salinity (~5–20‰) and to the highest tidal settings. Sometimes comprises > 80% of the foraminiferal faunas in the uppermost reaches of estuaries (Hayward et al., 1999). In a scale of preference for increasing salinity, *T. salsa/irregularis* represents the least saline end member. Concerning the tidal exposure, the *Trochamminita* association ranges between MSL and extreme high water spring – EHWS (Hayward et al., 1999; Sen Gupta, 2002). Near monospecific assemblages have been recorded at the marsh-to-upland transition, close to MHHW, where *J. macrescens* is the species more commonly found (e.g. Scott and Medioli, 1978; Scott and Medioli, 1980; Gehrels, 1994; Horton and Culver, 2008). Although, *T. salsa/irregularis* seems to substitute *J. macrescens*, *T. inflata* or *Miliammina obliqua* dominated-faunas under lower salinity conditions at this tidal high levels, often where freshwater seepage is significant (Hayward et al., 2010; Hayward, 2014). *Trochamminita salsa* is present under low salinity conditions in the Caminha high marsh dead assemblages (lower Minho estuary), associated with *H. manilaensis*, *H. wilberti* and *P. limnetis* (Fatela et al., 2014). It is also present (living and dead) at mid estuarine marshes, as accessory species, from mud flat to high marsh in Tejo, Sado and Mira estuaries. Even though, it is most significantly associated with *J. macrescens* above highest high tide level in Mira, where it reaches 11% of dead assemblage and 23% of living assemblage (authors unpublished data).

References (Appendix 5.3)

Alve, E. and Murray, J.W., 1999. Marginal marine environments of the Skagerrak and Kattegat: a baseline study of living (stained) benthic foraminiferal ecology. Palaeogeography, Palaeoclimatology, Palaeoecology 146, 171–193.

Andersen, H.V., 1953. Two new species of Haplophragmoides from the Louisiana coast. Contributions from the Cushman Foundation for Foraminiferal Research, 4, 21–22.

Bartenstein, H. and Brand, E., 1938. Die Foraminiferen-Fauna des Jade-Gebietes. 1. *Jadammina polystoma* n. g. n. sp. Aus dem Jade-Gebiete (For.). Senckenbergiana 20, 381–385.

Brady, H.B., 1870. Analysis and descriptions of the foraminifera. Annals and Magazine of Natural History 4(6), 273–309.

Brönnimann, P., Whittaker, J.E. and Zaninetti, L., 1992. Brackish water foraminifera from mangrove sediments of southwestern Viti Levu, Fiji Islands, Southwest Pacific. Revue Paléobiologie 11, 13–65.

Brönnimann P., 1986. Paratrochammina (Lepidoparatrochammina) guaratibaensis n sp. from brackish waters of Brazil and a check-list of Recent trochamminaceans from brackish waters (Protista: Foraminifera). Revue de Paléobiologie 5, 221–229.

Cahill, N., Kemp, A.C., Horton, B.P. and Parnell, A.C., 2015. A Bayesian hierarchical model for reconstructing relative sea level: from raw data to rates of change. Climate of the Past Discussions 11, 4851–4893.

Camacho, S., Connor, S., Scott, D.B. and Boski, T., 2015. Taxonomy, ecology and biogeographical trends of dominant benthic foraminifera species from an Atlantic-Mediterranean estuary (the Guadiana, southeast Portugal). Palaeontologia Electronica 18.1.17A: 1–27.

Cushman, J.A. and Brönnimann, P., 1948a. Additional new species of arenaceous foraminifera from brackish water of Trinidad. Cushman Laboratory for Foraminiferal Research 24, 37–43.

Cushman, J.A. and Brönnimann, P., 1948b. Some new genera and species of foraminifera from shallow waters of Trinidad. Contributions from the Cushman Foundation for Foraminiferal Research Contributions 24, pp.12–21.

Culver, J. and Horton, B., 2005. Infaunal marsh foraminifera from the outer banks, North Carolina, U.S.A. Journal of Foraminiferal Research 35, 148–170.

Debenay, J.-P. and Guillou, J.J., 2002. Ecological transitions indicated by foraminiferal assemblages in paralic environments. Estuaries 25, 1107–1120.

Debenay, J.-P., Guiral, D. and Parra, M., 2002. Ecological factors acting on microfauna in mangrove swamps. The case of foraminiferal assemblages in French Guiana. Estuarine, Coastal and Shelf Science 55, 509–533.

Debenay, J.P., Guiral, D. and Parra, M., 2004. Behaviour and taphonomic loss in foraminiferal assemblages of mangrove swamps of French Guiana. Marine Geology 208, 295–314.

De Rijk, S., 1995a. Agglutinated foraminifera as indicators of salt marsh development in relation to late Holocene sea level rise (Great Marshes at Barnstable, Massachusetts), Febo, Utrecht, 188p.

De Rijk, S., 1995b. Salinity control on the distribution of salt marsh foraminifera (Great Marshes, Massachusetts). Journal of Foraminiferal Research 25, 156–166.

De Rijk, S. and Troelstra, S.R., 1997. Saltmarsh foraminifera from the Great Marshes, Massachusetts: environmental controls. Palaeogeography, Palaeoclimatology, Palaeoecology 130, 81–112.

Fatela, F., Moreno, J. and Antunes, C., 2007. Salinity influence on foraminiferal tidal marsh assemblages of NW Portugal: an anthropogenic constraint? Thalassas 23, 51–63.

Fatela, F., Moreno, J., Moreno, F., Araújo, M.F., Valente, T., Antunes, C., Taborda, R., Andrade, C. and Drago, T., 2009a. Environmental constraints of foraminiferal assemblages distribution across a brackish tidal marsh (Caminha, NW Portugal). Marine Micropaleontology 70, 70–88.

Fatela, F., Moreno, J., Antunes, C., Leorri, E., Taborda, R., Silva, A., Andrade, C. and Cearreta, A., 2009b. Foraminiferal assemblages distribution across the Sado estuary tidal marshes (SW Portugal): local assessment of regional palaeoenvironmental value. In G. Flor Rodriguez et al. (Eds), Nuevas contribuciones al Margen Ibérico Atlantico, 345–348.

Fatela, F., Moreno, J., Leorri, E. and Corbett, R., 2014. High marsh foraminiferal assemblages' response to intra-decadal and multi-decadal precipitation variability, between 1934 and 2010 (Minho, NW Portugal). Journal of Sea Research 93, 118–132.

Gehrels, W.R., 1994. Determining relative sea-level change from salt-marsh foraminifera and plant zones on the coast of Maine, USA. Journal of Coastal Research 10, 990–1009.

Goldstein, S.T. and Harben, E.B., 1993. Taphonomic implications of infaunal foraminiferal assemblages in a Georgia salt marsh, Sapelo Island. Micropaleontology 39, 53–62.

Goldstein, S. & Alve, E. 2011. Experimental assembly of foraminiferal communities from coastal propagule banks. Marine Ecology Progress Series, 437: 1–11.

Hayward, B.W., Grenfell, H.R., Reid, C.M. and Hayward, K.A., 1999. Recent New Zealand Shallow-Water Benthic Foraminifera: Taxonomy, Ecologic Distribution, Biogeography, and Use in Paleoenvironmental Assessments. Institute of Geological and Nuclear Sciences monograph, vol. 21. Lower Hutt, New Zealand, 258p.

Hayward, B.W., Scott, G.H., Grenfell, H.R., Carter, R. and Lipps, J.H., 2004. Techniques for estimation of tidal elevation and confinement (~salinity) histories of sheltered harbours and estuaries using benthic foraminifera: examples from New Zealand. The Holocene 14, 218–232.

Hayward, B.W., Grenfell, H.R., Sabaa, A.T., Kay, J. Daymond-King, R. and Cochran, U., 2010. Holocene subsidence at the transition between strike-slip and subduction on the Pacific-Australian plate boundary, Marlborough Sounds, New Zealand. Quaternary Science Reviews 29, 648–661.

Hayward, B.W., 2014. ''Monospecific'' and near-monospecific benthic foraminiferal faunas, New Zealand. Journal of Foraminiferal Research 44, 300–315.

Horton, B.P. and Culver, S.J., 2008. Modern intertidal foraminifera of the Outer Banks, North Carolina, USA and their applicability for sea-level studies. Journal of Coastal Research 24, 1110–1125.

Horton, B.P. and Edwards, R.J., 2006. Quantifying Holocene sea level change using intertidal foraminifera: lessons from the British Isles. Journal of Foraminiferal Research Special Publication 40, 1–97.

Loeblich, A.R. and Tappan, H., 1988. Foraminiferal Genera and their Classification: Van Nostrand Reinhold Company. v. 1, 970 p., v. 2, 847 pl.

Montagu, G., 1808. Supplement to Testacea Britannica. S. Woolmer, Exeter, 183p.

Moreno, J., Fatela, F., Andrade, C. and Drago, T., 2006. Distribution of "living" Pseudothurammina limnetis (Scott and Medioli): an occurrence on the brackish tidal marsh of Minho/Coura estuary – Northern Portugal. Révue de Micropaléontologie 49, 45–53.

Murray, J.W., 1971. An Atlas of British Recent Foraminiferids. Heinemann Educational Book, 244p.

Murray, J.W., 1991. Ecology and Palaeoecology of Benthic Foraminifera. Longman, Harlow, 397p.

Murray, J.W., 2006. Ecology and Applications of Benthic Foraminifera. Cambridge University Press, Cambridge, 426p.

Murray, J.W., 2013. Living benthic foraminifera: biogeographical distributions and the significance of rare morphospecies. Journal of Micropalaeontology 32, 1–58.

Murray, J.W. and Alve, E., 1999. Taphonomic experiments on marginal marine foraminiferal assemblages: how much ecological information is preserved? Palaeogeography, Palaeoclimatology, Palaeoecology 149, 183–197.

Phleger, F.B., 1970. Foraminiferal populations and marine marsh processes. Limnology and Oceanography 15, 522–534.

Phleger, F.B. and Walton, W.R., 1950. Ecology of marsh and bay foraminifera, Barnstable, Massachusetts. American Journal of Science 248, 274–294.

Saunders, J.B., 1957. Trochamminidae and certain Lituolidae (Foraminifera) from the recent brackish-water sediments of Trinidad, British West Indies. Smithsonian Miscellaneous Collections 134, 1–16.

Scott, D.B., 1976. Brackish-water foraminifera from southern California and description of *Polysaccammina ipohalina* n. gen., n. sp. Journal of Foraminiferal Research 6, 312–321.

Scott, D.B. and Medioli, F.S., 1978. Vertical zonation of marsh foraminifera as accurate indicators of former sea-level. Nature 272, 538–541.

Scott, D.B. and Medioli, F.S., 1980. Quantitative studies of marsh foraminiferal distributions in Nova Scotia: their implications for the study of sea-level changes. Cushman Foundation for Foraminiferal Research, Special Publication 17, 59p.

Scott, D.K., and Leckie, R.M., 1990. Foraminiferal zonation of Great Sippewissett salt marsh (Falmouth, Massachusetts). Journal of Foraminiferal Research 20, 248–266.

Sen Gupta, B.K., 2002. Foraminifera in marginal marine environments. In: Sen Gupta, B. (Ed.), Modern Foraminifera. Dordrecht, Kluwer Academic Publishers, p.141–159.

Todd, R. and Brönnimann, P., 1957. Recent foraminifera and thecamoebina from the eastern Gulf of Paria. Contributions from the Cushman Foundation for Foraminiferal Research, Special Publication 6, pp.1–43.

Varekamp, J.C., Thomas, E. and Van de Plassche, O., 1992. Relative sea-level rise and climate change over the last 1500 years. Global Change 4, 293–304.

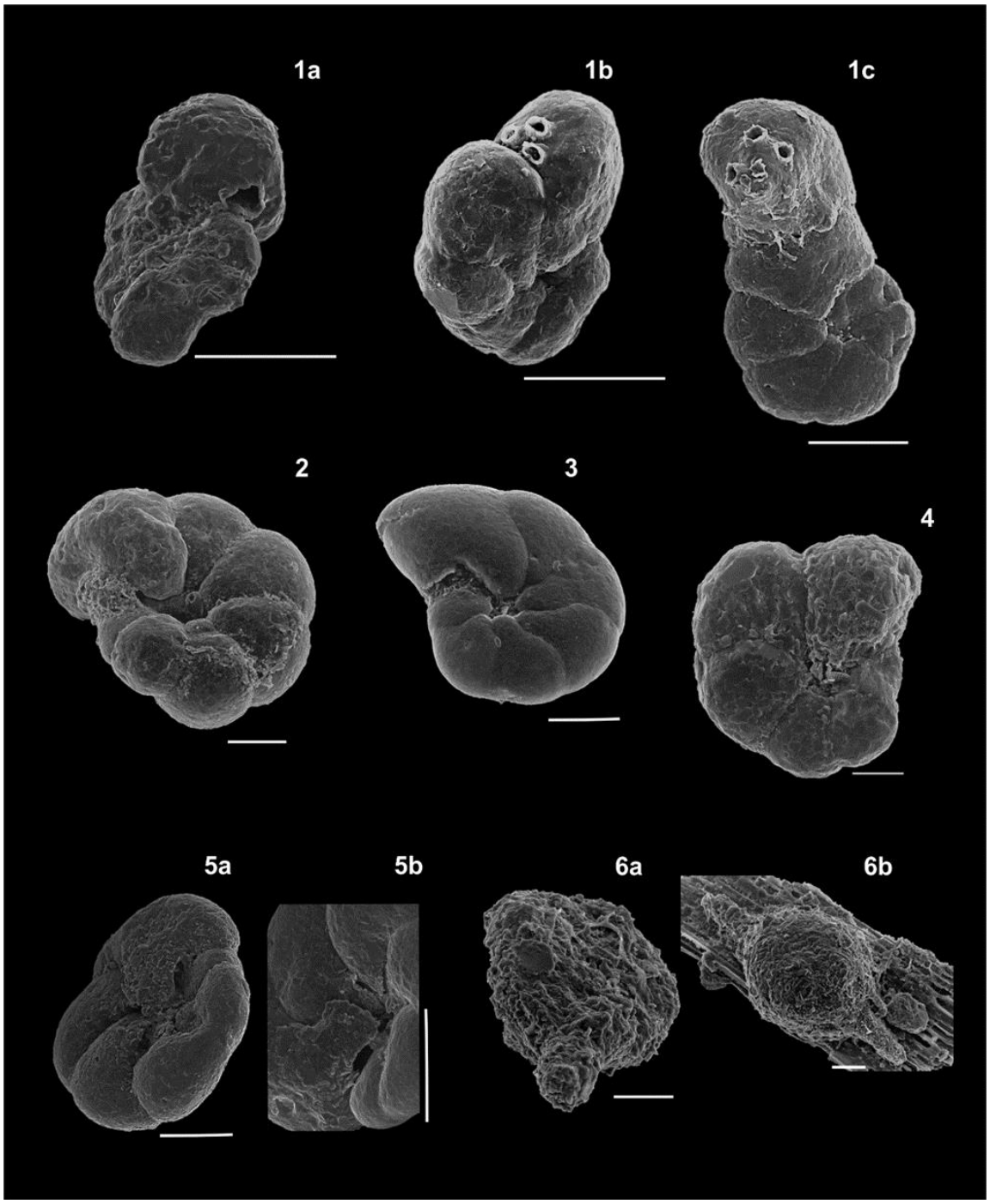

Plate 5.1. Scale bar 100 µm. 1a – *Trochamminita salsa/irregularis* (Cushman & Brönnimann, 1948),with a single aperture in the last chamber; 1b,c – *T. salsa/irregularis* irregular forms with backward secondary apertures in the last chamber; 2 – *Haplophragmoides manilaensis* Andersen, 1953; 3 – *Haplophragmoides wilberti* Andersen, 1953; 4 – *Haplophragmoides* sp.; 5a – *Tiphotrocha comprimata* (Cushman & Brönnimann, 1948), ventral face and oral view; 5b – *T. comprimata*, detail of secondary apertures; 6a – *Pseudothurammina limnetis* (Scott & Medioli, 1980), apertural view of a free specimen; 6b – *P. limnetis* sessile specimen attached to a marsh plant debris.

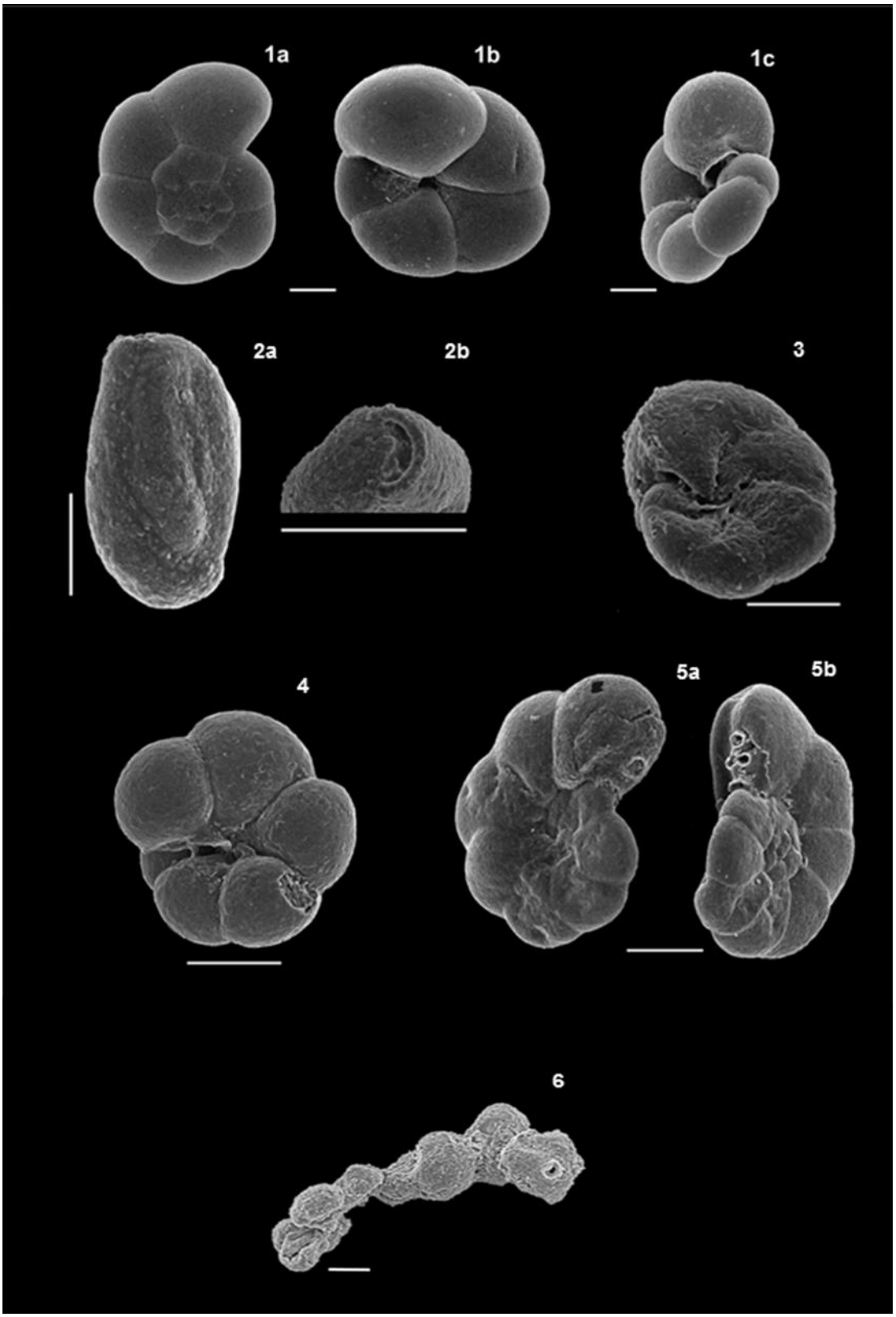

Plate 5.2. Scale bar 100 µm. 1a – *Trochammina inflata* (Montagu, 1808), dorsal face; 1b – *T. inflata*, ventral face; 1c – *T. inflata*, apertural view; 2a – *Milliammina fusca* (Brady, 1870); 2b – *M. fusca*, apertural view; 3 – *Paratrochammina guaratibaensis* Brönnimann, 1986, ventral face; 4 – *Siphotrochammina lobata* Saunders, 1957, ventral face; 5a – *Jadammina macrescens* (Brady, 1870), ventral face; 5b – *J. macrescens*, dorsal view; 6 – *Polysaccammina ipohalina* Scott, 1976. Scale bar 50 µm for plate figure 6.

6 A bi-proxy paleoclimatic reconstruction for the Entre-Douro-e-Minho region, northwest Portugal, from 1626 to 1820 – A search for evidence of solar forcing

J. Moreno [a,b] , F. Fatela [a,b], M.A. Gonçalves [a,b], E. Leorri [c], J.J. Gómez-Navarro [d], R. Brázdil [e,f], M.J. Ferreira [g], F. Moreno [h] and R.M. Trigo [i]

[a] IDL – Instituto Dom Luiz, Faculdade de Ciências, Universidade de Lisboa, Campo Grande, 1749-016 Lisboa, Portugal

[b] Departamento de Geologia da Faculdade de Ciências da Universidade de Lisboa, Campo Grande, 1749-016 Lisboa, Portugal

[c] East Carolina University, Department of Geological Sciences, Greenville, NC 27858-4353, USA

[d] University of Murcia, Department of Physics-Physics of the Earth, Campus de Espinardo, 30100 Murcia, Spain

[e] Institute of Geography, Masaryk University, 611 37 Brno, Czech Republic

[f] Global Change Research Institute, Czech Academy of Sciences, 603 00 Brno, Czech Republic

[g] Centro Algoritmi, Universidade do Minho, Campus de Azurém, 4800-058 Guimarães, Portugal

[h] Independent researcher, 4940-061 Paredes de Coura, Portugal

[i] DEGGE – Departamento de Engenharia Geográfica, Geofísica e Energia da Faculdade de Ciências da Universidade de Lisboa, Campo Grande, 1749-016 Lisboa, Portugal

Submitted to *Climate Research* the 26th September 2016 (presently under review)

"Feliz aquela que efabulou o romance/ Depois de o ter vivido/ A que lavrou a terra e construiu a casa/ Mas fiel ao canto estridente das sereias/ Amou a errância o caçador e a caçada/ E sob o fulgor da noite constelada/ À beira da tenda partilhou o vinho e a vida."

Sophia De Mello Breyner Andresen, Ode à Maneira de Horácio in O BÚZIO DE CÓS E OUTROS POEMAS

ABSTRACT

This work introduces a triennial-resolved wine production (WP) series from 1626 to 1820 based on hand-written Benedictine accounts from six monasteries of the Entre-Douro-e-Minho region (NW Portugal), and a new benthic foraminiferal record (AD 1654–1824) from the Caminha tidal marsh (Minho River lower

estuary). Spectral analysis of these two proxy time series shows statistically significant periodicities at ~13-year and ~60-year, falling in the range of the Schwabe and Lower Gleissberg solar cycles, respectively. Wavelet-based methods comparing these cycles in foraminifera with those in reconstructions of total solar irradiance, the North Atlantic Oscillation index, and a regional temperature climate model simulation revealed some highly coherent responses that can be linked to solar activity (SA). It is hypothesized that the inferred major solar-induced fluctuations in the WP trend have been modulated by the amplitude and phase interplay of the three solar dynamo natural oscillations (bi-decadal, semi-secular and secular). The likely socio-economic and political impacts on WP during the Little Ice Age, particularly in the Maunder and Dalton Minima, are also considered and contextualized based on the available documentary sources. Major WP loss in the Benedictine's possessions can be associated, besides climatic deterioration concomitant with documented agricultural crisis in Portugal, to local conflicts and international wars in which this country was involved. The analysis also provides evidence towards a SA–climate coupled primer control on the successful wine grape production trend. However, a key detrimental human impact on WP has to be accounted, particularly during the most acute crisis, which is difficult to isolate from the SA–climate factor.

Keywords: Wine production; benthic foraminifera; total solar irradiance; time–frequency analysis; solar–climate relationship; Little Ice Age.

6.1. Introduction

Wine production (WP) depends on a set of natural factors interacting with cultural traits and people's viticultural practices and expertise. This explains why "wine is a holistic result of nature and nurture" (Jones, 2014). In this interaction, known as the vineyard habitat or *terroir*, climate has a primary role in dictating the suitability of a region for viticulture at several spatiotemporal scales (Jones et al., 2012): warm and dry summers and cool and wet winters are recognized as suitable, ultimately promoting economic sustainability. Thus, climate has controlled the global distribution of the main wine-producing regions over historical times (Jones et al., 2012). Also, total solar irradiance (TSI) is crucial for grapevine since it is photoautotrophic, growing with CO_2 and light as the sole carbon and energy sources (Lima da Silva et al., 1996). From the incoming TSI, grapevine is mostly sensitive to the Photosynthetically Active Radiation (PAR), the energy source for the photosynthetic light-dependent reactions. Hence, TSI and PAR greatly affect grapevine and therefore WP. The sun's influence on viticulture has been addressed with data from wine-producing regions responding to climate changes related to solar activity (SA) (Jones et al., 2012). These authors described how WP extended as far north as the Baltic Sea coastlines and southern England during the warm Medieval Climatic Anomaly (900–1300), whereas during the Little Ice Age (LIA; 1350–1900) the dramatic temperature decline resulted in northern vineyards dying out, and growing seasons so short that harvesting even in southern Europe was difficult.

When the first wine was produced in Portugal remains uncertain, but by 1143 at this nation's birth a major portion of the best vineyard land between the Minho and Douro Rivers (Figure 6.1) – the so-called Entre-Douro-e-Minho (EDM) region – was owned by religious orders, including the Benedictines (Marques, 2011). In the Apocalypse of Lorvão, the famous 12th century illuminated manuscript from the Lorvão monastery (central Portugal) is possible to see grapes being harvested, in a reminiscence of the techniques and practices of that epoch (Figure 6.2). In the EDM region, Benedictines cultivated grapevines and produced wine, following the motto *Ora et Labora* ("pray and work"), also becoming promoters of an innovative viticulture (e.g., varietals and soils selection; trellis design and land terracing system introduction; Marques, 2011).

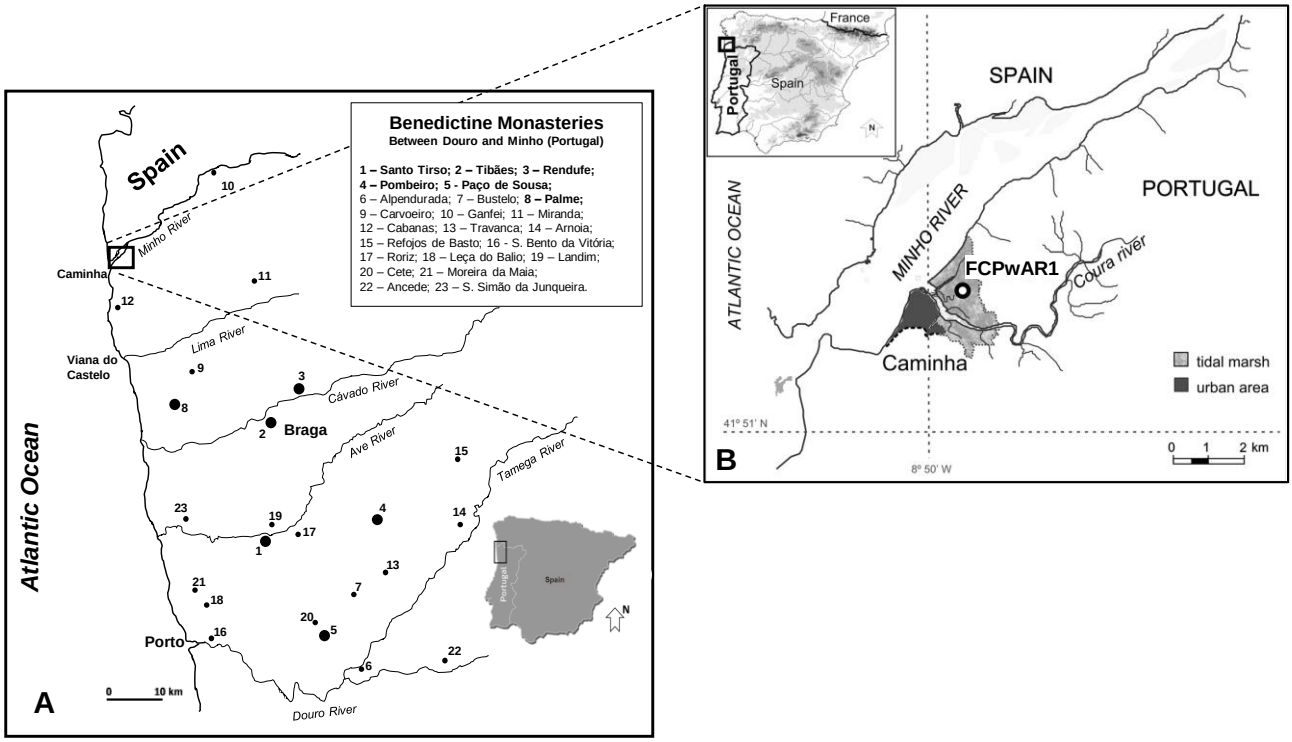

Figure 6.1. A – Geographical location of the Benedictine monasteries network established in the Entre-Douro-e-Minho (EDM) region (after Marques, 2011). The S. Martinho de Tibães monastery (Braga) was the head of the Benedictine Order in Portugal since 1569. It was in Tibães that, at every three years, the Orders' General Chapter meetings took place, in which the account reports (*Estados*) were presented. Bold dots represent the analyzed monasteries' wine productions; **B –** Location of core FCPwAR1 in the Caminha tidal marsh (Minho estuary, NW Portugal).

The climate of the EDM region, geographically overlapping the modern Minho Wine Region (MWR), has been a requisite for its wines' uniqueness ("Vinhos Verdes" *terroir*) (Fraga et al., 2014). But observations from other wine-growing regions confirmed that climate change is strongly affecting grapevine phenology and grapes composition, which may lead to great modifications in the aromatic profile of today's wines (Fraga et al., 2012). Increased complexity in grapevine agro-system has carried extra non-linearity to WP data when intending to link it to climate change. Hoyt and Schatten (1997) indicated that modern technological advances have triggered a partial uncoupling between

agricultural yields and climate, pointing that “the best chance of finding a solar connection in climate will come from the earlier records”.

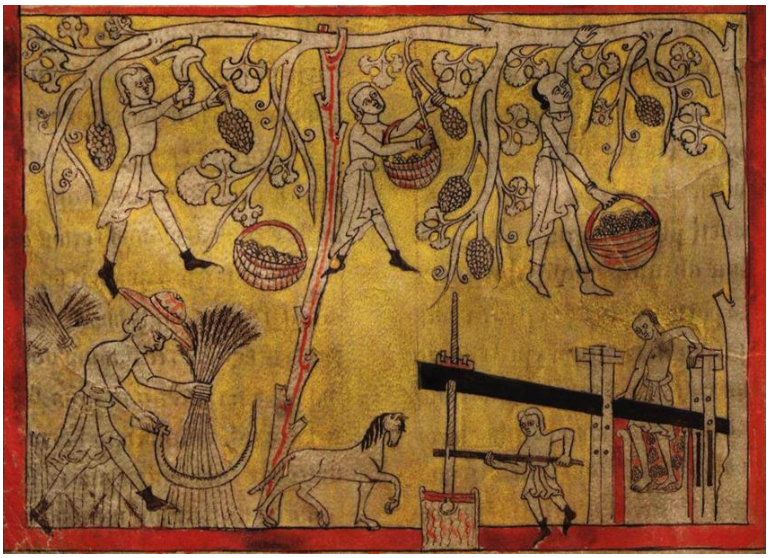

Figure 6.2. The Apocalypse of Lorvão, an early medieval (1189) illuminated manuscript from the *scriptorium* of the S. Mamede do Lorvão monastery (Central Portugal) and based on the 8th century codex *Commentarium in Apocalypsin* by Beatus of Liébana, shows the grape harvesting and other agricultural work according to the practices of the 12th century (in *Commentarium in Apocalypsin* of S. Mamede do Lorvão, Arquivo Nacional da Torre do Tombo Book 44, C.F.160, p 172v).

However, *Vitis vinifera* L. is considered as an accurate proxy for monitoring past climate fluctuations based on its long record (Le Roy Ladurie, 1967). Successful WP was always restricted to narrow geographical niches of suitable climate, which places grapevine cultivation at greater risk regarding short-term climate variability and long-term climate changes (Jones et al., 2005). As grapevine is a perennial crop, persisting productive for more than 50 years (Bindi et al., 1996), it is also one of the most sensitive to productivity constraints, less adaptable and thus, more susceptible to damage by climatic fluctuations (Lobell et al., 2006). Hence, the research on grapevine–climate relationships has great potential for climate reconstructions (Santos et al., 2011; Moreno et al., 2016; Možný et al., 2016).

Benthic foraminifera are also considered very suitable to describe paleoclimatic changes (Phleger, 1970; Murray, 2006). In brackish environments, they are considered as a proxy for salinity (Hayward et al., 1999), allowing to recognize variations in salt marshes’ hydrological balance related to regional temperature and precipitation patterns. Foraminiferal assemblages from Caminha high marsh (NW Portugal) reacted to the intra- and multi-decadal precipitation variability in the 1934–2010 period (Fatela et al., 2014). Salt marshes are under strong environmental variability caused by tides, however at higher elevations, where flooding frequency and duration is limited, the response provided by foraminiferal assemblages to climate fluctuations is highly valuable. Although, they present lower time resolution when compared to other proxies (e.g., tree rings, WP or grape harvest

dates) and a more thorough paleoclimatic reconstruction requires them to be presented with other proxies and/or historical archives.

Accordingly, this paper aims to (i) provide new climatic proxy data for the Portuguese EDM region, building a historical WP series, (ii) integrate these new data with benthic foraminiferal assemblages from Caminha, (iii) suggest a paleoclimatic framework for the studied region based upon the two proxies complemented with historical data and (iv) consider the SA potential impact on the EDM region climate, especially on grapevine historical production within the "Vinhos Verdes" *terroir*.

6.2. Data

6.2.1. WP data

The WP series for the EDM region is based on the available Benedictine hand-written records from 1626 to 1820, compiled by Oliveira (1979), Silva (1993) and Marques (2011). Those records correspond to the accounting reports (known as *Estados*) of each monastery, made public at every three years in Tibães. Thus, WP data follows the triennial resolution, with no acreages specified in the original source. *Estados* creation arose from an Order's major reorganization following a deep crisis – the *Comendatários Crisis*. This was a heavy and long-lasting process starting in 1566–1567 (Dias, 2011), which can explain the first report delay (1629). The last one is dated 1821, one year after the Liberal Revolution outbreak, whose outcome would dictate 13 years later the religious orders extinction in Portugal. Each report included a set of fixed items, namely about crops production (grain and wine) in the monastery's possessions.

Targeting to get the longest possible WP time series, the volumes of wine harvested as reported by six Benedictine monasteries: Tibães, Rendufe, Santo (S^{to}.) Tirso (Casa/Passais), Pombeiro, Paço de Sousa and Palme (Figure 6.1) were merged, generating a 194-year time series (Appendix 6.1). The final dataset encompasses triennial values (representing the sum of the three preceding years) starting in 1629 and ending in 1821 (i.e., 1626 to 1820 years), with two major gaps (shared by all monasteries) in the years of 1641–1644 and 1677–1710 (except of 1680–1682).

6.2.2. Sediment cores

The methodology for sediment cores collection and analysis from Caminha (41º52′37″ N, 8º49′28″ W; 1.55 m above mean sea-level; Figure 6.1), aiming to obtain foraminiferal, sedimentological, chronological and organic chemistry data, is described in detail at De la Rosa et al. (2012), Fatela et al. (2014) and Moreno et al. (2014). Here, we present a new record with a higher foraminiferal sampling resolution than prior studies. For this a PVC pipe (12 cm diameter; 30 cm long) was inserted in the sediment using a rubber hammer. The core was then recovered by

shovelling all sediment around the PVC pipe minimizing sediment disruption during collection, wrapped in a cling film to avoid desiccation and kept in a freezer until sliced into 0.5 cm intervals. A total of sixty new foraminiferal, *ca.* 56 cm^3, samples were analyzed.

The age-depth model is fully described in Moreno et al. (2014). The upper section of the core was dated via ^{210}Pb measured by alpha spectroscopy, ^{137}Cs, and total Pb activities with six additional samples analyzed for radiocarbon content (total organic) at Beta Analytic Inc. (USA). The age-depth model was developed using a Bayesian model (Bchron 3.2; Haslett and Parnell, 2008; Parnell et al., 2008). While the chronology provided seems accurate, the individual error for each sample averaged *ca.* 130 years (95% confidence interval). All the calendar ages obtained using this model are reported in *Anno Domini* (years AD).

6.2.3. Additional reconstructed and simulated climate series

The TSI reconstructed dataset is based on the works of Krivova et al. (2010) and Yeo et al. (2014) [hereafter referred as Krivova et al. (2010)] and covers the period from 1610 until present.

The North Atlantic Oscillation (NAO) index reconstruction by Luterbacher et al. (2002) is available from https://climexp.knmi.nl.

We also use a selection of the Xoplaki et al. (2005) and Luterbacher et al. (2006) gridded reconstruction of seasonal temperature for Europe, along with two series of simulated temperature and precipitation data for the area under consideration and achieved with a regional climate model driven by reconstructions of the external forcings (Gómez-Navarro et al., 2011, 2012).

6.3. Methods

6.3.1. WP reconstruction

The WP raw-dataset exhibits gaps for some monasteries, except for the two referred periods with gaps across all six. To take advantage from the monasteries network spatiotemporal range and develop a single (representative) WP series for the region, a stepwise regression-based approach was applied to fill the individual gaps (Appendix 6.1). Initially, correlation coefficients between the six WP series were computed, as a measure of their connexion. Then, the common data for the overlap period of the two best correlated monasteries were used in the linear least-squares fit reconstruction for filling the gaps from both series (when needed) giving the derived relationship. Two sub-periods (calibration/verification) have been considered for cross-calibration-verification procedures, with 50% random samples extracted from the period of common overlap (also known as full calibration period) for calibration, and remaining data for verification. Thus, the S^{to}. Tirso/Casa WP time series (most complete record) was selected to fill the gaps of the S^{to}. Tirso/Passais series based on their

strong correlation (r = 0.90, p < 0.05; Table 6.1). The other WP series were filled applying an iterative process and following the order shown in Table 6.2 until the reconstruction was accomplished. Finally, the six series were converted into a single one, expressed as the sum of corresponding values. This is considered representative for the EDM region during the 1626–1820 period, with a 6-year (1638–1643) and a 33-year (1674–1709, except 1680–1682) gaps. The advantage of merging local series into a regional dataset is its increased ability to represent the grapevines response to solar radiative forcing, minimizing most local distortions.

Table 6.1. Pearson correlation coefficients between 1629–1821 triennia of wine production raw data (p < 0.05).

	Rendufe_Passais	S^{to} Tirso_Casa	S^{to} Tirso_Passais	Pombeiro_Passais	Paço de Sousa_Passais	Palme_Passais	Tibães_Passais
Rendufe_Passais			0.42	0.60			0.54
S^{to} Tirso_Casa			0.90	0.64	0.72		0.56
S^{to} Tirso_Passais	0.42	0.90		0.57	0.62	0.56	0.68
Pombeiro_Passais	0.60	0.64	0.57		0.74		0.51
Paço de Sousa_Passais		0.72	0.62	0.74			0.73
Palme_Passais			0.56				0.64
Tibães_Passais	0.54	0.56	0.68	0.51	0.73	0.64	

Table 6.2. WP Reconstruction: calibration/verification statistics.

Reconstruction steps	WP series to be reconstructed	WP series used in the reconstruction	Calibration statistics			Verification statistics		Full calibration period		
			r^2	r^2 adjusted	DW test	RE	CE	r^2	r^2adjusted	DW test
1	S$^{to.}$ Tirso/ Passais	S$^{to.}$ Tirso/ Casa	0.62	0.59	1.206	0.90	0.90	0.82	0.81	1.993
2	Paço de Sousa	S$^{to.}$ Tirso/ Casa	0.51	0.48	1.415	0.47	0.33	0.42	0.40	1.840
3	Pombeiro	S$^{to.}$ Tirso/ Casa	0.48	0.45	1.510	0.33	0.32	0.41	0.39	1.457
4	Tibães	S$^{to.}$ Tirso/ Passais	0.41	0.34	1.661	0.50	0.37	0.47	0.44	1.792
5	Palme	Tibães	0.40	0.33	1.434	0.40	0.28	0.50	0.47	1.730
6	Rendufe	Pombeiro	0.38	0.33	1.189	0.20	0.12	0.31	0.28	1.368

As predictive ability measures, the reduction of error (RE), the coefficient of efficiency (CE) and the coefficient of determination (r^2 and r^2 adjusted) were evaluated (Cook et al., 1994). These parameters were calculated separately for each reconstruction step (Table 6.2). The Durbin-Watson (DW) test was used to detect the presence of first-order autocorrelation in the residuals. For small samples (< 200), lower and upper bounds for critical values of DW are tabulated. When the Durbin-Watson test gave inconclusive results, the Cochrane-Orcutt procedure was applied (Kutner et al., 2005).

6.3.2. Spectral analysis

The REDFIT tool in PAST (Schulz and Mudelsee, 2002; Hammer, 2012) was used to check significant cyclicity in the foraminiferal dataset. A multi-species assemblage comprised by *Jadammina macrescens* (Brady, 1870), *Trochammina inflata* (Montagu, 1808), *Tiphotrocha comprimata* (Cushman and Brönnimann, 1948), *Siphotrochammina lobata* (Saunders, 1957) and

Paratrochammina guaratibaensis (Brönnimann, 1986) was selected for this task, showing a clear response to salinity variations: these species abundances increase with brackish-to-normal salinity conditions, reflecting higher salinity episodes in the otherwise prevailing low-salinity (mesohaline) environment of the study site (Moreno et al., 2014). The spectral peaks' statistical significance was assessed by considering only those exceeding the critical false-alarm level (dependent on the time series length, i.e., 96.8% in our case; Schulz and Mudelsee, 2002). The power spectral density estimate of the WP series was obtained using the generalized Lomb-Scargle periodogram, as well as for the reconstructed TSI series (Krivova et al., 2010). The previous frequency-domain analysis is limited by sampling rate and Nyquist cut-off frequency. Though, for the foraminiferal data, short mean sampled intervals of 3–4 years are available for the last 4–5 decades. Overall, intervals of up to 7 years represent 80% of data, with a median of 5 years and a mode of 3 years.

6.3.3. Wavelet analysis

We use the continuous wavelet transform (CWT) approach, including cross wavelet transform (XWT) and wavelet coherence (WTC) methods, for quantifying the proxies' one-way causality with TSI and climate-related variables: reconstructed temperatures and the NAO index and simulated temperatures and precipitation. These calculations were performed with the MATLAB/R tool package (Grinsted et al., 2004). Prior to CWT, WP (1713–1821 triennia) and foraminiferal (1654–2010) series were interpolated using cubic splines (e.g., Debret et al., 2007) to obtain annual chronologies for the former and a regular time axis for the latter, as this is a method's requirement, which demands evenly spaced series. Such an interpolation is statistically similar to the one used in the Lomb-Scargle periodogram, and the quantified root mean squared deviation (RMSD) is half the standard deviation of the data using cross-validation procedures.

6.4. Results

6.4.1. WP series

Figure 6.3A and Appendix 6.1 show the reconstructed triennial WP series (1626–1820). Cross-calibration-verification results (Table 6.2) evidence a predictive ability reduction after the first reconstruction step (explaining 82% of variance). Following steps explained smaller variance in calibration (between 41–50%), reaching the lowest value in the final (31%). Up to 62% of the variance is verified in cross-validation in the first step, decreasing to 51–38% afterwards. The scores of r and r^2 together with RE and CE positive values fall within to conventional limits for uncertainty (Cook et al., 1994) and support the reconstructive confidence and usefulness of this approach for the period studied. DW values suggest no evidence of first order autocorrelation in the residuals at the 0.01 significance level.

Long-term WP evolution (Figure 6.3A) shows some irregularity with a mean 180,927 l, ranging between 80,438 l (1635) and 293,414 l (1773). Based on mean values, four periods can be identified (99% confidence level): WP1_1629–1683 (N = 15; mean = 132,430 l); WP2_1713–1752 (N = 14; mean = 169,776 l), WP3_1755–1794 (N = 14; mean = 239,665 l) and WP4_1797–1821 (N = 9; mean = 187,735 l). Higher WP values are shown from 1755 until 1773, in which four triennia 1755, 1758, 1767 and 1773 indicate good harvests. Conversely, the 1629 and 1635 triennia correspond to less WP.

6.4.2. High marsh benthic foraminiferal assemblages

The Caminha high marsh foraminiferal assemblages are dominated by agglutinated species, in which *Trochamminita salsa/irregularis* (Cushman and Brönnimann, 1948), *Haplophragmoides manilaensis* (Andersen, 1953), *Haplophragmoides wilberti* Andersen, 1953, *J. macrescens*, *T. inflata*, *T. comprimata*, *P. guaratibaensis*, *Polysaccammina ipohalina* Scott, 1976, *S. lobata*, *Pseudothurammina limnetis* (Scott and Medioli, 1980) and *Miliammina fusca* (Brady, 1870) are the most frequent (Figure 6.4). Although the whole core was included in REDFIT analysis, only the samples overlapping with WP series are discussed here. Accordingly, three Foraminiferal Assemblage Zones (FAZ) can be outlined regarding species presence, abundance and dominance (FAZ I, II and III; Figure 6.4, Appendix 6.2).

FAZ III (31–24.5 cm depth; AD 1650–1730): The foraminiferal assemblages primarily contain low-salinity (limnetic-mesohaline) species *T. salsa/irregularis*, followed by *H. wilberti*, *H. manilaensis* and *P. ipohalina*. There is a trend of increasing abundances of brackish-to-normal marine (mesohaline-euhaline) species towards the top of this FAZ.

FAZ II (24.5–19 cm; AD 1730–1790): This unit records the low-salinity species decline (16–40%) and a significant increase of moderate-brackish (oligohaline-mesohaline) plus brackish-to-normal salinity species (54–77%). Two major events can be recognised within this FAZ: an initial increase of moderate-brackish salinity mainly indicated by *H. wilberti* in AD 1730–1760 (30–62%); a subsequent increase of normal-salinity species in AD 1760–1790, reflected particularly by *J. macrescens* (2–31%) and secondary species *S. lobata*. It is noteworthy the spike in *T. comprimata* and *P. guaratibaensis* between these two steps.

FAZ I (19–16 cm; AD 1790–1824): Also two distinct events can be identified. The first one, around AD 1795, is recorded by one single sample and marked by a major reduction of the brackish-to-normal salinity marsh species *J. macrescens*, *T. comprimata*, *S. lobata* and an increment of *T. salsa/irregularis* and *H. wilberti*. The second (AD 1810–1820) shows a clear dominance of low-salinity species (52–61%), especially *T. salsa/irregularis*, *H. manilaensis*, and *P. ipohalina*, and a moderate-to-normal salinity species decrease, to a minimum of 28% around AD 1812, when *J. macrescens* is missing.

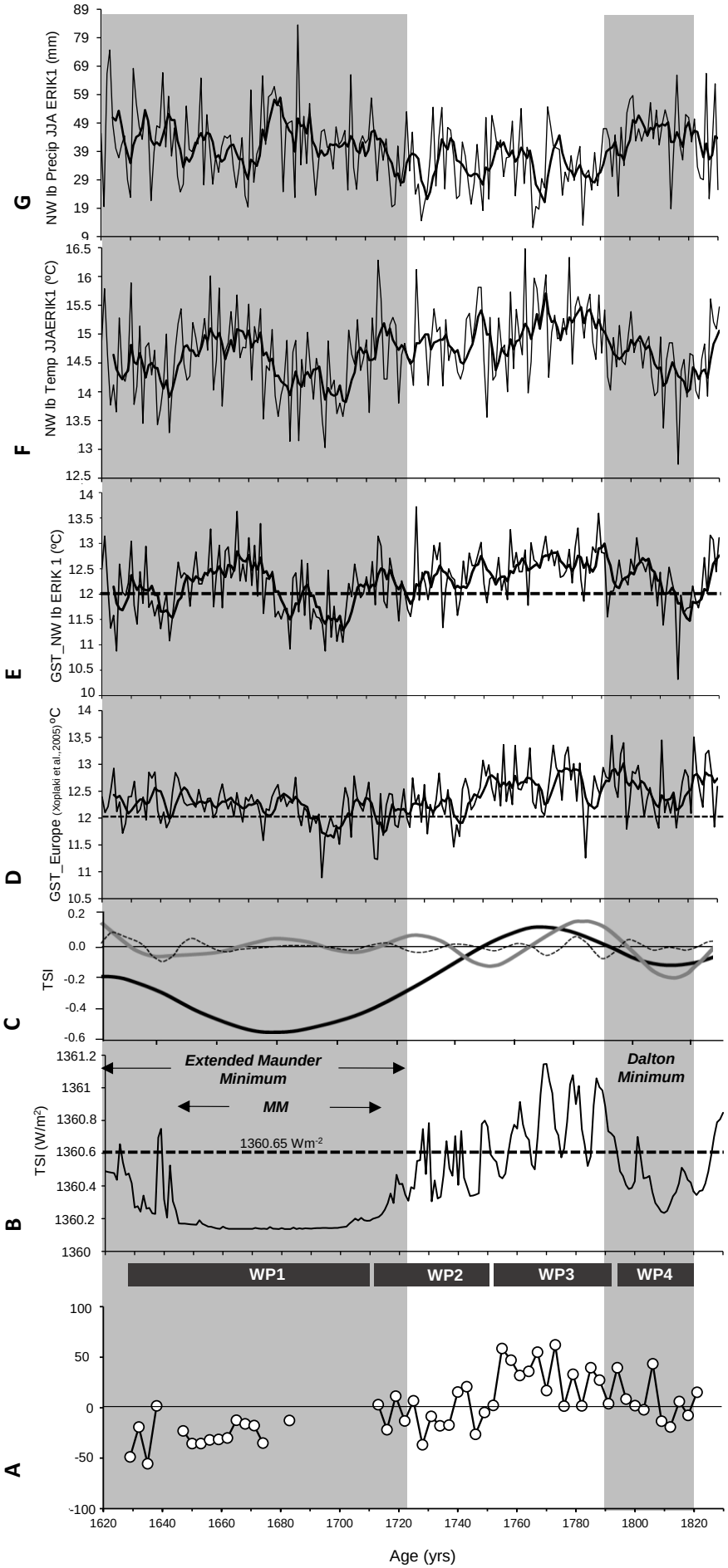

Figure 6.3. A – Wine production (WP) composite time series represented as deviations of the mean (%) for six Benedictine monasteries from the Entre-Douro-e-Minho (EDM) region. The periods WP1 to WP4 are distinguished based on differences of WP averages (arithmetic means) at the 99% level; **B –** Total solar irradiance (TSI) time series (Krivova et al., 2010); MM – Maunder Solar Minimum; Extended Maunder Minimum after Vaquero and Trigo (2015); **C –** Representation of the three solar dynamo natural oscillations in TSI raw data: black line - secular oscillation, grey line - semi-secular, dashed line - bi-decadal oscillation (after Duhau and Martínez, 2012); **D –** GST_Europe – European growing season temperatures (March to August) reconstruction (Xoplaki et al., 2005); black thicker line - 5 years running average; **E –** GST_NW IP ERIK1- NW Iberian (Ib) growing season temperatures (March to August) simulation (Gómez-Navarro, 2011, 2012); black thicker line - 5 years running average; **F –** NW Ib Temp JJA ERIK1 - NW Iberian summer temperatures simulation (Gómez-Navarro et al., 2011, 2012); black thicker line - 5 years running average; **G –** NW Ib Precip. JJA ERIK1 - NW Iberian summer precipitation

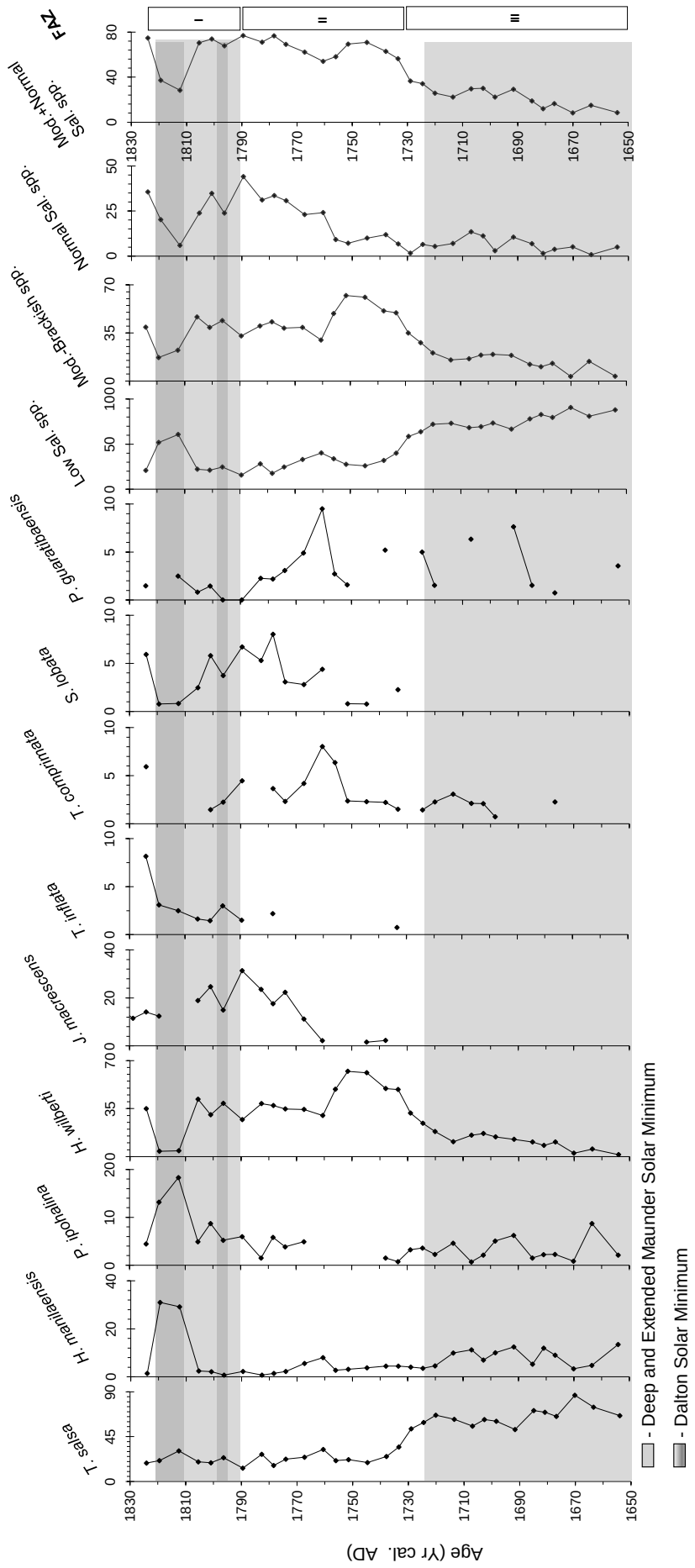

Figure 6.4. Summary of benthic foraminiferal data in core FCPwAR. Age (yr cal. AD) – age in calendar years AD; Salt marsh spp. – percentage distributions of the group of brackish salt marsh benthic species; Low Sal. spp. – percentage distributions of the group of low-salinity benthic species; Mod.-Brackish spp. – percentage distributions of the group of Brackish/Moderate-Brackish benthic species; Normal Sal. spp. – percentage distributions of the group of Brackish-to-Normal salinity benthic species; Mod.+Normal Sal. spp. – Brackish/Moderate plus Brackish-to-Normal salinity benthic species; FAZ – foraminiferal assemblage zones.

6.4.3. Spectral analysis

The WP series Lomb-Scargle spectrum reveals a significant peak at ~64 years (Figure 6.5A), while foraminifera REDFIT periodogram shows two: ~59 years and ~13 years (Figure 6.5B). Although the latter needs to be considered carefully, it is important to observe its consistency with other data. Both peaks also stand out in the TSI series Lomb-Scargle periodogram (~13-year and ~57-year; not shown).

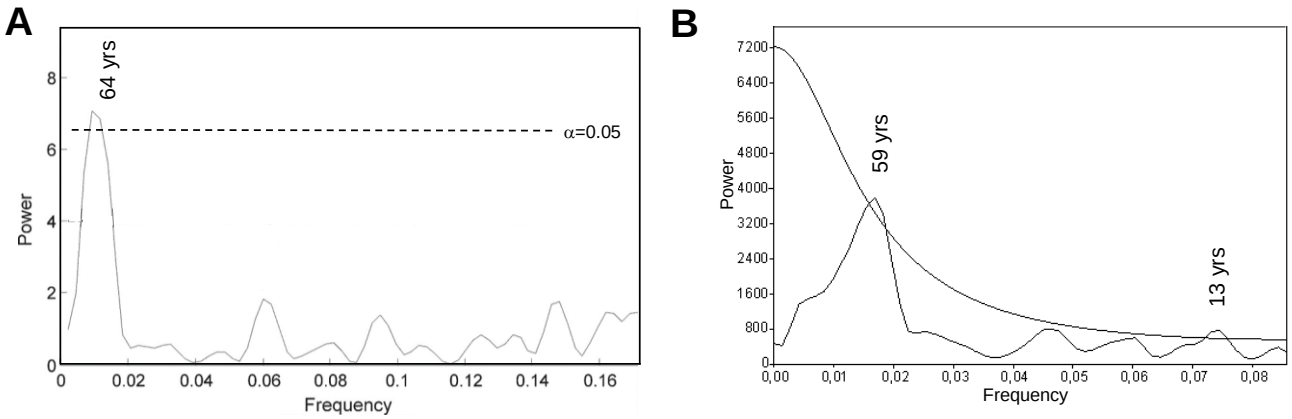

Figure 6.5. **A –** Lomb-Scargle periodogram of WP series for the 1713–1821 period; **B –** REDFIT periodogram of brackish/normal salinity species (*J. macrescens*, *T. inflata*, *T. comprimata*, *S. lobata* and *P. guaratibaensis*) for the period AD 1654–2010. The two statistically significant peaks registered at 59 years and 13 years are set at 96.8% level.

Figure 6.6 presents XWT and WTC calculations for benthic foraminifera *vs.* TSI (Figure 6.6A–B), the NAO index (Figure 6.6C–D) and simulated annual temperatures (Figure 6.6E–F). Although XWT detected further relationships between the combinations of the two proxies and climate-related variables (spring-summer temperature; annual and summer precipitation), they were not validated by WTC indicating non-significant coherence at the 0.05 significance level. Regrettably, CWT results concerning WP data were inconclusive due to the limited time span covered.

The spectral peaks found in foraminifera REDFIT periodogram are apparent in XWT and WTC graphs from Figure 6.6. They reveal common and highly significant cycle coherence in the quasi-decadal (centred at ~13-year) and quasi-bi-decadal bands (centred at ~22-year; sometimes extending until ~32-year) and also in the 40–80-year band (centred at ~64-year), depending on variables. The latter band is the only persistent, with the previous only visible over patchy temporal sectors, particularly around *ca.* 1700–1750, *ca.* 1800 and *ca.* 1850–1900. Furthermore, correlation patterns in these episodic, significant coherent regions (given by arrows directions) indicate that the interdependences between two variables are not phase-locked, but fluctuating between states.

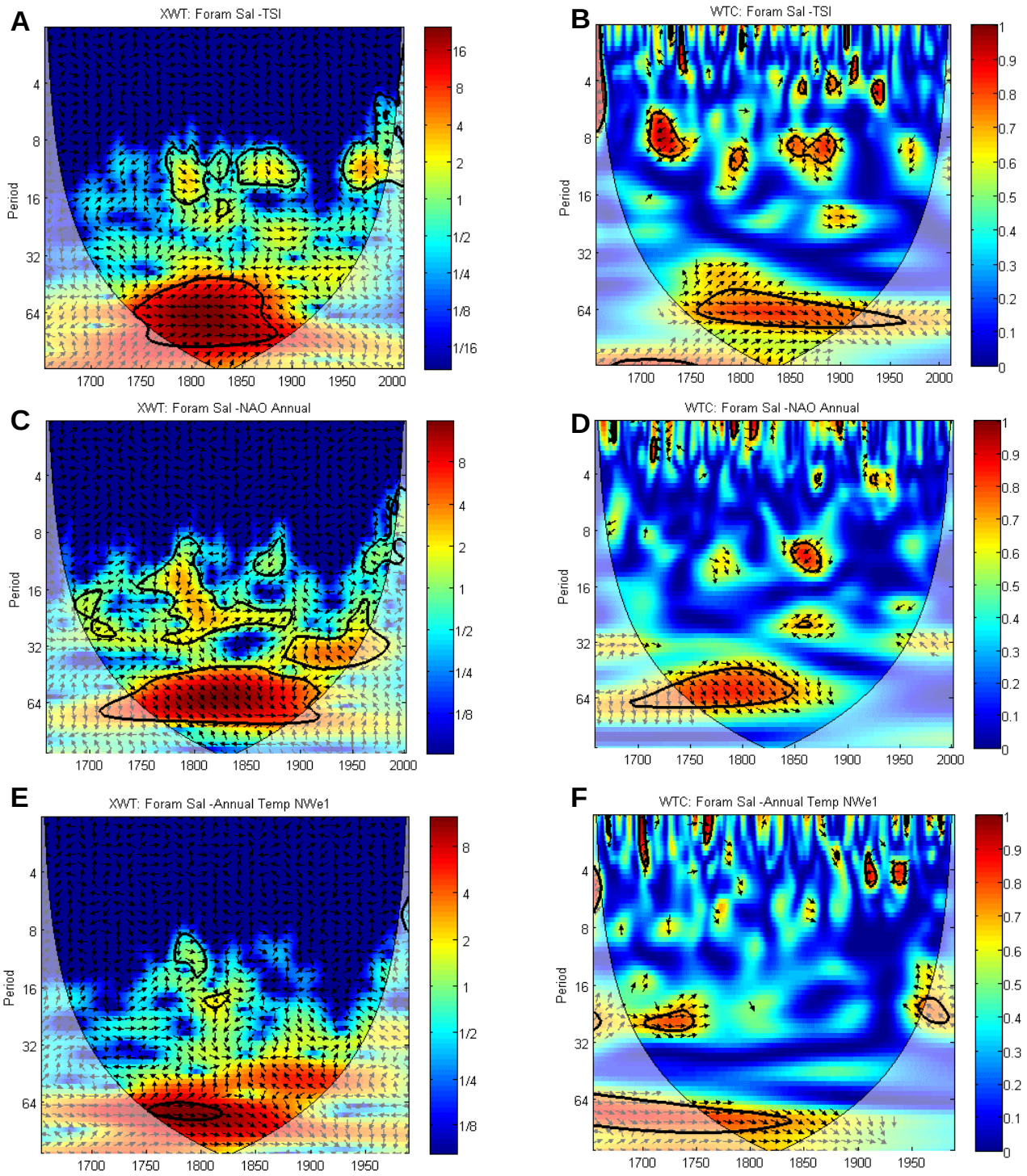

Figure 6.6. Results of the cross wavelet transform (XWT) and wavelet coherence (WTC). A) and B) Benthic foraminifera (*J. macrescens*, *T. inflata*, *T. comprimata*, *S. lobata* and *P. guaratibaensis)* (this work) *vs.* TSI (Krivova et al., 2010) for AD 1654–2010; C) and D) Benthic foraminifera *vs.* the NAO index (Luterbacher et al., 2002); E) and F) Benthic foraminifera *vs.* simulated annual temperature for NW IP (Gómez-Navarro et al., 2011, 2012). The color scale is proportional to the wavelet cross-correlation power. The black arrows indicate the relative phase relationship, with horizontal right-pointing arrows representing in-phase relationships and left-facing arrows denoting anti-phase; arrows pointing straight down indicate that the first series leads ahead the second by 90 degrees; arrows pointing vertically upward means the second series leads the first by 90 degrees. In all panels the black thick line is the 5% significance level using the red noise model. Shaded areas represent the cone of influence (COI) where edge effects may distort the results, so regions outside are discarded.

6.5. Discussion

6.5.1. Potential links between SA, climatic variables and proxies

The EDM region, reconstructed WP series starts and ends near two well-recognized periods of greatly reduced SA during the LIA: the Maunder Minimum (MM) and the Dalton Minimum (DM) (Figure 6.3). These Minima have distinct physical origin, occurring due to different features of the solar dynamo altogether (Duhau and de Jager, 2010). Thus, it may be assumed that this difference partially explains the magnitude of the reduced WP values on both Minima, significantly lower throughout the MM. Similarities between the overall WP long-term and variations in the three TSI oscillation components can be found (Figure 6.3A and C), which suggests a likely meaningful impact on WP. For instance, the WP3 period, with the highest WP (1750–1780), occurs when the semi-secular and secular component's amplitudes are clearly higher than the one of the decadal (~11-year) (Le and Wang, 2003). Wine abundance around 1780 is not a regional peculiarity as it was witnessed in France, Germany and Switzerland (Pfister, 1980). In particular, the 1773 WP maximum (Figure 6.3A) occurs during the common positive phase of the three TSI components, and following a reported maximum (*ca.* 1770) of the Gleissberg cycle (Figure 6.3C). This can indicate a direct SA influence on WP, with this responding to multi-decadal solar variability. Such assumption is reinforced by additional evidence, regarding new grapevines plantation (Figure 6.7). When survived, new vines may have taken up to 4–5 years to produce viable yields (Bindi et al., 1996), thus starting to affect WP amounts two triennia afterwards. Given missing information about acreages, these records help us to assess that the major WP fluctuations are not a straight result of planted areas, with new grapevines only affecting WP punctually (e.g., 1740–1743 and 1794 triennia).

The MM fits well the minimum values of the secular component, however other SA components still indicate variability (Figure 6.3C). In this context, it is interesting to note that WP records during the 1683 triennium match with the SA maximum in *ca.* 1680 on the bi-decadal (~22-year) cycle, and *ca.* 1684 on the ~11-year cycle, both detected in the ^{14}C production rate (Lundstedt et al., 2006). The latest was also detected by Vaquero et al. (2015) in reviewing Sunspot cyclic activity in the 1637–1715 period. This review suggests SA maxima of ~11-year cycles around 1639, 1655–1657, 1675, 1684 and 1705, and SA clustering in near 20-year intervals (1650–1670, 1670–1690 and 1690–1710). These studies indicate different levels of solar modulation throughout the MM to which grapevines may have reacted through productivity changes, ultimately leading to noticeable WP fluctuations. Despite the few records available in the EDM region at this period, our hypothesis finds support in the Swiss Plateau (1540–1820) wine yields series (Pfister, 1980), where a yield main positive persistent peak is observed between *ca.* 1675–1690.

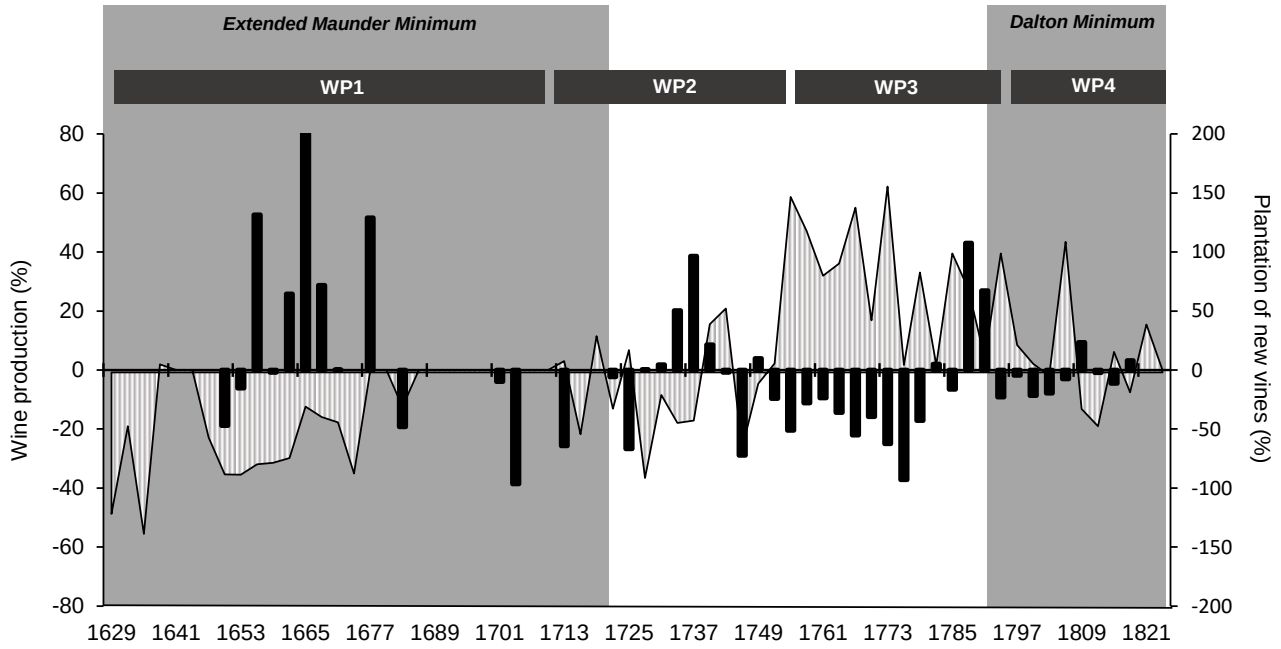

Figure 6.7. Wine production (WP) composite time series for six Benedictine monasteries from the Entre-Douro-e-Minho (EDM) region (line) and number of new planted vines (black bars). Time series represented as deviations of the mean (%), considering the Tibães, Rendufe, S.to Tirso (Casa/Passais), Pombeiro, Paço de Sousa and Palme monasteries (after Marques, 2011).

6.5.1.1. WP1 period (1626–1709 years): sun-climate impacts on WP and benthic foraminifera

The WP1 period covers the triennia between 1629 and 1710. During this time, WP mean values were just half of the production of the most productive period (WP3; 1755–1794; Figure 6.3A). This cannot be ascribed to the political status of the Benedictine Order, living in more auspicious years after the *Comendatários Crisis*, but rather to the LIA large climatic anomaly in Europe, particularly over the IP, resulting in frequently poor harvests (Oliveira, 1979; Font Tullot, 1988; Pfister and Brázdil, 1999). Furthermore, these lower WP values closely follow other adverse WP patterns in central Europe (Landsteiner, 1999), attributable to year-round variations in temperature and precipitation patterns. This had a significant social dimension (Pfister and Brázdil, 1999), besides being the cause of new cultural practices, namely the switch of wine to beer consumption, particularly due to critical wine years in the 1580s–1590s (Brázdil et al., 2008).

To assess the MM impact on WP1, we need to precisely constrain its timing. While Duhau and de Jager (2008) ascribe the MM (1645–1715; Eddy, 1976) to 1620-1715, Vaquero and Trigo (2015) suggested 1618–1723. Given these works, WP1 reflects right from its start the climatic conditions of the MM initial stages, included in the "Extended Maunder Minimum" (Vaquero and Trigo, 2015). Also Pfister (1980) referred to the 1618–1629 period as bad wine years preceding a wave of glacial activity after 1630, which falls within the MM "decay phase" (1618–1645; Vaquero and Trigo, 2015). A noticeable TSI reduction has occurred during the MM, with its absolute values well below the computed mean (1360.65 Wm^{-2}) for the 1724–1924 Regular Oscillations (Duhau and Martínez, 2012; Figure 6.3B). For these authors, SA is characterized by periods of Regular

Oscillations and Grand Episodes, to which the MM belongs. This decrease in TSI (available PAR) during the growing season, together with the consequent fluctuations in the global/regional temperature and precipitation annual/seasonal patterns (Moffa-Sánchez et al., 2014), forced decreased photosynthesis and then reduced harvests. The MM cooler-wetter and cloudy climatic setting (Soon and Yaskell, 2003) enhanced also the winter frosts, ill-timed rainfall, and fungal diseases risk usually linked to high humidity levels. Such broad adverse climatic patterns threatened the successful maturation of grapes, increasing the frequency of years with bad harvests and, subsequently, back-to-back crop failures as the MM progressed. In Portugal, a series of cold years, alternating from wet to dry, prevailed between 1640–1641 and 1665, which has continued from 1680 to at least 1712–1713, with some relaxation phases (Oliveira, 1979). The years of 1686 and 1693–1699 have been especially hard, regarding climatic patterns and agricultural outcomes, with reported subsistence crisis, followed by high prices, famines, epidemics and some conflicts in northern Portugal (Silva, 1859). A similar scenario is described by Le Roy Ladurie (1970) for France throughout the 1640s and 1690s. Also, in the 1640s seven barren years occurred in Bohemia, related mainly to damage by late spring frosts, similarly as in the 1660s in Moravia (Brázdil et al., 2008).

At this point, we can assume that the MM cumulative damage reached a climax for grapevine in the *terroir* of "Vinhos Verdes", coinciding with WP1 missing records. In fact, the two wine production gaps (WPG), registered simultaneously in all monasteries (WPG1: 1638–1643; WPG2: 1673–1709 except for the 1683 triennium), are well-matched with two phases of significantly low annual growing season temperatures (GST) in Europe / NW IP, identified in the modelled temperature simulation driven by variations in TSI (Figure 6.3D–E). In both periods, GST crossed down, almost uninterruptedly, the critical limit of 12ºC, considered as the lower temperature threshold for viticulture suitability (Jones et al., 2005). These GST were escorted by colder mid-summer patterns (Figure 6.3F), generally, largely responsible for WP fluctuations (Pfister, 1992).

The decline in the TSI (PAR range) absolute values (WPG1: mean 1360.5 ± 0.1 Wm^{-2}; WPG2: 1674–1679, mean 1360.1 ± 0.002 Wm^{-2} and 1683–1709, mean 1360.2 ± 0.004 Wm^{-2}) is simultaneous with a summer (and annual) precipitation increase in NW IP (Figure 6.3G), which could have had large negative implications, strongly reducing the photosynthetic ability of grapevines to provide a positive carbon balance and photoautotrophic growth. Moreover, an increase in summer precipitation is consistent with lower temperatures as an overall response to lower TSI during the LIA in NW IP (Gómez-Navarro et al., 2011, 2012). These authors indicated a summer precipitation increase for most of Iberia (up to 20%) during the MM in response to (lower) TSI, and a somewhat higher increase in winter precipitation for NW IP. The Caminha salt marsh foraminiferal record supports a precipitation increase in the studied area, which is reflected by the clear dominance of low-salinity marsh foraminiferal assemblages (FAZ III; Figure 6.4) in AD 1654–1725, in which *T. salsa/irregularis* prevails (87–52%; mean 66%). The current study refines the FAZs identified by

Moreno et al. (2014), specifying a concomitant change responsive to TSI oscillations. The wet patterns prevailed in the marsh area since the late 1300s, with WP1 matching with higher organic matter (OM) and bromine contents in its soils/sediments, representing rainy, colder conditions (Moreno et al., 2015). Geochemical data also evidenced a maximum of terrestrial OM contribution (De la Rosa et al., 2012), supporting an increased flux of continental runoff to the salt marsh.

The knowledge that grapevine canopy net photosynthesis is always light limited (Keller, 2015), supports reduced WP under those sun-climate coupled conditions. Therefore, the MM prevailing overcast weather (inferred from precipitation data), especially in the two WPGs (Figure 6.3F–G), can further deepened the typical radiative insufficiency for photosynthesis in grapevine. GST < 12ºC together with lower TSI likely disrupted the grapevine baseline climate, considered as the critical climatic conditions under which influence representative varietals are well-established (Irimia et al., 2014). Without the minimum thermal requirements, the planted varieties did not reach complete maturity, leading later on to WP breakdown and economic loss. This may have been quite dramatic within the “Vinhos Verdes” *terroir*, where, by that time, the vines were typically tall-trained vines (Figure 6.2), climbing by live tutors (trees) and reaching more than 4 m high. This viticultural design had major shortcomings, preventing the grapes full ripening (permanently shaded by the trees and their own leaves) and with vines absorbing much more humidity from surroundings (due to the greater number of stems) and therefore more prone to illnesses (Lobo, 1790).

Pfister (1980) reported a wine yield crisis at the Swiss Plateau near 1687 (“the barren 1690s”), when estimated mean annual temperatures dropped 2ºC below the 1901–1960 mean, together with a sudden increase in wetness. This partially coincides with the WPG2 in the EDM region, when summer temperatures in NW IP (*ca.* 1675–1710) concomitantly decreased with TSI (Gómez-Navarro et al., 2011, 2012). A 1670–1730 relatively cool period was recognized on reconstructed mean annual temperatures for the Lisbon region (Santos et al., 2015); this is also consistent with previous studies addressing the SA impact on global temperatures (Hoyt and Schatten, 1997).

Summarizing, a cold-wet WP1 period, reflecting a significant TSI decrease, affected the EDM region, with both proxies responding to the MM main climatic shifts, i.e., lower WP and higher abundance of low-salinity marsh benthic foraminiferal assemblages.

6.5.1.2. Historical events as potential drivers for the two WPGs in the WP1 period

We acknowledge that lack of data does not imply barren WP and that the historical contexts of the two data gaps (1638–1643 and 1673–1709) can help to better understand their origin.

The LIA deepest phase is recognized as a generalized crisis driven not only by climate, but also by a very instable socio-economic and political condition (the *General Crisis of the 17th Century*;

Parker, 2013). While some consider such a link highly controversial (Elliott, 2005), others see it as an example of cause-effect relationship (Zhang et al., 2011). The latter suggested that the cooling in 1560–1660 was in the origin of successive agro-ecological, socio-economic and demographic disasters, culminating in the major *17th Century Crisis*. In view of that, such a connection should also be investigated in the EDM region.

The WPG1 overlaps with two main events: (i) the popular insurrections occurring in northern Portugal (Viana do Castelo, 1636; Porto, 1638) that had indirect drawbacks on agricultural production (Oliveira, 2012), and (ii) the beginning of the Restauration War (1640–1668) between Portugal and Spain, when the turmoil caused by military recruitment, increased emigration and lack of skilled workers (exacerbated by overseas wars, mainly in west Africa) were at the origin of a severe decline in wine sector (Magalhães, 2010). Manpower shortage is a major cause for crop productivity loss in pre-industrial times, namely in the Early Modern period (Pfister, 2005). During WPG2, two historical sub-periods are noteworthy; (1) The agricultural production drop in northern Portugal after 1683, intensified during 1689–1691 and again at 1693–1694 (Oliveira, 1979). This condition extended until 1713 due to climate deterioration was aggravated by a coeval mortality crisis, largely affecting rural populations (Barbosa, 2001). In 1696, farmers from Lisbon surroundings stopped the work on vineyards due to the extreme dearth of this year and in previous years (Oliveira, 1979). This agricultural crisis post-1683 can be assessed by tithe proxy evidence (Figure 6.8). Tithes represented a tenth of the land production, and have been used to estimate the evolution of agricultural output at different time scales (Le Roy Ladurie and Goy, 1982). And (2), the 1704–1711 period, when Portugal was involved in the Spanish Succession War (1701–1714), with great instability, casualties and crops damage inflected by Franco-Spanish armies. Despite all these factors, harvests persisted, as expected in an ancient agrarian regime and during the WPG2 (1673–1709) the grain production although reduced, did not disappear from Tibães jurisdictions. While grapevine growth cycle does not necessarily mimic other crops (due to its own peculiarities responsible for WP short-term fluctuations), in exceptionally difficult years damage similarities can be observed (Oliveira, 1979). Thus, the two WPGs in the EDM region can illustrate how the MM stressful climatic baseline for WP (not fulfilling the minimum grapevine thermal requirements) has been worsened by different disruptive societal impacts, likely ending in collapse.

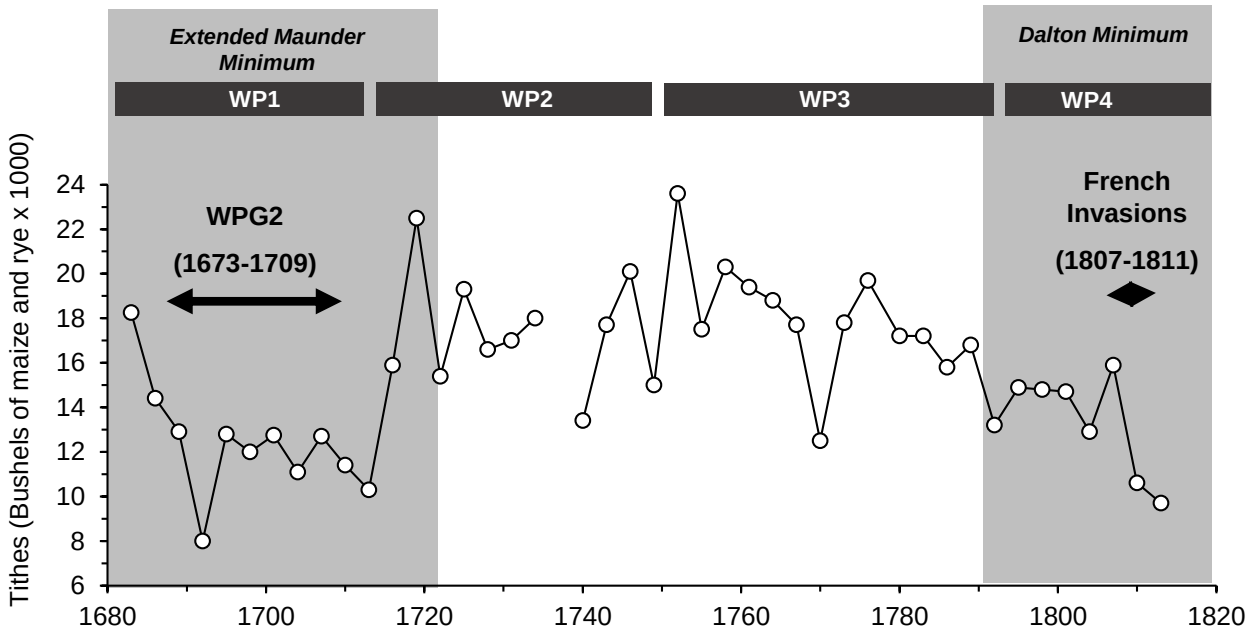

Figure 6.8. Triennial grain (maize and rye) tithe series from the Tibães parish churches from 1683 to 1813 (after Oliveira, 1979). WPG2 corresponds to the major gap on the Entre-Douro-e-Minho regional WP time series.

6.5.1.3. WP2 and WP3 periods (1713–1794 years)

The 1700–1723 period is a "recovery phase" within the MM, including two small amplitude ~11-year cycle, succeeding the ''Deep Maunder Minimum" (1645–1700; Vaquero and Trigo, 2015). The increasing SA, as recorded by the TSI reconstruction (Figure 6.3B), is mirrored in the EDM region by WP and foraminiferal records (Figures 6.3A and 6.4). The WP strengthening in the 1713 triennium (also observed in the Lisbon area; Oliveira, 1979) reproduce, in part, the light-temperature regime enhancement post-''Deep Maunder Minimum", with grapevine gradually profiting from the baseline climate restoration required for harvest stabilization. In addition to a TSI increase for photosynthesis, GST and mid-summer temperatures have risen in Europe and especially in NW IP (Figure 6.3D–E). This "standard" minimum requirement (GST) for wine grape production (Jones et al., 2005), has finally reached the 12ºC lower threshold by around 1700. This is perceived by the grapevine's "endogenous clock", triggering signalling cascades that finally influence plant's physiology (Keller, 2015). Also, the declining trend for summer precipitation in NW IP (Figure 6.3F) may have been positive for WP. This can be true given that wine yields in the modern MWR region are favoured by moderate water stress during growing season (Fraga et al., 2014) and many varietals in use nowadays were already cultivated at that time (CRVV, 2002). Such is supported by Tibães grain tithe series (Figure 6.8), upholding the synchronised reappearance of WP records by 1710 on all *Estados*, which we interpret as a signal of climate amelioration, and after a great increase in the Number of Active Days (days with sunspots reported on the solar disk) between 1700 and 1710 (Vaquero et al., 2015). The Number of Active Days is another SA index used by these authors to obtain an improved SA evolution report during the MM.

After 1713 a broad WP positive response to changing climate was also observed in several parts of Europe, followed by regional's ups and downs. For instance, Pfister (1980) indicated the overflow of wine between 1719 and 1729 from Lake Geneva to Rhineland, repeated around 1780. In the Czech Lands, Brázdil et al. (2008) reported good yields during the 1720s, although they also mentioned very bad ones particularly in 1757–1765. Labrousse (1944) refers to wine overproduction in northern France from 1778 to 1781 due to a sequence of hot years, which led to short-term price collapses and to a socio-economic crisis that he connected to the French Revolution (1789–1799). After 1784, WP decreased in the EDM region likely affected by several positive and negative rainfall extremes in continental Portugal in the 1780s (Alcoforado et al., 2012; Fragoso et al., 2015). Then a WP increase was recorded at the end of WP3, in the 1794 triennium, but most probably as a result of the plantation effort made in the 1788 triennium (Figure 6.7).

The Caminha high marsh foraminiferal assemblages also reacted to the climatic oscillations of the MM "recovery phase" although not steadily. An increment of the moderately brackish foraminiferal species around AD 1724, peaking AD 1751, was followed by a brackish-to-normal salinity species increase, with a maximum at AD 1790 (Figure 6.4). This shift towards higher salinity correlates with the modelled precipitation decrease and increase in summer temperature for NW IP (Figure 6.3F–G) that affected the marsh's hydrological balance, climatic conditions also reflected in the best triennia for WP (*ca.* 1755 to 1773). Furthermore, Abrantes et al. (2011), when studying two sediment cores recovered in the Portuguese inner continental shelf off Porto, described major changes in the North Atlantic Ocean circulation and upwelling-related conditions starting around 1730–1740. This transition was characterized by dry winters and coincided with a drought period that affected mainly the Atlantic sector of IP (Domínguez-Castro et al., 2010). The information provided by the Caminha foraminiferal record shows similarly a reasonable agreement with some SA key events reported by Duhau and de Jager (2010), who discussed the occurrence of a solar dynamo transition by *ca.* 1724. This was followed by a rapid decrease of the secular cycle's amplitude at the start of a Regular Episode, and again *ca.* 1788, when the semi-secular cycle was strong and positive, while the secular cycle continued in its weaker amplitude cycle, characteristic of a Regular Episode (Figure 6.3C).

6.5.1.4. WP4 (1795–1820 years) and the Dalton Minimum

WP4 is characterized by an overall WP declining trend that mimics the TSI decrease (Figure 6.3A–B). The only exception was the 1806 triennium, with remarkably higher WP values (Appendix 6.1). Such WP relative peak occurred after the TSI maximum (*ca.* 1360.58 Wm^{-2}; 1802–1803) in the solar cycle 5 (1798–1810), falling within the DM. While under the influence of new well-known SA minimum, WP shrinkage never reaches barren years as during the MM (Figure 6.3A). Is this an outcome of the DM not be a SA Grand Episode, as argued by Duhau and de Jager (2010)? More

than a TSI variation, Wagner and Zorita (2005) suggested that volcanic forcing was the main factor for the recorded temperature drop at global and regional scales, especially during the second half of the DM (1810–1830), while solar and atmospheric CO_2 variations were less important. More recently, Anet et al. (2014) concluded that an unusual (higher) volcanism could partially explain the cold period from 1809 onwards in different Northern Hemisphere temperature reconstructions, whereas lower temperatures remained after 1816 due to lower TSI values. Trigo et al. (2009) investigated the volcanic activity signal in IP during 1816, after the 1815 Mount Tambora eruption (one of the three known largest volcanic eruptions of the Holocene; Oppenheimer, 2003), and reported the detrimental effect that this cold and wet summer had on agricultural activity, seriously damaging production yields in IP. This major volcanic event could likewise had impacted the WP of the 1818 triennium, although not any direct reference to such connection has been found. Conversely, for Ruzmaikin and Feynman (2015), the DM is a case of a minimum in the secular Gleissberg cycle (see Figure 6.3C) which is coincidently associated, in combination with volcanic forcing, to severe weather extremes. Moreover, volcanism seems to have had an impact on precipitation patterns, leading to dryer winters and wetter summers over continental Europe up to 1–3 years after a volcanic eruption (Anet et al., 2014). Although our proxies cannot describe inter-annual climate variability, they reflect a response to the DM changing summer precipitation patterns (Figure 6.3F). In fact, the Caminha data display a clear double-step rise, one at AD 1796 by the dominance of moderate-brackish assemblages (mainly *H. wilberti* and *P. ipohalina*) and then at AD 1812 by the upsurge of low-salinity species (such as *T. salsa/irregularis* and *H. manilaensis*), mostly in the second half of the DM, indicative of more humid conditions enhancing continental runoff.

Throughout WP4, the Portuguese Benedictine Order life was deeply disturbed by the three French Invasions (1807–1808, 1809 and 1810–1811), with more detrimental effects on NW Portugal during 1809 (Marques, 2011). Then, several monasteries served as hospitals, to house soldiers, and a few, to organize armed resistance; some were attacked, occupied and robbed by French troops, with monks' killing (Araújo and Malheiro da Silva, 1985). In 1809, the Pombeiro monastery was burned by French troops in retreat to Spain. Despite the steeply WP reduction in the 1809 triennium and, even further, in the 1812 triennium, no barren years are identified throughout the DM (Figure 6.3A). According to Oliveira (1979), French Invasions cannot be considered the sole responsible for WP decline, with the first signs of a broader agricultural recession in Portugal becoming visible by around 1763–1764. The Tibães tithe series not only shows the farming's survival even in a war context (Figure 6.8), but also supports our assumption that climate have prevailed over societal impacts in the main Benedictines' viticultural achievements in the EDM region along the 1626–1820 period.

6.5.2. Cycles in paleoclimatic proxies and their relationship to SA

The two prominent cycles detected in WP and benthic foraminifera, ~13-years and ~60-years (Figures 6.5 and 6.6), also appear in the TSI dataset (Krivova et al., 2010) and correspond to the Schwabe (8–15-years) and Lower Gleissberg (50–80-years) bands, recognised by many authors in galactic cosmic rays (GCR) variations (McCracken et al., 2013) and in worldwide climatic (instrumental/proxy) series (Taricco et al., 2015).

While XWT analysis of WP *vs.* TSI evidences regions of high common power coinciding at the 95% confidence level on the Schwabe frequency band (not shown), this is not confirmed by WCT, indicating that they are not significantly locally correlated. This may occur because the grapevine response to TSI changes is a very dynamic (and non-linear) process, in which several phases, lasting from seconds to years, can be distinguished, leading to a novel homeostasis under the new (altered) conditions (Kosová et al., 2015). This lack of balanced co-variations at the quasi-decadal scale is also apparent in the foraminiferal wavelet coherence results, contrasting with the more regular and persistently observed ~60-year cycle (50–80-year band) (Figure 6.6A–F), which agrees with the stronger influence of external forcing on climate variability at lower-frequencies (Gómez-Navarro et al., 2012).

The shared periodicities at the Lower Gleissberg band, with a coherence coefficient of ≥ 0.7 (Figure 6.6B–6.6D–6.6F), can be analyzed in the context of the secular Gleissberg cycle being a complex characteristic of solar forcing with a bi-modal structure (i.e., involving two oscillation modes: 50–80-year and 90–140-year variations of the sunspot cycle), with reported evidence at high-latitudinal (Ogurtsov et al., 2015) and mid-latitudinal (Moffa-Sánchez et al., 2014) regions of the Northern Hemisphere. In these regions, the temporal structure (sign and amplitude) of the SA/GCR effects on troposphere pressure variations is closely related to the state of a stratospheric circumpolar cyclonic vortex (Veretenenko and Ogurtsov, 2014). They found that this vortex intensity reveals a clear ~60-year cycle affecting the evolution of the large-scale atmospheric circulation and the character of the SA/GCR effects (increased GCR flux at SA minima is accompanied by a strengthening of cyclogenesis at mid-latitudes), with positive NAO/AO (i.e., Arctic Oscillation) conditions connected with strong vortex conditions. Changes of the NAO under strong and weak vortex regimes then impact the mean latitudes of cyclone tracks (shifted to the north at the positive NAO), influencing temperature and precipitation/flood patterns over western and central Europe (Czymzik, et al. 2016).

Thus, a causal link between the NAO index and the temperature/precipitation regime affecting the Caminha tidal marsh hydrological balance provides a rationale for the pronounced ~60-year cycle is well pronounced in its foraminiferal records as well as why highly coherent near secular-scale co-variations are found in this paleoclimatic proxy within the studied period. As Figure 6.6 illustrates, foraminifera reveal maximum near secular-scale in phase correlations with (1) TSI,

appearing at *ca.*1750 and extending as far as *ca.* 1970 (with the last decades outside the cone of influence – COI), (2) the NAO index, from *ca.*1700 (outside the COI) to *ca.* 1850; after 1750 the arrows start to point right-down, indicating that the NAO shifts ahead, and (3) annual temperature starting before *ca.* 1650 (outside the COI) and persisting as much as *ca.* 1840. Such results, with foraminifera reproducing the near secular-scale regional climatic response to SA fluctuations, emphasize their skill as a paleoclimatic proxy. However, further research is warranted to consolidate the connections addressed here.

6.6. Conclusions

This study allowed to recognize encouraging solar forcing signals in two proxies (WP and benthic foraminifera) from the NW Portugal, considering the 1626–1820 period. A wide-scope assessment of the SA role in local and regional climate variability has been made, also including the historical socio-economic/political context of the large WP inter-decadal variability. The robustness of our results was impaired by proxies' resolution limitations, not allowing to fully explore the detected sun-climate coupled–WP/foraminifera relationships. However, the CWT approach confirmed prominent cyclicity in foraminifera, in connection with the Schwabe and Lower Gleissberg cycles. The former demonstrated more localized and intermittent coherent co-variations in contrast to the latter, showing more extended and stable spatiotemporal regions of coherent interdependence. This agrees with the insight of a differential sensitivity of terrestrial systems to SA changes, in the path of an adjustment to a new (non-) equilibrium state.

It is our expectation that the current analysis persuade others to re-examine their paleoclimatic sensitive archives in the search for more comprehensive signals of the SA–climate coupled system during this historical period in Europe and beyond.

Acknowledgments

This work was partly supported by IDL through the UID/GEO/50019/2013 program and is a contribution of the project WestLog (PTDC/CTE/105370/2008), both funded by the Portuguese Fundação para a Ciência e a Tecnologia (FCT). João Moreno benefits from a FCT PhD grant (SFRH/BD/ 87995/2012). R. Brázdil was supported by Grant Agency of the Czech Republic for the project no. 13-19831S. The authors would like to acknowledge to the proof-reader Carla Neves.

References

Abrantes, F., Rodrigues, T., Montanari, B., Santos, C., Witt, L., Lopes, C. and Voelker, A.H.L., 2011. Climate of the last millennium at the southern pole of the North Atlantic Oscillation: an inner-shelf sediment record of flooding and upwelling. Climate Research 48, 261–280.

Alcoforado, M.J., Vaquero, J.M., Trigo, R.M. and Taborda J.P., 2012. Early Portuguese meteorological measurements (18th century). Climate of the Past 8, 353–371.

Andersen, H.V., 1953. Two new species of *Haplophragmoides* from the Louisiana coast. Contributions from the Cushman Foundation for Foraminiferal Research 4, 21–22.

Anet, J.G., Muthers, S., Rozanov, E.V., Raible, C.C., Stenke, A., Shapiro, A.I., Brönnimann, S., Arfeuille, F., Brugnara, Y., Beer, J., Steinhilber, F., Schmutz, W. and Peter, T., 2014. Impact of solar *versus* volcanic activity variations on tropospheric temperatures and precipitation during the Dalton Minimum. Climate of the Past 10, 921–938.

Araújo, A.S. and Malheiro da Silva, A.B., 1985. Inventário do fundo monástico-conventual. Arquivo Distrital de Braga, Minho University, Braga, Portugal, 288p.

Barbosa, M.H.V., 2001. Crises de mortalidade em Portugal desde meados do século XVI até ao início do século XX. Monografias 10. Núcleo de Estudos de População e Sociedade Instituto de Ciências Sociais, Minho University, Guimarães, 78p.

Bindi, M., Fibbi, L., Gozzini, B., Orlandini, S. and Miglietta, F., 1996. Modelling the impact of future climate scenarios on yield and yield variability of grapevine. Climate Research 7, 213–224.

Brady, H.B., 1870. Analysis and descriptions of the Foraminifera. Annals and Magazine of Natural History 4, 273–309.

Brázdil, R., Zahradníček, P., Dobrovolný, P., Kotyza, O. and Valášek, H., 2008. Historical and recent viticulture as a source of climatological knowledge in the Czech Republic. Geografie 113, 351–371.

Brönnimann, P., 1986. Paratrochammina (Lepidoparatrochammina) guaratibaensis n. sp. from Brackish Waters of Brazil and a Check List of Recent Trochamminaceans from Brackish Waters (Protista: Foraminiferida). Revue Paléobiologie 5, 221–229.

Cook, E.R., Briffa, K.R. and Jones, P.D, 1994. Spatial regression methods in dendroclimatology: a review and comparison of two techniques. International Journal of Climatology 14, 379–402.

CRVV, 2002. Catálogo de Marcas da Região dos Vinhos Verdes. A Região Demarcada dos Vinhos Verdes - Um Século de História. Comissão de Viticultura da Região dos Vinhos Verdes, 72p.

Cushman, J.A. and Brönnimann, P., 1948. Some new genera and species of foraminifera from brackish water of Trinidad. Contributions from the Cushman Laboratory for Foraminiferal Research 24, 15–21.

Czymzik, M., Muscheler, R. and Brauer, A., 2016. Solar modulation of flood frequency in central Europe during spring and summer on interannual to multi-centennial timescales. Climate of the Past 12, 799–805.

de Jager, C. and Duhau, S., 2012. Sudden transitions and grand variations in the solar dynamo. Journal of Space Weather and Space Climate A07-8p.

De la Rosa, J.M., Araújo, M.F., González-Pérez, J.A., González-Vila, F.J., Soares, A.M., Martins, J.M., Leorri, E., Corbett, R. and Fatela, F., 2012. Organic matter sources for tidal marsh sediment over the past two millennia in the Minho River estuary (NW Iberian Peninsula). Organic Geochemistry 53, 16–24.

Debret, M., Bout-Roumazeilles, V., Grousset, F., Desmet, M., McManus, J.F., Massei, N., Sebag, D., Petit, J.-R., Copard, Y. and Trentesaux, A., 2007. The origin of the 1500-year climate cycles in Holocene North-Atlantic records. Climate of the Past 3, 569–575.

Dias, G.J.A.C., 2011. Quando os monges eram uma civilização. Edições Afrontamento, 333p.

Domínguez-Castro, F., García-Herrera, R., Ribera, P. and Barriendos, M., 2010. A shift in the spatial pattern of Iberian droughts during the 17th century. Climate of the Past 6, 553−563.

Duhau, S., and de Jager, C., 2008. The solar dynamo and its phase transitions during the last millennium, Solar Physics 250, 1–15.

Duhau, S., and de Jager, C., 2010. The forthcoming Grand Minimum of solar activity. Journal of Cosmology 8, 1983–1999.

Duhau, S. and Martínez, E.A., 2012. Solar dynamo transitions as drivers of sudden climate changes. INTECH, pp. 185–204.

Eddy, J.A., 1976. The Maunder Minimum. Science 192, 1189–1202.

Elliott, J.H., 2005. The general crisis in retrospect: a debate without end. In P. Benedict and M. P. Gutmann (Eds). Early Modern Europe: from crisis to stability. Newark, University of Delaware Press, pp. 31–51.

Fatela, F., Moreno, J., Leorri, E. and Corbett, R., 2014. High marsh foraminiferal assemblage's response to intra-decadal and multi-decadal precipitation variability, between 1934 and 2010 (Caminha, NW Portugal). Journal of Sea Research 93, 118–132.

Font Tullot, I., 1988. Historia del Clima de España. Madrid: Spanish Meteorological Institute (INM), 297p.

Fragoso, M., Marques, D., Santos, J.A., Alcoforado, M.J., Amorim, I., Garcia, J.C., Silva, L. and Nunes, M.F., 2015. Climatic extremes in Portugal in the 1780s based on documentary and instrumental records. Climate Research 66, 141–159.

Fraga, H., Malheiro, A.C., Moutinho-Pereira, J. and Santos, J.A., 2012. An overview of climate change impacts on European viticulture. Food Energy Security 1, 94–110.

Fraga, H., Malheiro, A.C., Moutinho-Pereira, J. and Santos, J.A., 2014. Climate factors driving wine production in the Portuguese Minho region. Agricultural and Forest Meteorology 185, 26–36.

Gómez-Navarro, J.J., Montávez, J.P., Jerez, S., Jiménez-Guerrero, P., Lorente-Plazas, R., González-Rouco, J.F. and Zorita, E., 2011. A regional climate simulation over the Iberian Peninsula for the last millennium. Climate of the Past 7, 451–472.

Gómez-Navarro, J.J., Montávez, J.P., Jiménez-Guerrero, P., Jerez, S., Lorente-Plazas, R., González-Rouco, J.F. and Zorita, E., 2012. Internal and external variability in regional simulations of the Iberian Peninsula climate over the last millennium. Climate of the Past 8, 25–36.

Grinsted, A., Moore, J.C., Jevrejeva, S., 2004. Application of the cross wavelet transform and wavelet coherence to geophysical time series. Nonlinear Processes in Geophysics 11, 561–566.

Hammer, Ø., 2012. PAST PAleontological STatistics Version 2.17, Reference manual. Natural History Museum University of Oslo, 229p.

Haslett, J. and Parnell, A., 2008. A simple monotone process with application to radiocarbon dated depth chronologies. Applied Statistics 57, 399–418.

Hayward, B.W., Grenfell, H.R., Reid, C.M. and Hayward, K.A., 1999. Recent New Zealand shallow-water benthic foraminifera: Taxonomy, Ecologic Distribution, Biogeography, and Use in Paleoenvironmental Assessments. Institute of Geological & Nuclear Sciences Monograph, vol. 21. Lower Hutt, New Zealand, 170p.

Hoyt, D.V. and Schatten, K.H., 1997. The Role of the Sun in Climate Change. Oxford University Press, New York, 279p.

Irimia, L.M., Patriche, C.V., Quénol, H., Planchon, O. and Sfâcă, L. 2014. Characteristics of the baseline climate of the Cotnari (Romania) wine growing region. Cercetări Agronomice în Moldova XLVII, 99–111.

Jones, G.V., White, M.A., Cooper, O.R. and Storchmann, K., 2005. Climate change and global wine quality. Climatic Change 73, 319–343.

Jones, G.V., Reid, R. and Vilks, A., 2012. Climate, grapes, and wine: structure and suitability in a variable and changing climate. In: The Geography of Wine. Regions, Terroir and Techniques, P.H. Dougherty (Ed.), Springer, pp. 109–133.

Jones, G.V., 2014. Climate, terroir and wine: what matters most in producing a great wine? EARTH 59, 36–43.

Keller, M., 2015. The science of grapevines. Anatomy and physiology. 2nd edition, Academic Press, 509p.

Kosová, K., Vítámvás, P., Urban, M.O., Klíma, M., Roy, A. and Prášil, I.T., 2015. Biological networks underlying abiotic stress tolerance in temperate crops. A proteomic perspective. International Journal of Molecular Sciences 16, 20,913–20,942.

Krivova, N.A., Vieira, L.E.A. and Solanki, S.K., 2010. Reconstruction of solar spectral irradiance since the Maunder Minimum. Journal of Geophysical Research: Space Physics 115, A12112.

Kutner, M.H., Nachtsheim, C.J., Neter, J. and Li, W., 2005. Applied Linear Statistical Models. McGraw-Hill, 5th edition, 1396p.

Labrousse, E., 1944. La crise de L'Économie Française ŕ la fin de L'Ancien Régime et au début de la Révolution. Tome I, Aperçus Généraux, Méthode, Objectifs. La Crise de la Viticulture, Presses Universitaires de France, Paris 664p.

Landsteiner, E., 1999. The crisis of wine production in late sixteenth-century central Europe: climatic causes and economic consequences. Climatic Change 43, 323–334.

Le, G.-M. and Wang, J.-L., 2003. Wavelet analysis of several important periodic properties in the relative sunspot numbers. Chinese Journal of Astronomy and Astrophysics 3, 391–394.

Le Roy Ladurie, E., 1967. Histoire du Climat Depuis l'an Mil. Flammarian, Paris, 381p.

Le Roy Ladurie, E., 1970. Pour une Histoire de L'environnement: la part du climat. In: Annales. Économies, Sociétés, Civilisations 5, 1459–1470.

Le Roy Ladurie, E. and Goy, J., 1982. Tithe and Agrarian History from the Fourteenth to the Nineteenth Centuries. An essay in comparative history. Cambridge University Press, 206p.

Lima da Silva, A., Hariscain, P., Ollatz, N. and Doazanz, J.P., 1996. Evaluation of the photoautotrophic ability of *Vitis* plantlets (rootstock var. Gravesac): set-up of a special open flow gas exchange system. Vitis 35, 73–78.

Lobo, C.B.L., 1790. Sobre a cultura das vinhas de Portugal. In: Memórias Económicas da Academia Real das Ciências de Lisboa, Tomo II, Lisboa, pp. 16–72.

Lobell, D.B., Field, C.B., Cahill, K.N. and Bonfils, C., 2006. Impacts of future climate change on California perennial crop yields: Model projections with climate and crop uncertainties. Agricultural and Forest Meteorology 141, 208–218.

Lundstedt, H., Liszka, L., Lundin, R. and Muscheler, R., 2006. Long-term solar activity explored with wavelet methods. Annales Geophysicae 24, 769–778.

Luterbacher, J., Xoplaki, E., Dietrich, D., Jones, P.D., Davies, T.D., Portis, D., Gonzalez-Rouco, J.F., von Storch, H., Gyalistras, D., Casty, C. and Wanner, H., 2002. Extending North Atlantic Oscillation reconstructions back to 1500. Atmospheric Science Letters 2, 114–124.

Luterbacher, J., Dietrich, D., Xoplaki, E., Grosjean, M. and Wanner, H., 2006. European Seasonal Temperature Reconstructions. IGBP PAGES/World Data Center for Paleoclimatology Data Contribution Series # 2006-060.NOAA/NCDC Paleoclimatology Program, Boulder CO, USA.

Magalhães, J.R., 2010. Do tempo e dos trabalhos: a agricultura portuguesa no século XVII. Revista Portuguesa de História 41, 59–72.

Marques, G.N.R.M., 2011. Do vinho de Deus ao vinho dos Homens: o vinho, os Mosteiros e o Entre Douro e Minho. Dissertação de Doutoramento em História apresentada à Faculdade de Letras do Porto. Porto: FLUP. 524p.

McCracken, K.G., Beer, J., Steinhilber, F. and Abreu, J., 2013. A phenomenological study of the cosmic ray variations over the past 9400 years, and their implications regarding solar activity and the solar dynamo. Solar Physics 286, 609–627.

Moffa-Sánchez, P., Born, A., Hall, I.R., Thornalley, D.J.R. and Barker, S., 2014. Solar forcing of North Atlantic surface temperature and salinity over the past millennium. Nature Geoscience 7, 275–278.

Montagu, G., 1808. Testacea Brittanica supplement, S. Woolmer, Exeter, England, 183p.

Moreno, J., Fatela, F., Leorri, E., De la Rosa, J., Pereira, I., Araújo, M.F., Freitas, M.C., Corbett, R. and Medeiros, A., 2014. Marsh benthic foraminifera response to estuarine hydrological balance driven by climate variability over the last 2000 years (Minho estuary, NW Portugal). Quaternary Research 82, 318–330.

Moreno, J., Fatela, F., Leorri, E., Araújo, M.F., Moreno, F., De la Rosa, J., Freitas, M.C., Valente, T. and Corbett, D.R., 2015. Bromine enrichment in marsh sediments as a marker of environmental changes driven by Grand Solar Minima and anthropogenic activity (Caminha, NW of Portugal). Science of the Total Environment 506–507, 554–566.

Moreno, J., Fatela, F., Moreno, F., Leorri, E., Taborda, R. and Trigo, R., 2016. Grape harvest dates as indicator of spring-summer mean maxima temperature variations in the Minho region (NW of Portugal) since the 19th century. Global and Planetary Change 141, 39–53.

Možný, M., Brázdil, R., Dobrovolný, P., Trnka, M., 2016. April–August temperatures in the Czech Lands, 1499–2015, reconstructed from grape-harvest dates. Climate of the Past 12, 1421–1434.

Murray, J.W., 2006. Ecology and Applications of Benthic Foraminifera. Cambridge University Press, Cambridge, UK, 426p.

Oliveira, A., 1979. A Abadia de Tibães (1630–1813): Propriedade e Exploração Agrícola no Vale do Cávado no Antigo Regime. PhD Thesis, Porto University, Porto, FLUP. Vol. 2, 798p.

Oliveira, A., 2012. Vinhos em Portugal antes das regiões demarcadas. ROTUR/Revista de Ocio Y Turismo 5, 161–178.

Oppenheimer, C., 2003. Climatic, environmental and human consequences of the largest known historic eruption: Tambora volcano (Indonesia) 1815. Progress in Physical Geography 27, 230–259.

Ogurtsov, M.G., Lindholm, M., Jalkanen, R. and Veretenenko, S., 2015. Evidence for the Gleissberg solar cycle at the high-latitudes of the Northern Hemisphere. Advances in Space Research 55, 1285–1290.

Parker, G., 2013. Global Crisis. War, Climate Change and Catastrophe in the Seventeenth Century. Yale University Press, New Haven and London, 871p.

Parnell, A., Haslett, J., Allen, J., Buck, C. and Huntley, B., 2008. A flexible approach to assessing synchroneity of past events using Bayesian reconstruction of sedimentation history. Quaternary Science Reviews 27, 1872–1885.

Pfister, C., 1980. The Little Ice Age: Thermal and wetness indices for Central Europe. The Journal of Interdisciplinary History 10, 665–696.

Pfister, C., 1992. Monthly temperature and precipitation in central Europe 1525-1979: quantifying documentary evidence on weather and its effects. In: Bradley, R.S. and Jones, P.D. (Eds.), Climate since A.D. 1500. Routledge London, pp. 118–142.

Pfister, C., 2005. Weeping in the Snow. The Second Period of Little Ice Age-type Impacts, 1570–1630. In: Behringer, W., Lehmann, H. and Pfister, C. (Eds.), Cultural Consequences of the “Little Ice Age”. Vandenhoeck & Ruprecht, Göttingen, pp. 31–86.

Pfister, C. and Brázdil, R., 1999. Climatic variability in sixteenth-century Europe and its social dimension: a synthesis. Climatic Change 43, 5–53.

Phleger, F.B., 1970. Foraminiferal populations and marine marsh processes. Limnology and Oceanography 15, 522–534.

Ruzmaikin, A. and Feynman, J., 2015. The Earth’s climate at minima of centennial Gleissberg cycles. Advances in Space Research 56, 1590–1599.

Santos, J.A., Malheiro, A., Karremann, M. and Pinto, J., 2011. Statistical modelling of grapevine yield in the Porto Wine region under present and future climate conditions. International Journal of Biometeorology 55, 119–131.

Santos, J.A., Carneiro, M.F., Correia, A., Alcoforado, M.J., Zorita, E. and Gómez-Navarro, J.J., 2015. New insights into the reconstructed temperature in Portugal over the last 400 years. Climate of the Past 11, 825–834.

Saunders, J.B., 1957. *Trochamminidae* and certain *Lituolidae* (Foraminifera) from the recent brackish-water sediments of Trinidad, British West Indies. Smithsonian Miscellaneous Collection 134, 1–23.

Schulz, M. and Mudelsee, M., 2002. REDFIT: estimating red-noise spectra directly from unevenly spaced paleoclimatic time series. Computers & Geosciences 28, 421–426.

Scott, D.B., 1976. Brackish-water foraminifera from Southern California and description of *Polysaccammina ipohalina* n. Gen., n. sp. Journal of Foraminiferal Research 6, 312–321.

Scott, D.B. and Medioli, F.S., 1980. Quantitative studies of marsh foraminiferal distributions in Nova Scotia: implications for sea level studies. Special Publication - Cushman Foundation for Foraminiferal Research 17, 58p.

Silva, J.J.A., 1859. Collecção Chronologica da Legislação Portugueza compilada e anotada. Collecção de Legislação Portuguesa (1683-1700). Vol. 10, Imprensa Nacional, Lisboa, 515p.

Silva, C.M.T., 1993. O Mosteiro de Ganfei. Propriedade, produção e rendas no Antigo Regime (1629-1683 e 1716-1822). Dissertação de Mestrado em História Moderna apresentada ŕ Faculdade de Letras do Porto. Porto, FLUP, 284p.

Soon, W. W.-H. and Yaskell, S.H., 2003. The Maunder Minimum and the Variable Sun-Earth Connection. World Scientific, Singapore, 278p.

Taricco, C., Mancuso, S., Ljungqvist, F.C., Alessio, S. and Ghil, M., 2015. Multispectral analysis of Northern Hemisphere temperature records over the last five millennia. Climate Dynamics 45, 83–104.

Trigo, R.M., Vaquero, J.M., Alcoforado, M.J., Barriendos, M., Taborda, J., García-Herrera, R., and Luterbacher, J., 2009. Iberia in 1816, the year without a summer. International Journal of Climatology 29, 99–115.

Vaquero, J.M., Kovaltsov, G.A., Usoskin, I.G., Carrasco, V.M.S. and Gallego, M.C., 2015. Level and length of cyclic solar activity during the Maunder minimum as deduced from the active day statistics. Astronomy & Astrophysics 577, A71-6p.

Vaquero, J.M. and Trigo, R.M., 2015. Redefining the limit dates for the Maunder Minimum. New Astronomy 34, 120–122.

Veretenenko, S. and Ogurtsov, M., 2014. Stratospheric polar vortex as a possible reason for temporal variations of solar activity and galactic cosmic ray effects on the lower atmosphere circulation. Advances in Space Research 54, 2467–2477.

Wagner, S. and Zorita, E., 2005. The influence of volcanic, solar and CO_2 forcing on the temperatures in the Dalton Minimum (1790–1830): a model study. Climate Dynamics 25, 205–218.

Xoplaki, E., Luterbacher, J., Paeth, H., Dietrich, D., Steiner, N., Grosjean, M. and Wanner, H., 2005. European spring and autumn temperature variability and change of extremes over the last half millennium. Geophysical Research Letters 32, L15713-4p.

Yeo, K.L., Krivova, N.A., Solanki, S.K. and Glassmeier, K.H., 2014. Reconstruction of total and spectral solar irradiance from 1974 to 2013 based on KPVT, SoHO/MDI, and SDO/HMI observations. Astronomy & Astrophysics 570, A85-18p.

Zhang, D.D., Lee, H.F., Wang, C., Li, B., Pei, Q., Zhang, J. and An, Y., 2011. The causality analysis of climate change and large-scale human crisis. Proceedings of the National Academy of Sciences 108, 17,296–17,301.

lasp.colorado.edu/lisird/tsi/historical_tsi.html
ftp://ftp.ncdc.noaa.gov/pub/data/paleo/historical/europe-seasonal.txt
https://climexp.knmi.nl
http://www.pol.ac.uk/home/research/waveletcoherence/
http://www.atmos.ucla.edu/tcd/ssa/

Appendix 6.1. Benedictine wine production in litres (bold- reconstructed values).

Triennia	Sto. Tirso Casa	Paço_de_Sousa	Sto. Tirso Passais	Pombeiro	Tibães	Palme	Rendufe	Total Wine Production
1629	32292	6120	**4691**	15660	**20826**	**7574**	**5578**	92741
1632	58860	3564	**23033**	8082	**38106**	**10744**	**4002**	146391
1635	**30999**	4374	**3798**	**9559**	**19985**	**7420**	**4309**	80438
1638	69120	5400	**30116**	17100	**44780**	**11968**	**5878**	184361
1647	57645	5040	**22194**	3600	**37316**	**10599**	**3069**	139463
1650	44766	8100	**13303**	8640	**28939**	**9062**	**4118**	116928
1653	44235	**7927**	**12936**	9684	**28594**	**8999**	**4335**	116710
1656	45000	5850	**13464**	15210	**29092**	**9090**	**5484**	123190
1659	45576	7380	**13862**	13500	**29466**	**9159**	**5129**	124072
1662	47916	5940	**15477**	12240	**30988**	**9438**	**4867**	126866
1665	56448	7092	**21368**	**20167**	**36538**	**10456**	**6515**	158583
1668	51480	9476	20700	**18096**	**35909**	**10341**	**6085**	152086
1671	48222	**8779**	14400	29700	**29973**	**9252**	**8499**	148825
1674	**42444**	**7544**	11700	**14329**	**27430**	**8785**	**5301**	117534
1683	55260	**10284**	**20547**	**19672**	**35765**	**10314**	**6412**	158255
1713	64098	**12173**	**26649**	**23355**	**41513**	**11369**	**7179**	186337
1716	53316	**9868**	**19205**	10080	**34501**	**10082**	**4417**	141470
1719	68940	**13209**	**29992**	**25374**	**44663**	**11947**	**7599**	201722
1722	57006	**10657**	**21753**	14400	**36901**	**10523**	5922	157161
1725	67176	**12831**	**28774**	22140	**43515**	**11736**	7020	193193
1728	39654	**6948**	**9773**	19440	**25615**	**8452**	4788	114670
1731	58608	**11000**	**22859**	19206	**37943**	**10714**	5301	165630
1734	62478	**11827**	15012	17100	**30550**	**9358**	2106	148431
1737	52668	**9730**	**18758**	**18591**	**34079**	**10005**	**6188**	150019
1740	75510	**14613**	34506	16920	**48915**	**12727**	**5840**	209031
1743	86724	**17010**	28080	24840	**42861**	**11616**	**7488**	218620
1746	45216	**8137**	11880	23238	**27599**	**8816**	8244	133130
1749	**61373**	10818	**24768**	**22220**	**39741**	**11044**	2594	172569
1752	69840	14841	25758	**25749**	34560	8370	5760	184878
1755	94482	17010	50400	33696	68760	14868	7920	287136
1758	86922	18540	42840	31680	61920	**15112**	9000	266014
1761	80802	15894	36720	38700	51282	8820	6480	238698
1764	90144	13923	46080	**34212**	41400	13788	6606	246153
1767	90162	17631	46080	43560	59760	13338	9900	280431
1770	80802	13554	36720	26280	37656	**10661**	5760	211433
1773	90882	18216	48600	**34520**	72180	20196	8820	293414
1776	65952	7200	31086	27684	32760	10098	9180	183960
1779	86094	13680	39600	38466	39240	13050	10548	240678
1782	59346	8100	24480	31950	39960	11160	9000	183996
1785	70290	16920	35604	38700	60120	19800	10980	252414
1788	68706	14040	33840	29124	60120	15300	9360	230490
1791	69966	**13428**	22500	24300	43200	7596	7038	188028
1794	72810	**14036**	37944	33318	66600	12672	15084	252464
1797	67086	16866	32220	18000	39600	12600	9900	196272
1800	63450	12222	28584	29520	31284	10620	9000	184680
1803	53946	14004	19260	28269	44244	10800	6894	177417
1806	76842	15768	41976	29520	65880	**15839**	13788	259613
1809	53586	9900	18630	16200	40320	12420	5940	156996
1812	54360	9198	19494	19800	30528	7866	5292	146538
1815	63306	17280	28440	19566	**43201**	11880	8388	192061
1818	56898	11484	**21678**	**20354**	**36830**	11520	8460	167225
1821	62946	14706	28080	35640	**42861**	**11616**	12960	208810

Appendix 6.2. Percentage distribution of benthic foraminifera in core FCPwAR1. Age (yr AD) – age in calendar years AD; Salt marsh spp. – distributions of the group of low-salinity benthic species – Low Salinity spp.; – distribution of the group of moderate-brackish benthic species; Mod. Brackish spp. – distribution of the group of brackish-to-normal salinity benthic species; Brackish to Normal Salinity spp.; – distribution of the group of brackish-to-normal salinity benthic species plus the group of moderate-brackish benthic species; Mod. Brackish+Brackish-to-normal Salinity spp.

Age (yr AD)	*Paratr* spp.	*Troch* spp.	*H. manilaensis*	*T. salsa*	*M. fusca*	*J. macrescens*	*T. inflata*	*P. limnetis*	*H. wilberti*	*T. comprimata*	*S. lobata*	*P. guaratibaensis*	*P. ipohalina*	*Miliammina. spp.*	Low Salinity spp.	Mod. Brackish spp.	Brackish to Normal Salinity spp.	Mod. Brackish+Brackish to Normal Salinity ssp.
1824			1.5	18.5	0.7	14.1	8.1		34.8	5.9	5.9	1.5	4.4		20.7	39.3	35.6	74.8
1819	3.9		31.0	20.9		12.4	3.1		3.9		0.8		13.2		51.9	17.1	20.2	37.2
1812			29.2	30.8			2.5		4.2		0.8	2.5	18.3	0.8	60.8	22.5	5.8	28.3
1805			2.5	19.7		18.9	1.6		41.8		2.5	0.8	4.9		22.1	46.7	23.8	70.5
1801			2.2	18.8		24.6	1.4		30.4	1.4	5.8	1.4	8.7		21.0	39.1	34.8	73.9
1796			0.7	23.9		14.9	3.0		38.8	2.2	3.7	0.0	5.2		24.6	44.0	23.9	67.9
1789			2.2	13.4		31.3	1.5		26.9	4.5	6.7	0.0	6.0		15.7	32.8	44.0	76.9
1783			0.8	27.3		23.5			38.6		5.3	2.3	1.5		28.0	40.2	31.1	71.2
1778			1.5	16.1		17.5	2.2		37.2	3.6	8.0	2.2	5.8		17.5	43.1	33.6	76.6
1774			2.3	22.3		22.3			34.6	2.3	3.1	3.1	3.8		24.6	38.5	30.8	69.2
1767			5.6	24.5	1.4	11.2			34.3	4.2	2.8	4.9	4.9	1.4	32.9	39.2	23.1	62.2
1761			8.0	32.1		2.2			29.9	8.0	4.4	9.5			40.1	29.9	24.1	54.0
1756			2.7	20.9	1.8				49.1	6.4		2.7		8.2	33.6	49.1	9.1	58.2
1751		2.4	3.1	22.0	2.4				62.2	2.4	0.8	1.6			27.6	62.2	7.1	69.3
1745	5.3		3.8	19.1	3.1	1.5			61.1	2.3	0.8				26.0	61.1	9.9	71.0
1738	2.2		4.4	25.2	2.2	2.2			49.6	2.2		5.2	1.5		31.9	51.1	11.9	63.0
1733	2.3		4.5	34.6			0.8		48.9	1.5	2.3		0.8	0.8	39.8	49.6	6.8	56.4
1729	1.6		4.1	52.8					31.7				3.3	1.6	58.5	35.0	1.6	36.6
1725	0.0		3.6	59.3					24.3	1.4		5.0	3.6	0.7	63.6	27.9	6.4	34.3
1720	1.5		4.5	66.7	0.8				18.2	2.3		1.5	2.3		72.0	20.5	5.3	25.8
1714	3.8		10.0	62.3	0.8				10.8	3.1			4.6		73.1	15.4	6.9	22.3
1707	1.4	3.5	11.3	55.6	1.4				15.5	2.1		6.3	0.7		68.3	16.2	13.4	29.6
1703	7.7	1.4	7.0	62.2					16.8	2.1			2.1		69.2	18.9	11.2	30.1
1698	1.4	0.7	10.1	60.4	1.4				14.4	0.7			5.0	1.4	73.4	19.4	2.9	22.3
1692		2.8	12.5	52.1	2.1				12.5			7.6	6.3		66.7	18.8	10.4	29.2
1685		5.3	5.3	71.2					10.6			1.5	1.5	1.5	78.0	12.1	6.8	18.9
1681	1.5		11.9	69.4	0.7				8.2				2.2	0.7	82.8	10.4	1.5	11.9
1677		0.8	9.0	65.4	3.8				10.5	2.3		0.8	2.3	1.5	79.7	12.8	3.8	16.5
1670	5.0		3.4	86.6	0.8				2.5				0.8		90.8	3.4	5.0	8.4
1663	0.8		4.8	74.6					5.6				8.7	1.6	81.0	14.3	0.8	15.1
1654	1.4		13.5	66.0	2.8				1.4			3.5	2.1	5.7	87.9	3.5	5.0	8.5

7 Marsh benthic Foraminifera response to estuarine hydrological balance driven by climate variability over the last 2000 yr (Minho estuary, NW Portugal)

João Moreno [a,*], Francisco Fatela [a], Eduardo Leorri [b], José M. De la Rosa [c], Inês Pereira [d,1], M. Fátima Araújo, M. Conceição Freitas [a], D. Reide Corbett [b], Ana Medeiros [d]

[a] Universidade de Lisboa, Faculdade de Ciências, Centro de Geologia, Departamento de Geologia, Campo Grande, 1749-016 Lisboa, Portugal

[b] East Carolina University, Department of Geological Sciences, Greenville, NC 27858-4353, USA

[c] Instituto de Recursos Naturales y Agrobiología de Sevilla, Av. Reina Mercedes 10, 41012 Sevilla, Spain

[d] Universidade de Lisboa, Instituto Superior Técnico, Centro de Ciências e Tecnologias Nucleares, Estrada Nacional 10, km 139,7, 2695-066 Bobadela LRS, Portugal

Published in: Quaternary Research 82 (2014) 318–330

http://dx.doi.org/10.1016/j.yqres.2014.04.014

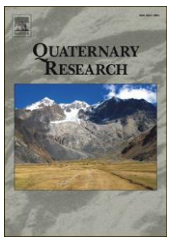

"Fossil foraminiferal faunas can provide assessments, at varying levels of accuracy, of a number of paleoenvironmental factors of value to geological, paleoclimatic and paleoceanographic studies."

B. W. Hayward, H R. Grenfell, C. M. Reid and K. A. Hayward in RECENT NEW ZEALAND SHALLOW-WATER BENTHIC FORAMINIFERA: Taxonomy, Ecologic Distribution, Biogeography, and Use in Paleoenvironmental Assessment (1999), p. v.

ABSTRACT

A high-resolution study of a marsh sedimentary sequence from the Minho estuary provides a new paleoenvironmental reconstruction from NW Iberian based on geological proxies supported by historical and instrumental climatic records. A low-salinity tidal flat, dominated by *Trochamminita salsa/irregularis*, *Haplophragmoides* spp. and *Cribrostomoides* spp., prevailed from AD 140–1360 (Roman Warm Period, Dark Ages, Medieval Climatic Anomaly). This sheltered environment was affected by high hydrodynamic episodes,

marked by the increase in silt/clay ratio, decrease of organic matter, and poor and weakly preserved foraminiferal assemblages, suggesting enhanced river runoff. The establishment of low marsh began at AD 1380. This low salinity environment, marked by colder and wet conditions, persisted from AD 1410–1770 (Little Ice Age), when foraminiferal density increased significantly. *Haplophragmoides manilaensis* and *Trochamminita salsa/irregularis* mark the transition from low to high marsh at AD 1730. Since AD 1780 the abundances of salt marsh species (*Jadammina macrescens*, *Trochammina inflata*) increased, accompanied by a decrease in foraminiferal density, reflecting climate instability, when droughts alternate with severe floods. SW Europe marsh foraminifera respond to the hydrological balance, controlled by climatic variability modes (e.g., the NAO) and solar activity, thus contributing to the understanding of NE Atlantic climate dynamics.

Keywords: Marsh foraminifera, Hydrological balance, Paleoenvironmental reconstruction, Climate variability, RWP to Present, Minho estuary, NW Iberian region.

7.1. Introduction

Tidal marshes are dynamic ecosystems, considered critical transition zones between adjacent terrestrial and marine environments within the estuarine landscape. These environments have been the source of considerable benefits, both social and economic. The human impact on tidal marshes started a long time ago (e.g., drainage and agriculture, grazing, saltpans), and increased in modern times (dredging, harbors, heavy industries, communication routes and urban settlement, agriculture, sewages and industrial effluents). Identifying past environmental changes that influenced the estuarine margins, whether triggered by natural internal processes (e.g., sediment supply), external forcing (e.g., solar irradiance, volcanic aerosols, atmospheric circulation patterns) or by persistent human impact (e.g., anthropogenic induced climate warming), is essential to understand global and regional climatic variability and the relationship between climate and sea-level during the last two millennia.

Since the pioneering works of Phleger (1965) and Scott and Medioli (1978, 1980), tidal marsh foraminiferal assemblages have been used as paleoenvironmental proxies and sea-level indicators in Holocene intertidal deposits (e.g., Gehrels, 1994; Hayward et al., 1999; Horton, 1999; Scott et al., 2001; Gehrels and Newman, 2004; Horton and Edwards, 2005; Fatela et al., 2009; Leorri et al., 2010a, 2011). The distribution of foraminiferal species across tidal marshes around the world exhibits a vertical zonation with respect to the tidal frame that depends on abiotic and biotic factors and allows the recognition of foraminiferal assemblage characteristics of a narrow zone (high marsh) between mean high water (MHW) and mean high water spring (MHWS). They also provide an efficient method to reconstruct water circulation patterns in estuaries and the interplay between marine and freshwater inflow (e.g., Hayward et al., 1999; Leorri and Cearreta, 2009a). The study of modern foraminiferal patterns can be used to interpret fossil brackish foraminiferal faunas and they are of

special relevance to recent methods of determining rates of Quaternary changes in sea-level, climate and geohistory (e.g., Hayward et al., 1999; Hippensteel et al., 2005; Alday et al., 2006; Drago et al., 2006; Horton and Murray, 2006; Horton and Culver, 2008; Leorri and Cearreta, 2009b; Leorri et al., 2013).

In the present work, foraminiferal data are combined with both descriptive documental records and instrument-based observations (i.e., meteorological and hydrological) to improve the understanding of climate variability in the NW of Portugal over the last 2000 yr. Further comparison with historical climatic information from the Iberian Peninsula (e.g., Font Tullot, 1988; Benito et al., 1996, 2008, 2010; Bernárdez et al., 2008a; Martín-Chivelet et al., 2011) and paleoclimatic reconstructions from offshore Atlantic Iberian margin (Lebreiro et al., 2006; Rodrigues et al., 2009; Abrantes et al., 2011) was made to recognize and characterize the potential of marsh foraminiferal assemblages as a proxy for major shifts in climate. Notwithstanding the uncertainties inherent to the dating methods, especially sub-centennial scale chronologies based on radiocarbon dating, foraminiferal changes over the last two millennia might reflect climatic changes such as Roman Warm Period (RWP), Dark Ages (DA), Medieval Climatic Anomaly (MCA), Little Ice Age (LIA), the solar activity cycles (maxima and minima), the present warming pulse, as well as extreme climatic events.

7.2. Study area

The Minho River runs through the NW of Portugal (Figure 7.1), defining 77 km of the political border with Spain, just before reaching the Atlantic Ocean near the ancient fortress town of Caminha. It drains a carbonate depleted Variscan basement across the rainiest area of Portugal, with an average annual precipitation of 1780 mm (maxima 3470 mm; http://snirh.pt). The annual average fluvial discharge is approximately 300 m^3/s and the winter peak discharge (December to March) generally exceeds 1000 m^3/s; the 100-yr flood recorded 6100 m^3/s (Bettencourt et al., 2003). In spite of the construction of several dams since AD 1951, a correlation between river flow and precipitation of r = 0.85 (Fatela et al., 2013) to r = 0.88 (Gómez-Gesteira et al., 2011) was found in Minho, as well as a correlation between winter precipitation and NAO index of r = −0.70 (Fatela et al., 2013).

The Minho estuary presents a semi-diurnal high-mesotidal regime where astronomical tides range between 2 m and almost 4 m under neap or spring waters, respectively. However, tidal levels are often amplified by storm surges (Taborda and Dias, 1991). The dynamic tide is felt up to 40 km up stream (Alves, 1996). The upstream limit of marine water is recorded up to 6–9 km (Fatela et al., 2009). This estuary is shallow, as a result of widespread siltation, and semi-enclosed by a mouth bar, exposing a considerable part of the bottom during low water spring tide. The lower estuary extends a few kilometers from the mouth and behaves as “partially mixed” (Brown et al., 1991; Moreno et al., 2005c). The most extensive marsh development occurs in the south bank of the Minho

estuary, at the confluence with the Coura River (hereafter referred to as the Caminha tidal marsh), providing an adequate site to investigate the current and past distribution of foraminiferal assemblages (Figure 7.1).

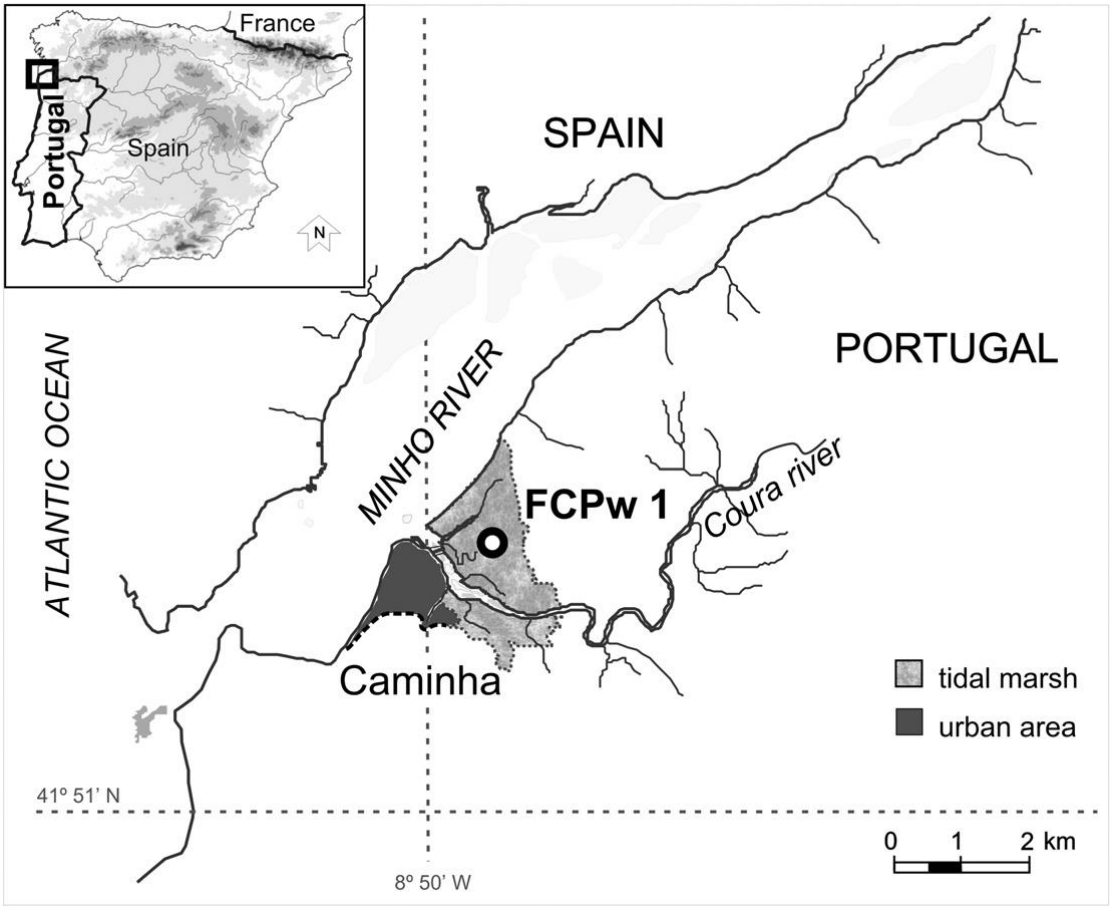

Figure 7.1. Location of core FCPw1 in the Caminha tidal marsh (Minho estuary, NW Portugal).

7.3. Surface foraminiferal distribution at the Caminha marsh

Several studies related to the living and dead marsh foraminiferal assemblage zonation and their environmental constraints (Moreno et al., 2005a, 2005b, 2005c, 2006, 2007; Fatela et al., 2007, 2009) and Holocene sea-level changes (Leorri et al., 2010a, 2011, 2013) have been carried out. The main control to the general composition of the foraminiferal assemblages is salinity and submersion time (e.g., Fatela et al., 2009). However, these assemblages are also controlled by calcite undersaturation in these brackish marshes and tidal flats, where marine water is the major source of carbonates (Moreno et al., 2007; Valente et al., 2009). While with each tidal cycle salinity present large changes, foraminifera live infaunally (i.e., inhabit the sediment) and the controls are exerted by interstitial pore water that buffer these drastic changes (Fatela et al., 2009). The particular conditions (e.g., undersaturation in calcite, low pore-water pH) of the interstitial water have led to foraminiferal assemblages strongly dominated by robust agglutinated foraminifera, since calcareous foraminifera

dissolve and most fragile marsh agglutinated tests disaggregate in response to these geochemical conditions.

Low-salinity conditions limit the elevation at which foraminiferal assemblages can be found. In fact, in this region the typical highest high marsh zone is absent and it is instead colonized by terrestrial vegetation. A pronounced dilution of marine water, caused by plentiful rain, in conjunction with the morphology of the estuary, limits the tidal salt wedge penetration landwards and residence time of marine waters within the estuarine space.

Following the tidal marsh foraminiferal zonation previously defined by the seminal work of Scott and Medioli (1980), a study of forty-eight surface sediment samples (from the spring and fall of 2002; Fatela et al., 2009), shows that Caminha assemblages from the high marsh IB subzone, between mean high waters (MHW) and mean high waters spring (MHWS), are dominated by *Haplophragmoides* sp. and *Haplophragmoides manilaensis* (Andersen, 1953), together with *Pseudothurammina limnetis* (Scott and Medioli, 1980) as a co-dominant species in the living assemblage. The low marsh zone II is characterized by the dominance of *Miliammina fusca* (Brady, 1870). This zone may be subdivided into a IIA upper subzone, between MHW and mean high waters neap (MHWN), where *M. fusca* is accompanied by secondary species *P. limnetis*, and a lower subzone IIB defined by *M. fusca* and secondary *Psammosphaera* sp. This subzone is located between MHWN and the mean tide level (MtL, i.e., mean water level inside the estuary). *Haplophragmoides manilaensis* characterizes the elevation range between MHW and MHWS (0.99 m to 1.11 m above Minho estuarine MtL). It is the most abundant in both the living (stained) and dead assemblages. Because of its dominance and limited vertical range, *H. manilaensis* is an important sea-level and low-salinity high marsh indicator (Fatela et al., 2009).

A new set of eighteen surface samples was collected in May 2010 to improve the understanding of the Caminha high marsh assemblage (Fatela et al., 2013). Correspondence Analysis (CA) integrating dead benthic foraminiferal results from both the 2002 and 2010 samples resulted in 3 defined groups according to foraminiferal assemblage distribution across the tidal marsh zonation, with a significant correlation with submersion time (Fatela et al., 2013). However, a difference is evident between the two sampling periods when the dominant salt marsh species are evaluated; for instance, *Trochammina inflata* (Montagu, 1808) and *Jadammina macrescens* (Brady, 1870) were absent in 2002 but are common in 2010. This decline of lower salinity species (*Haplophragmoides* sp., *H. manilaensis*, *H. wilberti* and *P. limnetis*) abundances is seen as a direct consequence of the salinity increase of the interstitial water in the marsh, which reflects a decrease in the regional precipitation regime during the 8 years that separate the samplings (Fatela et al., 2013). This observation points out that the records of benthic foraminifera from Caminha high marsh represent an important proxy for high-resolution studies of climate variability (Fatela et al., 2013).

7.4. Materials and methods

The Caminha high marsh sediment core FCPw1 was collected with a manual Auger sampler (5 replicated cores, one-meter-long each) at 1.55 m above mean sea-level (41º52′37″ N and 8º49′28″ W; Figure 7.1), and transferred to a half PVC pipe and wrapped with cling film to protect it during transport and minimize desiccation.

7.4.1. Foraminifera

In the laboratory, the core was carefully sliced into 1-cm intervals and 56 samples (*ca.* 25 cm^3) were analyzed for foraminiferal purposes. Samples were taken every centimeter to a depth of 30 cm, below which samples were collected every other cm down to 50-cm depth and alternating 2 cm from 50 cm to the core bottom. Each sample corresponds to a circular slice of sediment with a volume of *ca.* 25 cm^3. Samples were wet sieved to remove clay and silt material (63 μm mesh). At least 100 individuals were wet picked with a micropipette in each sample, a number fully adequate to characterize the low-diversity assemblages of tidal marshes (Fatela and Taborda, 2002). When the number of specimens was too low, the trichloroethylene (density = 1.46 g/cm^3) flotation procedure was used to separate foraminiferal tests from sand particles (Murray, 2006). All specimens contained in that fraction were picked. Foraminiferal identification followed Loeblich and Tappan (1988) to generic classification and several published papers regarding tidal marsh foraminifera for specific classification (e.g., Murray, 1971; Scott and Medioli, 1978, 1980; Hayward et al., 1999; Debenay et al., 2002). The specimens picked per sample were archived in a micropaleontological Plummer cell slide.

7.4.2. Sedimentology and geochemistry

Two replicate cores were sliced every centimeter for geochemical and sedimentological purposes. All samples were frozen and then freeze-dried prior to the analyses. Organic matter (OM) content was determined by loss on ignition methodology (LOI), using a 2 g of bulk sediment dried and oven-heated at a temperature range of 490–510ºC, for about 2 h. Sediment pH was determined using the electrometric method (Head, 1980) with an inoLab WTW series pH730 model. Wet sieving was used to separate and determine the ratio of coarse (> 63 μm): fine (< 63 μm) particles, and the silt and clay fractions were determined using a Malvern laser particle analyzer and Mastersizer 2000 software. Selected samples of one of the replicates were sieved to remove the coarser particles larger than 2 mm. The remaining material (< 2 mm) was dried, ground in an agate mill, and a portion was homogenized and compacted into pressed pellets for analysis by Energy-Dispersive X-Ray Fluorescence Spectrometry (EDXRF) using a KEVEX 771 spectrometer. Spectral data were acquired for the quantification of Al, Si, S, Cl, K, Ca, Ti, Cr, Mn, Fe, Ni, Cu, Zn, Br, Rb, Sr, Zr, and Pb. A detailed description on the sample preparation, analytical conditions, detection limits and the

accuracy and precision of the overall procedure has been published elsewhere (Araújo et al., 1998, 2003). In this multi-proxy analysis, special focus was made on the elements recognized as proxies of marine and continental inputs.

7.4.3 Chronology

The upper section of the core was dated via ^{210}Pb measured by alpha spectroscopy following the methodology of Nittrouer et al. (1979). In this approach, unsupported ^{210}Pb ($^{210}Pb_{Excess}$) is determined as the difference of ^{210}Pb activity *versus* ^{226}Ra, assumed to be in equilibrium at depth within the core (Nittrouer et al., 1979). ^{137}Cs (Smith, 2001) and total Pb activities (Leorri et al., 2008; Leorri and Cearreta, 2009b) were used to support the ^{210}Pb-derived chronology based on the constant rate of supply model (CRS; Appleby and Oldfield, 1992), as it has been shown to be the most suitable for the region (Leorri et al., 2010b). The radionuclide ^{137}Cs was determined by its gamma emissions at 662 KeV (Appendix 7.1). Samples were counted for 24 h to the depth of limit of measurable fallout ^{210}Pb or ^{137}Cs, i.e., until activity concentrations of both radionuclides dropped below the minimum detectable activity (Leorri et al., 2010b). Six additional samples (40–41 cm, 44–45 cm, 63–64 cm, 66–67 cm, 81–82 cm and 90–91 cm depth) were analyzed for radiocarbon content (total organic) at Beta Analytic Inc. (USA) (Table 7.1) to extend the chronology down-core (Figure 7.2). The interpolation of the data has been performed using a Bayesian age-depth model (Bchron 3.2; Haslett and Parnell, 2008; Parnell et al., 2008) to provide age and associated errors to the environmental reconstructions. The lowermost 10 cm (91–100 cm depth) has been extrapolated by linear regression from the Bchron calculation between 81 and 91 cm depth. This section has to be considered carefully as errors cannot be calculated. The obtained calendar ages are presented in years of Anno Domini (AD).

Table 7.1. Radiocarbon ages data determined in the Laboratory "Beta Analytic Inc.". (AMS – standard delivery).

Sample	Depth (cm)	δ^{13}C ‰	Conventional radiocarbon age	Δ14C ‰	Calibrated years AD (2 sigma range)
CM 41	40–41	−26.7	380 ± 30 BP	−46.20 ± 3.6	1490 to 1666
CM 45	44–45	−26.8	650 ± 35 BP	−84.57 ± 3.9	1330 to 1453
CM 64	63–64	−25.9	1010 ± 50 BP	−122.49 ± 1.9	1032 to 1197
CM 67	66–67	−25.9	1030 ± 34 BP	−124.97 ± 1.9	934 to 1082
CM 82	81–82	−25.8	1570 ± 40 BP	−181.66 ± 1.9	463 to 650
CM 91	90–91	−27.2	1760 ± 30 BP	−196.80 ± 3.0	215 to 429

^{210}Pb CRS chronology supported by ^{137}Cs and total Pb concentrations of Caminha high marsh sediment core (FCPw1) are available in Appendix 7.1.

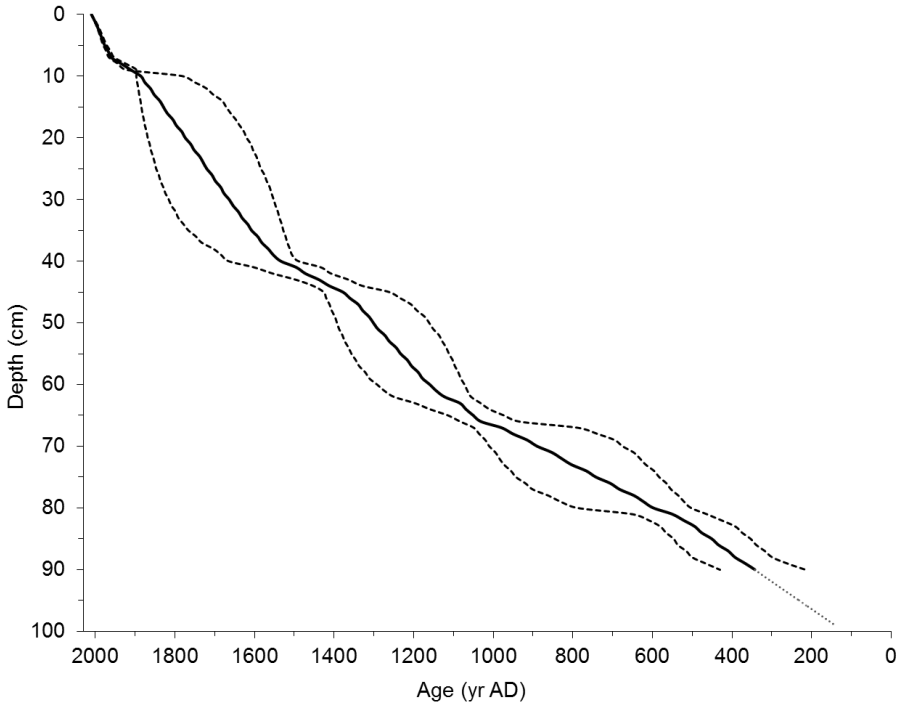

Figure 7.2. Age model for the core FCPw1 and estimated 2σ errors, based on six AMS-^{14}C dates, performed on total organic sediment, and ^{210}Pb chronology. The data interpolation was obtained with Bchron 3.2 software. The lowermost 10 cm has been extrapolated from the Bchron calculation between 81 and 91 cm depth by linear regression.

7.4.4. Historical and instrumental records

The last two millennia comprise five well-known climatic historical periods: 1) Roman Warm Period (RWP, AD 0–400; e.g., Lamb, 1985); 2) Dark Ages Cold Period (DA, AD 400–700; e.g., Keigwin and Pickart, 1999); 3) Medieval Climatic Anomaly (MCA, AD 900–1300; e.g., Stine, 1994; Mann et al., 2009; Trouet et al., 2009; Cook et al., 2010; Graham et al., 2011); 4) Little Ice Age (LIA, AD 1350–1900; e.g., Bradley and Jones, 1993) and 5) 20th century warming (Present Warm Period – PWP), as recorded by instrumental temperature measurements over the last two centuries. These climate changes were also recognized by several authors that have studied the variability of the climatic conditions in Northern Iberian Peninsula during the late Holocene until present using proxies like organic and inorganic geochemistry, sedimentology and micropaleontology (e.g., Martínez Cortizas et al., 1999; Luque and Juliá, 2002; Desprat et al., 2003; Pla and Catalan, 2005; Lebreiro et al., 2006; Burdloff et al., 2008; Martín-Chivelet et al., 2011; González-Álvarez, 2013). In addition, several extreme local climatic events, like strong flooding episodes, are documented (e.g., Marquina, 1949; Benito et al., 1996, 2008; Abrantes et al., 2011). These events have typically occurred at times of transition between climatic periods (e.g., AD 500–600, AD 1100–1200, AD 1450–1600). For example, alternating periods of intensive precipitation and thunderstorms with severe droughts were common during the 18th and 19th centuries as recorded in Portugal (e.g., Marques, 2001; Do Ó and Roxo, 2008; Pfister et al., 2010) and several localities from southern and northern Spain (e.g., Riera

et al., 2004; Llasat et al., 2005; Vicente-Serrano and Cuadrat, 2007; Benito et al., 2008, 2010; Domínguez-Castro et al., 2008; Gil-Garcia et al., 2008; Martin-Puertas et al., 2008).

Solar activity cycles (maxima and minima) are based on Versteegh (2005), Usoskin et al. (2007), Scaffeta (2012), Steinhilber et al. (2012), WDC and NOAA (2013). Precipitation data were compiled from the monthly records of meteorological stations from the Minho region since 1930. The available data from the Portuguese sectors of Minho and Lima basins were merged in order to obtain the longest and the most representative record of the area (http://snirh.pt). This series of precipitation data from 1932 to 2010 was used to compute the SPI (McKee et al., 1993; Moreira et al., 2012) with a freeware program (SPI_SL_6.exe) available at the National Drought Mitigation Center of the University of Nebraska–Lincoln, USA (http://drought.unl.edu). The SPI allows the identification of drought events and classifies their severity according to defined drought classes. The wide use of this index comes from its reliability and relatively easy comparison between different locations and climates (http://drought.unl.edu). Moreira et al. (2012) determined the SPI from Porto (Serra do Pilar: 41º08′19.20″ N–08º36′09.68″ W), *ca.* 80 km south of Caminha, based on the precipitation record from 1863 to 2007. Considering the good correlation (r = 0.85) between SPI from Minho region and Porto, the latter was used as representative of severe and extreme droughts that occurred in NW Portugal. In this work, the SPI 12-month period was used because it reflects long term precipitation patterns and identifies dryer periods of long duration with impact in the hydrological regime (e.g., McKee et al., 1993; Moreira et al., 2012; http://drought.unl.edu). The identification of the severe and extreme drought periods between 2007 and 2010 in NW Portugal was completed with the on-line SPI data provided by the Instituto Português do Mar e da Atmosfera (IPMA, 2013).

7.5. Results

Based on foraminiferal assemblages (defined in terms of species presence, abundance, dominance and density – number of foraminifera per cm^3; Appendix 7.2), the Caminha marsh core (FCPw1) can be divided into six different Foraminiferal Assemblage Zones (FAZ VI to I; Table 7.2). This division is also supported by sedimentological and geochemical data (Table 7.2, Appendix 7.3).

Table 7.2. Summary of micropaleontological and sedimentological data. The values represent the average (bold) and the range; Low Sal. spp. % – low-salinity species group; Salt marsh spp. % – "normal"-salinity species group; NF – number of foraminifera; S – number of species; assemblages dominant species (bold).

FAZ	Depth cm	Age yr AD	Benthic foraminifera %	Low sal. spp. %	Salt marsh spp. %	NF/cm^3	S	pH	OM %	Mud %
I	0–4	2010	***H. manilaensis*** (**49**; 40–56); ***Haplophragmoides* spp** (**23**; 2–65),	**84**	**12**	**253**	**9**	**5.1**	**53**	**63**
		1985	***M. fusca*** (**12**; 2–20) and ***T. salsa/irregularis*** (**9**; 7–11), *Cribrostomoides* spp.(**5**; 210), *T. inflata* (**7**; 2–13); *H. wilberti*, *P. limnetis*, *T. comprimata*, *J. macrescens* and *P. guaratibaensis* ≤5	77–88	8–21	22–498	7–11	4.6–5.4	46–65	50–69
II	4–10	1985	***H. manilaensis***, (**35**; 16–63), ***T. salsa/irregularis*** (**11**; 4–15),	**58**	**37**	**168**	**9**	**5.4**	**38**	**74**
		1900	*M. fusca* (**6**; 5–6), associated with ***T. inflata*** (**12**; 3–41), ***J. macrescens*** (**11**; 3–14), *T. comprimata* (**4**; 1–8) *H. wilberti* (**8**; 4–13); *P. guaratibaensis*, *S. lobata* and *P. limnetis* ≤5	36–78	14–59	68–252	7–10	5.1–5.7	36–40	51–88
III	10–20	1900	***H. manilaensis*** (**32**; 21–51), ***T. salsa/irregularis*** (**19**; 10–32),	**57**	**35**	**79**	**8**	**5.7**	**33**	**79**
		1780	*M. fusca* (**4**; 1–8), **Haplophragmoides spp** (46); *J. macrescens* (**17**; 12–23), *T. inflata* (**12**; 3–22), *T. comprimata* (**7**; 3–13); *Cribrostomoides* spp., *H. wilberti*, *P. guaratibaensis*, *P. ipohalina* and *P. limnetis* ≤5	44–78	10–47	17–205	6–9	5.7–5.8	22–40	66–88
IV	20–29	1780	***T. salsa/irregularis*** (**59**; 16–74), ***H. manilaensis***, (**26**; 6–63),	**91**	**4**	**244**	**6**	**5.8**	**30**	**86**
		1690	***M. fusca*** (**5**; 1–16); *Cribrostomoides* spp., *H. wilberti*, *P. limnetis* and *T. comprimata*, *J. macrescens*, *T. inflata*, *P. guaratibaensis*, *P. ipohalina* ≤5	84–95	1.3–11	161–345	4–9	5.7–5.9	25–38	81–90
V	29–46	1690	***T. salsa/irregularis*** (**77**; 74–92), ***M. fusca*** (**7**; 1–16),	**88**	**4**	**260**	**5**	**6.1**	**19**	**91**
		1380	*Haplophragmoides* spp (**4**;0.7–12), *Cribrostomoides* spp. (**4**;0.8–9), *T. comprimata* (**4**; 0.7–6); *H. manilaensis*, *P. limnetis*, *P. guaratibaensis*, *S. lobata*, *J. macrescens*, *T. Inflata*, *P. ipohalina* ≤5	82–95	1.4–9	63–609	4–8	5.8–6.6	12–24	80–95
VI	46–100	1380	***T. salsa/irregularis*** (**59**; 21–80), ***Cribrostomoides* spp.** (**14**; 2–42),	**76**	**3**	**3**	**3**	**4.8**	**8**	**97**
		140	***Haplophragmoides* spp** (**10**; 4–26), *J. macrescens* (**3**; 1–7); *M. fusca*, *T. Inflata*, *P. ipohalina* ≤5	59–88	0.8–8	0.1–13	2–5	3.8–6.7	6–13	93–100

FAZ VI (100 cm to 46 cm depth) ranges from AD 140 to 1380, encompassing the RWP, DA cold period and the MCA. The foraminiferal assemblages are scarce (average 3 tests/cm^3), often exhibiting poorly preserved tests and low diversity (average 3 species/sample). Assemblages are composed primarily by the upstream low-salinity species *Trochamminita salsa/irregularis* (Cushman and Brönnimann, 1948), followed by *Cribrostomoides* spp. and *Haplophragmoides* spp. (Table 7.2). *Jadammina macrescens* is also present (7%) at AD 1070.

Sediment is essentially mud (average 97%) and the OM content ranges between 6% and 13%; the pH values are generally low, exhibiting an average of 4.8 (Table 7.2; Appendix 7.3); the higher concentration of Zr is recorded in this FAZ (average 213 ppm; Appendix 7.3). In this zone, some interval barren of foraminifera tend to be related with higher silt/clay ratio (Appendix 7.2 and 7.3), namely at AD 190, 800, 1140, 1270 and two in the interval AD 1310−1340.

FAZ V (46 cm to 29 cm depth) ranges from AD 1380 to 1690 and is included within the LIA period. This unit records a strong increase in the density of the assemblages (average 260 tests/cm^3), but low species richness remains (average 5 species/sample). The low-salinity species still dominate (82–95%), namely *T. salsa/irregularis* and *M. fusca*, with minor presence of *Haplophragmoides* spp., *Cribrostomoides* sp., *H. manilaensis* and *P. limnetis*. Salt marsh species *Tiphotrocha comprimata* (Cushman and Brönnimann, 1948), *Paratrochammina guaratibaensis* (Brönnimann, 1986), *Polysaccammina ipohalina* Scott, 1976 and *Siphotrochammina lobata* (Saunders, 1957) join *J. macrescens* and *T. inflata* (Table 7.2; Appendix 7.2).

Concomitant with FAZ V, mud percentage decreases (average 91%) while OM content (12% to 24%) and pH values (average 6.1; Table 7.2) increase; the average concentration of Zr falls in

this zone to 161 ppm, whereas Br exhibits an opposite trend rising from an average content of 148 ppm (FAZ VI) to 483 ppm (FAZ V; Appendix 7.3).

The FAZ IV (29 cm to 20 cm depth) spans from AD 1690 to 1780 (LIA). Foraminifera in this unit are still abundant (average 244 tests/cm^3). The assemblages have low diversity (average 6 species/sample) and they are still dominated by low-salinity species (84–95%), *T. salsa/irregularis*, *H. manilaensis* and *M. fusca*, along with secondary species *Cribrostomoides* sp., *H. wilberti* and *P. limnetis* (Table 7.2). Salt marsh foraminifera, *T. comprimata*, *J. macrescens*, *T. inflata*, *P. guaratibaensis* and *P. ipohalina*, are also found. The increasing trend of OM towards the top of the core is significant, reaching 25–38% in this FAZ (Table 7.2). Likewise, the sediment texture continues the tendency of coarsening towards the top of the core (average mud percentage 86%), but the coarse fraction is mainly represented by plant debris. Br presents its highest content, with 1300 ppm (average 927 ppm), and the concentration of Zr continues falling in this FAZ (average 143 ppm; Appendix 7.3).

FAZ III (20 cm to 10 cm depth) extends between AD 1780 and 1900 (LIA). Low foraminiferal diversity (8 species/sample) prevails and density exhibits a significant drop (average 79 tests/cm^3). Low-salinity species (*H. manilaensis*, *T. salsa/irregularis*, *M. fusca* and *Haplophragmoides* spp.) dominate (average 57%), but in this FAZ the “normal”-salinity species (*J. macrescens*, *T. inflata* and *T. comprimata*) become a significant part of the assemblages (average 35%). Minor species are represented in this FAZ by *Cribrostomoides* spp., *H. wilberti*, *P. guaratibaensis*, *P. ipohalina* and *P. limnetis* (Table 7.2). The OM content remains high (average 33%) and the average mud content decreases to 79% (Table 7.2). Br still exhibits high concentration (average 605 ppm).

FAZ II (10 cm to 4 cm depth) spans from AD 1900 to 1985 (PWP). Foraminiferal assemblages reach the highest number of species (9), but have similarly low diversity and exhibit a consistent density increase, with an average of 168 tests/cm^3. Low-salinity species represent 58% (average) of the assemblages and “normal”-salinity species 37% (average; Table 7.2). This FAZ records the only interval (8–9 cm; AD 1934) where “normal”-salinity species became dominant (59%), marked by the acme of *T. inflata*. Mud percentage and Zr sediment content present the same trend as in the previous FAZ III, while OM and Br content increase, the latter achieving the average of 919 ppm (Table 7.2; Appendix 7.3).

FAZ I (4 cm to 0 cm depth), from AD 1985 to 2010, shows that diversity of foraminiferal assemblages is still low until present (maximum 11 species) but their density increases to an average of 253 tests/cm^3 (Table 7.2). The lower faunal densities occur between AD 1995 (22 tests/cm^3) and AD 2002 (99 tests/cm^3). In this FAZ, the high marsh foraminiferal assemblages are dominated by the low-salinity species *H. manilaensis*, *Haplophragmoides* spp., *M. fusca* and *T. salsa/irregularis*, representing 77% to 88% of the assemblage, with *Cribrostomoides* spp., *H. wilberti* and *P. limnetis* as minor representatives as well as the “normal”-salinity marsh species *T. comprimata*, *J.*

macrescens and *P. guaratibaensis*. *Trochammina inflata* is the most representative of this group (average 7%; Table 7.2), reaching the highest percentages at the uppermost sample (AD 2010), although its presence is significantly reduced from FAZ II to FAZ I. The coarsening upwards trend is clear in FAZ I (average 63% mud), as well as the increase of OM content (average of 53%), reflecting the observed increase of marsh plant debris. Zr and Br trends change, with the gradual decrease of Zr from the bottom to the top of the core (average 115 ppm) and the Br content increasing to an average of 1120 ppm (Appendix 7.3).

7.6. Discussion

The sediment texture of core FCPw1 and the OM content (Table 7.2) indicate the development of a tidal flat (FAZ VI) that lasted over 1200 yr (AD 140–1380). During this period, foraminiferal assemblages present low density, with a dominance of few low-salinity species (Figure 7.3). However these originally scarce assemblages, like in the tidal flats modern analogs (Fatela et al., 2009), are often poorly preserved, suggesting a diagenetic alteration, probably related to the low values of sediment pH (Table 7.2) that seem to reflect a strong fluvial influence. In fact, minimum pH values of 4.33 have been recently measured in the Coura river waters (Moreno et al., 2005a). Alternatively, foraminifera are absent from this depositional setting probably due to low salinity. These low abundances tend to be correlated with higher silt/clay ratio (Figure 7.4). Silt/clay ratio could be used as a proxy of hydrodynamic energy, where higher silt content could be associated to periods of rainfall/flood intensification, mainly at AD 140–190, AD 320 and AD 800, AD 1140, AD 1270 and AD 1310–1340. Desprat et al. (2003) identified the development of temperate vegetation during Roman colonization in Galicia (RWP, peaking at AD 150), suggesting that this period presented humid conditions. Moreover the paleotemperature records from speleothem materials located in the North of Spain (Martín-Chivelet et al., 2011) show some marked negative anomalies for the late RWP period, namely AD 90 and 250 (Figure 7.3).

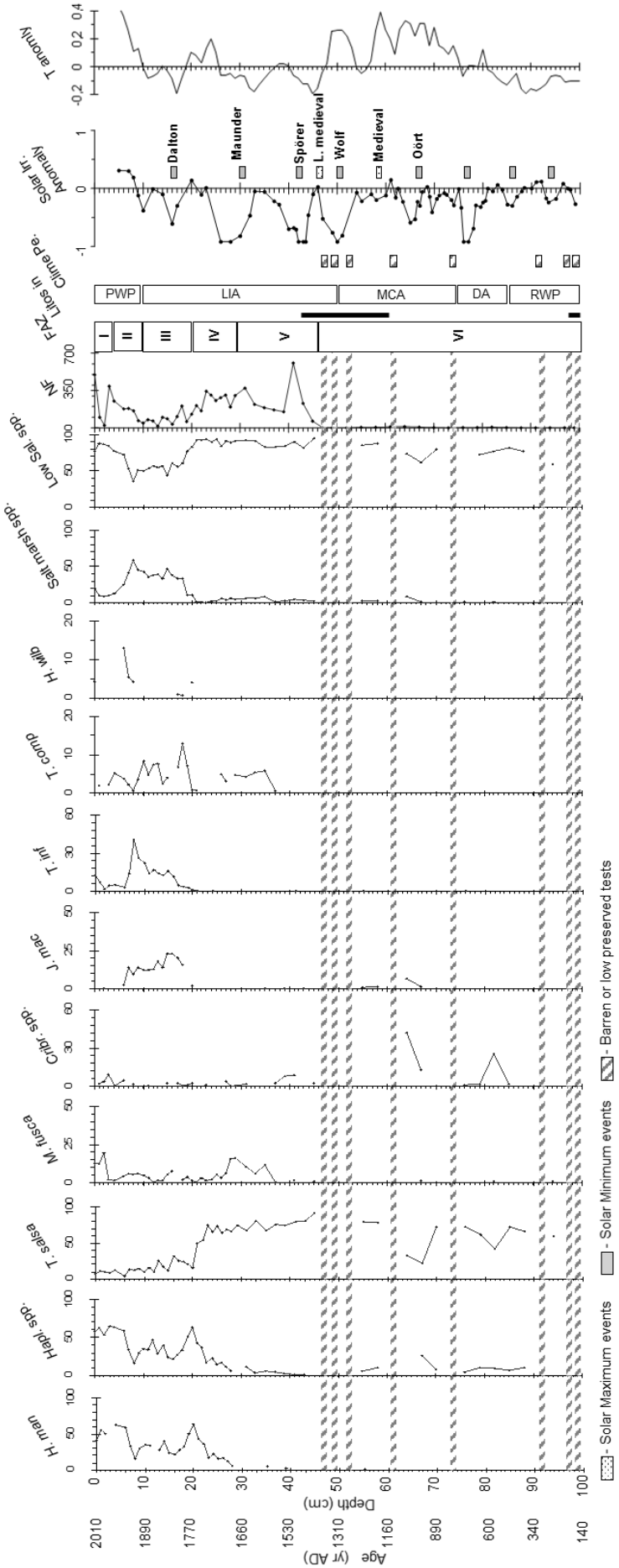

Figure 7.3. Percentage distribution of benthic foraminifera in core FCPw1. Age (yr AD) – age in calendar years AD; Salt marsh spp. – distributions of the group of brackish salt marsh benthic species; Low Sal. spp. – distributions of the group of low-salinity benthic species; NF – number of foraminifera per cm^3; FAZ – foraminiferal assemblage zones; Litos in – periods of continental lithogenic inputs to the shelf (see references in the text and Appendix 7.5); Clime Pe. – Climate periods in the last 2 millennia (see references in the text); Solar Irr. Anomaly – solar irradiance anomaly using a 22-yr running average reconstruction (after Steinhilber et al., 2012); Solar Ev. – Solar events (see references in the text); T anomal. – Temperature anomaly using a 10-yr running average reconstruction (after Martín-Chivelet et al., 2011).

The combined effect of high precipitation and changes in land use (e.g., deforestation and farming, associated with the mining exploitation, intensified soil erosion) carried out by Romans in NW Iberia, and more specifically in the Minho river catchment area, led to a higher loading of terrestrial-derived sediments transported to the shelf by the rivers. A significant increase in river borne detrital material in sediments to the W Iberian shelf is broadly recognized during the RWP (e.g., Lebreiro et al., 2006: 50 BC; Bernárdez et al., 2008a; Bernárdez et al., 2008b: 50 BC–AD 250; Abrantes et al., 2005; Rodrigues et al., 2009; Mohamed et al., 2010: AD 0–550). Foraminiferal data suggests increased fluvial influence at AD 230–280 as indicated by low-salinity species (*T. salsa/irregularis* and *M. fusca*) and the low density. This contrasts with a previous study devoted to the identification of OM sources by using lipid biomarker analysis (De la Rosa et al., 2012) performed at the same location that pointed to an increase contribution of marine phytoplankton to the organic pool at that time. This disagreement can be explained by the complex processes that control salt marsh settings. For instance, while increase river flow might provide the ecological framework, more frequent or intense storms (recorded between AD 50–300; Behre, 2007) could deposit marine phytoplankton, leaving a geochemical signal but without modifying the brackish conditions. Overwash deposits found at AD 180–310, 40 km south of the Minho estuary (Granja, 1999), support this hypothesis.

The uppermost FAZ VI (AD 1080 to 1380) is coeval with the later part of the MCA and the transition to the LIA. The new climatic conditions are reflected in the core sediments in four episodes of very low abundance and poorly preserved foraminifera. The first occurrence at AD 1140 is coeval with a maximum in carbon isotopic composition ($\delta^{13}C$; De la Rosa et al., 2012; Appendix 7.4) and organic carbon to total nitrogen ratio (C_{org}/N), indicating a major input from terrestrial plants at AD 1140–1160 (Appendix 7.4). This is further supported by the lipid content, average chain length of n-alkanes (ACL) and terrigenous/aquatic ratio of n-alkanes (TAR) values that also suggest an increase in the continental discharges at that time, which is contemporary with major river flood events reported for the same period in this area (De la Rosa et al., 2012). This event could be related with the Oört Solar Minimum (AD 1040–1080), if the date uncertainties are considered. The following episodes occurred at AD 1270, AD 1310 and AD 1340 (Figure 7.3), might be related to the Wolf Solar Minimum (AD 1280–1350). Historical records of the 12th and 13th centuries confirm that the Atlantic Iberian region experienced severe winter floods in the years of AD 1102, 1168, 1178, 1181, 1201, 1203, 1207, 1258, 1264 and 1310 (Font Tullot, 1988; Benito et al., 2008). Sediment cores from the shelf Douro Mud Patch allowed the recognition of abnormal precipitation events resulting in fluvial flooding recorded at AD 1100–1200, coeval with well-marked sea-surface temperature (SST) decreases, shifts in solar activity and more persistent NAO negative phases (Abrantes et al., 2011). Low-salinity foraminiferal assemblages are only well preserved between AD 1190 and 1230, in a period that corresponds to the Medieval Solar Maximum (AD 1100–1250).

In summary, FAZ VI records a prevailing fluvial contribution, leading to a low-salinity environment in spite of the proximity to the river mouth (*ca.* 3.5 km). If stronger marine input existed, namely at RWP and MCA, it did not last long enough in order to change the environmental conditions of the tidal flats in this sector of the estuary.

Above the tidal flat represented by FAZ VI, a tidal marsh develops (FAZ V) still under low-salinity conditions from AD 1380 to 1690, where foraminiferal assemblages exhibit low diversity but significantly higher density. This suggests that sedimentation rates are large enough to gain elevation in relation to the tidal frame. Salt marsh species *T. comprimata* tends to increase towards the top of this section (36–29 cm depth) after AD 1610 (4–6%; Figure 7.3), suggesting that the low marsh environment was already installed, growing from the lower IIB zone (between MtL and MHWN) to IIA zone (between MHWN and MHW) and marking the increase of the marsh paleoelevation. This important step in Caminha marsh evolution was accompanied by a significant increase in OM and Br content followed by the opposite trend in Zr concentration (Figure 7.4; Appendix 7.3). Positive correlations between Br and OM contents in soils and marine sediments were documented at least since the 1970s (e.g., Yamada, 1968; Price et al., 1970). More recent studies have shown that Br cycling in marine and terrestrial ecosystems is strongly influenced by OM (e.g., Leri et al., 2010; Leri and Myneni, 2012). According to these authors the relative ease of natural Br oxidation seems to promote its biogeochemical transformation from inorganic to organic forms, conducting to the incorporation into OM through enzymatic processes related to plant litter decay. Salt marshes are areas of high primary productivity and OM accumulation, thus presenting relatively high amounts of Br, supplied by seawater inundation, in both sediment and flora (Rhew et al., 2002). Considered together, the density of foraminiferal assemblages, the OM and Br data suggest the development of a vegetated low marsh. The up-core lowering of Zr content, observed from the base of FAZ V (Appendix 7.3), provides another evidence of an energy drop caused by the development of vegetation on the marsh surface and consequent flat energy gradients. In fact, heavy minerals like zircon require strong hydrodynamic forces for mobilization and transport and serve as a geochemical proxy of depositional energy (e.g., Dellwig et al., 2000; Kolditz et al., 2012). The accumulation of plant debris and particulate OM, following the development of the low marsh, directly contributes to the increase in sediment coarse particles, preventing the use of silt/clay ratio as a runoff proxy after AD 1380. Geochemical data also record the more depleted values of $\delta^{13}C$ accompanied by high C_{org}/N ratios, suggesting that a maximum of terrestrial contribution and lipid biomarkers (C_{31}/C_{27}al, $CPI^{o/e}$ and ACL_{al}) indicate that grass vegetation prevails (De la Rosa et al., 2012; Appendix 7.4) during this FAZ.

After the former phase of uncovered tidal flat conditions, FAZ V marks an important step with the onset of a vegetated low marsh surface after AD 1380, despite the persistent high rainfall, fluvial runoff and intense floods recorded during the LIA (e.g., Benito, 2006; Benito et al., 2008; Bernárdez

et al., 2008a; Burdloff et al., 2008; Abrantes et al., 2011; González-Álvarez, 2013; Appendix 7.5). Halophytic plants buffer the energy in the system trapping sediment, which increases the marsh vertical elevation. However, other factors such as deforestation, agriculture and mining play a significant role in sedimentation rates. These factors were exacerbated since the Roman times, which, associated with low energetic conditions, lead to the siltation of tide dominated estuaries (Poirier et al., 2011). This filling up of the Portuguese coastal systems has been reported in many other locations, namely in Caminha at AD 1541, 1575 and 1582 (Granja, 1990, 2007; Granja and Carvalho, 1992). For instance, in the Royal Courts of Évora (AD 1436), the ship-owners from Viana do Castelo, Ponte de Lima and Vila do Conde stated that they were already silted, preventing the access of larger ships. In fact, the forests depletion in northern Portuguese hinterland attained a critical point that necessitated the import of timber from the north of Spain, France, England and Flanders in order to supply the growing shipbuilding industry (Devy-Vareta, 1986). This was also a period of increased formation of transgressive dune fields. A generalized phase of intense aeolian activity is also distinguished along the Portuguese coast, marked by dune development and enhancement of westerly winds and storminess throughout the LIA, compatible with prolonged negative phases of the NAO (e.g., Clarke and Rendell, 2006; Clemmensen et al., 2009; Costas et al., 2012).

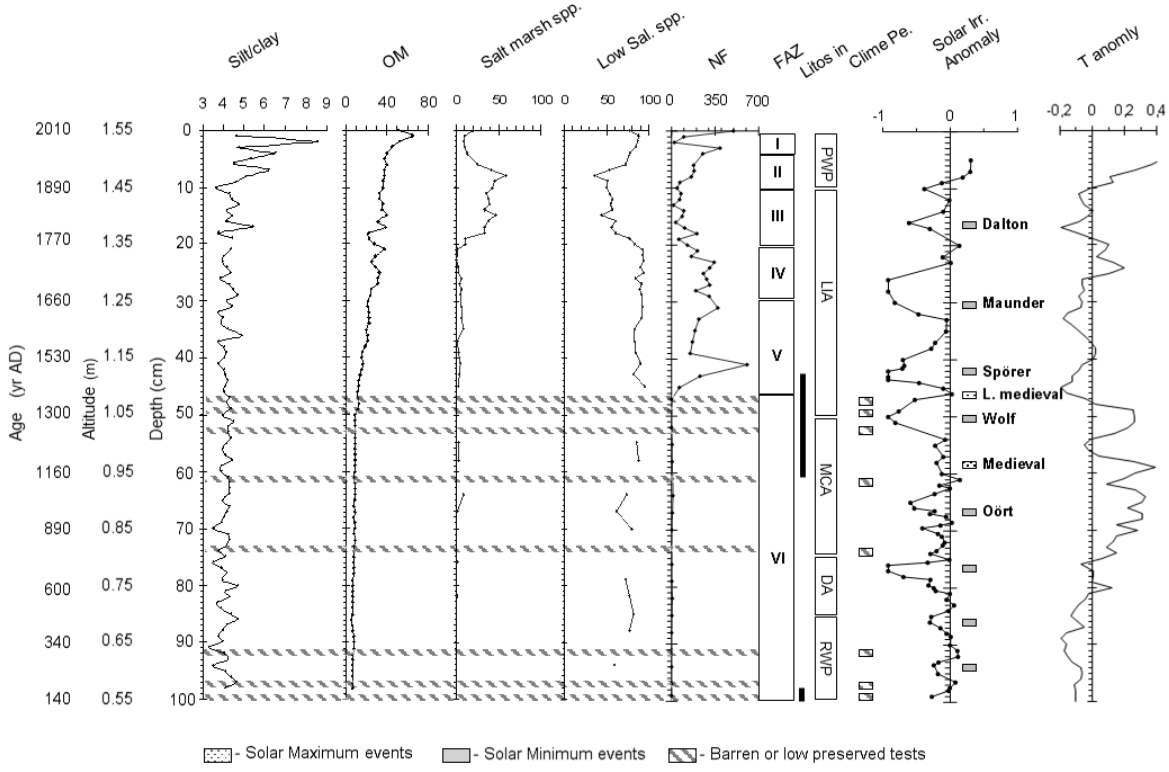

Figure 7.4. Sedimentological, geochemical and summary of benthic foraminiferal data in core FCPw1. Age (yr AD) – age in calendar years AD; Salt marsh spp. – percentage distributions of the group of brackish salt marsh benthic species; Low Sal. spp. – percentage distributions of the group of low-salinity benthic species; NF – number of foraminifera per cm3; FAZ – foraminiferal assemblage zones; Litos in – periods of continental lithogenic inputs to the shelf (see references in the text and Appendix 7.5); Clime Pe. – Climate periods in the last 2 millennia (see references in the text); Solar Irr. Anomaly – solar irradiance anomaly using a 22-yr running average reconstruction (after Steinhilber et al., 2012); T anomal. – Temperature anomaly using a 10-yr running average reconstruction (after Martín-Chivelet et al., 2011).

The transition between FAZ V and FAZ IV is marked by the species *T. comprimata* and *P. ipohalina* (AD 1690–1730) and *J. macrescens*, *H. wilberti*, *P. limnetis* and *T. inflata* at the top of FAZ IV (AD 1770). This distribution suggests a gradual evolution from low marsh zone IIA to high marsh zone IB (between MHW and MHWS). It still portrays a markedly low-salinity environment, but the presence (even in low percentage) of these salt marsh species suggests increasing salinity in the area, that might be related to sea-level changes.

The transition from low to high marsh occurs mostly during the Maunder Solar Minimum (AD 1645–1715). The grain size and OM content is still increasing in this FAZ, Br presents its highest content and foraminiferal density remains high, probably reflecting a denser marsh plant cover. During this period, there was a wet phase recorded in Galician continental vegetation (Schellekens et al., 2011), concomitant with the coldest phase of the LIA in Europe that peaked around AD 1700 (e.g., Desprat et al., 2003; Lockwood, 2012; Lockwood et al., 2010; Luterbacher et al., 2001).

FAZ III to I also correspond to a high marsh depositional environment, recording frequent increments of salt marsh species and low foraminiferal density episodes, under general conditions of low salinity. Such variability of assemblages is associated with the end of the LIA and beginning of the PWP, characterized by alternating wet and dry years, namely dryer winter conditions (e.g., Marques, 2001; Abrantes et al., 2011). This reduced river discharge leads to an increase in the marine influence inside the estuary. The beginning of meteorological instrumental record in the NW of Portugal in AD 1864 (FAZ III) allows a better interpretation of proxy data.

The high marsh (foraminiferal IB zone) recorded at FAZ III, is mostly represented by low-salinity assemblages. The species associated with salt marshes are meaningful but with lower percentages: *J. macrescens* (12–23%), *T. inflata* (3–22%) and *T. comprimata* (3–13%). The assemblages still have low diversity and density exhibits a significant drop for most of FAZ III (Table 7.2). The lower density levels, 59 tests/cm^3 (AD 1780) and 34 tests/cm^3 (AD 1820), tend to be associated with the Dalton Solar Minimum (AD 1790–1820) transitions. Other low values are recorded throughout this event: 17 tests/cm^3 (AD 1850) and 44 tests/cm^3 (AD 1890). This disparate record between 17 and 205 test/cm^3 suggests a biotic response to more stressful conditions, induced by alternating periods of intense rainfall/floods and droughts. In fact, it was a time of major river floods in northern Portugal, as recorded at Douro basin (e.g., Rodrigues et al., 2003; Araújo, 2005). The record of floods from the Atlantic Iberian Rivers (south basins included) also suggests higher flood intensification during the periods AD 1730–1760, AD 1780–1810 and AD 1870–1900 (Marques, 2001; Rodrigues et al., 2003; Benito et al., 2008; Appendix 7.5). This alternating climatic pattern switches the system from essentially fluvial controlled to more marine, with increasing salinity in the high marsh ecosystem as a result of higher evaporation rates and higher inputs of marine water into the estuary.

Alternations in the C/N and $\delta^{13}C$ values through the 18th and 19th centuries were consistent with fluctuations in the n-alkyl parameters. These proxies also document regular intensive rainfall alternating with severe droughts (De la Rosa et al., 2012). Events like storms, cold persistent rains, wet and cool summers, and droughts that caused wine harvest delays, crop loss and famines, high prices of cereals, and plagues are documented for the Minho region throughout the 18th century and the beginning of the 19th century, as well as religious services pro-pluvia and pro-serenitate (Marques, 2001). These historical records therefore corroborate the climatic pattern suggested by geochemical and foraminiferal proxies.

The lowest foraminifera density level recorded in FAZ II (68 tests/cm^3) occurs at AD 1900, probably linked to the solar minimum of AD 1900–1920 (Scaffeta, 2012). Major flooding events of the NW Portuguese main rivers are recorded in the transition from the 19th to the 20th century, like in the Douro (e.g., Rodrigues et al., 2003; Araújo, 2005; Appendix 7.5) and Lima basins: the higher mark of the 20th century Lima river flood, from 1909, may be directly observed on the medieval tower wall of Ponte de Lima.

The analysis of the drought events, based on standardized precipitation index (SPI_12-month) for the series of Porto meteorological stations data (1922–2005), reveals that droughts begun in the mid-1930s, attaining their most significant expression (severe to extreme droughts: SPI ≤ −1.5) in the 1940s and 1950s (1944/1945, 1949, 1953/1954 and 1957; Domingos, 2006). Moreira et al. (2012) noted the same severe and extreme droughts until 1956, followed by a period of decrease in drought episodes. Besides its severity, the Palmer Drought Severity Index (PDSI) notes that the duration of these droughts was the most striking of the instrumental record: 1933–1935, 26 months; 1943–1946, 36 months and 1953–1955, 25 months (Pires et al., 2010). The salt marsh species acme (AD 1934) may therefore be the corollary of these dryer conditions (Figure 7.5), probably associated with the solar maximum of AD 1940–1950 (Scaffeta, 2012). After AD 1960, the foraminiferal assemblages gradually become dominated by low-salinity species (> 70%) until AD 1983, during the solar minimum AD 1960–1980. This transition points towards a higher fluvial influence in the lower estuary. In fact, the instrumental precipitation recorded in the Minho region (available since 1934; http://snirh.pt) shows persistent positive anomalies from 1955 to 1983 (Fatela et al., 2013) and the SPI_12 of Porto exhibits the lowest drought indices (Figure 7.5). Besides the direct effect of this high precipitation, the river flow and seepage inputs are also enhanced over the high marsh zone, creating ecological conditions that lead to a major presence of low-salinity species.

The enhanced Br concentration shows a direct relation with OM contents throughout this FAZ (10–4 cm depth; AD 1900 to 1985) with higher values at 4–5 cm depth, AD 1983 (Appendix 7.3). The organic geochemical results obtained by De la Rosa et al. (2012) showed a decrease in the terrestrial OM component and an increase of plankton-derived lipid contribution at AD 1960–1985. This was interpreted as a possible enhancement of marine input probably associated with a

reduction in the Minho River discharge due to the construction of many major dams or with diagenetic processes induced by the selective degradation of different minerals in sediments affecting, for instance, the C_{org}/N. While the presence of dams might reduce the relationship between precipitation and runoff, the good correlation between these two parameters (DeCastro et al., 2006; Gómez-Gesteira et al., 2011; Fatela et al., 2013) suggests that this is not the case here. Also, it should be noted that the intense dredging in the Minho lower estuary, mainly between 1960 and 1990 (Alves, 1996; Delgado, 2011), caused an intense remobilization of sediments. The process of sand extraction also included the wash of these materials leaving the mud fraction (OM included) inside the estuary during rising tides. These anthropogenic activities likely promoted remobilization, transport and redeposition of the mud fraction, contributing to the intensification of the geochemical marine signal in the tidal marshes. The foraminiferal assemblages highlight that rainfall increased the brackish ecological conditions at the high marsh, in spite of the enhanced marine geochemical records for this time.

Increase fluvial influence is also recorded in FAZ I by the OM proxies (De la Rosa et al., 2012). Foraminiferal assemblages are consistent with the present-day high marsh zone IB. This assemblage reflects the modern hydroclimatic balance in the Minho lower estuary, where low-salinity species prevail at higher high marsh zones (Figure 7.3; Table 7.2), mostly under brackish/fresh estuarine water. The lowest values of foraminiferal density reflect the precipitation positive anomalies and the intensification of flood events (Fatela et al., 2013).

Brackish conditions have persisted in the Minho estuary at least since AD 140. The intertidal sedimentary record highlights two main steps – tidal flat and marsh – where the preservation of proxies' information, namely benthic foraminifera, is quite distinct. The tidal flat assemblages are poorly preserved and often absent, in this environment where the hydrogeochemical pattern is marked by a general baseline depleted in calcium carbonate (Moreno et al., 2007; Valente et al., 2009). Even so, it is clear that the residual assemblages are predominantly composed by low-salinity species. The sediment accretion leads to the marsh installation after AD 1380 and the development of a plant cover that reduces hydrodynamics energy, acts as a sediment trap and improves the assemblages' preservation. Marsh foraminiferal response firstly reflects the elevation change from tidal flat to high marsh and the hydrological balance inside the estuary.

The hydrological balance is closely connected to climate variability during the last millennia and its dependent on the fluctuations in solar activity (e.g., Duhau, 2006; Jager and Duhau, 2009; Jager and Nieuwenhuijzen, 2013; Keller, 2004; Lean, 2010; Mörner, 2010; Shindell et al., 2001; Usoskin, 2013; Versteegh, 2005; Wanner et al., 2008), which drives the position, migration and stability of atmospheric systems (e.g., Haigh, 2007) and oceanic circulation (e.g., Mörner, 2010). According to Shindell et al. (2001) and Martín-Puertas et al. (2012), the modeling of climate response to periods of low solar activity coupled with low NAO index and led to a southward displacement of the westerlies.

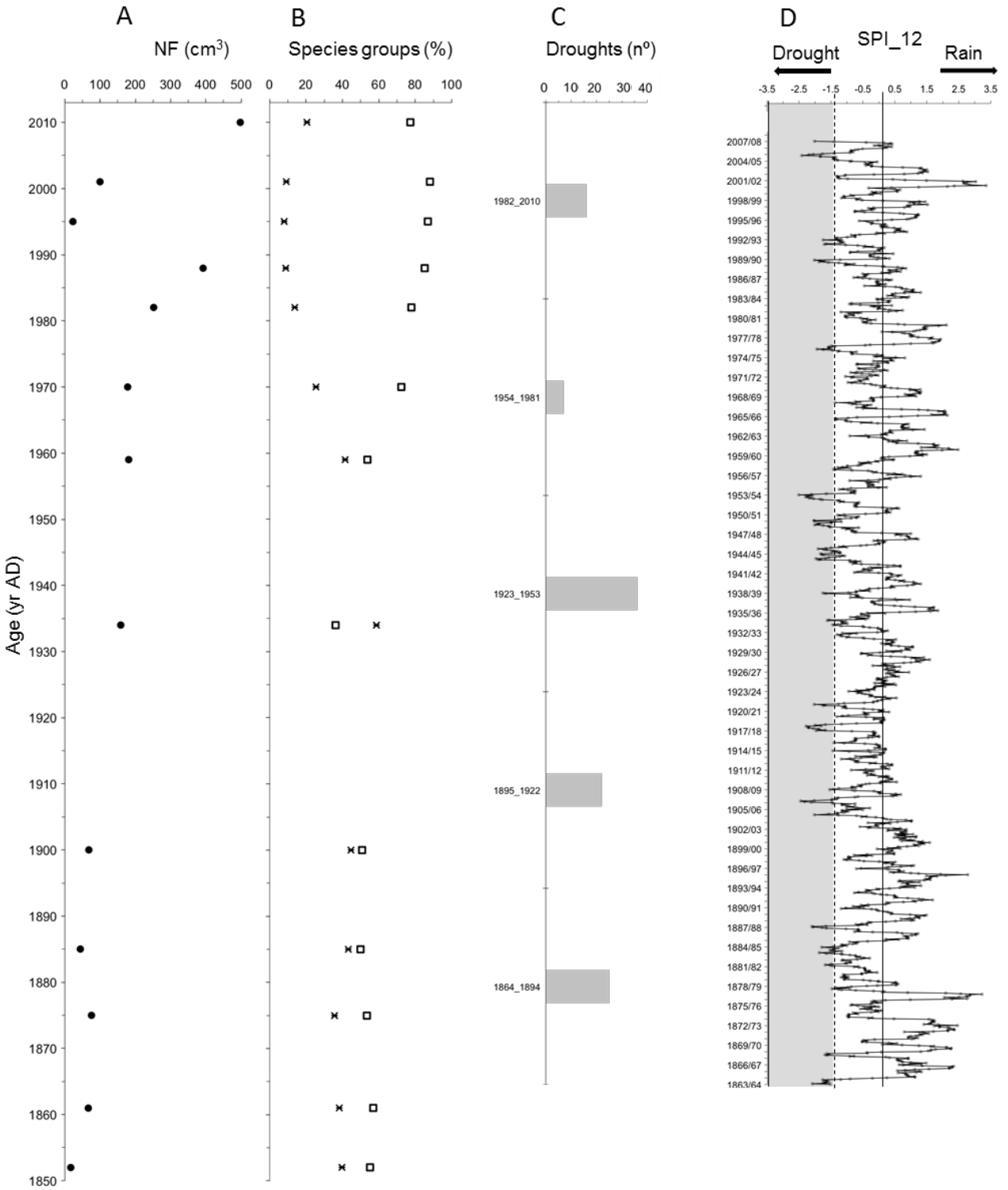

Figure 7.5. Relationship between foraminiferal data and Standardized Precipitation Index (12-months: SPI_12), after Moreira et al. (2012), from Porto (Serra do Pilar: 41º08′19.20″ N–08º36′09.68″ W). **A –** number of foraminifera per cm^3; **B –** percentage of "normal" (stars) and "low" salinity (open squares) species; **C –** number of severe and extreme droughts (grey bars) calculated with the SPI_12, grouped in intervals of *ca.* 30 yrs., from 1864 to 1894, 1895 to 1922, 1923 to 1953 and 1982 to 2010; **D –** SPI_12 time series, from hydrological year 1863/1864 to 2007/2008), grey column represents the field of severe and extreme droughts (SPI ≤ −1.5).

Therefore, as a response to reduced solar activity, European mid-latitudes experienced colder temperatures and increased humidity. The paleoclimatic records of the Iberian Peninsula continental shelf reveal increased river discharge during periods of negative NAO (Álvarez et al.,

2005; Lebreiro et al., 2006; Bernárdez et al., 2008b; Abrantes et al., 2011; González-Álvarez, 2013) and the instrumental data show good correlations between negative phases of NAO index and winter precipitation and river flow in NW Iberia, namely in Minho river basin (e.g., Trigo et al., 2004; DeCastro et al., 2006; Fatela et al., 2013). The hydrological balance recorded by the Caminha marsh foraminiferal and sedimentological proxies is controlled by the atmospherical modes, reflecting the NE Atlantic climate dynamic, namely from LIA to present.

7.6. Conclusions

Foraminiferal assemblages reveal the paleoenvironmental evolution of NW Portugal estuaries, primarily in the intertidal zone. The assemblages, associated with sedimentological and geochemical proxies, provided a detailed reconstruction for the last two millennia. Six Foraminiferal Assemblage Zones (FAZ) have been considered in this period. The tidal flat environment prevailed in the riverbanks of Minho low estuary until the end of the 14th century, when vertical accretion led to the colonization by halophyte plants and the development of a stable low marsh environment. The natural continuity of this process, probably enhanced by anthropogenic activities, resulted in the establishment of the high marsh zone, beginning at about the 18th century. Foraminiferal species and the density of their assemblages revealed to be a fundamental tool to the recognition of the estuarine hydrological balance, namely between predominantly marine or fluvial conditions as result of wet or dry periods. Estuarine evolution mainly occurred under brackish conditions reflected by the dominance of low-salinity species, where the flood events created a drop in the foraminiferal density. The drought periods are marked by an increase in the proportion of salt marsh species that dominated the assemblages during the most severe events recorded in the middle of 20th century. The stronger influence of marine or fluvial conditions inside the estuary over RWP, MCA, LIA and PWP appears closely connected to climate variability (in dependence upon the fluctuations in solar activity), highlighting the contribution of marsh foraminifera from SW Europe to the understanding of NE Atlantic regional climate evolution.

Acknowledgments

This work is a contribution of the WestLog (PTDC/CTE/105370/2008) project, funded by the Fundação para a Ciência e a Tecnologia – FCT, that includes the grants of João Moreno, Inês Pereira and Ana Medeiros. Jose de la Rosa's participation was funded through the Ciência 2008 framework (FCT) at IST/CTN. It is also a contribution to the IGCP Project 588, Northwest Europe working group of the INQUA Commission on Coastal and Marine Processes and the Geo-Q Zentroa Research Unit (Joaquín Gómez de Llarena Laboratory), Sociedad de Ciencias Aranzadi. We are grateful to Elsa Moreira (Centro de Matemática e Aplicações, Faculdade de Ciências e Tecnologia

– UNL) who kindly provided SPI data series from Porto. We also thank Peter Langdon, Derek Booth and two anonymous reviewers for their comments that improved the final manuscript.

References

Abrantes, F., Lebreiro, S., Rodrigues, T., Gil, I., Bartels-Jónsdóttir, H., Oliveira, P., Kissel, C., Grimalt, J.O., 2005. Shallow marine sediment cores record climate variability and earthquake activity off Lisbon (Portugal) for the last 2,000 years. Quaternary Science Reviews 24, 2477–2494.

Abrantes, F., Rodrigues, T., Montanari, B., Santos, C., Witt, L., Lopes, C., Voelker, A.H.L., 2011. Climate of the last millennium at the southern pole of the North Atlantic Oscillation: an inner-shelf sediment record of flooding and upwelling. Climate Research 48, 261–280.

Alday, M., Cearreta, A., Cachão, M., Freitas, M.C., Andrade, C., Gama, C., 2006. Micropalaeontological record of Holocene estuarine andmarine stages in the Corgo do Porto rivulet (Mira River, SW Portugal). Estuarine, Coastal and Shelf Science 66, 532–543.

Álvarez, M., Flores, J., Sierro, F., Diz, P., Francés, G., Pelejero, C., Grimalt, J., 2005. Millennial surface water dynamics in the Ría de Vigo during the last 3000 years as revealed by coccoliths and molecular biomarkers. Palaeogeography, Palaeoclimatology, Palaeoecology 218, 1–13.

Alves, A., 1996. Causas e Processos da Dinâmica Sedimentar na Evolução Actual do Litoral do Alto Minho. Unpublished PhD Thesis, Universidade do Minho, Braga, Portugal. 442p.

Andersen, H.V., 1953. Two new species of Haplophragmoides from the Louisiana coast. Contributions from the Cushman Foundation for Foraminiferal Research 4, 21–22.

Appleby, P.G., Oldfield, F., 1992. Application of ^{210}Pb to sedimentation studies. In: Ivanovich, M. and Harmon, R.S. (Eds.), Uranium Series Disequilibrium. Oxford University Press, Oxford, pp. 731–778.

Araújo, E.L.S., 2005. Geoturismo: Conceptualização, Implementação e Exemplo de Aplicação ao Vale do Rio Douro no Sector Porto-Pinhão. Unpublished MSc Thesis, Universidade do Minho, Braga, 213p.

Araújo, M.F., Valério, P., Jouanneau, J.-M., 1998. Heavy metal assessment in sediments of the Ave river basin (Portugal) by EDXRF. X-Ray Spectrometry 27, 305–312.

Araújo, M.F., Conceição, A., Barbosa, T., Lopes, M.T., Humanes, H., 2003. Elemental composition of marine sponges from the Berlengas natural park, western Portuguese coast. X-Ray Spectrometry 32, 428–433.

Behre, K.-E., 2007. A new Holocene sea-level curve for the southern North Sea. Boreas 36, 82–102 (January).

Benito, G., 2006. Paleofloods and historical flood records along the middle Tagus river catchment: climatic and flood hazard implications. Tagus Floods Abstracts, p. 35.

Benito, G., Machado, M.J., Pérez-González, A., 1996. Climate change and flood sensitivity in Spain. In: Branson, J., Brown, A.G. and Gregory, K.J. (Eds.), Global Continental Changes: The Context of Palaeohydrology. Geological Society Special Publication, 115, pp. 95–98.

Benito, G., Thorndycraft, V.R., Rico, M., Sánchez-Moya, Y., Sopeña, A., 2008. Palaeoflood and floodplain records from Spain: evidence for long-term climate variability and environmental changes. Geomorphology 101, 68–77.

Benito, G., Rico, M., Sánchez-Moya, Y., Sopeña, A., Thorndycraft, V.R., Barriendos, M., 2010. The impact of late Holocene climatic variability and land use change on the flood hydrology of the Guadalentín River, southeast Spain. Global and Planetary Change 70, 53–63.

Bernárdez, P., González-Álvarez, R., Francés, G., Prego, R., Bárcena, M.A., Romero, O.E., 2008a. Late Holocene history of the rainfall in the NW Iberian peninsula – evidence from a marine record. Journal of Marine Systems 72, 366–382.

Bernárdez, P., González-Álvarez, R., Francés, G., Prego, R., Bárcena, M.A., Romero, O.E., 2008b. Palaeoproductivity changes and upwelling variability in the Galicia Mud Patch during the last 5000 years: geochemical and microfloral evidence. The Holocene 18, 1207–1218.

Bettencourt, A., Ramos, L., Gomes, V., Dias, J.M.A., Ferreira, G., Silva, M., Costa, L., 2003. In: INAG (Ed.), Estuários Portugueses. Ministério das Cidades, Ordenamento do Território e Ambiente, Lisboa, 311p.

Bradley, R.S., Jones, P.D., 1993. 'Little Ice Age' summer temperature variations: their nature and relevance to recent global warming trends. The Holocene 3, 367–376.

Brady, H.B., 1870. Analysis and descriptions of the Foraminifera. Annals and Magazine of Natural History 4, 273–309.

Brönnimann, P., 1986. Paratrochammina (Lepidoparatrochammina) guaratibaensis n. sp. from Brackish Waters of Brazil and a Check List of Recent Trochamminaceans from Brackish Waters (Protista: Foraminiferida). Revue Paleobiologie 5, 221–229.

Brown, J., Colling, A., Park, D., Philips, J., Rothery, D., Wright, J., 1991. Waves, Tides and Shallow-water Processes. The Open University, 187p.

Burdloff, D., Araújo, M.F., Jouanneau, J.-M., Mendes, I., Monge Soares, A.M., Dias, J.M.A., 2008. Sources of organic carbon in the Portuguese continental shelf sediments during the Holocene period. Applied Geochemistry 23, 2857–2870.

Clarke, M.L., Rendell, H.M., 2006. Effects of storminess, sand supply and the North Atlantic Oscillation on sand invasion and coastal dune accretion in western Portugal. The Holocene 16, 341–355.

Clemmensen, L.B., Murray, A., Heinemeier, J., de Jong, R., 2009. The evolution of Holocene coastal dune fields, Jutland, Denmark: a record of climate change over the past 5000 years. Geomorphology 105, 303–313.

Cook, E.R., Seager, R., Heim Jr., R.R., Vose, R.S., Herweijer, C., Woodhouse, C., 2010. Megadroughts in North America: placing IPCC projections of hydroclimatic change in a long-term palaeoclimate context. Journal of Quaternary Science 25, 48–61.

Costas, S., Jerez, S., Trigo, R.M., Goble, R., Rebêlo, L., 2012. Sand invasion along the Portuguese coast forced by westerly shifts during cold climate events. Quaternary Science Reviews 42, 15–28.

Cushman, J.A., Brönnimann, P., 1948. Some new genera and species of foraminifera from brackish water of Trinidad. Contributions from the Cushman Laboratory for Foraminiferal Research 24, 15–21.

De Jager, C. and Duhau, S., 2009. Episodes of relative global warming. Journal of Atmospheric and Solar-Terrestrial Physics 71, 194–198.

De Jager, C. and Nieuwenhuijzen, H., 2013. Terrestrial ground temperature variations in relation to solar magnetic variability, including the present Schwabe cycle. Natural Science 5, 1112–1120.

De la Rosa, J.M., Araújo, M.F., González-Pérez, J.A., González-Vila, F.J., Soares, A.M., Martins, J.M., Leorri, E., Corbett, R., Fatela, F., 2012. Organic matter sources for tidal marsh sediment over the past two millennia in the Minho River estuary (NW Iberian Peninsula). Organic Geochemistry 53, 16–24.

Debenay, J.-P., Guiral, D., Parra, M., 2002. Ecological factors acting on microfauna in mangrove swamps. The case of foraminiferal assemblages in French Guiana. Estuarine, Coastal and Shelf Science 55, 509–533.

DeCastro, M., Lorenzo, M., Taboada, J.J., Sarmiento, M., Alvarez, I., Gómez-Giesteira, M., 2006. Influence of teleconnection patterns of precipitation variability and on river flow regimes in the Miño River basin (NW Iberian Peninsula). Climate Research 32, 63–73.

Delgado, A., 2011. Caracterização hidrodinâmica e sedimentar do estuário do rio Minho. Unpublished MSc Thesis, Universidade do Porto, Portugal, 197p.

Dellwig, O., Hinrichs, J., Hild, A., Brumsack, H.-J., 2000. Changing sedimentation in tidal flat sediments of the southern North Sea fromthe Holocene to the present: a geochemical approach. Journal of Sea Research 44, 195–208.

Desprat, S., Goñi, M.F.S., Loutre, M.-F., 2003. Revealing climatic variability of the last three millennia in northwestern Iberia using pollen influx data. Earth and Planetary Science Letters 213, 63–78.

Devy-Vareta, N., 1986. Para uma geografia histórica da floresta portuguesa. do declínio das matas medievais à política florestal do renascimento (séc. xv e xvi). Revista da Faculdade de Letras — Geografia. I Série, vol. I. Porto, pp. 5–37.

Domingos, S.I.S., 2006. Análise do índice de seca Standardized Precipitation Index (SPI) em Portugal Continental e sua comparação com o Palmer Drought Severity Index (PDSI). Unpublished Msc Thesis, Universidade de Lisboa, Portugal, 53p.

Domínguez-Castro, F., Santisteban, J.I., Barriendos,M., Mediavilla, R., 2008. Reconstruction of drought episodes for central Spain from rogation ceremonies recorded at Toledo Cathedral from 1506 to 1900: a methodological approach. Global and Planetary Change 63, 230–242.

Do Ó, A., Roxo, M.J., 2008. Drought events in Southern Portugal from the 12th to the 19th centuries: integrated research from descriptive sources. Natural Hazards 47, 55–63.

Drago, T., Freitas, M.C., Rocha, F., Cachão, M., Moreno, J., Naughton, F., Fradique, C., Araújo, F., Silveira, T., Oliveira, A., Cascalho, J., Fatela, F., 2006. Paleoenvironmental evolution of estuarine systems during the last 14 000 years — the case of Douro estuary (NW Portugal). Journal of Coastal Research, SI 39, 186–192.

Duhau, S., 2006. Solar activity, Earth's rotation rate and climate variations in the secular and semi-secular time scales. Physics and Chemistry of the Earth 31, 99–108.

Fatela, F., Taborda, R., 2002. Confidence limits of species proportions in microfossil assemblages. Marine Micropaleontology 45, 169–174.

Fatela, F., Moreno, J., Antunes, C., 2007. Salinity influence on foraminiferal tidal marsh assemblages of NW Portugal: an anthropogenic constraint?. Thalassas, An International Journal of Marine Sciences 23, 51–63.

Fatela, F., Moreno, J., Moreno, F., Araújo, M.F., Valente, T., Antunes, C., Taborda, R., Andrade, C., Drago, T., 2009. Environmental constraints of foraminiferal assemblages distribution across a brackish tidal marsh (Caminha, NW Portugal). Marine Micropaleontology 70, 70–88.

Fatela, F., Moreno, J., Leorri, E., Corbett, R., 2013. High marsh foraminiferal assemblages response to intra-decadal and multi-decadal precipitation variability, between 1934 and 2010 (Minho, NW Portugal). Journal of Sea Research. http://dx.doi.org/10. 1016/j.seares.2013.07.021.

Font Tullot, I., 1988. Historia del clima de España. Spanish Meteorological Institute (INM), Madrid, 297p.

Gehrels, W.R., 1994. Determining relative sea level change from salt marsh foraminifera and plant zones on the coast of Maine, USA. Journal of Coastal Research 10, 990–1009.

Gehrels, W.R., Newman, S.W.G., 2004. Salt-marsh foraminifera in Ho Bugt, western Denmark, and their use as sea-level indicators. Danish Journal of Geography 104, 49–58.

Gil-Garcia, M.J., Ruiz Zapata, M.B., Mediavilla, R., Santisteban, J.I., Dominguez-Castro, F., Dabrio, C.J., 2008. Registro de los cambios humanos y naturales en el humedal de las Tablas de Daimiel (Ciudad Real, España). Geo-Temas 10, 1471–1474.

Gómez-Gesteira,M., Gimeno, L., de Castro, M., Lorenzo, M.N., 2011. The state of climate in NW Iberia. Climate Research 48, 109–144.

González-Álvarez, R., 2013. Cambios climáticos de pequeña magnitude durante el Holoceno: sus efectos en la paleoceanografía de la plataforma continental gallega. Unpublished PhD Thesis, Universidade de Vigo, España, 306p.

Graham, N.E., Ammann, C.M., Fleitmann, D., Cobb, K.M., Luterbacher, J., 2011. Support for global climate reorganization during the “Medieval Climate Anomaly”. Climate Dynamics 37, 1217–1245.

Granja, H.M., 1990. Representar a geodinâmica da zona costeira: o passado e o presente; que futuro? Unpublished PhD Thesis, Universidade do Minho, Braga, Portugal, 347p.

Granja, H.M., Carvalho, G.S., 1992. Dunes and Holocene deposits of the coastal zone of Portugal, north Mondego Cape. In: Carter, R.W.G., Curtis, T.G.F. and Sheehy-Skeffington, M.J. (Eds.), Coastal Dunes: Geomorphology, Ecology and Management for Conservation. Proceedings of the Third European Dune Congress, Galway, Ireland, pp. 43–50.

Granja, H.M., 1999. Evidence for Late Pleistocene and Holocene sea-level, neo-tectonic and climatic control in the coastal zone of northwest Portugal. Geologie en Mijnbouw 77, 233–245.

Granja, H.M., 2007. Multidisciplinary analysis of historical sources – The geomorphological approach. European Seaport Systems in the early modern age. A comparative approach. International Workshop Proceedings. Porto, IHM-UP, pp. 70–78.

Haigh, J.D., 2007. The sun and the earth's climate. Living Reviews in Solar Physics 4, 1–64 (URL accessed 03.12.13: http://www.livingreviews.org/lrsp-2007-2).

Haslett, J., Parnell, A., 2008. A simple monotone process with application to radiocarbon dated depth chronologies. Applied Statistics 57, 399–418.

Hayward, B.W., Grenfell, H.R., Reid, C.M., Hayward, K.A., 1999. Recent New Zealand Shallow-water Benthic Foraminifera: Taxonomy, Ecologic Distribution, Biogeography, and Use in Paleoenvironmental Assessment, Institute of Geological & Nuclear Sciences, Lower Hutt, New Zealand (monograph 21, 264p).

Head, K., 1980. Manual of soil laboratory testing. Volume 1: Soil Classification and Compaction Tests, Pentech Press, London, 339p.

Hippensteel, S.P., Martin, R.E., Harris, M.-S., 2005. Records of prehistoric hurricanes on the South Carolina coast based on micropaleontological and sedimentological evidence, with comparison to other Atlantic Coast records: discussion. Geological Society of America Bulletin 117, 250–253.

Horton, B.P., 1999. The distribution of contemporary intertidal foraminifera at Cowpen Marsh, Tees Estuary, UK: implications for studies of Holocene sea-level changes. Palaeogeography, Palaeoclimatology, Palaeoecology 149, 127–149.

Horton, B.P., Edwards, R.J., 2005. The application of local and regional transfer functions to the reconstruction of Holocene sea levels, north Norfolk, England. The Holocene 15, 216–228.

Horton, B.P., Murray, J.W., 2006. Patterns in cumulative increase in live and dead species from foraminiferal time series of Cowpen Marsh, Tees Estuary, UK: implications for sea-level studies. Marine Micropaleontology 58, 287–315.

Horton, B.P., Culver, S.J., 2008. Modern intertidal foraminifera of the Outer Banks, North Carolina, U.S.A. and their applicability for sea-level studies. Journal of Coastal Research 24, 1110–1125.

Keigwin, L.D., Pickart, R.S., 1999. Slope water current over the Laurentian Fan on interannual to millennial time scales. Science 286, 520–523.

Keller, C., 2004. 1000 years of climate change. Advances in Space Research 34, 315–322.

Kolditz, K., Dellwig, O., Barkowski, J., Bahlo, R., Leipe, T., Freund, H., Rgen Brumsack, H.-J., 2012. Geochemistry of Holocene salt marsh and tidal flat sediments on a barrier island in the southern North Sea (Langeoog, North-west Germany). Sedimentology 59, 337–355.

Lamb, H.H., 1985. Climate History and the Future, Princeton University Press, 835p.

Lean, J.L., 2010. Cycles and trends in solar irradiance and climate.WIREs: Climate Change 1, 111–122. http://dx.doi.org/10.1002/wcc.018.

Lebreiro, S.M., Frances, G., Abrantes, F., Diz, P., Bartels-Jónsdóttir, H.B., Stroynowski, Z.N., Gil, I.M., Pena, L.D., Rodrigues, T., Jones, P.D., Nombela, M.A., Alejo, I., Briffa, K.R., Harris, I., Grimalt, J.O., 2006. Climate change and coastal hydrographic response along the Atlantic Iberian margin (Tagus Prodelta and Muros Ría) during the last two millennia. The Holocene 16, 1003–1015.

Leorri, E., Horton, B.P., Cearreta, A., 2008. Development of a foraminifera-based transfer function in the Basque marshes. Marine Geology 251, 60–74.

Leorri, E., Cearreta, A., 2009a. Quantitative assessment of the salinity gradient within the estuarine systems in the southern Bay of Biscay using benthic foraminifera. Continental Shelf Research 29, 1226–1239.

Leorri, E., Cearreta, A., 2009b. Recent sea-level changes in the southern Bay of Biscay: transfer function reconstructions from salt-marshes compared with instrumental data. Scientia Marina 73, 287–296.

Leorri, E., Gehrels, W.R., Horton, B.P., Fatela, F., Cearreta, A., 2010a. Distribution of foraminifera in salt marshes along the Atlantic coast of SW Europe: tools to reconstruct past sea-level variations. Quaternary International 221, 104–115.

Leorri, E., Cearreta, A., Corbett, R., Blake, W., Fatela, F., Gehrels, R., Irabien, M.J., 2010b. Identification of suitable areas for high-resolution sea-level studies in SW Europe using commonly applied ^{210}Pb models. Geogaceta 48, 35–38.

Leorri, E., Fatela, F., Cearreta, A., Moreno, J., Antunes, C., Drago, T., 2011. Assessing the performance of a foraminifera-based transfer function to estimate sea-level changes in northern Portugal. Quaternary Research 75, 278–287.

Leorri, E., Drago, T., Fatela, F., Bradley, S., Moreno, J., Cearreta, A., 2013. Late Glacial and Holocene coastal evolution in the Minho estuary (N. Portugal): implications for understanding sea-level changes in Atlantic Iberia. The Holocene 23, 352–362.

Leri, A.C., Myneni, S.C.B., 2012. Natural organobromine in terrestrial ecosystems. Geochimica et Cosmochimica Acta 77, 1–10.

Leri, A.C., Hakala, A., Marcus, M.A., Lanzirotti, A., Reddy, C.M., Myneni, S.C.D., 2010. Natural organobromine in marine sediments: new evidence of biogeochemical Br cycling. Global Biogeochemical Cycles 24 (GB4017), 1–15.

Llasat, M.-C., Barriendos, M., Barrera, A., Rigo, T., 2005. Floods in Catalonia (NE Spain) since the 14th century. Climatological and meteorological aspects from historical documentary sources and old instrumental records. Journal of Hydrology 313, 32–47.

Lockwood, M., 2012. Solar Influence on Global and Regional Climates. Surveys in Geophysics 33, 503–534. http://dx.doi.org/10.1007/s10712-012-9181-3.

Lockwood, M., Harrison, R.G., Woollings, T., Solanki, S.K., 2010. Are cold winters in Europe associated with, low solar activity? Environmental Research Letters 5 (024001), 1–7. http://dx.doi.org/10.1088/1748-9326/5/2/024001.

Loeblich Jr., A.R., Tappan, H., 1988. Foraminiferal Genera and their Classification, v. 1. Van Nostrand Reinhold Company (970p., v. 2, 847 pl.).

Luque, J.A., Juliá, R., 2002. Lake sediment response to land-use and climate change during the last 1000 years in the oligotrophic Lake Sanabria (northwest of Iberian Peninsula). Sedimentary Geology 148, 343–355.

Luterbacher, J., Rickli, R., Xoplaki, E., Tinguely, C., Beck, C., Pfister, C., Wanner, H., 2001. The Late Maunder Minimum (1675–1715) – a key period for studying decadal scale climatic change in Europe. Climatic Change 49, 441–462.

Mann, M.E., Zhang, Z., Rutherford, S., Bradley, R.S., Hughes, M.K., Shindell, D., Ammann, C., Faluvegi, G., Ni, F., 2009. Global signatures and dynamical origins of the little ice age and medieval climate anomaly. Science 326, 1256–1260.

Marques, J., 2001. Estados do Tempo e Outros Fenómenos na Região de Braga, no Século XVII, Vol. L, n. 2. Bracara Augusta, pp. 104–105 (117–118).

Marquina, J.R., 1949. Crecidas Extraordinarias del Rio Duero. Revista de Obras Públicas I (3), 202–213.

Martín-Chivelet, J., Muñoz-García, M.B., Edwards, R.L., Turrero, M.J., Ortega, A.I., 2011. Land surface temperature changes in Northern Iberia since 4000 yr BP, based on δ13C of speleothems. Global and Planetary Change 77, 1–12.

Martínez Cortizas, A., Pontevedra-Pombal, X., Garcia-Rodeja, E., Novoa-Muñoz, J.C., Shotyk, W., 1999. Mercury in a Spanish peat bog: archive of climate change and atmospheric metal deposition. Science 284, 939–942.

Martin-Puertas, C., Valero-Garces, B.L., Mata, M.P., Gonzalez-Samperiz, P., Bao, R., Moreno, A., Stefanova, V., 2008. Arid and humid phases in Southern Spain during the last 4000 years: the Zonar Lake record, Cordoba. The Holocene 18, 1–15.

Martín-Puertas, C., Matthes, K., Brauer, A., Muscheler, R., Hansen, F., Petrick, C., Aldahan, A., Possnert, G., van Geel, B., 2012. Regional atmospheric circulation shifts induced by a grand solar minimum. Nature Geoscience 5, 397–401.

McKee, T.B., Doesken, N.J., Kleist, J., 1993. The relationship of drought frequency and duration to time scales. 8th Conference on Applied Climatology. American Meteoreological Society, Boston, pp. 179–184.

Mohamed, K.J., Rey, D., Rubio, B., Vilas, F., Frederichs, T., 2010. Interplay between detrital and diagenetic processes since the last glacial maximum on the northwest Iberian continental shelf. Quaternary Research 73, 507–520.

Montagu, G., 1808. Testacea Brittanica supplement, S. Woolmer, Exeter, England (183 pp.). Moreira, E.E., Mexia, J.T., Pereira, L.S., 2012. Are drought occurrence and severity aggravating? A study on SPI drought class transitions using log-linear models and ANOVA-like inference. Hydrological Earth System Sciences 16, 3011–3028.

Moreno, F., Araújo, M.F., Moreno, J., Fatela, F., Drago, T., 2005b. Caracterização geoquímica de sedimentos superficiais do estuário do rio Minho e do sapal de Caminha (NW de Portugal) – estimativa do potencial de stress biológico. XIV Semana de Geoquímica & VIII Congreso de Geoquímica dos Países de Língua Portuguesa. Universidade de Aveiro, Portugal, pp. 675–678.

Moreno, F., Moreno, J., Fatela, F., Valente, T., Guise, L., Araújo, M.F., Drago, T., 2005c. Geoquímica de sedimentos em ambientes típicos de sapal – o exemplo do sapal de Caminha (NW de Portugal). XIV Semana

de Geoquímica & VIII Congresso de Geoquímica dos Países de Língua Portuguesa. Univ. Aveiro, Portugal, pp. 661–664.

Moreno, J., Fatela, F., Andrade, C., Cascalho, J., Moreno, F., Drago, T., 2005a. Living Foraminiferal assemblages from Minho/Coura estuary (Northern Portugal): a stressfull environment. Thalassas 21, 17–28.

Moreno, J., Fatela, F., Andrade, C., Drago, T., 2006. Distribution of "living" *Pseudothurammina limnetis* (Scott and Medioli): an occurrence on the brackish tidal marsh of Minho/Coura estuary — Northern Portugal. Revue de Micropaleontologie 49, 45–53.

Moreno, J., Valente, T., Moreno, F., Fatela, F., Guise, L., Patinha, C., 2007. Calcareous foraminifera occurrence and calcite-carbonate equilibrium conditions – a case study in Minho/Coura estuary (N Portugal). Hydrobiologia 597, 177–184.

Mörner, N.-X., 2010. Solar Minima, Earth's rotation and Little Ice Ages in the past and in the future. The North Atlantic-European case. Global and Planetary Change 72, 282–293.

Murray, J.W., 1971. An Atlas of British Recent Foraminiferids. Heinemann Educational Books, 244p.

Murray, J.W., 2006. Ecology and Applications of Benthic Foraminifera. Cambridge University Press, Cambridge, 438p.

Nittrouer, C.A., Sternberg, R.W., Carpenter, R., Bennett, J.T., 1979. The use of ^{210}Pb geochronology as a sedimentological tool: application to the Washington Continental Shelf. Marine Geology 31, 297–316.

Parnell, A., Haslett, J., Allen, J., Buck, C., Huntley, B., 2008. A flexible approach to assessing synchroneity of past events using Bayesian reconstructions of sedimentation history. Quaternary Science Reviews 27, 1872–1885.

Pfister, C., Garnier, E., Alcoforado, M.-J., Wheeler, D., Luterbacher, J., Nunes, M.F., Taborda, J.P., 2010. The meteorological framework and the cultural memory of three severe winter-storms in early eighteenth-century Europe. Climatic Change 101, 281–310.

Phleger, F.B., 1965. Patterns of marsh foraminifera, Galveston Bay, Texas. Limnology and Oceanography 10, 169–180.

Pires, V.C., Álvaro, S., Mendes, L., 2010. Riscos de secas em Portugal continental. Territorium 17, 27–34.

Pla, S., Catalan, J., 2005. Chrysophyte cysts from lake sediments reveal the sub millennial winter/spring climate variability in the northwestern Mediterranean region throughout the Holocene. Climate Dynamics 24, 263–278.

Poirier, C., Chaumillon, E., Arnaud, F., 2011. Siltation of river-influenced coastal environments: respective impact of late Holocene land use and high-frequency climate changes. Marine Geology 290, 51–62.

Price, N.B., Calvert, S.E., Jones, P.G.W., 1970. Distribution of iodine and bromine in sediments of the south western Barents Sea. Journal of Marine Research 28, 22–34.

Rhew, R.C., Miller, B.R., Bill, M., Goldstein, A.H., Weiss, R.F., 2002. Environmental and biological controls on methyl halide emissions from southern California coastal salt marshes. Biogeochemistry 60, 141–161.

Riera, S., Wansard, G., Juliá, R., 2004. 2000-year environmental history of a karstic lake in the Mediterranean Pre-Pyrenees: the Estanya lakes (Spain). Catena 55, 293–324.

Rodrigues, R., Brandão, C., Costa, J., 2003. As cheias no Douro, ontem, hoje e amanhã. In: Ministério das Cidades (Ed.), Ordenamento do território e Ambiente. Instituto da Água, Lisboa, 29p.

Rodrigues, T., Grimalt, J.O., Abrantes, F.G., Flores, J.A., Lebreiro, S.M., 2009. Holocene interdependences of changes in sea surface temperature, productivity, and fluvial inputs in the Iberian continental shelf (Tagus mud patch). Geochemistry, Geophysics, Geosystems 10, 1–17.

Saunders, J.B., 1957. Trochamminidae and certain Lituolidae (Foraminifera) from the recent brackish-water sediments of Trinidad, British West Indies. Smithsonian Miscellaneous Collection 134 (5), 1–23.

Scaffeta, N., 2012. Multi-scale harmonic model for solar and climate cyclical variation throughout the Holocene based on Jupiter–Saturn tidal frequencies plus the 11-year solar dynamo cycle. Journal of Atmospheric and Solar — Terrestrial Physics 80, 296–311.

Schellekens, J., Buurman, P., Fraga, I., Martínez-Cortizas, A., 2011. Holocene vegetation and hydrologic changes inferred from molecular vegetation markers in peat, Penido Vello (Galicia, Spain). Palaeogeography, Palaeoclimatology, Palaeoecology 299, 56–69.

Scott, D.B., 1976. Brackish-water foraminifera from Southern California and description of Polysaccammina ipohalina n. Gen., n. sp. Journal of Foraminiferal Research 6 (4), 312–321.

Scott, D.B., Medioli, F.S., 1978. Vertical zonations of marsh foraminifera as accurate indicators of former sea-levels. Nature 272, 528–531.

Scott, D.B., Medioli, F.S., 1980. Quantitative studies of marsh foraminiferal distributions in Nova Scotia: implications for sea level studies. Special Publication – Cushman Foundation for Foraminiferal Research 17, 58.

Scott, D.B., Medioli, F.S., Schafer, C.T., 2001. Monitoring in Coastal Environments Using Foraminifera and Thecamoebian Indicators. Cambridge University Press, USA, 177p.

Shindell, D.T., Schmidt, G.A., Mann, M.E., Rind, D., Waple, A., 2001. Solar forcing of regional climate change during the Maunder Minimum. Science 294, 2149–2152.

Smith, J.N., 2001. Why should we believe ^{210}Pb sediment geochronologies? Journal of Environmental Radioactivity 55, 121–123.

Steinhilber, F., Abreu, J.A., Beer, J., Brunner, I., Christl, M., Fischer, H., Heikkilä, U., Kubik, P. W., Mann, M., McCracken, K.G., Miller, H., Miyahara, H., Oerter, H., Wilhelms, F., 2012. 9,400 years of cosmic radiation and solar activity from ice cores and tree rings. PNAS 109, 5967–5971.

Stine, S., 1994. Extreme and persistent drought in California and Patagonia during Medieval Time. Nature 369, 546–549.

Taborda, R., Dias, J.M.A., 1991. Análise da sobre-elevação do nível do mar de origem meteorológica durante os temporais de 1978 e 1981. Geonovas, SI, 1 pp. 89–97.

Trigo, R.M., Pozo-Vázquez, D., Osborn, T.J., Castro-Díez, Y., Gámis-Fortis, S., Esteban-Parra, M.J., 2004. North Atlantic Oscillation influence on precipitation, river flow and water resources in the Iberian Peninsula. International Journal of Climatology 24, 925–944.

Trouet, V., Esper, J., Graham, N.E., Baker, A., Scourse, J.D., Frank, D.C., 2009. Persistent positive North Atlantic Oscillation mode dominated the medieval climate anomaly. Science 324, 78–80.

Usoskin, I.G., Solanki, S.K., Kovaltsov, G.A., 2007. Grand minima and maxima of solar activity: new observational constraints. Astronomy & Astrophysics 471, 301–309.

Usoskin, I., 2013. A history of solar activity over millennia. Living Reviews in Solar Physics 10, 1–94 (URL accessed 25th November, 2013: http://www.livingreviews.org/lrsp-2013-1).

Valente, T., Fatela, F., Moreno, J., Moreno, F., Guise, L., Patinha, C., 2009. A comparative study of the influence of geochemical parameters on the distribution of foraminiferal assemblages in two distinctive tidal marshes. Journal of Coastal Research, SI 56, 1439–1443.

Versteegh, G.J.M., 2005. Solar forcing of climate. 2: evidence from the past. Space Science Reviews 120, 243–286.

Vicente-Serrano, S.M., Cuadrat, J.M., 2007. North Atlantic oscillation control of droughts in north-east Spain: evaluation since 1600 A.D Climatic Change 85, 357–379.

Wanner, H., Beer, J., Bütikofer, J., Crowley, T., Cubasch, U., Flückiger, J., Goosse, H., Grosjean, M., Joos, F., Kaplan, J., Küttel, M., Müller, S., Prentice, I., Solomina, O., Stocker, T., Tarasov, P., Wagner, M., Widmann, M., 2008. Mid- to Late Holocene climate change: an overview. Quaternary Science Reviews 27, 1791–1828.

Yamada, Y., 1968. Occurrence of bromine in plants and soil. Talanta 15, 1135–1141.

http://snirh.pt (18th June 2012).
http://drought.unl.edu (22th May 2013).
IPMA, 2013. http://www.ipma.pt/pt/oclima/observatorio.secas/spi/apresentacao/evolu.historica/ (5th June 2013).
WDC and NOAA, 2013. ftp://ftp.ncdc.noaa.gov/pub/data/paleo/climate_forcing/solar_variability/steinhilber2009tsi.txt (25th November 2013).

Appendix 7.1. $^{210}Pb_{Excess}$ and ^{137}Cs content (Bq kg^{-1}) in the FCPw1 core – Caminha tidal marsh.

$^{210}Pb_{Excess}$ and ^{137}Cs content (Bq kg−1)				
Depth (cm)	$^{210}Pb_{Excess}$	error	^{137}Cs	error
0.5	328.8	38.3		
1.5	250.7	29.7		
2.5	166.1	20.9		
3.5	121.1	16.4	16.7	1.7
4.5	113.6	15.6	17.7	1.7
5.5	108.9	15.3	20.0	1.7
6.5	88.2	13.0	28.5	1.7
7.5	125.9	16.8	40.5	1.3
8.5	66.8	10.9	74.4	2.7
9.5	30.5	7.4	45.7	1.7
10.5	12.5	5.6		
11.5	5.0	4.9		
12.5	2.4	4.6		
13.5	2.1	4.6		

Appendix 7.2. Foraminiferal data (%) from core FCPw1 – Caminha tidal marsh.

Depth (cm)	*Cribro*. spp.	*Hapl*. spp.	*H. man*	*T. salsa/irreg.*	*M. fusca*	*J. macrescens*	*T. inflata*	*P. limnetis*	*H. wilberti*	*T. comprimata*	*S. lobata*	*P. guaratibaensis*	*P. ipohalina*	Low Salinity spp.	Salt marsh spp.	NForam/cm^3	AD Age
0-1		17.0	40.4	7.1	12.8		12.8	3.5	4.3					77.3	20.6	498.0	2010
1-2	2.0	6.6	55.6	11.3	12.6		7.3			2.0				88.1	9.3	98.8	2002
2-3	4.3	2.2	50.7	10.1	19.6	0.7	2.2	2.2			0.7	2.2		87.0	8.0	22.1	1995
3-4	9.7	64.9		8.2	2.2		4.5	1.5		2.2	0.7			85.1	9.0	391.4	1988
4-5	0.9		63.2	12.0	1.7		5.1	0.9		5.1		2.6		77.8	13.7	251.7	1983
5-6																	1976
6-7	4.6		59.2	3.8	4.6	3.1	3.1	0.8	13.1	3.8		1.5		72.3	25.4	178.3	1967
7-8			33.8	13.8	6.2	13.8	13.8	0.8	5.4	2.3	3.8	1.5		53.8	41.5	181.7	1960
8-9	2.2		15.9	12.3	5.8	9.4	40.6		4.3	0.7	1.4	2.2		36.2	58.7	159.1	1934
9-10			29.8	14.9	6.1	14.0	26.3	0.9		3.5				50.9	44.7	67.8	1910
10-11			35.0	10.0	5.0	12.5	22.5			8.3				50.0	43.3	44.1	1885
11-12	0.8		34.1	15.5	3.1	12.4	14.0	0.8		4.7	3.9			53.5	35.7	75.8	1876
12-13		46.3		9.8	0.8	13.0	17.1			7.3	0.8			56.9	38.2	66.3	1861
13-14			28.0	25.4	1.7	17.8	14.4			7.6				55.1	39.8	16.7	1852
14-15			39.3	16.4	1.6	13.9	13.1			2.5	0.8	3.3		57.4	33.6	100.1	1838
15-16	2.5		23.8	12.3	5.7	23.0	16.4			4.1	0.8		2.5	44.3	46.7	84.8	1829
16-17			21.2	31.7	7.7	23.1	11.5	1.9			1.9			60.6	38.5	34.0	1819
17-18	2.5		27.5	25.8		20.0	5.0	0.8	0.8	6.7				55.8	33.3	105.9	1805
18-19	0.8		33.1	24.1	2.3	15.8	3.8		0.8	12.8			0.8	60.2	33.8	205.3	1796
19-20	1.6		51.2	20.8	4.0		3.2			7.2				77.6	10.4	58.5	1783
20-21	2.4		63.4	16.3	1.6	2.4	1.6	1.6	4.1	0.8				83.7	10.6	127.4	1774
21-22			43.5	48.9	0.8		0.8			0.8				93.1	1.5	209.2	1761
22-23			36.2	53.7	3.4							1.3		93.3	1.3	160.6	1751
23-24	1.6		17.2	74.2	1.6									94.5		344.7	1738
24-25			22.9	64.9	2.3		0.8					0.8	0.8	90.1	2.3	308.4	1729
25-26			15.2	73.6	5.6							1.6	0.8	94.4	2.4	257.2	1720
26-27			16.9	64.1	3.5					4.9			0.7	84.5	5.6	282.6	1707
27-28	3.8		11.5	69.2	6.9					3.1			0.8	91.5	3.8	307.4	1698
28-29	0.8		6.3	66.4	15.6							3.1	2.3	89.1	5.5	196.0	1685
29-30	0.8			74.6	16.2					4.6				91.5	4.6	303.9	1677
30-31																	1663
31-32	2.1	11.9		67.8	10.5					4.2		0.7	1.4	92.3	6.3	372.3	1654
32-33																	1640
33-34		3.9		81.3	6.3					5.5				91.4	5.5	221.3	1631
34-35																	1617
35-36			5.1	66.9	11.8	0.7				5.9			2.2	83.8	8.8	189.9	1607
36-37																	1592
37-38	2.7	4.1		75.3	0.7					0.7			0.7	82.9	1.4	169.6	1582
38-39																	1565
39-40	8.1		2.4	74.2		0.8							1.6	84.7	2.4	149.8	1552
40-41																	1533
41-42	8.8	0.7		79.4	1.5		0.7	0.7			0.7		2.9	90.4	5.1	609.1	1495
42-43																	1472
43-44		1.5		80.2		0.8							2.3	81.7	3.1		1438
44-45																	1412
45-46	2.8			91.7	0.9								1.9	95.4	1.9	63.1	1378
46-47																	1360
47-48																1.7	1339
48-49																	1328
49-50																1.0	1312
50-51																	1301
51-52																	1290
52-53																1.3	1272
53-54																	1261
54-55																	1244
55-56		3.5	1.7	80.0		0.9	0.9							85.2	1.8	4.4	1233
56-57																	1216
57-58																	1205
58-59		9.8		78.6		1.8								88.4	1.8	3.9	1189
59-60																	1178
60-61																	1159
61-62																9.0	1143
62-63																	1122
63-64																	1084
64-65	41.6			32.7		6.9							1.0	74.3	7.9	12.5	1069
65-66																	1050
66-67																	1031
67-68	13.1	26.2		21.3	1.6	1.6								62.3	1.6	6.3	979
68-69																	950
69-70																	914
70-71		8.3		71.9									2.1	80.2		1.6	890
71-72																	853
72-73																	828
73-74																0.9	803
74-75																	766
75-76																	742
76-77	1.6	4.9		72.4			0.8							78,9	0.8	1.9	706
77-78																	682
78-79																	646
79-80	1.7	10.3		61.2										73.2		1.6	622
80-81																	598
81-82																	550
82-83	25.8	9.0		41.6	1.1								1.1	77.5	1.1	6.4	522
83-84																	494
84-85																	477
85-86	2.1	7.0		72.7										81.8		1.5	451
86-87																	434
87-88																	409
88-89		10.5		66.7									1.0	77.2		0.9	393
89-90																	367
90-91																	343
91-92																0.2	321
92-93																	299
93-94																	277
94-95				59.0	1.0									59.0		0.1	254
95-96																	232
96-97																	210
97-98																0.6	187
98-99																	165
99-100																0.2	143

Appendix 7.3. Sedimentological and geochemical data from core FCPw1 – Caminha tidal marsh.

Depth (cm)	OM %	pH	H_2O%	S (wt%)	Cl (wt%)	Ca (wt%)	Br (mg/kg)	Sr (mg/kg)	Zr (mg/kg)	Mud %	Silt/ Clay	AD Age
0-1	51.4	4.61	75.6	0.46	0.68	0.33	779	123	99	67.1		2010
1-2	64.5	4.99	75.3	0.56	0.52	0.38	1100	138	119	67.1	4.59	2002
2-3	52.1	5.39	74.8	0.60	0.65	0.35	1100	129	119	50.2	8.51	1995
3-4	45.3	5.41	73.5	0.58	0.46	0.36	1100	126	123	69.1	4.74	1988
4-5	39.9	5.27	73.2	0.56	0.63	0.37	1100	123	122	51.0	6.49	1983
5-6	37.7	5.11	53.9	0.45	0.54	0.36	900	113	111	84.6	5.31	1976
6-7	39.7	5.24	68.9							87.9	4.42	1967
7-8	37.3	5.50	69.8	0.41	0.49	0.28	948	113	114	66.5	6.14	1960
8-9	37.6	5.66	67.7	0.39	0.34	0.26	831	113	145	84.0	5.01	1934
9-10	35.7	5.69	67.9	0.40	0.46	0.25	817	117	153	67.6	4.60	1910
10-11	35.7	5.83	62.8	0.34	0.24	0.2	690	138	173	75.1	3.56	1885
11-12	32.1	5.70	61.1	0.30	0.31	0.18	540	118	157	80.6	4.25	1876
12-13	32.3	5.67	62.4	0.31	0.23	0.19	566	120	160	77.9	4.39	1861
13-14	35.6	5.69	64.8	0.35	0.39	0.2	611	116	152	65.5	4.71	1852
14-15	35.3	5.70	65.5	0.34	0.28	0.2	603	121	157	81.4	4.13	1838
15-16	39.8	5.65	63.0	0.31	0.28	0.2	624	120	151	83.6	4.38	1829
16-17	31.6	5.67	61.0	0.30	0.38	0.18	585	116	143	70.0	4.14	1819
17-18	38.4	5.69	60.8	0.28	0.26	0.19	615	131	161	88.2	5.39	1805
18-19	22.6	5.72	61.1	0.29	0.27	0.19	586	121	157	83.3	3.72	1796
19-20	22.4	5.66	63.4	0.30	0.33	0.19	633	120	160	86.0	4.35	1783
20-21	26.9	5.80	65.7	0.34	0.52	0.19	805	113	137	86.6		1774
21-22	37.5	5.82	61.5	0.29	0.31	0.2	693	115	170	86.5	4.29	1761
22-23	28.4	5.73	62.4	0.33	0.32	0.2	758	118	142	80.9	4.02	1751
23-24	25.4	5.88	62.2	0.33	0.50	0.2	836	113	144	84.9	3.90	1738
24-25	28.7	5.81	61.7	0.30	0.36	0.2	818	111	143	88.9	4.12	1729
25-26	31.9	5.87	65.9	0.35	0.47	0.21	1100	113	145	86.3	4.29	1720
26-27	30.8	5.84	66.4	0.36	0.47	0.21	1300	118	138	88.0	3.78	1707
27-28	31.8	5.85	64.2	0.37	0.45	0.22	1100	120	151	91.3	4.28	1698
28-29	25.2	5.87	62.2	0.33	0.65	0.21	931	119	152	83.7	4.46	1685
29-30	24.2	5.85	60.3	0.31	0.43	0.21	806	122	154	86.4	4.63	1677
30-31	21.6	5.77	60.4							91.7	4.13	1663
31-32	21.3	5.79	60.1	0.28	0.45	0.21	712	122	157	91.9	4.38	1654
32-33	21.9	5.84	59.1							91.9	3.73	1640
33-34	21.9	5.89	60.3							90.3	3.96	1631
34-35	22.2	5.88	59.4							79.5	3.85	1617
35-36	19.7	5.88	61.3	0.19	0.67	0.19	234	107	180	89.9	4.19	1607
36-37	21.5	5.94	62.7							93.6	4.83	1592
37-38	20.8	5.94	61.3							92.5	3.74	1582
38-39	19.0	6.02	58.2	0.26	0.82	0.21	487	115	147	92.8	4.01	1565
39-40	15.7	6.03	57.3							92.8	4.11	1552
40-41	15.3	6.62	53.8							88.5	4.01	1533
41-42	15.8	6.60	52.9							95.2	3.73	1495
42-43	14.5	6.30	52.3	0.20	0.73	0.18	366	114	161	90.2	3.97	1472
43-44	13.8	6.56	50.6							94.1	4.05	1438
44-45	12.1	6.61	49.8							93.6	4.21	1412
45-46	13.0	6.64	46.8	0.18	0.63	0.18	294	114	169	94.0	4.07	1378
46-47	10.7	6.68	47.4							94.2	3.98	1360
47-48	10.8	6.70	46.5	0.19	0.49	0.19	260	110	199	95.5	4.26	1339
48-49	12.5	6.68	45.6	0.30	0.87	0.23	646	122	142	94.0	4.09	1328
49-50	10.8	6.69	45.8	0.19	0.52	0.19	211	106	180	95.1	4.32	1312
50-51	9.0	6.56	45.0							93.4	3.91	1301
51-52	8.4	6.64	40.8							97.1	4.43	1290
52-53	8.3	6.61	41.5	0.18	0.66	0.19	142	110	225	96.2	4.19	1272
53-54	8.7	6.58	40.4							97.3	4.16	1261
54-55	8.2	5.76	39.8							95.8	4.31	1244
55-56	8.2	6.30	39.1	0.47	0.47	0.19	78	110	229	97.3	4.09	1233
56-57	8.4	6.14	39.3							94.7	3.92	1216
57-58	8.4	6.19	39.3							96.8	4.07	1205
58-59	8.5	6.10	38.3							98.0	4.40	1189
59-60	8.6	5.54	38.2	0.24	0.59	0.2	82	114	236	97.6	3.85	1178
60-61	8.7	5.63	37.2							96.1	3.87	1159
61-62	8.1	5.33	37.1	0.24	0.41	0.21	68	115	235	95.9	4.20	1143
62-63	9.1	5.18	37.5	0.30	0.56	0.21	71	113	224	93.7	4.25	1122
63-64	9.2	5.05	37.6							96.9	4.24	1084
64-65	8.4	5.01	37.7							97.7	4.24	1069
65-66	8.9	4.73	36.5							98.6	3.89	1050
66-67	8.1	4.82	36.3	0.43	0.53	0.21	77	115	217	97.3	4.24	1031
67-68	8.6	4.16	36.3							98.6	4.12	979
68-69	8.0	4.19	35.7							98.0	4.02	950
69-70	8.3	4.01	35.2							97.8	3.84	914
70-71	8.3	3.87	34.5							98.6	3.49	890
71-72	7.8	3.82	32.0	0.21	0.61	0.2	127	110	224	97.9	4.17	853
72-73	8.2	3.94	31.5							95.7	4.24	828
73-74	7.0	4.16	31.7							97.6	4.15	803
74-75	7.3	3.88	32.6							97.6	3.72	766
75-76	7.7	3.80	34.7	0.52	0.46	0.21	107	113	211	98.6	4.04	742
76-77	7.3	3.75	35.9							96.8	3.47	706
77-78	7.8	3.82	36.2							96.6	3.87	682
78-79	7.4	3.90	35.9							97.7	4.14	646
79-80	5.7	3.95	34.6							98.4	3.95	622
80-81	6.1	4.15	34.5	0.47	0.50	0.21	85	112	221	97.3	4.63	598
81-82	6.2	4.35	33.9							99.2	4.06	550
82-83	6.2	4.38	33.0							98.6	4.25	522
83-84	6.0	4.44	28.0	0.40	0.45	0.2	77	111.27	235	98.6	3.69	494
84-85	6.1	4.29	34.0							98.8	3.84	477
85-86	5.9	4.77	33.9							97.7	4.31	451
86-87	5.5	4.35	33.9							98.5	4.63	434
87-88	5.8	4.19	34.6	0.47	0.53	0.19	87	111	210	98.7	4.12	409
88-89	6.8	4.02	36.1							99.1	3.91	393
89-90	6.9	3.98	37.1	0.51	0.61	0.23	99	116	211	98.9	3.72	367
90-91	7.3	3.90								99.2	3.91	343
91-92	7.2	4.08								99.7	3.29	321
92-93	6.6	3.99								98.6	3.99	299
93-94	6.6	3.97								97.7	4.21	277
94-95	6.2	4.07								98.5	3.44	254
95-96	6.7	4.31								98.9	4.08	232
96-97	6.0	4.52								98.0	4.31	210
97-98	6.0	4.30								98.9	4.58	187
98-99	6.3	4.51								98.4	4.05	165
99-100												143

Appendix 7.4. Data from organic geochemistry proxy core FCPw1 (after De la Rosa et al., 2012) – Caminha tidal marsh.

Depth	Age	C_{org}/N	$\delta^{13}C$	n-Alkanes				n-Alkan-2-ones	
cm	Cal AD		‰	CPI ALKa (o/e)	TAR ALK b	ACL ALK d	C_{31}/C_{27}	CPI KET g (o/e)	C_{25}/C_{27}
0-2	2010-2002	16.5	-26.6	3.0	7.5	27.4	3.6	3.4	0.5
4-6	1983-1977	12.1	-25.0						
10-12	1885-1876	18.0	-26.6	3.0	11.7	28.3	5.0	2.9	0.5
14-16	1838-1829	17.0	-26.1						
20-22	1774-1761	17.4	-26.9	3.1	13.5	28.6	4.8	3.3	0.4
24-26	1729-1720	16.5	-27.4						
30-32	1663-1654	16.2	-27.2	3.5	15.1	28.7	6.7	3.5	0.3
34-36	1617-1607	18.9	-27.4						
40-42	1533-1495	17.5	-27.4	1.8	8.0	28.0	3.4	2.7	0.4
44-46	1412-1378	17.9	-27.1						
50-52	1301-1290	18.5	-27.1	2.0	3.8	26.9	3.3	3.2	0.3
54-56	1244-1233	19.0	-26.5						
60-62	1159-1143	19.9	-26.6	2.4	14.2	28.2	3.0	4.0	0.4
64-66	1069-1050	16.9	-26.3						
70-72	890-853	16.4	-26.8	2.7	13.8	27.3	3.9	4.4	0.4
74-76	766-742	17.9	-26.1						
80-82	598-550	17.0	-26.8	2.2	7.9	27.2	2.9	4.4	0.4
84-86	477-451	18.5	-26.9						
90-92	343-321	13.4	-26.7	2.9	9.9	27.3	3.9	4.0	0.5
94-96	254-232	15.0	-25.5						
98-100	165-143	13.8	-26.4	2.9	8.0	27.1	3.6	4.1	0.4

Appendix 7.5. Chronology of main floods and paleofloods from the Iberian Atlantic and NW Portuguese regions.

NW Portuguese River floods	Iberian Atlantic River floods
2002-03 (a)	1989 (h)
1989, 1987 (a)	1981 (h)
1962, 1959 (a)	1980 - 1960 (g)(i); 1978, 1979 (h)
1909-10 (a)	1950 - 1930 (g)(i); 1947,1941, 1940 (h)
1888, 1877, 1865, 1860 (b)	1912 (h); 1900 (i)
1859, 1855, 1853, 1850, 1843 (b)	1895, 1876, 1855, 1823 (h); 1870 (i)
1825, 1823 (b)	1810 (g)(i); 1808 (h)
1788, 1779, 1727, 1739 (b)	1780 (g)(i); 1760, 1730 (i)
1582 (c)	1640 (i); 1610 (g)(i)
1575 (c); 1573 (d)	1597 (d); 1590 (g)(i); 1573 (d)
1526 (b); 1529 (d)	1540 (i)
1453 (e); 1450 (to 1150) lithos shelf (f)	1290 (g)
1402 (e)	1258 (j)
1207 (g)	1211 (j); 1210 (i); 1200 (j)
1181, 1178, 1168 (g)	1181, 1178, 1168 (j)
1150 (to 1450) lithos shelf (f)	1160 - 1150 (g)(i)
1094 - 1088 (e)	1113 (j)
AD 250 - BC 50 lithos shelf (f)	

(a) Araújo, 2005; (b) Rodrigues et al., 2003; (c) Granja, 2007; (d) Marques, 2001; (e) Abrantes et al., 2011; (f) Bernárdez et al., 2008a; (g) Benito et al., 2008; (h) Loureiro, J., M., 2009. Rio Tejo As Grandes Cheias 1800–2007, ARH Tejo, 79p.; (i) Benito, 2006 (j) De Villalta, F. & Benito, G., 2001. Historical Flood Data Analysis Using a GIS: The Paleotagus Database In: T. Glade et al. (Eds.), The use of Historical Data in Natural Hazard Assessments, pp. 101–112. Kluwer Academic Publishers, Netherlands.

Appendix 7.6. Foraminifera faunal list from core FCPw1 – Caminha tidal marsh.

SPECIES	Citation
Cribrostomoides sp.	
Haplophragmoides manilaensis Andersen, 1953	*Haplophragmoides manilaensis* Andersen, 1953: p. 22, pl. 4, fig. 7, 8. Remarks: interspecific variability in this species includes forms with lobate periphery, depressed straight sutures and forms with almost smooth periphery and slightly depressed, curved sutures. Multiple apertures with supplementary areal pore(s) can also be present especially in lobate forms.
Haplophragmoides sp.	
Haplophragmoides wilberti Andersen, 1953	*Haplophragmoides wilberti* Andersen, 1953: p. 21, pl. 2, figs. 5, 6, pl. 3, figs. 9-16.
Jadammina macrescens (Brady, 1870)	*Trochammina inflata* (Montagu) var. *macrescens* Brady, 1870: p. 290, pl. 11, figs. 5a-c. *Jadammina polystoma* Bartenstein and Brand, 1938: p. 381, text-figs. 1-3. *Trochammina macrescens* Brady; Phleger and Walton, 1950: p. 281, pl. 2, figs. 6, 7. *Jadammina macrescens* (Brady); Murray, 1971: p. 41, pl. 13, figs. 1-5.
Lepidodeuterammina ochracea (Williamson, 1858)	*Rotalia ochracea* Williamson, 1858: p. 55, pl. 4, fig. 112, pl. 5, fig. 113. *Trochammina ochracea* (Williamson 1858); Murray, p. 37, pl. 11, fig. 1-5. *Lepidodeuterammina ochracea* (Williamson 1858); Loeblich & Tappan, p. 127, pl. 135, fig. 10-14.
Miliammina fusca (Brady, 1870)	*Quinqueloculina fusca* Brady, 1870: p. 286, pl. 11, fig. 2a-c. *Miliammina fusca* (Brady); Horton and Edwards, 2006: p. 68, pl. 1, figs. 5a, b.
Paratrochammina guaratibaensis Brönnimann, 1986	*Paratrochammina guaratibaensis* Brönnimann, 1986; Debenay et al., 2002: p. 531, pl. 2, figs. 11-14.
Polysaccammina ipohalina Scott, 1976	*Polysaccammina ipohalina* Scott, 1976: p. 318, pl. 2, fig.1-4, text-figs. 4a-c; Zaninetti et al., 1977: p. 176, pl.1, fig. 7; Scott and Medioli, 1980, p. 43, pl. 2, fig. 8-9.
Psammosphaera sp.	
Pseudothurammina limnetis (Scott and Medioli, 1980)	*Thurammina*? *limnetis*, Scott and Medioli, 1980: p. 43, pl. 1, figs. 1-3. *Pseudothurammina limnetis*, (Scott and Medioli); De Rijk, 1995: p. 28, pl. 1, figs. 15, 16.
Saccammina sp.	
Siphotrochammina lobata Saunders, 1957	*Siphotrochammina lobata* Saunders, 1957: p. 9-10, pl. 3, fig. 1-2; Brönnimann et al., 1992, p. 31, pl. 4, fig. 1-2; De Rijk, 1995, p. 33, pl. 3, figs. 9, 11-13.
Tiphotrocha comprimata (Cushman and Brönnimann, 1948)	*Trochammina comprimata* Cushman and Brönnimann, 1948: p. 41, pl. 8, figs. 1-3. *Tiphotrocha comprimata* (Cushman and Brönnimann); Horton and Edwards, 2006: p. 69, pl. 2, figs. a-e.
Trochammina inflata (Montagu, 1808)	*Nautilus inflatus* Montagu, 1808: p. 81, pl. 18, fig. 3. *Trochammina inflata* (Montagu); Horton and Edwards, 2006: p. 69, pl. 2, figs. 8a-d.
Trochamminita salsa/irregularis (Cushman and Brönnimann, 1948)	*Labrospira salsa* Cushman and Brönnimann 1948 b, p.16, p l.3, fig. 5, 6. *Alveophragmium salsum* (Cushman and Brönnimann). Todd and Brönnimann 1957, p. 23, pl. 2, fig. 3. *Trochamminita salsa* (Cushman and Brönnimann). Saunders 1957, p. 6, pl. 1, fig. 3-8. *Trochamminita irregularis* Cushman and Brönnimann 1948b, p. 17, pl. 4, fig. 1-3. - Saunders, 1957, p. 4, pl. 2, fig. 3-8. - Todd and Brönnimann 57, p. 30, pl. 4, fig. 19-22.- Topping 1973, p. 21, pl. 3, fig. 4-7. Remarks: *T. salsa* and *T. irregularis* are considered as synonymous in several works (e.g., Hayward et al., 1994; Guilbault et al., 1995); in this work they are identified separately but considered as one single group for interpretation. *Trochamminita salsa/irregularis* is abundant in the low salinity environment at the head of estuaries and in the mouth of small streams; mostly occurs at or above mean high waters, under plentiful freshwater seepage or groundwater and stream discharge, but also lives subtidally (e.g., Hayward et al., 1994, 1999). This species was not present in Caminha coarse sandy subtidal and tidal flat surface sediment.

8 Bromine enrichment in marsh sediments as a marker of environmental changes driven by Grand Solar Minima and anthropogenic activity (Caminha, NW of Portugal)

J. Moreno [a], F. Fatela [a], E. Leorri [b], M.F. Araújo [c], F. Moreno [c], J. De la Rosa [d], M.C. Freitas [a], T. Valente [e], D.R. Corbett [b]

[a] Universidade de Lisboa, Faculdade de Ciências, Centro e Departamento de Geologia, Campo Grande, 1749-016 Lisboa, Portugal

[b] East Carolina University, Department of Geological Sciences, Greenville, NC 27858-4353, USA

[c] Universidade de Lisboa, Instituto Superior Técnico, Centro de Ciências e Tecnologias Nucleares, Estrada Nacional 10, km 139,7, 2695-066 Bobadela LRS, Portugal

[d] Instituto de Recursos Naturales y Agrobiología de Sevilla, Av. Reina Mercedes 10, 41012 Sevilla, Spain

[e] Universidade do Minho, Centro de Investigação Geológica, Ordenamento e Valorização de Recursos (CIG-R), Departamento de Ciências da Terra, CIG-R, 4710

Published in: *Science of the Total Environment* 506–507 (2015) 554–566

http://dx.doi.org/10.1016/j.scitotenv.2014.11.062

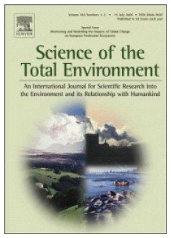

"Bromine (…) received attention as potential contributor to stratospheric ozone loss. In this context, the importance of organohalogen compounds lies in their ability to transfer halogen from the Earth's surface reservoirs, of which the ocean is the most important, to the lower and upper atmosphere."

R.M. Moore in THE HANDBOOK OF ENVIRONMENTAL CHEMISTRY Vol. 3, Part P (2003), p. 86.

ABSTRACT

A sediment core collected in the Caminha tidal marsh, NW Portugal, was used to assess the bromine (Br) signal over the last *ca.* 1700 years. The Br temporal variability reflects its close relationship with

soil/sediment organic matter (OM) and also alterations in Br biogeochemical recycling in marsh environment. The highest Br enrichment in sediments was found during the Maunder Solar Minimum, a major solar event characterized by lower irradiance (TSI) and temperature, increased cloudiness and albedo. The obtained results suggest that those climate-induced changes weakened the natural mechanisms that promote Br biochemical transformations, driven by both living plants metabolism and plant litter degradation, with the ensuing generation of volatile methyl bromide (CH_3Br). It seems that the prevailing climate conditions during the Maunder favoured the retention of more Br in marsh ecosystem, ultimately decreasing the biogenic Br emissions to the atmosphere. During the 20th century, the Br pattern in sediments appears to mirror likewise anthropogenic sources. The significant correlation ($p < 0.05$) between Br/OM ratios and Pb contents in sediments after 1934 suggests a common source. This is most probably related with the rise, massive consumption and prohibition of leaded gasoline, where ethylene dibromide was added as lead scavenger to antiknock mixtures. More regionally, the concerted use of flame retardants on forest fire management, covering the 1980s through mid-1990s in the North of Portugal and Galicia, could be responsible for the observed increase of sediment Br (relatively to Pb) pool of this tidal marsh. Although human-made brominated compounds are being phased-out since the inception of the 1992 Montreal Protocol, the Caminha tidal marsh sedimentary record showed that Br levels only started to decline after 2002.

Keywords: Bromine, tidal marsh, biogenic CH_3Br emissions, solar activity, anthropogenic impacts, NW Iberia.

8.1. Introduction

Salt marshes are very dynamic ecosystems, quickly responding to changing environmental conditions (Costanza et al., 1997). While these environments occupy a very small proportion of the ocean surface (between 22,000 and 400,000 km^2 depending on the estimates), they are ranked between the most valuable ecosystems on Earth mainly due to its capability for providing goods and services (Costanza et al., 1997; Duarte et al., 2013). They generate high biological productivity (between 440 and 1585 g C/m^2/year), they are important carbon sinks (218 ± 24 g C/m^2/year), and they play an important role protecting the coast from flooding and erosion (Fagherazzi et al., 2013). They also mediate some key biogeochemical cycles with repercussions at large scale (e.g., potential for mitigating climate change; Duarte et al., 2013).

The work from Rhew et al. (2000, 2002) and all the succeeding investigation (Cox et al., 2004; Drewer et al., 2006; Manley et al., 2006; Wishkerman et al., 2008; Rhew and Mazéas, 2010; Rhew et al., 2014) highlighted that salt marshes are also sources of some potentially hazardous chemicals, amongst them, methyl bromide (CH_3Br). CH_3Br is a trace gas considered as the single largest carrier of bromine (Br) from the terrestrial and marine environments to the atmosphere. Once there, CH_3Br is photo dissociated to form reactive radical species BrOx (Br + BrO), extremely effective in catalyzing tropospheric ozone (O_3) loss (Toyota et al., 2011). These species take part in many reaction cycles involving O_3, the O_3 photolysis product, the hydroxyl radical (OH), and nitrogen

oxides ($NO+NO_2$=NOx), making bromine even more “aggressive” than chlorine on a per-atom basis for global ozone depletion (Platt and Hönninger, 2003; Monks, 2005).

Bromine can be widely found in nature as soluble bromide salts in seawater, salt lakes and underground brine deposits associated with oil (Lyday, 2000). There are also numerous known organobromine (Br_{org}) compounds (around 2000, until now), synthesized by living organisms or formed during natural abiotic processes like forest fires or volcanic eruptions (Gribble, 2003), or even in early diagenetic processes in soils and sediments (Keppler et al., 2000). The studies regarding Br biogeochemistry support i) the Br cycling through biomass and organic matter (OM) formation/degradation in soils and sediments (Mayer et al., 1981; Malcolm and Price, 1984; Gerritse and George, 1988 and references therein) and ii) the ready uptake (and bioaccumulation) of Br by terrestrial plants and hydrophytes (Jemison and Fox, 1991; Xu et al., 2004), questioning some persistent beliefs, such as, that environmental Br occurs largely as inorganic bromine (Br_{inorg}) and that bromide (Br^-) is an excellent hydrological conservative tracer.

Recently, research based on the application of a set of sensitive X-ray spectroscopic techniques to coastal and marine sediment cores (Leri et al., 2010) and to a soil profile (Leri and Myneni, 2012) allowed to successfully determine Br speciation in samples and showed that Br_{inorg} can be biochemically converted to Br_{org} through natural mechanisms. According to these authors, natural bromination reactions (in sediments/soils, plant and animal debris, algae and fungi) can explain the ubiquitous appearance of Br_{org} in diverse sedimentary environments, in association with organic carbon (C_{org}) through strong covalent C–Br bonds.

Salt marshes, with concomitantly high C_{org} content and relatively elevated concentrations of readily available Br^- (derived from seawater flooding), are privileged settings for Br recycling between inorganic and organic forms. The plant life cycle and plant litter decay processes ultimately promote Br transfer to atmosphere, through the production of volatile methyl bromide. In fact, salt marshes are the largest natural transitional (from land to sea) source of CH_3Br, although emission rates can vary widely around the world (Rhew and Mazéas, 2010; Rhew et al., 2014). Emissions derived from salt marshes located in warmer areas (Mediterranean climate) can be up to two orders of magnitude higher than fluxes from temperate or cooler regions (Blei et al., 2010).

In 2006, Manley and co-workers estimated that over 90% of the CH_3Br released by a salt marsh ecosystem is produced by halophytic vegetation. This inherent ability is, however, highly plant species-dependent (e.g., succulent/non succulent), which is probably a major cause for the high spatial flux variability detected within these ecosystems. The remaining 10% are a contribution from the mid and upper marsh soils/sediments, with no measurable involvement of mud flats (Manley et al., 2006). These results agree with the former thesis that marsh sediments, even organic-rich, more than sources seem to be good candidates for sinks as they can anaerobically degrade CH_3Br by

nucleophilic substitution reactions with sulphide and, in a lesser extent, with chloride (Oremland et al., 1994).

Up to date, there are two well-established pathways for the production of CH_3Br, acting simultaneously in biological systems: (1) biotic production by living plants in their cells as result of the enzymatically mediated methylation of Br^- (Wuosmaa and Hager, 1990; Saini et al., 1995) and (2) abiotically, when Br^-, dissolved in the tissue water of the plant, reacts with the methyl moiety of methoxyl groups ($–OCH_3$) of the pectin molecule, an abundant plant cell-stabilizing component (Hamilton et al., 2003; Keppler et al., 2004). Moreover, it was recognized that this latest reaction takes place at ambient temperatures in senescent and plant leaf litter. Thus, the occurrence of this abiotic process on dry and dead plant material in salt marshes can be, by its own side, responsible for the formation of a quantifiable proportion of CH_3Br, very dependent on temperature in the range of 25–50ºC (Wishkerman et al., 2008).

The phytogenic CH_3Br emission trends from a given salt marsh are complex but they display strong temporal variations linked to both seasonal and diurnal cycles. These are directly related with factors like bromide and water contents of plants, plant growing season, ambient temperature, daylight hours and solar irradiance/sunshine conditions (Rhew et al., 2000, 2002, 2014; Cox et al., 2004; Drewer et al., 2006; Manley et al., 2006; Wishkerman et al., 2008; Rhew and Mazéas, 2010). Taken together, these sightings have conducted to a final assumption, i.e., CH_3Br emissions by salt marshes have strong climate dependence, related mostly with both temperature and insolation (Rhew et al., 2014).

Over the last 100 years, in addition to natural sources, the presence of Br in the atmosphere has had a gradually larger input from a broad number of anthropogenic sources (Montzka et al., 2003; Yvon-Lewis et al., 2009). It was in the first half of the 20th century that bromine-based compounds started to be synthesized worldwide on a commercial basis (Wisniak, 2002), mainly related to the production of leaded gasoline (after 1922) as well as grain and soil fumigants (in the 1930s). In the early 1970s, the demand for flammable commodities has conducted to an extensive use of brominated flame retardants – BFRs (Rahman et al., 2001). This panoply of human-made brominated compounds rapidly achieved notoriety as persistent pollutants especially owing to their great ozone depletion potential and toxicological properties with probable harmful effects in human health (Rahman et al., 2001). All are phased-out under the amended 1992 Montreal Protocol (World Meteorological Organization (WMO), 2002). These policies were responsible for the decline of the atmospheric CH_3Br burden in recent years (Yvon-Lewis et al., 2009). The atmospheric Br content in Europe further diminished as a result of the steadily decrease in the consumption of leaded gasoline since the 1970s, which the UE mandated to be replaced by unleaded gasoline by the year 2005. On the contrary, the annual global consumption of polybrominated diphenyl ethers, one of the most used

halogenated flame retardants, was approximately 40,000 tons in 1992, but increased to more than 65,000 tons in 2001 (de Wit, 2002).

An outcome of the international restrictions imposed to Br anthropogenic sources was the increase of the relative contribution of naturally produced brominated compounds for the stratospheric reactive Br budget. So, undoubtedly, more attention should be paid to its natural terrestrial and marine sources. Specifically for CH_3Br, there is a well-recognized large missing source. Using best estimates, the global CH_3Br budget displays an imbalance with sinks outweigh the sources by around 32 Gg/year, corresponding to approximately 25% of the total annual flux (Yvon-Lewis et al., 2009).

Although salt marshes are generally regarded as net sources of CH_3Br (14.6 Gg/year and 24 Gg/year as best estimates, respectively, from Rhew et al., 2002; Manley et al., 2006), as aforementioned, their land–atmosphere flux rates are under the control of major environmental factors impacting on the halophytic vegetation activity and on the decaying of Br-enriched organic debris. This means that the plant derived fluxes of CH_3Br from a salt marsh are arbitrated by the biogeochemical cycling of Br in such ecosystems.

Under the present global warming trend it seems important to better understand the influence of past climate forcing in global and regional cycles and how they might have altered the Br source/sink dynamics of salt marsh ecosystems through time. In this context, the present work aims to deconvolve the link between the Br record on tidal marsh sediments and past climatic shifting (solar cycles) and anthropogenic fingerprints over the last 1700 years in the Minho River estuary (NW Iberian coast).

8.2. Materials and methods

8.2.1. Study area

The Minho River is an Iberian river with *ca.* 340 km of length that defines in its final stretch (*ca.* 75 km) the border between Portugal and Spain–Galicia (Figure 8.1). The river begins in Serra da Meira (Lugo, Spain) and reaches the Atlantic Ocean near the municipalities of Caminha (Portuguese side) and La Guardia (Spanish side).

The Minho River drains mostly igneous and metamorphic rock formations, including granites, quartz-diorites, greywackes and schists (IGME, 1986; Pereira et al., 1989). It flows in the rainiest region of the country, where the average annual precipitation is around 1800 mm but may reach more than 3500 mm (Fatela et al., 2014), under a wet Atlantic climate. The largest extension of tidal marsh environment (with around 6 km^2) occurs in the south margin of the low-estuary, at the confluence of the Minho River with its tributary, the Coura River (Caminha marsh; Figure 8.1).

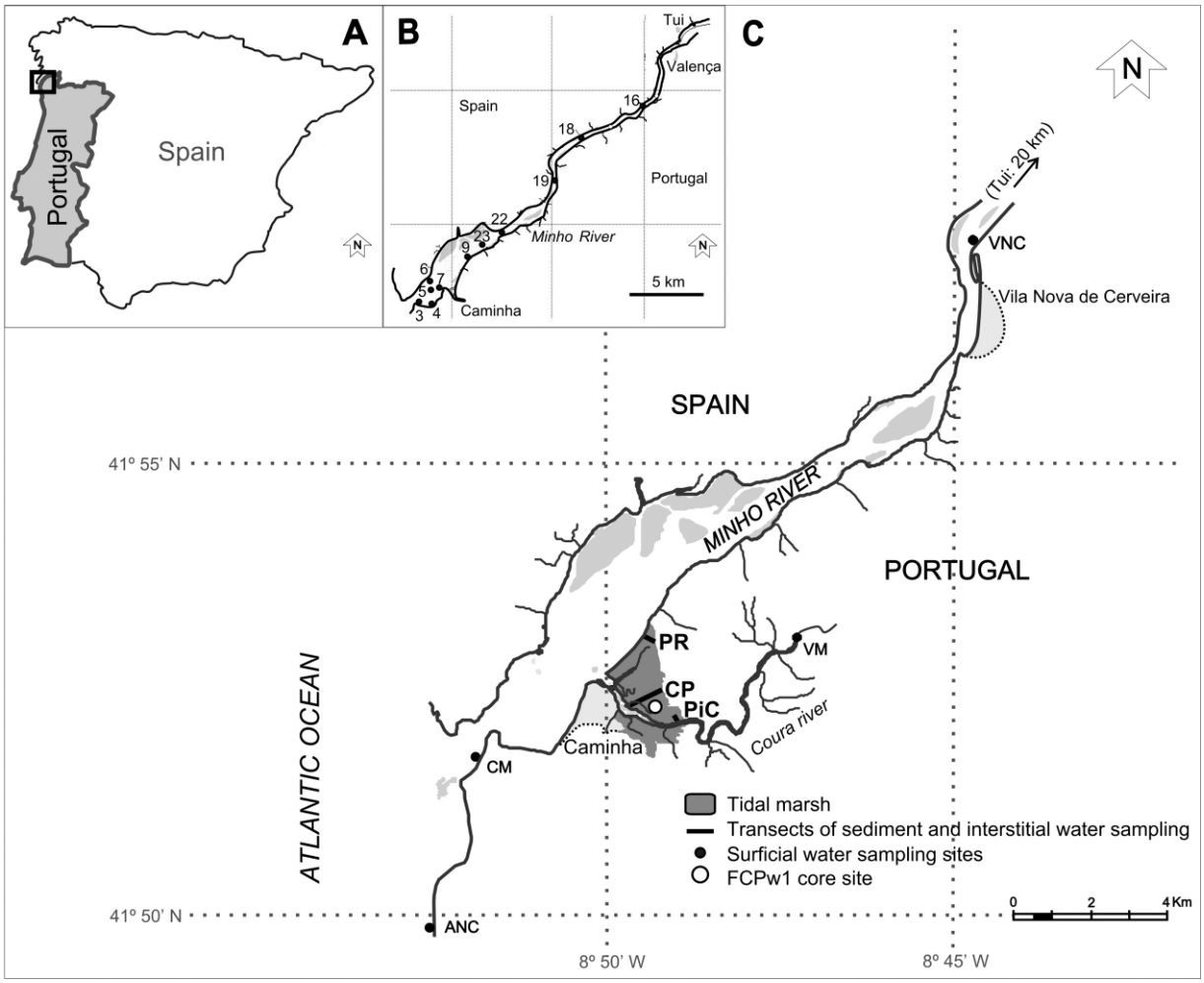

Figure 8.1. **A –** Location of the study area in Portugal. **B –** Location of Minho estuary bottom sediment samples and water analyzed for geochemistry. **C –** Minho estuary and Coura tributary sampling. Dark grey area represents the Caminha tidal marsh. Estuarine water samples CM – Camarido, VNC – Vila Nova de Cerveira and VM – Vilar de Mouros. Surface sediment and interstitial water sampling transects PR – Pedras Ruivas, CP – railway bridge and PiC – Pinelas. FCPw1 – sediment core location.

According to Moreno et al. (2005, 2006), marine water is completely flushed out from the lower estuary during each ebb cycle, leading to a full replacement by fluvial waters. The low salinity conditions are reflected in the prevailing marsh plant cover of sea rush *Juncus maritimus* and *Phragmites australis* on a typically halophytic phytocoenosis of reed meadows (Honrado et al., 2004). Likewise, the dominance of brackish agglutinated foraminifera *Haplophragmoides manilaensis* Andersen 1953, *Trochamminita salsa/irregularis* (Cushman and Brönnimann, 1948), *Pseudothurammina limnetis* (Scott and Medioli, 1980) *and Miliammina fusca* (Brady, 1870) in the marsh assemblages is a reflection of low salinities in this marsh setting (Fatela et al., 2014; Moreno et al., 2014).

8.2.2. Sampling and analytical procedures

8.2.2.1. Sediment surface samples

Twenty-two surface composite sediment samples, each one corresponding to five subsamples of the top 4–5 cm were collected, in 2003, with a small plastic shovel, in an area of a half square meter, on the Caminha intertidal domain (creek, tidal flat, low marsh and high marsh environments), along three cross shore transects: Pedras Ruivas (PR), Railway Bridge (CP) and Pinelas (PiC). These transects represent different estuarine conditions, in terms of hydrodynamics, salt water wedge penetration, tides and plant cover. Additionally, twelve samples of the uppermost *ca.* 5 cm of sediment were collected using a Van Veen grab sampler in the Minho River main channel (Figure 8.1).

After collection, sediments were stored in plastic boxes and kept at -20ºC till freeze drying prior to analysis. The dry bulk sediment was sieved to separate the particles coarser than 2 mm. The undersized fraction was ground in an agate mortar and around 2 g of material was homogenized, dried and compacted into pressed pellets to be analyzed by Energy-Dispersive X-Ray Fluorescence Spectrometry (EDXRF), using a KEVEX 771 spectrometer. Certified reference materials (SGR1 River Sediment from the United States Geological Survey (USGS); SRM 2704 River Sediment and SRM1646 Estuarine Sediment from the National Institute for Standards and Technology (NIST)) were also prepared as pressed pellets and used to calibrate the spectrometer and to determine the accuracy and precision of the overall procedure. Corrections for matrix effects were made by a calibration method (O'Reilly and King, 1986) that calculates the relation of the incoherent and coherent scattered radiation with the atomic number of the elements constituents of the sediments. Samples and certified reference materials were irradiated under different excitation conditions allowing the determination of a set of elements, amongst which the Br and Pb contents. Accuracy and precision measured in the certified reference materials for Pb are better than 10%, although for the SRM 1646 precision is poorer (~14%) derived from counting statistics, due to the low elemental content and peak overlap (As and Pb). Br content is below quantification limits for the SRM 2704 and is not certified in the SRM 1646, however, comparison with available previous published values (Doff, 1989) indicate an accuracy of 6% and a precision of 7% (Appendix 8.1). A detailed description of the equipment, analytical conditions, spectral evaluation, and calibration and quantification procedures has been published elsewhere (Araújo et al., 1998, 2003).

The organic matter (OM) content was estimated by Loss-on-Ignition methodology (LOI). An aliquot of bulk sediment sample (2.0 g) was dried and oven-heated at a temperature of 500ºC ± 50ºC for about 2 h (Moreira et al., 2009). After cooling, the samples were re-weighed and the percentage loss in weight was calculated. Quality control was assured by means of duplicate analysis (30% of the total) with a maximum acceptable coefficient of variation of 20%. LOI measurement errors were

less or equal to 5.0% for 87% of the samples and between 5.1% and 10% in the remaining 13%, with an average error of 2.5% for all the analysis.

8.2.2.2. Water samples

Ten interstitial water samples from tidal marsh transects (CP, PR and PiC; Figure 8.1) were collected and analyzed in 2003 for bromide contents (amongst other major anions). These marsh interstitial waters were sampled during low tide, using a perforated PVC tube inserted into the sediment. The tube was top covered until the water percolated inside allowing the collection of 1000 mL with a plastic syringe. In order to characterize the two possible end-members of water inputs to tidal marsh, marine seawater and fluvial freshwater, a coastal marine (ANC; Figure 8.1), a mouth estuary (CM; Figure 8.1) and two river water samples (VM and VNC; Figure 8.1) were also collected *ca.* 20 cm below surface.

After collection, water samples were immediately refrigerated, transported in polyethylene bottles kept in the dark and stored at 4ºC until analysis. Prior to the analysis and immediately after arriving to the laboratory water samples were filtered through 0.45 µm pore diameter cellulose ester membrane filters, following preconditioning the filter with a small amount of sample. The filtrate was then analyzed for Br^- by ion chromatography (IC) with suppressed conductivity detection (761 Compact IC Metrohm), with raw data being processed with Metrohm Metrodata 1.1 (Valente et al., 2009). The IC method no. S-73, developed by Metrohm for the determination of anions in seawater, was used for the most saline waters. Analytical conditions included the use of a 6.1006.100 Metrosep anion dual 2 column, with a flow of 0.8 mL/min and an injection volume of 20 µg/L. An internal calibration was performed in the range 1–40 mg/L, using multi element ion chromatography solutions (Fluka Analytical). During the analysis sequence, a standard solution of 20 mg/L was included periodically amongst the samples (every five samples). Between samples ultrapure water (Mili Q) was injected for cleaning the system. The detection limit was 0.01 mg/L and the measurement precision was within 5% RSD for all determinations.

8.2.2.3. Sediment core

A series of five one-meter-long sediment cores was collected, at the same FCPw1 sampling site, in the high marsh zone of the Caminha tidal marsh with a manual Auger sampler, 1.55 m above mean sea-level, at 41º52'37″ N and 8º49′28″ W (Figure 8.1), in the year of 2010. After sampling, the cores were transferred to a PVC half pipe stand and wrapped with cling film to protect it during transport and avoid desiccation. The methodologies used for the study of the foraminiferal assemblages and in the acquisition of sedimentological, chronological and organic chemistry data in core samples are fully described elsewhere (De la Rosa et al., 2012; Fatela et al., 2014; Moreno

et al., 2014). One of the cores was sliced every centimeter for the determination of Br and Pb concentrations, following the same techniques used for surface sediment samples.

8.2.3. Solar activity and paleotemperature data

The definition of the Grand Solar Minima events is based on the reconstruction of sunspot number series as referred on Versteegh (2005) and Usoskin et al. (2007). The solar activity reconstruction data (total solar irradiance – TSI) used here are based on a high-resolution galactic cosmic ray (GCR) produced radionuclides ^{10}Be and ^{14}C records from Steinhilber et al. (2012). These cosmogenic isotopes are produced in the Earth's atmosphere by nuclear reactions of cosmic ray particles with atmospheric nitrogen and oxygen, and stored on polar ice (^{10}Be) and tree rings (^{14}C). The solar wind and the solar magnetic field provide protection to Earth from GCRs. There is, therefore, an inverse relationship between solar activity and the production rates of these nuclides.

It was also used a dataset of surface paleotemperatures from northern Iberia determined by a high- resolution study of carbon stable isotope (^{13}C/^{12}C; δ^{13}C) records of stalagmites (Martín-Chivelet et al., 2011). U-dated stable isotope speleothem series are frequently studied in order to generate high- resolution archives as a sensitive tool of climatic or environmental changes (Martín-Chivelet et al., 2011).

8.2.4. Chronology

The final chronology has been created using a Bayesian age-depth model (Bchron 3.2; Haslett and Parnell, 2008; Parnell et al., 2008) based on ^{210}Pb derived sedimentation rates (supported by ^{137}Cs and total Pb chronological markers) and six radiocarbon dates (in total organics). This model provides age and associated errors to every sample (error ranges are presented in Figure 8.2, according to Moreno et al., 2014). ^{210}Pb was measured by alpha spectroscopy following the methodology of Nittrouer et al. (1979). ^{137}Cs was determined by its gamma emissions at 662 keV ^{137}Cs (Smith, 2001) and total Pb concentrations (Appendix 8.2; Leorri et al., 2008; Leorri and Cearreta, 2009) suggest that the constant rate of supply model (CRS; Appleby and Oldfield, 1992) is the most accurate ^{210}Pb derived chronology, as it has been shown to be the most suitable in the region (Leorri et al., 2010). The radiocarbon samples (40–41 cm, 44–45 cm, 63–64 cm, 66–67 cm, 81–82 cm and 90–91 cm depth) were analyzed at Beta Analytic Inc. (USA) (Table 8.1) to extend down-core the chronology (Figure 8.2). The obtained calendar ages are presented in years of Anno Domini (years AD).

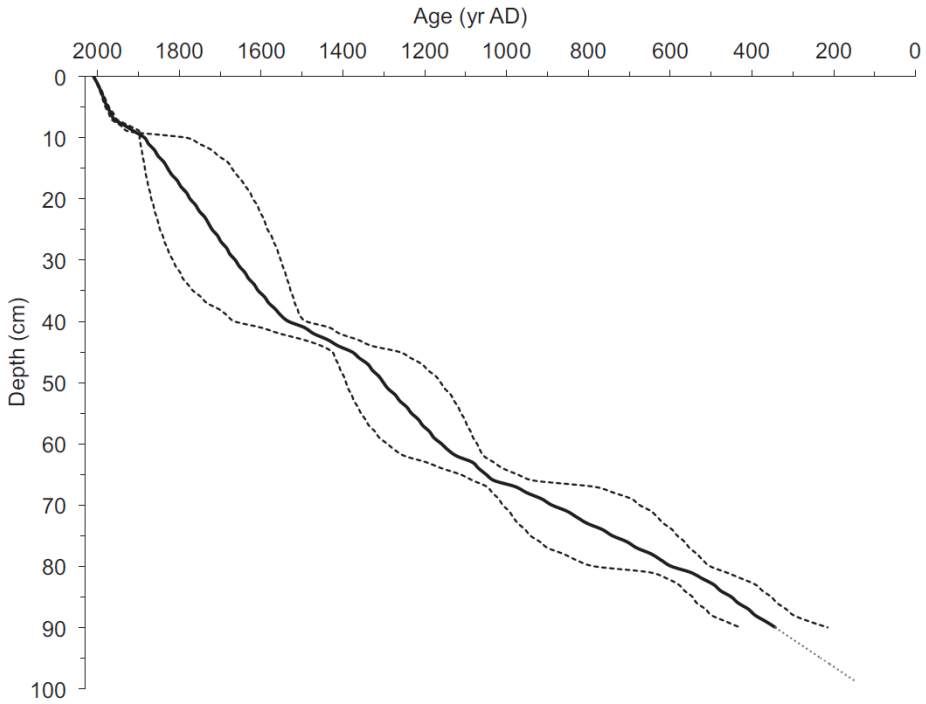

Figure 8.2. Age model for the core FCPw1 and estimated 2σ errors, based on six AMS–^{14}C dates, performed on total organic sediment, and ^{210}Pb chronology. The data interpolation was obtained with Bchron 3.2 software.

Table 8.1. Radiocarbon age data determined in the Laboratory "Beta Analytic Inc." (AMS – standard delivery).

Sample	Depth (cm)	δ^{13}C ‰	Conventional radiocarbon age	Δ^{14}C ‰	Calibrated years AD (2 Sigma range)
CM 41	40–41	−26.7	380 ± 30 BP	−46.20 ± 3.6	1490 to 1666
CM 45	44–45	−26.8	650 ± 35 BP	−84.57 ± 3.9	1330 to 1453
CM 64	63–64	−25.9	1010 ± 50 BP	−122.49 ± 1.9	1032 to 1197
CM 67	66–67	−25.9	1030 ± 34 BP	−124.97 ± 1.9	934 to 1082
CM 82	81–82	−25.8	1570 ± 40 BP	−181.66 ± 1.9	463 to 650
CM 91	90–91	−27.2	1760 ± 30 BP	−196.80 ± 3.0	215 to 429

^{210}Pb CRS chronology supported by ^{137}Cs and total Pb concentrations of Caminha high marsh sediment core (FCPw1) are available in Appendix 8.2.

8.3. Results and discussion

8.3.1. Br concentrations in surface samples

The analytical dataset, including Br^- contents in Caminha tidal marsh interstitial waters, fluvial waters (Minho and Coura Rivers) and coastal seawater, and Br concentrations in estuarine and marsh sediments, is summarized in Table 8.2.

Table 8.2. Geochemical data from Minho estuary. A – Surface and marsh interstitial water; B – Surface sediments.

A Samples	Zone	OM %	Br mg/l	Pb mg/l
PR1	Tidal Flat		49	240
PR2	Tidal Flat		56	340
PR5	Low Marsh		77	390
PR6	Low Marsh		69	320
PR7	HLow Marsh		64	370
PR8	High Marsh		58	250
PR10	High Marsh		49	240
CP5	Low Marsh		83	d.l.
CPAS	High Marsh		62	d.l.
PIC6	HLow Marsh		62	160
VM	River		d.l.	d.l.
VNC	River		d.l.	d.l.
CM	Estuary Mouth		141	530

B Samples	Zone	OM %	Br mg/kg	Pb mg/kg
Minho3	Low Estuary		72	19
Minho4	Low Estuary		37	30
Minho5	Low Estuary		d.l.	29
Minho6	Low Estuary		d.l.	30
Minho7	Low Estuary		20	42
Minho9	Middle Estuary		d.l.	1
Minho16.1	Upper Estuary		d.l.	41
Minho16	Upper Estuary		d.l.	40
Minho18	Upper Estuary		13	12
Minho19	Upper Estuary		14	39
Minho22	Middle Estuary		20	42
Minho23	Middle Estuary		d.l.	18
PR2	Tidal Flat	1.7	15	32
PR3	Tidal Flat	1.7	20	21
PR4	Low Marsh	9.0	89	26
PR5	Low Marsh	10.8	95	21
PR6	Low Marsh	11.7	147	43
PR7	HLow Marsh	11.9	134	26
PR8	High Marsh	32.6	482	36
PR10	High Marsh	38.8	407	39
CP1	Tidal Flat	0.6	30	27
CP2	Tidal Flat	1.5	11	25
CP3	Low Marsh	15.7	165	39
CP4	Low Marsh	19.2	174	61
CP5	Low Marsh	18.9	373	38
CP6	HLow Marsh	24.4	411	25
CP7	HLow Marsh	19.6	695	80
CPAS	High Marsh	27.7	389	44
PIC1	Tidal Flat	1.5	27	40
PIC3	Low Marsh	11.9	77	30
PIC4	Low Marsh	5.9	62	39
PIC5	High Marsh	17.9	188	55
PIC6	HLow Marsh	20.5	406	80
PIC7	High Marsh	10.6	162	24

d.l.: <detection limit.

Br^- concentrations in coastal seawater (ANC) and estuary mouth (CM) samples are 197 mg/L and 141 mg/L, respectively, while the concentrations in freshwater (VM and VNC) are below detection limits (lower than 0.01 mg/L). Mean concentration of Br in seawater, mostly in the form of Br^-, ranges from 65 mg/L to well over 80 mg/L in some confined sea areas (Al-Mutaz, 2000). An explanation for the measured higher levels of bromide is the existence in the study area of a large

biological Br pool in waters in relation with the extensive macroalgal richness of the northern Portuguese shore and the strong seasonal (spring-summer) coastal upwelling. These factors are recognized for stimulating the supersaturation in brominated organic compounds of coastal regions (Quack and Wallace, 2003; Sturrock et al., 2003), including Portuguese offshore (Raimund et al., 2011). The main chemical degradation pathways of the brominated organic compounds dissolved in seawater are hydrolysis and chloride substitution, both having bromide anions as reaction product, as shown below for CH_3Br:

$$CH_3Br + Cl^- \rightarrow CH_3Cl + Br^-$$
$$CH_3Br + H_2O \rightarrow CH_3OH + H^+ + Br^-.$$

Caminha tidal marsh interstitial water values of Br^- (min–max: 49–83 mg/L) seem to be largely dictated by marine influence, with the highest values found in two samples from the low marsh (CP5 and PR5; Table 8.2) and the lower ones in the high marsh zone (PR 8 and PR10; Table 8.2). Distinctively, surface sediments present increasing Br concentrations from the low marsh (range: 62–373 mg/kg; average: 146 mg/kg) towards the high marsh (162–695 mg/kg; 393 mg/kg). Longer submersion times by salty water, with a high load of Br^-, can considerably contribute to the sediment/soil Br pools from this marsh zone. The samples from higher low marsh transition zone and from high marsh are more enriched in Br^-, with greater values on the CP transect (Table 8.2). It is also in this transect that Br concentration in superficial sediments reaches a maximum of 695 mg/kg in the transition to high marsh. The lowest concentrations are found in the bottom sediments of the Minho River estuary (10–72 mg/kg; 29 mg/kg) and at tidal flats (11–30 mg/kg; 21 mg/kg). The highest Br contents in estuarine sediments occur in two samples from the lower estuary (Minho 3 and Minho 4; Table 8.2), chiefly in relation with the proximity to estuary mouth.

A literature review shows that total Br contents in soils and sediments can vary remarkably, with reported concentrations in soils from as low as 0.3 mg/kg to more than 800 mg/kg (Flury and Papritz, 1993). Analyzing a set of Japanese soils, Yuita (1983) concluded that coastal soils may accumulate significant Br, up to 495 mg/kg, mainly in the top horizon, and also that those contents were generally higher in coastal than inland areas. In marine sediments, total Br can surpass 100 mg/kg (Leri et al., 2010) and in salt marsh superficial sediments from Seine (France) and Medway (SE England) estuaries, Cundy et al. (2005) have obtained values ranging between 29–255 mg/kg and 117–1090 mg/kg, respectively. In the majority of these studies, significant direct correlations between Br and C_{org} contents were also stated.

The OM spatial pattern is similar to the one of Br in the Caminha tidal marsh, with a clear differentiation across the marsh and concentrations in sediments correlated ($r = 0.86$; $p < 0.001$; $N = 21$) along surface transects. Not surprisingly, the OM lowest values (0.6 to 1.7%; average: 1.4%)

occur at the tidal flat, intermediate values (5.9–19.2%; avg.: 12.9%) at the low marsh and the highest values (10.6–38.8%; avg.: 22.7%) in samples taken at the high marsh. The Br^- supplied by seawater to the marsh environment during tidal flooding, is readily absorbed by halophytic plants through the roots and leaves. The literature indicates that this uptake mechanism followed by upward translocation towards shoots explains why all marsh plant tissues have relatively high natural Br concentrations, greater in leaves, and why Br concentrations in halophytes (very close to 740 mg/kg) are about two orders of magnitude higher than in glycophytes (Yuita, 1994). Also, amongst halophytic plants is possible to find variations, with more succulent species having higher Br^- tissue levels (Manley et al., 2006), for instance.

Leri and Myneni (2012) detected that all Br in isolated humic substances, decaying plant material and organic fraction of soils/sediments is covalently bonded to carbon, stating that the Br^- absorbed by living plants is ultimately converted to Br_{org} during plant litter decay and then incorporated in OM (excluding volatile species like CH_3Br). Since OM inputs in tidal marsh sediments strongly reflect the accumulation of leaves, root and rhizome biomass produced in situ (Blum, 1993), the occurrence of plenty Br-enriched plant material deposited locally could explain the higher total Br concentrations found in sediments from the Caminha high marsh zone, where plant density is greater. However, it is not completely excluded the possibility of some new Br_{org} might be produced during decay and/or leaching of soluble Br_{inorg}, revealing more refractory Br_{org} that had been present all along in the plant tissue (Leri and Myneni, 2012).

The conversion of Br_{inorg} to Br_{org} and its presence in OM is linked to the relative ease of the Br^- abiotic oxidation by hydrogen peroxide (H_2O_2) within plants. H_2O_2 is generated in plant cells under steady-state conditions predominantly during photosynthesis and photorespiration and, additionally, as a physiological response under stress conditions (Ślesak et al., 2007). Photosynthetic H_2O_2 is used routinely by enzymes like bromoperoxidases that can catalyze the oxidation of Br^- to hypobromous acid (HOBr) according to the following reaction:

$$H_2O_2 + Br^- + H^+ = HOBr + H_2O.$$

HOBr is a powerful brominating/oxidizing agent, which can promptly react, in a number of ways, with natural OM to form organobromine compounds:

$$HOBr + AH = ABr + H_2O$$ (where A represents an organic substrate).

Likewise, H_2O_2 can be produced in the water–soil binomium from standard metabolic processes of fungi and bacteria (under aerobic conditions) and freely diffuse across the cell membrane into the surrounding milieu (Li et al., 2012).

Therefore, natural oxidative bromination processes (enzymatic and/or abiotic) taking place in living plants and in humified plant material seem to be a very feasible source of Br_{org} to OM. This pathway converts plant litter and OM in Br_{org} reservoirs, contributing to the Br pool of soils/sediments (Leri et al., 2010). Reductive debromination of Br_{org} upon degradation of OM could induce the release of some of this Br later on, as Br_{inorg}. Nevertheless, natural organobromine compounds, like their persistent hazardous man-made analogues, should be resistant to biodegradation, representing a relatively stable form of carbon in soils/sediments (Leri and Myneni, 2012), including in marsh environments.

8.3.2. Br variability in core sediment samples

8.3.2.1. Relationships with OM content

The down-core profiles of Br and OM until 75 cm depth (AD 742) are presented in Figure 8.3 together with the corresponding Br/OM ratios.

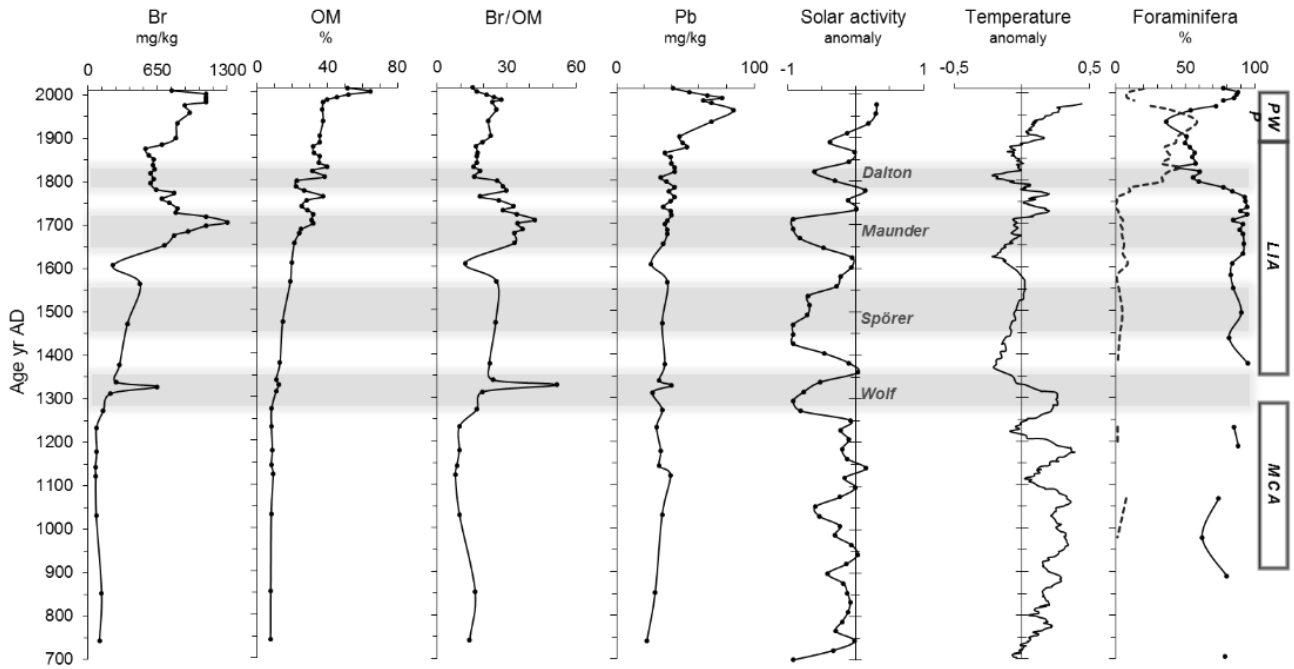

Figure 8.3. FCPw1 core data of bromine (Br), organic matter (OM), Br/OM ratio, lead (Pb) and summary of benthic foraminiferal assemblages (dashed line: distribution of salt marsh species; solid line: distribution of low-salinity marsh species); solar activity – solar irradiance anomaly using a 22-year running average reconstruction (after Steinhilber et al., 2012); temperature anomaly – 10-year running average reconstruction (after Martín-Chivelet et al., 2011); grey bars – solar minima events (references in the text); PWP – Present Warm Period; LIA – Little Ice Age; MCA – Medieval Climatic Anomaly.

The Br contents in cored sediments vary between 68 and 1300 mg/kg (Table 8.3), with values remaining fairly constant (68–127 mg/kg; avg.: 87 mg/kg) from the base (AD 370) to approximately the middle of the core (AD 1230). In the upper section, after AD 1270 and until AD 2010, the Br pattern becomes irregular but it is clear a general increase towards the top (142–1300 mg/kg; Figure

8.3, Table 8.3). In fact, in the upper section of the core the averaged Br concentration (717 mg/kg) is about an order of magnitude higher than in the lower section (87 mg/kg), between AD 370 and AD 1270. Thus, in this period the sediments of the area would have had much lower Br contents, like the ones obtained in the present low marsh environments (Tables 8.2 and 8.3).

The significant direct correlation between Br and OM detected in surface samples remains strong in the cored sediments ($r = 0.83$; $p < 0.001$; $N = 49$). Christiansen et al. (2002) have obtained an even better correlation in sediments from a core collected in Skallingen salt marsh (Denmark), with Br and OM contents in the interval 100–600 mg/kg and 2–14%, respectively. In the current case, and given that the Br enrichment after AD 1300 is synchronous with an important increase in OM (from around 8% to 11%), we consider that both are interrelated and linked to the changes introduced by the invasion of the intertidal flats by vegetation. These inferences are supported by a previous paleoenvironmental reconstruction, based on benthic foraminiferal assemblages, sedimentological and geochemical data, suggesting the presence of a tidal flat since AD 370, when fluvial influence prevailed, and its subsequent transition to a low marsh, which appears clearly established by the 1300s (Moreno et al., 2014). Based on these findings, it is advanced that, at that time, the Br enrichment in paleorecord indicates the transition from an exposed tidal flat to a vegetated surface. After this environmental change, marsh vegetation life cycles and plant debris humification triggered the Br biogeochemical recycling between Br_{inorg} and Br_{org}, influencing its behavior/mobility. This affects the Br net source/sink balance in the marsh ecosystem and, accordingly, the amounts of Br persisting retained in soils/sediments or released to atmosphere (as CH_3Br).

8.3.2.2. Br enrichment peaks in association with solar cycles

Once settled the marsh environment, the first Br enrichment peak (646 mg/kg) occurs at AD 1330, within a general trend of increasing Br concentrations in sediments (Figure 8.3, Table 8.3). Based on the modelled chronology, a match between this Br enrichment and the Wolf Solar Minimum (AD 1280–1350) may be suggested.

Through the Little Ice Age (LIA; AD 1350–1900; Bradley and Jones, 1993), Br concentrations although irregular continue relatively high (range: 234–1300 mg/kg; average: 680 mg/kg), with greater values generally in phase with increasing OM contents (Figure 8.3, Table 8.3). During this period, however, the relationship between the two, Br and OM, is not sufficient to fully explain the higher Br levels in marsh sediments, with almost 40% of the samples falling outside the upper 95% confidence interval of its correlation coefficient, which denotes an excess of Br relatively to OM. These samples shape a strong Br enrichment (931–1300 mg/kg) between AD 1677 and AD 1783 peaking at AD 1698–1720, concomitant with the Maunder Solar Minimum (AD 1645–1715). This is known as a 70-year period of persistent reduced solar activity, when sunspots vanished (Eddy, 1976; Beer et al., 2006). Another Br minor peak, occurring during the LIA at AD 1770 (805 mg/kg), might

be connected to the transition to the Dalton Solar Minimum (AD 1790–1820). This peak has a clearer expression in the Br/OM ratios diagram until AD 1796 (Figure 8.3). The same relationship may be pointed out to the Spörer Minimum, nevertheless a denser sampling should be implemented.

It has been proposed that a reduction in total solar irradiance (TSI) during the period between AD 1645 and AD 1715 has contributed to the important decline in European temperature and significant climatic variability (Pfister, 1992; Shindell et al., 2001; Luterbacher et al., 2004; Wirth et al., 2013). Although most climatic models cannot explain how relatively small alterations in solar irradiance alone can force modifications in climate, it seems that there might be at least two amplifying factors. Firstly, a reduction of solar activity would be responsible for an increase in cosmic ray intensity, stimulating cloud formation and precipitation. Alterations in cloudiness alter the albedo and can potentially cause a significant climatic change (Scaffeta, 2012). Secondly, a decrease in solar UV intensity, causing a decline on the ozone formation and cooling, could have resulted in less absorption of sunlight during the Maunder (Van Geel et al., 2000).

Climatic reconstructions show, conversely, that past global climate changes have a strong regional expression (Ahmed et al., 2013). This seems particularly right for the LIA in the NW Iberia, as revealed by several works, based on mercury, pollen and lipid biomarkers proxies (Martinez-Cortizas et al., 1999; Muñoz Sobrino et al., 2005; Ortiz et al., 2010). Lower temperatures and high climatic instability distinguished the period from AD 1650 to AD 1850 (Martinez-Cortizas et al., 1999), with a dry period from AD 1720 to AD 1870 (Ortiz et al., 2010). Regional paleoclimate modelling for Iberian Peninsula (winter and summer surface atmospheric temperature (SAT) and precipitation) allowed in particular the identification of some pronounced cold periods, such as the Spörer, Maunder and Dalton Solar Minima, occurring associated with a concomitant reduction in TSI (Gómez-Navarro et al., 2012). Those models also make possible to recognize that, in such periods, the repercussion of external forcing (solar activity) seems to be more relevant in summer SAT simulations. They additionally allow us to identify winter and summer positive precipitation anomalies in the Maunder Minimum, with an increase in precipitation of about 20% for most of the Iberian Peninsula, during summer, and slightly higher (in W Iberian Peninsula) in winter (Gómez-Navarro et al., 2011). Despite these specificities, a broad reconstruction of the spatiotemporal patterns on past climate variability (seven continental-scale regions) shows generally cold conditions between AD 1580 and AD 1880 (Ahmed et al., 2013). Furthermore, historical data indicate that the LIA climate deterioration was felt in Galicia mainly after AD 1565. In this region, climate conditions worsen through the 17th century, when 33 years of heavy rainfall and summer storms was registered. These circumstances frequently prevented crop maturation, being directly accountable by heavy losses to agriculture, and by the decline of vineyard cultivation and olive grove (Font Tullot, 1988).

The strong climate variability during the LIA must also have affected salt marsh vegetation life cycles, concerning to biosynthesis of CH_3Br. Wishkerman et al. (2008) found that the abiotic

reaction taking place in halophytic plants involving Br and methoxyl groups, with the volatilization of CH_3Br, is very sensitive to variations in temperature. These authors report a double increase in CH_3Br emissions by plants every 5ºC rise. They also discovered that this same reaction is influenced by the water content of plants, becoming more efficient as plants dry out. By their side, Manley et al. (2006) reported maximum CH_3Br emissions during the flowering period in the reproductive phase, connecting, by this way, the magnitude of salt marsh emissions to plant growth and reproduction.

The combination of lower temperatures and lower TSI during Grand Solar Minima has certainly reduced the overall metabolism of marsh plants, slowing down the entire dynamics involved in the bioaccumulation and biochemical transformation of Br and favouring its retention as Brorg in soils/sediments over its transfer to atmosphere (as CH_3Br). Thus, it is plausible to assume that through the Maunder Solar Minimum sediments sequestered more Br by overcoming the biogenic flux to the atmosphere. Considering the Br enrichment observed in the core sediments during the Maunder, it suggests that Caminha tidal marsh was a net sink of Br through this solar event and it might have also been during any Grand Solar Minima. We propose that the variation observed in the Br pattern contents from Caminha tidal marsh sediments, rather than the result of increased seawater intrusion in the estuary, is mainly a biogeochemical response to climate change. This hypothesis is supported by the dominance of low-salinity benthic marsh foraminiferal assemblages (Figure 8.3; Moreno et al., 2014) and by the origin of OM, primarily derived from terrestrial sources and reaching its maximum signature during the LIA, with n-alkane lipid biomarkers showing the dominance of grass vegetation (Appendix 8.3; De la Rosa et al., 2012). Furthermore, these results are in agreement with the evidences collected by Wirth et al. (2013) that indicate that Grand Solar Minima triggered higher annual flood frequency and summer flood intensity in Central Europe for the last 800 years.

Towards the end of the LIA, around AD 1860–1880, the Br content in sediments is marked by a slightly decline (566–540 mg/kg). This can be interpreted as an outcome of the amelioration of climatic conditions and its effect, with the gradual restoration of the biogenic Br recycling promoted by marsh vegetation, in the transition to the Present Warm Period (20th century warming).

Table 8.3. Geochemical and foraminiferal assemblage data from sediment core FCPw1.

Depth cm	OM %	Br mg/kg	Br/OM	Pb mg/kg	Low Salinity species %	Salt marsh species %	AD Age years
0-1	51.4	779	15.2	41	77.3	20.6	2010
1-2	64.5	1100	17.1	53	88.1	9.3	2002
2-3	52.1	1100	21.1	66	87.0	8.0	1995
3-4	45.3	1100	24.3	77	85.1	9.0	1988
4-5	39.9	1100	27.5	63	77.8	13.7	1983
5-6	37.7	900	23.9	69			1976
6-7	39.7				72.3	25.4	1967
7-8	37.3	948	25.4	85	53.8	41.5	1960
8-9	37.6	831	22.1	69	36.2	58.7	1934
9-10	35.7	817	22.9	46	50.9	44.7	1910
10-11	35.7	690	19.4	48	50.0	43.3	1885
11-12	32.1	540	16.8	51	53.5	35.7	1876
12-13	32.3	566	17.5	35	56.9	38.2	1861
13-14	35.6	611	17.2	39	55.1	39.8	1852
14-15	35.3	603	17.1	40	57.4	33.6	1838
15-16	39.8	624	15.7	42	44.3	46.7	1829
16-17	31.6	585	18.5	42	60.6	38.5	1819
17-18	38.4	615	16.0	32	55.8	33.3	1805
18-19	22.6	586	26.0	36	60.2	33.8	1796
19-20	22.4	633	28.3	42	77.6	10.4	1783
20-21	26.9	805	29.9	38	83.7	10.6	1774
21-22	37.5	693	18.5	42	93.1	1.5	1761
22-23	28.4	758	26.7	39	93.3	1.3	1751
23-24	25.4	836	32.9	34	94.5		1738
24-25	28.7	818	28.5	39	90.1	2.3	1729
25-26	31.9	1100	34.5	40	94.4	2.4	1720
26-27	30.8	1300	42.2	37	84.5	5.6	1707
27-28	31.8	1100	34.6	35	91.5	3.8	1698
28-29	25.2	931	36.9	37	89.1	5.5	1685
29-30	24.2	806	33.2	37	91.5	4.6	1677
30-31	21.6						1663
31-32	21.3	712	33.4	34	92.3	6.3	1654
32-33	21.9						1640
33-34	21.9				91.4	5.5	1631
34-35	22.2						1617
35-36	19.7	234	11.9	25	83.8	8.8	1607
36-37	21.5						1592
37-38	20.8				82.9	1.4	1582
38-39	19.0	487	25.7	37			1565
39-40	15.7				84.7	2.4	1552
40-41	15.3						1533
41-42	15.8				90.4	5.1	1495
42-43	14.5	366	25.2	33			1472
43-44	13.8				81.7	3.1	1438
44-45	12.1						1412
45-46	13.0	294	22.5	35	95.4	1.9	1378
46-47	10.7						1360
47-48	10.8	260	24.1	31			1339
48-49	12.5	646	51.6	40			1328
49-50	10.8	211	19.5	26			1312
50-51	9.0						1301
51-52	8.4						1290
52-53	8.3	142	17.2	33			1272
53-54	8.7						1261
54-55	8.2						1244
55-56	8.2	78	9.5	29	85.2	1.8	1233
56-57	8.4						1216
57-58	8.4						1205
58-59	8.5				88.4	1.8	1189
59-60	8.6	82	9.5	32			1178
60-61	8.7						1159
61-62	8.1	68	8.4	31			1143
62-63	9.1	71	7.8	39			1122
63-64	9.2						1084
64-65	8.4				74.3	7.9	1069
65-66	8.9						1050
66-67	8.1	77	9.5	33			1031
67-68	8.6				62.3	1.6	979
68-69	8.0						950
69-70	8.3						914
70-71	8.3				80.2		890
71-72	7.8	127	16.4	28			853
72-73	8.2						828
73-74	7.0						803
74-75	7.3						766
75-76	7.7	107	13.9	22			742
76-77	7.3				78,9	0.8	706
77-78	7.8						682
78-79	7.4						646
79-80	5.7				73.2		622
80-81	6.1	85	14.0	34			598
81-82	6.2						550
82-83	6.2				77.5	1.1	522
83-84	6.0	77	12.8	26			494
84-85	6.1						477
85-86	5.9				81.8		451
86-87	5.5						434
87-88	5.8	87	15.0	20			409
88-89	6.8				77.2		393
89-90	6.9	99	14.3	26			367

3.2.3. Br enrichment linked to anthropogenic activity

In the most recent section of the core, the sediments representing the interval AD 1982–2002 exhibit another Br peak (1100 mg/kg), though Br content is already significantly high (948 mg/kg) by AD 1960. During this period of time the anthropogenic inputs of Br to the marsh environment should have become increasingly dominant, much likely surpassing the natural signal. During the 20th century warming, the pattern of Br/OM ratios in these marsh sediments is concomitant with a Pb concentration enhancement (Figure 8.3). Total Pb concentrations vary very little (37 ± 5 mg/kg) since the tidal marsh setting stabilized *ca.* AD 1300 until AD 1876 (51 mg/kg), when Pb content rises until it reaches its highest concentration between AD 1960 (85 mg/kg) and AD 1988 (77 mg/kg). Then Pb content decreases till AD 2010, when it returns to pre-industrial (prior to 1850s) concentrations (41 mg/kg). Pb is seen as a global scale contaminant that can be traced back to Roman Ages (Rosman et al., 1997). Though, total Pb concentrations recorded in sediments from salt marshes prior to AD 1800 are difficult to be differentiated from background values. Results from a salt marsh core in Northern Spain suggest that the anthropogenic sources recorded from the sediments were *ca.* 90% by AD 1975. However, the influence of leaded gasoline increased from almost negligible in AD 1930 to 13–24% by AD 1975 (Leorri et al., 2014). Similar values are reported from an estuarine system in NW of Spain (Alvarez-Iglesias et al., 2012) closer to our study site. On the other hand, a peat bog from NW Spain (Martinez-Cortizas et al., 2012) and other European records (Shotyk et al., 1998; Dunlap et al., 1999) suggest greater contributions from leaded gasoline. Regionally, the Pb concentration peak has been reported to be at 1955–1962 (Olid et al., 2010; Alvarez-Iglesias et al., 2012), comparable to Caminha (AD 1960), which might point to a significant input from local sources. The profile of total Pb from Caminha increases from AD 1930 towards 1960s and 1970s and then decreases, following a similar pattern than those found elsewhere (see references above).

Global Pb emissions from leaded gasoline started in the 1920s, peaked in Europe by the 1950s (Dunlap et al., 1999), and then dropped since the 1970s, mainly as a result of the European Union regulation (von Storch et al., 2003) (Figure 8.4).

Similarly to the abandonment of leaded gasoline, all human-made organobromine chemicals are under phase-out schedule, with some exceptions for critical usages, considering their negative impact as Class I ozone-depleting substance, according to the 1992 Montreal Protocol. This has conducted to cut in the production and import of methyl bromide, being virtually unavailable since 2005 (Figure 8.5). Though, the phase-out of CH_3Br fumigant or specific BFRs has been constrained by the apparent lack of viable alternatives (efficient and economical). Despite these drawbacks, the global atmospheric load of Br peaked in 1998 and has declined since then (Montzka et al., 2003). In the Caminha tidal marsh sediments, Br and Pb profiles parallel each other since *ca.* 1930, with both (Br/OM ratios and Pb contents) presenting a strong direct correlation ($r = 0.79$; $p < 0.05$; $N = 8$). This

implies a major common anthropogenic source, most probably the use of ethylene dibromide in leaded gasoline and vehicle-related emissions of volatile brominated compounds (e.g., CH_3Br).

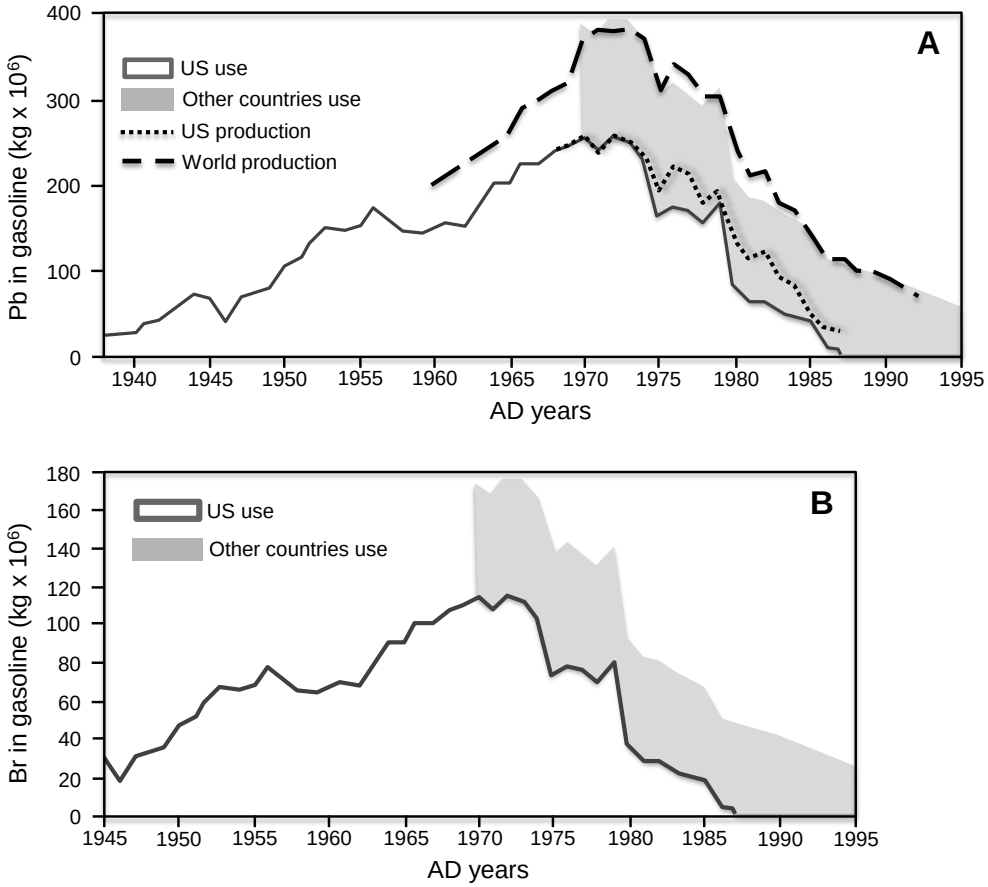

Figure 8.4. **A –** Production and use of lead in gasoline from *ca.* 1935 to 1995; **B –** Estimated use of bromine in leaded gasoline, based on data in **A** (adapted from Thomas et al., 1997).

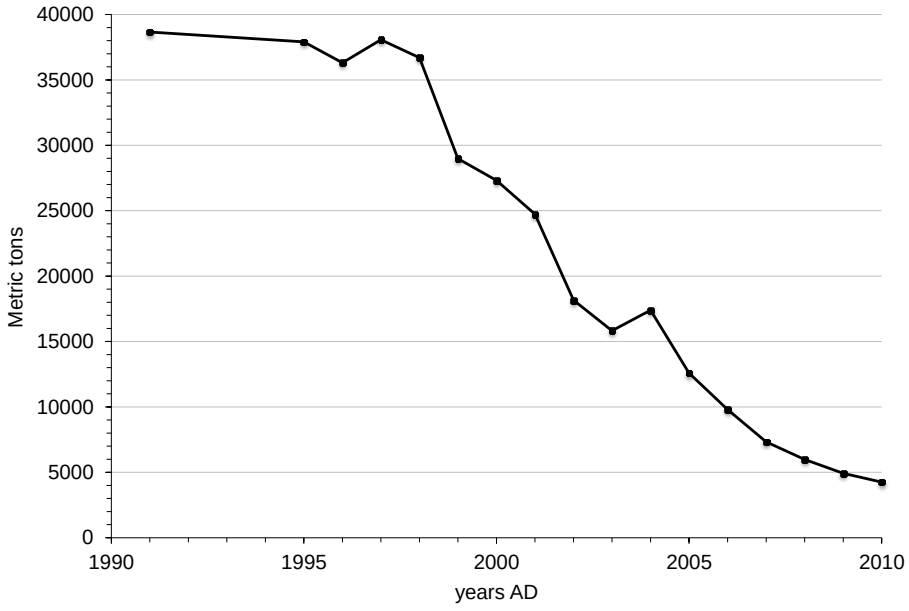

Figure 8.5. World consumption phase-out of methyl bromide (raw data source: United Nations Environment Programme, Ozone Secretariat, Data Access Centre).

However, the correlation of Br/OM ratio with Pb does not exclude the existence of other potential regional anthropogenic sources of Br to this tidal marsh. The sample corresponding to AD 1983 lies outside the upper limit of the 95% confidence interval of Br/OM–Pb correlation coefficient. This surplus of Br might be assumed as a consequence of the addition of brominated substances to water, to increase its effectiveness as forest fire extinction agent. This has been a common practice since the beginning of the 1930s (Giménez et al., 2004). For instance, more than 2000 tons of fire retardants have been used, annually, to combat fires in the Mediterranean zones (Luna et al., 2007). In Portugal, the large-range missions of forest fire attack with flame retardants began precisely in the year 1982 and were in the course until mid-90s. So, the atmospheric deposition and washed-out of BFRs directly added to forests and soils, in Portuguese (and Galician) mountains during strategic fire-fight actions, could have also contributed, in some extent, to the most recent Br enrichment registered in the Caminha tidal marsh sediments.

8.4. Conclusions

The Br record of the Caminha tidal marsh sediments has provided promising information concerning the biogeochemical responses to climatic forcing in the last 1700 years and the overlaid anthropogenic signature.

The results obtained indicate that climate condition deterioration felt during the Little Ice Age is particularly marked by the enrichment of sediments in Br, in which maxima occur within the Maunder Solar Minimum.

The most recent research, regarding Br recycling in terrestrial and marine environments, leads us to suggest that the Br enhancement in these tidal marsh sediments during past Grand Solar Minima is interrelated with changes in biogeochemical processes driven by solar activity, which constrains the Br release to atmosphere. Caminha tidal marsh has been acting as a sink of Br more than a source, through these periods.

Additionally, the Br pattern in sediments along the 20th century, corresponding to the Present Warm Period, may be related with the history of human-made organic brominated compounds and to its anthropogenic fingerprints in the tidal marsh environment.

The investigation in progress on several salt marshes from the SW Portuguese coast can supply further insights, improving the present approach and upholding it with more widespread data, concerning the use of Br content changes in marsh sediments as a proxy of climatic changes and anthropogenic impacts.

Acknowledgments

This work is a contribution of the WestLog (PTDC/CTE/105370/ 2008) project, funded by the Fundação para a Ciência e a Tecnologia (FCT). João Moreno benefits from a PhD grant (SFRH/BD/87995/2012) from FCT and Jose de la Rosa's participation was funded through the Ciência 2008 framework (FCT) at IST/CTN. It is also a contribution to the IGCP Project 588, Northwest Europe working group of the INQUA Commission on Coastal and Marine Processes and the Geo-Q Zentroa Research Unit (Joaquín Gómez de Llarena Laboratory), Sociedad de Ciencias Aranzadi. We thanks Inês Pereira and Ana Medeiros for carrying out the sedimentological and geochemical analysis. We are also very grateful to the anonymous reviewers for their comments that greatly improved the final manuscript.

References

Ahmed M, et al. Continental-scale temperature variability during the past two millennia. Nat. Geosci. 2013; 6: 339–46.

Al-Mutaz IS. Water desalination in the Arabian Gulf region. In: Goosen MFA, Shayya WH, editors. Water Management, Purification and Conservation in Arid Climates. Water Purification Basel: Technomic Publishing; 2000. p. 245–65.

Alvarez-Iglesias P, Rubio B, Millos J. Isotopic identification of natural *vs.* an anthropogenic lead sources in marine sediments from the inner Ria de Vigo (NW Spain). Sci. Total Environ. 2012; 437: 22–35.

Appleby PG, Oldfield F. Application of ^{210}Pb to sedimentation studies. In: Ivanovich M, Harmon RS, editors. Uranium Series Disequilibrium. Oxford: Oxford University Press; 1992. p. 731–78.

Araújo MF, Valério P, Jouanneau J-M. Heavy metal assessment in sediments of the Ave river basin (Portugal) by EDXRF. X-Ray Spectrom. 1998; 27: 305–12.

Araújo MF, Conceição A, Barbosa T, Lopes MT, Humanes H. Elemental composition of marine sponges from the Berlengas Natural Park, Western Portuguese Coast. X-Ray Spectrom. 2003; 32: 428–33.

Beer J, Vonmoos M, Muscheler R. Solar variability over the past several millennia. Space Sci. Rev. 2006; 125: 67–79.

Blei E, Heal MR, Heal KV. Long-term CH_3Br and CH_3Cl flux measurements in temperate salt marshes. Biogeosciences 2010; 7: 3657–68.

Blum LK. Spartina alterniflora root dynamics in a Virginia marsh. Mar. Ecol. Prog. Ser. 1993; 102: 169–78.

Bradley RS, Jones PD. 'Little Ice Age' summer temperature variations: their nature and relevance to recent global warming trends. The Holocene 1993; 3: 367–76.

Christiansen C, Bartholdy J, Kunzendorf H. Effects of morphological changes in a salt marsh sediment of the Skallingen peninsula, Denmark. Wetl. Ecol. Manag. 2002; 10: 11–23.

Costanza R, d'Arge R, deGroot R, Farber S, Grasso M, Hannon B, Limburg K, Naeem S, O'Neill RV, Paruelo J, Raskin RG, Sutton P, Van Den Belt M. The value of the world's ecosystem services and natural capital. Nature 1997; 387: 253–60.

Cox ML, Fraser PJ, Sturrock GA, Siems ST, Porter LW. Terrestrial sources and sinks of halomethanes near Cape Grim, Tasmania. Atmos. Environ. 2004; 38: 3839–52.

Cundy AB, Hopkinson L, Lafite R, Spencer K, Taylor JA, Ouddane B, Heppell CM, Carey PJ, Charman RO, Shell D, Ullyott JS. Heavy metal distribution and accumulation in two Spartina sp.-dominated macrotidal salt marshes from the Seine estuary (France) and the Medway estuary (UK). Appl. Geochem. 2005; 20: 1195–208.

De la Rosa JM, Araújo MF, González-Pérez JA, González-Vila FJ, Soares AM, Martins JM, Leorri E, Corbett R, Fatela F. Organic matter sources for tidal marsh sediment over the past two millennia in the Minho River estuary (NW Iberian Peninsula). Org. Geochem. 2012; 53: 16–24.

de Wit CA. An overview of brominated flame retardants in the environment. Chemosphere 2002; 46: 583–624.

Doff DH. Determination of bromine and iodine in four marine sediment reference samples by Energy-Dispersive X-Ray Fluorescence Spectrometry. Geostand. Newslett. 1989; 13: 75–7.

Drewer J, Heal MR, Heal KV, Smith KA. Temporal and spatial variation in methyl bromide flux from a salt marsh. Geophys. Res. Lett. 2006; 33:L16808. http://dx.doi.org/10. 1029/2006GL026814.

Duarte CM, Losada IJ, Hendriks IE, Mazarrasa I, Marbà N. The role of coastal plant communities for climate change mitigation and adaptation. Nat. Clim. Chang. 2013; 3: 961–8. http://dx.doi.org/10.1038/nclimate1970.

Dunlap CE, Steinnes E, Russel Flegal A. A synthesis of lead isotopes in two millennia of European air. Earth Planet. Sci. Lett. 1999; 167: 81–8.

Eddy JA. The Maunder Minimum. Science 1976; 192: 1189–202.

Fagherazzi S, Wiberg PL, Temmerman S, Struyf E, Zhao Y, Raymond PA. Fluxes of water, sediments, and biogeochemical compounds in salt marshes. Ecol. Process. 2013; 2: 3.

Fatela F, Moreno J, Leorri E, Corbett R. High marsh foraminiferal assemblages response to intra-decadal and multi-decadal precipitation variability, between 1934 and 2010 (Caminha, NW Portugal). J. Sea Res. 2014; 93: 118–32.

Flury M, Papritz A. Bromide in natural environment: occurrence and toxicity. J. Environ. Qual. 1993; 22: 747–58.

Font Tullot I. Historia del clima de España. Madrid: Spanish Meteorological Institute (INM); 1988 (297 pp.).

Gerritse RG, George RJ. The role of soil organic matter in the geochemical cycling of chloride and bromide. J. Hydrol. 1988; 101 (1–4): 83–95.

Giménez A, Pastor E, Zárate L, Plananas E, Arnaldos J. Long-term forest retardants: a review of quality, effectiveness, application and environmental considerations. Int. J. Wildland Fire 2004; 13: 1–15.

Gómez-Navarro JJ, Montávez JP, Jerez S, Jiménez-Guerrero P, Lorente-Plazas R, González-Rouco JF, Zorita E. A regional climate simulation over the Iberian Peninsula for the last millennium. Clim. Past 2011; 7: 451–72.

Gómez-Navarro JJ, Montávez JP, Jiménez-Guerrero P, Jerez S, Lorente-Plazas R, González- Rouco JF, Zorita E. Internal and external variability in regional simulations of the Iberian Peninsula climate over the last millennium. Clim. Past 2012; 8: 25–36.

Gribble G. The diversity of naturally produced organohalogens. Chemosphere 2003; 52: 289–97.

Hamilton JTG, McRoberts WC, Keppler F, Kalin RM, Harper DB. Chloride methylation by plant pectin: an efficient environmentally significant process. Science 2003; 301: 206–9.

Haslett J, Parnell A. A simple monotone process with application to radiocarbon-dated depth chronologies. Appl. Stat. 2008; 57: 399–418.

Honrado J, Alves P, Alves HN, Torres J, Caldas FB. A Flora e a vegetação do Minho internacional — Diversidade, ecologia e valor para conservação. Melgaço, Portugal: Atas do Congresso Internacional Sobre o Rio Minho; 2004 (5 pp.).

IGME, 1986.Mapa geológico de la Peninsula Ibérica, Baleares y Canarias (1:1 000 000). Ed Instituto Geologico y Minero de España.

Jemison Jr JM, Fox RH. Corn uptake of bromide under greenhouse and field conditions. Commun. Soil Sci. Plant Anal. 1991; 22: 283–97.

Keppler F, Eiden R, Niedan V, Pracht J, Scholer HF. Halocarbons produced by natural oxidation processes during degradation of organic matter. Nature 2000; 403:298–301.

Keppler F, Kalin RM, Harper DB, McRoberts WC, Hamilton JTG. Carbon isotope anomaly in the major plant C1 pool and its global biogeochemical implications. Biogeosciences 2004; 1: 123–31.

Leorri E, Cearreta A. Recent sea-level changes in the southern Bay of Biscay: transfer function reconstructions from salt-marshes compared with instrumental data. Sci. Mar. 2009; 73: 287–96.

Leorri E, Horton BP, Cearreta A. Development of a foraminifera-based transfer function in the Basque marshes. Mar. Geol. 2008; 251: 60–74.

Leorri E, Cearreta A, Corbett R, Blake W, Fatela F, Gehrels R, Irabien MJ. Identification of suitable areas for high-resolution sea-level studies in SW Europe using commonly applied ^{210}Pb models. Geogaceta 2010; 48: 35–8.

Leorri E, Mitra S, Irabien MJ, Zimmerman AR, William WH, Cearreta A. A 700 year record of combustion-derived pollution in northern Spain: tools to identify the Holocene/Anthropocene transition in coastal environments. Sci. Total Environ. 2014; 470–471: 240–7.

Leri AC, Myneni SCB. Natural organobromine in terrestrial ecosystems. Geochim. Cosmochim. Acta 2012; 77: 1–10.

Leri AC, Hakala JA, Marcus MA, Lanzirotti A, Reddy CM, Myneni SCB. Natural organobromine in marine sediments: new evidence of biogeochemical Br cycling. Glob. Biogeochem. Cycles 2010; 24: GB4017. http://dx.doi.org/10.1029/2010GB003794.

Li H-P, et al. Bacterial production of organic acids enhances H2O2-dependent iodide oxidation. Environ. Sci. Technol. 2012; 46: 4837–44.

Luna B, Moreno JM, Cruz A, Fernández-González F. Effects of a long-term fire retardant (Fire-Trol 934) on seed viability and germination of plants growing in a burned Mediterranean area. Int. J. Wildland Fire 2007; 16: 349–59.

Luterbacher J, Dietrich D, Xoplaki E, Grosjean M, Wanner H. European seasonal and annual temperature variability, trends, and extremes since 1500. Science 2004; 303: 1499. http://dx.doi.org/10.1126/science.1093877.

Lyday PA. Bromine. U.S. Geological Survey Minerals Yearbook–2000; 2000. p. 15.2–7.

Malcolm SJ, Price NB. The behaviour of iodine and bromine in estuarine surface sediments. Mar. Chem. 1984; 15: 263–71.

Manley SL, Wang N-Y, Walser ML, Cicerone RJ. Coastal salt marshes as global methyl halide sources from determinations of intrinsic production by marsh plants. Glob. Biogeochem. Cycles 2006; 20: GB3015. http://dx.doi.org/10.1029/2005GB002578.

Martín-Chivelet J, Muñoz-García MB, Edwards RL, Turrero MJ, Ortega AI. Land surface temperature changes in Northern Iberia since 4000 yr. BP, based on δ^{13}C of speleothems. Glob. Planet. Chang. 2011; 77: 1–12.

Martinez-Cortizas A, Pontevedra-Pombal X, García-Rodeja E, Nóvoa-Muñoz JC, ShotykW. Mercury in a Spanish peat bog: archive of climate change and atmospheric metal deposition. Science 1999; 284: 939–42.

Martinez-Cortizas A, Peiteado Varela PE, Bindler R, Biester H, Cheburkin A. Reconstructing historical Pb and Hg pollution in NW Spain using multiple cores from the Chao de Lamoso bog (Xistral Mountains). Geochim. Cosmochim. Acta 2012; 82: 68–78.

Mayer LM, Macko SA, MookWH, Murray SM. The distribution of bromine in coastal sediments and its use as a source indicator for organic matter. Org. Geochem. 1981; 3: 37–42.

Monks PS. Gas-phase radical chemistry in the troposphere. Chem. Soc. Rev. 2005; 34: 376–95. http://dx.doi.org/10.1039/b307982c.

Montzka SA, Butler JH, Hall BD, Mondeel DJ, Elkins JW. A decline in tropospheric organic bromine. Geophys. Res. Lett. 2003; 30 (15): 1826. http://dx.doi.org/10.1029/ 2003GL017745.

Moreira S, Freitas MC, Araújo MF, Andrade C, Munhá J, Fatela F, Cruces A. Contamination of intertidal sediments — the case of Sado estuary (Portugal). J. Coast. Res. Spec. Issue 2009; 56: 1380–4.

Moreno F, Moreno J, Fatela F, Valente T, Guise L, Araújo MF, Drago T. Geoquímica de sedimentos em ambientes típicos de sapal — o exemplo do sapal de Caminha (NW de Portugal). XIV Semana de Geoquímica & VIII Congresso de Geoquímica dos Países de Língua Portuguesa. Portugal: Universidade de Aveiro; 2005. p. 661–4.

Moreno J, Fatela F, Leorri E, De la Rosa J, Pereira I, Araújo MF, Freitas MC, Corbett R, Medeiros A. Marsh benthic Foraminifera response to estuarine hydrological balance driven by climate variability over the last 2000 years (Minho estuary, NW Portugal). Quat. Res. 2014. http://dx.doi.org/10.1016/j.yqres.2014.04.014.

Muñoz Sobrino C, Ramil-Rego P, Gómez-Orellana L, Varela AD. Palynological data on major Holocene climatic events in NW Iberia. Boreas 2005; 34: 381–400. http://dx.doi.org/10.1080/03009480510013006.

Nittrouer CA, Sternberg RW, Carpenter R, Bennett JT. The use of ^{210}Pb geochronology as a sedimentological tool: application to the Washington Continental Shelf. Mar. Geol. 1979; 31: 297–316.

Olid C, Garcia-Orellana J, Martinez-Cortizas A, Masque P, Varela PE, Sanchez-Cabeza J-A. Multiple site study of recent atmospheric metal (Pb, Zn and Cu) deposition in the NW Iberian Peninsula using peat cores. Sci. Total Environ. 2010; 408: 5540–9.

O'Reilly T, King BSW. Use of scattered secondary target radiation in EDXRF analysis: a fundamental parameter method for matrix correction. Adv. X-ray Anal. 1986; 30: 165–74.

Oremland RS, Miller LG, Strohmaier FE. Degradation of methyl bromide in anaerobic sediments. Environ. Sci. Technol. 1994; 28: 514–20. http://dx.doi.org/10.1021/ es00052a026.

Ortiz JE, Gallego JLR, Torres T, Diaz-Bautista A, Sierra C. Palaeoenvironmental reconstruction of Northern Spain during the last 8000 cal yr BP based on the biomarker content of the Ronanzas peat bog (Asturias). Org. Geochem. 2010; 41: 454–66.

Parnell A, Haslett J, Allen J, Buck C, Huntley B. A flexible approach to assessing synchronicity of past events using Bayesian reconstructions of sedimentation history. Quat. Sci. Rev. 2008; 27: 1872–85.

Pereira, E., Ribeiro, A., Carvalho G. and Monteiro, H., 1989. Carta Geológica de Portugal (1:200 000), folha 1. Ed. Serviços Geológicos de Portugal.

Pfister C. Monthly temperature and precipitation patterns in Central Europe from 1525 to the present. In: Bradley RS, Jones PD, editors. A Methodology for Quantifying Man-made Evidence on Weather and Climate. London and New York: Routledge; 1992. p. 118–42.

Platt U, Hönninger G. The role of halogen species in the troposphere. Chemosphere 2003; 52:325–38.

Quack B, Wallace DWR. Air–sea flux of bromoform: controls, rates, and implications. Glob. Biogeochem. Cycles 2003; 17: 1023. http://dx.doi.org/10.1029/2002GB001890.

Rahman F, Langford KH, Scrimshaw MD, Lester JN. Polybrominated diphenyl ether (PBDE) flame retardants. Sci. Total Environ. 2001; 275: 1–17.

Raimund S, Quack B, Bozec Y, Vernet M, Rossi V, Garçon V, Morel Y, Morin P. Sources of short-lived bromocarbons in the Iberian upwelling system. Biogeosciences 2011; 8: 1551–64. http://dx.doi.org/10.5194/bg-8-1551-2011.

Rhew RC, Mazéas O. Gross production exceeds gross consumption of methyl halides in northern California salt marshes. Geophys. Res. Lett. 2010; 37:L18813. http://dx.doi. org/10.1029/2010GL044341.

Rhew RC, Miller BR, Weiss RF. Natural methyl bromide and methyl chloride emissions from coastal salt marshes. Nature 2000; 403: 292–5.

Rhew RC,Miller BR, Bill M, Goldstein AH, Weiss RF. Environmental and biological controls on methyl halide emissions from southern California coastal salt marshes. Biogeochemistry 2002; 60: 141–61. http://dx.doi.org/10.1023/A:1019812006560.

Rhew RC, Whelan ME, Min D-H. Large methyl halide emissions from south Texas salt marshes. Biogeosciences Discussions 2014; 11: 9451–70. http://dx.doi.org/10.5194/ bgd-11-9451-2014. (www.biogeosciences-discuss.net/11/9451/2014/).

Rosman KJR, Chisholm W, Hong SM, Candelone JP, Boutron CF. Lead from Carthaginian and Roman Spanish mines isotopically identified in Greenland ice dated from 600 BC to 300 AD. Sci. Total Environ. 1997; 31: 3413–6.

Saini HS, Attieh JM, Hanson AD. Biosynthesis of halomethanes and methanethiol by higher plants via a novel methyltransferase reaction. Plant Cell Environ. 1995; 18: 1027–33.

Scaffeta N. Multi-scale harmonicmodel for solar and climate cyclical variation throughout the Holocene based on Jupiter–Saturn tidal frequencies plus the 11-year solar dynamo cycle. J. Atmos. Solar Terr. Phys. 2012; 80: 296–311.

Shindell DT, Schmidt GA, Mann ME, Rind D, Waple A. Solar forcing of regional climate change during the Maunder Minimum. Science 2001; 294: 2149.

Shotyk W, Weiss D, Appleby PG, Cheburkin AK, Frei R, Gloor M. History of atmospheric lead deposition since 12,370 C-14 yr. BP from a peat bog, Jura Mountains, Switzerland. Science 1998; 281: 635–40.

Ślesak I, Libik M, Karpinska B, Karpinski S, Miszalski Z. The role of hydrogen peroxide in regulation of plant metabolism and cellular signalling in response to environmental stresses. Acta Biochim. Pol. 2007; 54: 39–50.

Smith JN. Why should we believe ^{210}Pb sediment geochronologies? J. Environ. Radioact. 2001; 55: 121–3.

Steinhilber F, Abreu JA, Beer J, Brunner I, ChristIM, Fischer H, Heikkilä U, Kubik PW, Mann M, McCracken KG, Miller H, Miyahara H, Oerter H,Wilhelms F. 9,400 years of cosmic radiation and solar activity from ice cores and tree rings. PNAS 2012; 109: 5967–71.

Sturrock GA, Reeves CE, Mills GP, Penkett SA, Parr CR, McMinn A, Corno G, Tindale NW, Fraser PJ. Saturation levels of methyl bromide in the coastal waters off Tasmania. Glob. Biogeochem. Cycles 2003; 17(4): 101. http://dx.doi.org/10. 1029/2002GB002024.

Thomas VM, Bedford JA, Cicerone RJ. Bromine emissions from leaded gasoline. Geophys. Res. Lett. 1997; 24: 1371–4.

Toyota K, McConnell JC, Lupu A, Neary L, McLinden CA, Richter A, Kwok, Semeniuk K, Kaminski JW, Gong S-L, Jarosz J, Chipperfield MP, Sioris CE. Analysis of reactive bromine production and ozone depletion in the Arctic boundary layer using 3-D simulations with GEM-AQ: inference from synoptic-scale patterns. Atmos. Chem. Phys. 2011; 11: 3949–79. http://dx.doi.org/10.5194/acp-11-3949-2011.

Usoskin IG, Solanki SK, Kovaltsov GA. Grand minima and maxima of solar activity: new observational constraints. Astron. Astrophys. 2007; 471: 301–9.

Valente T, Fatela F, Moreno J, Moreno F, Guise L, Patinha C. A comparative study of the influence of geochemical parameters on the distribution of foraminiferal assemblages in two distinctive tidal marshes. J. Coast. Res. SI 2009; 56: 1439–43.

Van Geel B, Heusser C, Renssen H, Schuurmans C. Climatic change in Chile at around 2700 BP and global evidence for solar forcing: a hypothesis. The Holocene 2000; 10: 659–64.

Versteegh GJM. Solar forcing of climate. 2: evidence from the past. Space Sci. Rev. 2005; 120: 243–86.

von Storch H, Costa-Cabral M, Hagner C, Feser F, Pacyna J, Pacyna E, Kolb S. Four decades of gasoline lead emissions and control policies in Europe: a retrospective assessment. Sci. Total Environ. 2003; 311: 151–76.

Wirth SB, Gilli A, Simonneau A, Ariztegui D, Vannière B, Glur L, Chapron E, Magny M, Anselmetti FS. A 2000 year long seasonal record of floods in the southern European Alps. Geophys. Res. Lett. 2013; 40 (4025–4029). http://dx.doi.org/10.1002/grl.50741.

Wishkerman A, Gebhardt S, McRoberts CW, Hamilton JTG, Williams J, Keppler F. Abiotic methyl bromide formation from vegetation and its strong dependence on temperature. Environ. Sci. Technol. 2008; 42: 6837–42.

Wisniak J. The history of bromine from discovery to commodity. Indian J. Chem. Technol. 2002; 9: 263–71.

World Meteorological Organization (WMO). Scientific assessment of ozone depletion: 2002. Global Ozone Research Monitoring Project Report 47. Geneva: Switzerland Protection Agency; 2002.

Wuosmaa AM, Hager LP. Methyl chloride transferase: a carbocation route for biosynthesis of halometabolites. Science 1990; 249: 160–2.

Xu S, Leri A, Myneni S, Jaffé P. Uptake of bromide by two wetland plants (*Typha latifolia L.* and *Phragmites australis (Cav.) Trin. ex Steud*). Environ. Sci. Technol. 2004; 38: 5642–8.

Yuita K. Iodine, bromine and chlorine contents in soils and plants of Japan: III. Iodine, bromine and chlorine contents in the andosols and in plants of central Honshu. Soil Sci. Plant Nutr. 1983; 29: 403–28.

Yuita K. Overview and dynamics of iodine and bromine in the environment 1. Dynamics of iodine and bromine in soil-plant system. Jpn. Agric. Res. Q. 1994; 28: 90–9.

Yvon-Lewis SA, Saltzman ES, Montzka SA. Recent trends in atmospheric methyl bromide: analysis of post-Montreal protocol variability. Atmospheric Chemistry and Physics 2009; 9: 5963–74. http://dx.doi.org/10.5194/acp-9-5963-2009. (http://ozone.unep.org/new_site/en/ozone_data_tools_access.php).

Appendix 8.1. Comparative values of the measured and certified concentrations of geological standard reference materials (SRM 2704 and SRM 1646).

	SRM 2704			**SRM 1646**		
	(n=20)			(n=10)		
	(certified)	(measured)	(% error)	(certified)	(measured)	(% error)
Br (mg/kg)	7	>10	-	(101±4)*	95±7	7
Pb (mg/kg)	161	168±10	6	28	26±4	15

* Doff (1989)

Appendix 8.2. ^{210}PbExcess and ^{137}Cs content (Bq kg^{-1}) in the FCPw1 core – Caminha tidal marsh.

$^{210}Pb_{Excess}$ and ^{137}Cs content (Bq kg−1)				
Depth (cm)	$^{210}Pb_{Excess}$	error	^{137}Cs	error
0.5	328.8	38.3		
1.5	250.7	29.7		
2.5	166.1	20.9		
3.5	121.1	16.4	16.7	1.7
4.5	113.6	15.6	17.7	1.7
5.5	108.9	15.3	20.0	1.7
6.5	88.2	13.0	28.5	1.7
7.5	125.9	16.8	40.5	1.3
8.5	66.8	10.9	74.3	2.7
9.5	30.5	7.4	45.7	1.7
10.5	12.5	5.6		
11.5	5.0	4.9		
12.5	2.4	4.6		
13.5	2.1	4.6		

Appendix 8.3. Organic matter data from the core FCPw1 (after De la Rosa et al., 2012) – Caminha tidal marsh.

Depth cm	Age Cal AD	C_{org}/N	$\delta^{13}C$ ‰	n-Alkanes				n-Alkan-2-ones	
				CPI ALKa (o/e)	TAR ALK b	ACL ALK d	C_{31}/C_{27}	CPI KET g (o/e)	C_{25}/C_{27}
0-2	2010-2002	16.5	-26.6	3.0	7.5	27.4	3.6	3.4	0.5
4-6	1983-1977	12.1	-25.0						
10-12	1885-1876	18.0	-26.6	3.0	11.7	28.3	5.0	2.9	0.5
14-16	1838-1829	17.0	-26.1						
20-22	1774-1761	17.4	-26.9	3.1	13.5	28.6	4.8	3.3	0.4
24-26	1729-1720	16.5	-27.4						
30-32	1663-1654	16.2	-27.2	3.5	15.1	28.7	6.7	3.5	0.3
34-36	1617-1607	18.9	-27.4						
40-42	1533-1495	17.5	-27.4	1.8	8.0	28.0	3.4	2.7	0.4
44-46	1412-1378	17.9	-27.1						
50-52	1301-1290	18.5	-27.1	2.0	3.8	26.9	3.3	3.2	0.3
54-56	1244-1233	19.0	-26.5						
60-62	1159-1143	19.9	-26.6	2.4	14.2	28.2	3.0	4.0	0.4
64-66	1069-1050	16.9	-26.3						
70-72	890-853	16.4	-26.8	2.7	13.8	27.3	3.9	4.4	0.4
74-76	766-742	17.9	-26.1						
80-82	598-550	17.0	-26.8	2.2	7.9	27.2	2.9	4.4	0.4
84-86	477-451	18.5	-26.9						
90-92	343-321	13.4	-26.7	2.9	9.9	27.3	3.9	4.0	0.5
94-96	254-232	15.0	-25.5						
98-100	165-143	13.8	-26.4	2.9	8.0	27.1	3.6	4.1	0.4

9 Bromine soil/sediment enrichment in tidal salt marshes as a potential indicator of climate changes driven by solar activity: New insights from W coast Portuguese estuaries

J. Moreno [a,b,*], F. Fatela [a,b], E. Leorri [c], F. Moreno [d], M.C. Freitas [a,b], T. Valente [e,f], M.F. Araújo [g], J.J. Gómez-Navarro [h], L. Guise [i], W.H. Blake [j]

[a] IDL - Instituto Dom Luiz, Universidade de Lisboa, Campo Grande, 1749-016 Lisboa, Portugal

[b] Departamento de Geologia da Faculdade de Ciências da Universidade de Lisboa, Campo Grande, 1749-016 Lisboa, Portugal

[c] East Carolina University, Department of Geological Sciences, Greenville, NC 27858-4353, USA

[d] Independent Researcher, Caminho da Portela, 97, 4940-061 Bico PCR, Portugal

[e] Instituto de Ciências da Terra (ICT), Polo da Universidade do Minho, Campus de Gualtar, 4710-057 Braga, Portugal

[f] Centro de Investigación para la Ingenieria en Mineria Sostenible (CIPIMS), Universidad de Huelva, Ctra. Palos Fra. s/n, 21819 Palos de la Frontera, Huelva, Spain

[g] Universidade de Lisboa, Instituto Superior Técnico, Centro de Ciências e Tecnologias Nucleares (C2TN), Estrada Nacional 10, km 139,7, 2695-066 Bobadela LRS, Portugal

[h] University of Murcia, Department of Physics-Physics of the Earth, Campus de Espinardo, 30100 Murcia, Spain

[i] Departamento de Ciências da Terra, Universidade do Minho, Campus de Gualtar, 4710-057 Braga, Portugal

[j] School of Geography, Earth and Environmental Sciences, Plymouth University, Plymouth, Devon PL4 8AA, UK

Published in: *Science of Total Environment* 580 (2017), 324–338

http://dx.doi.org/10.1016/j.scitotenv.2016.11.130

"The ubiquitous abundance of the four halides (fluoride, chloride, bromide and iodide) has resulted in the evolution of organohalogens in all regions of our earth, both biogenic and abiotic."

G.W. Gribble in NATURALLY OCCURRING ORGANOHALOGEN COMPOUNDS – A Comprehensive Update, p. 3.

GRAPHICAL ABSTRACT

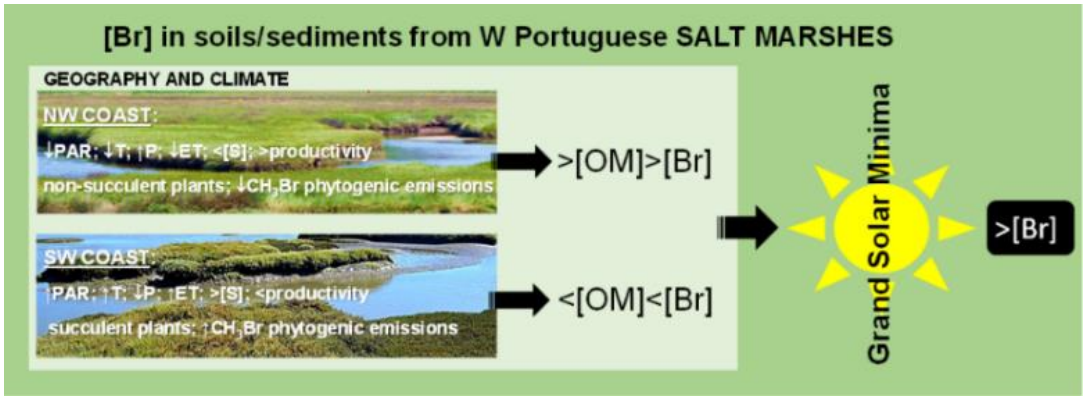

ABSTRACT

This paper aims at providing insight about bromine (Br) cycle in four Portuguese estuaries: Minho, Lima (in the NW coast) and Sado, Mira (in the SW coast). The focus is on their tidal marsh environments, quite distinct with regard to key biophysicochemical attributes. Regardless of the primary bromide (Br^-) common natural source, i.e., seawater, the NW marshes present relatively higher surface soil/sediment Br concentrations than the ones from SW coast. This happens in close connection with organic matter (OM) content, and is controlled by their main climatic contexts. Yet, the anthropogenic impact on Br concentrations cannot be discarded. Regarding [Br] spatial patterns across the marshes, the results show a general increase from tidal flat toward high marsh. Maxima [Br] occur in the upper drift line zone, at transition from highest low marsh to high marsh, recognized as a privileged setting for OM accumulation. Based on the discovery of OM ubiquitous bromination in marine and transitional environments, it is assumed that this Br occurs mainly as organobromine. Analysis of two dated sediment cores indicates that, despite having the same age (AD ~1300), the Caminha salt marsh (Minho estuary) evidences higher Br enrichment than the Casa Branca salt marsh (Mira estuary). This is related to a greater Br storage ability, which is linked to OM build-up and rate dynamics under different climate scenarios. Both cores evidence a fairly similar temporal Br enrichment pattern, and may be interpreted in light of the sun–climate coupling. Thereby, most of the well-known Grand Solar Minima during the Little Ice Age appear to have left an imprint on these marshes, supported by higher [Br] in soils/sediments. Besides climate changes driven by solar activity and impacting marsh Br biogeodynamics, those Br enrichment peaks might also reflect inputs of enhanced volcanic activity covarying with Grand Solar Minima.

Keywords: Salt marshes; Br cycle; OM storage; Grand Solar Minima; Climate modelling; Climate variability.

9.1. Introduction

Wetlands play an important role on the biogeochemical cycle of elements such as carbon, nitrogen, phosphorus, sulphur and mercury at local, regional and even global scales (e.g., Marques et al., 2011; Neubauer et al., 2013). A considerable amount of research has revealed that this is also true for bromine (Br) (Varner et al., 1999; Keppler et al., 2000; Rhew et al., 2000, 2002, 2014; Dimmer

et al., 2000; Drewer et al., 2006; Manley et al., 2006; Martínez-Cortizas et al., 2007; Hardacre et al., 2009; Blei et al., 2010; Hardacre and Heal, 2013). Specifically, coastal wetlands, in which tidal marshes are included, represent important land–ocean–atmosphere interfaces that allow to capture spatiotemporal variability in chemical fluxes. In these habitats, Br, mainly supplied by seawater, interacts with both halophytes and the relatively large pool of soil/sediment organic matter (OM). This connection occurs through, although still poorly understood, bromination processes that contribute to the production of organobromine compounds, which have detrimental effects on the atmosphere. For instance, salt marshes have been identified as globally significant natural sources of methyl bromide (CH_3Br) (Rhew et al., 2014, and references therein), a reactive trace gas contributing to ozone loss processes in the stratosphere (e.g., Chipperfield, 2015). On the other hand, significant widespread bromination of natural OM may significantly impact the preservation and/or degradation of organic carbon (C_{org}) in soils/sediments (Leri and Myneni, 2012), therefore affecting the recognized salt marsh ecosystem's role on climate and carbon sequestration. It is also known that in coastal (and open ocean) areas, bromine-radical chemistry provides alternative reaction pathways in the marine atmospheric boundary layer for (i) sulphur cycling, with associated implications for aerosol production (and growth), radiative heat transfer and climate (Keene et al., 2007), and (ii) mercury (Hg) cycling (Obrist et al., 2011; Tas et al., 2012), with Br-induced Hg oxidation as a likely important Hg source to world's oceans, which can contribute to human Hg exposure by seafood consumption (Sunderland, 2007). Taking together the previous findings about the Br influence on other key element biogeochemical cycles in the marine domain, and the knowledge that natural CH_3Br emissions are contributing to increase the stratospheric reactive Br budget (e.g., Carpenter et al., 2014), establishing the foundations of the Br biogeochemical cycle in coastal areas and tidal marsh habitats has gained a renewed significance.

Traditionally, Br has been used in conjunction with chlorine (Cl) as a geochemical proxy for seawater intrusion in coastal areas (e.g., Jones et al., 1999; Alcalá and Custodio, 2008), and alone as a paleosalinity indicator and a stratigraphic marker in brine cores (Adams, 1969; Ziegler et al., 2008). An alternative interpretation regarding Br concentrations and fluxes has been proposed by Moreno et al. (2015) when studying the sedimentary record recovered from the high marsh zone on a tidal salt marsh located in the NW coast of Portugal (Caminha, in the Minho River estuary). They suggested that the most prominent Br enrichment peaks between AD ~1300 (tidal marsh settlement) and AD ~1800 (considered as the beginning of industrialization) were primarily driven by a series of biogeochemical processes rather than an indication of seawater intrusion events in the Minho estuary. Those processes responded to significantly prolonged environmental (e.g., temperature and precipitation) shifts triggered by Grand Minima Episodes of solar activity (SA) during the Little Ice Age (LIA), namely the Wolf and Maunder Minima, as well as the Dalton Minimum. Such episodes corresponded to periods of solar minimal energy output, as demonstrated by long-term records of SA proxies (e.g. Usoskin et al., 2007), affecting Earth's climate. Prolonged changes in environmental

conditions can lead to significant responses at all levels of ecosystem organization, generating persistent alterations in its biogeochemical functioning (e.g., Keller et al., 2006; Neubauer et al., 2013). Accordingly, and based on Moreno et al. (2015) that linked Br biogeodynamics to past SA, the impact of the sun–climate coupling at Grand Solar Minima resulted in cascading effects on Br cycling in the Caminha salt marsh, in parallel with rate changes in OM bromination, which ultimately weakened the marsh's role as a source for CH_3Br.

Following the study conducted in Caminha, the current contribution expands and generalises the analysis, including three other Portuguese estuaries (Figure 9.1): the Lima estuary, also in the NW coast, and the Sado and Mira estuaries, both located in the SW coast. Broadly, the Portuguese W coast is typically characterized by an Atlantic climate, though two main climatic regions can be distinguished. Compared to the NW coast, climate in SW coast has drier summers, lower annual precipitation as well as higher annual temperatures and insolation. Therefore, the aim of this work is twofold: (i) acquire a wider latitudinal range of Br measurements in waters (superficial and interstitial) and marsh soils/sediments in order to infer trends associated to the biogeomorphological settings and climatic variability, and (ii) improve the understanding of bromine-climate relationships driven by SA, also providing new independent data and source insight to the still ongoing debate about the "missing source" for the CH_3Br global budget (Yvon-Lewis et al., 2009).

9.2. Regional setting

9.2.1. NW coast

Taken together, the Minho and Lima watersheds cover an area of 19,550 km^2 under an Atlantic wet climate, relatively exposed to maritime winds, high mean annual precipitation (Minho: 1200–2400 mm; Lima: 1300–4200 mm), mild summers (mean temperatures from *ca.* 18–22ºC) and relatively low mean annual insolation (2200–2500 h) (APA, 2011).

The Minho estuary (23 km^2) is oriented NE–SW and presents a semidiurnal, high-mesotidal regime in which vertical stratification occurs during periods of large freshwater discharge. The mean annual freshwater inflow is around 300 m^3/s (Ferreira et al., 2003). The highest high water spring (HHWS) is 4 m height, but this is often amplified by storm surges (Taborda and Dias, 1991), which we observed during field work. The mean tidal range is of about 2.0 m. The upstream limit of the tidal salt wedge in the Minho River is 9 km (Fatela et al., 2009). Large tidal flat and tidal marsh surfaces (*ca.* 6 km^2) occur in the Minho estuary's banks, with its largest expansion along the left bank – Caminha tidal marsh (ca. 2.5 km^2) – at the confluence with the Coura tributary (Figure 9.1). Lately, Reis et al. (2014) updated the estuary ecological quality to "moderately to remarkably polluted" based on metal concentrations guidelines (SFT TA-1467/1997). Moreover, the use of ethylene dibromide in leaded gasoline and the vehicle emissions since 1930, a shared Br and Pb

anthropogenic source, appears to have had a significant impact on the Caminha salt marsh (Moreno et al., 2015).

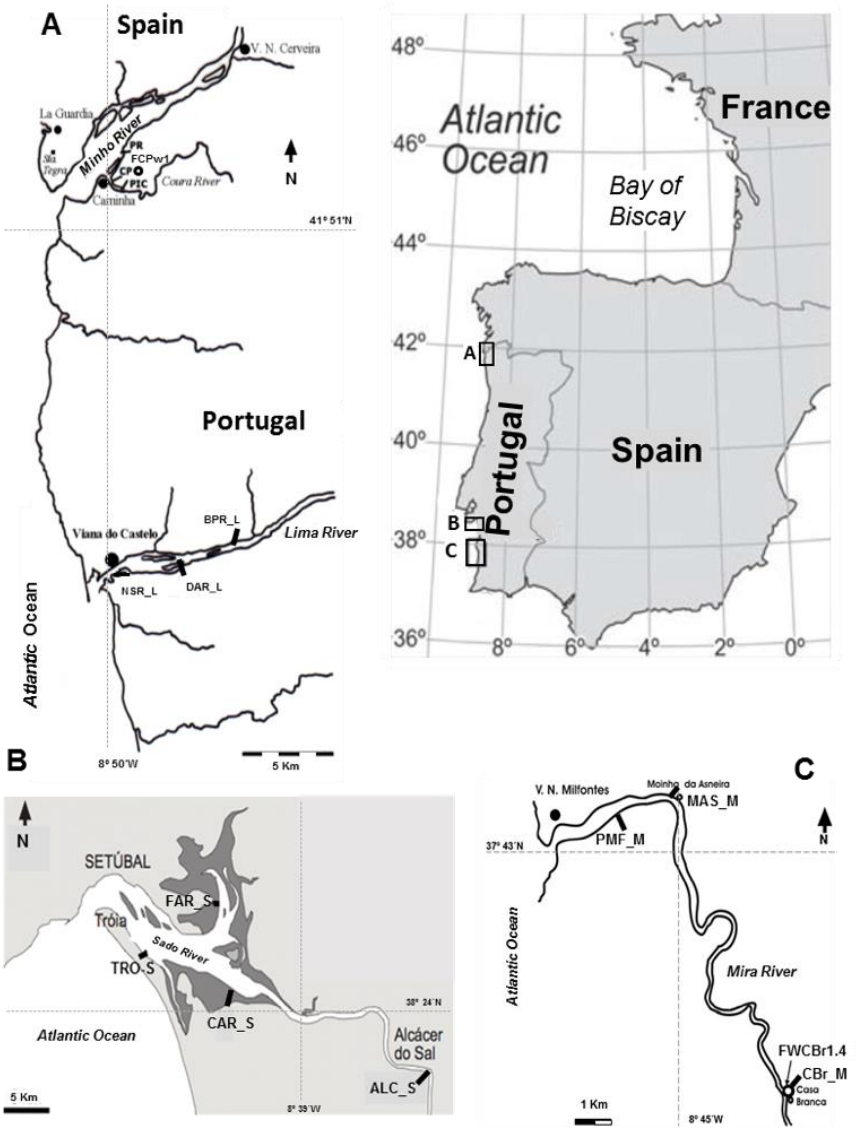

Figure 9.1. **A –** Study areas general location; **B –** Minho and Lima estuaries (NW coast); **C –** Sado estuary (SW coast); **D –** Mira estuary (SW coast). The location of the complete sampling set is also indicated. This includes thirteen surface sampling transects across the four tidal salt marshes (where both interstitial waters and sediments have been collected), and the two sediment cores obtained in the high marsh zones of the Caminha (FCPw1; Minho estuary; 1.55 m above mean sea-level; 41º52′37.0″ N and 8º49′28.0″ W) and Casa Branca (FWCBr1.4; Mira estuary; 1.74 m above mean sea-level; 37º40′03.7″ N and 8º43′12.7″ W) salt marshes.

The Lima estuary (5 km^2), located 20 km south of Minho, is oriented ENE–WSW and it is a semidiurnal mesotidal estuary, with a mean tidal range of about 2.5 m and a HHWS of 3.7 m (Vale and Dias, 2011). The mean annual freshwater inflow is 50 m^3/s (Vale and Dias, 2011). Here the tidal salt wedge effect is noticed to 3–5 km upstream in winter and no more than 15 km in summer (Alves, 2003). Intertidal areas extend over more than 2 km^2 on the banks of the Lima estuary, including the Nossa Senhora do Rosário salt marsh (NSR; Figure 9.1). The Lima lower estuary's ecological status

was considered “moderate” by Costa-Dias et al. (2010). This results from the significant impact on the estuary of the harbour activities, leading to continuous petrochemical contamination (Lima et al., 2007), and diffuse pollution from agriculture, domestic, and industrial waste discharges, including a paper mill (Costa-Dias et al., 2010).

The salt marshes of these two NW sites are classified as Eurosiberian, based on their plant communities (Costa et al., 2009), with abundant reed meadows where the presence of *Juncus maritimus* Lam. (C3 plant; non-succulent; perennial) is ubiquitous (Honrado et al., 2004; Almeida et al., 2011). Although, other plant species can also be found such as the non-native *Triglochin striatum* Ruiz & Pav. (C3 plant; succulent; perennial), the invasive *Phragmites australis* (Cav.) Trin ex. Steud. (C3 plant) and the weed *Spartina patens* (Aiton) Muhl (C4 plant; non-succulent; perennial) (Almeida et al., 2011).

9.2.2. SW coast

The SW coast of Portugal, where the Sado and Mira estuaries are located, is under a subhumid Mediterranean climate, with mean values of annual precipitation around 600–700 mm (Bettencourt et al., 2003). Mean air surface temperatures are near 23ºC in the hottest months (July and August), with a yearly average number of sunshine hours ranging 2900–3000 (APA, 2011), also showing almost permanent maritime moist winds (APA, 2011). The size of Sado and Mira rivers watersheds is 6700 km^2 and 1576 km^2, respectively.

The Sado estuary (170 km^2), the second largest estuarine system in Portugal, is located about 40 km south of Lisbon (Figure 9.1). It is a well-mixed estuary under normal river flow conditions, however, high discharge in some winter months may cause moderate stratification locally (Ferreira et al., 2003). It has a complex morphology generally oriented NW–SE and presents wide tidal flats as well as narrow and discontinuous coastal salt marshes covering around 7.2 km^2 (Moreira, 1992). The tidal pattern is semi-diurnal, with a mean tidal range of about 2.7 m and a HHWS of 3.2 m (Martins et al., 2001). The maximum salt-wedge limit is 70 km upstream. The mean annual freshwater input is *ca.* 40 m^3/s, exhibiting large interannual fluctuations. The lower estuary behaves as a coastal lagoon, while the upper reaches present a greater fluvial influence (Martins et al., 2001). In general, the Sado estuary can be classified as “moderately contaminated”, but the lower estuary and some segments near industrial areas have revealed levels of concern for several contaminants both organic and inorganic, with adverse toxicological effects to biota (e.g., Neuparth et al., 2005).

Finally, the vertically well-mixed Mira estuary (4.5 km^2) is a narrow incised estuary oriented NE–SW (e.g., Paula et al., 2006). It presents a semi-diurnal mesotidal regime with a mean tidal range of about 2.4 m and a HHWS of 3.5 m (Amaral et al., 2007). The salt edge may reach 32 km from the river mouth (Bettencourt et al., 2003). The lower section of the estuary has a dominant

marine influence due to low, seasonal and limited freshwater input by the Mira River (2.9 m^3/s). This characteristic has allowed the development, in the lower 8 km long, of large intertidal and homogenous seagrass meadows of *Zostera noltii* Hornemann, 1832 (e.g., Cunha et al., 2013). The estuarine area is also characterized by bare sandy areas and muddy substrates, with a 2.9 km^2 area of fringing salt marshes occurring as far as 15–20 km upstream (Costa et al., 2001). These salt marshes have remained nearly unchanged since 1958, with the entire ecosystem relatively undisturbed by anthropogenic activities (Castro and Freitas, 2006).

As oppose to the NW sites, the SW salt marshes studied here belong to the Biogeographic Mediterranean region (Costa et al., 2009). The halophytic community is mixed including perennial succulent species such as *Halimione portulacoides* (L.) Aellen (C3 plant), *Sarcocornia fruticose* (L.) A.J. Scott (C3 plant), *Sarcocornia perennis* (Mill.) A.J. Scott (C3 plant) in the high marsh and the annuals *Spartina maritima* (Curtis) Fernald (C4 plant) and *Salicornia fragilis* P. W. Ball & Tutin (C3 plant) in the low marsh (e.g., Costa, 2001).

9.3. Materials and methods

9.3.1. Water and sediment samples

The methodologies used for sampling and analysis of water (superficial and interstitial) and sediments (surface and cored) in the Lima, Sado and Mira estuaries follow Moreno et al. (2015) and are fully described therein. Figure 9.1 and Tables 9.1 and 9.2 summarize the new samples analyzed here: eight interstitial water samples from three salt marsh transects (NSR_L, TRO_S, PMF_M), ninety-one sediment surface samples from the intertidal domain (tidal flat, devoid of vascular plants; low marsh and high marsh zones with typical halophytic vegetation), along ten cross-shore transects, as well as a one-meter-long sediment core (hereafter FWCBr) recovered with a manual Auger sampler from the Casa Branca salt marsh (1.74 m above mean sea-level; 37º40′03.7″ N and 8º43′12.7″ W), located on the Mira River estuary. A total of thirty sliced (1 cm thick) samples were analyzed for Br and LOI. The FCPw1 core from Moreno et al. (2015), located in the Caminha high marsh zone (1.55 m above mean sea-level; 41º52′37.0″ N and 8º49′28.0″ W), is also indicated in Figure 9.1.

In order to characterize the two possible end-members (fluvial and marine) of biogeochemical sources to salt marshes, four marine seawater and four fluvial freshwater samples were collected (Table 9.1).

Water sample analyses: The filtrate was analyzed for bromide (Br^-), among other anions, by ion chromatography (IC) with suppressed conductivity detection (761 Compact IC Metrohm), and raw data processed with Metrohm Metro data 1.1. The IC method no. S-73, developed by Metrohm to determine anions in seawater, was used for the most saline waters (see Valente et al., 2009 and

Moreno et al., 2015 for detailed information). A set of standards was prepared to make a 6-point calibration curve covering the range of Br^- (and Cl^-) concentrations in water samples. The IC method not only allows an efficient separation of the Br^- and Cl^- peaks, but has also the advantage of measuring both anions in the same sample preventing the errors introduced by dilution. A standard (20 mg/L) was run independently of the calibration curve to check for accuracy (every two samples) and sample replicates were run to check for precision. The precision was within the relative standard deviation (RSD) of 5% for all determinations and results were accurate within precision.

Sediment sample analysis: Br concentrations in cored samples, along with the collected surface sediments, were determined by Energy-Dispersive X-Ray Fluorescence Spectrometry (EDXRF), using a KEVEX 771 spectrometer. To calibrate the spectrometer and verify the accuracy and precision of the overall procedure three certified reference materials were analyzed: SGR1 (Green River Shale from the United States Geological Survey – USGS), SRM 2704 (Buffalo River Sediment) and SRM1646 (Estuarine Sediment), both from the National Institute for Standards and Technology (NIST). A complete description of the equipment, analytical conditions and spectral evaluation, along with the calibration and quantification techniques, is available in Araújo et al. (1998, 2003). Accuracy and precision on the Br determinations are better than 10% as previously fully described in Moreno et al. (2015). The OM content was estimated from Loss-on-Ignition (LOI), with an aliquot of bulk sediment sample (2.0 g) dried and oven-heated at a temperature of 500ºC ± 50ºC for about 2 h (Moreira et al., 2009). Quality control was checked by replicate analysis (40% of the total), with errors lying in the interval 0.1%–15.0% (average: 5.7%) of the measured value. In an attempt to test the reliability of LOI data for the estimation of C_{org} content, a regression analysis was performed for LOI *vs.* C_{org} for the FCPw1 core, with C_{org} data taken from De la Rosa et al. (2012). A strong statistically significant direct correlation ($r = 0.97$, $N = 19$; $p < 0.001$) between LOI and C_{org} was achieved, ensuring that LOI results are reflecting mostly C_{org} (%OM).

In order to characterize OM quality, i.e., the percentages of labile and recalcitrant OM, the stepwise thermogravimetric procedure (STG) of Kristensen (1990) was applied to the cored samples from the Casa Branca salt marsh. According to this method, these OM fractions are defined as the percentage weight losses after ignition at 280ºC and 520ºC, respectively. In short, samples of 0.5 g were grounded and pre-dried at 105ºC for 6 h. After cooling in a desiccator, the sample weight was determined with a precision of 0.1 mg. Next, the samples were combusted at precisely 280ºC for 6 h in a computer controlled Heraeus MR 170 muffle furnace. After cooling in a desiccator and re-weighting, the samples returned to the muffle furnace and combusted at 520ºC for 6 h. After cooling in a desiccator the final ash weight was determined (Kristensen, 1990).

9.3.2. Solar activity, temperature and precipitation climatic modelled data

The reconstructed dataset chosen for this work is the total solar irradiance (TSI), considered as a proxy for SA, from Steinhilber et al. (2012). This reconstruction is based on time series of ^{14}C stored in tree rings and of ^{10}Be extracted from polar ice cores, and was downloaded from the NOAA web page (http://www.noaa.gov/).

Aiming to compare the Br and OM records with climate variables, this study also incorporates temperature and precipitation time series from both study areas, reconstructed by a high-resolution regional climate model (Gómez-Navarro et al., 2011) that encompasses the whole Iberian Peninsula (IP) and spans the second millennium entirely. The model simulates coherently the evolution of most relevant climate variables, and in particular reproduces the physically constrained coevolution of temperature and precipitation, as well as their relation with large-scale dynamics (e.g., the North Atlantic Oscillation – NAO). It is jointly driven by reconstructions of the variability of three external forcings: TSI, greenhouse gas concentrations and the effect of volcanic activity.

9.3.3. Chronology

The geochronology of the top 15 cm of the FWCBr core was calculated from the ^{210}Pb profile using the constant rate of supply method (CRS) (Appleby and Oldfield, 1978) supported by ^{137}Cs. Samples for ^{210}Pb and ^{137}Cs were analyzed following the methodology described by Appleby (2001) at the University of Plymouth (UK) Consolidated Radioisotope Facility, using an EG&G Ortec planar (GEM-FX8530-S N-type) HPGe gamma spectrometry system built to ultra-low background specification for ^{210}Pb detection. Additional information regarding the technique is provided in Appendix 9.1. This core presented an unsupported ^{210}Pb ($^{210}Pbxs$) profile that suggested some changes in the sediment accumulation rate in the upper section (*ca.* 150 years), although they could also reflect sediment mixing or disruption of the sedimentation. While the available elemental data is limited and presents generally low concentrations, the Pb profile shows slightly higher values above 18 cm that could be coincident with the initial stages of the industrial revolution (unclear date for this region but *ca.* AD 1800), which would be in agreement with the CRS model used here. However, the inflexion indicated by the model for the two older samples should be considered carefully (Leorri et al., 2010). To extend the chronology down-core, two samples (69–70 cm, 90–91 cm depth) of total organic carbon (TOC) were ^{14}C dated by accelerator mass spectrometry – AMS at Beta Analytic Inc. (USA). The chronology for the FWCBr core was created using a Bayesian age-depth model (Bchron 4.1; Haslett and Parnell, 2008; Parnell et al., 2008) (Appendix 9.1). The model provides ages with an individual error for each sample averaging 73 years for a 95% confidence interval. The obtained calendar ages are presented in years of Anno Domini (years AD).

The chronology of the FCPw1 core can be found in Moreno et al. (2015), but also relies on the combination of ^{210}Pb and ^{14}C data from TOC.

9.4. Results and discussion

9.4.1. Br^- in surface and interstitial water samples

The results of Br^- concentrations in surface and interstitial waters are presented in Table 9.1. Freshwater samples show Br^- contents between < 0.01 mg/L (Minho River) and a maximum of 0.8 mg/L (Sado River). On the other hand, marine surface water samples throughout the W coast have Br^- contents ranging from 185 to 197 mg/L (Table 9.1). Such high values, outside the typical marine [Br^-] range: 60–80 mg/L, are somewhat expected and linked to the known supersaturation in brominated organic compounds in the Portuguese offshore (Raimund et al., 2011). This one is, in turn, related to the presence of strong macroalgal sources and to the Iberian Peninsula coastal upwelling, as discussed previously by Moreno et al. (2015). Brominated organic compounds (also including CH_3Br) are produced and degraded at relatively fast rates in the coastal ocean, with their degradation mechanisms (e.g., hydrolysis and chloride exchange reactions) in the water column as major suppliers of bromide anions to seawater. Our hypothesis – linking the Br^- enrichment of western Portuguese superficial coastal waters to loss reactions of brominated organic compounds in seawater column – may be supported by other authors' findings. Namely, Hu et al. (2010) discovered for the east coast of United States evidence of a vertical distribution in the CH_3Br saturation anomalies, with highest concentrations in the subsurface seawater below the mixed layer, due to high degradation rates near the surface. An analogous subsurface seawater enhancement in depth profiles of two of the most important short-lived carriers of atmospheric Br, i.e., dibromomethane (CH_2Br_2) and bromoform ($CHBr_3$), was described by Raimund et al. (2011) when sampling the Iberian Peninsula upwelling system off the coast of Portugal.

Table 9.1. Bromide concentrations in surface water (river freshwater, estuarine and coastal seawater) samples and in marsh interstitial water samples (Minho, Lima, Sado and Mira tidal salt marshes).

Surface and interstitial waters	NW coast				SW coast			
	Minho		Lima		Sado		Mira	
Zone	Br^- (mg/L)	Salinity (‰)	Br^- (mg/L)	Salinity (‰)	Br^- (mg/L)	Salinity (‰)	Br^- (mg/L)	Salinity (‰)
River	<d.l.	0.0	0.07	0.0	0.8	0.3	0.5	0.2
Estuary mouth	141	32.5	—	—	—	—	—	—
Coastal seawater	197	35.2	197	35.2	185	35.7	197	35.4
Tidal flat	52 (48-55)*	9.5 (2-17)*	48	24.6	177	31.8	—	—
Low marsh	71 (64-83)*	14.5 (10-18)*	70	14.4	171	31.4	195	37.0
High marsh	56 (49-62)*	12.6 (11-15)*	87	13.5	54	26.6	59	30.6
Marsh transect references	PR; CP; PIC		NSR_L		TRO_S		PMF_M	
Distance to river mouth (km)	3.8 - 4.8		2.0		14.0		2.0	

*Average from three transects and range

d.l. detection limit (0.01 mg/L Br^-)

The detected Br^- enrichment in the nearshore surface water samples also implies that marine water would have Cl^-/Br^- mass ratios lower than the reported value for the average seawater

(typically 290 ± 4; e.g., Katz et al., 2011). This chemical signature in our water samples is presented in the plot of Cl^-/Br^- mass ratios *versus* Cl^- in Figure 9.2, along with a typical marine water sample (TA_SW: [Cl^-] = 19,353 mg/L and [Br^-] = 67 mg/L; Millero, 2013). The clusters displayed by the Cl^-/Br^- *vs.* Cl^- plot allow to identify freshwater (with consistently lower levels of Cl^- and Br^-) from marine and brackish waters reflecting an increase in Cl^- (Figure 9.2A). In addition, it is possible to differentiate between the interstitial water samples of the NW coast salt marshes (Minho and Lima) and the SW coast samples (Sado and Mira) (Figure 9.2B). This suggests that beyond the inferred common main source of Br^- (and Cl^-), i.e., seawater (theoretical ranges after Panno et al., 2006), a clear North–South differentiation can be established based on the relationship between the chemical indicators chloride and bromide. As shown in Figure 9.2B, the Sado and Mira interstitial waters, ranging from polyhaline (18–30‰) to euhaline (30–40‰), can be considered closer, based on these anions, to marine water samples (all clustering together; Figure 9.2B) than the ones from the Caminha and Lima salt marshes (mostly mesohaline: 5–18‰). These results are symptomatic of a stronger mixing with freshwater, originated by higher inputs of rainfall-land runoff production to the NW coast salt marshes, leading to salt dilution and lower ionic concentrations.

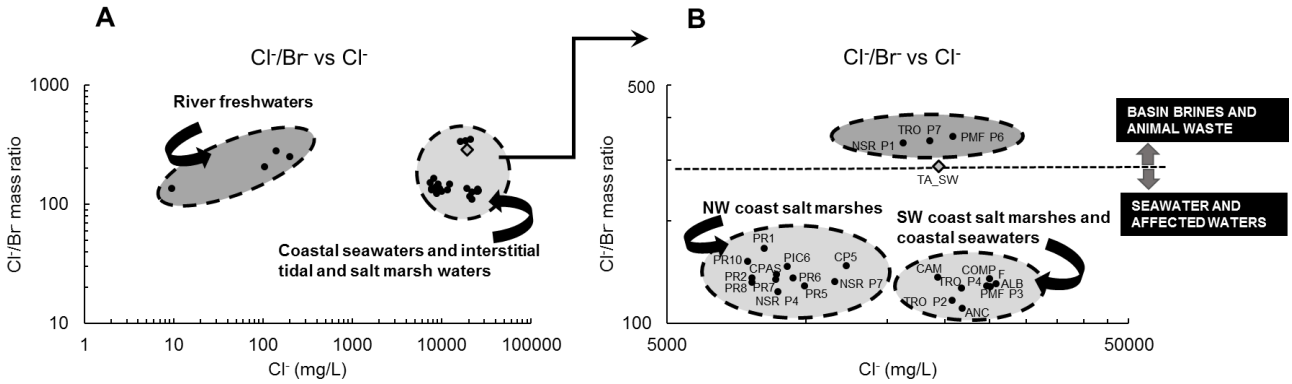

Figure 9.2. Cl^-/Br^- mass ratios *vs.* Cl^- concentrations of (surface and interstitial) water samples and potential sources (zones and theoretical limits from Panno et al., 2006). **A –** Clusters of freshwater (riverine), marine, and impacted water samples (i.e., tidal and salt marsh interstitial waters) are indicated. **B –** Clusters of interstitial waters from NW and SW coastal salt marshes. Marine water samples are in the same group as the SW coast salt marshes interstitial waters. A group of three anomalous samples (TRO_P7, NSR_P1 and PMF_P6) is also identified. The diamond represents a typical marine sample.

At this point, it must be emphasized that a rising body of evidence suggests that Br^- does not act conservatively in soils or water. Br^- can be (re)actively involved in OM cycling (e.g., Gerritse and George, 1988; Mahn and Gieskes, 2001; Biester et al., 2004, 2006; Leri et al., 2010, 2014), and it is frequently related to Fe and Mn cycling (e.g., Leri et al., 2010). This could diminish the "sensitivity" of the ratio Cl^-/ Br^-, and limits its applicability as an inorganic tracer of marine intrusion. However, plotting Cl^-/Br^- ratios provides insight into the Br^- (and Cl^-) major sources in the sampled salt marshes. Panno et al. (2006) proposed Cl^-/Br^- fingerprinting as a valuable diagnostic method in the identification of anthropogenic sources of salinization; though additional analysis should be required

to complement this technique, and thus determine more accurately the source of the contaminant present in water samples. For instance, Figure 9.2B depicts a group of samples that evidence an anthropogenic impact based on this methodology – NSR_P1 (tidal flat; Lima), TRO_P7 (high marsh zone; Sado) and PMF_P6 (high marsh zone; Mira). The three fit in the "basin brines and animal waste" water-type (Panno et al., 2006). In addition, the sample TRO_P7 presents a measurable [NO_3^-] of 54 mg/L, by opposition to the other two, both with [NO_3^-] < 0.01 mg/L (results not shown). Historical Br anthropogenic sources such as emissions from an antiknock additive in leaded gasoline, flame retardants, dyes, pharmaceuticals or pesticides in agriculture are well-known (e.g., Flury and Papritz, 1993), and while some were phased-out, others are still in use (e.g., Shawet al., 2010). As briefly pointed in Section 9.2, the Lima, Sado and Mira estuaries have their specific histories of anthropogenic disturbances, but the effort to better distinguish the likely detected Br^- contamination in water samples (Figure 9.2B) is beyond the scope of the present study.

9.4.2. Br–OM relationships in marsh surface environments

A trend of [Br^-] interstitial water was previously detected in the Caminha salt marsh, mostly assigned to the marine influence (periodic tidal flooding) on the marsh (Moreno et al., 2015). There, higher [Br^-] was found in the low marsh zone (average 71 mg/L; Table 9.1), exposed to longer inundation periods by seawater and, consequently, prone to greater inflow of Br^- brought in by incoming tides. This was correlated with the calculated relative submersion times (annual basis) for Caminha, with more than 53% for tidal flat, *ca.* 53–10% for low marsh and *ca.* 10–2% for high marsh (Fatela et al., 2009), confirming this way an increasing gradient of nontidal exposure to which Br^- seems coupled.

The tidal Br^- entering salt marshes can be cycled by several biotic and abiotic OM bromination mechanisms (e.g., Keppler et al., 2000, 2004; Hamilton et al., 2003; Saito and Yokouchi, 2006; Wishkerman et al., 2008; Leri et al., 2010; Leri and Myneni, 2012; Leri and Ravel, 2015). All include the production of an oxidized form of Br that reacts with electron-rich organic molecules, with the subsequent formation of organobromine by-products (Leri et al., 2014). Among them, it is the highly volatile gas CH_3Br (e.g., Wuosmaa and Hager, 1990; Hamilton et al., 2003; Keppler et al., 2000, 2004; Saito and Yokouchi, 2006). Therefore, both the halophytic vegetation cover and the soil/sediment organic fraction of tidal salt marshes are the main settings and substrates for the conversion of inorganic Br (Br_{inorg}) into organic Br (Br_{org}), which can largely contribute to their Br pool (Moreno et al., 2015). It also explains why the total [Br] in (coastal) soils/sediments might not necessarily correlate with [Br^-] in water (Leri and Ravel, 2015). This lack of correlation is clear in the investigated salt marshes, where some mismatch is observed between [Br^-] in interstitial waters and the total [Br] gradient in surface soils/sediments (Tables 9.1 and 9.2; Figure 9.3). The highest total Br concentrations were found in the high marsh zones from Minho (average: 389 mg/kg) and Mira

(avg.: 233 mg/kg) estuaries, while in their respective low marshes these contents did not exceed, on average, 133 mg/kg and 152 mg/kg (Table 9.2). Salt marshes from the Sado are the most depleted in both Br and OM, with average (median) values of 53 mg/kg and 8.2% (low marsh), and 81 mg/kg and 11.7% (high marsh), respectively. In the Lima estuary, Br trends are quite distinct (Table 9.2). This might be somewhat explained by the dominance of a coarser soil/sediment fraction (mainly sands) in the samples from these salt marshes transects (results not shown). Since a direct correlation has been well-established and widely accepted between mud (clay and/or silt) grain size fractions and both Br (e.g., Correns, 1956; Vinogradov, 1959; Martínez-Cortizas et al., 2016) and OM (e.g., Buchanan and Longbottom, 1970; Mayer, 1994) contents, Br concentrations can be diluted in the coarse-grained samples. The NSR_L transect is additionally impacted by a dredged sand processing facility located in the marsh surrounding area, causing resuspension of large quantities of sediment and disturbing this salt marsh (Cardoso et al., 2008).

Table 9.2. Bromine and organic matter contents in the surface sediment cross-shore transects from the Minho, Lima, Sado and Mira intertidal domains (tidal flat, low marsh and high marsh).

Surface sediment samples / Estuaries	NW coast				SW coast			
	Minho		Lima		Sado		Mira	
Zone	Br (mg/kg)	OM (%)	Br (mg/kg)	OM (%)	Br (mg/kg)	OM (%)	Br (mg/kg)	OM (%)
Tidal Flat	21 (11-30)*	1.4 (0.6-1.7)*	71 (31-79)*	8.6 (2.7-10.1)*	83 (19-226)**	11.5 (1.7-15.0)**	158 (75-318)*	8.8 (7.7-9.9)*
Low Marsh	133 (62-695)*	15.0 (5.9-24.4)*	110 (64-296)*	11.0 (5.5-20.2)*	53 (17-456)**	8.2 (0.8-21.8)**	152 (80-224)*	11.2 (9.7-12.8)*
High Marsh	389 (162-482)*	27.7 (10.6-38.8)*	49 (45-900)*	13.3 (5.9-38.9)*	81 (10-252)**	11.7 (3.3-16.3)**	233 (85-693)*	16.9 (11.2-38.3)*
Marsh transect/cores surface references	PR; CP; PIC		NSR_L; DAR_L; BPR_L		TRO_S; CAR_S; FAR_S; ALC_S		PMF_M; MAS_M; CBr_M	
Distance to river mouth (km)	3.8 - 4.8		2; 5; 8.5		14; 19; 24; 43.5		2; 3.5; 13	
Correlation coeficient Br vs.OM (p < 0.001)	0.86 (N= 21)		0.89 (N= 28)		0.67 (N= 34)		0.79 (N= 29)	

*Average (median) from three transects and range

**Average (median) from four transects and range

The spatial pattern across soil/sediment surface transects (Figure 9.3) presents a strong direct correlation between Br and OM (Lima: $r = 0.89$; $N = 28$; $p < 0.001$; Minho: $r = 0.86$; $N = 21$; $p < 0.001$; Mira: $r = 0.79$; $N = 29$; $p < 0.001$, and Sado $r = 0.67$; $N = 34$; $p < 0.001$; tidal flat samples are also included in the computed correlation coefficients). These results are in good agreement with other studies (e.g., Cundy et al., 2005), indicating that elevation is a key factor controlling the soil/sediment C_{org} pools of tidal salt marshes as suggested by Spohn and Giani (2012) and Spohn et al. (2013). These authors not only found higher C_{org} stocks in the high marsh zones with limited flooding, but a major contribution of autochthonous (in situ) OM inputs of the halophytic plant cover to soils and sediments at higher elevation within the tidal frame. Such findings could likewise enlighten the preferential total Br enrichment in the surface soils/sediments from the studied high marshes. Assuming that this Br is present mainly as organobromine, the higher concentrations found in the high marsh zones, typically characterized by greater density of stems and litter, can be associated to the relatively fast oxidation of part of Br^-, which seems to lead to a rapid conversion to Br_{org} (Leri and Myneni, 2012).

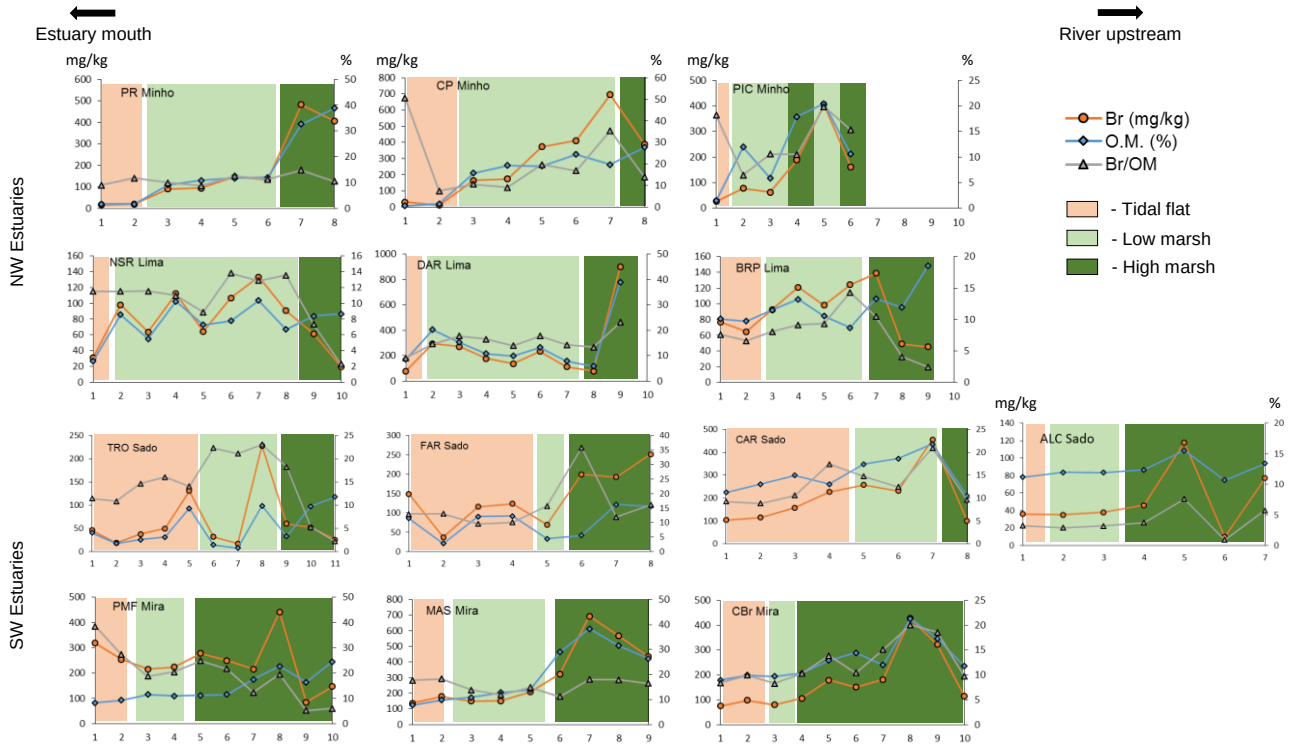

Figure 9.3. Bromine and organic matter (OM) contents of superficial tidal salt marsh sediment transects from Minho, Lima, Sado and Mira estuaries.

Similarly, the vegetation might play a significant role and the differences between locations need to be indicated. The ubiquity of non-succulent perennial species (*J. maritimus*) in the Caminha and Lima salt marshes contrasts with the dominance of succulent species (e.g., from the *Sarcocornia*/*Salicornia* genera) in Sado and Mira salt marshes. Manley et al. (2006) and Blei et al. (2010) found relatively higher Br contents in succulent species, which (succulence) results from their strategy to survive in saline soils by maintaining a large amount of tissue water. According to Manley et al. (2006), high Br tissue levels would make of these succulent halophytes prolific CH_3Br producers, although further suggesting that each plant species has very different intrinsic abilities to produce CH_3Br. Conversely, Rhew et al. (2014) estimated that only around 0.17% Br^- in the leaf tissue of *Batis maritima* L. (known as one of the CH_3Br greatest producers in salt marshes) is daily removed via CH_3Br emissions, mentioning the need of a separated "active" Br^- pool to impact this halide availability. This is a major controlling factor of the total [Br^-] budget that might be converted into Br_{org} in a given marsh. Finally, we would like to draw attention to the extensive intertidal habitat of *Zostera noltii* in the Sado and Mira estuaries (Cunha et al., 2013), and its possible impact on the Br estuarine cycling. This seagrass along with *Zostera marina* Linnaeus 1753, which though very rare occurs as well in the Mira estuary (Cunha et al., 2013), also have been identified as producers/emitters of volatile Br compounds, such as CH_3Br and $CHBr_3$ (Weinberg et al., 2013, 2015).

Interestingly, maximum Br soil/sediment enrichment in all studied salt marshes occurs in the highest low marsh transitioning to high marsh, in the so-called upper driftline zone (Adam, 1990; Gerlach, 1999; Persicke et al., 1999; Lefeuvre et al., 2000; Gettner, 2003). These areas represent a tidal-terrestrial/freshwater transition interface, where most drift litter accumulates, usually containing a high concentration of seeds and vegetative material (Mineke and Bakker, 2002). While this litter is effectively taken out of the estuarine circulation (e.g., Boorman, 2003), it becomes potentially accessible for promoting the magnification of the local C_{org} pool of soils/sediments. As a result, and even if the understanding of the internal marsh processes affecting OM accumulation and turnover is limited (Fagherazzi et al., 2013) – identical to the mechanisms regulating Br^- fluxes –, it seems plausible to consider the upper driftline zones as promising Br_{org} sink areas, from the standpoint of the current knowledge about OM bromination. Driftline zones could also be natural laboratories for studying the short and longer-term impacts of counterbalancing controls, like temperature, moisture and inundation (e.g., Lewis et al., 2014) as well as priming (e.g., Gontikaki et al., 2013) on OM mineralization, distressing Br sequestration and its fate in coastal environments.

Finally, the identified Br reduction in the soils/sediments collected at the highest high marsh (Figure 9.3) can be attributed to the increased influence of adjacent terrestrial uplands, taking into account the principle that the terrestrial environment, and thus terrestrial OM, is relatively poorer in bromine (Mayer et al., 2007). Very recently, Martínez-Cortizas et al. (2016), studying OM-rich colluvial soils, the Atlantic rankers from Galicia (NW Spain), stated that the estimations of the Br/C ratio from Mayer et al. (2007) used as representative end-members for terrestrial and marine OM may be biased by the average age of the terrestrial OM reaching the marine environment. Therefore, this sharp [Br] change recorded in our salt marshes transects needs a more thorough analysis, also taking into consideration the “upland border in the high salt marsh” as a coastal ecotone, with biological and physicochemical conditions distinct from those of the adjacent marsh plain and upland (Traut, 2005).

9.4.3. Br temporal trends in SW (Mira estuary) and NW (Minho estuary) coasts

9.4.3.1. Comparing Br enrichment in relation to the long-term OM storage ability from salt marshes in their soils/sediments

Casa Branca salt marsh (FWCBr core; Mira estuary) down-core profiles of Br and OM up to 89 cm depth (AD 1190) are presented in Figure 9.4, along with the profiles previously obtained from the Caminha salt marsh up to 62 cm depth (AD 1143) (FCPw1 core; Figure 8.3 of this PhD dissertation). Also shown in Figure 9.4 are the corresponding computed Br/OM ratio trends for both cores.

The FWCBr core presents Br concentrations in the range 129–560 mg/kg while the OM content varies between 4.9% and 23.6% (Appendix 9.2), with values uniform from the base (AD

1190) until around AD 1920 (Br: 129–215 mg/kg; average 161 ± 5 mg/kg; OM: 4.9–8.3%; average 6.7 ± 0.2%). Then, in the core's uppermost part, both Br and OM increase significantly, with two peaks at AD 1984 and AD 2010. This depth profile contrasts with the wider range and higher average Br content recorded in the FCPw1 core (Caminha): average concentration of 747 mg/kg after the tidal marsh set up in AD 1380; minimum of 68 mg/kg, AD 1143, and maximum of 1300 mg/kg by AD 1700 (Moreno et al., 2015). It seems important to mention the concomitant tidal marsh build-up in both places, as indicated by the core's analysis of preserved benthic foraminiferal assemblages: AD 1380 in Caminha (Moreno et al., 2014) and AD 1323 in Casa Branca (unpublished data). This event occurs during the transition from the Medieval Climatic Anomaly (MCA; 900–1300) to the LIA (1350–1900) and it is likely related to the main MCA–LIA shifts in local-to-regional hydro-climatic conditions in Iberian Peninsula (e.g., Lebreiro et al., 2006; Moreno et al., 2012).

The strong direct Br–OM correlation identified in surface marsh environments is preserved in the cored sediment samples with depth ($r = 0.91$; $N = 30$; $p < 0.001$), like previously described for the Caminha salt marsh ($r = 0.83$; $N = 49$; $p < 0.001$). This Br–OM correlation occurs independently of the large differences observed between the two cores regarding their Br and OM inventories (Figure 9.4). Indeed, and regardless of the evidence provided herein showing that the Mira estuary is subject to greater influence from Br^- enriched coastal waters than Minho, the FWCBr core is relatively depleted in total Br (Appendix 9.2), which also occurs despite the slightly greater percentage of the < 63 μm size fraction in its samples (FWCBr median: 99.2%, N = 91 against the FCPw1 median: 94.7%, N = 99). This depletion is also true for the long-term OM storage in both salt marshes soils/sediments. While in the FCPw1 core near 45% of the samples can be labelled as highly organic (OM > 30%) and *ca.* 41% as organic (OM range: 15%–30%), in the FWCBr core almost 94% of the samples can be classified as mineral soils with organics (OM > 3% and ≤ to 15%) (Huang et al., 2009). Therefore, and consistent with the Br–OM relationship (leading to the production of organobromine compounds) found in the surface/modern marsh habitats, it can be hypothesized that the primary driver of the whole dissimilar Br pool size of these two coastal tidal marshes is their C_{org} sink capacity, constraining the amount of C_{org} that is sequestered in each. Generally, decomposition rates in salt marshes are lower than OM inputs (allochthonous and autochthonous), the reason why they are recognized as one of the most powerful C_{org} sinks on the planet (e.g., Macreadie et al., 2013). However, it is expected that at a regional scale, soil/sediment C_{org} pools are dependent upon several decomposition rate modifiers (e.g., litter chemical composition, climate, nutrient availability, communities of soil/sediment organisms, and site-specific factors), creating diverse geographic patterns as regards C_{org} sequestration. Among those controls, salinity seems to be a major factor in tidal marshes, and it is suggested that on these environments soil C_{org} sequestration increases with decreasing salinity (e.g., Poffenbarger et al., 2011; Van de Broek et al., 2016). Actually, salinity seems to have an even stronger impact than elevation on the soil/sediment OM pools of tidal marshes, inhibiting above-ground biomass and by enhancing OM

mineralization (Hansen, 2015). In the climatic context of the Mira estuary, the evapotranspiration rates usually exceed precipitation, with tidal seawater supplying most of the moisture to the Casa Branca salt marsh soils/sediments. This induces high salinity even on the high marsh (Table 9.1), with Fatela et al. (2016) referring the occurrence of modern hypersaline conditions, with maxima records of 48‰, in the Mira lower estuary. Foraminiferal evidence (that will be discussed elsewhere) supports the idea that the (higher) Mira salinity baseline has been dominant across the time frame investigated, with the prevalence of brackish-to-normal salinity assemblages dominated by *Jadammina macrescens* (Brady, 1870) and *Trochammina inflata* (Montagu, 1808) (average 92–94%) (Unpublished data). Such high salinity baseline is, in turn, a possible explanation to the lower OM in-depth concentrations from the FWCBr profile, which agrees with results from other studies (e.g., Van de Broek et al., 2016 and references therein).

Moreover, climate has a fundamental influence on the quantity (and quality) of inputs to the soil OM pool, with C_{org} stocks being largest toward cooler and wetter locations, and smallest at hotter and drier regions, as established by other studies of terrestrial ecosystems (e.g., Jenny, 1941; Meentemeyer, 1978; Liu et al., 2012, and references therein). These climatic gradients may have left their signature on the temporal evolution of the C_{org} storage in the Caminha and Casa Branca study sites. This is revealed by their individual temporal soil/sediment OM patterns, developed in response to the long-term climatic gradient between the NW and SW coasts of rising temperature and decreasing precipitation (as can be observed in Figure 9.4), with probable direct implications on Br longer-time-scale trend, as explained before.

The strong direct Br–OM correlation holds for both the labile ($r = 0.92$, $N = 30$; $p < 0.001$) and the relatively more recalcitrant OM ($r = 0.88$; $N = 30$; $p < 0.001$) fractions from the Casa Branca salt marsh soils/sediments (data not shown). This result is consistent with recent investigation, in which a series of model experiments allowed to establish the existence of a natural, abiotic mechanistic source both of aliphatic (more labile) and aromatic (more recalcitrant) forms of Br_{org} in plant debris and humic substances in soil environment (Leri et al., 2014), and marine particulate OM (Leri and Ravel, 2015). The soil humic substances showed a recalcitrant aromatic Br_{org} speciation, leading Leri et al. (2014) to suggest that this might provide a useful proxy for evaluating the rate of OM burial in sediments. In this direction, is worth mentioning the work by Biester et al. (2004, 2006) and Martínez-Cortizas et al. (2007, 2016) in organic (i.e., peatlands) and mineral continental soils to study the temporal trends of the more stable Br_{org} compounds and the role of the main pedogenetic processes involved on Br accumulation. Altogether, this analysis can help future investigation on the Br–OM link in tidal marshes, needed to support the use of Br in tidal marsh soils/sediments as a paleoclimatic indicator. In this context, also the role of the soils/sediments main chemistry should be assessed since this can have an influence on Br accumulation (e.g., by differences in the mechanisms stabilizing the brominated-OM; Martínez-Cortizas et al., 2016).

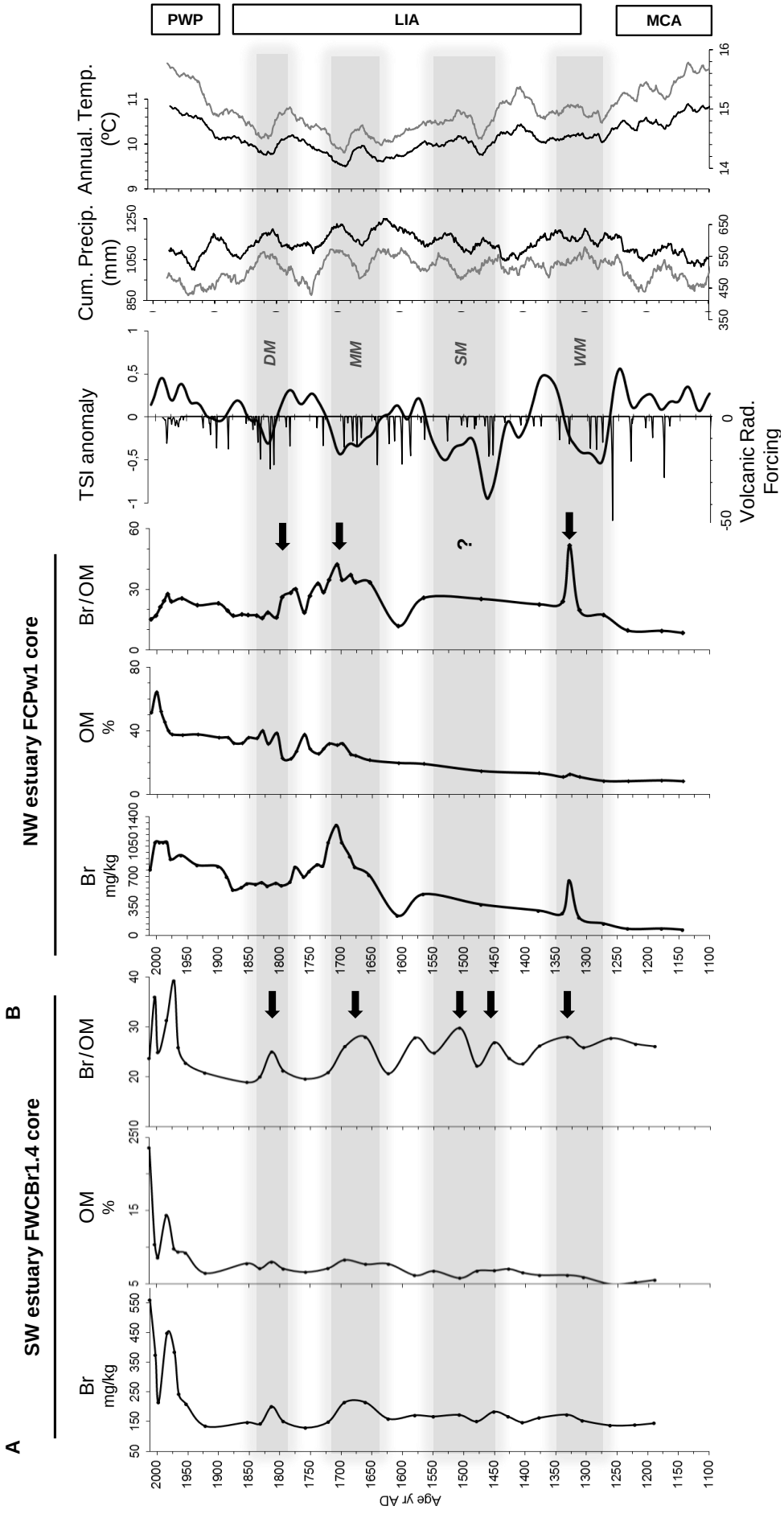

Figure 9.4. FWCBr1.4 and FCPw1 cores geochemical data: Br (mg/kg), OM (%) and Br/OM ratios. Other data represented are: TSI anomaly using a 21-year running average reconstruction (Steinhilber et al., 2012); volcanic radiative forcing (black bars) after Crowley (2000); cumulative precipitation and annual temperature (31-year running averages) for NW coast (black lines and top axis) and SW coast (grey lines and bottom axis) of Portugal (Gómez-Navarro et al., 2011). DM – Dalton Minimum; MM – Maunder Minimum; SM – Spörer Minimum; WM – Wolf Minimum.

Finally, we propose a conceptual model for the salt marshes Br cycle in our case study (NW Caminha and SW Casa Branca) in order to summarize the interplay between the forcing factors analyzed along the lines of the previous discussion. The interactions illustrated in Figure 9.5 are, in our view, the most likely to have a strong influence on salt marshes short and even longer-term role to act as a source and/or as a sink for Br. Accordingly, NW coast high marshes under the sustained influence of concomitant lower photosynthetically active radiation (PAR), this one corresponding to the spectral range of solar radiation from 400 to 700 nm that is used in photosynthesis reactions (e.g., Mariscal et al., 2000), and colder wetter conditions developed lower salinity baselines where the vegetation cover largely consists of non-succulents. These lower salinity (mesohaline) tidal marshes have typically higher rates of plant productivity and lower decomposition rates of dead and senescing plant material, leading to higher accumulation of soil/sediment OM (e.g., Morrisey et al., 2014). Collectively, these processes culminate in lesser CH_3Br atmospheric emissions from marshes and higher Br_{org} concentration in their soils/sediments. Instead, the SW coast high marshes, settled under higher available PAR conditions and a hotter and dryer climate, show higher (polyhaline to euhaline) salinity baselines and consequently lower productivity, being mostly colonized by succulent plants more adapted to saline conditions and greater emitters of CH_3Br. These conditions finally lead to a lower long-term storage of OM and Br_{org} in soils/sediments.

The afore-described model establishes a connection with the analysis of the Br temporal variability in light of the past SA–climate link made in the next section.

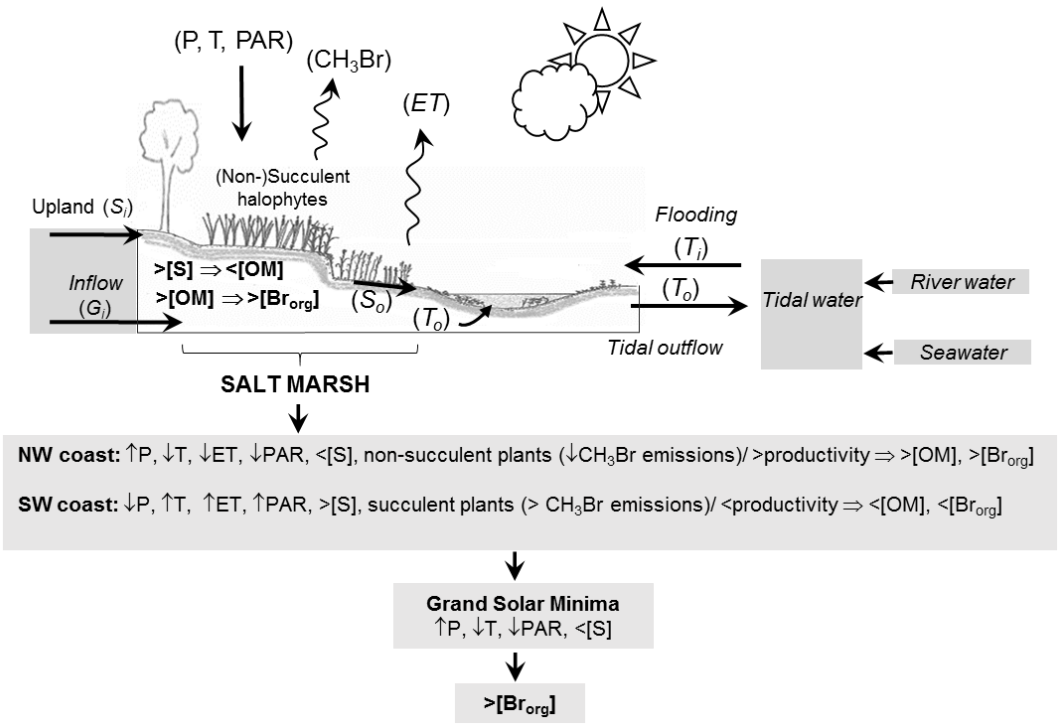

Figure 9.5. Conceptual model for the Br cycling in the W Portuguese coast saltmarshes, including the most important elements influencing the Br pool in soils/sediments (P – Precipitation; T – Temperature; PAR – Photosynthetically Active Radiation; ET – Evapotranspiration; S_i – Surface water inflow; S_o – Surface water outflow; G_i – Ground water inflow; T_i – Tidal water outflow; T_o – Tidal water outflow; [S] – Salinity; [OM] – Soil/Sediment Organic Matter content; [Br_{org}] – Soil/Sediment Organic Bromine content).

9.4.3.2. Br enrichment peaks in association with Grand Minima of solar activity

The manifestation of solar activity (SA) Grand Minima in terrestrial climate has been established after the work of Eddy (1976). The most recent Grand Minima in reconstructed SA, as expressed by the TSI variation (Steinhilber et al., 2012), are presented in Figure 9.4 (Maunder Minimum – MM; 1645–1715; Spörer Minimum – SM; 1450–1550; and Wolf Minimum – WM; 1282–1342). Note that the Dalton Minimum (DM; 1790–1820) has a distinct physical origin (Duhau and de Jager, 2010) and, for that reason, it is not regarded today as a Grand Episode of SA.

Understanding the Sun–Earth's climate coupling system is both an essential and an urgent issue, with great progress achieved over the last decades (e.g., Haigh, 2007; Soon et al., 2014 for a review). Recently, Brugnara et al. (2013) referred that the Euro-Atlantic sector, in which Portugal is located, seems to be a region with a particularly strong solar influence on the troposphere, finding a significant change in the mean late winter circulation over Europe, which culminates in detectable impacts on the near-surface climate. Jiang et al. (2015) suggested that (i) climate in the northern North Atlantic regions follows SA fluctuations on multidecadal to centennial time scales, and (ii) it is more susceptible to the influence of those fluctuations throughout cool periods with, for instance, less vigorous ocean circulation. Similar results were found by Gómez-Navarro et al. (2012) in the context of climate simulations for the second millennium over the Iberian Peninsula, recognizing that temperature and precipitation variability is significantly affected at centennial time scales by variations in the SA.

Grand Minima and Dalton-type Minimum scenarios are broadly characterized by (i) lower TSI (i.e., lower available PAR) (Lean, 1991, and references therein), (ii) development of cloudiness (e.g., Usoskin and Kovaltsov, 2008), and (iii) decreased global/regional air surface temperatures (e.g., Neukom et al., 2014) in tandem with greater regional precipitation variability. In the Iberian Peninsula, according with the modelled results from Gómez-Navarro et al. (2011), precipitation could have increased in response to reduced solar forcing (Figure 9.4), prompting greater river discharges. Also Cruz et al. (2015) related maxima rainfall episodes with other Grand Solar Minima (recognized in stalagmite record), suggesting a strong coupling between SA and precipitation over northern Iberia, which agrees with Gómez-Navarro et al. (2012) outcomes in the standpoint of climate simulations.

The connections between solar phenomena and the lower atmosphere processes can be explained by two kind of mechanisms: (i) "top-to-down", influencing the pole-to-equator temperature gradient and exerting an impact on the modulation of the atmospheric circulation cells, weakening or strengthening the zonal winds, and (ii) "bottom-to-up" that directly impact on the radiation fluxes, energy balance and temperatures on the ground. Both finally impact the atmospheric circulation modes responsible for the global/regional precipitation and temperature patterns (e.g., Gray et al., 2010; Martin-Puertas et al., 2012; Thiéblemont et al., 2015).

Therefore, if solar variations are an important source of regional climate variability, we might expect that paleoclimate proxies reproduce somewhat the climatic response to SA changes. In line with this, Moreno et al. (2015) suggested that Br soil/sediment enrichment in the Caminha salt marsh (NW coast) is, at least partially, related to the SA pattern over the last almost 800 years. This can be extended to the Casa Branca salt marsh (SW coast), essentially through a SA control on (i) available PAR fluctuations and (ii) regional temperature and precipitation regimes, affecting evapotranspiration rates and, consequently, interstitial water salinity at the upper elevations within the marsh. Indeed, the relationship between the records presented in Figure 9.4 is clear, with periods of highest Br enrichment (FCPw1 and FWCBr) agreeing with major excursions in SA. This means that the TSI negative anomalies (Steinhilber et al., 2012) from the Dalton, Maunder, Spörer and Wolf Solar Minima, to which correspond periods of both modelled lower temperature and increased precipitation in the NW and SW of Portugal (Gómez-Navarro et al., 2011), are marked by Br enrichment peaks in marshes soils/sediments, more clearly observed in Br/OM record to account for changes in OM content (see black arrows). Considering only the group of samples from the FWCBr core falling within the LIA (with stronger impacts on the climate of Europe and other regions neighbouring the North Atlantic during the 16th–19th centuries; e.g., Mann et al., 2009), three display a more pronounced Br excess relative to OM, lying outside the upper 95% confidence limit of their linear regression interval: AD 1451 (Spörer Minimum), and AD 1694 and AD 1660 (both in the Maunder Minimum). These sedimentary records, considered altogether with other climatic proxies for the NW of Portugal, strongly suggest that the LIA resulted in a wetter and cool climate in this southwestern European region, triggering major hydrological changes present in paleoecological records, namely from high marsh benthic foraminifera (Moreno et al., 2014). Specifically, climatic shifts driven by Grand Minima on western Portuguese coast could have forced a deceleration of the whole dynamics involving the net CH_3Br phytogenic emissions to the atmosphere, thus favouring Br sequestration and storage (as Br_{org}) in marsh soils/sediments. Throughout SA Grand Minima (↓TSI/PAR), the climate controls departed from normal values (↓T; ↓ET; ↑P; see Figure 9.5), inducing a decrease in marsh interstitial salinity. This certainly resulted in higher plant productivity peaks (e.g., De Leeuw et al., 1990), thereby causing a rise in salt marsh sediment C_{org} accumulation over time, with plant debris more enriched in Br and liable to further bromination during the humification process.

Rhew et al. (2014) emphasized that CH_3Br phytogenic emissions from coastal salt marshes present a dramatic inter- and intra-marshes variability, in relation to magnitude (subtropical salt marshes showing much higher emission rates than temperate salt marshes) and seasonality. They recorded maxima CH_3Br emission fluxes in peak summer growing season (July) and lowest at the end of the growing season (November). The latter were registered during the morning and coincident with the high tide. They also found a pronounced mid-day peak, overlapping in time the highest

ambient air and surface soil temperatures, in the diurnal CH_3Br emission trend, with this one mirroring the variation of PAR.

Considering both CH_3Br phytogenic emissions and the ubiquity of soil/sediment OM bromination, and applying them to a Grand Minima scenario (↓TSI/available PAR; ↓air surface temperatures; shorter growing seasons, ↑rainfall leading to soil/sediment saturation), a reliable framework for the Br enrichment in temperate marsh habitats triggered by climatic shifts driven by SA can be proposed (see Figure 9.5), while recognizing that further work would be required to completely prove this assumption.

Volcanic eruptions may also have been an alternative source of Br to salt marshes during Grand Minima Episodes (see Figure 9.4). The first discovery of volcanic BrO (Bobrowski et al., 2003), and its subsequent measurement in many volcanic plumes around the globe (e.g., Roberts et al., 2014) demonstrates the formation of reactive bromine (firstly as Br_2, which then converts into other forms including Br, BrO, HOBr, $BrONO_2$) during these events, which can be removed (at least partially) from gaseous phase by aerosol, water and ice-uptake (followed by particle sedimentation) (Fernandez et al., 2014; Jourdain et al., 2015). Reactive bromine acts as a catalyst to its own formation, leading to an exponential growth called “bromine explosion”. The LIA Grand Minima have been punctuated by considerable volcanic activity (e.g., D’Arrigo et al., 2013; Figure 9.4). D’Arrigo et al. (2013) highlighted, as two of the major volcanic events over the past millennium, the eruptions of 1453 (Kuwae Volcano, Vanuatu; Spörer Minimum) and 1815 (Mount Tambora, Indonesia; Dalton Minimum). Such episodes of great volcanic activity and their worldwide effects (e.g., Trigo et al., 2009; Koffman et al., 2013) might also have had the potential for causing disruption on the Br cycling in Caminha and Casa Branca salt marshes, contributing to some extent for their soils/sediments Br enrichment throughout Grand Minima.

9.5. Conclusions

The present study addresses major topics concerning the Br cycling in contrasting salt marshes environments of four western Portuguese estuaries – Minho, Lima, Sado and Mira –, drawing attention for its complexity and linkages with OM dynamics. We provided evidence that besides the marine influence, the Br enrichment of these marshes is ultimately connected to their ability for long-term C_{org} storage. A clear difference between the marshes from NW and SW coasts stands out, with the former being more enriched in both OM and total Br. This opposing behaviour is driven by distinct climatic conditions in the two regions that favour more strongly the mechanisms and processes of OM production, burial, and preservation (with concomitant incorporation of Br) in the northwestern coastal salt marshes, in contrast with the SW coast, most probably as an outcome of the higher salinity (lesser productivity) of the latter. Seemingly, this same NW climatic setting inhibits the emission of comparatively larger phytogenic CH_3Br fluxes to atmosphere. This might be

intensified as a result of the marshes colonization by non-succulent species (less efficient in the CH_3Br production), further promoting the Br enrichment of soil/sediment OM.

Although the applied approach is constrained by chronological uncertainties, cores sampling resolution or the (relatively short) time series lengths, preventing the application of enhanced methodologies in the time–frequency domain, the Br temporal variability in the Caminha and Casa Branca salt marshes can be related to SA oscillations, showing greater Br enrichment during Grand Minima or Minima-like Episodes. This can be explained in connection with the changing temperature (decrease) and precipitation (increase) regimes in the NW and SW coasts of Portugal induced by lower TSI (available PAR), as pointed out by previous studies and supported by climate simulations. The potential contribution of major tropical volcanic explosions at Grand Solar Minima, during the registered higher Br enrichment in both Portuguese salt marshes, is also considered.

Finally, we expect that the issues encompassed here can be deepened in upcoming research about the Br biogeochemical cycle in salt marshes worldwide. The proposed conceptual framework identifies several stimuli capable of imbalance the Br–OM interconnections and helps to prioritize which are likely to play key roles on salt marshes Br recycling, in order to improve, henceforward, its reliability as a marker of climate change driven by past SA. In consonance, it is important to bear in mind that for robustly test solar–climate signals in Br tidal salt marsh records, large and widespread ensembles of well-dated data are required along with high-resolution sampling.

Acknowledgments

This work was partly supported by IDL through the UID/GEO/50019/ 2013 program, by C2TN through the UID/Multi/04349/2013 program, and is a contribution of the project WestLog (PTDC/CTE/105370/2008), funded by the Fundação para a Ciência e a Tecnologia (FCT). João Moreno benefits from a FCT PhD grant (SFRH/BD/87995/2012). The authors would like to express their sincere gratitude to Inês Pereira, Ana Medeiros and Vera Lopes for carrying out the soils and sediments geochemical analysis, and the proof-reader Carla Neves. J.J. Gómez-Navarro acknowledges the funding provided through the contract for the return of experienced researches, resolution R-735/2015 of the University of Murcia. Additionally, the authors would like to thank the handling editor, and the two anonymous reviewers for their valuable comments.

References

Adam, P., 1990. Salt Marsh Ecology. Cambridge University Press, Cambridge, UK, 461p.

Adams, S.S., 1969. Bromine in the Salado Formation, Carlsbad Potash District, New Mexico. State Bureau of Mines and Mineral Resources, Bulletin 93, Socorro, New Mexico, 122p.

Alcalá, F.J., Custodio, E., 2008. Using the Cl/Br ratio as a tracer to identify the origin of salinity in aquifers in Spain and Portugal. J. Hydrol. 359, 189–207.

Almeida, C.M.R., Mucha, A.P., Vasconcelos, M.T., 2011. Role of different salt marsh plants on metal retention in an urban estuary (Lima estuary, NW Portugal). Estuar. Coast. Shelf Sci. 91, 243–249.

Alves, A.M.C., 2003. O estuário do rio Lima: pressão antrópica e caracterização ambiental. Ciências da Terra (UNL), Lisboa, pp. H5–H9 special n°. V, CD-ROM.

Amaral, V., Queiroga, H., Skov, M., Paula, J., 2007. Planktonic availability and settlement of Carcinus maenas megalopae at high temporal resolution in the lower Mira Estuary (SW Portugal). Mar. Ecol. Prog. Ser. 348, 239–248.

APA, 2011. Sistema Nacional de Informação de Ambiente da Agência Portuguesa do Ambiente (SNIAmb). http://sniamb.apambiente.pt/.

Appleby, P.G., 2001. Chronostratigraphic techniques in recent sediments. In: Last, W.M. and Smol, J.P. (Eds.), Tracking Environmental Change Using Lake Sediments, 1. Kluwer Academic Publishers, Dordrecht, The Netherlands, pp. 171–203.

Appleby, P.G., Oldfield, F., 1978. The calculation of lead-210 dates assuming a constant rate of supply of unsupported ^{210}Pb to the sediment. Catena 5, 1–8.

Araújo, M.F., Valério, P., Jouanneau, J.-M., 1998. Heavy metal assessment in sediments of the Ave river basin (Portugal) by EDXRF. X-Ray Spectrom. 27, 305–312.

Araújo, M.F., Conceição, A., Barbosa, T., Lopes, M.T., Humanes, H., 2003. Elemental composition of marine sponges from the Berlengas Natural Park, Western Portuguese Coast. X-Ray Spectrom. 32, 428–433.

Bettencourt, A., Ramos, L., Gomes, V., Dias, J.M.A., Ferreira, G., Silva, M., Costa, L., 2003. Estuários Portugueses. Ed. INAG – Ministério das Cidades, Ordenamento do Território e Ambiente, Lisboa (311 p).

Biester, H., Keppler, F., Putschew, A., Martínez-Cortizas, Petri, M., 2004. Halogen retention, organohalogens, and the role of organic matter decomposition on halogen enrichment in two Chilean peat bogs. Environmental Science & Technology 38, 1984–1991.

Biester, H., Selimović, D., Hemmerich, S., Petri, M., 2006. Halogens in pore water of peat bogs – the role of peat decomposition and dissolved organic matter. Biogeosciences 3, 53–64.

Blei, E., Heal, M.R., Heal, K.V., 2010. Long-term CH3Br and CH3Cl flux measurements in temperate salt marshes. Biogeosciences 7, 3657–3668.

Bobrowski, N., Hönninger, G., Galle, B., Platt, U., 2003. Detection of bromine monoxide in a volcanic plume. Nature 423, 273–276.

Boorman, L.A., 2003. Saltmarsh review. An overview of coastal saltmarshes, their dynamic and sensitivity characteristics for conservation and management. JNCC Report, No. 334 113p.

Brugnara, Y., Brönnimann, S., Luterbacher, J., Rozanov, E., 2013. Influence of the sunspot cycle on the Northern Hemisphere wintertime circulation from long upper-air data sets. Atmos. Chem. Phys. 13, 6275–6288.

Buchanan, J.B., Longbottom, M.R., 1970. The determination of organic matter in marine muds: the effect of the presence of coal and the routine determination of protein. J. Exp. Mar. Biol. Ecol. 5, 158–169.

Cardoso, R., Araújo, M.F., Freitas, M.C., Fatela, F., 2008. Geochemical characterisation of sediments from marginal environments of Lima Estuary (NW Portugal). e-Terra, Revista Electrónica de Ciências da Terra Volume 5 – N° 6. GEOTIC – Sociedade Geológica de Portugal (11 p).

Carpenter, L.J., Reimann, S., Burkholder, J.B., Clerbaux, C., Hall, B.D., Hossaini, R., Laube, J.C., Yvon Lewis, S.A., 2014. Ozone-Depleting Substances (ODSs) and Other Gases of Interest to the Montreal Protocol. Chapter 1 in Scientific Assessment of Ozone Depletion: 2014, Global Ozone Research and Monitoring Project-Report N° 55. World Meteorological Organization, Geneva, Switzerland.

Castro, P., Freitas, H., 2006. Anthropogenic effects and saltmarsh loss in the Mondego and Mira estuaries (Portugal). Web Ecology 6, 59–66.

Chipperfield, M.P., 2015. Global atmosphere – the Antarctic ozone hole. Still Only One Earth: Progress in the 40 years Since the First UN Conference on the Environment, 2015, pp. 1–33.

Correns, C.W., 1956. The geochemistry of halogens. In: Ahrens, L.H., Rankama, K. and Rancorn, S.K. (Eds.), Physics and Chemistry of the Earth, Vol. 1. Pergamon Press, New York, pp. 181–233.

Costa, J.C., 2001. Tipos de vegetação e adaptações das plantas do litoral de Portugal continental. In: Albergaria Moreira, M.E., Casal Moura, A., Granja, H.M. and Noronha, F. (Eds.), Homenagem (in Honorio) Professor Doutor Soares de Carvalho. Universidade do Minho, Braga, pp. 283–299.

Costa, M.J., Catarino, F., Bettencourt, A., 2001. The role of salt marshes in the Mira estuary (Portugal). Wetl. Ecol. Manag. 9, 121–134.

Costa, J.C., Arsénio, P., Monteiro-Henriques, T., Neto, C., Pereira, E., Almeida, T., Izco, J., 2009. Finding the boundary between Eurosiberian and Mediterranean salt marshes. Journal of Coastal Research SI 56, 1340–1344.

Costa-Dias, S., Ronaldo Sousa, R., Antunes, C., 2010. Ecological quality assessment of the lower Lima Estuary. Mar. Pollut. Bull. 61, 234–239.

Crowley, T.J., 2000. Causes of climate change over the past 1000 years. Science 289, 270–277.

Cruz, J.A., Turrero,M.J., Cáceres, J.O., Marín-Roldán, A., Ortega, A.I., Garralón, A., Sánchez, L., Gómez, P., Munõz-García, M.B., Edwards, R.L., Martín-Chivelet, J., 2015. Long-term hydrological changes in northern Iberia (4.9–0.9 ky BP) from speleothem Mg/Ca ratios and cave monitoring (Ojo Guarenã Karst Complex, Spain). Environmental Earth Sciences 74, 7741–7753.

Cundy, A.B., Hopkinson, L., Lafite, R., Spencer, K., Taylor, J.A., Ouddane, B., Heppell, C.M., Carey, P.J., Charman, R.O., Shell, D., Ullyott, J.S., 2005. Heavy metal distribution and accumulation in two Spartina sp.-dominated macrotidal salt marshes from the Seine estuary (France) and the Medway estuary (UK). Appl. Geochem. 20, 1195–1208.

Cunha, A.H., Assis, J.F., Serrão, E.A., 2013. Seagrasses in Portugal: a most endangered marine habitat. Aquat. Bot. 104, 193–203.

D'Arrigo, R., Wilson, R., Anchukaitis, K.J., 2013. Volcanic cooling signal in tree ring temperature records for the past millennium. Journal of Geophysical Research: Atmospheres 118, 1–11.

De la Rosa, J.M., Araújo, M.F., González-Pérez, J.A., González-Vila, F.J., Soares, A.M., Martins, J.M., Leorri, E., Corbett, R., Fatela, F., 2012. Organic matter sources for tidal marsh sediment over the past two millennia in the Minho River estuary (NW Iberian Peninsula). Org. Geochem. 53, 16–24.

De Leeuw, J., Olff, H., Bakker, J.P., 1990. Year-to-year variation in peak above-ground biomass of six salt-marsh angiosperm communities as related to rainfall deficit and inundation frequency. Aquat. Bot. 36, 139–151.

Dimmer, C.H., Simmonds, P.G., Nickless, G., Nickless, M.R., 2000. Biogenic fluxes of halomethanes from Irish peatland ecosystems. Atmos. Environ. 35, 321–330.

Drewer, J., Heal, M.R., Heal, K.V., Smith, K.A., 2006. Temporal and spatial variation in methyl halide flux from a salt marsh. Geophys. Res. Lett. 33, L16808-5p.

Duhau, S., De Jager, C., 2010. The forthcoming Grand Minimum of solar activity. Journal of Cosmology 8, 1983–1999.

Eddy, J.A., 1976. The Maunder Minimum. Science 192, 1189–1202.

Fagherazzi, S., Wiberg, P.L., Temmerman, S., Struyf, E., Zhao, Y., Raymond, P.A., 2013. Fluxes of water, sediments, and biogeochemical compounds in salt marshes. Ecol. Process. 2, 1–16.Fatela, F., Moreno, J., Moreno, F., Araújo, M.F., Valente, T., Antunes, C., Taborda, R., Andrade, C., Drago, T., 2009. Environmental constraints of foraminiferal assemblages distribution across a brackish tidal marsh (Caminha, NW Portugal). Mar. Micropaleontol. 70, 70–88.

Fatela, F., Moreno, J., Cabral, M.C., 2016. Salinity and temperature water assessment of the tidal marshes from the W Portuguese coast, as an ecological tool to palaeoenvironmental reconstructions based on foraminifera and ostracoda assemblages. Estudos do Quaternário 14. http://www.apeq.pt/ojs/index.php/apeq.

Fernandez, R.P., Salawitch, R.J., Kinnison, D.E., Lamarque, J.-F., Saiz-Lopez, A., 2014. Bromine partitioning in the tropical tropopause layer: implications for stratospheric injection. Atmospheric Chemistry and Physics 14, 13391–13410.

Ferreira, J.G., Simas, T., Nobre, A., Silva, M.C., Shifferegger, K., Lencart-Silva, J., 2003. Identification of Sensitive Areas and Vulnerable Zones in Transitional and Coastal Portuguese Systems. INAG, Lisboa 151p.

Flury, M., Papritz, A., 1993. Bromide in the natural environment: occurrence and toxicity. J. Environ. Qual. 22, 747–758.

Gerber, E.P., Butler, A., Calvo, N., Charlton-Perez, A. Giorgetta, M., Manzini, E., Perlwitz, J., Polvani, L.M., Sassi, F., Scaife, A.A., Shaw, T.A., Son, S.-W. and Watanabe, S., 2012. Assessing and understanding the impact of stratospheric dynamics and variability on the Earth system. Bulletin of American Meteorological Society 93, 845–859.

Gerlach, A., 1999.Winter driftline debris on the Wadden Island of Mellum, Germany; distribution, quantity and decomposition. Abhandlungen Naturwissenschaftliches Verein Bremen 44, 707–724.

Gerritse, R.G., George, R., 1988. The role of soil organic matter in the geochemical cycling of chloride and bromide. J. Hydrol. 101, 83–95.

Gettner, S., 2003. Untersuchungen des Zusammenhangs zwischen Treibselmengen und Vorlandnutzung an der Westküste Schleswig-Holsteins. Kieler Notizen Pflanzenkunde Schleswig Holstein Hamburg 31, 57–71.

Gómez-Navarro, J.J., Montávez, J.P., Jerez, S., Jiménez-Guerrero, P., Lorente-Plazas, R., González-Rouco, J.F., Zorita, E., 2011. A regional climate simulation over the Iberian Peninsula for the last millennium. Clim. Past 7, 451–472.

Gómez-Navarro, J.J., Montávez, J.P., Jiménez-Guerrero, P., Jerez, S., Lorente-Plazas, R., González-Rouco, J.F., Zorita, E., 2012. Internal and external variability in regional simulations of the Iberian Peninsula climate over the last millennium. Clim. Past 8, 25–36.

Gontikaki, E., Thornton, B., Huvenne, V.A.I., Witte, U., 2013. Negative priming effect on organic matter mineralisation in NE Atlantic slope sediments. PLoS One 8, e67722-9p.

Gray, L.J., Beer, J., Geller, M., Haigh, J.D., Lockwood, M., Matthes, K., Cubasch, U., Fleitmann, D., Harrison, G., Hood, L., Luterbacher, J., Meehl, G.A., Shindell, D., van Geel, B., White, W., 2010. Solar influences on climate. Rev. Geophys. 48, RG4001-53p.

Haigh, J.D., 1996. The impact of solar variability on climate. Science 272, 981–984.

Haigh, J.D., Blackburn, M. and Day, R., 2005. The response of tropospheric circulation to perturbations in lower-stratospheric temperature. Journal of Climate 18, 3672–3685.

Haigh, J.D., 2007. The sun and the earth's climate. Living Review Solar Physics 4:1e64 (Online article). Available at: http://www.livingreviews.org/lrsp-2007-2 (accessed 08.05.2016).

Hamilton, J., McRoberts, W., Keppler, F., Kalin, R., Harper, D., 2003. Chloride methylation by plant pectin: an efficient environmentally significant process. Science 301, 206–209.

Hansen, K., 2015. Ecosystem Functions of Tidal Marsh Soils of the Elbe Estuary. Dissertation. Fachbereich Geowissenschaften, Universität Hamburg Hamburger Bodenkundliche Arbeiten 76, XX + 161p.

Hardacre, C.J., Heal, M.R., 2013. Characterization of methyl bromide and methyl chloride fluxes at temperate freshwater wetlands. Journal of Geophysical Research: Atmospheres 118, 977–991.

Hardacre, C.J., Blei, E., Heal, M.R., 2009. Growing season methyl bromide and methyl chloride fluxes at a sub-arctic wetland in Sweden. Geophys. Res. Lett. 36, L12401-5p.

Haslett, J., Parnell, A., 2008. A simple monotone process with application to radiocarbon dated depth chronologies. Appl. Stat. 57, 399–418.

Honrado, J., Alves, P., Alves, H.N., Torres, J., Caldas, F.B., 2004. A Flora e a vegetação do Minho internacional – Diversidade, ecologia e valor para conservação. Atas do Congresso Internacional Sobre o Rio Minho, Melgaço, Portugal 5p. http://www.noaa.gov/.

Hu, L., Yvon-Lewis, S.A., Liu, Y., Salisbury, J.E., O'Hern, J.E., 2010. Coastal emissions of methyl bromide and methyl chloride along the eastern Gulf of Mexico and the east coast of the United States. Biogeochemical Cycles 24, GB1007-10p.

Huang, P.-T., Patel, M., Santagata, M.C., Bobet, A., 2009. Classification of organic soils. FHWA/IN/JTRP-2008/2. Purdue University 170p.

Jenny, H., 1941. Factors of Soil Formation - A System of Quantitative Pedology. Dover Publications, Inc., New York 291p.

Jiang, H., Muscheler, R., Björck, S., Seidenkrantz, M.-S., Olsen, J., Sha, L., Sjolte, J., Eiríksson, J., Ran, L., Knudsen, K.-L., Knudsen, M.F., 2015. Solar forcing of Holocene summer sea surface temperatures in the northern North Atlantic. Geology http://dx.doi.org/10.1130/G36377.1.

Jones, F., Vengosh, A., Rosenthal, E., Yechieli, Y., 1999. Geochemical investigation of groundwater quality. Proceeding: Seawater Intrusion in Coastal Aquifers - Concepts, Methods and Practices. Kluwer Academic, Dordrecht, pp. 51–71.

Jourdain, L., Roberts, T.J., Pirre, M., Josse, B., 2015. Modeling the reactive halogen plume from Ambrym volcano and its impact on the troposphere with the CCATT-BRAMS mesoscale model. Atmospheric Chemistry and Physics Discuss 15, 35313–35381.

Katz, B.G., Eberts, S.M., Kauffman, L.J., 2011. Using Cl/Br ratios and other indicators to assess potential impacts on groundwater quality from septic systems: a review and examples from principal aquifers in the United States. J. Hydrol. 397, 151–166.

Keene, W.C., Stutz, J., Pszenny, A.A.P., Maben, J.R., Fischer, E.V., Smith, A.M., von Glasow, R., Pechtl, S., Sive, B.C., Varner, R.K., 2007. Inorganic chlorine and bromine in coastal New England air during summer. Journal of Geophysical Research 112, D10S12 (15 p).

Keller, J.K., Bauers, A.K., Bridgham, S.D., Kellogg, L.E., Iversen, C.M., 2006. Nutrient control of microbial carbon cycling along an ombrotrophic-minerotrophic peatland gradient. Journal of Geophysical Research 111, G03006-14p.

Keppler, F., Eiden, R., Niedan, V., Pracht, J., Scholer, H.F., 2000. Halocarbons produced by natural oxidation processes during degradation of organic matter. Nature 403, 298–301.

Keppler, F., Kalin, R.M., Harper, D.B., McRoberts, W.C., Hamilton, J.T.G., 2004. Carbon isotope anomaly in the major plant C1 pool and its global biogeochemical implications. Biogeosciences 1, 123–131.

Kodera, K., and Kuroda, Y., 2002. Dynamical response to the solar cycle: Winter stratopause and lower stratosphere, Journal of Geophysical Research 107, 4749-12p.

Koffman, B.G., Kreutz, K.J., Kurbatov, A.V., Dunbar, N.W., 2013. Impact of known local and tropical volcanic eruptions of the past millennium on the WAIS Divide micro particle record. Geophys. Res. Lett. 40, 4712–4716.

Kristensen, E., 1990. Characterization of biogenic organic matter by stepwise thermogravimetry (STG). Biogeochemistry 9, 135–159.

Lean, J., 1991. Variations in the sun's radiative output. Rev. Geophys. 29, 505–535.

Lebreiro, S.M., Francés, S.G., Abrantes, F.F.G., Diz, P., Bartels-Jónsdóttir, H.B., Stroynowski, Z.N., Gil, I.M., Pena, L.D., Rodrigues, T., Jones, P.D., Nombela, M.A., Alejo, I., Briffa, K.R., Harris, I., Grimalt, J.O., 2006. Climate change and coastal hydrographic response along the Atlantic Iberian margin (Tagus Prodelta and Muros Ría) during the last two millennia. The Holocene 16, 1003–1015.

Lefeuvre, J.-C., Bouchard, V., Feunteun, E., Grare, S., Laffaille, P., Radureau, A., 2000. European salt marshes diversity and functioning: the case study of the Mont Saint-Michel bay, France. Wetland Ecology and Management 8, 147–161.

Leorri, E., Freitas, M.C., Zourarah, B., Andrade, C., Mellas, S., Cruces, A., Griboulard, R., Lopes, V., 2010. Multiproxy approach to characterize an overwash deposit: Oualidia lagoon (Moroccan Atlantic coast). Geogaceta 48, 7–10.

Leri, A.C., Myneni, S.C.B., 2012. Natural organobromine in terrestrial ecosystems. Geochimica and Cosmochimica Acta 77, 1–10.

Leri, A.C., Ravel, B., 2015. Abiotic bromination of soil organic matter. Environmental Science & Technology 49, 13350–13359.

Leri, A.C., Hakala, J.A., Marcus, M.A., Lanzirotti, A., Reddy, C.M., Myneni, S.C.B., 2010. Natural organobromine in marine sediments: new evidence of biogeochemical Br cycling. Glob. Biogeochem. Cycles 24, GB4017-15p.

Leri, A.C., Mayer, L.M., Thornton, K.R., Ravel, B., 2014. Bromination of marine particulate organic matter through oxidative mechanisms. Geochim. Cosmochim. Acta 142, 53–63.

Lewis, D.B., Brown, J.A., Jimenez, K.L., 2014. Effects of flooding and warming on soil organic matter mineralization in Avicennia germinans mangrove forests and Juncus roemerianus salt marshes. Estuar. Coast. Shelf Sci. 139, 11–19.

Lima, I., Moreira, S.M., Osten, J.R.-V., Soares, A.M.V.M., Guilhermino, L., 2007. Biochemical responses of the marine mussel Mytilus galloprovincialis to petrochemical environmental contamination along the North-western coast of Portugal. Chemosphere 66, 1230–1242.

Liu, Z.P., Shao, M.A., Wang, Y.Q., 2012. Large-scale spatial variability and distribution of soil organic carbon across the entire Loess Plateau, China. Soil Research 50, 114–124.

Macreadie, P.I., Hughes, A.R., Kimbro, D.L., 2013. Loss of "blue carbon" from coastal salt marshes following habitat disturbance. PLoS One 8, e69244-8p.

Mahn, C.L., Gieskes, J.M., 2001. Halide systematics in comparison with nutrient distributions in sites 1033B and 1034B, Saanich Inlet: ODP Leg 169S. Mar. Geol. 174, 323–339.

Manley, S.L., Wang, N.-Y., Walser, M.L., Cicerone, R.J., 2006. Coastal salt marshes as global methyl halide sources from determinations of intrinsic production by marsh plants. Glob. Biogeochem. Cycles 20, GB3015-13p.

Mann, M.E., Zhang, Z., Rutherford, S., Bradley, R.S., Hughes, M.K., Shindell, D., Ammann, C., Faluvegi, G., Ni, F., 2009. Global signatures of the Little Ice Age and Medieval climate anomaly and plausible dynamical origins. Science 326, 1256–1260.

Mariscal, M.J., Orgaz, F., Villalobos, F.J., 2000. Modelling and measurement of radiation interception by olive canopies. Agric. For. Meteorol. 100, 183–197.

Marques, B., Lillebø, A.I., Pereira, E., Duarte, A.C., 2011. Mercury cycling and sequestration in salt marshes sediments: an ecosystem service provided by Juncus maritimus and Scirpus maritimus. Environ. Pollut. 159, 1869–1876.

Martínez-Cortizas, A., Biester, H., Mighall, T., Bindler, R., 2007. Climate-driven enrichment of pollutants in peatlands. Biogeosciences 4, 905–911.

Martínez-Cortizas, A., Vázquez, C.F., Kaal, J., Biester, H., Casais, M.C., Rodríguez, T.T., Lado, L.R., 2016. Bromine accumulation in acidic black colluvial soils. Geochim. Cosmochim. Acta 174, 143–155.

Martin-Puertas, C., Matthes, K., Brauer, A., Muscheler, R., Hansen, F., Petrick, C., Aldahan, A., Possnert, G., van Geel, B., 2012. Regional atmospheric circulation shifts induced by a grand solar minimum. Nat. Geosci. 5, 397–401.

Martins, F., Leitão, P., Silva, A., Neves, R., 2001. 3D modelling in the Sado estuary using a new generic vertical discretization approach. Oceanol. Acta 24, 1–12.

Mayer, L.M., 1994. Relationships between mineral surfaces and organic carbon concentrations in soils and sediments. Chem. Geol. 114, 347–363.

Mayer, L.M., Schick, L.L., Allison, M.A., Ruttenberg, K.C., Bentley, S.J., 2007. Marine *vs.* terrigenous organic matter in Louisiana coastal sediments: the uses of bromine:organic carbon ratios. Mar. Chem. 107, 244–254.

Meentemeyer, V., 1978. Macroclimate and lignin control of litter decomposition rates. Ecology 59, 465–472.

Millero, F.J., 2013. Chemical Oceanography. Fourth ed. CRC Press, Boca Raton 571p.

Mineke, W., Bakker, J.P., 2002. Soil seed bank and driftline composition along a successional gradient on a temperate salt marsh. Appl. Veg. Sci. 5, 55–62.

Moreira, M.E.S.A., 1992. Recent saltmarsh changes and sedimentation rates in the Sado estuary, Portugal. J. Coast. Res. 8, 631–640.

Moreira, S., Freitas, M.C., Araújo, M.F., Andrade, C., Munhá, J., Fatela, F., Cruces, A., 2009. Contamination of intertidal sediments – The case of Sado estuary (Portugal). J. Coast. Res. SI 56, 1380–1384.

Moreno, A., Pérez, A., Frigola, J., Nieto-Moreno, V., Rodrigo-Gámiz, M., Martrat, B., González-Sampériz, P., Morellón, M., Martín-Puertas, C., Corella, J.P., Belmonte, Á, Sancho, C., Cacho, I., Herrera, G., Canals, M., Grimalt, J.O., Jiménez-Espejo, F., Martínez-Ruiz, F., Vegas-Vilarrúbia, T., Valero-Garcés, B.L., 2012. The Medieval Climate Anomaly in the Iberian Peninsula reconstructed from marine and lake records. Quat. Sci. Rev. 43, 16–32.

Moreno, J., Fatela, F., Leorri, E., De la Rosa, J., Pereira, I., Araújo, M.F., Freitas, M.C., Corbett, R., Medeiros, A., 2014.Marsh benthic foraminifera response to estuarine hydrological balance driven by climate variability over the last 2000 years (Minho estuary, NW Portugal). Quat. Res. 82, 318–330.

Moreno, J., Fatela, F., Leorri, E., Araújo, M.F., Moreno, F., De la Rosa, J.M., Freitas, M.C., Valente, T., Corbett, R., 2015. Bromine enrichment in marsh sediments as a marker of environmental changes driven by grand solar minima and anthropogenic activity (Caminha, NW of Portugal). Sci. Total Environ. 506–507, 554–566.

Morrisey, E.M., Gillespie, J.L., Morina, J.C., Franklin, R.B., 2014. Salinity affects microbial activity and soil organic matter content in tidal wetlands. Glob. Chang. Biol. 20, 1351–1362.

Neubauer, S.C., Franklin, R.B., Berrier, D.J., 2013. Saltwater intrusion into tidal freshwater marshes alters the biogeochemical processing of organic carbon. Biogeosciences Discussions 10, 10685–10720.

Neukom, R., Gergis, J., Karoly, D.J., Wanner, H., Curran, M., Elbert, J., González-Rouco, F., Linsley, B.K., Moy, A.D., Mundo, I., Raible, C.C., Steig, E.J., van Ommen, T., Vance, T., Villalba, R., Zinke, J., Frank, D., 2014. Inter-hemispheric temperature variability over the past millennium. Nat. Clim. Chang. 4, 362–367.

Neuparth, T., Correia, A.D., Costa, F.O., Lima, G., Costa, M.H., 2005. Multi-level assessment of chronic toxicity of estuarine sediments with the amphipod Gammarus locusta: I. Biochemical endpoints. Mar. Environ. Res. 60, 69–91.

Obrist, D., Tas, E., Peleg, M., Matveev, V., Faïn, X., Asaf, D., Luria, M., 2011. Bromine-induced oxidation of mercury in the mid-latitude atmosphere. Nat. Geosci. 4, 22–26.

Panno, S.V., Hackley, K.C., Hwang, H.H., Greenberg, S.E., Krapac, I.G., Landsberger, S., O'Kelly, D.J., 2006. Characterization and identification of Na-Cl sources in ground water. Ground Water 44, 176–187.

Parnell, A., Haslett, J., Allen, J., Buck, C., Huntley, B., 2008. A flexible approach to assessing synchronicity of past events using Bayesian reconstructions of sedimentation history. Quat. Sci. Rev. 27, 1872–1885.

Paula, J., Silva, I.C., Francisco, S.M., Flores, A.V., 2006. The use of artificial benthic collectors for assessment of spatial patterns of settlement of megalopae of Carcinus maenas (L.) (Brachyura: Portunidae) in the lower Mira Estuary, Portugal. Hydrobiologia 557, 69–77.

Persicke, U., Gerlach, A., Heiber, W., 1999. Zur botanischen Zusammensetzung von Treibsel der niedersachsischen Deichvorlander und Deichabsnitte. Drosera 1, 23–34.

Poffenbarger, H.J., Needelman, B.A., Megonigal, J.P., 2011. Salinity influence on methane emissions from tidal marshes. Wetlands 31, 831–842.

Raimund, S., Quack, B., Bozec, Y., Vernet, M., Rossi, V., Garçon, V., Morel, Y., Morin, P., 2011. Sources of short-lived bromocarbons in the Iberian upwelling system. Biogeosciences 8, 1551–1564.

Reis, P.A., Guilhermino, L., Antunes, C., Sousa, R., 2014. Assessment of the ecological quality of the Minho estuary (Northwest Iberian Peninsula) based on metal concentrations in sediments and in *Corbicula fluminea*. Limnetica 33, 161–174.

Rhew, R.C., Miller, B.R., Weiss, R.F., 2000. Natural methyl bromide and methyl chloride emissions from coastal salt marshes. Nature 403, 292–295.

Rhew, R.C., Miller, B.R., Bill, M., Goldstein, A.H., Weiss, R.F., 2002. Environmental and biological controls on methyl halide emissions from southern California coastal salt marshes. Biogeochemistry 60, 141–161.

Rhew, R.C., Whelan, M.E., Min, D.-H., 2014. Large methyl halide emissions from south Texas saltmarshes. Biogeosciences 11, 6427–6434.

Roberts, T.J., Martin, R.S., Jourdain, L., 2014. Reactive bromine chemistry in Mount Etna's volcanic plume: the influence of total Br, high-temperature processing, aerosol loading and plume–air mixing. Atmos. Chem. Phys. 14, 11201–11219.

Saito, T., Yokouchi, Y., 2006. Diurnal variation in methyl halide emission rates from tropical ferns. Atmos. Environ. 40, 2806–2811.

Shaw, S.D., Blum, A., Weber, R., Kannan, K., Rich, D., Lucas, D., Koshland, C.P., Dobraca, D., Hanson, S., Birnbaum, L.S., 2010. Halogenated flame retardants: do the fire safety benefits justify the risks? Rev. Environ. Health 25, 261–305.

Soon, W., Velasco Herrera, V.M., Selvaraj, K., Traversi, R., Usoskin, I., Chen, C.-T.A., Lou, J.-Y., Kao, S.-J., Carter, R.M., Pipin, V., Severi, M., Becagli, S., 2014. A review of Holocene solar-linked climatic variation on

centennial to millennial timescales: physical processes, interpretative frameworks and a new multiple cross-wavelet transform algorithm. Earth-Sci. Rev. 134, 1–15.

Spohn, M., Giani, L., 2012. Carbohydrates, carbon and nitrogen in soils of a marine and a brackish marsh as influenced by inundation frequency. Estuar. Coast. Shelf Sci. 107, 89–96.

Spohn, M., Babka, B., Giani, L., 2013. Changes in soil organic matter quality during sea-influenced marsh soil development at the North Sea coast. Catena 107, 110–117.

Steinhilber, F., Abreu, J.A., Beer, J., Brunner, I., Christl, M., Fischer, H., Heikkilä, U., Kubik, P.W., Mann, M., McCracken, K.G., Miller, H., Miyahara, H., Oerter, H., Wilhelms, F., 2012. 9,400 years of cosmic radiation and solar activity from ice cores and tree rings. Proc. Natl. Acad. Sci. 109, 5967–5971.

Sunderland, E.M., 2007. Mercury exposure from domestic and imported estuarine and marine fish in the U.S. seafood market. Environ. Health Perspect. 115, 235–242.

Taborda, R., Dias, J.M.A., 1991. Análise da sobre-elevação do nível do mar de origem meteorológica durante os temporais de 1978 e 1981. Geonovas, SI 1, 89–97.

Tas, E., Obrist, D., Peleg, M., Matveev, V., Faïn, X., Asaf, D., Luria, M., 2012. Measurement based modelling of bromine-induced oxidation of mercury above the Dead Sea.

Atmos. Chem. Phys. 12, 2429–2440.

Thiéblemont, R., Matthes, K., Omrani, N.-E., Kodera, K., Hansen, F., 2015. Solar forcing synchronizes decadal North Atlantic climate variability. Nat. Commun. 6, 8268-8p.

Traut, B.H., 2005. The role of coastal ecotones: a case study of the salt marsh/upland transition zone in California. J. Ecol. 93, 279–290.

Trigo, R.M., Vaquero, J.M., Alcoforado, M.J., Barriendos, M., Taborda, J., García-Herrera, R., Luterbacher, J., 2009. Iberia in 1816, the year without a summer. Int. J. Climatol. 29, 99–115.

Usoskin, I.G., Kovaltsov, G.A., 2008. Cosmic rays and climate of Earth: possible connection. Compt. Rendus Geosci. 340, 441–450.

Usoskin, I.G., Solanki, S.K., Kovaltsov, G.A., 2007. Grand minima and maxima of solar activity: new observational constraints. Astrono. Astrophys. 471, 301–309.

Vale, L.M., Dias, J.M., 2011. The Effect of Tidal Regime and River Flow on the Hydrodynamics and Salinity Structure of the Lima Estuary: Use of a Numerical Model to Assist on Estuary Classification, SI 64 (Proceedings of the 11th International Coastal Symposium). Szczecin, Poland, pp. 1604–1608.

Valente, T., Fatela, F., Moreno, J., Moreno, F., Guise, L., Patinha, C., 2009. A comparative study of the influence of geochemical parameters on the distribution of foraminiferal assemblages in two distinctive tidal marshes. J. Coast. Res. SI 56, 1439–1443.

Van de Broek, M., Temmerman, S., Merckx, R., Govers, G., 2016. The importance of an estuarine salinity gradient on soil organic carbon stocks of tidal marshes. Biogeosci. Discuss. http://dx.doi.org/10.5194/bg-2016-285.

Varner, R.K., Crill, P.M., Talbot, R.W., 1999.Wetlands: a potentially significant source of atmospheric methyl bromide and methyl chloride. Geophys. Res. Lett. 26, 2433–2435.

Vinogradov, A.P., 1959. The Geochemistry of Rare and Dispersed Elements in Soils. Second ed. Consultants Bureau, New York 209p.

Weinberg, I., Bahlmann, E., Michaelis, W., Seifert, R., 2013. Determination of fluxes and isotopic composition of halocarbons from seagrass meadows using a dynamic flux chamber. Atmos. Environ. 73, 34–40.

Weinberg, I., Bahlmann, E., Eckhardt, T., Michaelis, W., Seifert, R., 2015. A halocarbon survey from a seagrass dominated subtropical lagoon, Ria Formosa (Portugal): flux pattern and isotopic composition. Biogeosciences 12, 1697–1711.

Wishkerman, A., Gebhardt, S., McRoberts, C.W., Hamilton, J.T.G., Williams, J., Keppler, F., 2008. Abiotic methyl bromide formation from vegetation and its strong dependence on temperature. Environmental Science & Technology 42, 6837–6842.

Wuosmaa, A.M., Hager, L.P., 1990. Methyl chloride transferase: a carbocation route for biosynthesis of halometabolites. Science 249, 160–162.

Yvon-Lewis, S.A., Saltzman, E.S., Montzka, S.A., 2009. Recent trends in atmospheric methyl bromide: analysis of post-Montreal Protocol variability. Atmos. Chem. Phys. 9, 5963–5974.

Ziegler, M., Jilbert, T., de Lange, G.J., Lourens, L.J., Reichart, G.-J., 2008. Bromine counts from XRF scanning as an estimate of the marine organic carbon content of sediment cores. Geochemistry Geophysics Geosystems 9, Q05009-6p.

Appendix 9.1. Age model for the core FWCBr and estimated 2σ errors, based on two AMS ^{14}C dates, performed on total organic sediment, and ^{210}Pb and ^{137}CS chronology. The data interpolation was obtained with Bchron 4.1 software.

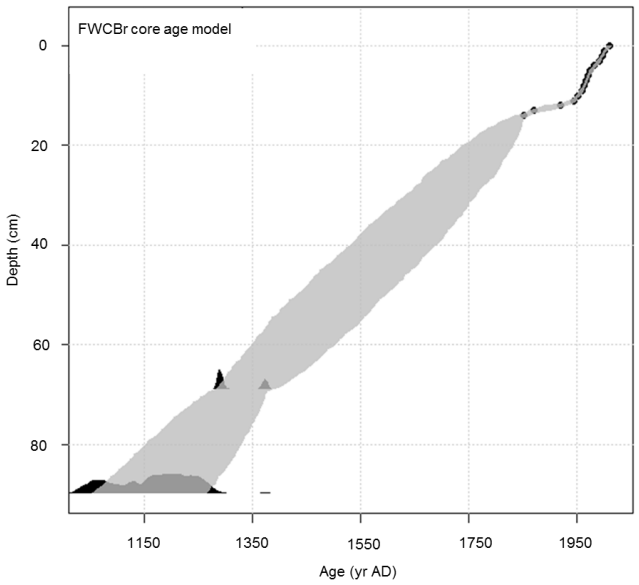

Depth (cm)	^{137}Cs	2-sigma	^{210}Pb	2-sigma	^{214}Pb	2-sigma	$^{210}Pb_{excess}$
0.5	5.56	2.27	152.5	30.6	37.5	6.76	115
1.5	5.44	1.6	84.52	20.11	40.02	3.78	44.5
2.5	6.95	1.63	72.48	20.36	38.38	3.9	34.1
3.5	8.78	2.13	98.24	21.85	37.22	5.58	61.02
4.5	10.64	2.18	70.55	21.47	34.65	5.25	35.9
5.5	13.23	2.23	53.13	21.05	32.45	4.79	20.68
6.5	19.19	2.32	48.51	25.88	34.29	3.97	14.22
7.5	23.69	2.73	46.97	17.43	36.53	6.44	10.44
8.5	14.41	2.04	54.26	18.92	42.94	5.77	11.32
9.5	6.74	1.81	58.57	20.37	41.42	4.24	17.15
10.5	6.4	1.72	52.57	18.23	40.33	4.8	12.24
11.5	5.45	1.65	65.43	19.23	41.41	3.99	24.02
12.5	2.92		65.13	22.17	47.18	4.21	17.95
13.5	2.37		53.57	21.12	51.31	5.19	2.26
14.5	2.58		56.08	21.57	52.17	5.83	3.91
15.5	2.5		41.48	19.35	43.05	4.29	-1.57

Pb and Cs isotopes contents (Bq kg−1)

Core/Sample	Depth (cm)	$\delta^{13}C$ ‰	Conventional radiocarbon age	$\Delta^{14}C$ ‰	Calibrated years AD (2 Sigma range)
FW CBr 2.0 CM 70	69-70	-25.0	720 +/- 30 BP	-85.7±3.4	1260 to 1295
FW CBr 2.0 CM 91	90-91	-25.6	920 +/- 30 BP	-108.2±3.3	1025 to 1190

Appendix 9.2. Geochemical data from the FWCBr sediment core (Casa Branca salt marsh; Mira estuary).

Depth (cm)	Br (mg/kg)	OM (%)	Br/OM	Age (AD years)
0-1	560	23.6	23.7	2012
1-2	374	10.4	36.0	2003
2-3	214	8.6	24.9	1998
4-5	448	14.3	31.2	1984
6-7	385	9.8	39.3	1972
8-9	242	9.4	25.8	1965
10-11	209	9.2	22.7	1953
12-13	134	6.5	20.7	1921
14-15	147	7.8	18.8	1853
16-17	142	7.1	20.0	1832
18-19	200	8.0	24.9	1813
20-21	150	7.1	21.2	1794
24-25	129	6.6	19.5	1758
28-29	149	7.1	20.9	1721
31-32	215	8.3	26.0	1694
35-36	214	7.7	27.9	1660
39-40	159	7.7	20.6	1623
43-44	171	6.2	27.8	1580
47-48	167	6.7	24.8	1549
52-53	172	5.8	29.7	1507
55-56	150	6.8	22.1	1479
58-59	183	6.8	26.9	1451
61-62	166	7.0	23.6	1427
64-65	147	6.5	22.6	1404
68-69	162	6.2	26.2	1377
72-73	173	6.2	28.0	1332
75-76	153	5.9	25.9	1306
80-81	137	4.9	27.7	1261
85-86	138	5.2	26.5	1221
89-90	144	5.5	26.0	1190

10 Marsh benthic foraminiferal evidence for environmental changes driven by the sun-climate coupling: application to the western coast of Portugal from the 14th century to present

J. Moreno [a,b], F. Fatela [a,b], E. Leorri [c], F. Moreno [d], J.J. Gómez-Navarro [e], M.F. Araújo [f], M.C. Freitas [a,b], R.M. Trigo [g] and W.H. Blake [h]

[a] IDL - Instituto Dom Luiz, Universidade de Lisboa, Campo Grande, 1749-016 Lisboa, Portugal

[b] Departamento de Geologia da Faculdade de Ciências da Universidade de Lisboa, Campo Grande, 1749-016 Lisboa, Portugal

[c] Department of Geological Sciences, East Carolina University, Greenville, NC 27858-4353, USA

[d] Independent researcher, Caminho da Portela, 97, 4940-061 Bico PCR, Portugal

[e] Department of Physics, University of Murcia, E-30100 Murcia, Spain

[f] Instituto Superior Técnico, Centro de Ciências e Tecnologias Nucleares (C2TN), Universidade de Lisboa, Estrada Nacional 10, km 139,7, 2695-066 Bobadela LRS, Portugal

[g] DEGGE - Departamento de Engenharia Geográfica, Geofísica e Energia da Faculdade de Ciências da Universidade de Lisboa, Campo Grande, 1749-016 Lisboa, Portugal

[h] School of Geography, Earth and Environmental Sciences, Plymouth University, Plymouth, Devon PL4 8AA, UK

Submitted to *Palaeogeography, Palaeoclimatology, Palaeoecology* the 21st January 2017

"The final conclusion is that: through the analysis of changes in abundance of marker species; the introduction of new species or serious loss of previously existing species; and changes in species diversity, dominance, and abundance that extend well outside the established limits of variability, it is possible to document the extent of environmental changes that have taken (or are taking) place."

J. W. Murray in ENVIRONMENTAL MICROPALEONTOLOGY – *The Application of Microfossils to Environmental Geology* (2000), p. 34.

ABSTRACT

This study presents a paleoclimatic reconstruction for the west Portuguese coast during the last six centuries based on benthic foraminiferal records preserved on two dated sediment cores, from the Casa Branca (Mira estuary, southwest coast) and Caminha (Minho estuary, northwest coast) high marshes, supported by geochemical–sedimentological data. The results from Casa Branca, shown here for the first time, are compared with published data for Caminha, to provide a comprehensive overview of the environmental evolution in the west Iberian margin.

It was found that both marshes were formed in the AD 1300s, highlighting a major episode of sediment yield increase on lower estuaries, associated to climatically driven enhanced continental runoff, at the transition of the Medieval Climatic Anomaly to the Little Ice Age. Since then, the two have evolved under different climatic scenarios, as expressed by their foraminiferal assemblages, more saline in Casa Branca (with *Jadammina macrescens* and *Trochammina inflata* as dominant species) than in Caminha (where *Haplophragmoides* spp. dominates). We suggest that this microfaunal contrast was mainly triggered by a relatively long-term trend of net gain from evapotranspiration over precipitation in the former, prompting a higher marsh salinity baseline. Besides, we propose *T. inflata* as an indicator of drier periods in the studied area, associated to key events of aeolian large-dust input. The influence of the most important driving climate mechanisms was evaluated, particularly external (solar) and internal (North Atlantic Oscillation – NAO) forcings.

Spectral and wavelet transform coherence analysis were used to detect the solar imprint on the foraminiferal time series. Two significant periodicities were identified, close to the Hale and Lower Gleissberg cycles, the latter impacting the annual NAO and regional climate (namely, modelled annual mean temperatures) after 1700–1750, which can be linked to the known broad upward trend of the secular oscillations in the total solar irradiance.

Keywords: Southwest Europe; interstitial salinity; dust events; Grand Minima; LIA; Gleissberg cycle.

10.1. Introduction

The geological record provides an excellent archive of changes in Earth's climate and environment (Williams et al., 2007). In this field, research depends on a range of biological and chemical systems, which have responded to changes in climate and left a record in sediments (Vaughan, 2007). These proxies are carefully chosen according to their sensitivity to environmental changes, geographic distribution, as well as temporal range and resolution, but each one is, ultimately, an inevitable imperfect representation of past climate. In fact, all paleoecological and paleoclimatic proxy data come with a degree of uncertainty, in both the measurements of the proxies themselves and in their age estimates (Blaauw, 2012). Such awareness has been central to the ongoing efforts to improve proxy acquisition, interpretation and application (Smerdon and Pollack, 2016).

Benthic foraminifera proved to be reliable paleoclimate proxies, as they offer many valuable clues about the ecosystems where they live in (e.g., Phleger, 1970; Cearreta, 1989; Murray, 1991, 2006; Debenay and Guiral, 2006). In the intertidal zone, they are closely linked to specific elevational ranges relative to mean sea-level (MSL) and local tidal regimes (e.g., Scott and Medioli, 1978; Hayward et al., 1999), with the former operating as the ultimate base level (Plater and Kirby, 2011). As a result, their use as relative MSL change indicators has attracted great attention, with a rising number of publications in the last two decades (Barlow et al., 2013 for a review). Such corpus of research give emphasis to elevation (while a proxy for tidal flooding) as a major control of foraminiferal distribution within the intertidal zone, with salinity as the next most significant variable (e.g., Horton and Culver, 2008). However, long-term monitoring programs are lacking from these habitats and, at best, there have been multi-year seasonal studies (e.g., Hippensteel et al., 2002).

The work conducted in the Caminha salt marsh (Minho estuary, NW Portugal) since 2002 has revealed a systematic response from the foraminiferal assemblages characteristic of the high marsh zone, such as *Haplophragmoides manilaensis* (Andersen, 1953) *Jadammina macrescens* (Brady, 1870) or *Trochammina inflata* (Montagu, 1808), to the estuarine hydrological balance, inducing marsh interstitial water salinity variations and thus affecting their ecological niches. This has been linked to the impact of alternating wetter/drier periods on the salt marsh habitat, together with changes in the depositional environment over the last 2000 years (Fatela et al., 2014; Moreno et al., 2014). More recently, an attempt has been made to connect temporal shifts on a particular brackish foraminiferal group, defined by *J. macrescens*, *T. inflata*, *Tiphotrocha comprimata* (Cushman and Brönnimann, 1948), *Siphotrochammina lobata* (Saunders, 1957) and *Paratrochammina guaratibaensis* (Brönnimann, 1986), to the occurrence of Sun's Grand Minima activity states during the Little Ice Age (LIA; 1350–1900) and their effects on terrestrial climate (Moreno et al., submitted, [**Chapter 6**]). But establishing such a link can be quite challenging, with the recognition that the ecological consequences of solar-induced climatic changes remain poorly understood during the Holocene (e.g., Kern et al., 2013).

The present study explores the marsh benthic foraminifera's sensitivity to changes in environmental parameters through a paleoclimatic reconstruction based on both single species and grouped species abundance. For this, the record of a dated marsh sediment core recovered on the high marsh zone of the Casa Branca salt marsh, Mira estuary, southwest of Portugal, has been studied. The main objectives are: (i) characterize the southwest Portuguese coastal climatic and environmental evolution for the second millennium based on their high marsh foraminiferal assemblages, (ii) compare the southwest record with the one obtained earlier for the NW coast (Moreno et al., 2014, Moreno et al., submitted, [**Chapter 6**]), (iii) acquire an evolutionary perspective of this microfaunal latitudinal record in relation with simulated regional past climate variability (temperature and precipitation; Gómez-Navarro et al., 2011) and, finally, (iv) establish a link between

our foraminifera-based paleoclimatic reconstruction approach for the western Portuguese estuaries and solar activity (SA).

10.2. Regional setting

The west Portuguese coast faces the northeast Atlantic Ocean and develops from around 37º00' N to 41º50' N and between 8º40' W and 9º30' W, over more than 700 km long, often intersected by estuaries, among them the Minho (northwest coast) and Mira (southwest coast) estuaries (Figure 10.1; Fatela et al., 2016). Tides present a semi-diurnal high-mesotidal regime along this coast. The tidal range varies between 2 m, during neap waters, and almost 4 m in spring waters, with the astronomical tide levels often incremented by storm surges (e.g., Canas et al., 2009; Araújo et al., 2011). Since both study sites have been thoroughly described in earlier papers (e.g., Moreno et al., 2017a), here we only present a brief characterization, according to Table 10.1.

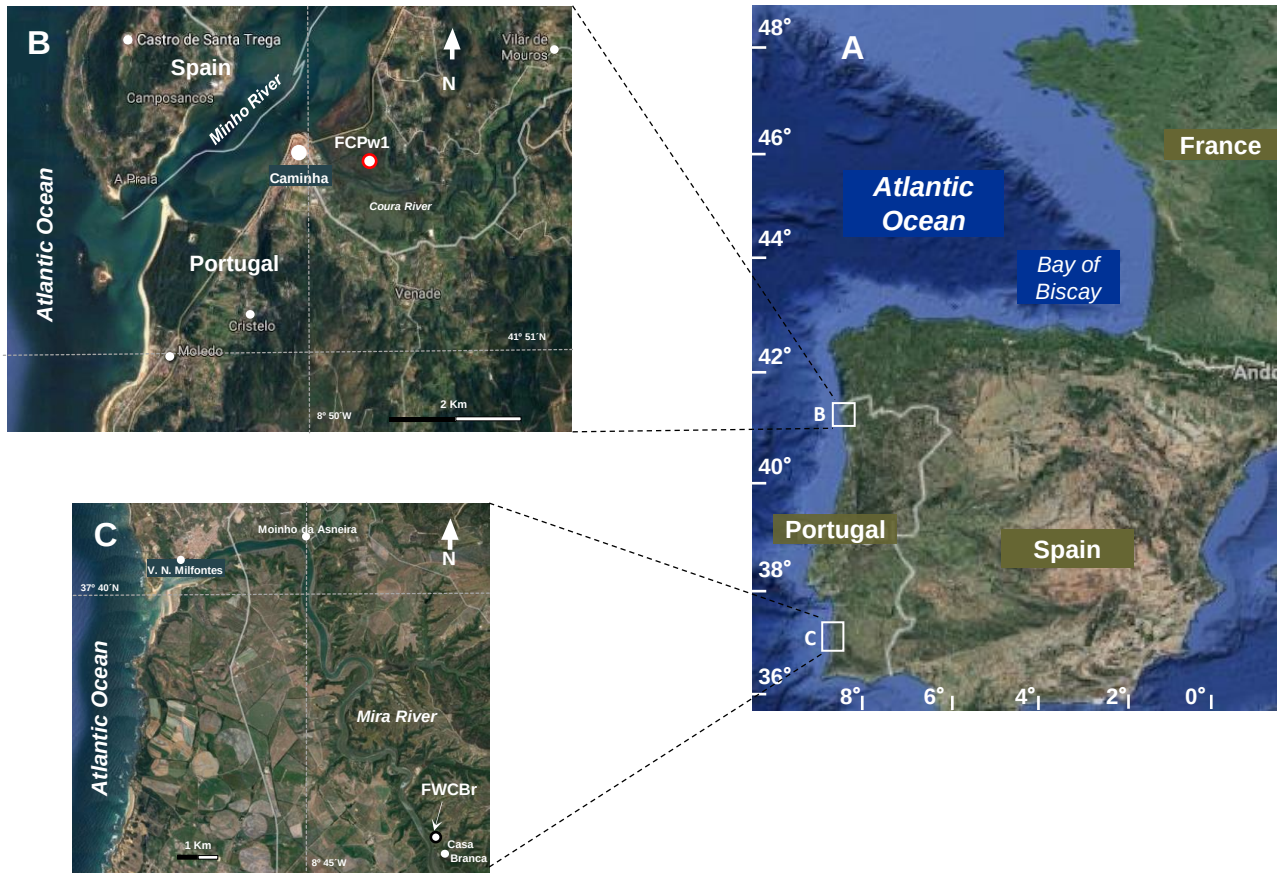

Figure 10.1. **A –** Study areas general location; **B –** Minho estuary (northwest coast); **C –** Mira estuary (southwest coast). The location of the two sediment cores is also indicated: FCPw1 (Caminha, Minho estuary; 1.55 m above mean sea-level; 41º52′37.0″ N and 8º49′28.0″ W) and FWCBr (Casa Branca, Mira estuary; 1.74 m above mean sea-level; 37º40′03.7″ N and 8º43′12.7″ W).

Table 10.1. Summary of the main characteristics of the two studied regions in the west coast of Portugal.

Characteristics	Northwest Coast (Minho Estuary)	Southwest Coast (Mira Estuary)
Climate	C_{fb}	C_{sa}
Mean annual precipitation	1200–2400 mm	600–700 mm
Summer mean temperature	ca. 18–22ºC	23ºC
Mean annual insolation	2200–2500 h	2900–3000 h
Estuary area	23.0 km^2	4.5 km^2
Mean annual freshwater inflow	300 m^3/s	2.9 m^3/s
Highest high water spring (HHWS)	4.0 m	3.5 m
Mean tidal range	2.0 m	2.4 m
Salt wedge penetration	9.0 km	32.0 km
Marsh size	*ca.* 2.5 km^2	*ca.* 2.9 km^2
Distance from the core site to the estuary mouth	*ca.* 3.5 km	*ca.* 13.0 km
Biogeographic (floral) region	Eurosiberian	Mediterranean
River basin geology	Carbonate depleted rocks of igneous and metamorphic nature, namely granites, greywackes and schists	Carbonate depleted metamorphic rocks namely greywakes, clay schists; metavulcanic rocks; sands, sanstones and conglomerates

* Climate key: C, Temperate; f, without dry season; s, with dry season; a, hot summer; b, warm summer

10.3. Materials and methods

10.3.1. Sampling and analytical techniques

10.3.1.1. Sediment coring

Core sampling in the southwest coast was conducted on the Casa Branca salt marsh, located 13 km upstream of the Mira River's mouth. Two cores, FWCBr 1.4 and FWCBrAR, with respectively 100 cm and 28.5 cm long, were recovered at the same high marsh site (1.74 m above MSL; 37º40′03.7″ N, 08º43′12.7″ W; Figure 10.1). The complete description of the methodological approach can be found in prior works (e.g., Fatela et al., 2014; Moreno et al., 2014, 2017a). FWCBrAR was collected and sampled every 0.5 cm aiming to improve the foraminiferal study resolution of the FWCBr1.4 core top 28.5 cm. Thus, here, we present the combined results provided by both cores and hereafter referred as FWCBr core.

Also the collection and analytical methodologies implemented in the study of two sediment cores (FCPw1 and FCPwAR) from the northwest Portuguese coast, including foraminiferal, sedimentological, chronological and chemistry data acquisition have been earlier explained (De la Rosa et al., 2012; Fatela et al., 2014; Moreno et al., 2014, Moreno et al., 2017b). Both cores were recovered on the high marsh zone of the Caminha salt marsh, in the Minho River lower estuary, near the confluence with its tributary, the Coura River (1.55 m above MSL, at 41º52′37″ N and 8º49′28″ W; Figure 10.1).

10.3.1.2. Chronology

The FWCBr core's chronology has been modelled using a Bayesian statistical approach (Bchron 4.1; Haslett and Parnell, 2008; Parnell et al., 2008). The model provides ages with an individual error for each sample averaging 73 years (95% confidence interval). The whole chronological information is given in Moreno et al. (2017a). The same is true for the FCPw1 core (Moreno et al., 2014). The obtained calendar ages are presented herein in years of Anno Domini (years AD).

10.3.1.3. Geochemical and sedimentological analyses

Thirty samples from the FWCBr core were analyzed by Energy-Dispersive X-Ray Fluorescence Spectrometry (EDXRF). Spectral data were acquired for Al, K, Zr and Rb quantification, with an analytical precision better than 10%, and an accuracy better than 5%, tested against certified reference materials. Methodological details can be found in Araújo et al. (2003). Those elements have been successfully applied (combined in elemental ratios) in interpreting paleoclimatic and paleoceanographic variability in marine sediments, in relation with different sediment-transport (aeolian and/or riverine) pathways (e.g., Calvert and Pederson, 2007; Nieto-Moreno et al., 2011). Here, we use the Rb/Al, K/Al and K/Zr ratios as proxies for terrestrial/riverine runoff contributions and the Zr/Rb and Zr/Al as proxies for aeolian dust transport inputs. Dust material mainly falls into the silt fraction (2–63 μm), with most of the mineral-dust particles normally not exceeding 20 μm when transported over long distances (Middleton et al., 2001, and references therein). However, there are also aeolian-dust records having considerable amounts of coarse silt and fine sand, i.e., particles well above the theoretic 20 μm size limit of sorted particle-size distribution (Stuut and Prins, 2014; Van der Does et al., 2016). Therefore, the grain-size distributions of the sample's < 63 μm fraction were determined by laser-diffraction using a Malvern Mastersizer 2000 analyser. Frequencies were computed for six intervals (< 2 μm, 2–4 μm, 4–8 μm, 8–16 μm, 16–32 μm and 32–63 μm), with the final grain-size distributions/histograms as the mean of 5 runs.

10.3.1.4. Multivariate (Factor) analysis (FA)

The dataset including foraminifera (*T. inflata)*, Rb/Al, K/Al, K/Zr, Zr/Rb and Zr/Al ratios data as well as the six grain-size fractions obtained by laser-diffraction along with the fraction > 63 μm was processed by Factor analysis (R-mode) Varimax normalized rotation with principal components extraction. This was done to assess links between sediment characteristics and *T. inflata*'s abundance in the Casa Branca sedimentary record, also trying to better disentangle potential proxies' imprints; these not only often reflect superimposing signals, but dissimilar environmental drivers can end in an analogous elemental response.

10.3.1.5. Reconstruction of solar activity and climate simulations

The total solar irradiance (TSI) reconstruction we use is the one of Steinhilber et al. (2012). The dataset is based on a reconstruction of historical TSI across various thousands of years by correlating solar variability, estimated over the 400-year sunspot record, with cosmogenic-isotope depositions determined from polar ice cores (^{10}Be) and tree rings (^{14}C).

Our study also considers series for annual temperature and precipitation in both study areas, as reproduced by a high-resolution regional climate model (RCM) simulation. It was produced with a climate version of the mesoscale model MM5, using a simulation run with the global model ECHO-G as source of initial and boundary conditions during the second millennium entirely (details in Gómez-Navarro et al., 2011).

10.3.1.6. Spectral (REDFIT) analysis

The Spectral analysis of the benthic foraminiferal records from the FWCBr (this work) and FCPw1 (Moreno et al., submitted, [**Chapter 6**]) cores was conducted using the REDFIT module from PAST (Hammer et al., 2001). In the FWCBr's case, this analysis was performed on single species, i.e., *J. macrescens* or *T. inflata*; the two are the most responsive to variations in interstitial salinity, which depends on temporal changes in the precipitation minus evapotranspiration (P–ET) balance of the high marsh. Instead, in the FCPw1's record such influences are better shown by a foraminiferal group (*J. macrescens* + *T. inflata* + *T. comprimata* + *S. lobata* + *P. guaratibaensis*), as already stated in the Introduction. These species showed a convergent response to increased (brackish-to-normal) salinity conditions, capturing higher salinity episodes in its usual low salinity baseline (Moreno et al., 2017b).

A Monte Carlo simulation was used on the resultant power spectra to test the time series under white-noise conditions (Hammer, 2012). The valid peaks considered as statistically significant were the ones exceeding the critical false-alarm level, dependent on time series lengths (Schulz and Mudelsee, 2002). This kind of analysis is constrained by sampling rates and to the frequencies above the Nyquist frequency. Although foraminiferal data are unevenly spaced in time, short average sampled intervals of 3–4 years are available in the FWCBr core for the last six decades. Overall, intervals of up to 7 years represent 70% of observed data, with a median of 5 years and a mode of 4 and 5 years.

10.3.1.7. Coherence-cross wavelet (WTC) analysis

The wavelet transform coherence (WTC) method was adopted here to identify and test the common power significance between the TSI reconstructed dataset (Steinhilber et al., 2012) and foraminifera (*T. inflata*), being also applied to the annual North Atlantic Oscillation (NAO) index

reconstruction by Luterbacher et al. (2002). To perform WTC, we used the Matlab free software package from Grinsted et al. (2004). Preceding the analysis, the southwest foraminiferal time series (AD 1323–2010) and the TSI dataset were transformed to equidistant time (annual) intervals via a cubic spline interpolation, similarly to other authors (e.g., Naidu and Malmgren, 1995; Debret et al., 2007). This is a mandatory step due to the technique's inability to process unequally spaced data. Such a type of interpolation is not statistically different from the one used in the Lomb-Scargle periodogram, and the quantified root mean squared deviation (RMSD) is below the standard deviation (SD) of the FWCBr core's foraminiferal data using cross-validation procedures (i.e., RMSD = 13.7 and SD = 16.1).

10.4. Results

10.4.1. Foraminiferal, geochemical and sedimentological evidence from the Casa Branca coring site at the Mira River lower estuary

10.4.1.1. Characterization of the high marsh foraminiferal assemblages

Agglutinated foraminifera considerably dominate the Casa Branca salt marsh cores to a depth of 1.0 m, but below 74 cm (AD 1323) there are few individuals and these sporadic low preserved assemblages are not considered suitable for our investigation. Throughout the studied period (AD 1323–2012), the assemblages are characterized by low diversity (2 to 8 species), with *J. macrescens* and *T. inflata* clearly dominant (Figure 10.2, Appendix 10.1). In fact, these species represent together 94% (median) and 92% (mean) of the foraminiferal assemblages. However, as can be seen in Figure 10.2, they show important opposite trends, particularly in AD 1568, AD 1677, AD 1763–1823 and AD 1934. *Pseudothurammina limnetis* (Scott and Medioli, 1980), *Miliammina fusca* (Brady, 1870), *H. manilaensis*, *Haplophragmoides wilberti* Andersen, 1953, *S. lobata* and *Trochamminita salsa/irregularis* (Cushman and Brönnimann, 1948) are also present. Among them, *P. limnetis* is the most significant species, occurring from AD 1323 to AD 1532 (5.0%–40.3%). *Trochamminita salsa/irregularis* is concentrated (11%–13%) from AD 1972–1975 and at the surface (12%; AD 2012).

10.4.1.2. Statistical evidence provided by Factor analysis

Table 10.2 and Figure 10.3 summarize the main results obtained with FA. Four factors were retained based on the Cattell's (1966) scree-plot test. The total variance in the dataset explained by this four-factor (F1, F2, F3 and F4) model is 87.6%, with F1-to-F4 contributing with 41.7%, 22.3%, 14.7 % and 8.9%, respectively. F1 exhibits high negative loadings for the very coarse (32–63 μm)/coarse (16–32 μm) silts, as opposed to the fine (4–8 μm)/very fine (2–4 μm) silts (Figure 10.3); high loadings for Zr/Al and Zr/Rb (negative) as well as for K/Zr (positive) are also shown in this factor.

F2 evidences high positive loadings for Rb/Al and K/Al in addition to the > 63 μm fraction. F3 presents a high positive loading for the medium silt (8–16 μm) and negative loadings for the clay (< 2 μm) and very fine silt (2–4 μm) grain-size fractions. Lastly, F4 shows high negative loadings for T. inflata as well as for Zr/Al and Zr/Rb, and a positive loading for K/Zr.

10.4.1.3. Geochemical and sedimentological tracers

Figure 10.4 and Appendix 10.2 display the results from the Zr/Rb, Zr/Al, Rb/Al, K/Al and K/Zr ratios obtained for the FWCBr core. As we can see, the temporal patterns of the Zr/Rb and Zr/Al ratios (as aeolian proxies) almost mimic each other, with a stable period between AD 1360 and 1690, and punctuated by relative minima in AD 1832, AD 1921, AD 1984 and AD 2012. Relative maxima occur at AD 1310, AD 1721–1813 (longest period of relative maximum), AD 1853, AD 1965 and AD 1998 (absolute maximum). The age profiles of the Rb/Al, K/Al and K/Zr ratios (as fluvial input proxies) demonstrate a general opposing trend to the Zr/Rb and Zr/Al profiles, with the first two presenting a more irregular pattern than K/Zr (Figure 10.4).

Grain-size analysis indicates that the cored sediment samples are silt-dominated (71.8%–90.5%; avg.: 86.6%), followed by the clay fraction (9.4%–25.7%; avg.: 13.0%). In the silt range, sizes vary as follows, very coarse silt (32–63 μm): 0.8%–11.8%, avg. 2.9%; coarse silt (16–32 μm): 6.3%–21.1%, avg. 11.0%; medium silt (8–16 μm): 17.2%–28.7%, avg. 24.0%; fine silt (4–8 μm): 18.6%–33.1%, avg. 28.3% and very fine silt (2–4 μm): 12.6%–24.1%, avg. 19.1% (data not shown). From these silt-fractions, we have selected two as the most explanatory regarding the coupled foraminiferal (*T. inflata*)/environment fluctuations over time, i.e., the coarse-to-medium (16–32/8–16 μm; Appendix 10.3) silt-sizes, although some discrepancies exist between the records (Figure 10.4). Considering Figure 10.4, similarly we can find in these two fractions some common relevant peaks (relative maxima), in association with the aeolian signal (Zr/Rb and/or Zr/Al), namely in the period between the Maunder (1618–1723; Vaquero and Trigo, 2015) and the Dalton (1790–1830) Solar Minima, i.e., from AD 1721 to 1794, in AD 1853, AD 1965, AD 1972 (only in the 8–16 μm) and AD 1998 (only in the 16–32 μm). Significant prior common relative maxima occur earlier than AD 1300 (not shown), at AD 1427 (Zr/Rb and 8–16 μm), AD 1532–1549 and AD 1623 (Zr/Rb and 8–16 μm) (Figure 10.4).

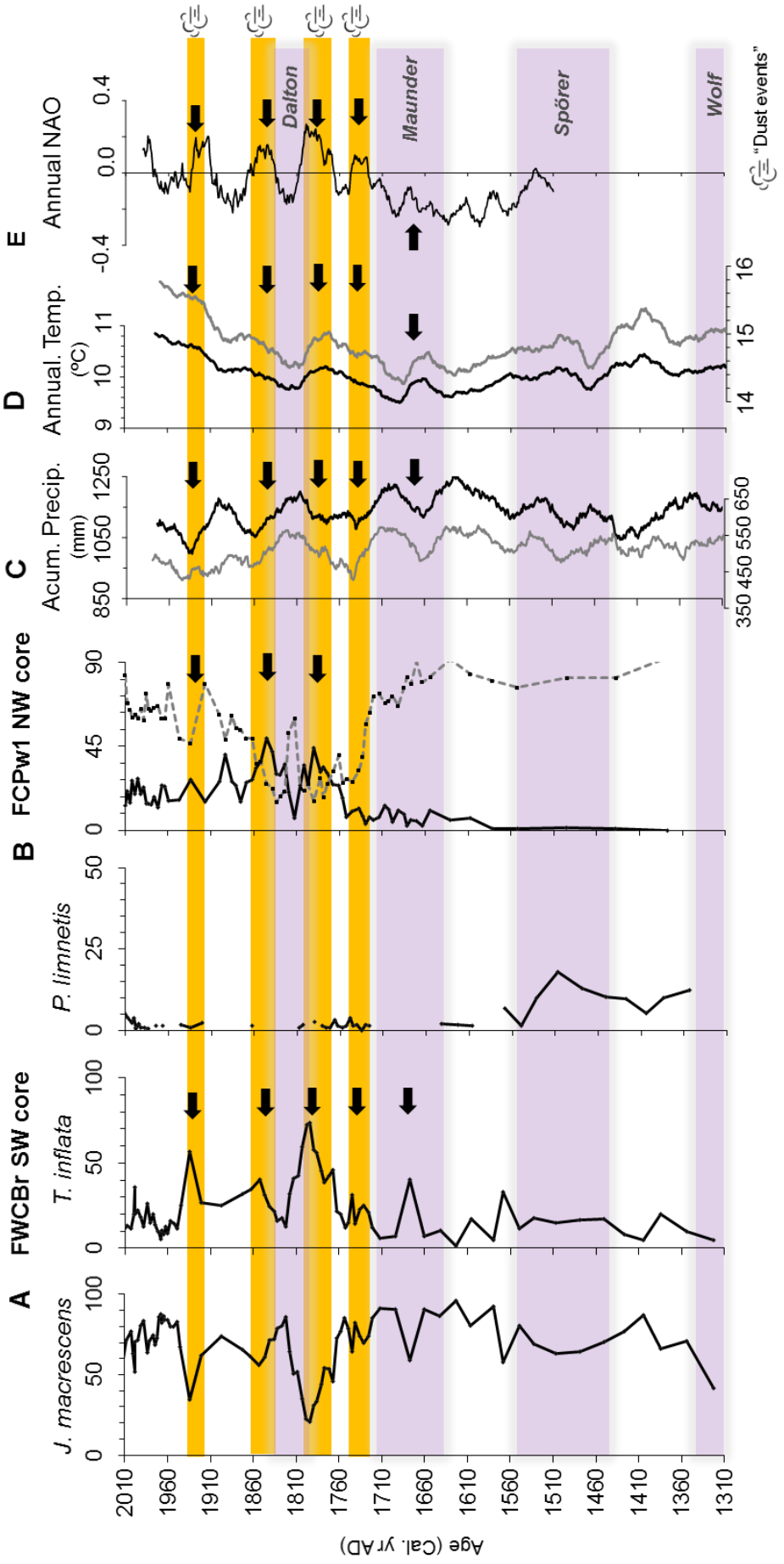

Figure 10.2. A – Summary of dominant benthic foraminifera data in the southwest (SW) FWCBr core. **B –** Percentage distributions of the groups of brackish-to-normal salinity (black line) and brackish-low salinity benthic species (grey dashed line) in the northwest (NW) FCPw1 core; **C –** Accumulated annual precipitation simulation ERIK1 (Gómez-Navarro et al., 2011, 2012) - northwest Iberia black line; southwest Portugal grey line; **D –** Annual temperature simulation ERIK1 (Gómez-Navarro et al., 2011, 2012) - northwest Iberia black line; southwest Portugal grey line; **E –** annual North Atlantic Oscillation (NAO) index reconstruction (Luterbacher et al. 2002). - 21 years running average; Purple shadows represent Grand Solar Minima; Yellow bars represent drier/dust periods; Black arrows mark the *T. inflata* episodes in FWCBr; Age (yr cal. AD) – age in calendar years AD.

Table 10.2. Factor analysis (FA) based on the geochemical and sedimentological proxies chosen in estimating the respective riverine and aeolian contribution.

Variable	F1	F2	F3	F4
T. inflata	0.172	-0.090	0.003	**-0.706**
Zr/Al	**-0.602**	0.041	-0.009	**-0.709**
Zr/Rb	**-0.541**	-0.370	0.000	**-0.700**
Rb/Al	0.080	**0.962**	-0.032	0.188
K/Al	-0.052	**0.821**	-0.270	0.245
K/Zr	**0.548**	0.236	-0.057	**0.736**
>63 µm	-0.032	**0.905**	0.132	-0.043
32-63 µm	**-0.907**	-0.041	-0.096	-0.238
16-32 µm	**-0.906**	-0.018	0.340	-0.105
8-16 µm	0.045	0.036	**0.954**	0.136
4-8 µm	**0.960**	0.001	0.047	0.069
2-4 µm	**0.769**	-0.179	**-0.550**	-0.178
<2 µm	0.272	0.280	**-0.778**	0.371
Expl.Var	4.226	2.734	2.039	2.390
Prp.Totl	0.325	0.210	0.157	0.184
Eigenvalue	5.42	2.90	1.91	1.16
Cumulative	5.42	8.32	10.23	11.39
% Total	41.70	22.27	14.69	8.94
Cumulative	41.70	63.97	78.66	87.61

Expl.Var. – particular component variance; Prp.Totl. – total amount of the explained variance

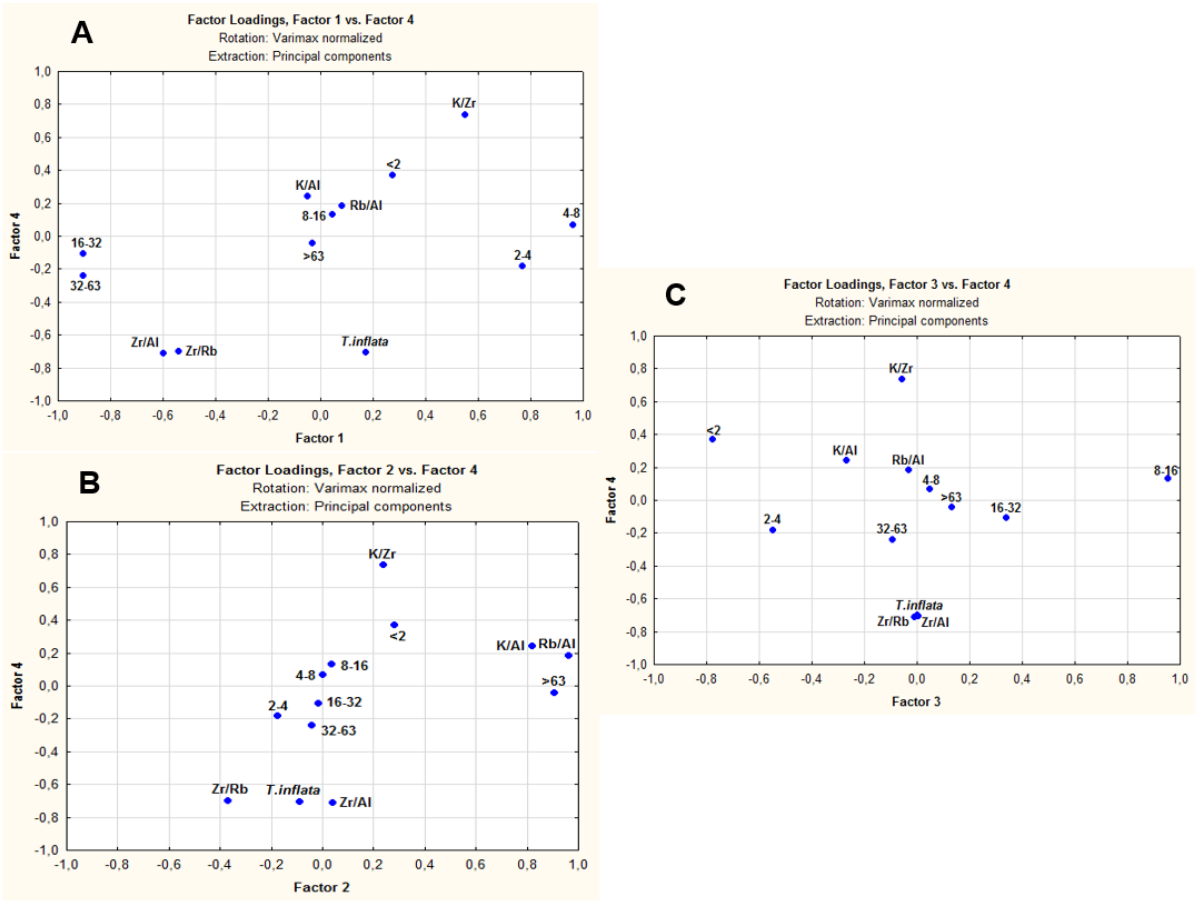

Figure 10.3. Factor analysis (FA) of the *T. inflata*, geochemical and sedimentological data from the FWCBr core. Biplots showing: **A –** Factors F1 *vs*. F4; **B –** Factors F2 *vs*. F4; **C –** Factors F3 *vs*. F4.

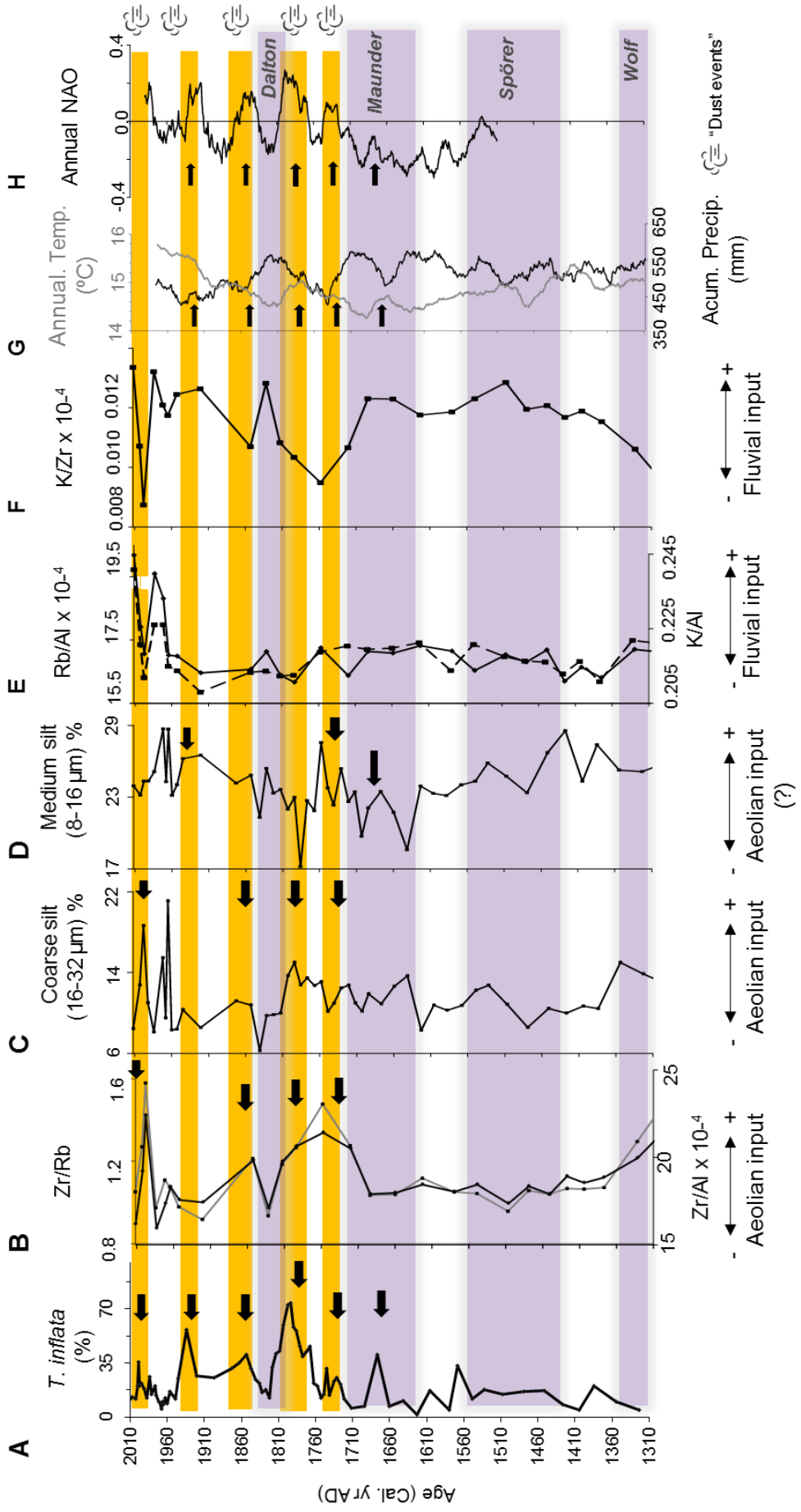

Figure 10.4. A – *Trochammina inflata* occurrence in the southwest (SW) FWCBr core; **B –** Zr/Rb ratio (black line); Zr/Al ratio (gray line); **C –** Percentage of coarse silt fraction; **D –** Percentage of medium silt fraction; **E –** Rb/Al ratio (black line); K/Al ratio (dashed line); **F –** K/Zr ratio; **G –** Accumulated annual precipitation (black line) and annual temperature simulation (gray line) ERIK1 (Gómez-Navarro et al., 2011, 2012) for southwest Portugal; **H –** annual North Atlantic Oscillation (NAO) index reconstruction (Luterbacher et al., 2002) - 21 years running average; Purple shadows represent Grand Solar Minima; Yellow bars represent drier/dust periods; Black arrows mark the *T. inflata* episodes; Age (yr cal. AD) – age in calendar years AD.

10.4.1.4. Spectral analysis (REDFIT) of the benthic foraminiferal time series

The results of the spectral analysis carried on, individually, on the species *J. macrescens* and *T. inflata* from the Casa Branca salt marsh for the AD 1323–2012 period are presented in Figure 10.5A–B. The REDFIT spectra reveal the presence of statistically significant variability on near bi-decadal and near semi-secular time-scales in the foraminiferal species distribution. In fact, the frequency values of the *J. macrescens* and *T. inflata* periodograms indicate shared statistically relevant peaks above the critical false-alarm level (i.e., 97.4%), respectively at *ca.* 70 years and *ca.* 23 years (both validated by the Monte Carlo test, at a confidence level higher than 90% and 80%, respectively), and an additional peak at *ca.* 29 years, just held up by *J. macrescens*.

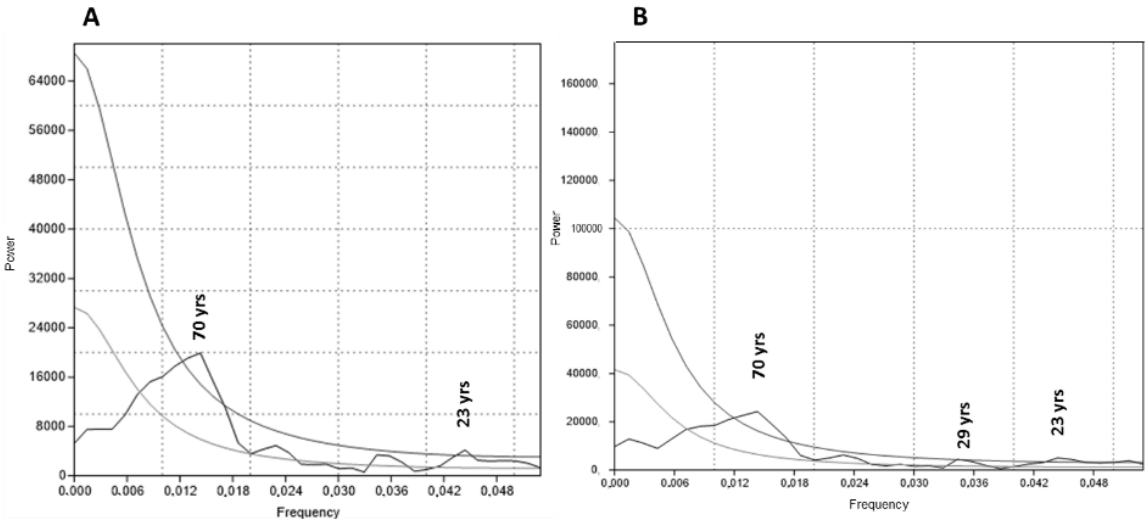

Figure 10.5. A – REDFIT periodogram of *T. inflata*; **B –** REDFIT periodogram of *J. macrescens;* both for the AD 1323–2012 period. The statistically significant peaks registered at 70, 29 and 23 years are set at 97.4% level.

10.4.1.5. WTC analysis: marsh benthic foraminifera and sun–climate variables

WTC of *T. inflata vs.* TSI has the most significant coherence at the *ca.* 50–80-year band (centred at *ca.* 64 years), while the *ca.* 23-year band is only significant transiently, around 1550 and 1930 (Figure 10.6A). The former, although continuous, does not encompass the entire period of time analyzed, and it is significant from *ca.* 1700 to present (already outside the cone of influence – COI), when it shows to be mainly in-phase for *T. inflata vs.* TSI. The WTC calculations for the NAO index *vs.* TSI reveal common and significant cyclic co-variations in the *ca.* 50–80-years band, noticeable in the *ca.* 1700–1800 period and extending to *ca.* 1950, while for the *ca.* 23-year band, it is identified rather by patchy sectors, more persistent around 1550–1600, when the phase-angle relation suggests a non-linear relationship leaded by the TSI (Figure 10.6B). Consistently, it is in the 1700–2012 period (after *ca.* 1890 outside the COI) that an almost perfect in-phase relationship between the TSI and the simulated annual temperatures for the southwest Portugal (Gómez-Navarro et al., 2011) is observed at the *ca.* 50–80-year band (Figure 10.6C). This is accompanied by a *T.*

inflata/mean annual temperatures in-phase relationship (after *ca.* 1650), leaded by temperature (Figure 10.6D).

10.5. Discussion

10.5.1. Identifying foraminifera-based paleoclimatic trends in the west coast of Portugal

10.5.1.1. Casa Branca (southwest) and Caminha (northwest) salt marshes settlement as inferred from their foraminiferal record

The preserved foraminiferal record from the FWCBr core (Casa Branca) begins in AD 1323 (Figure 10.2A), similarly to the one of the FCPw1 core (AD 1380, Caminha; Moreno et al., 2014), overlapping the transition period between two "solar-controlled climate change epochs" (Soon and Lüning, 2013) in the second millennium – the Medieval Climatic Anomaly (MCA, *ca.* AD 900–1300) and the LIA. It is thought that this last pulse of marshland creation evidenced on both cores happened likely associated to enhanced river runoff influence, driven by major flooding periods (e.g., Abrantes et al., 2005, 2011), and to widespread siltation in the lower estuaries, both increasing intertidal ecosystems elevation relative to the tidal frame. This assumption is supported by other authors' findings, ascribing salt marsh formation primarily to high sedimentation rates promoted by sustained physical deposition in sheltered areas, while vegetation encroachment on the newly established platform is important only in the last phase of marsh emergence (Fagherazzi, 2006, 2007; Gunnell et al., 2013). It is also in agreement with the results from Muñoz Sobrino et al. (2014) studying two sedimentary sequences from the Ría de Vigo (northwest Spain), and located at *ca.* 40 km North of Caminha, where an almost simultaneous phase (*ca.* AD 1100–1300) of stronger continental contribution has been distinguished and which they related to the increasing intensity of storms throughout the MCA–LIA transition. Further North, in the Basque coast (northern Spain) the foraminiferal record of the Kanala salt marsh core starts with a marsh dominated by *M. fusca* at AD 1300 (Leorri et al., 2013, 2014), presumably reflecting higher river discharge. In fact, the LIA enhanced storminess has been interpreted as a consequence of more intense, rather than more frequent winter storms, linked to the major mid-latitude anticyclones breakdown (Raible et al., 2007; Trouet et al., 2012). The climatic shift from a drier/arid MCA to a wetter LIA along the western Portuguese coast (Abrantes et al., 2005; Lebreiro et al., 2006; Rodrigues et al., 2009) appears to have been a widespread climatic condition across the Iberian Peninsula (IP), although with slight moisture nuances indicated by opposing hydrographic and climatic scenarios recorded, simultaneously, at different latitudes, along the Atlantic Iberian coastline (Lebreiro et al., 2006; Moreno et al., 2012; Nieto-Moreno et al., 2013; Muñoz Sobrino et al., 2014; Sánchez-López et al., 2016). It is well-established that the climate of the IP is modulated by just a small number of large-scale patterns or modes including the North Atlantic Oscillation (NAO; Hurrell, 1995), but also the

East Atlantic (EA) and Scandinavian (SCA) patterns (Trigo et al., 2008; Jerez and Trigo, 2013). The combined role of large-scale climatic patterns such as the interplay between the NAO and the EA pattern was suggested to explain the reported main differences in the IP wetness during this transitional period, with NAO^{+}–EA^{+} and NAO^{-}–EA^{-} interactions dominating during the MCA and LIA, respectively (e.g., Sánchez-López et al., 2016).

Finally, it is worth mentioning that high-energy events (intensification of hurricane activity), occurring through the MCA–LIA transition in the eastern coast of the USA, were suggested by van de Plassche et al. (2004) as responsible for erosive hiatus found in the peat stratigraphy and marsh-accumulation record from New England salt marshes. On the studied marshes (Succotash, Rhode Island; Hammock and East River, Connecticut), they found, following marsh erosion, first plant growths at the AD 1290–1400 and AD 1390–1450 periods, respectively in Rhode Island and Connecticut, comparable to our tidal marshes development after AD 1300. Martin et al. (2002) found similar paleoenvironmental responses between Clinton, CT and Bombay Hook, DE (USA eastern coast), which the authors suggested was a reflection of regional to basin-scale forcings that may reflect coupled, multidecadal-to-centennial scale ocean–atmosphere interactions. Also, it may be inferred from foraminiferal data from the Connecticut's East River marsh (Kemp et al., 2015) an increase of *Haplophragmoides spp.* around AD 1050 and from AD 1259 to AD 1308, representing a likely stronger fluvial impact on this coastal marsh at the MCA–LIA transition, which therefore seems to have happened on a wider scale, on both sides of the Atlantic Ocean basin.

10.5.1.2. Foraminiferal trends on Casa Branca (and Caminha) and their relationship with the physical factors influencing the P–ET balance of high marsh(es)

The foraminiferal records from the FWCBr core (this work; Figure 10.2A; Appendix 10.1) and the FCPw1 core (Moreno et al., 2014, Moreno et al., 2017b) reveal important assemblages' differences, which may be interpreted in the framework of climate evolution. Such interpretation is supported by (i) the knowledge about the existence of two main regions (North and South) in the modern broad Atlantic climatic setting of the western Portuguese coast, and (ii) the increase/decrease of a long-term latitudinal gradient of temperature/precipitation from the northwest coast towards the southwest coast, as shown by the regional climate model of Gómez-Navarro et al. (2011, 2012), and discussed before by Moreno et al. (2017a). In view of these premises, one can consider that the LIA has left a stronger and more persistent (until AD 1730) wetter signal in the northwest coast, as evidenced by the brackish-to-low salinity foraminiferal group (Moreno et al., submitted, [**Chapter 6**]; see also Figure 10.2B), while in the southwest coast it is only noticeable until AD 1570. This is supported by *P. limnetis*, one of the species present in the FWCBr record (mean 4.4%; median 2.0%). Considering its temporal distribution trend (Figure 10.2), it can be seen that *P. limnetis* marks the low to high marsh transition (2–40%) at AD 1323, and the settlement of the lower

high marsh up to AD 1568. This likely happened at lower salinities than the ones prevailing today, since this species is cited as living in the low salinity estuarine upper reaches (e.g., Hayward et al., 1999). Likewise, in Caminha the presence of *P. limnetis* is characteristic of the higher low marsh transitioning into high marsh under a possible salinity optimum, between 8‰ and 14‰, in association with *H. manilaensis* and *Haplophragmoides* spp. (Moreno et al., 2006; Fatela et al., 2009). In our studies of superficial sediment samples from several southwest Portuguese salt marshes, it was found that *P. limnetis* occurs in low abundance (< 2%) in the boundary between the middle and lower estuary (e.g., Tejo and Sado Rivers). However, in the Mira middle estuary, this species' abundance reaches 37% in the lower high marsh, where interstitial salinity is *ca.* 4 ‰ (authors' unpublished data).

Besides a potential sea-level indicator along the FWCBr core, *P. limnetis* could also point toward higher river influx, with reduced salinity conditions, peaking in AD 1323–1384, AD 1427–1532 and AD 1568. The factor F2 of the Factor analysis (Table 10.2; Figure 10.3), consisting of the (fluvial-derived) elemental ratios (Rb/Al and K/Al) as well as the > 63 μm fraction, seems to define the major freshwater signal on the Casa Branca high marsh environment, including coarser terrigenous material, likely suggesting the contribution of (sand-sized) detrital K-feldspars, also well-known as the most important Rb-carrying minerals. River floods generate high-energy flows to estuarine marshlands, and can considerably alter the (mineral/organic) sedimentary fluxes in the high marsh. These are otherwise controlled by fine-grained materials (e.g., de Groot et al., 2011), with the sediment supply largely organic (e.g., Turner et al., 2000; Chmura and Hung, 2004). The Casa Branca high marsh is not an exception, with a very uniform grain-size distribution down-core, characterized by a < 63 μm fraction median value of 99.2% (data not shown). However, greater freshwater contribution (expressed by higher abundance of *P. limnetis*) is not clearly established in the simulated annual precipitation for the southwest Portugal (Figure 10.2). Even so, wetness fluctuations may be observed in the fluvial proxies for this period (AD 1323–1568), with increasing trends of K/Zr, Rb/Al and K/Al ratios, since AD 1262 (not shown), indicating enhanced runoff conditions, these last two more seemingly during the Wolf (1282–1342) and Spörer (1450–1550) Grand Solar Minima (Figure 10.4), and matching with the maximum occurrence of *P. limnetis* (Figure 10.2).

The FWCBr foraminiferal record is dominated (mean 92%; median 94%) by *J. macrescens* and *T. inflata* (Appendix 10.1; Figure 10.2). It is thought that this continued dominance offers a long-term insight on the control of brackish-to-normal salinity assemblages at the Casa Branca high marsh environment. Such suggestion is reinforced by the measured ecological parameters influencing the modern assemblages (Fatela et al., 2016) and the modelled annual precipitation and temperatures for this coastal area (Figure 10.2; Gómez-Navarro et al., 2011, 2012). In the southwest coast these two climatic variables display, in that order, sustained lower and higher values than in northwest

coast, where, in an analogous study, the foraminiferal record of the FCPw1 core has revealed a persistent prevalence of brackish-to-low salinity assemblages, in which *T. salsa/irregularis* and *H. manilaensis* stands out, and *J. macrescens* plus *T. inflata* reach a mean and median of 18% and 16%, respectively, in the high marsh (Moreno et al., submitted, [**Chapter 6**]). This foraminiferal assemblages' main composition was then interpreted (applying the same criteria as in the present work) as following the modelled precipitation and temperature regimes, in association to well-known atmospheric circulation modes (Fatela et al., 2014; Moreno et al., 2017b).

Hence, a first outcome from the current northwest–southwest Portuguese coasts' comparison is the identification of two rather steady foraminiferal assemblages' distributions over the studied period of time, with a more noteworthy ecological variability in the northwest. Furthermore, a clear distinction in the assemblages' composition of the two cores can be made, which is assumed to be mainly driven by the precipitation/temperature spatial distribution in mainland Portugal, dictating interstitial salinity in high marshes that results from the interaction among the opposing forces of P and ET. As the precipitation decreases towards South, the hydrological regime becomes more irregular (Portela and Quintela, 2006), and thus more prone to droughts (Santos et al., 2010), with greater marine influence felt up within the estuarine domain. This is what happens nowadays in the Mira estuary, where ET usually exceeds freshwater inputs (low river flow and low precipitation), and tidal seawater is the main responsible for wetting the Casa Branca high marsh habitat. This combination of factors eventually leads to increased salt concentrations in its soils/sediments. In fact, a dominance of hypersaline conditions in this estuary has been reported recently by Fatela et al. (2016), with maximum salinity records of *ca.* 48‰ in high marsh zones of the lower estuarine section.

In summary, a long-term averaged negative P–ET balance in the southwest coast of Portugal forced a higher salinity baseline in the Casa Branca high marsh, which is expected to be one key driver for the underlying *J. macrescens* and *T. inflata* greater abundance over time, when compared to the northwest Caminha high marsh, showing usually mesohaline conditions, upheld by persistent P excess, accompanied by greater stream flow (Fatela et al., 2016).

10.5.1.3. Potential proxies of dust events associated to drier conditions in the southwest coast of Portugal: examining the role of Trochammina inflata

The following discussion is based on published references regarding the ability of the two dominant species – *J. macrescens* and *T. inflata* – to adapt to extreme and highly variable ecological conditions and, as a result, to live within a wider amplitude shifts in environmental parameters. We chose to focus our attention on *T. inflata* as this species (when compared to *J. macrescens*) shows a larger salinity range and tidal exposure tolerance. As such, it can characterize the transition to dry fields, where the environmental changes resultant from aerial exposure are stronger (e.g., Hayward

et al., 1999; Debenay and Guillou, 2002), being one of the species adapted to desiccation in higher salinity conditions (Hayward, 2014). As seen in Figure 10.2, the peaks of relative abundance of *T. inflata* in the Casa Branca high marsh approximately match (or arise soon after) modelled higher annual temperatures and lower annual precipitation periods in southwest Portugal. Despite the limitations from each proxy record, one can also notice several other peak-to-peak correlations from AD 1570 onwards, when lower salinity conditions begin to be less evident (gaps or strong decrease on the abundance of *P. limnetis*). Namely, the most prominent relative maxima of *T. inflata*, i.e., AD 1767–1798, AD 1934, AD 1853, and AD 1677, by decreasing order of importance, roughly agree with higher (lower) aeolian (riverine) inputs, more evident in the Zr/Rb, Zr/Al (aeolian) and K/Zr (fluvial) ratios age/depth profiles, a relationship that is captured by the factor F4 of the FA, though only explaining a small proportion (8.9%) of the variance of the dataset (Table 10.2). Concomitant phases of increased aeolian input (Zr/Al) were detected by Nieto-Moreno et al. (2013) studying marine records from the Alboran Sea basin. These major *T. inflata* peaks are emphasized by increases of the coarse silt (16–32 μm) or medium silt (8–16 μm), depending on the dynamics associated to the particles' uptake and transportation, and mainly occurring in the NAO^+ phases or in less deeply negative NAO^- phases (Figure 10.4). This connection to the NAO index is not fortuitous. The NAO exerts a strong influence on the large-scale variations of both the atmospheric circulation and the hydrological cycle in the Northern Hemisphere (Hurrell, 1995), Mediterranean basin (e.g., Cook et al., 2016) and more specifically in the IP (e.g., Trigo et al., 2004), and mineral dust export from Africa is somewhat correlated with it: enhanced dust transport from the Saharan region over the North Atlantic Ocean and the Mediterranean Sea has been reported during the NAO^+ phases (e.g., Moulin et al., 1997; Ginoux et al., 2004; Nakamae and Shiotani, 2013), with some authors even describing a time-lagged relationship between the frequency Sahara-dust events in summer and the NAO conditions during the preceding October–December period (Laken et al., 2013). Cusack et al. (2012) stated that when the NAO was more intensely positive, the likelihood of transporting air masses from North Africa towards the IP was higher, and when the NAO is negative, intense Atlantic Advection directed over the IP can block North African air masses, preventing them moving northward; they also point out that this NAO influence varies locally across the IP, weakening as the distance to Atlantic Ocean increases.

In the European setting, large-dust (coarse and very coarse silt: 16–62 μm) is produced "in continent" (Stuut et al., 2009). But, presently, the only notable source of large-dust in Europe seems to be the Po River Valley in northern Italy (Husar et al., 2000). Therefore, it is recognized that modern aeolian large-dust in Europe mostly indicates incursion from Saharan material dispersed by variable winds across the continent and dominating the dry deposition flux (Guerzoni et al., 1997). In fact, where Africa and Europe are close, as in the southwest IP, most of the dust-laden winds transport considerable amounts of African large-dust, mostly in summer, thus representing a significant contribution to soils (Stuut et al., 2009). But as stated by Muhs (2013), the identification of dust

accretion to soils poses relevant problems, with the recognition of exotic dust particles normally demanding exhaustive (mineralogical, geochemical and isotopic) analyses. In spite of these constraints, an aeolian source is suggested to the coarse silt range (16–32 μm) represented in Figure 10.4, mainly on the basis of the FA results. F1, including this grain-size fraction, the very coarse silt (32–63 μm) as well as the Zr/Al and Zr/Rb ratios (aeolian proxies), all with high negative loadings (Table 10.2; Figure 10.3), seems to us to gather suitable aeolian material characteristics, thus highlighting this source's contribution to sedimentation in the Casa Branca high marsh. According to Evans et al. (2004), the 16–32 μm fraction lies at a compromise point among the several modal sizes of sedimentary particle that are settled in motion during dust transportation events: smaller particles are difficult to lift due to the increase in cohesion, and larger particles are difficult to lift because of weight; as a result, once the land surface is disturbed, the ideal lift is in the coarse-silt particle range. The medium silt size range appears in the factor F3, separated from the clay and very fine silt fractions (see Table 10.2; Figure 10.3), which might be related, at least to some extent, to the formerly proposed existence (in the middle of the noise of the particulate systems) of certain mode sizes revealing different genetic processes involved in the shaping of clastic sedimentary particles (e.g., Tanner, 1958). Evans et al. (2004) considered the 8–16 μm range as separating large (20–60 μm) from small (< 10 μm; the PM10) dust populations, a major size distinction in the world of dust (Stuut et al., 2009). Small dust not only consists of single mineral particles in the silt size range, but also of clay particles that often occur in agglomerates of fine or very fine-silt size (Evans et al., 2004), and probably responsible for the link between the two (< 2 μm and 2–4 μm), as beheld in factor F3 (Table 10.2; Figure 10.3).

As may be perceived, either the linkages between climate and desert dust fluxes or the mechanisms involved in dust production are highly complex (or both), with many variables eventually affecting, directly and/or indirectly, the dust cycle under any specific climate scenario, which also makes the paleoclimatic interpretation of the dust records a very difficult assignment (Maher et al., 2010). Fortunately, in the Casa Branca salt marsh record, the *T. inflata* most striking peak (AD 1767–1798) matches with the largest feature observed in a dust record spanning the last millennium from an Alpine ice core, i.e., between *ca.* 1780 and 1800 (Thevenon et al., 2009, 2012). These authors stated that the quantity of dust deposited during that outstanding Sahara-dust event was nearly comparable to the amount of dust deposited from the beginning of their record to the industrial revolution (AD *ca.*1000–1850), proposing its use as a reference horizon for dating other European (ice and sediment) records that lack further suitable dating tools. In tandem, one can find a correlation between such *T. inflata* peak in the Casa Branca record and an increase in the abundance of the brackish-to-normal salinity group (from AD 1761–1801) in the Caminha record (Figure 10.2; Fatela et al., 2014; Moreno et al., 2014, submitted, [**Chapter 6**]). This partially coincides with a wider period of megadrought (1779 to 1827) reported by Cook et al. (2015) in their "Old World Drought Atlas" (OWDA) for Europe and the Mediterranean basin, and matching with the interval of highest

reconstructed NAO^+ values (Luterbacher et al., 2002) observed in Figure 10.2. This large-scale atmospheric circulation pattern leads to drought conditions in Portugal, more strongly in southern region (Trigo et al., 2004; Santos et al., 2005; Santos et al., 2011), and in northern Africa, enhancing desert dust production and subsequent transport northward to the European continent (e.g., Moulin et al., 1997; Goudie and Middleton, 2001). The long-term record of droughts in northwest Africa (Touchan et al., 2008, 2011), consisting in a reconstructed spatially-complete gridded Palmer Drought Severity Index (PDSI) over Morocco, Algeria, and Tunisia spanning 1179–2002, enables us to demonstrate that some of the most severe multi-year drought events in the western area (Morocco), particularly in the mid-18th and mid-19th centuries, may have had an impact on the Casa Branca high marsh. Both periods are marked in the FWCBr record by highest values of Zr/Rb and Zr/Al in AD 1758 and AD 1853, and greater coarse silt input in a wide period extending from AD 1721 to AD 1794 as well as around AD 1873. The agreement between the southwest and northwest foraminiferal records, evidencing dryer phases, repeats as well at AD 1853 (Casa Branca), with expression in Caminha at AD 1845–1852 (Figure 10.2; Fatela et al., 2014; Moreno et al., submitted, [**Chapter 6**]), and again at AD 1934 on both marshes. Interestingly, these specific climatic shifts are also pointed out by higher grapevine growing season (March–August) temperatures in a reconstruction for the northwest Portugal (Moreno et al., 2016a).

In the most recent period of our record, the AD 1934 relative maxima of *T. inflata* could draw a period (the 1930s–1950s) of several extreme droughts in Portugal, with a duration lying among the most notable of the instrumental record and affecting both the southern and northern regions of the country (Pires et al., 2010). Besides, one of the highest peaks in the aeolian proxies (Zr/Rb, Zr/Al and 16–32 μm fraction) temporal trends from Casa Branca occurs at AD 1998 (Figure 10.4). This accords with published drought data putting the 1990's between the most notable decades concerning droughts frequency, severity and duration in southern Portugal (Pires et al., 2010) and the 1990–1995 period as the one corresponding to the longest drought from the last 75 years affecting mostly the centre and the south of Spain (Domínguez-Castro et al., 2012). In the same way, Touchan et al. (2011) emphasizes the latter half of the 20th century as one of the driest from the last 900 years in northwest Africa, when considering their PDSI reconstruction at the regional scale. They argued that this shift to drier conditions, with the most severe multi-year drought in the 1999–2002 period, also spanning the United States, southern Europe and southwest Asia, was possibly related to anthropogenic climate change, as earlier suggested by Hoerling and Kumar (2003). Although the *T. inflata* temporal trend from the Casa Branca high marsh exhibits a clear relative maxima at this time (AD 1998), its size does not reproduce this drought phase's magnitude, at least not in the same manner as the aeolian proxies (Figure 10.4). There may be some plausible explanations for this inferred "underestimation" (e.g., foraminiferal spatial heterogeneity on salt marsh or changes on its water storage capacity). Likewise, and taking into account the change on MSL data, one can recognize a period (1997–1999) of sudden increase on the trend of global rise

acceleration for the 20th century (e.g., Church and White, 2011), and a steeply rise oscillation for the 1995–1997 record on the Cascais (Portugal) tide gauge (Silva et al., 2008; Antunes and Taborda, 2009). This may have triggered more frequent salt marsh's flooding and the alteration of the past relationship between high marsh elevation and climate. It is also worth noticing that in latest decades, the frequency of Sahara-dust events has varied strikingly in response not only to climatic factors such as drought, but also to anthropogenic disturbance of desert marginal surfaces (Goudie and Middleton, 2001), which implies that our aeolian proxies, unlike *T. inflata*, can likewise mirror the increment of particulate matter (made available by human mismanagement) in the contemporary global atmospheric dust budget.

An additional line of evidence linking the major excursions of *T. inflata* to the prevalence of (coarser) Sahara-dust events/drought conditions comes, although incidentally, from the work of Costas et al. (2012). These authors, after studying sand invasion and dune field progression on a cliff-top dune 20 km South of Lisbon, have identified two key pulses of aeolian activity in the Portuguese coast on the second millennium – 1560 and 1710 –, which were forced by enhanced zonal westerly winds and storminess during cold climate events compatible with prolonged winter NAO^- phases. However, none of our aeolian proxies display those pulses in the Casa Branca record (Figure 10.4) which, in our perspective, points towards a divergent climatic scenario (of dryness) from the one described by Costas et al. (2012).

Taken together the preceding considerations, we may hypothesize that the *T. inflata* record from the FWCBr core is somewhat related to major regional and more widespread climatic changes, occurring in response to persistent NAO^+ phases, which promote large-dust mobilization over the Sahara Desert and its transportation by winds from the South quadrant (SW/S/SE) until the Casa Branca salt marsh region. Likewise, it suggests drier conditions prevailing in the southwest Portuguese coast, mostly between AD 1721–1813, AD 1853 and AD 1934, and, moreover, in the most plausible dust source area, i.e., northwest Africa. In tandem, the FCPw1 foraminiferal record shows an enhancement of the brackish-to-normal salinity group, mainly after the mid-18th century, indicative of drier conditions also in the northwest coast of the country (Moreno et al., 2014, submitted, [**Chapter 6**]).

To substantiate our paleoclimatic interpretation and the assigned climatic-driven signs of Sahara-dust events in the Casa Branca salt marsh sedimentary record – by replicate the cores and comparing the results with more specific fingerprints of large-dust source areas over northern Africa as well as with local/regional (background) sources – further diagnosis studies are needed, specifically regarding mineralogical (e.g., clay/silt mineralogy) and isotopic ratios composition (e.g., $^{87}Sr/^{86}Sr$; $^{143}Nd/^{144}Nd$).

10.5.2. Identifying imprints of the solar–terrestrial climate link in the Casa Branca coastal salt marsh environment

The most remarkable feature that has emerged from the solar activity (SA) research is its (quasi-)cyclic character (Attolini et al., 1988). After the *ca.* 11-year cycle's discovery (Schwabe, 1843), much of the investigation on Holocene climatic variability has sought to identify characteristic periodicities in proxy climate data, with the bulk of the detected quasi-cyclic variances being assigned to solar forcing (e.g., Engels and van Geel, 2012). Hypothetical cycles of solar origin have also been searched in the geological record using several (terrestrial and marine) paleoenvironmental proxies (e.g., Galloway et al., 2013; Auer et al., 2015). But get SA fingerprints in these proxies has major shortcomings, with several works drawing attention to (i) the considerable time and amplitude heterogeneity on solar cyclicity (e.g., Ogurtsov et al., 2002) and (ii) the fact that the signal-to-noise ratio in proxies is often very low, with these ones associated to chronological errors that may obscure this kind of connections (Swindles et al., 2013). For instance, Ogurtsov et al. (2002) showed the complexity of the secular Gleissberg cycle (*ca.* 88-year; Gleissberg, 1939, 1958), consisting of a wide frequency band with a double structure: 50–80-year (Lower Gleissberg) and 90–140-year (Upper Gleissberg) periodicities. On the other hand, high-quality proxies can be limited (e.g., Neukom and Gergis, 2012). In this field, the development and application of enhanced spectral (Shultz and Mudelsee, 2002) and wavelet (Torrence and Compo, 1998; Grinsted et al., 2004) techniques have been of major importance, being, at present, a key tool for identifying periodic patterns in sedimentary sequences.

The spectral analysis of the *T. inflata* and *J. macrescens* assemblages from the FWCBr core reveals a main statistically significant spectral power at *ca.* 70 years and, marginally, at *ca.* 23 years (Figure 10.5). This happens nearly the lower Gleissberg cycle (50–80-year) and, at higher frequencies, the bi-decadal (Hale) solar cycle, and can be interpreted as evidence for solar-forced climate changes affecting the Casa Branca salt marsh ecosystem. Such an impact could be achieved by a complex succession of ocean–atmosphere feedback mechanisms driven largely by ultraviolet radiation and solar wind changes, with the subsequent variation in atmospheric circulation, temperature and precipitation regimes (e.g., Bond et al., 2001). This ultimately provokes shifts in high marsh hydrology and consequent responses, for instance, from the "dry-sensitive" *T. inflata,* capturing bi-decadal to quasi-secular solar variability. The presence of bi-decadal and quasi-secular peridiocities in the European and North American drought/hydro-climate variability has been reported extensively in the literature, also in connection to solar forcing (e.g., Cook et al. 1997, 2015; 2016; Yu and Ito, 1999; Herweijer et al., 2007). In this context, it seems relevant to refer as well a pioneer study from Nigam et al. (1995), using benthic foraminifera as proxies for paleomonsoons, and detecting a *ca.* 77-year cyclic recurrence of dry conditions in India. A linkage between SA and

the Indian monsoon precipitation has been suggested, with correlations being found in several time-scales (e.g., Agnihotri et al., 2002, 2011; Fleitmann et al., 2003).

The WTC spectra from Figure 10.6A show how the two dominant time-scales of *T. inflata* variability change with time. While the bi-decadal cycle is mostly characterized by very short-lived transient components (AD *ca.* 1550s and AD *ca.* 1930s), preventing other inferences, the main 50–80-year band is robust and phase-locked with solar force after *ca.* 1700, which is in accord with a detected general upward trend of the secular oscillations in TSI from AD 1705 onward, after a solar dynamo chaotic ascending transition (in which the dominant periodicities change abruptly in time) that lasted around 30 years (Duhau and Martínez, 2012). These authors also found a good agreement between the secular oscillation in TSI and global surface temperatures. Similarly, the almost concomitant statistically significant coherent response of the NAO index and the modelled temperatures for the southwest region with TSI changes on the Lower Gleissberg cycle time-scale between *ca.* 1720 and *ca.* 1900–1950 (inside the COI) and thereafter (outside the COI) (Figure 10.6B–C) can reconcile the *ca.* 70 years periodicity (detected by REDFIT analysis in our *T. inflata* record and evidenced by the 50–80-year band after *ca.* 1700 in the WTC spectrum), with dominant quasi-secular solar modulation of some foraminiferal distributions on high marsh, and occurring also in the Caminha salt marsh, as argued by Moreno et al., submitted [**Chapter 6**]. The comparison of the WTC spectra of the benthic foraminifera *vs.* TSI on the two sedimentary records, for the common AD 1610–2010 period, is presented in Figure 10.6E. It highlights that the northwest coast foraminiferal group (brackish-to-normal salinity) clearly exhibits a similar *ca.* 64 year centred band by *ca.* 1750 extending to *ca.* 1970 (already outside the COI). Therefore, we can document that either the single species (*T. inflata*; southwest record) or the group of species (brackish-to-normal salinity group; northwest record), taken as indicators of drier (or saltier) conditions, equally reflect an (non-stationary) in-phase statistically significant periodicity within the range of the Gleissberg cycle, particularly after the Maunder Minimum. This leads us to suggest that the hydro-climate of the west Portuguese coast and, hence, the P–ET balance on both high marshes might have responded reliably to the quasi-secular oscillations of SA for the last nearly 300 years through changes in the NAO framework and features related to the circumpolar cyclonic vortex's expansion/contraction, as earlier proposed for the USA (e.g., Stine, 1994; Nichols and Huang, 2012) and the eastern Mediterranean–Middle East and North Africa (Touchan et al., 2010).

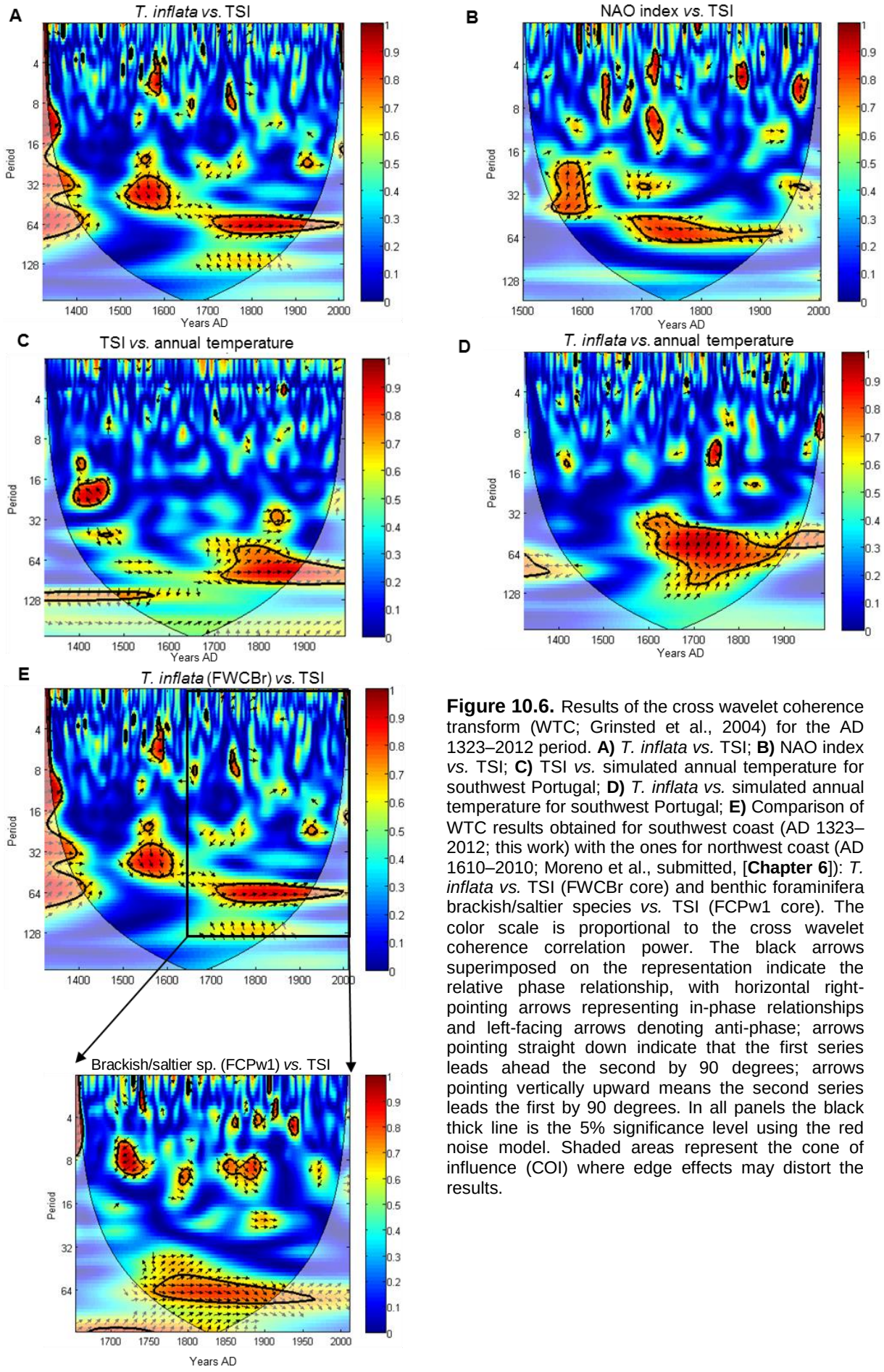

Figure 10.6. Results of the cross wavelet coherence transform (WTC; Grinsted et al., 2004) for the AD 1323–2012 period. **A)** *T. inflata vs.* TSI; **B)** NAO index *vs.* TSI; **C)** TSI *vs.* simulated annual temperature for southwest Portugal; **D)** *T. inflata vs.* simulated annual temperature for southwest Portugal; **E)** Comparison of WTC results obtained for southwest coast (AD 1323–2012; this work) with the ones for northwest coast (AD 1610–2010; Moreno et al., submitted, [**Chapter 6**]): *T. inflata vs.* TSI (FWCBr core) and benthic foraminifera brackish/saltier species *vs.* TSI (FCPw1 core). The color scale is proportional to the cross wavelet coherence correlation power. The black arrows superimposed on the representation indicate the relative phase relationship, with horizontal right-pointing arrows representing in-phase relationships and left-facing arrows denoting anti-phase; arrows pointing straight down indicate that the first series leads ahead the second by 90 degrees; arrows pointing vertically upward means the second series leads the first by 90 degrees. In all panels the black thick line is the 5% significance level using the red noise model. Shaded areas represent the cone of influence (COI) where edge effects may distort the results.

10.6. Conclusions

In this study, we examined the potential of salt marsh benthic foraminifera as paleoclimatic indicators, considering the longer-term distribution (from the mid-14th century onward) of the most common assemblages inhabiting in two distinct temperate high marshes from the west coast of Portugal. The preserved foraminiferal record points to the 1300s as the age at which both marshes were settled, closely following a broad climate shift, from dryer-to-wetter conditions and increased storms' intensity, illustrative of the MCA–LIA transitional period in the IP. The results revealed two characteristic high marsh foraminiferal assemblages, dominated by *J. macrescens* and *T. inflata* in the southwest coast, and *H. manilaensis* and *T. salsa/irregularis* in the northwest coast, dependent on the prevailing climatic conditions at both sites, which prompt different interstitial salinity in the high marsh environment via the net balance between precipitation and evapotranspiration. The higher humidity context of the LIA in this Iberian region is more remarkable and persistent in the northwest, as expressed by the foraminiferal assemblages of the Caminha (FCPw1) core, lasting until the mid-18th century, whereas in the southwest coast wetter conditions, as given by the *P. limnetis* record on Casa Branca (FWCBr core), only prevailed until the mid-16th century. Drier phases can be identified, in both cores, by increments of *T. inflata*, being this species in the southwest possibly connected to large Sahara-dust intrusion events, as further supported by geochemical–sedimentological evidence. Moreover, either the brackish-to-normal salinity group (in the northwest) or the *T. inflata* (in the southwest) reveal a similar response to solar forcing, suggesting a major influence of the Lower Gleissberg cycle on the local/regional hydro-climate variability after *ca.* 1700, i.e., succeeding the Maunder Minimum.

Our findings are a contribution to the research pursuing sensitive proxies for Holocene hydro-climate variability at secular time-scales, possibly through modulation of atmospheric dynamics (namely, of the NAO) by solar forcing. Clearly, the results achieved here are not definitive until they can be replicated in new locations. Thus, more extensive coring (intra- and inter-marsh) is needed to proceed with the recognition of marsh benthic foraminiferal single species/group of species as a consistent proxy, suitable for the evaluation of this Sun-terrestrial climate link, and sustain their role in enlightening on the mechanisms by which such connection may be implemented.

Acknowledgments

This work was partly supported by IDL through the UID/GEO/50019/2013 program, by C2TN through the UID/Multi/04349/2013 program, and is a contribution of the project WestLog (PTDC/CTE/105370/2008), funded by the Fundação para a Ciência e a Tecnologia (FCT). João Moreno is supported by a FCT PhD fellowship (SFRH/BD/ 87995/2012). J.J. Gómez-Navarro thanks the CARM for the funding provided through the Seneca Foundation (project 20022/SF/16). The authors would like to express their sincere gratitude to Mário Gonçalves, Inês Pereira, Ana Medeiros,

Maria Quintela and Vera Lopes for their technical support. Many thanks to Vanesa Nieto-Moreno for sharing some cores' geochemical data from the Alboran Sea.

References

Abrantes, F., Lebreiro, S.M., Rodrigues, T., Gil, I., Bartels-Jónsdóttir, H., Oliveira, P., Kissel, C. and Grimalt, J.O., 2005. Shallow-marine sediment cores record climate variability and earthquake activity off Lisbon (Portugal) for the last 2000 years. Quaternary Science Reviews 24, 2477–2494.

Abrantes, F., Rodrigues, T., Montanari, B., Santos, C., Witt, L., Lopes, C. and Voelker, A.H.L., 2011. Climate of the last millennium at the southern pole of the North Atlantic Oscillation: an inner-shelf sediment record of flooding and upwelling. Climate Research 48, 261–280.

Agnihotri, R., Dutta K., Bhushan, R. and Somayajulu B.L.K., 2002. Evidence for solar forcing on the Indian monsoon during the last millennium. Earth and Planetary Science Letters 198, 521–527.

Agnihotri, R., Dutta, K. and Soon, W., 2011. Temporal derivative of Total Solar Irradiance and anomalous Indian summer monsoon: An empirical evidence for a Sun–climate connection. Journal of Atmospheric and Solar-Terrestrial Physics 73, 1980–1987.

Antunes, C. and Taborda, R., 2009. Sea level at Cascais Tide Gauge: Data, analysis and results: Journal of Coastal Research SI 56, 218–222.

Andersen, H. V., 1953. Two new species of Haplophragmoides from the Louisiana coast. Contributions from the Cushman Foundation for Foraminiferal Research 4, 21–22.

Araújo, M.F., Conceição, A., Barbosa, T., Lopes, M.T. and Humanes, H. 2003. Elemental composition of marine sponges from the Berlengas Natural Park, Western Portuguese Coast. X-Ray Spectrometry 32, 428–433.

Araújo, M.A.V.C., Mazzolari, A. and Trigo-Teixeira, A., 2011. Wave set-up in the modelling of storm surge at Viana do Castelo (Portugal). Journal of Coastal Research SI 64, 971–975.

Attolini, M.R., Cecchini, S., Castagnoli, G.C., Galli, M. and Nanni, T., 1988. On the existence of the 11-year cycle in solar activity before the Maunder Minimum. Journal of Geophysical Research 93, 12729–12734.

Auer, G., Piller, W.E. and Harzhauser, M., 2015. Two distinct decadal and centennial cyclicities forced marine upwelling intensity and precipitation during the late Early Miocene in central Europe. Climate of the Past 11, 283–303.

Barlow, N.L.M., Shennan, I., Long, A.J., Gehrels, W.R., Saher, M.H, Woodroffe, S.A. and Hillier, C., 2013. Salt marshes as late Holocene tide gauges. Global and Planetary Change 106, 90–110.

Blaauw, M., 2012. Out of tune: the dangers of aligning proxy archives. Quaternary Science Reviews 36, 38–49.

Bond, G.G., Kromer, B., Beer, J., Muscheler, R., Evans, M., Showers, W., Hoffmann, S., Lotti-Bond, R., Hajdas, I. and Bonani, G., 2001. Persistent solar influence on North Atlantic climate during the Holocene. Science 294, 2130–2136.

Brady, H.B., 1870. Analysis and descriptions of the foraminifera. Annals and Magazine of Natural History 4, 273–309.

Brönnimann, P., 1986. *Paratrochammina* (*Lepidoparatrochammina*) *guaratibaensis* n sp. from brackish waters of Brazil and a check-list of Recent trochamminaceans from brackish waters (Protista: Foraminifera). Revue de Paléobiologie 5, 221–229.

Calvert, S.E. and Pedersen, T.F., 2007. Elemental proxies for palaeoclimatic and palaeoceanographic variability in marine sediments: interpretation and application. In: Hillaire-Marcel, C. and Vernal, A.D. (Eds.), Proxies in Late Cenozoic Paleoceanography. Elsevier, Amsterdam, pp. 567–644.

Canas, A., Santos, A. and Leitão, P., 2009. Effect of large scale atmospheric pressure changes on water level in the Tagus estuary. Journal of Coastal Research SI 56, 1627–1631.

Cattell, R.B., 1966. The scree test for the number of factors. Multivariate Behavioral Research 1, 245–276.

Cearreta, A., 1989. Foraminiferal assemblages in the ria of San Vicente de la Barquera (Cantabria, Spain). Revista Española de Micropaleontologia 21, 67–80.

Chmura, G.L. and Hung, G.A., 2004. Controls on salt marsh accretion: a test in salt marshes of eastern Canada. Estuaries 27, 70–81.

Church, J.A. and White, N.J., 2011. Sea-level rise from the late 19th to the early 21st century. Surveys in Geophysics 32, 585–602.

Cook, E.R., Meko, D.M. and Stockton, C.W., 1997. A new assessment of possible solar and lunar forcing of the bidecadal drought rhythm in the western United States: Journal of Climate 10, 1343–1356.

Cook, E.R., Seager, R., Kushnir, Y., Briffa, K.R. and others, 2015. Old World megadroughts and pluvials during the Common Era. Science Advances 1:e1500561-9p.

Cook, B.I., Anchukaitis, K.J., Touchan, R., Meko, D.M. and Cook, E.R., 2016. Spatiotemporal drought variability in the Mediterranean over the last 900 years, Journal of Geophysical Research: Atmospheres 121, 2060–2074.

Costas, S., Jerez, S., Trigo, R.M., Goble, R. and Rebêlo, L., 2012. Sand invasion along the Portuguese coast forced by westerly shifts during cold climate events. Quaternary Science Reviews 42, 15–28.

Cusack, M., Alastuey, A., Pérez, N., Pey, J. and Querol, X., 2012. Trends of particulate matter (PM2.5) and chemical composition at a regional background site in the Western Mediterranean over the last nine years (2002–2010). Atmospheric Chemistry and Physics 12, 8341–8357.

Cushman, J.A. and Brönnimann, P., 1948. Additional new species of arenaceous foraminifera from brackish water of Trinidad. Cushman Laboratory for Foraminiferal Research 24, 37–43.

de Groot, A.V., Veeneklaas, R.M. and Bakker, J.P., 2011. Sand in the salt marsh: Contribution of high-energy conditions to salt-marsh accretion. Marine Geology 282, 240–254.

De la Rosa, J.M., Araújo, M.F., González-Pérez, J.A., González-Vila, F.J., Soares, A.M., Martins, J.M., Leorri, E., Corbett, R. and Fatela, F., 2012. Organic matter sources for tidal marsh sediment over the past two millennia in the Minho River estuary (NW Iberian Peninsula). Organic Geochemistry 53, 16–24.

Debenay, J.-P. and Guillou, J.-J., 2002. Ecological transitions indicated by foraminiferal assemblages in paralic environments. Estuaries 25, 1107–1120.

Debenay, J.-P. and Guiral, D., 2006. Mangrove swamp foraminifera, indicators of sea level or paleoclimate? Revue de Paléobiologie 25, 567–574.

Debret, M., Bout-Roumazeilles, V., Grousset, F., Desmet, M., McManus, J.F., Massei, N., Sebag, D., Petit, J.R., Copard Y. and Trentesaux, A., 2007. The origin of the 1500-year climate cycles in Holocene North-Atlantic records. Climate of the Past 3, 569–575.

Domínguez-Castro, F., Ribera, P., García-Herrera, R., Vaquero, J.M., Barriendos, M., Cuadrat, J.M. and Moreno, J.M., 2012. Assessing extreme droughts in Spain during 1750–1850 from rogation ceremonies. Climate of the Past 8, 705–722.

Duhau, S. and Martínez, E.A., 2012. Solar dynamo transitions as drivers of sudden climate changes. INTECH, pp. 185–204.

Engels, S. and van Geel, B., 2012. The effects of changing solar activity on climate: contributions from palaeoclimatological studies. Journal of Space Weather and Space Climate 2, A09-9p.

Evans, R.D., Jefferson, I.F., Kumar, R., O'Hara-Dhand, K. and Smalley, I.J., 2004. The nature and early history of airborne dust from North Africa; in particular the Lake Chad basin. Journal of African Earth Sciences 39, 81–87.

Fagherazzi, S., Carniello, L., D'Alpaos, L. and Defina, A., 2006. Critical bifurcation of shallow microtidal landforms in tidal flats and salt marshes. Proceedings of the National Academy of Sciences of the United States of America 103, 8337–8341.

Fagherazzi, S., Palermo, C., Rulli, M.C., Carniello, L. and Defina, A., 2007. Wind waves in shallow microtidal basins and the dynamic equilibrium of tidal flats: Journal of Geophysical Research 112, F02024-12p.

Fatela, F., Moreno, J., Moreno, F., Araújo, M.F., Valente, T., Antunes, C., Taborda, R., Andrade, C., Drago, T., 2009. Environmental constraints of foraminiferal assemblages' distribution across a brackish tidal marsh (Caminha, NW Portugal). Marine Micropaleontology 70, 70–88.

Fatela, F., Moreno, J., Leorri, E. and Corbett, R. 2014. High marsh foraminiferal assemblage's response to intra-decadal and multi-decadal precipitation variability, between 1934 and 2010 (Caminha, NW Portugal). Journal of Sea Research 93, 118–132.

Fatela, F., Moreno, J. and Cabral, M.C., 2016. Salinity and temperature water assessment of the tidal marshes from the W Portuguese coast, as an ecological tool to palaeoenvironmental reconstructions based on foraminifera and ostracod assemblages. Estudos do Quaternário, APEQ 14, 73–81.

Fleitmann, D., Burns, S.J., Mudelsee, M., Neff, U., Kramers, J., Mangini, A. and Matter, A., 2003. Holocene forcing of the Indian monsoon recorded in a stalagmite from southern Oman. Science 300, 1737–1740.

Galloway, J.M., Wigston, A. Patterson, R.T., Swindles, G.T., Reinhardt, E. and Roe, H.M., 2013. Climate change and decadal to centennial-scale periodicities recorded in a late Holocene NE Pacific marine record: Examining the role of solar forcing. Palaeogeography, Palaeoclimatology, Palaeoecology 386, 669–689.

Ginoux, P., Prospero J.M., Torres O. and Chin, M., 2004. Long-term simulation of global dust distribution with the GOCART model: correlation with North Atlantic Oscillation. Environmental Modelling & Software 19, 113–128.

Gleissberg, W., 1939. A long-periodic fluctuation of the sun-spot numbers. The Observatory 62, 158–159.

Gleissberg, W., 1958. The eighty-year sunspot cycle, Journal of the British Astronomical Association 68, 148–152.

Gómez-Navarro, J.J., Montávez, J.P., Jerez, S., Jiménez-Guerrero, P., Lorente-Plazas, R., González-Rouco, J.F. and Zorita, E., 2011. A regional climate simulation over the Iberian Peninsula for the last millennium. Climate of the Past 7, 451–472.

Gómez-Navarro, J.J., Montávez, J.P., Jiménez-Guerrero, P., Jerez, S., Lorente-Plazas, R., González-Rouco, J.F. and Zorita, E., 2012. Internal and external variability in regional simulations of the Iberian Peninsula climate over the last millennium. Climate of the Past 8, 25–36.

Goudie, A.S. and Middleton, N.J., 2001. Saharan dust storms: nature and consequences. Earth-Science Reviews 56, 179–204.

Grinsted, A., Moore, J.C. and Jevrejeva, S., 2004. Application of the cross wavelet transform and wavelet coherence to geophysical time series. Nonlinear Processes in Geophysics 11, 561–566.

Guerzoni, S., Molinaroli, E. and Chester, R., 1997. Saharan dust inputs to the western Mediterranean Sea: depositional patterns, geochemistry and sedimentological implications. Deep-Sea Research Part II: Topical Studies in Oceanography 44, 631–654.

Gunnell, J.R., Rodriguez, A.B., and McKee, B.A., 2013. How a marsh is built from the bottom up. Geology 41, 859–862.

Hammer, Ø., Harper, D.A.T. and Ryan, P.D., 2001. PAST: Paleontological statistics software package for education and data analysis. Palaeontologia Electronica, http://paleoo-electronica.org, 9 p.

Hammer, Ø., 2012. PAST PAleontological STatistics Version 2.17, Reference manual. Natural History Museum University of Oslo, 229p.

Haslett, J. and Parnell, A., 2008. A simple monotone process with application to radiocarbon dated depth chronologies. Applied Statistics 57, 399–418.

Haslett, S.K., Davies, P., Curr, R.H.F., Davies, C.F.C, Kennington, K., King, C.P. and Margetts, A. J. 1998. Evaluating Late Holocene relative sea-level change in the Somerset Levels, southwest Britain. The Holocene 8, 197–207.

Hayward, B.W., Grenfell, H.R., Reid, C.M. and Hayward, K.A., 1999. Recent New Zealand Shallow-Water Benthic Foraminifera: Taxonomy, Ecologic Distribution, Biogeography, and Use in Paleoenvironmental Assessments. Institute of Geological and Nuclear Sciences monograph, vol. 21. Lower Hutt, New Zealand, 258 p.

Hayward, B.W., 2014. ''Monospecific'' and near-monospecific benthic foraminiferal faunas, New Zealand. Journal of Foraminiferal Research 44, 300–315.

Herweijer, C., Seager, R., Cook, E.R. and Emile-Geay, J., 2007. North American droughts of the last millennium from a gridded network of tree-ring data. Journal of Climate 20, 1353–1376.

Hippensteel, S.P., Martin, R.E., Nikitina, D. and Pizzuto, J.E., 2002. Interannual variation of marsh foraminiferal assemblages (Bombay Hook National Wildlife Refuge, Smyrna, De): Do foraminiferal assemblages have a memory? Journal of Foraminiferal Research 32, 97–109.

Hoerling, M. and Kumar, A., 2003. The Perfect Ocean for Drought. Science 299, 691–694.

Horton, B.P. and Culver, S.J., 2008. Modern intertidal foraminifera of the Outer Banks, North Carolina, USA and their applicability for sea-level studies. Journal of Coastal Research 24, 1110–1125.

Hurrell, J.W., 1995. Decadal trend in the North Atlantic Oscillation: Regional temperatures and precipitations. Science 269, 676–679.

Husar, R.B., Husar, J.D. and Martin, L., 2000. Distribution of continental surface aerosol extinction based on visual range data. Atmospheric Environment 34, 5067–5078.

Jerez, S. and Trigo, R.M., 2013. Time-scale and extent at which large-scale circulation modes determine the wind and solar potential in the Iberian Peninsula, Environmental Research Letters 8, 044035-11p.

Kemp, A.C., Hawkes A.D., Donnelly, J.P., Vane, C.H., Horton, B.P., Hill T.D., Anisfeld, S.C., Parnell, A.C., and Cahill, N., 2015. Relative sea-level change in Connecticut (USA) during the last 2200yrs. Earth and Planetary Science Letters 428, 217–229.

Kern, A.K., Harzhauser, M., Soliman, A., Piller, W.E. and Mandic, O., 2013. High-resolution analysis of upper Miocene lake deposits: Evidence for the influence of Gleissberg-band solar forcing. Palaeogeography, Palaeoclimatology, Palaeoecology 370, 167–183.

Laken, B.A., Parviainen, H., Pallé, E. and Shahbaz, T., 2013. Saharan mineral dust outbreaks observed over the North Atlantic island of La Palma in summertime between 1984 and 2012. Quarterly Journal of the Royal Meteorological Society DOI:10.1002/qj.2170.

Lebreiro, S.M., Frances, G., Abrantes, F., Diz, P., Bartels- Jónsdóttir, H.B., Stroynowski, Z.N., Gil, I.M., Pena, L.D., Rodrigues, T., Jones, P.D., Nombela, M.A., Alejo, I., Briffa, K.R., Harris I. and Grimalt, J.O., 2006. Climate change and coastal hydrographic response along the Atlantic Iberian margin (Tagus Prodelta and Muros Ría) during the last two millennia, Holocene 16, 1003–1015.

Leorri, E., Cearreta, A., Garcia-Artola, A., Irabien, M.J. and Blake, W.H., 2013. Relative sea-level rise in the Basque coast (N Spain): Different environmental consequences on the coastal area. Ocean & Coastal Management 77, 3–13.

Leorri, E., Mitra, S., Irabien, M.J., Zimmerman, A.R., Blake, W.H. and Cearreta, A., 2014. A 700 year record of combustion-derived pollution in northern Spain: Tools to identify the Holocene/Anthropocene transition in coastal environments. Science of the Total Environment 470-471, 240–247.

Luterbacher, J., Xoplaki, E., Dietrich, D., Jones, P.D., Davies, T.D., Portis, D., Gonzalez-Rouco, J.F., von Storch, H., Gyalistras, D., Casty, C. and Wanner, H., 2002. Extending North Atlantic Oscillation reconstructions back to 1500. Atmospheric Science Letters 2, 114–124.

Maher, B.A., Prospero, J.M., Mackie, D., Gaiero, D., Hesse, P.P. and Balkanski, Y., 2010. Global connections between aeolian dust, climate and ocean biogeochemistry at the present day and at the last glacial maximum. Earth-Science Reviews 99, 61–97.

Martin, R.E., Hippensteel, S.P., Nikitina, D. and Pizzuto, E., 2002. Artificial time-averaging of marsh foraminiferal assemblages: linking the temporal scales of ecology and paleoecology. Paleobiology 28, 263–277.

Middleton, N.J., Betzer, P.R. and Bull, P.A., 2001. Long-range transport of “giant” aeolian quartz grains: linkage with discrete sedimentary sources and implications for protective particle transfer. Marine Geology 177, 411–417.

Montagu, G., 1808. Supplement to Testacea Britannica, S. Woolmer, Exeter, 183p.

Moreno, A., Pérez, A., Frigola, J., Nieto-Moreno, V., Rodrigo-Gámiz, M., Martrat, B., González-Sampériz, P., Morellón, M., Martín-Puertas, C., Corella, J.P., Belmonte, Á., Sancho, C., Cacho, I., Herrera, G., Canals, M., Grimalt, J.O., Jiménez-Espejo, F., Martínez-Ruiz, F., Vegas-Vilarrúbia, T. and Valero-Garcés, B.L., 2012. The Medieval Climate Anomaly in the Iberian Peninsula reconstructed from marine and lake records. Quaternary Science Reviews 43, 16–32.

Moreno, J., Fatela, F., Andrade, C. and Drago, T., 2006. Distribution of “living” *Pseudothurammina limnetis* (Scott and Medioli): an occurrence on the brackish tidal marsh of Minho/Coura estuary – Northern Portugal. Révue de Micropaléontologie 49, 45–53.

Moreno, J., Fatela, F., Leorri, E., De la Rosa, J., Pereira, I., Araújo, M.F., Freitas, M.C., Corbett, R. and Medeiros, A., 2014. Marsh benthic foraminifera response to estuarine hydrological balance driven by climate variability over the last 2000 years (Minho estuary, NW Portugal). Quaternary Research 82, 318–330.

Moreno, J., Fatela, F., Moreno, F., Leorri, E., Taborda, F., R. and Trigo, R., 2016a. Grape harvest dates as indicator of spring-summer mean maxima temperature variations in the Minho region (NW Portugal) since the 19th century. Global and Planetary Change 141, 39–53.

Moreno, J., Fatela, F., Leorri, Moreno, F., Freitas, M.C., Valente, T., Araújo, M.F., Gómez-Navarro, J.J., Guise, L. and Blake, W.H., 2017a. Bromine soil/sediment enrichment in tidal salt marshes as a potential indicator of climate changes driven by solar activity: new insights from W coast Portuguese estuaries. Science of the Total Environment 580, 324–338.

Moreno, J., Fatela, F., Leorri, E. and Moreno, F., 2017b. Temperature change as a control on marsh development: benthic foraminifera compared with reconstructed grapevines growing season maxima temperatures and its application to the hydro-climatic evolution of the Minho region (NW Portugal) from 1856 to 2009. Journal of Foraminiferal Research 47, 208–218.

Moreno, J., Fatela, F., Gonçalves, M.A Ferreira, M.J. Gómez-Navarro J.J., Leorri, E., Moreno, F. and Trigo, R., (submitted). A paleoclimatic reconstruction for the Entre-Douro-e-Minho region (NW Portugal) from AD 1626 to AD 1820: searching evidence of solar forcing. (Climate Research).

Moulin, C., Lambert, C.E., Dulac, F. and Dayan, U., 1997. Control of atmospheric export of dust from North Africa by the North Atlantic Oscillation. Nature 387, 691–694.

Muhs, D.R., 2013. The geologic records of dust in the Quaternary. Aeolian Research 9, 3–48.

Muñoz Sobrino, C., García-Moreiras, I., Castro, Y., Martínez Carreño, N., de Blas, E., Fernandez Rodríguez, C., Judd, A. and García-Gil, S., 2014. Climate and anthropogenic factors influencing an estuarine ecosystem from NW Iberia: New high resolution multiproxy analyses from San Simon Bay (Ría de Vigo). Quaternary Science Reviews 93, 11–33.

Murray, J. W., 1991. Ecology and Palaeoecology of Benthic Foraminifera: Longman, Harlow, 397 p.

Murray, J.W., 2006. Ecology and Applications of Benthic Foraminifera. Cambridge University Press, Cambridge, UK, 426 p.

Naidu, P.D. and Malmgren, B. A., 1995. A 2,200 years periodicity in the Asian monsoon system. Geophysical Research Letters 22, 2361–2364.

Nakamae, K. and Shiotani, M. 2013. Interannual variability in Saharan dust over the North Atlantic Ocean and its relation to meteorological fields during northern winter. Atmospheric Research 122, 336–346.

Neukom, R. and Gergis, J., 2012. Southern Hemisphere high-resolution palaeoclimate records of the last 2000 years, Holocene 22, 501–524.

Nichols, J. and Huang, Y., 2012. Hydroclimate of the northeastern United States is highly sensitive to solar forcing. Geophysical Research Letters 39, L04707-5p.

Nieto-Moreno, V., Martínez-Ruiz, F., Giralt, S., Jiménez-Espejo, F., Gallego-Torres, D., Rodrigo-Gámiz, M., García-Orellana, J., Ortega-Huertas, M. and de Lange, G.J., 2011. Tracking climate variability in the western Mediterranean during the Late Holocene: a multiproxy approach. Climate of the Past 7, 1395–1414.

Nieto-Moreno, V., Martinez-Ruiz, F., Giralt, S., Gallego-Torres, D., García-Orellana, J., Masqué, P. and Ortega-Huertas, M., 2013. Climate imprints during the 'Medieval Climate Anomaly' and the 'Little Ice Age' in marine records from the Alboran Sea basin. The Holocene 23, 1227–1237.

Nigam, R., Khare, N. and Nair, R.R., 1995. Foraminiferal evidences for 77-year cycles of droughts in India and its possible modulation by the Gleissberg solar cycle. Journal of Coastal Research 11, 1099–1107.

Ogurtsov, M.G., Kocharov, G.E., Lindholm, M., Meriläinen, J., Eronen, M. and Nagovitsyn, Y.A., 2002. Evidence of solar variation in tree-ring-based climate reconstructions. Solar Physics 205, 403-417.

Parnell, A., Haslett, J., Allen, J., Buck, C. and Huntley, B., 2008. A flexible approach to assessing synchroneity of past events using Bayesian reconstructions of sedimentation history. Quaternary Science Reviews 27, 1872–1885.

Phleger, F.B., 1970, Foraminiferal populations and marine marsh processes. Limnology and Oceanography, v. 15, p. 522–534.

Pires, V.C., Álvaro, S. and Mendes, L., 2010. Riscos de secas em Portugal continental. Territorium 17, 27–34.

Plater, A.J. and Kirby, J.R., 2011. Sea-Level Change and Coastal Geomorphic Response. In: Wolanski, E. and McLusky, D.S. (Eds.), Treatise on Estuarine and Coastal Science. Elsevier Academic Press, Volume 3, pp. 39–72.

Portela, M.M. and Quintela, A.C., 2006. Estimação em Portugal Continental de escoamentos e de capacidades úteis de albufeiras de regularização na ausência de informação. Recursos Hídricos 27, 7–18.

Raible, C., Yoshimori, M., Stocker, T. and Casty, C., 2007. Extreme midlatitude cyclones and their implications for precipitation and wind speed extremes in simulations of the Maunder Minimum *versus* present day conditions. Climate Dynamics 28, 409–423.

Rodrigues, T., Grimalt, J.O., Abrantes, F.G., Flores, J.A. and Lebreiro, S.M., 2009. Holocene interdependences of changes in sea surface temperature, productivity, and fluvial inputs in the Iberian continental shelf (Tagus mud patch). Geochemistry Geophysics Geosystems 10, Q07U06-17p.

Sánchez-López, G., Hernández, A., Pla-Rabes, S., Trigo, R.M., Toro, M., Granados, I., Sáez, A., Masqué, P., Pueyo, J.J., Rubio-Inglés, M.J. and Giralt, S., 2016. Climate reconstruction for the last two millennia in central Iberia: The role of East Atlantic (EA), North Atlantic Oscillation (NAO) and their interplay over the Iberian Peninsula. Quaternary Science Reviews 149, 135–150.

Santos, J.A., Corte-Real, J. and Leite, S.M., 2005. Weather regimes and their connection to the winter rainfall in Portugal. International Journal of Climatology 25, 33–50.

Santos, J.F., Pulido-Calvo, I. and Portela, M.M., 2010. Spatial and temporal variability of droughts in Portugal. Water Resources Management 46, W03503-13p.

Santos, J.F., Portela, M.M. and Pulido-Calvo, I., 2011. Regional Frequency Analysis of Droughts in Portugal. Water Resources Management 25, 3537–3558.

Saunders, J.B., 1957. Trochamminidae and certain Lituolidae (Foraminifera) from the recent brackish-water sediments of Trinidad, British West Indies. Smithsonian Miscellaneous Collections 134, 1–16.

Schulz, M. and Mudelsee, M., 2002. REDFIT: estimating red-noise spectra directly from unevenly spaced paleoclimatic time series. Computers & Geosciences 28, 421–426.

Schwabe, M., 1843. Die Sonne. Astronomische Nachrichten 20, p. 283.

Scott, D.B. and Medioli, F.S., 1978. Vertical zonation of marsh foraminifera as accurate indicators of former sea-level. Nature 272, 538–541.

Scott, D.B. and Medioli, F.S., 1980, Quantitative studies of marsh foraminiferal distributions in Nova Scotia: their implications for the study of sea-level changes. Cushman Foundation for Foraminiferal Research, Special Publication 17, 59p.

Silva, A.A.A., Freire, E. and Crisóstomo, G., 2008. Variações do nível médio anual do mar em Cascais: características e tendências. Estudos do Quaternário 5, 51–66.

Smerdon, J.E. and Pollack, H.N., 2016. Reconstructing Earth's surface temperature over the past 2000 years: the science behind the headlines, WIREs Climate Change 7, 746–771.

Soon, W. and Lüning, S., 2013. Solar forcing of climate. In: Karnick, S.T. and Bast, D.C. (Eds.), Climate Change Reconsidered II: Physical Science. Fifth Assessment Report of the Intergovernmental Panel on Climate Change, Heartland Institute, pp. 247–348.

Steinhilber, F., Abreu, J.A., Beer, J., Brunner, I., Christl, M., Fischer, H., Heikkilä, U., Kubik, P.W., Mann, M., McCracken, K.G., Miller, H., Miyahara, H., Oerter, H. and Wilhelms, F., 2012. 9,400 years of cosmic radiation and solar activity from ice cores and tree rings. Proceedings of the National Academy of Sciences 109, 5967–5971.

Stine, S., 1994. Extreme and persistent drought in California and Patagonia during Mediaeval time. Nature 369, 546–549.

Stuut, J.-B.W., Smalley, I. and O'Hara-Dhand, K., 2009. Aeolian dust in Europe: African sources and European deposits. Quaternary International 198, 234–245.

Stuut, J.-B.W. and Prins, M.A, 2014. The significance of particle size of long-range transported mineral dust. Science Highlights: Dust, Pages Magazine 22, 71–72.

Swindles, G.T. et al., 2013. Centennial-scale climate change in Ireland during the Holocene. Earth-Science Reviews 126, 300–320.

Tanner, W.F., 1958. The zig-zag nature of Type I and Type IV curves. Journal Sedimentary Petroleum 28, 372–375.

Thevenon, F., Anselmetti, F.S., Bernasconi, S.M. and Schwikowski, M., 2009. Mineral dust and elemental black carbon records from an Alpine ice core (Colle Gnifetti glacier) over the last millennium. Journal of Geophysical Research 114, ID D17102-11p.

Thevenon, F., Chiaradia, M., Adatte, T., Hueglin, C. and Poté, J., 2012. Characterization of modern and fossil mineral dust transported to high altitude in the western Alps: Saharan sources and transport patterns. Advances in Meteorology 2012, ID 674385-14p.

Touchan, R., Anchukaitis, K.J., Meko, D.M., Attalah, S., Baisan, C. and Aloui, A., 2008. Long term context for recent drought in northwestern Africa. Geophysical Research Letters 35, L13705-5p.

Touchan, R., Anchukaitis, K.J. and Meko, D.M., 2010. Drought history from tree rings in the Mediterranean region. American Geophysical Union, Fall Meeting 2010, abstract A33J-05.

Touchan, R., Anchukaitis, K.J., Meko, D.M., Sabir, M., Attalah, S. and Aloui, A., 2011. Spatiotemporal drought variability in northwestern Africa over the last nine centuries. Climate Dynamics 37, 237–252.

Torrence, C. and G.P., Compo, 1998. A practical guide to wavelet analysis. Bulletin of the American Meteorological Society 79, 61-78.

Trigo, R.M., Pozo-Vazquez, D., Osborn, T.J., Castro-Diez, Y., Gamiz-Fortis, S. and Esteban-Parra, M.J., 2004. North Atlantic Oscillation influence on precipitation, river flow and water resources in the Iberian Peninsula. International Journal of Climatology 24, 925–944.

Trigo, R.M., Valente, M.A., Trigo, I.F., Miranda, M., Ramos, A.M., Paredes, D. and García-Herrera, R., 2008. North Atlantic wind and cyclone trends and their impact in the European precipitation and Atlantic significant wave height. Annals of the New York Academy of Sciences 1146, 212–234.

Trouet, V., Scourse, J.D. and Raible, C.C., 2012. North Atlantic storminess and Atlantic meridional overturning circulation during the last millennium: reconciling contradictory proxy records of NAO variability. Global and Planetary Change 84–85, 48–55.

Turner, R.E., Swenson, E.M. and Milan, C.S., 2000. Organic and inorganic contributions to vertical accretion in salt marsh sediments. In: Weinstein, M. and Kreeger, D.A. (Eds.), Concepts and Controversies in Tidal Marsh Ecology. Kluwer Academic Publishing, Dordrecht, Netherlands, pp. 583–595.

Van de Plassche, O., Wright, A.J., van der Borg, K. and de Jong, A.F.M., 2004. On the erosive trail of a 14th and 15th century hurricane in Connecticut (USA) salt marshes. Radiocarbon 46, 775–784.

Van der Does, M., Korte, L.F., Munday, C.I., Brummer, G.-J.A. and Stuut, J.-B.W., 2016. Particle size traces modern Saharan dust transport and deposition across the equatorial North Atlantic. Atmospheric Chemistry and Physics 16, 13697–13710.

Vaquero, J.M. and Trigo, R.M., 2015. Redefining the limit dates for the Maunder Minimum. New Astronomy 34, 120-122.

Vaughan, A.P.M., 2007. Climate and Geology – A Phanerozoic Perspective. In: Williams, M., Haywood, A.M., Gregory, F.J. and Schmidt, D.M. (Eds.), Deep-time Perspectives on Climate Change: Marrying the Signal from Computer Models and Biological Proxies. The Micropaleontological Society Special Publications. The Geological Society, London, pp. 5–59.

Williams, M., Haywood, A.M., Gregory, F.J. and Schmidt, D.M., 2007. Deep-time Perspectives on Climate Change: An Introduction. In: Williams, M., Haywood, A.M., Gregory, F.J. and Schmidt, D.M. (Eds.), Deep-time Perspectives on Climate Change: Marrying the Signal from Computer Models and Biological Proxies. The Micropaleontological Society Special Publications. The Geological Society, London, pp. 1–3.

Yu, Z. and Ito, E., 1999. Possible solar forcing of century-scale drought frequency in the northern Great Plains. Geology 27, 263–266.

https://www.ncdc.noaa.gov
http://www.pol.ac.uk/home/research/waveletcoherence/

Appendix 10.1. Percentage distribution of benthic foraminifera in Casa Branca marsh cores. Age (yr AD) – age in calendar years AD; H. spp. – *Haplophragmoides* spp.

Depth (cm)	Age (yr AD)	*J. macrescens*	*T. inflata*	*P. limnetis*	*H. manilaensis*+*H.* spp	*H. wilberti*	*M. fusca*	*Miliammina* spp.	*T. salsa*	*S. lobata*
0.0	2012	60	10	6		5	3	1	11	
0.5	2008	72	13	4	1		2	1	1	1
1.0	2003	77	12	2		1	1	1	4	1
1.5	2000	63	20	4		2	2	3	1	3
2.0	1998	52	36	1			4		7	
2.5	1995	72	22	2					1	
3.0	1992	80	18	1					1	
3.5	1988	83	13	1	1				1	
4.0	1984	64	26	1	2				6	
4.5	1981	71	15		3				6	
5.0	1977	74	20					1	2	
5.5	1975	69	14	1	2				10	
6.0	1972	73	10						13	
6.5	1970	86	9		1	0			3	
7.0	1968	88	5						2	
7.5	1967	82	10	2					0	
8.0	1965	86	8						4	
8.5	1963	84	13							
9.0	1960	84	9						2	
9.5	1957	80	16							
10.0	1953	80	14							
10.5	1949	83	12						1	
11.0	1945	67	25	2					2	
11.5	1934	35	57	1					3	
12.0	1921	62	27	2					4	
12.5	1897	74	25						1	
13.0	1873	66	32							
13.5	1863	61	35	2					2	
14.0	1853	56	40						3	
14.5	1847	61	32						2	
15.0	1841	71	24						4	
15.5	1836	72	22						4	
16.0	1832	78	16						3	
16.5	1827	80	18			1				
17.0	1823	86	13						1	
17.5	1818	64	32						1	1
18.0	1813	50	41			1			6	
18.5	1808	52	43	1					0	2
19.0	1803	35	59	2					3	
19.5	1798	23	73		3					2
20.0	1794	20	74			2			3	
20.5	1790	31	58	3		3			2	1
21.0	1786	33	56			7				
21.5	1781	44	45	2		4			1	2
22.0	1777	54	39	1		2			2	
22.5	1772	54	42	1					2	
23.0	1767	46	46	3	1	2				
23.5	1763	73	22	2	1			1		
24.0	1758	77	20	1						1
24.5	1753	85	12	2						
25.0	1749	79	15	4						1
25.5	1745	64	31	1						
26.0	1741	83	14	2						
26.5	1736	74	23	0					1	
27.0	1731	70	25	2						
27.5	1726	74	21	2						
28.0	1721	85	12							
29.0	1712	91	6							
31.0	1694	91	7							
33.0	1677	59	40				1			
35.0	1660	91	7							
37.0	1642	86	10	2			1			
39.0	1623	96	2	2						
41.0	1606	81	17	1						
43.0	1580	92	5							
45.0	1568	58	33	7			1			
47.0	1549	81	12	2						
49.0	1532	69	18	10					1	
52.0	1507	63	15	18			1			
55.0	1479	64	17	13						
58.0	1451	70	17	10			1			
61.0	1427	77	8	10			4			1
64.0	1404	87	5	5			1			
67.0	1384	66	20	10			3			
70.0	1354	71	10	12			3			1
73.0	1323	42	5	40			2			
76.0	1297									
79.0	1270									
82.0	1243									
85.0	1221									
88.0	1197									

Appendix 10.2. Aeolian and fluvial geochemical indicators in the Casa Branca marsh core. Age (yr AD) – age in calendar years AD.

Depth (cm)	Age (yr AD)	Zr/Rb	Zr/Al x 10^{-4}	K/Zr x 10^{-4}	Rb/Al x 10^{-4}	K/Al
0	2012	0.894	18.0	0.0134	20.2	0.2409
1	2003	1.151	20.6	0.0107	17.9	0.2207
2	1998	1.422	24.3	0.0087	17.1	0.2119
4	1984	0.874	17.1	0.0132	19.6	0.2260
6	1972	0.995	18.7	0.0121	18.8	0.2261
8	1965	1.076	18.3	0.0117	17.0	0.2149
10	1953	1.011	17.2	0.0124	17.0	0.2137
12	1921	1.000	16.5	0.0126	16.5	0.2080
14	1853	1.204	19.9	0.0107	16.6	0.2133
16	1832	0.973	16.7	0.0128	17.1	0.2136
18	1813	1.198	19.6	0.0108	16.4	0.2123
20	1794	1.273	20.6	0.0103	16.2	0.2125
24	1758	1.338	23.1	0.0095	17.2	0.2188
28	1721	1.263	20.7	0.0107	16.4	0.2204
31	1694	1.041	17.8	0.0123	17.1	0.2194
35	1660	1.047	17.9	0.0123	17.1	0.2198
39	1623	1.087	18.8	0.0118	17.3	0.2212
43	1580	1.052	18.0	0.0119	17.1	0.2138
47	1549	1.085	17.9	0.0123	16.5	0.2208
52	1507	0.994	16.9	0.0128	17.0	0.2175
55	1479	1.078	18.1	0.0119	16.8	0.2163
58	1451	1.042	17.9	0.0121	17.2	0.2160
61	1427	1.126	18.2	0.0117	16.2	0.2128
64	1404	1.094	18.2	0.0119	16.6	0.2162
68	1377	1.121	18.3	0.0115	16.3	0.2108
72	1332	1.216	20.9	0.0106	17.2	0.2219
75	1306	1.310	22.5	0.0099	17.1	0.2213
80	1261	1.320	20.6	0.0103	15.6	0.2110
85	1221	1.402	24.9	0.0088	17.8	0.2189
89	1190	1.298	21.2	0.0101	16.3	0.2152

Appendix 10.3. Relative percentage distribution of the sand and silt (coarse and medium) fractions in Casa Branca marsh cores. Age (yr AD) – age in calendar years AD.

Depth (cm)	Age (yr AD)	16-32 µm	8-16 µm
		Coarse silt	Medium silt
0	2012	8	24
1	2003	13	23
2	1998	19	24
3	1992	11	24
4	1984	8	25
6	1972	15	29
7	1968	10	24
8	1965	21	29
9	1960	8	23
10	1953	8	24
11	1945	10	26
12	1921	9	27
13	1873	11	24
14	1853	11	25
15	1841	6	21
16	1832	10	25
17	1823	10	23
18	1813	10	24
19	1803	14	22
20	1794	15	23
21	1786	13	17
22	1777	13	23
23	1767	13	22
24	1758	13	28
25	1749	10	24
26	1741	11	22
27	1731	12	25
28	1721	13	23
29	1712	11	23
30	1703	10	20
31	1694	12	22
33	1677	11	23
35	1660	13	22
37	1642	14	19
39	1623	8	24
41	1606	11	23
43	1588	10	23
45	1568	11	24
47	1549	12	24
49	1532	13	26
52	1507	11	25
55	1479	9	23
58	1451	10	27
61	1427	10	29
64	1404	11	24
67	1384	10	27
70	1354	15	25
73	1323	14	25
76	1297	13	26
79	1270	14	26
82	1243	18	25
85	1221	16	24
88	1197	13	25
90	1178	13	23

11 Concluding remarks

11.1. General conclusions

The focus of the most recent research on the solar–terrestrial climate interaction has turned towards regional climate responses, instead of global ones, as various studies (some of them mentioned along this manuscript) emphasized the importance of the solar forcing for regional climate variability. As a result, there is a need for local/regional paleoenvironmental and paleoclimatic studies to better disentangle the intricate mechanisms of the Sun–Earth system. To a certain degree the current effort adds new data worthy of debate in a wider forum.

This PhD dissertation presents novel records of (paleo)biological, geochemical, sedimentological and historical data of climatological interest from a suite of multi-proxy studies of the west Portuguese coast, which have been analyzed in relation with SA. The high-resolution records preserved in two dated-sediment cores taken on the high marsh zone of the Caminha and Casa Branca tidal marshes, in the northwest and southwest coast, respectively, were primarily used to answer the key motivating question: *Is there a relationship between the paleoecology of marsh benthic foraminifera and climatic indices?* Important answers were achieved contributing to increase the knowledge on the west Iberian margin's paleoclimatic evolution in the context of the northeast Atlantic region. Aiming to get the best possible answer, other datasets have been incorporated to the research – instrumental climate data, GHD, WP, historical *pro-pluvia* and *pro-serenitate* rogations, modelled temperatures and precipitation, atmospheric circulation modes, solar and geochemical-sedimentological proxies, in order to constrain both, the evolution of local/regional climate regimes and the NW *vs.* SW coast response along the common record for the last two millennia.

Present environmental conditions (Table 11.1):

⇒ The study of the seasonal variations of water temperature and salinity performed along three estuaries of the W Portuguese coast (Minho, Tejo and Mira) allowed to conclude that the modern dissimilar climate from the northern and southern coastlines introduces significant changes in the hydrological balance of the W coast estuaries. The freshwater drainage's contribution to the estuaries is reflected in the tidal marshes' interstitial waters, with prevailing mesohaline conditions in the marsh interstitial waters of the Minho lower estuary and euhaline to hypersaline for the Tejo and Mira lower estuaries. The seasonal cycle is also well noticeable either in the NW, under warm

summers and no dry season (C_{fb} climate type) or in the SW, under hot and dry summers (C_{sa} climate type). In the low-salinity baseline of the Caminha tidal marsh, living foraminifera are essentially composed by the agglutinated species *Haplophragmoides manilaensis*, *Miliammina fusca*, *Pseudothurammina limnetis*, *Psammosphaera* sp. and *Trochamminita salsa/irregularis*. In both, the Tejo and Mira salt marshes, *Ammonia beccarii*, *Ammonia tepida*, *Haynesina germanica*, *Jadammina macrescens* and *Trochammina inflata* are the dominant foraminifera.

Table 11.1. Climate types of the NW and SW Portuguese coasts and main features, as defined based on the studies performed at the marshes surface and estuaries.

SURFACE	NW coast	SW coast	
Climate	C_{fb}	C_{sa}	**Chapter 2**
Flooding waters' salinity	Limnetic to euhaline	Euhaline to slightly polyhaline	
Sediment interstitial waters' salinity	Mesohaline	Polyhaline to hypersaline	
Foraminifera dominant species	*H. manilaensis, M. fusca, P. limnetis, Psammosphaera* sp., *T. salsa*	*J. macrescens, T. inflata, A. beccarii, A. tepida, H. germanica*	
Br^- marsh interstitial waters (mg/L)	51 to 87*	54 to 195*	**Chapters 8** and **9**
Br marsh sediments (mg/kg)	49 to 389*	53 to 233*	

Climate key: C, Temperate; f, without dry season; s, with dry season; a, hot summer; b, warm summer
* Minimum and maximum of average median values from low and high marsh

⇒ As regards Br biogeochemical cycling on the salt marshes of the western Portuguese coast, four estuaries (Minho/Lima, NW coast and Sado/Mira, SW coast) provided evidence that beyond the Br common (marine) source, its enrichment chiefly derives from the interconnection with the organic component of soils/sediments. A clear difference between the marshes from the NW and SW coasts is noteworthy, with the Minho and Lima marsh sediments more enriched in both OM and total Br. This can be interpreted on the light of paleoclimate evolution, with the conceptual model of **Chapter 9** providing the major insights. Accordingly, the size of the marshes' Br pools mainly reflect the enrichment in OM and depositional conditions (e.g., salinity, vegetation type), as well as the production rates of volatile organobromine species under two different climate types. However, the human impact on the most recent Br enrichment (post-industrial) cannot be discarded, as can be seen in the high-resolution records from the two studied cores.

The high-resolution cores, FCPw1 – Caminha and FWCBr – Casa Branca (Figure 11.1):

⇒ The NW high marsh foraminiferal assemblages seem to well capture the precipitation/river flow seasonal (decadal) shorter-term variability in the period AD 1934–2010. When one compares the Caminha foraminiferal and the precipitation instrumental records on the Portuguese sectors of Minho and Lima basins, a direct relationship between the abundance of low-salinity species (*H.*

manilaensis, *H. wilberti*, *T. irregularis*, *P. limnetis*) and the inter- and intra-decadal precipitation became clear in the years of heavy rainfall recorded during dryer periods. On the other hand, a steady low precipitation throughout a period of 4 or 5 years appears enough to increase the presence of high marsh brackish-to-normal salinity species, namely *T. inflata* and *J. macrescens*. The statistically significant direct relationship found between the Minho–Lima winter precipitation and the winter NAO index reflects its connection with the climate dynamics of the North Atlantic region, and seems to reveal that the benthic foraminiferal record from the Caminha high marsh may contribute to high-resolution studies of SW Europe climate evolution (**Chapter 3**).

⇒ The historical report of 154 years on GHD for the MWR is a product from a combination of local and regional newspapers consulted in several archives and the proceedings from a Wine Cooperative (Ponte de Lima). This dataset allowed to reconstruct high-resolution growing season (March–August) temperatures (mean maxima) back to 1856, based on a simple linear regression model. GSTmax seem to express the complex interaction between different low frequency modes of atmospheric circulation and regional spring-summer mean maximum temperature variation patterns, in which the SCA mode revealed a particular importance (**Chapter 4**).

⇒ By combining GSTmax with Caminha tidal marsh foraminiferal assemblages' data (AD 1824–2010), it was possible to obtain a characterization of the main hydro-climatic episodes in the Minho region for the same period. Benthic foraminifera have responded to the interplay between atmospheric circulation (associated with the precipitation regime) and temperature variation patterns, affecting the water balance in the high marsh. An increase in the proportion of the foraminiferal species indicative of brackish-to-normal salinity occurred in periods of rainfall deficit, associated to higher GSTmax, after saltier conditions had been promoted by enhanced evapotranspiration (**Chapter 5**).

⇒ This climatic conditioning on the marsh benthic foraminiferal assemblages was supported further back, for the period 1626 to 1820, by a triennial-resolved wine production (WP) series based on hand-written Benedictine accounts from six monasteries of the Entre-Douro-e-Minho region (NW Portugal) and modelled precipitation and temperature data. Spectral analysis of these two proxy time series shows statistically significant peridiocities around 13-year and 60-year. The application of wavelet-based methods comparing these cycles in foraminifera with the ones in TSI and NAO reconstructions, as well as in a regional temperature climate model simulation, revealed some highly coherent responses that can be linked to SA. Despite impaired by proxies' resolution limitations, the CWT approach confirmed prominent cyclicity in foraminifera, essentially in connection with the Lower Gleissberg cycle (50–80 years). Although this research has provided

evidence towards a SA–climate coupled primer control on the Benedictine's WP trend, a key (harmful) human influence must be taken into account (particularly during the most acute reported crisis), even though hard to separate from the natural factor (**Chapter 6**).

⇒ The foraminiferal records have shown that both NW and SW marshes were formed in the 1300s, highlighting a major episode of sediment yield increase on lower estuaries driven by enhanced continental runoff. This closely followed a widespread climate shift – from dryer-to-wetter conditions and increased storms' intensity – illustrative of the MCA–LIA transitional period in Iberia, which seems to have happened on an even broader scale, on both sides of the Atlantic Ocean basin, as revealed by several marsh records in the eastern coast of the United States. After formation, the two marshes have evolved under different climatic scenarios, as expressed by more saline foraminiferal assemblages in Casa Branca (with *J. macrescens* and *T. inflata* as dominant species) than in Caminha (where *H. manilaensis and T. salsa/irregularis* dominate). Such difference has been mainly triggered by a relatively long-term trend of net gain from evapotranspiration over precipitation in Casa Branca, prompting an upper salinity baseline in the high marsh. Also according to the foraminiferal record of the two cores, it appears that the higher humidity context of the LIA in this Iberian region persisted differently in the NW coast (until the mid-18th century) and in the SW coast (until the mid-16th century). Drier phases have been identified, in both cores, by increases of *T. inflata*, being this species in the SW coast possibly related to large Sahara-dust intrusion events, as further supported by geochemical–sedimentological evidence (Zr/Rb, Zr/Al and 16–32 μm fraction). Lastly, either the brackish-to-normal salinity group (in the NW) or *T. inflata* (in the SW) reveal an analogous response to solar forcing, indicative of a major influence of the Lower Gleissberg cycle on the local/regional (hydro)climate variability after *ca.* 1700, i.e., next the Maunder Minimum (**Chapters 7** and **10**).

⇒ The Caminha Br pattern for the 20th century record appears to reflect as well anthropogenic sources: (i) globally, the use of leaded gasoline after 1934, where ethylene dibromide was added as lead scavenger to antiknock mixtures, and (ii) regionally, the application of flame retardants on forest fire management, encompassing the 1980s through mid-1990s in northern Portugal and Galicia (**Chapter 8**).

⇒ Regardless of the NW–SW different size of the Br pools, two similar Br temporal patterns in the Caminha and Casa Branca salt marshes emerged. They can be related to major SA oscillations (Grand Solar Minima) affecting the mid-latitudes climate, as described to some extent in **Chapter 1**, and responsible for decreased temperature and increased precipitation in the W coast of

Portugal. To this, one must add enhanced volcanic activity covarying with Grand Solar Minima and also potentially enriching salt marshes in Br (**Chapter 9**).

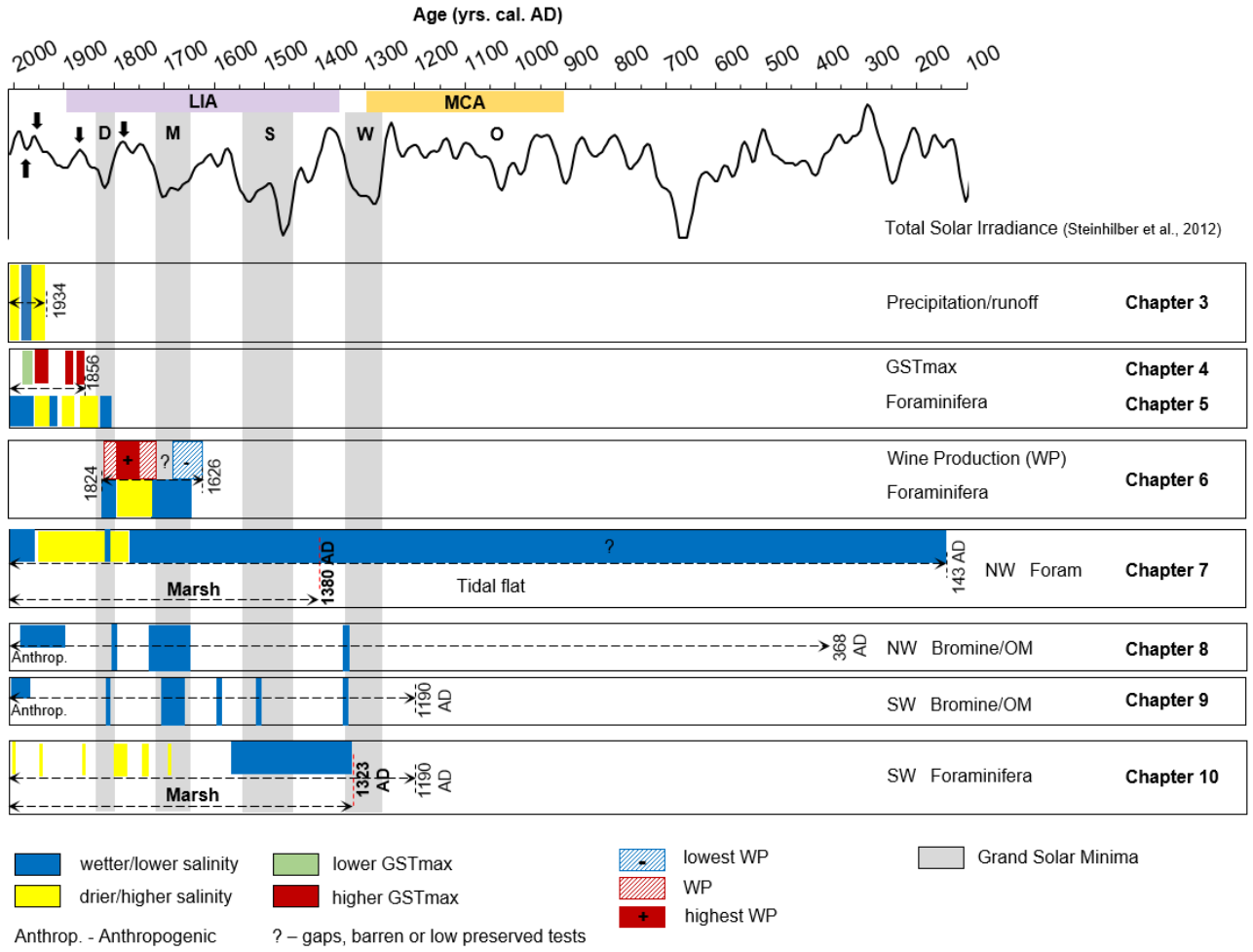

Figure 11.1. Main paleoclimate evolution characteristics of the NW and SW coasts as defined based on the down-core studies.

Although the results accomplished with the current investigation are not definitive until they can be replicated in new sites, as previously mentioned, they draw attention to the importance of taking into consideration additional influences, besides sea-level changes, when analysing the foraminiferal records of coastal wetlands, as other drivers can also be meaningful in dictating assemblages' distribution and composition. To end, it seems relevant to evoke that (paleo)climate science more than ever demands integrated interdisciplinary cooperation and holistic approach to deal with the challenges of the projections of future climate change, as well as upcoming policies. In this sense "it is impossible to separate the geological from the meteorological, as the two are expressions of the results of the same forces" as the meteorologist Sir Napier Shaw (1854–1945) once remarked.

11.2. Prospective

There are several research topics that can be addressed in order to improve the accuracy of the applied paleoenvironmental proxies and validate the results now obtained, namely:

(1) Further investigate and extend to the southern Portuguese regions the collection of GHD, to reconstruct growing season temperatures in a context of climate change.

(2) More extensive coring (intra- and inter-marsh) is necessary to improve the recognition of marsh benthic foraminifera (single species/group of species) as reliable proxies, to be used in the study of the Sun–terrestrial climate connection.

(3) Since no significant results were achieved in the current research concerning the solar cycles' influence on the Earth's climate via ocean–atmosphere interaction, specifically when exploring the relationships between the marsh foraminiferal record and (i) the SST and (ii) the Atlantic Multidecadal Oscillation (AMO) index – which happened possibly due to a lag response or internal dynamics stronger signal imposition –, it would be important to apply other statistical tools aiming to capture such connection.

(4) It also should be fundamental in the future to investigate more deeply the interaction climate–Br/OM in recent and pre-industrial sedimentary records from the Portuguese estuaries.

Additionally, it would be of great importance to advance more research dealing with:

(5) The climate impact on past human mortality and diseases as a tool of climate reconstruction and its relation with solar activity, volcanic activity and dust events in historical times; this also would lead to a sustained and comprehensive basis of any strategies for adapting and mitigating to climate change, so as to defend the health of present and future generations.

Appendices

Appendix A1. Systematic List

Systematic list of the dominant or diagnostic foraminiferal marsh species in the assemblages of cores' FCPw1, FCPwAR (Caminha), FWCBr1.4 and FWCBrAR (Casa Branca).

Suprageneric classification of agglutinated foraminifera (Textulariia) follows Debenay (2012) and Kaminski (2004).

Class FORAMINIFERA d'Orbigny, 1826

Subclass TEXTULARIIA

Order ASTRORHIZIDA Lankester, 1885

Suborder Saccamminina Lankester, 1885

Superfamily Saccamminacea Brady, 1881

Family Saccamminidae Brady, 1884

Subfamily Saccammininae Brady, 1884

Genus *Saccammina* Carpenter, 1869

***Saccammina* sp.**

Plate 3.2, Figure 3a,b, p. 94

Subfamily Thuramminінae Miklukho-Maklay, 1963

Genus *Pseudothurammina* Scott, Medioli & Williamson, 1981

Pseudothurammina limnetis Scott & Medioli, 1980

Plates 3.1 and 5.1, Figures 6a,b, p. 93, 152

1980 *Thurammina* ? *limnetis* Scott and Medioli, p. 43, pl. 1, figs. 1-3.

1995a *Pseudothurammina limnetis* (Scott and Medioli) - De Rijk, p. 29, pl. 1, figs. 15-16.

1999 *Pseudothurammina limnetis* (Scott & Medioli) - Hayward *et al*., p. 80; pl. 1, figs. 1-2.

Superfamily Psammosphaeracea Haeckel, 1894

Family Polysaccamminidae Loeblich & Tappan, 1984

Subfamily Polysaccammininae Loeblich & Tappan, 1984

Genus *Polysaccammina* Scott, 1976

Polysaccammina ipohalina Scott, 1976

Plate 5.2, Figure 6, p. 153

1976 *Polysaccammina ipohalina* Scott, p. 318, pl. 2, figs. 1-4.

1980 *Polysaccammina ipohalina* Scott, 1976 - Scott and Medioli, p. 38, pl. 2, figs. 8-9.

Family Psammosphaeridae Haeckel, 1894

Subfamily Psammosphaerinae Haeckel, 1894

Genus *Psammosphaera* Schulze, 1875

***Psammosphaera* sp.**

Plate 3.2, Figure 4a,b, p. 94

Order LITUOLIDA Lankester, 1885

Suborder *Rzehakinina Saidova,* 1981

Superfamily Rzehakinacea Cushman, 1933

Family Rzehakinidae Cushman, 1933

Subfamily Miliammininae Saidova, 1981

Genus *Miliammina* Heron-Allen & Earland, 1930

Miliammina fusca (Brady, 1870)

Plates 3.2 and 5.2, Figures 2a,b, p. 94, 153

1870 *Quinqueloculina fusca* Brady, p. 286, pl. 11, figs. 2a-c.

1980 *Miliammina fusca* (Brady) - Scott & Medioli, p. 40; pl. 2, figs. 1-3.

2006 *Miliammina fusca* (Brady) - Horton and Edwards, p. 68, pl. 1, figs. 5a-b.

Suborder Lituolina Lankester, 1885

Superfamily Lituolacea de Blainville, 1827

Family Haplophragmoididae Maync, 1952

Genus *Haplophragmoides* Cushman, 1910

Haplophragmoides wilberti Andersen, 1953

Plates 3.1 and 5.1, Figures 3, p. 93, 152

1953 *Haplophragmoides wilberti* Andersen, p. 21, pl. 2, figs. 5-6, pl. 3, figs. 9-16.

1999 *Haplophragmoides wilberti* Andersen, 1953 - Hayward et al., pl. 1, figs. 25–26

Haplophragmoides manilaensis Andersen, 1953

Plates 3.1 and 5.1, Figures 2, p. 93, 152

1953 *Haplophragmoides manilaensis* Andersen, p. 22, pl. 4, figs. 7-8.

1957 *Haplophragmoides bonplandi* Todd and Brönnimann, p. 23, pl. 2.

1980 *Haplophragmoides bonplandi* Todd and Brönnimann, 1957 - Scott and Medioli, p. 40, pl. 2, fig. 4-5.

Genus *Trochamminita* Cushman and Brönnimann, 1948

Trochamminita salsa/irregularis (Cushman and Brönnimann, 1948)

Plates 3.1 and 5.1, Figures 1a,b,c, p. 93, 152

1948b *Labrospira salsa* Cushman and Brönnimann, p.16, p l.3, figs. 5-6.

1957 *Alveophragmium salsum* (Cushman and Brönnimann) - Todd and Brönnimann, p. 23, pl. 2, fig. 3.

1957 *Trochamminita salsa* (Cushman and Brönnimann) - Saunders 1957, p. 6, pl. 1, figs. 3-8.

1999 *Trochamminita salsa* (Cushman and Brönnimann) - Hayward et al., p. 217, pl. 1, figs. 30-32.

1948b *Trochamminita irregularis* Cushman and Brönnimann, p. 17, pl. 4, fig. 1-3.

1957 *Trochamminita irregularis* Cushman and Brönnimann - Saunders, p. 4, pl. 2, figs. 3-8.

1957 *Trochamminita irregularis* Cushman and Brönnimann - Todd and Brönnimann, p. 30, pl. 4, figs. 19-22.

Suborder Trochamminina Saidova, 1981

Superfamily Trochamminacea Schwager, 1877

Family Trochamminidae Schwager, 1877

Subfamily Trochammininae Schwager, 1877

Genus *Paratrochammina* Brönnimann, 1979

Paratrochammina* (*Lepidoparatrochammina*) *guaratibaensis Brönnimann, 1986

Plates 3.2 and 5.2, Figures 5 and 3, p. 94, 153

2002 *Paratrochammina guaratibaensis* Brönnimann, 1986 - Debenay et al., p. 531, pl. 2, figs. 11-14.

Genus *Trochammina* Parker & Jones, 1859

Trochammina inflata (Montagu, 1808)

Plates 3.2 and 5.2, Figures 1a,b,c, p. 94, 153

1808 *Nautilus inflatus* - Montagu, p. 81; pl. 18, fig. 3.

1980 *Trochammina inflata* (Montagu) - Scott & Medioli, p. 44; pl. 3, figs. 12-14; pl. 4, figs. 1-3.

2002 *Trochammina inflata* (Montagu) - Debenay *et al*.; pl. 1, figs. 20, 21.

2006 *Trochammina inflata* (Montagu, 1808) - Horton and Edwards, p. 69, pl. 2, figs. 8a-d.

Subfamily Jadamminininae Saidova, 1981

Genus *Jadammina* Bartenstein & Brand, 1938

Jadammina macrescens (Brady, 1870)

Plates 3.2 and 5.2, Figures 7a,b; 5a,b, p. 94, 153

1870 *Trochammina inflata* (Montagu) var. *macrescens* - Brady, p. 290; pl. 11, fig. 5.

1938 *Jadammina polystoma* Bartenstein and Brand, p. 381, text-figs. 1-3.

1950 *Trochammina macrescens* Brady - Phleger and Walton, p. 281, pl. 2, figs. 6-7.

1971 *Jadammina macrescens* (Brady) - Murray, p. 41, pl. 13, figs. 1-5.

1980 *Trochammina macrescens* Brady - Scott & Medioli, p. 44; pl. 3, figs. 1-12.

1999 *Jadammina macrescens* (Brady) - Hayward *et al*., p. 83; pl. 1, figs. 27-29.

The present trend that includes *Jadammina macrescens* in the genus *Enzia* is not followed because the proposal of Holzmann et al. (2012) is not supported by a reliable result. Quoting their abstract "A molecular investigation of *Entzia* based on partial SSU rDNA sequences reveals that specimens of *Entzia* are genetically more or less identical to *Jadammina macrescens* sampled from Dovey Estuary"…

Subfamily Rotaliammininae Saidova, 1981

Genus *Siphotrochammina* Saunders, 1957

Siphotrochammina lobata Saunders, 1957

Plates 3.2 and 5.2, Figures 6; 4, p. 94, 153

1957 *Siphotrochammina lobata* - Saunders, p. 9; pl. 3, figs. 1, 2.

1992 *Siphotrochammina lobata* Saunders - Brönnimann *et al*., p. 21; pl. 4, figs. 1-2.

1995a *Siphotrochammina lobata* Saunders, 1957 - De Rijk, p. 33, pl. 3, figs. 9, 11-13.

Genus *Tiphotrocha* Saunders, 1957

Tiphotrocha comprimata (Cushman and Brönnimann, 1948)

Plates 3.1 and 5.1, Figures 5a,b, p. 93, 152

1948a *Trochammina comprimata* Cushman and Brönnimann, p. 41, pl. 8, figs. 1-3.

2006 *Tiphotrocha comprimata* (Cushman and Brönnimann) - Horton and Edwards p. 69, pl. 2, figs. a-e.

Order ROTALIIDA Lankester, 1885

Suborder Rotaliina Delage and Herouard, 1896

Superfamily Rotaliacea Ehrenberg, 1839

Family Rotaliidae Ehrenberg, 1839

Subfamily Pararotaliinae Reiss, 1963

Genus *Ammonia* Brünnich, 1772

Ammonia beccarii (Linné, 1758)

1758 *Nautilus beccarii* Linnaeus, p. 720.

1995 *Ammonia beccarii* (Linné) – Yassini and Jones, p. 175, figs. 994-999.

1999 *Ammonia beccarii* (Linné) – Alve and Murray, p.180, pl.2, fig.1.

Ammonia tepida (Cushman, 1926)

1926 *Rotalia beccarii* (Linné) var. t*epida* Cushman, p. 79, pl. 1.

1990 *Ammonia tepida* (Cushman, 1926) - Walton e Sloan, p. 133, Pl. 1, figs. 1 – 3, Pl. 2, figs. 2.

1995 *Ammonia tepida* (Cushman, 1926) - Pawlowski et al., p. 173, fig. 3.1 e 3.2.

Superfamily: Nonionacea Schultze, 1854

Family: Nonionidae Schultze, 1854

Subfamily: Nonioninae Schultze, 1854

Genus: Haynesina Banner and Culver, 1978

Haynesina germanica (Ehrenberg, 1840)

1840 Nonionina germanica Ehrenberg, p. 23, pl. 2, figs. 1a–g.

1930 Nonion germanicum (Ehrenberg) - Cushman, p. 8, 9, pl. 3, fig. 5.

1965 Protelphidium anglicum - Murray, p. 149–150, pl. 25, figs. 1–5, pl. 26, figs. 1–6.

1978 Haynesina germanica - Banner e Culver, , p. 191, Pl. 4, figs. 1-6, Pl. 5, figs. 1-8, Pl. 6, figs. 1-7, Pl. 7, figs. 1-6, Pl. 8, figs. 1-10, Pl. 9, figs. 1-11,15,18.

Alphabetic list of identified species

This list includes minor species identified from the 91,529 specimens studied. The names of the species included in the preceding Systematic List, are in bold.

Ammobaculites exiguus Cushman and Brönnimann, 1948

Ammonia beccarii (Linné, 1758)

Ammonia tepida (Cushman, 1926)

Ammoscalaria runiana (Heron-Allen and Earland, 1916)

Ammotium cassis (Parker, 1870)
Ammotium salsum (Cushman and Brönnimann, 1948)
Arenoparrella mexicana (Kornfeld, 1931)
Asterigerinata mamilla (Williamson, 1858)
Aubignyna sp.
Aubignyna hamblensis Murray, Whittaker and Alve, 2000
Balticammina pseudomacrescens Lutze and Whittaker, 1989
Birsteiniolla macrostoma Yankovskaya and Mikhalevich, 1972
Bolivina difformis (Williamson, 1858)
Bolivina dilatata Reuss, 1850
Bolivina ordinaria Phleger and Parker, 1952
Bolivina pseudoplicata Heron-Allen and Earland, 1930
Bolivina striatula Cushman, 1922
Bulimina elongata d'Orbigny, 1846
Bulimina elongata var. lappa Cushman and Parker, 1937
Bulimina marginata d'Orbigny, 1826
Cassidulina carinata Silvestri, 1896
Cassidulina laevigata d'Orbigny, 1826
Cassidulina teretis Tappan, 1951
Cibicides refulgens Montfort, 1808
Cibicidoides pseudoungeriana (Cushman, 1922)
Cribroelphidium incertum Williamson, 1858
Cribroelphidium selseyense (Heron-Allen and Earland, 1911)
Cribrostomoides sp.
Cribrostomoides jeffreysii (Williamson, 1858)
Deuterammina cf. *celtica* Brönnimann and Whittaker, 1990
Eggerelloides scaber (Williamson, 1858)
Elphidium excavatum (Terquem, 1875)
Elphidium gunteri Cole, 1931
Elphidium pulvereum Todd, 1958
Elphidium williamsoni Haynes, 1973
Gavelinopsis praegeri (Heron-Allen & Earland, 1913)
Glabratella brasiliensis Boltovskoy, 1959
Globocassidulina crassa (d'Orbigny, 1839)
Globocassidulina minuta (Cushman, 1933)
Globocassidulina subglobosa (Brady, 1881)
Haplophragmoides spp.
Haplophragmoides manilaensis Andersen, 1953
Haplophragmoides wilberti Andersen, 1953
Haynesina depressula (Walker & Jacob, 1798)

Haynesina germanica (Ehrenberg, 1840)

Helenina andersoni (Warren, 1957)

Hyalinonetrion gracillima (Seguenza, 1862)

Jadammina macrescens (Brady, 1870)

Lepidodeuterammina ochracea (Williamson, 1858)

Lobatula lobatula (Walker and Jacob, 1798)

Miliammina fusca (Brady, 1870)

Miliammina obliqua Heron-Allen and Earland, 1930

Miliammina spp.

Morulaeplecta bulbosa Höglund, 1947

Nonion pauperatus (Balkwill and Wright, 1885)

Nonionoides turgidum (Williamson, 1858)

Paratrochammina* (*Lepidoparatrochammina*) *guaratibaensis Brönnimann, 1986

Paratrochammina spp.

Planorbulina mediterranensis d'Orbigny, 1826

Patellina corrugata Williamson, 1858

Polysaccammina ipohalina Scott, 1976

Portatrochammina murrayi Brönnimann and Zaninetti, 1984

Procerolagena clavata (d'Orbigny, 1846)

***Psammosphaera* sp.**

Pseudothurammina limnetis Scott and Medioli, 1980

Quinqueloculina sp.

Rectuvigerina phlegeri Le Calvez, 1959

Remaneica helgolandica Rhumbler, 1938

Reophax curtus Cushman, 1920

Reophax dentaliformis de Montfort, 1808

Reophax nana Rhumbler, 1913

Reophax nodulosus Brady, 1879

Reophax scorpiurus de Montfort, 1808

Saccammina sp.

Scherochorella moniliforme (Siddall, 1886)

Septotrochammina gonzalesi (Seiglie, 1964)

Sigmoilopsis sp.

Siliconodosarina delicatula Colom, 1963

Siphotrochammina lobata Saunders, 1957

Stainforthia fusiformis (Williamson, 1848)

Svratkina tuberculata (Balkwill and Wright, 1885)

Tiphotrocha comprimata (Cushman and Brönnimann, 1948)

Textularia earlandi Parker, 1952

Trochammina inflata (Montagu, 1808)

Trochammina sp.

Trochamminita salsa (Cushman and Brönnimann, 1948)

References

Alve, E. and Murray, J.W. 1999. Marginal marine environments of the Skagerrak and Kattegat: a baseline study of living (stained) benthic foraminiferal ecology. Palaeogeography, Palaeoclimatology, Palaeoecology, 146, 171–193.

Andersen, H.V., 1953. Two new species of Haplophragmoides from the Louisiana coast. Contributions from the Cushman Foundation for Foraminiferal Research 4, 21–22.

Balkwill, F.P., and Wright, J. 1885. Report on some Recent foraminifera found off the coast of Dublin and in the Irish Sea. Transactions of the Royal Irish Academy, 28, 317–368.

Banner, F.T. and Culver, S.J. 1978. Quaternary Haynesina n. gen. and Paleogene Protelphidium Haynes; their morphology, affinities and distribution. Journal of Foraminiferal Research, 8, 177–207.

Bartenstein, H. and Brand, E., 1938. Die Foraminiferen-Fauna des Jade-Gebietes. 1. *Jadammina polystoma* n. g. n. sp. Aus dem Jade-Gebiete (For.). Senckenbergiana 20, 381–385.

Berthois, L. and Le Calvez, Y., 1959. Deuxième contribution à l'étude de la sédimentation dans le golfe de Gascogne. Revue des Travaux de l'Institut des Pêches Maritimes, 23, 3, 323–375.

Boltovskoy, E. 1959. Foraminíferos recientes del Sur del Brasil y sus relaciones con los de Argentina e India del Este. Serv. Hidrogr. Nav. Secret. Mar., Rep. Argentina, H. 1005, 1–124.

Brady, H.B., 1870. Analysis and descriptions of the foraminifera. Annals and Magazine of Natural History 4(6), 273–309.

Brady, H.B. 1879. Notes on some of the reticularian Rhizopoda of the “Challenger” Expedition. Part 1. On new or little known arenaceous types. Quarterly Journal of Microscopical Science, new series, 19, 20–63.

Brady, H.B. 1881. Notes on some of the reticularian Rhizopoda of the Challenger Expedition. Part III. 1. Classification. 2. Further notes on new species. 3. Note on Biloculina mud. Quarterly Journal of Microscopical Science, new series, 21, 31–71.

Cole, W. S. 1931. The Pliocene and Pleistocene foraminifera of Florida. Florida State Geological Survey Bulletin, 6, 1–79.

Colom, G., 1963. The Foraminifera of the bay of Vigo. J Invest Pesquera 23, 71–89.

Cushman, J.A. 1920. Foraminifera of the Atlantic Ocean, Part 2. Lituolidae. Bulletin of the United States National Museum, 104(2), 1–143.

Cushman, J.A. 1922. The Foraminifera of the Atlantic Ocean, pt. 3, Textulariidae. — U.S. Nat. Mus. Bull., 104, 1–149.

Cushman, J.A., Bronnimann, P., 1948a. Additional new species of arenaceous foraminifera from brackish water of Trinidad. Cushman Laboratory for Foraminiferal Research 24, 37–43.

Cushman, J.A., Bronnimann, P., 1948b. Some new genera and species of foraminifera from shallow waters of Trinidad. Contributions fromthe Cushman Foundation for Foraminiferal Research Contributions. 24, 12–21.

Cushman, J.A., and Parker, F.L., 1937. Notes on some European species of Bulimina. Contributions from the Cushman Laboratory for Foraminiferal Research, 12, 5–10.

Balkwill F. P., Wright J., 1885. Report on some Recent foraminifera found off the coast of Dublin in the Irish Sea. Transactions of the Royal Irish Academy, 28, 317–368.

Brönnimann P., 1986. Paratrochammina (Lepidoparatrochammina) guaratibaensis n sp. from brackish waters of Brazil and a check-list of Recent trochamminaceans from brackish waters (Protista: Foraminifera). Revue de Paléobiologie 5, 221–229.

Bronnimann, P. & Whittaker, J.E, 1990. Revision of the Trochamminacea and Remaneicacea of the Plymouth District, SW England, Described by Heron-Allen and Earland (1930). P. 105-137, In: Hemleben, C. et al. (Eds.), Paleoecology, Biostratigraphy, Paleoecography and Taxonomy of agglutinated Foraminifera. Kluwer. Netherlands.

Brönnimann, P., Lutze, G.F., and Whittaker, J.E. 1989. Balticammina pseudomacrescens, a new brackish water trochamminid from the western Baltic Sea, with remarks on the wall structure. Meyniana, 41, 167–177.

Brönnimann, P., Whittaker, J.E. and Zaninetti, L., 1992. Brackish water foraminifera from mangrove sediments of southwestern Viti Levu, Fiji Islands, Southwest Pacific. Revue Paléobiologie 11, 13–65.

Brönnimann, P. and Zaninetti, L. 1984. Agglutinated foraminifera mainly Trochamminacea from the Baia de Sepetiba, near Rio de Janeiro, Brazil. Revue de Paléobiologie, Généve, 3, 63–115.

Cushman, J.A. 1926. Recent foraminifera from Porto Rico: Publications of the Carnegie Institution of Washington, 342, 73–84.

Cushman, J.A. 1930. The foraminifera of the Atlantic Ocean, Part 7: Nonionidae, Camerinidae, Peneroplidae, and Alveolinellidae. Smithsonian Institute. United States National Museum Bulletin, 104(7), 1–79.

Cushman J. A., 1933. Some new Recent foraminifera from the tropical Pacific. Contributions from the Cushman Laboratory for Foraminiferal Research, 9, 77–95.

Cushman, J.A. and Brönnimann, P., 1948a. Additional new species of arenaceous foraminifera from brackish water of Trinidad. Cushman Laboratory for Foraminiferal Research 24, 37–43.

Cushman, J.A. and Brönnimann, P., 1948b. Some new genera and species of foraminifera from shallow waters of Trinidad. Contributions from the Cushman Foundation for Foraminiferal Research Contributions 24, pp.12–21.

d'Orbigny A., 1826. Tableau méthodique de la classe des Céphalopodes, 3e Ordre, Foraminifères. Annales de Sciences Naturelles, 7, 254–314.

d'Orbigny, A., 1839. Voyage dans l'Amérique méridionale, foraminifères. Levrault, Paris and Strasbourg, vol. 5, 86p.

De Montfort, P. D., 1808. Conchyliologie systématique et classification méthodique des coquilles, t. 1. Paris, France, F. de Schoell ed., 1–410.

d'Orbigny, A., 1846. Foraminiferes fossiles du Bassin Tertiaire de Vienne (Autriche). i-xxxvi, 312 p., Gide & Co., Paris.

Debenay, J.-P., Guiral, D. and Parra, M., 2002. Ecological factors acting on microfauna in mangrove swamps. The case of foraminiferal assemblages in French Guiana. Estuarine, Coastal and Shelf Science 55, 509–533.

Debenay, J.-P., 2012. A Guide to 1,000 Foraminifera from Southwestern Pacific: New Caledonia. IRD Editions, 378p.

De Rijk, S., 1995a. Agglutinated foraminifera as indicators of salt marsh development in relation to late Holocene sea level rise (Great Marshes at Barnstable, Massachusetts), Febo, Utrecht, 188p.

Ehrenberg, C.G. 1840. Eine, weitere Erlauterung des Organismus meherer in Berlin lebend beobachteter Polythalamien der Nordesee. Abhandlungen der Königlichen Akademie der Wissenschaften, Berlin, 18–23.

Haynes, J.R. 1973. Cardigan Bay recent foraminifera. Bulletin of the British Museum of Natural History (Zoology), supplement 4, 1–245.

Hayward, B.W., Grenfell H.R., Ried C.M. and Hayward, K.A., 1999. Recent New Zealand Shallow-Water Benthic Foraminifera: Taxonomy, Ecologic Distribution, Biogeography, and Use in Paleoenvironmental Assessment. *Institute of Geological and Nuclear Sciences monographs* 21, pp.1–264.

Heron-Allen, E., and Earland, A., 1911. On Recent and fossil foraminifera of the shore sands of Selsey Bill, Sussex VIII: Journal of the Royal Microscopical Society, v. 1911, 436–498.

Heron-Allen, E. and Earland, A. 1913. Clare Island Survey: part 64 -Foraminifera Proc. R. Ir. Acud., Dublin, 31 (sect. 3), 1–188, pls. 1-13.

Heron-Allen, E. and Earland, A., 1916. The foraminifera of the west coast of Scotland. Transactions of the Linnean Society of London, Zoology, series 2, 11, 197–299.

Heron-Allen, E., and Earland, A., 1930. Some new foraminifera from the South Atlantic, Part 3. Journal of the Royal Microscopical Society, London, 50, 38–45.

Höglund, H. 1947. Foraminifera in the Gullmar Fjord and Skagerrak. Zoologiska bidrag från Uppsala, 26, 1–328.

Holzmann, M., Kaminski, M., Filipescu, S., Pawlowski, J. 2012. A molecular comparison of *Entzia tetrastomella* and *Jadammina macrescens*. Abstract in Alegret, Ortiz & Kaminski (Eds.), 2012. Ninth International Workshop on Agglutinated Foraminifera, Abstract Volume. p.42.

Horton, B.P. and Edwards, R.J., 2006. Quantifying Holocene sea level change using intertidal foraminifera: lessons from the British Isles. Journal of Foraminiferal Research Special Publication 40, 1–97.

Kaminski, M., 2004. The year 2000 classification of the agglutinated foraminifera. In: Bubík M., Kaminski M. A. (Eds): *Proceedings of the Sixth International Workshop on Agglutinated Foraminifera*. Grzybowski Foundation Special Publication 8, 237–255.

Kornfeld, M.M., 1931. Recent littoral foraminifera from Texas and Louisiana. Standford University Department of Geology Contributions, 1 (3), 77–101.

Linnaeus, C. 1758. Systema Naturae per regna tria naturae, secundum classes, ordines, genera, species, cum characteribus, differentiis, synonymis, locis. Editio decima, reformata. Laurentius Salvius: Holmiae. ii, 824p.

Monfort, D. de, 1808 – Conchyliologie systématique et classification méthodique des coquilles. Paris, Schoell.

Montagu, G., 1808. Supplement to Testacea Britannica. S. Woolmer, Exeter, 183p.

Murray, J. W., 1965. Two new species of British Recent Foraminiferida. Contributions from the Cushman Foundation for Foraminiferal Research, 16, 148–150.

Murray, J.W., 1971. An Atlas of British Recent Foraminiferids. Heinemann Educational Book, 244p.

Murray, J. W., Whittaker, J. E., Alve, E., 2000. On the type species of Aubignyna and a description of A. hamblensis, a new microforaminifer from temperate shallow waters. Journal of Micropalaeontology, 19(1), 61–67.

Parker, W.K. 1870. In Dawson, G.M. On the foramininifera of the Gulf and River St. Lawrence. Canadian Naturalist and Quarterly Journal of Science, new series, 5, 172–177.

Pawlowski, J., Bolivar, I., Fahrni, J.F., and Zaninetti, L. 1995. DNA analysis of “Ammonia beccarii” morphotypes: one or more species? Marine Micropaleontology, 26, 171–178.

Phleger, F.B. and Parker, F.L. 1952. Ecology of foraminifera, northwest Gulf of Mexico. Part 2. Foraminifera species. Geological Society of America Memoir, 46, 1–64.

Phleger, F.B. and Walton, W.R., 1950. Ecology of marsh and bay foraminifera, Barnstable, Massachusetts. American Journal of Science 248, 274–294.

Reuss, A.E., 1850. Neue Foraminiferen aus den Schichten des österreichischen Tertiärbeckens. Denkschriften der mathematisch-naturwissenschaftlichen Classe der kaiserlichen Akademie der Wissenschaften (1849), 1, 360–395.

Rhumbler, L. 1913. Die foraminiferen (Thalamorphoren) der Plankton-Expedition: Ergebnisse der Plankton-Expedition der Humboldt-Stiftung, 3, Lief. C.

Rhumbler, L. 1938. Foraminiferen aus dem Meeressand von Helgoland, gesammelt von A. Remane Kiel). Kieler Meeresforschungen, 2, 157–222.

Saunders, J.B., 1957. Trochamminidae and certain Lituolidae (Foraminifera) from the recent brackish-water sediments of Trinidad, British West Indies. Smithsonian Miscellaneous Collections 134, 1–16.

Scott, D.B., 1976. Brackish-water foraminifera from southern California and description of *Polysaccammina ipohalina* n. gen., n. sp. Journal of Foraminiferal Research 6, 312–321.

Scott, D.B. and Medioli, F.S., 1980. Quantitative studies of marsh foraminiferal distributions in Nova Scotia: their implications for the study of sea-level changes. Cushman Foundation for Foraminiferal Research, Special Publication 17, 59p.

Seguenza G., 1862. Dei terreni Terziarii del distretto di Messina; Parte II - Descrizione dei foraminiferi monotalamici delle marne Mioceniche del distretto di Messin. Messina. T. Capra.

Seiglie, G. A., 1964. New and rare foraminifers from Los Testigos Reefs, Venezuela. Caribbean Journal of Science, 4, 497–512.

Siddall, J.D. 1886. Report on the foraminifera of the Liverpool Marine Biology Committee District. Proceedings of the Literary and Philosophical Society, Liverpool, 40 appendix 4, 2–71.

Silvestri, A., 1896. Foraminiferi pliocenici di Siena. Part I. Memorie dell' Accademia Pontificia dei Nuovi Lincei 12, 1–224.

Tappan, H. 1951. Northern Alaska index Foraminifera. Contributions from the Cushman Foundation for Foraminiferal Research, Lawrence, Kansas, 2, 1, 1–8.

Terquem, O. 1875. Essai sur le classement des animaux qui vivent sur la plage et dans les environs de Dunquerque, Memoirs de la Society Dunkerquoise (1876), 19, 405–447.

Todd, R. 1958. Foraminifera from Western Mediterranean Deep-sea Cores. Rep. Swedish Deep-Sea Exped., 8 (2), 167–216.

Todd, R. and Brönnimann, P., 1957. Recent foraminifera and thecamoebina from the eastern Gulf of Paria. Contributions from the Cushman Foundation for Foraminiferal Research, Special Publication 6, 1–43.

Walton, W. and Sloan, B. 1990. The genus AmmoniaBrünnich, 1772: its geographic distribution and morphological variability. Journal of Foraminiferal Research, 20, 128–156.

Warren A.D., 1957. Foraminifera of the Buras-Scofield Bayou region, southeast Louisiana. Contributions from the Cushman Foundation for Foraminiferal Research, 8 (1), 29–40.

Walker G., and Jacob E., 1798. In Adams, G.: Essays on the Microscope, 2nd edition. London. 712p.

Williamson, W.C., 1848. On the Recent British species of the genus Lagena. Annals and Magazine of Natural History, series 2, 1, 1–20.

Williamson, W.C., Medioli, F.S., Schafer, C.T., 1858. On the Recent Foraminifera of Great Britain. Ray Society, London, 107p.

Yankovskaya, A.I., and Mikhalevich, V.I., 1972. Foraminifery ozera Issyk-kul' gruntovykh vod sredney Azii [Foraminifera from Lake Issyk-kul' and ground water of central Asia], Doklady Akademii Nauk SSSR, 205, 1005–1008.

Yassini, I. and Jones, B.G. 1995. Foraminiferida and Ostracoda from Estuarine and Shelf Environments on the Southeastern Coast of Australia. University of Wollongong Press, Australia, 484p.

Appendix A2. List of the scrutinized local/regional newspapers.

Newspaper title	Years	Documentary source
O Lethes	1865–1870	Arquivo Municipal de Ponte de Lima
Echo do Lima	1866–1882	Arquivo Municipal de Ponte de Lima
Estrella do Lima	1868	Arquivo Municipal de Ponte de Lima
O Commercio do Lima	1879–1919	Arquivo Municipal de Ponte de Lima
Jornal do Minho	1884	Arquivo Municipal de Ponte de Lima
O Lima	1894–1962	Arquivo Municipal de Ponte de Lima
O Comércio do Lima 2ª Série	1906 to 1914	Arquivo Municipal de Ponte de Lima
Cardeal Saraiva	1910 to 1939	Arquivo Municipal de Ponte de Lima
Democracia do Lima	1921-1922	Arquivo Municipal de Ponte de Lima
Rio Lima	1922-1935	Arquivo Municipal de Ponte de Lima
Caminhense	1971 to 1983	Biblioteca Municipal de Caminha
Echo do Lima	1866–1891	Biblioteca Nacional de Portugal
Echo do Lima	1905–1906	Biblioteca Nacional de Portugal
A Voz do Lima	1886–1892	Biblioteca Nacional de Portugal
A Estrela de Caminha	1882–1895	Biblioteca Nacional de Portugal
O Valenciano	1880–1919	Biblioteca Nacional de Portugal
O Noticioso	1869–1898	Biblioteca Nacional de Portugal
Comércio do Minho	1873–1921	Biblioteca Nacional de Portugal
Correio do Minho	1926 to present	Biblioteca Nacional de Portugal
Diário do Minho	1919 to present	Biblioteca Nacional de Portugal
O Comércio de Braga	1890–1891	Biblioteca Nacional de Portugal
O Amarense	1898–1905	Biblioteca Nacional de Portugal
O Comércio do Vez	1884–1906	Biblioteca Nacional de Portugal
Jornal dos Arcos	1896–1903	Biblioteca Nacional de Portugal
A Voz do Minho	1862–1869	Biblioteca Nacional de Portugal
Notícias dos Arcos	1931 to present	Biblioteca Nacional de Portugal
A folha de Vila Verde	1885–1948	Biblioteca Nacional de Portugal
A Semana	1892–1904	Biblioteca Nacional de Portugal
O Valenciano	1880–1919	Biblioteca Nacional de Portugal
A Grinalda	1895	Biblioteca Nacional de Portugal
Boletim Oficial de Braga	1846	Arquivo Distrital de Braga
Crónica Nacional de Braga	1846	Arquivo Distrital de Braga
A Gazeta de Braga	1846; 1864–1865	Arquivo Distrital de Braga
O Barqueiro do Cávado	1853	Arquivo Distrital de Braga
O Moderado	1853–1856	Arquivo Distrital de Braga
O Pharol do Minho	1854–1855	Arquivo Distrital de Braga
O Bracarense	1855	Arquivo Distrital de Braga
O Independente	1855–1861	Arquivo Distrital de Braga
O Bracarense	1862, 1864, 1865; 1899	Arquivo Distrital de Braga
O Comércio de Braga	1862	Arquivo Distrital de Braga
A Revista de Braga	1862	Arquivo Distrital de Braga
O Clamor doNorte	1863	Arquivo Distrital de Braga
O Distrito de Braga	1863	Arquivo Distrital de Braga
O Progresso	1863–1865	Arquivo Distrital de Braga
Gazeta de Braga	1864–1866	Arquivo Distrital de Braga
A União Progressista	1865–1866	Arquivo Distrital de Braga
O Comércio	1869	Arquivo Distrital de Braga
Gazeta do Minho	1871	Arquivo Distrital de Braga
O Comércio do Minho	1873–1915	Arquivo Distrital de Braga
Jornal do Minho	1875	Arquivo Distrital de Braga
Diário do Minho	1877–1976	Arquivo Distrital de Braga
A Correspondência do Norte	1880–1883	Arquivo Distrital de Braga
O Constituinte	1883	Arquivo Distrital de Braga
Folha de Vila Verde	1885–?	Arquivo Distrital de Braga
O Campo	1891	Arquivo Distrital de Braga
O Comércio de Braga	1892	Arquivo Distrital de Braga
Correio do Minho	1902–1966	Arquivo Distrital de Braga
O Jornal de Braga	1902	Arquivo Distrital de Braga
Ecos do Minho	1911	Arquivo Distrital de Braga
Jornal do Norte	1924	Arquivo Distrital de Braga
O Rural	1966	Arquivo Distrital de Braga
O Vilaverdense	1966	Arquivo Distrital de Braga
O Cávado	1974–1975	Arquivo Distrital de Braga
A Aurora do Lima	1966–1991	Arquivo Distrital de Braga
A Aurora do Lima	1856–1870	Biblioteca Pública Municipal do Porto
A Razão	1857–1862	Biblioteca Pública Municipal do Porto
A Voz do Minho	1862–1870	Biblioteca Pública Municipal do Porto
O Bracarense	1855–1862	Biblioteca Pública Municipal do Porto